Modelling runoff generation and connectivity for semi-arid hillslopes and small catchments

Simeon Matthew Reaney

Submitted in accordance with the
requirements for the degree of
Doctor of Philosophy

University of Leeds
School of Geography

October 2003

Abstract

The processes relating to runoff generation in a semi-arid environment at the hillslope scale are poorly understood. This research considers the amount and origin of water reaching the channel during a storm event using a combination of field experiments and computer simulation techniques.

From the field experiments, it was found that the key controls on runoff generation at the point scale are the surface cover of rock fragments, vegetation cover, slope gradient and surface roughness. The effect of land management was found to be greater than geology.

The simulation modelling work investigated the controls on runoff generation at the hillslope and small catchment scales. It was found that the storm characteristics are far more important than surface properties in determining the amount of discharge from a slope. The temporal fragmentation of the rainfall was found to control the distribution of flow path lengths and hence the amount of discharge leaving a slope. The key surface controls on the form of the discharge hydrograph are slope length, slope gradient and the hydrological properties at the base of the slope.

The origin of runoff was investigated using autonomous software agents able to trace the flow of water through a catchment. This technique is able to give a unique picture of the origin of runoff within a catchment. It was shown that the spatial pattern of the origin of runoff is complex and varies significantly between catchments.

This research has shown that there are two key themes in determining the amount of runoff reaching the channel network: the interplay between the distribution of flow path lengths generated during a storm and the distributions of flow lengths to the channel as a function of the landscape. The second theme relates to the importance of the spatial structure of hydrological areas within the landscape.

Acknowledgements

I would like to thank Prof. Mike Kirkby and Dr. Louise Bracken for their support, guidance and encouragement throughout the course of this research. This work was funded by a School of Geography, University of Leeds studentship and financial support from the EU PESERA project.

Many people have helped with this research whose assistance I would like to acknowledge. Julie Shannon at King's College London supplied the rainfall time series and geospatial data on the distribution of land use in the catchment. Dr. Nick Drake, also at King's, loaned equipment used on the field work which was extremely useful. I would like to thank Kathy Hayes, Mercedes del Rio and Rachel Harrison for help with field work in Spain. I would also like to thank David Ashley for pointing me in the right direction in the laboratory and Alan Cundill for helping with the laboratory analysis.

Mike Crabtree, John Dodds, Andy Evans, John Harrison and Zia have provided valuable IT assistance and make a powerful machine available for the modelling work. Over the course of my time in Leeds, I am sure that I took up a disproportionate amount of their time, for which I apologise.

In the preparation of this thesis, David Appleyard and Mark Newcombe assisted with a number of the graphics and Helen Aslett, Richard Austen, Louise Bracken, Kerry Gleeson, Brian Irvine, Kath Roberts, Claire Seymore and Ramsay Reaney all helped with the editing of the thesis.

Many people have helped with personal support, mainly in the form of cups of coffee and beer. I would like to thank, in alphabetical order: Helen Aslett, Richard Austen, Lydia Bruce-Burgess, Alison Heppenstall, Suzie Hewitt, Louise Mackay, Hazel Parry, Hamish Pritchard, Ruth Schofield and Lizzie Sagoo for keeping me sane and for encouragement when times were dark.

Finally I would like to thank the people that have helped me to get to this point: Prof. John Thornes and Dr. Mark Mulligan at King's College London for inspiration and for introducing me to modelling and most importantly my parents, Hilary and Ramsay Reaney, for their support and encouragement throughout the course of my PhD and my first degree. Without their support, none of this would have been possible.

Table of Contents

List of Figures

List of Tables

Symbols used

β	=	Surface gradient
ff	=	The Darcy-Weisbach friction factor
g	=	Gravity constant.
i	=	Infiltration
i_c	=	Infiltration capacity (mm hr^{-1})
i_r	=	Infiltration rate (mm hr^{-1})
K	=	Hydraulic conductivity
K_s	=	Saturated hydraulic conductivity
m	=	Metres
R	=	Hydraulic radius
rc	=	Runoff coefficient
rf	=	Rainfall
rf_d	=	Rainfall depth
rf_i	=	Rainfall intensity
RPM	=	Rectangular Pulse Model
RR	=	Random Roughness
s	=	Slope of the energy gradient.
S_p	=	Sorpivity
t	=	Time (seconds)
t_p	=	Time to ponding
v	=	Flow velocity
z	=	Vertical distance
z_f	=	Vertical depth of the wetting front
θ	=	Moisture volume per unit volume of soil
Ψ	=	Soil matrix potential

1 Introduction

1.1 Background

Many semi-arid areas are subject to intense storm events which can lead to catastrophic flooding with significant economic, social and geomorphological impacts. These events are driven by the generation of runoff on the hillslopes within the catchments. Despite the importance of these events, the process of runoff generation at the hillslope and small catchment scale is poorly understood. This is because of the change in the system dynamics with the increase in spatial scale from the point scale to the hillslope scale (Cammeraat and Imeson 1999).

Semi-arid regions are an important global environment covering 17 % of the global land surface (UNEP 1992). These regions are characterised by annual potential evaporation rates which far exceed the annual rainfall resulting in a large water deficit and the variability of environmental factors over a range of spatial and temporal scale (Thornes 2001). There are strong seasonal and annual variations in rainfall and the storm water can be delivered at extremely high intensities. These factors combine to give a spatially non-uniform response to rainfall (Cerdá 1995).

The amount of water which leaves a slope is controlled by the connectivity of the runoff generating areas. Both the characteristics of the landscape and the storm will control the strength and development of hydrological connectivity. This will, therefore, determine the amount of water reaching the channel network during a storm event. The connectivity of flow will determine if the runoff generated at a certain point will reach the channel. It is possible that the areas which produce the greatest amount of runoff may never connect to the channel. The source of channel flow may then come from areas which generate smaller amounts of runoff but are better connected. The origin of the channel flow is not always clear and thus needs detailed consideration.

1.2 Research Aim and Objectives

The aim of this research is "to understand the amount and origin of water contributing to channel flow during a storm event in a semi-arid environment".

In order to accomplish this aim, the following research objectives have been defined

1. To identify the key variables controlling runoff generation in the field (chapters 2, 3 and 4).

2. To develop a hydrology model to forecast runoff generation and transmission at the hillslope and small catchment scale (chapter 5).

3. To investigate the surface and storm controls on the form of the discharge hydrograph using the model developed in objective 2 (chapters 6 and 7).

4. To trace the origin of runoff for a flood event on hillslopes and catchments using the model developed in objective 2 (chapter 8).

1.3 Research Approach

The research approach adopted in this study is a combination of field work and mathematical simulation modelling. This dual approach results in a powerful combination of techniques that provides insight into the mechanisms of runoff generation and connectivity in a semi-arid environment at the spatial scale of hillslopes and small catchments.

The field experiments form the foundation of the research into the generation of runoff. These experiments consider the actual physical processes operating in the field and hence are able to give a large amount of information on the controls of runoff generation. However, due to practical and financial constraints, there were limits on the number and scale of experiments that could be performed. These constraints limited the number of factors that were investigated and the level of detail of the experiments. The modelling approach is free from many of these limitations and hence many more factors and land surface configurations can be investigated. However, for the modelling results to be valid there needs to be a strong link between the modelling work and the real world. This link is generated by using the field experiments on the hydrological factors of interest to inform the design and parameterisation of the hydrological model.

The field data are used to guide both the development and the parameterisation of the model. The data from the field experiments have been analysed to determine the most significant controls on the generation of runoff. These significant factors are incorporated into the model structure. The measurement of certain factors showed that there is a stochastic element in their distribution due to both measurement errors and spatial variability, such as vegetation patterns and the surface roughness. Any stochastic behaviour may then determine how the investigations into these factors are handled in the modelling experiments. The field experiments give measured parameter values for the process representation equations in the model. Many modelling experiments consider the system response over a range of parameter values.

Knowledge of the measured values therefore places the field site within the model parameter phase space.

The aim of the modelling work within this thesis is to test and generate hypotheses about the hydrological functioning of the semi-arid hydrological system. Therefore, the aim of the model is to increase understanding of the hydrological system rather than to make precise predictions. The results of interest are the change in output with a change in input rather than the absolute output value. This will give information of the relative importance of different controls on runoff generation. Since any model is an abstraction of the real physical system, the model results must be viewed critically and related to physical measurements for the modelling derived conclusions to be valid.

Any modelling work requires a consistent set of parameter values at the spatial and temporal scale of the model application. The field work section of this research is able to provide this parameter set. Although there is a large number of parameter values reported in the literature, these have been measured at different places, times and scales and these differences mean that the parameter values will not be compatible. The uncertainty associated with reported values in the literature is not always detailed. As Beven (2002b) states: "there is no guarantee that bringing together parameter *values* from different sources will lead to acceptable simulations". Therefore, a set of field experiments gives a consistent parameter set with an understanding of the uncertainty associated with each and is an improvement on taking values from the literature. This field derived parameter set provides the necessary basis for modelling work.

Mathematical simulation modelling is a powerful technique for the investigation of the controls on runoff generation. Since the simulated environment can be precisely controlled, the sensitivity of the model to individual factors can be investigated. Therefore, the influence of, for example, surface roughness can be separated from slope gradient. This is always not possible using field experiments. For the results to be meaningful, the range of surface roughness values and slope gradient values must be related to those found in the field.

Using simulation modelling techniques, it is possible to undertake experiments not feasible in the field. These experiments include looking at the hydrological behaviour over longer spatial and temporal scales than is possible in field experiments. It is also possible to consider historical events so that the contributing areas during real storm events can be simulated.

1.4 Thesis Structure

The first section of this thesis examines the real world processes related to runoff generation and transmission. This is achieved through reviewing available literature on the processes which control runoff generation and transmission in chapter 2. The second method is through field

investigations, which are detailed in chapters 3 and 4. In chapter 3, the selection of the field site and the field techniques are presented whilst chapter 4 contains the analysis of the field results.

The results presented in chapter 4 are at the point or plot scale. In order to up-scale the results to the hillslope and small catchment scale, a hydrological model has been used. The development of the model and the selection of the process representation equations are presented in chapter 5. The model is then used to investigate the surface and storm controls on the discharge hydrograph from a hillslope. The surface controls are presented in chapter 6 and the storm controls in chapter 7. Chapter 8 then investigates the origin of runoff within the catchment.

The first two model results chapters (chapters 6 and 7) consider the fundamental controls on runoff generation and transmission. As such, these chapters consider idealised environments and storm forms. The final model results chapter aims to apply these results and the model to real catchments with a real storm. Therefore, the research moves towards the detail and complexity found in the natural world as presented in chapters 2, 3 and 4. The implications of the research findings for semi-arid hydrology and the research conclusions are presented in chapter 9.

2 Semi-Arid Runoff Generation

2.1 Introduction

This chapter reviews the processes leading to the generation of runoff in semi-arid environments. The main focus of this chapter is south-east Spain but examples are drawn from comparable global semi-arid environments. The general characteristics of semi-arid areas are discussed in section 2.2, the climate and rainfall regime is presented in section 2.3 and the main hydrological processes are examined in the following sections. The key areas covered are interception (section 2.4), infiltration (section 2.5) and overland flow (section 2.6). In section 2.7, the effects of up-scaling from the point and plot scale are considered. The impact of land use and management is described in section 2.8. A summary is presented in section 2.9 and the conclusions and research gaps are presented in section 2.10.

2.2 Characteristics of Semi-Arid Hydrology

There have been complex geological, pedological and management histories in many semi-arid areas (Fitzjohn et al. 1998) which resulted in spatial variability in hydrological properties at the landscape scale. This variability is coupled with the highly variable rainfall on both spatial and temporal scales (Thornes 2001). Taken together, these factors give a non-uniform hydrological response to rainfall events (Cerdá 1995; Bergkamp et al. 1996).

Figure 2.1 presents a conceptual model of the vertical hydrological system in a semi-arid area. As the rainfall is sequentially partitioned, a percentage is first intercepted by the vegetation canopy and the remainder falls directly onto the soil surface. The water that is intercepted may be stored temporarily or drain from the canopy either directly to the soil surface or by flowing down the stems of the vegetation. The water held in either the canopy or stem stores may be evaporated during or after the storm event. Water reaching the soil surface may infiltrate or be held in the surface depression store. When the surface depression store overflows, runoff is generated. The main process by which runoff is generated is infiltration excess or Hortonain overland flow (Yair and Lavee 1985; Beven 2002a). The rate at which the water may enter the soil matrix store is influenced by the presence of a surface crust, stone cover, air entrapment and macropores. Water may then leave the soil matrix store as recharge to ground water or by evaporation.

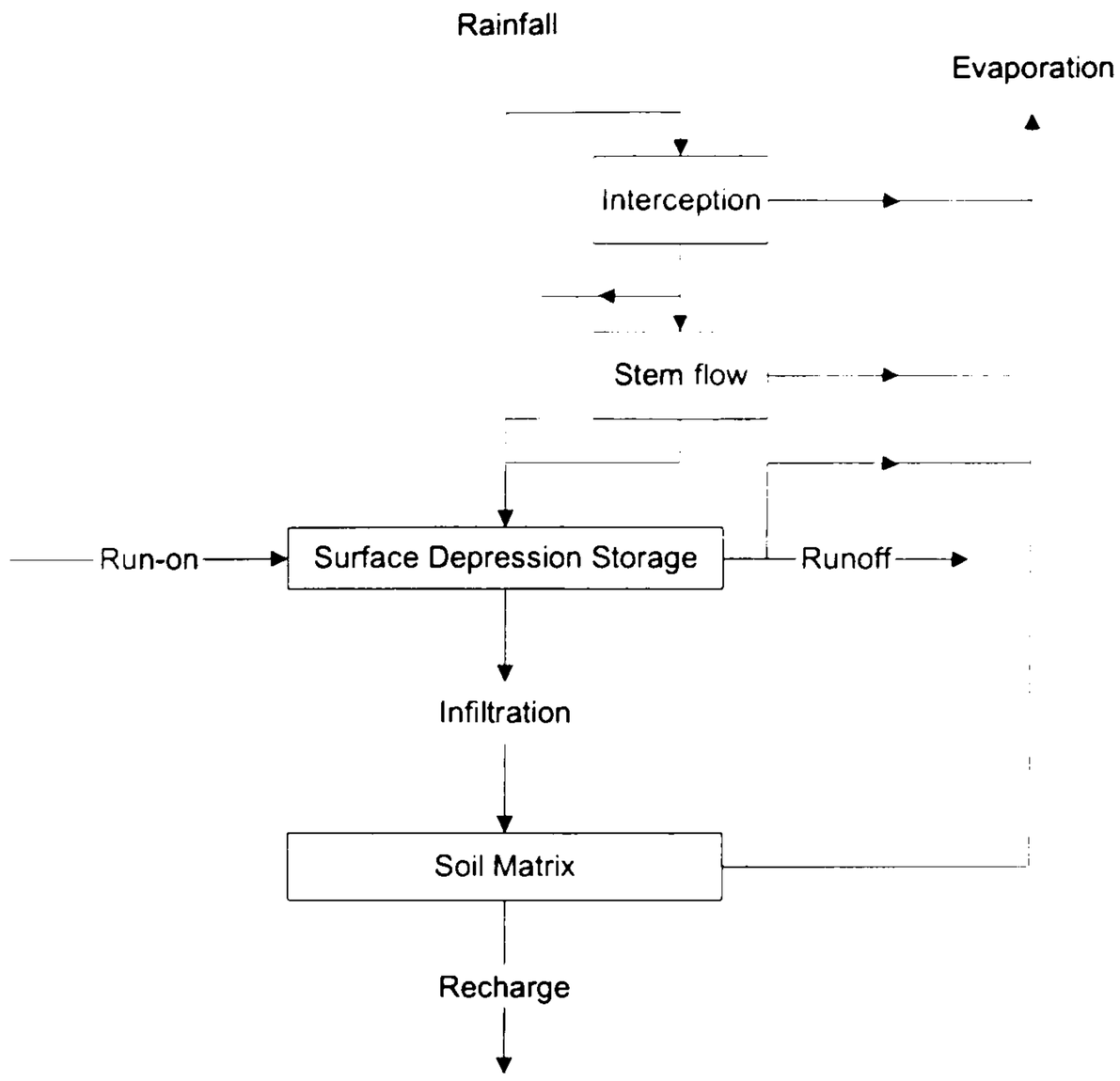

Figure 2.1 Conceptual model of semi-arid hydrology

The main difference between this conceptual model of semi-arid hydrology compared to one for temperate hydrology is the nature of the horizontal fluxes. The high potential evaporation rates, far exceed the annual rainfall resulting in a large water deficit (Thornes 2001), so that the soils are below field capacity for most of the year. Therefore through-flow only occurs under very special circumstances and hence the soil system can be considered as behaving in a cellular rather than catena fashion (Mulligan and Thornes in press).

Each of the different processes in the hydrological system operates at a different time scale. The flow velocities of overland flow are many orders of magnitude greater than the rates of evaporation. For the study of the system response to single storm events, the processes which operate at this time scale will have far greater importance than those operating on longer time scales. Therefore, the emphasis will be upon the infiltration and runoff processes rather than recharge and evaporation.

Semi-arid regions cover 17.7 % of the global land surface area (UNEP 1992) and their global distribution is shown in Figure 2.2. This work will focus on south east Spain. This area is representative of many semi-arid regions, much research has been undertaken in this area and it is easily accessible from the UK.

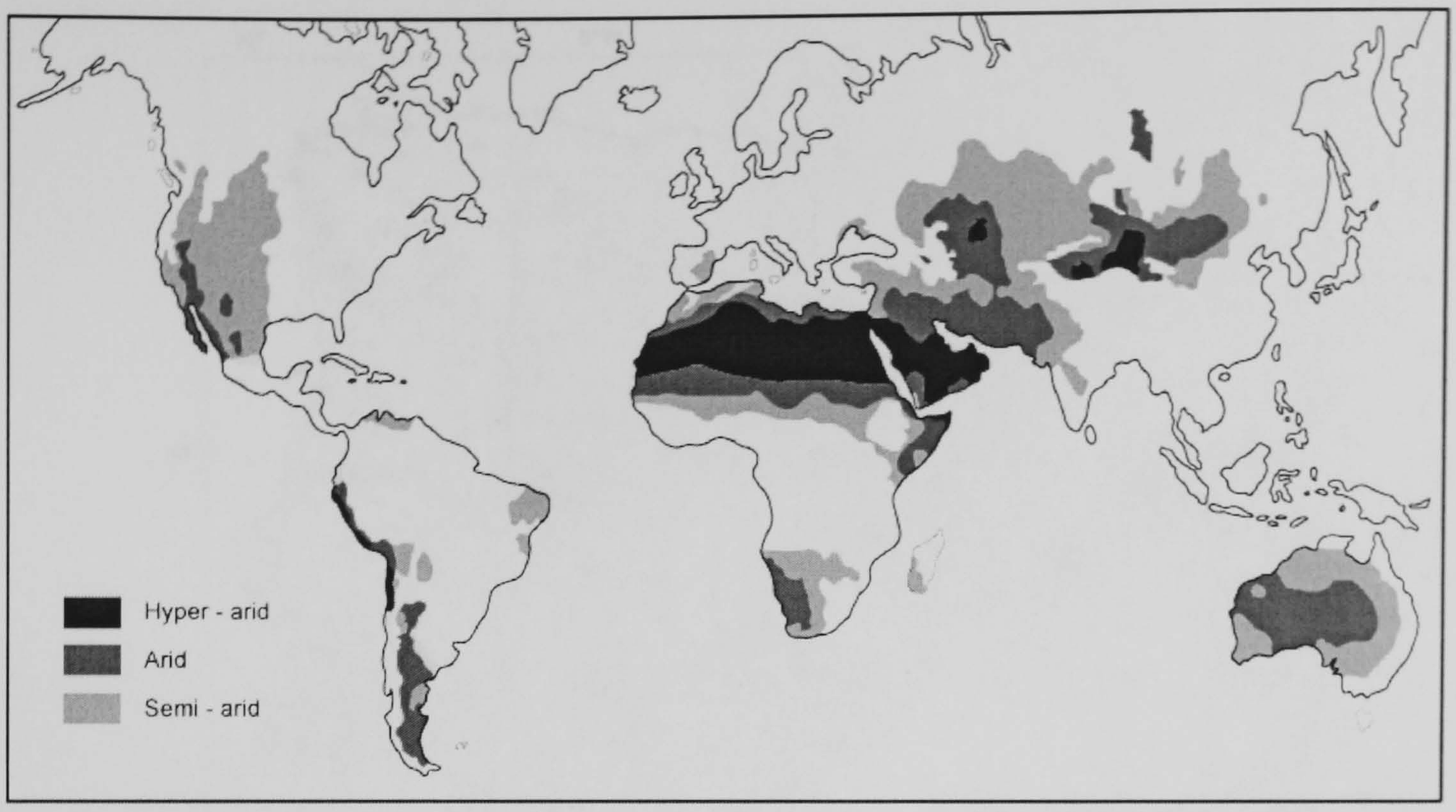

Figure 2.2 Global distribution of arid areas (UNEP 1992)

2.3 Mediterranean Climate and Rainfall

The Mediterranean is located between a temperate maritime climate and an arid subtropical desert climate. The transition between these climates is controlled by westerly wind patterns in winter and by subtropical anticyclones in the summer (Barry and Chorley 1992). This leads to hot, dry summers and mild, relatively wet winters (Allen 2001).

The switch between the dominant climates occurs suddenly with the change into winter occurring when the summer eastern extension of the Azores high-pressure cell collapses. In the western Mediterranean, a sudden drop in air pressure occurs around the 20 October and is associated with an increase in the probability of precipitation. The probability of rainfall in a five day period before the pressure cell collapse is 50 – 90 % and this rises to 90 % after the collapse (Barry and Chorley 1992). During the winter, the sea surface temperature is up to 2 °C warmer than the air temperature. With the incursion of cold fronts, this leads to convective instability along the front and hence frontal and orographic rainfall. The summer weather is dominated by the expansion of the Azores high-pressure system into the Mediterranean. This results in stable conditions with hot dry weather (Allen 2001).

2.3.1 Spatial and Temporal Variability of Rainfall

The amount of precipitation is a function of both large scale climatic patterns and the local relief. The complex pattern of annual rainfall totals for the Iberian Peninsula is shown in Figure 2.3. This shows the large range of rainfall depths received. For example, Navacerrada, located at 1860 m, received 1300 mm of rainfall, compared to the 430 mm received in Madrid located only 50 km away (Allen 2001).

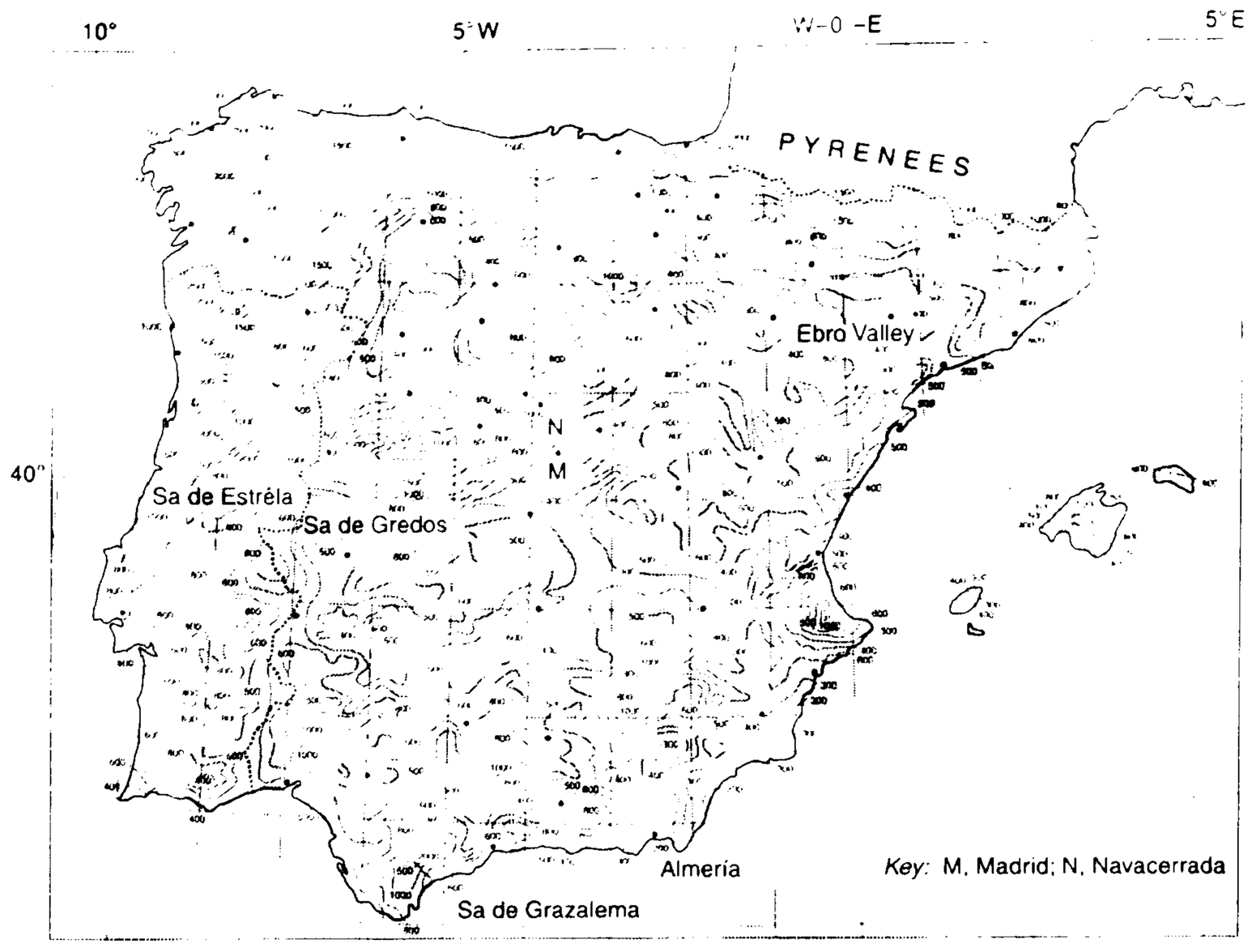

Figure 2.3 Annual rainfall totals for the Iberian Peninsula for the period 1931 – 1960 (Allen 2001)

At the spatial scale of a small catchment, the spatial variability of received rainfall is large, especially for convectional events (Beven 2002a). The spatial variability of the rainfall intensity from a convectional storm cell was shown by Goodrich et al. (1997) for a storm in the Walnut Gulch catchment, Arizona. Goodrich et al. (1997) observed differences in total rainfall depth for a single storm event of over 65 mm over a distance of 3 km (Figure 2.4). Due to the limited extent of the convectional storm cell (3-10 km in diameter), there are great differences in the amount of rainfall received across a catchment. The life span of a cell may vary from a few minutes to an hour and the cell may move at 500 to 1600 m min^{-1} (8.3 - 26.6 m s^{-1}) (Yair and Lavee 1985). The spatial extent of the rainfall is greater during frontal rainfall events than under convectional events, however, there are still complex patterns of rainfall intensities and amounts. The spatial pattern is controlled by the surface topography, with the slope gradient and the aspect influencing the amount of rainfall received. The temporal structure is made up of a series of rainfall pulses. These spatial and temporal variations in the rainfall amounts and intensities lead to spatial and temporal discontinuities in the generation and transmission of runoff. Due to the short bursts of runoff generating rainfall, the time when runoff can be generated is short and hence the time available for flow transmission is also limited. Therefore, the overland flow travel distances are short since the water will infiltrate after the end of the rainfall pulse and hence the flow may not reach the channel (Yair and Lavee 1985).

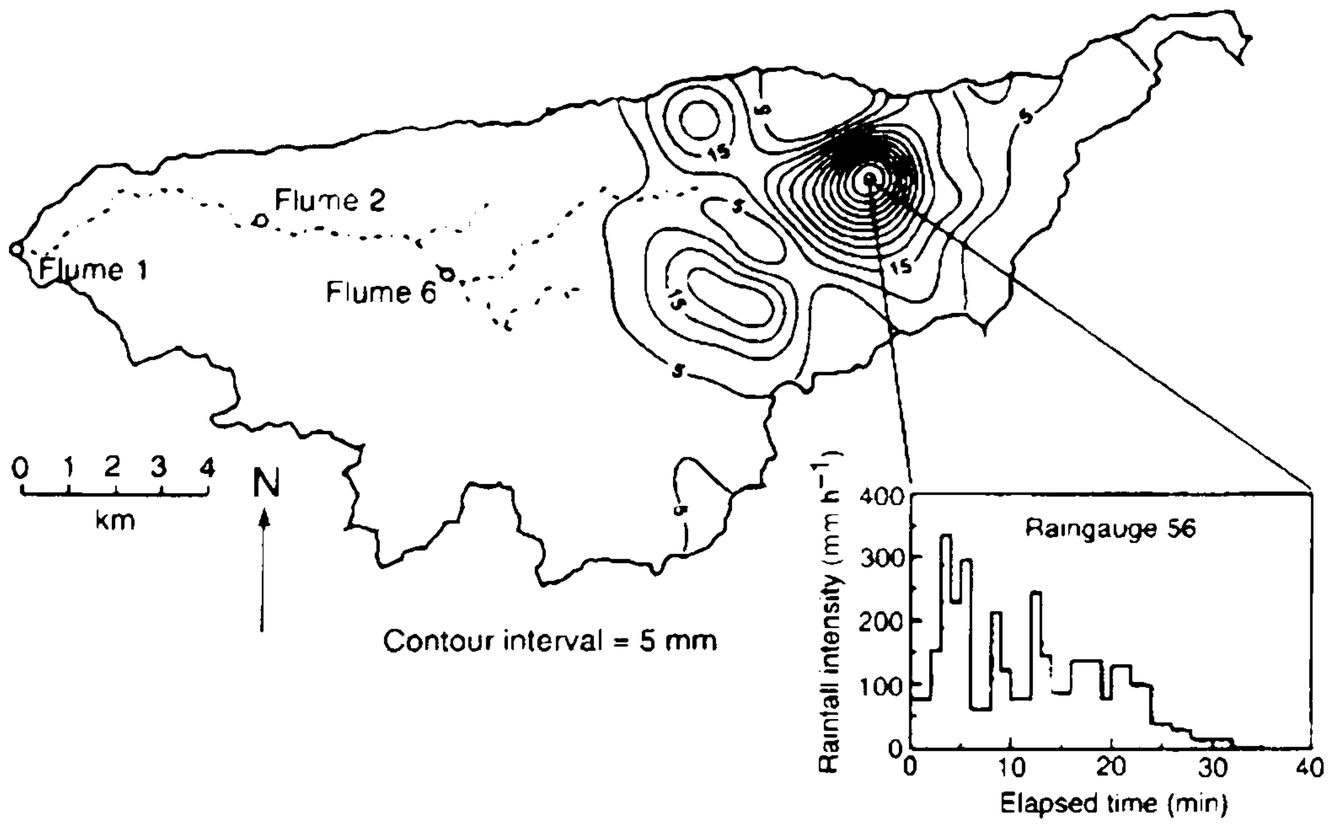

Figure 2.4 Pattern of rainfall depths for a storm at the Walnut Gulch catchment, Arizona (Goodrich et al. 1997)

The rainfall regime in Spain shows variability on various temporal scales. Over the previous centuries, there have been a number of periods with statistically different climates. For example, the Little Ice Age in Spain (AD 1590 – 1649) was characterised by wet conditions with higher flood frequencies (Rodrigo et al. 2000). Over the course of the twentieth century, there have been marked fluctuations in the temperature and precipitation regimes (Allen 2001). These fluctuations are most pronounced in changes in the seasonality of the climate. In Portugal and southern Spain there was a reduction in rainfall in March for the 1961-90 period compared to the 1932-60 period. Between the same periods, there was a slight increase in autumn and winter precipitation (Corte-Real et al. 1998). On the longer time scale of 1880 – 1992, Esteban-Parra et al. (1998) found a significant decrease in precipitation for the Mediterranean regions of Spain. This was related to variations in the large scale circulation patterns over Western Europe and the North Atlantic.

There is often high inter-annual variability in the total annual rainfall. This is shown in Figure 2.5 using standardised anomaly indices (SAI) of annual rainfall for the western Mediterranean (Corte-Real et al. 1998). The use of SAI allows the use of difference rainfall time series in a single index and thus is able to give the regional pattern of change.

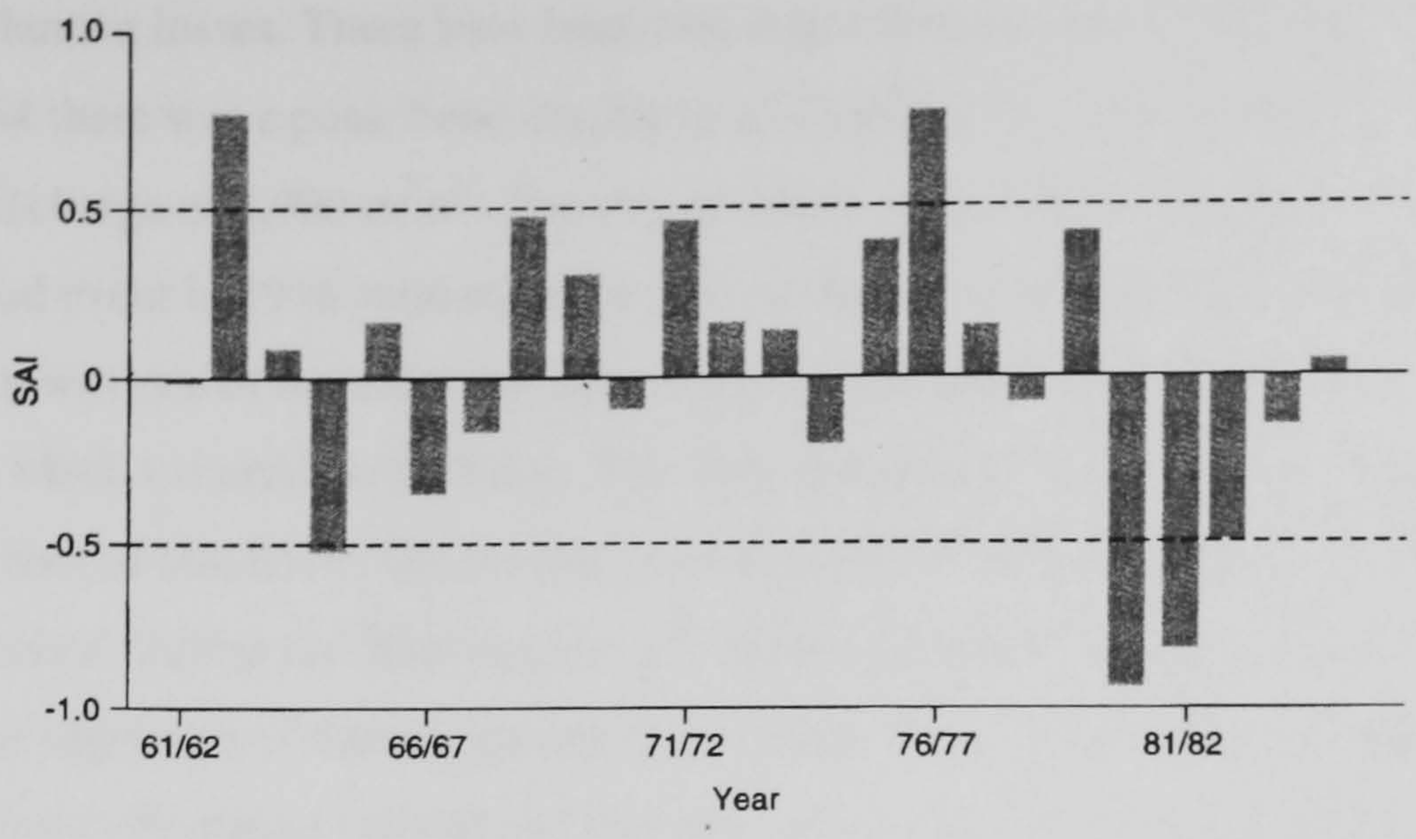

Figure 2.5 Standardised anomaly indices of annual rainfall for the western Mediterranean (Corte-Real et al. 1998)

2.3.2 Extreme Events and Flooding

The rainfall in many Mediterranean areas can be extreme. Poesen and Hooke (1997) list many high magnitude rainfall events from across southern Europe. Since 1970 there have been over ten significant flood events in south east Spain and the synoptic climatic conditions associated with these have been summarised by Alonso-Sarria et al. (2002). At the surface level, a low cell originating over Morocco or the Gulf of Cadiz produces an incursion of warm air from North Africa. This crosses the Mediterranean Sea and hence accumulates much moisture. This wave of warm air may be met by an arctic trough and the resultant instability can produce extreme storm events. Full details and a number of case studies are given in Alonso-Sarria et al. (2002). These events result in high magnitude floods with large geomorphic, economic and social impacts (Lopez-Bermudez et al. 2002), as shown in Figure 2.6. The floods generated in ephemeral streams are "especially rapid, violent and therefore dangerous" (Camarada and Segura 2001).

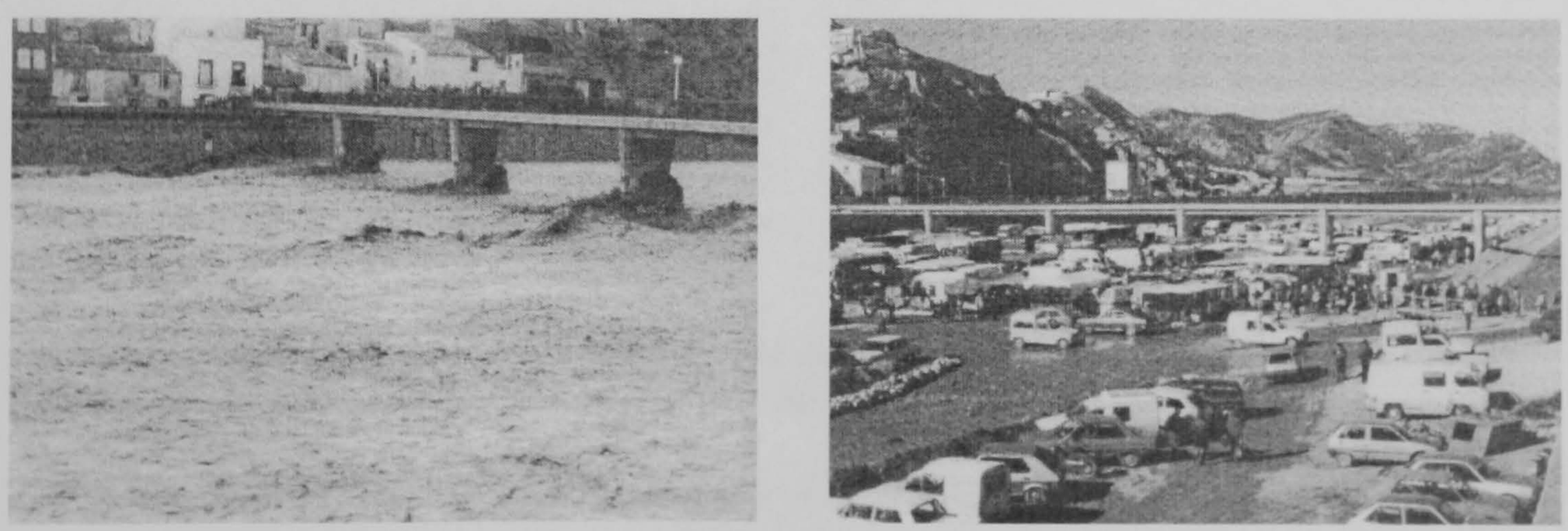

Figure 2.6 Flood event at the outflow of the Rambla de Nogalte catchment, 7 September 1989, and human activity in the same channel, 26 January 1990 (Lopez-Bermudez et al. 2002)

There have been many high magnitude flood events in south east Spain and the details of the key events have been reported by Lopez-Bermudez et al. (2002). Some examples from Lopez-Bermudez et al. (2002) are as follows. The city of Valencia has had a long history of flood events. The last major event occurred in 1957 with a peak discharge of 4,000 $m^3 s^{-1}$ and caused severe

economic and human losses. There have been two major flood events on the Rio Jucar. In September 1864 there was a peak flood discharge of 12,000 $m^3 s^{-1}$ and in October 1982 there was a peak flood discharge of 5,000 $m^3 s^{-1}$. The city of Alcria was completely destroyed by a flood in 1472 and a flood event in 1916 submerged the city under 8.5 m of water. During the 19th century, the Guadalentin was one of the most energetic rivers in Western Europe. There have been two notable floods which occurred in the basin. The first occurred in 1802 when the Puentes reservoir broke with the loss of 604 lives. The second occurred in 1879 where a total of 58 M m^3 of flow occurred in 8 hours. During the 20th century, 22 significant flood events occurred in the basin. One of the most important of these occurred in October 1973 at the Rambla de Nogalte catchment, Murcia, when over 100 mm of rainfall fell in a day. This event had a peak discharge which was in excess of 2,000 $m^3 s^{-1}$ and resulted in the loss of many lives (Lopez-Bermudez et al. 2002).

2.3.3 Climate Change

Most scientists agree that climate will change over the next 100 years as a result of anthropogenic activities (IPCC 2001). The impacts of increased CO_2 on the climate have been investigated using general circulation models (GCM) of the atmosphere and oceans. The UK Hadley Centre has performed a 75 year transient increase in CO_2 experiment using their GCM. In this experiment, the CO_2 concentration was increased by 1 % per year such that a CO_2 concentration double that was present in pre-industrial times was reached in the 70th model year. For south-east Spain, the GCM showed an increase in temperature of nearly 2 °C by the 70th year and a decrease in the average rainfall per day of 0.275 mm, as shown in Figure 2.7. There is a clear trend for hotter, drier conditions although this change will be non-linear in time (Goodess et al. 1998).

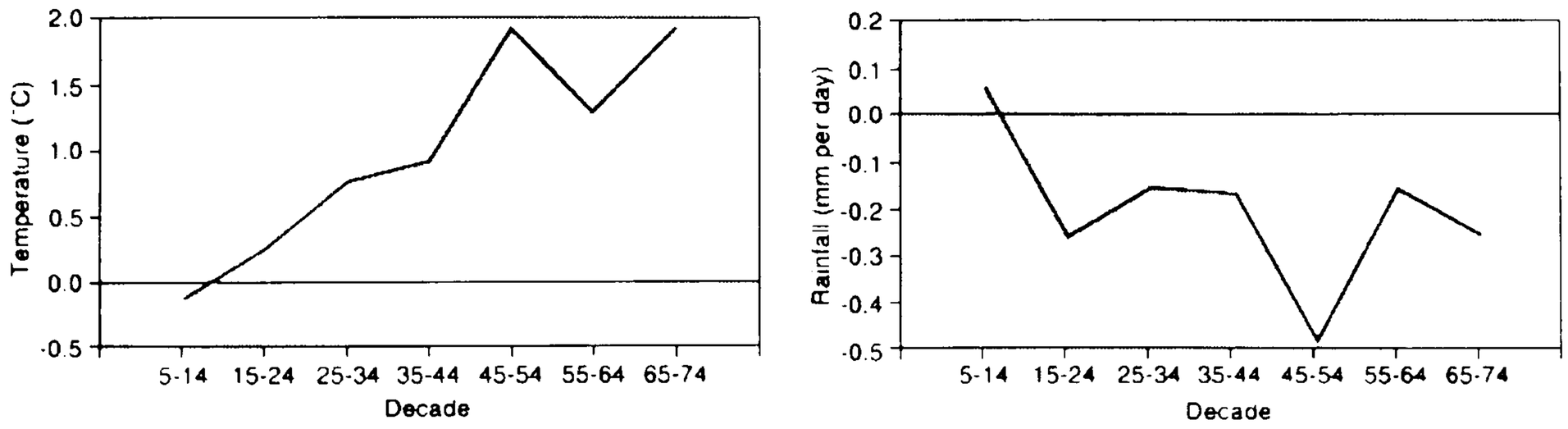

Figure 2.7 Predicted changes in temperature and rainfall for southern Spain under double CO_2 from the Hadley Centre GCM (Goodess et al. 1998).

The impact of climate change on the magnitude of rainfall events can be investigated through the analysis of circulation patterns. These are generated by the GCM and can be compared to observed circulation patterns and the weather related to them (Wilby 1995). Using this approach, it has been found that in southern Spain there could be fewer rain days in the spring, thus reducing the amount of water available for agriculture and ground water recharge. However, there may also be an increase in the number of rain days in the summer when potential evaporation rates are at their

highest and the soil surface is most vulnerable to erosion (Goodess and Palutikof 1998). The net influence of these factors will lead to a reduction in the available soil moisture.

2.4 Interception

The retention and subsequent evaporation of water droplets from the vegetation surface is termed interception. This process has been extensively studied, but is still one of the more poorly understood processes in hydrology (Calder 1996). Although it operates at the scale of a single plant it can be crucial in understanding the hydrological response of heterogeneous landscapes (Domingo et al. 1998). Interception influences the amount and distribution, both spatially and temporally, of water reaching the soil surface. A conceptual diagram of the stores and pathways involved is shown in Figure 2.8.

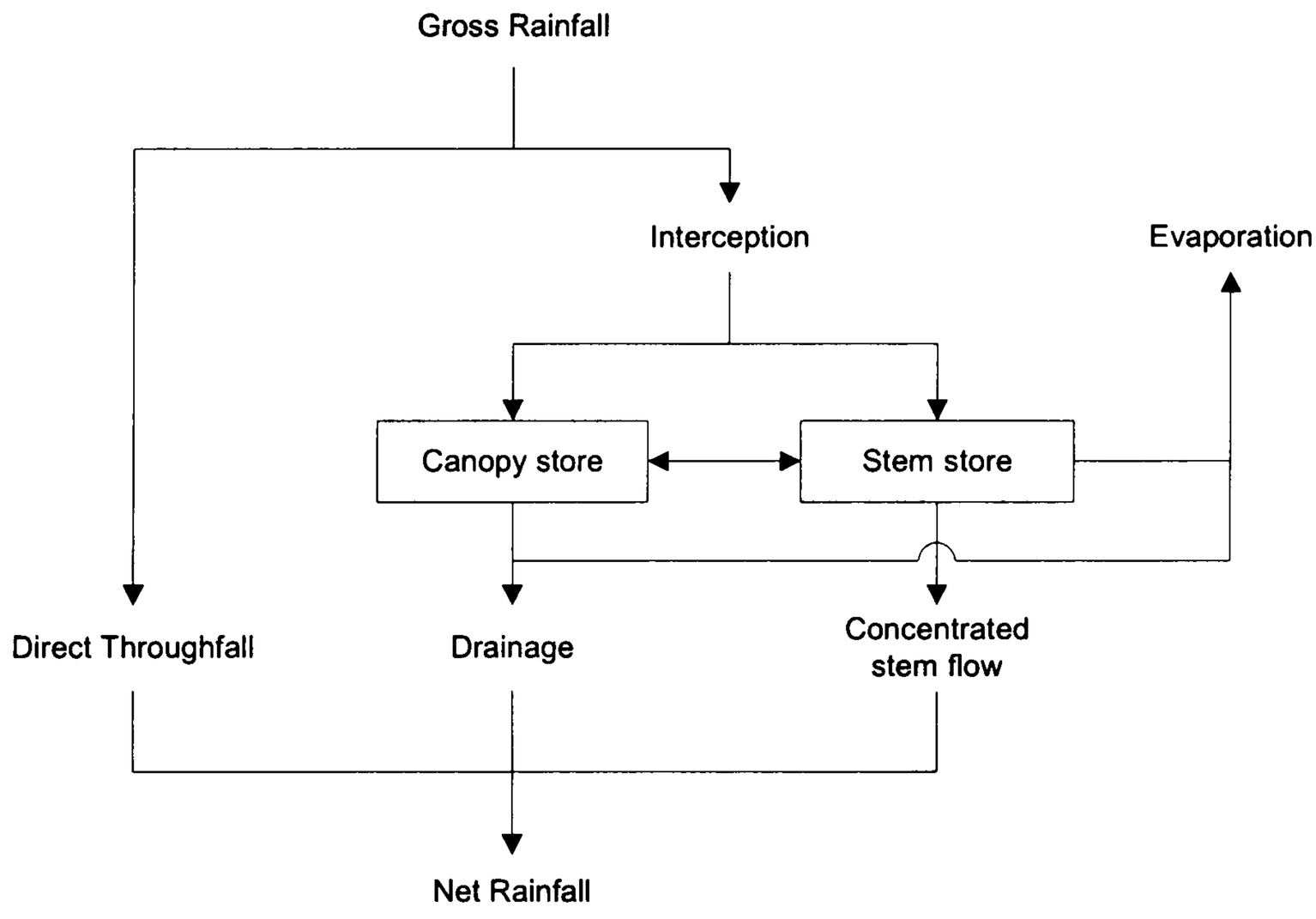

Figure 2.8 Conceptual model of rainfall interception

The first stage of the process is the separation of the direct throughfall (rf_d) from the intercepted fraction. This can be related to the percentage of the ground area covered by the canopy elements, the percentage canopy gap fraction (gf). The amount of direct throughfall can then be calculated from the gross rainfall (rf_g) using:

$$rf_d = rf_g . \frac{gf}{100}$$

Equation 2.1

However, this relationship will be modified by the 3D structure of the canopy and the angle of incidence of the rainfall on the canopy surface (Herwitz and Slye 1995). Gap fraction values for typical semi-arid vegetation species are given in Table 2.1.

A fraction of the rainfall intercepted by the canopy may be held in the canopy store. This is expressed as the equivalent depth of water per unit area and values for a number of semi-arid vegetation types are given in Table 2.1. The leaf area, tree species, storm intensity, surface tension forces resulting from leaf surface configuration, liquid viscosity and mechanical activity determines the capacity of this store (Aston 1979).

The canopy storage capacity is variable on the temporal scale of a storm event. The force with which a raindrop impacts upon the canopy will influence the storage. This is related to wind speed, rainfall intensity and the drop size distribution, all of which are highly variable on both spatial and temporal scales (Hall et al. 1996). Wind speed will influence the movement of the vegetation and hence higher wind speeds will result in lower canopy storage due to shaking of the vegetation (Pearce 1987).

There are three pathways through which the water may leave the canopy store. The first is evaporation and accounts for the interception loss, typical losses are given in Table 2.1. This can occur during the storm event, especially from rough canopies under windy conditions when the air next to the canopy is not saturated with water (Beven 2002a). The second method is from drainage from the canopy store as throughfall (rf_t). The simulation of this process has received much attention in the literature (Rutter et al. 1971; Gash 1979; Calder 1986; Calder 1996) and a number of models have been developed. The applicability of these models to a semi-arid environment is discussed in chapter 5.

The third pathway out of the canopy store is via the stems of the vegetation. Typical amounts of water flowing along this pathway are given in Table 2.1. Stem flow results in a concentration of water at the plant base with an effective intensity many times greater than the rainfall intensity. Many semi-arid plants have evolved structures that channel the intercepted water through the plant and to the plant roots (Domingo et al. 1998). In water scarce environments, this can give a significant survival advantage.

The interception of rainfall on the canopy and the subsequent drainage alters the raindrop size and velocity distributions (Brandt 1989) which in turn results in a reduction in the amount of energy reaching the soil surface. Wainwright et al. (1999) found a 30 % reduction in energy under creosote bushes. This decrease in energy reduces the ability of the rainfall to develop soil surface crusts and leads to an increased infiltration capacity relative to the inter-plant areas (Abrahams and Parsons 1991). The shading effect of the vegetation reduces the solar energy reaching the surface and hence decreases the soil evaporation (Pariente 2002). These two factors increase the amount of water available to the plant and hence increase its chances of survival.

Vegetation	Location	Gap Fraction (gf) (%)	Canopy storage depth (mm)	Stem flow (%)	Interception loss (%)	Source
Stipa tenacissima L.	Spain	10	2.44 ± 0.27	20	40	(Domingo et al. 1998)
Anthyllis cytisoides L.	Spain	10	1.8 ± 0.21	-	-	(Domingo et al. 1998)
Retama sphaerocarpa L.	Spain	70	0.29 ± 0.02	7	21	(Domingo et al. 1998)
Tamaulipan matorral thorn scrub	Mexico	14.65	-	0.6	16.4	(Navar et al. 1999)
Olive	Spain	-	1.96	-	8	(Gomez et al. 2001)

Table 2.1 Rainfall interception parameters for semi-arid vegetation

2.5 Infiltration

Infiltration is the process by which water enters the soil. This is a key process since it partitions rainfall between the soil store and the water available for the generation of runoff. The rate at which water may enter the soil is determined by effects of gravity and pressure forces acting on the water at the surface (Dingman 1994). The nature of these forces is determined by:

- The rate at which water arrives at the soil surface or the depth of ponding.
- The saturated conductivity of the soil surface.
- The soil moisture at the start of the infiltration event.
- The slope gradient and roughness of the soil surface.

The effects of each of these factors on the nature of the infiltration process will be examined in urn in the following sub-sections.

The observed infiltration capacities for semi-arid environments show a wide range of values (Table 2.2). The infiltration capacities range from 2.7 mm hr^{-1} on a decalcified marl to 650.6 mm hr^{-1} on sands and gravels (Scoging and Thornes 1980). At single locations, the variability of the measured values can be high. Cerdá (1997) reported on infiltration rates on bare areas in Murcia with a mean of 26.17 mm hr^{-1} and a standard deviation of 10.93 mm hr^{-1}. Whilst Leonard and Andrieux (1998) found that the average infiltration rate in a vineyard in southern France was 16.6 mm hr^{-1} with a standard deviation of 18.9 mm hr^{-1}.

The factors influencing the generation of runoff may be divided into three groups determined by the spatial scale at which the factor operates. The first set of factors operates at the point scale and includes the rate of water delivery to the soil surface, the soil matrix hydrological properties, the antecedent soil moisture and the entrapment of air in the soil matrix. These factors are discussed in

section 2.5.1. The second group of factors operates at the plot scale which is considered to be 0.5 by 0.5 m. This group includes the effects of macropores, crust development. vegetation, rock fragments and surface roughness. These factors are discussed in section 2.5.2. The final set of factors may be considered topographic factors and covers the impact of slope gradient and aspect on the infiltration capacity. These factors are discussed in section 2.5.3.

Location	Land use	Infiltration Rate (mm hr^{-1}, stdev in brackets)	Technique Used	Source
Benidorm, south eastern Spain	Bare	23.89 (7.12)	Rainfall simulation	(Cerdá 1997)
	Herbs	53.56 (2.28)		
	Tussock	54.43 (0.99)		
Murcia, south eastern Spain	Bare	26.17 (10.93)	Rainfall simulation	(Bergkamp et al. 1999)
	Tussock	46.36 (1.22)		
Albaceta, Central Spain	Scrub	56		
	Scrub	42		
	Scrub	67		
South eastern Spain	Decalcified marl	2.7 (min)	Rainfall simulation	(Scoging and Thornes 1980)
South eastern Spain	Sands and gravel	650.6 (max)		
Walnut Gulch, Arizona	Natural scrub	44.94 (8.74)	Rainfall simulation	(Wainwright et al. 2000)
Caceres, Extremadura, south western Spain	Hillslope grass	23.63	Rainfall simulation	(Cerdá et al. 1997b)
	Bottom grass	28.47		
	Tree cover	24.29		
	Sheep trails	26.26		
	Shrub cover	39.99		
South eastern France	Agricultural, field A	176.5 (77.0)	Ponded infiltration test	(Wainwright 1996)
	Agricultural, field A	87.1 (17.0)	Natural rainfall	
	Agricultural, field B	737.6 (283.4)	Ponded infiltration test	
	Agricultural, field B	87.9 (42.7)	Natural rainfall	
Southern France	Vineyard	16.6 (18.9)	Rainfall simulation	(Leonard and Andrieux 1998)

Table 2.2 Observed infiltration rates for semi-arid environments

2.5.1 Point Scale Factors

The Rate of Water Delivery

It is possible to define three conditions under which infiltration may occur (Dingman 1994): Firstly the rainfall intensity (rf_i) may be less than the infiltration capacity (ic), $rf_i <= ic$, resulting in all of the water being infiltrated into the soil and no ponding of water at the soil surface. Secondly,

the condition that $rf_i > ic$ may exist when a fraction of the water will directly infiltrate and the remaining water will either pond and infiltrate at a later time or become overland flow which may infiltrate further down slope or reach a channel. This situation leads to the runoff generation mechanism termed infiltration excess or Hortonain overland flow. Thirdly, the soil may be saturated, leading to the condition $ic = 0$. Therefore, all of the water will pond or runoff. This leads to the runoff generation mechanism termed saturated infiltration excess overland flow.

As the rainfall rate increases, the area over which ponding occurs increases. This means that more of the surface is infiltrating at the maximum rate and it can also infiltrate on parts of the surface that are not influenceed by a soil crust (Fox et al. 1998). This leads to an increase in the infiltration rate and is discussed further in section 2.5.2.

Soil Matrix Hydrological Properties

The movement of water through the soil matrix is dependent upon three factors, the soil moisture content (θ), the soil water potential (Ψ) and the hydraulic conductivity of the soil (K). The soil water potential is the force by which the water is held in the soil and the hydraulic conductivity is the rate at which water can move through the soil.

The soil moisture content is expressed as the degree of saturation of the soil. There is a lower limit beyond which plants are no longer able to extract water from the soil. This is termed the wilting limit. This point varies between plants but is normally taken as 1.5 MPa of matrix potential (Brady 1990). Another important soil moisture value is the residual soil moisture (field capacity). This point is reached when there is no longer continuity in the soil moisture content between the pores in the soil (Dingman 1994).

The soil moisture content is modified by capillary action and gravity. The capillary action moves water through the soil due to the attraction between the water molecules and the walls of the channels through which it moves. This attraction is greater than the force of gravity and hence water can move up through the profile. The rate of movement is controlled by the size of the channels and hence is dependent upon soil texture. The smaller the channels, the greater the amount of movement. Gravity moves the water down through the soil profile.

The soil hydraulic conductivity in saturated soils is determined by the soil texture since texture determines the size of the channels. In unsaturated flow, both the texture and the soil moisture will determine the rate of movement. There is an increase in conductivity with increasing soil moisture to a maximum at saturation (Ksat).

There is a curvilinear relationship between the soil moisture content and the soil water potential (Figure 2.9). The form of this relationship is influenceed by the soil texture and structure and hence a curve is specific to a certain soil. The relationship between the hydraulic conductivity and

the soil moisture is non-linear (Figure 2.9). The conductivity is low at low to medium soil moisture contents but then increases non-linearly with increasing soil moisture. The integrated response of these two factors leads to a decrease in the infiltration capacity since the reduction in soil water potential dominates (Figure 2.10).

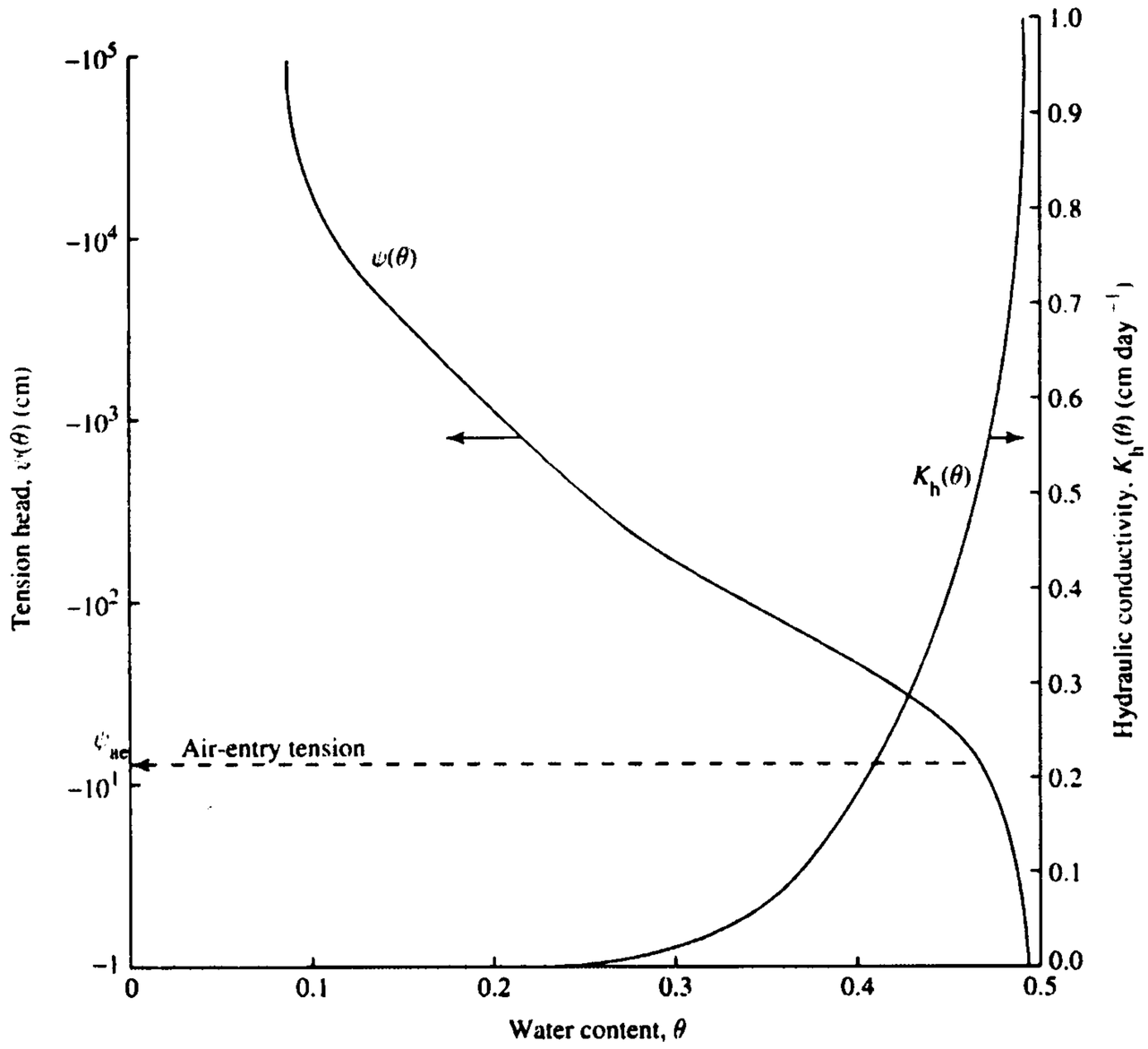

Figure 2.9 Relationship between soil moisture, soil water potential and hydraulic conductivity (Dingman 1994)

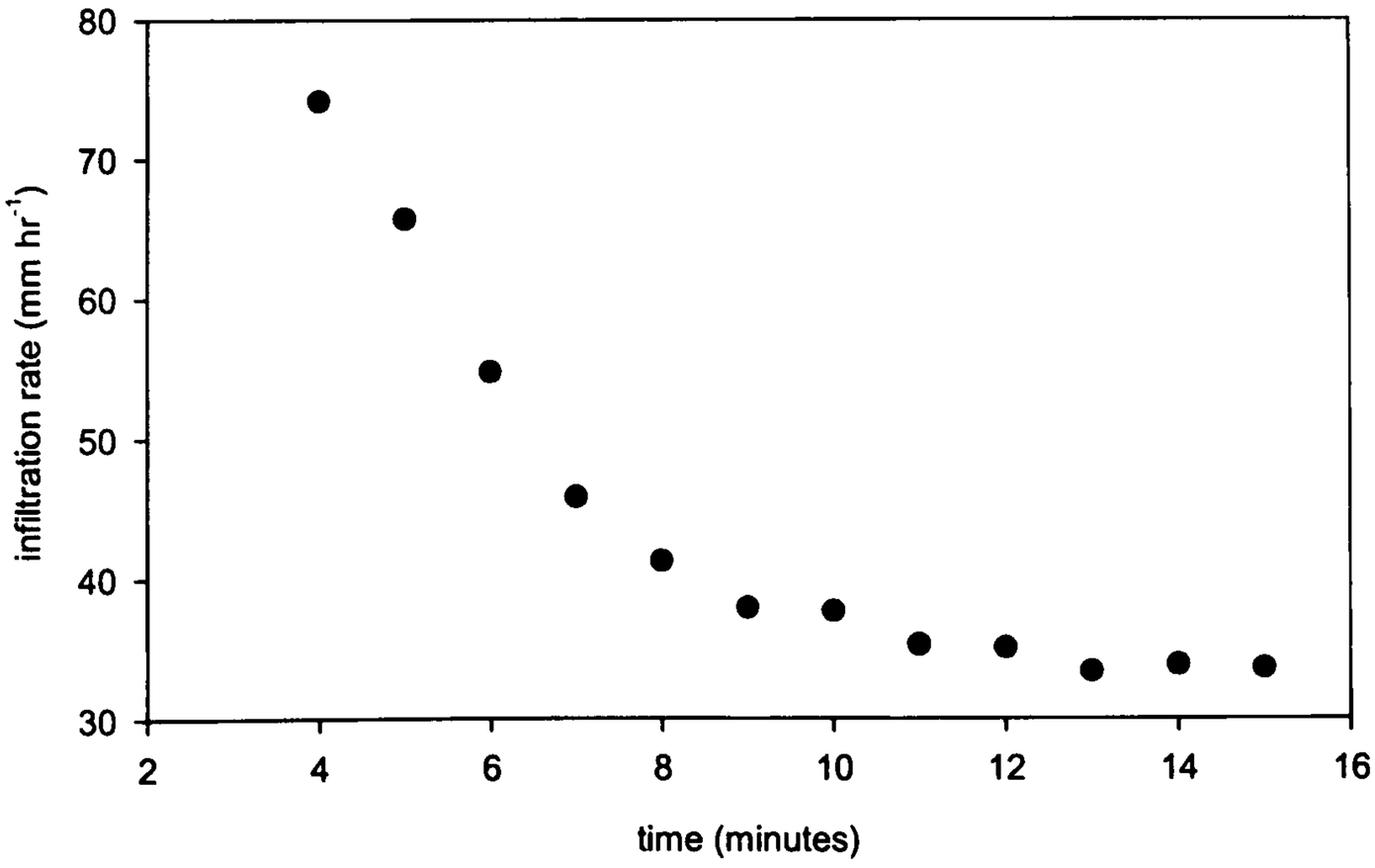

Figure 2.10 Changes in infiltration capacity with time for a standard soil with grass surface cover (Dingman 1994)

The soil moisture at the start of the infiltration event is a key factor in determining the response of the soil to the event (Fitzjohn et al. 1998). If the soil is near saturation at the start of the infiltration event, it is more likely that saturated conditions will develop and hence leads to ponding and the generation of runoff. The influence of antecedent soil moisture conditions on the infiltration rate

during the summer is low, but there is a relationship during the winter when the soil moisture is greater (Nicolau et al. 1996).

2.5.2 Plot Scale Factors

Macropores

The presence of macropores in the soil is an important control on the soil infiltration rate (Beven 2002a). Since the flow rate within a cylinder varies with the fourth power of the radius, larger pores can transport large amounts of water and hence strongly influence the infiltration rate. Micropores are capable of holding water under capillary tension and hence a macropore is defined as a pore space which allows water to move under gravity without being restrained by capillary tension (Beven and Germann 1982).

Macropores are formed by both biological and physical methods. Physical processes include the cracking of the surface material (Navar et al. 2002) and preferential flow paths along the sides of embedded rock fragments (Poesen et al. 1990). Biological processes include biotic activity such as ants (Eldridge 1993), earthworms (Oades 1993) and burrowing mammals (Hangen et al. 2002) and the spaces left by dead roots (Passioura 1991). Macropore systems which only extend a short distance into the soil matrix may have a limited effect on the infiltration rate. This is because their effect will be constrained by the infiltration rates into the surrounding matrix rather than the potential flow rate. However, some root systems, earthworm and ant burrows extend for many metres below the surface and can have a significant effect on the infiltration rate (Beven 2002a).

Imeson et al. (1992) found that water did not infiltrate as a flat wetting front but as a discontinuous wetting front along macropores. These macropores routed the water through an overlaying hydrophobic layer directly into a lower level in the soil at ~30 cm. It was found that 5 – 10 % of the soil surface was covered with macropores. Imeson et al. (1992) also found that areas that had recently undergone fire had a greater number of macropores near vegetation and that the porosity of the soil was 25 % lower than the site which was not burnt.

Eldridge (1994) investigated the influence of macropores created by ants and termites in a semi-arid woodland in eastern Australia. The experiments used disc infiltrometers to assess the infiltration rates and it was found that the average infiltration rate was 1,026 mm hr^{-1} at sites with nest entrances compared to 120 mm hr^{-1} at sites without.

Crust Development

Surface crusts are discontinuities in the vertical soil profile characterised by lower hydraulic conductivities than the parent soil (Bradford and Huang 1992). The presence of a soil crust can therefore significantly reduce the infiltration capacity of the soil. Crusts formed in the Tengger Desert, China, reduced infiltration rates by 36 – 74 % compared to a non-crusted site (Li et al.

2001). In semi-arid Niger, it has been found that the hydraulic conductivity of the sedimentary crust were very low, covering the range 6-4 – 5-5 mm hr^{-1} (Bromley et al. 1997b).

There are two types of crusts, physical and biological. The formation of physical surface crusts is dependent on both rainfall characteristics and the chemical and physical properties of the soil. The main process for physical crust formation is the breakdown of soil aggregates. The processes involved in the breakdown of aggregates are numerous and complex (Le Bissonnais 1996). Biological crusts develop by the accumulation of filaments of cyanobacteria and algae and thalli of lichen and moss combined with soil particles. The accumulation creates a physical discontinuity in the surface profile with greater concentrations of clay, silt and potentially hydrophobic organic matter (Williams et al. 1999). Physical crusts are the most comment and hence the discussion here is focused on physical crusts.

Soil texture has the greatest influence on the soil crusting process (Bradford and Huang 1992) with crusts forming more readily on soil with a high silt content (Tackett and Pearson 1965). The silt content determines the resistance of soil aggregates to breakdown by raindrop impact, surface flow and slaking. There is a negative relationship between the potential for crust formation and aggregate stability. The main factors that influence aggregate stability are the soil texture, clay mineralogy, organic matter content, type and concentration of cations, sesquioxide content and $CaCO_3$ content. There are then interactions between these factors that influence their individual influence (Le Bissonnais 1996).

There are four mechanisms by which the breakdown of aggregates can occur. The first is slaking caused by the compression of air trapped within the aggregate. The second is by differential swelling. The third is raindrop impact and the fourth method is physico-chemical dispersion due to osmotic stress (Le Bissonnais 1996). The initial moisture content of soil aggregates will greatly influence the resistance to breakdown. The breakdown mechanism is controlled by the moisture content. For initially dry aggregates, the mechanism is mainly slaking (Le Bissonnais 1990). The aggregate stability has been found to be sensitive to the effects of fire with the stability decreasing following a fire event (Cerdá et al. 1995).

Soils with smaller aggregate sizes, and hence lower surface roughness, are more disposed to form surface crusts. Farres (1978) showed that a soil with a mean aggregate size of 3.3 mm formed crusts faster than a soil with a mean aggregate size of 6.7 mm. As the surface roughness increases, the depth of the depression store will also increase. This can have the effect of protecting the

aggregates from raindrop impact. The greater roughness decreases surface flow volumes and velocities and this leads to a reduction in the effects of flow on the breakdown of aggregates.

Physico-chemical dispersion results from the reduction of the attractive forces between colloidal particles during wetting (Emerson 1995). The dispersion of the soil is influenceed by the electrolyte concentration of both the soil and the applied water (Agassi et al. 1985). Dispersion breaks the aggregates down into elementary particles rather than micro-aggregates. Hence it is one of the most effective processes of aggregate breakdown and greatly increases the effect of the other processes (Bresson and Boiffin 1990).

The effect of surface gradient on the formation of surface crusts was investigated by De Ploey and Poesen (1985) using rainfall simulation. For soils that were highly susceptible to surface sealing, it was found that the surface seal intensity was inversely proportional to slope gradient. The increase in surface gradient results in greater amounts overland flow on steeper slopes which is able to erode the crust and increase the rill density. The increase in slope gradient decreases the projected surface area and hence there is a decrease in the number of raindrop impacts. Surface runoff can selectively remove the fine material from the soil resulting in a greatly increased soil stone cover. The impact of this is discussed in the next section.

The depth of the surface crust will vary across a soil surface and is strongly related to the micro-topography due to the formation of sedimentary crusts in surface depressions and structural crusts in other areas. Although other types of crusts may exist, the sedimentary and structural crusts are the most important. This two phase pattern has the effect that as the ponding depth increases, areas with a greater infiltration capacity are inundated and this leads to a significant increase in the infiltration rate (Fox et al. 1998). The increase in the infiltration rate was also found to be related to the increase in the pressure head with greater ponding depth (Fox et al. 1998).

Vegetation Effects

Vegetation cover has been shown to be the single most important factor in determining the infiltration capacity in semi-arid areas (Thornes 1976; Wood et al. 1987; Wilcox et al. 1998). The soils under the vegetation contain a higher percentage of sand and organic matter and the soils are disturbed by biotic activity. This results in a lower soil bulk density and hence an increase in the infiltration capacity (Lyford and Qashu 1969).

Many Mediterranean areas are characterised by a semi-natural scrubland termed matorral which develops in areas with 350 – 1500 mm $year^{-1}$ of rainfall. Matorral is characterised by shrubs whose above ground parts are not differentiated into trunks and branches, whose leaves are sclerophyllous and whose growth habit may be upright or prostrate (Allen 2001). The ground cover may be dense, discontinuous or scattered depending on the climate and there may be trees present. The key matorral species found in south east Spain include *Stipa tenacissima* L., *Anthyllis*

cytisoides L., *Rosmarinus* L. and *Thymus* L. Under more favourable climatic conditions forests of oak (*Quercus coccifera* L.) or Aleppo Pine (*Pinus halepensis* L) have developed. A detailed description of the ecogeography of the Mediterranean can be found in Allen (2001).

The vegetation reduces the amount of rain splash and hence decreases the rate of crust formation. This is due to the reduction in the rainfall kinetic energy and the changes to the drops size distribution. The effects of lower plants can have both positive and negative effects on the infiltration capacity. Crptograms can reduce infiltration by binding the soil surface and blocking soil pores (Greene et al. 1990). However, they can also increase surface roughness and hence the amount of ponding (Blackburn 1975). If the surface has grasses, it is likely that the soil will have macropores which can greatly increase the infiltration capacity (Abrahams et al. 1994).

Lyford and Qashu (1969) studied the infiltration rates at points radiating out from plants in a semi-arid environment. They defined three areas, directly under the plant, the area between plants and the intermediate point between these two domains. The species considered were creosotebush and paloverde. Their results showed that infiltration rate in the under plant zone was three times that of the inter-shrub area and 1.6 times that rate in the intermediate area for paloverde. Under creosotebushes, the rate was 2.6 times the intermediate area and 2.4 times the interplant area. These changes in the infiltration rate were related to differences in the bulk density, organic matter and gravel content of the soil. The bulk density was found to be greater in the interplant areas than under the plants and was not influenceed by plant species. The organic matter content was greater under the plants and the gravel content was greater in the inter-plant area.

The hydraulic conductivity of the soil under plants was found to be greater by Nicolau et al. (1996). The key factor which controls the rate of infiltration under plants was identified as the amount of organic matter. It was also found that the vegetation increased the surface roughness and hence increased the infiltration capacity.

The effect of vegetation structure on the generation of runoff was investigated by Quinton et al. (1997). The study investigated *Artemisia* L., *Anthyllis cytisoides* L., *Plantage* L. and S*tipa tenacissima* L. using rainfall simulation. Of the variables investigated, only the percentage canopy cover was statistically significantly related to the runoff. It was found that there was a positive relationship between the percentage canopy cover and the infiltration capacity.

Soils with waxy organic substances produced by vegetation and micro-organisms may have hydrophobic behaviour. The contact angle between the waxy surface and the water is negative, and hence the water tends to 'bead up' rather than being drawn into the soil by surface tension forces. During a fire these compounds are vaporised and condense on the bare soil resulting in hydrophobic soils and can significantly reduce the infiltration capacity (Dingman 1994).

The removal of vegetation by fire results in a reduction of organic matter, a decrease in aggregate stability, an increase in hydrophobic substances and surface crust development (Cerdá 1998). The development of a hydrophobic layer reduces the point scale infiltration capacity and hence increases runoff generation. The rate of recovery following a fire event is rapid. Cerdá (1998) found that runoff decreased from 45 % of rainfall after the fire, to less than 6 % after six and half years. The first two years showed a rapid recovery of the infiltration rate as a result of the rapid response of the vegetation.

The presence of hydrophobic soils does not always result in an increase in runoff from a hillslope. Doerr et al. (1996) found that a plot scale site in Portugal which had high levels of hydrophobic soils produced little runoff. The effects of hydrophobic soils decrease with wetting and thus fire can have a relatively small effect (Beven 2002a).

Rock Fragments

The presence of rock fragments on the soil surface can have both positive and negative correlations with the infiltration capacity (Abrahams and Parsons 1991). Poesen et al. (1990) reports on 17 studies, 10 showing negative relationships and 7 showing positive relationships. There are many pathways that water can take in a soil containing rock fragments (Figure 2.11). These are (1) absorption into the rock fragments, (2) interception and rock surface depression storage, (3) flow across the rock surface, (4) evaporation, (5) infiltration, (6) percolation, (7) overland flow and (8) capillary rise.

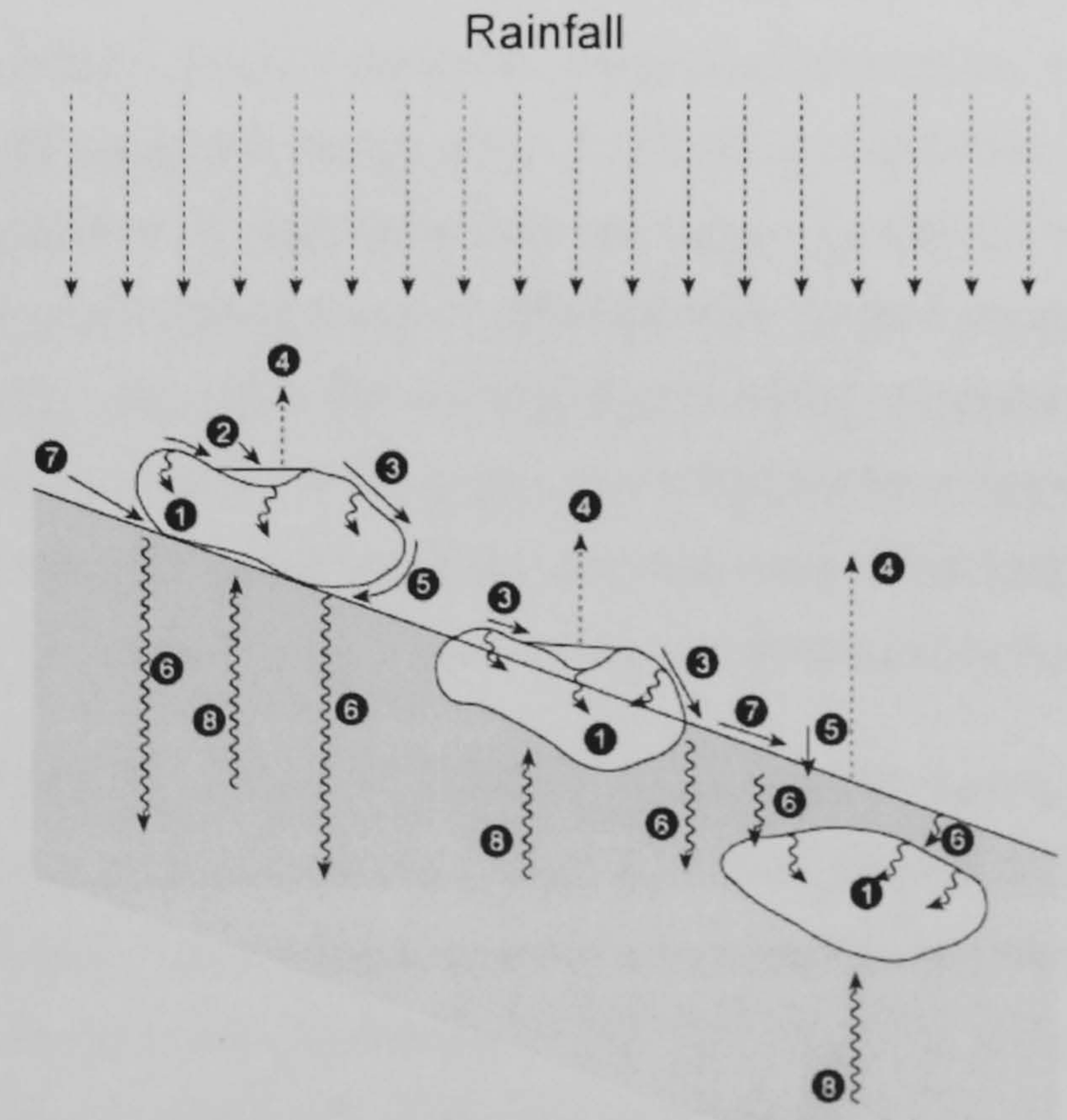

Figure 2.11 Hydrological pathways in a soil containing rock fragments

If the rock fragments are resting on the surface, they protect the soil from rain drop impact and hence reduce surface sealing. This leads to positive correlation with the infiltration capacity. If the rock fragments are embedded into the soil, they reduce the area over which water can infiltrate this and results in a negative correlation with the infiltration capacity (Poesen et al. 1990). However, macropores can develop along the edges of rock fragments resulting in an increase in the infiltration capacity (Poesen et al. 1990). If there are large individual rock fragments, they may deliver water from a large area to a single point on the soil surface. This therefore results in localised high intensity water input and hence can lead to local runoff generation (Poesen and Lavee 1994). Poesen et al. (1990) undertook a series of laboratory experiments to investigate the effect of rock position upon the infiltration rate in a soil susceptible to surface sealing. For a surface with 65 % rock fragment cover, the position of the rock fragments causes the runoff coefficient to vary over more than an order of magnitude.

Agassi and Levy (1991) investigated the effects of the level of stone cover and stone size upon infiltration, erosion and rain splash. They used a laboratory based rainfall simulator and asbestos cement plates to simulate stone cover. They found that an increase in stone cover increased infiltration and reduced erosion. Many small plates opposed to a small number of larger ones with the same percentage cover, resulted in less rain splash and hence a decrease in surface sealing and erosion.

Abrahams and Parsons (1991) undertook a study in southern Arizona to consider the relationship between stone cover and infiltration capacity including the effects of vegetation. The results showed a negative correlation between infiltration capacity and the surface stone cover and a positive correlation with vegetation canopy cover. The positive correlation with canopy cover was related to the accumulation of fine sediments under the canopy by differential splash. This leads to a higher percentage of sand and hence higher infiltration rates. In the inter-shrub areas, these fine sediments are removed by rain splash and overland flow resulting in a gravel lag layer. The vegetation was found to be effective at dissipating the rainfall kinetic energy and hence reduces soil surface seal formation. This study contrasts with other work which only considers inter-shrub areas where a positive correlation between stone cover and infiltration capacity has been reported.

Descroix et al. (2001) monitored runoff generation at 45 plots under natural rainfall conditions in the Western Sierra Madre, northwest Mexico. It was found that embedded gravel, the soil sand content and the percentage of grass cover were positively related to the amount of runoff. The presence of free pebbles and blocks, an increase in the percentage tree cover and the organic matter content of the soil resulted in a reduction in the amount of runoff.

The effects of rock fragment cover on infiltration and runoff were investigated by Cerdá (2001) on scrub slopes in Valencia, southeast Spain. The experiments were undertaken using rainfall

simulation on 26 plots. It was found that surface rock fragments impeded surface ponding and runoff and increased the steady state infiltration rate. This, therefore, led to a reduction in discharge, sediment concentration and erosion rates.

Poesen et al. (1998) found that the spatial distribution of rock fragments on semi-arid hillslopes is largely controlled by surface gradient. The total cover of rock fragments increases in a convex upward curve with hillslope gradient, whereas, the median size of the rock fragments increases linearly with slope gradient. It was also found that aspect influences the rock fragment cover with south facing slopes having slightly higher cover percentages. The local geology was found to control the fragment size distribution but not the cover percentage.

The presence of rock fragments within the soil is an important aspect of semi-arid hydrological systems. The rock fragments can both increase and decrease the infiltration capacity and result in locialsied concentrations of rainfall and hence localised runoff.

Surface Roughness

Soil surfaces have varying degrees of surface roughness which influences the amount of surface depression storage, the fraction of the surface covered by water, the amount of rainfall excess required to start runoff and the overland flow velocity (Moore and Larson 1979). The amount of storage is highly dependent on the recent history of the surface as it is modified by rainfall, wind and cultivation. The hydrological processes of infiltration, surface runoff and erosion are all related to, and influenceed by, the nature of the surface roughness (Zobeck and Onstad 1987).

Moore and Larson (1979) described the hydrological steps during a storm which lead to the initiation of runoff from a rough surface. As soon as the rainfall rate exceeds the infiltration rate, surface depressions start to fill. Since depressions are of different sizes some will begin to overflow before others are filled, initiating runoff. Moore and Larson (1979) noted that micro-relief depressions are both superimposed and interconnected and that each depression has a definite drainage area of its own. Therefore, the process of initiating runoff from a rough surface is complex.

Römkens and Wang (1986) identified several types of surface roughness. Each type represents a different order of magnitude and reflects a systematic variation in surface relief due to cultivation practices. They are:

- Micro-relief variations due to individual grains or micro aggregates. This type of roughness is uniform in all directions. Horizontal surface variations are of the order of 1 mm and vertical variations are of the order of 0 to 2 mm.

- Surface variations due to soil cloddiness. This is usually the result of soil break-up by tillage implements. Horizontal surface variations are of the order of 100 mm and vertical

variations are of the order of 200 mm. This type of roughness is non-directional and is often referred to as random roughness.

- Systematic variation in the surface form created by agricultural implements such as the furrows created by ploughing. These marks are uni-directional extending over the whole field and have vertical variation of the order of 100 to 200 mm. This type of roughness is also referred to as oriented roughness (Allmaras et al. 1966).
- Higher order roughness, represents elevation variations at the field, basin or landscape level. These variations in elevations may be very substantial and usually non-directional.

A number of indices have been developed for the description of surface roughness. A frequently used index is the Random Roughness (RR) index of Allmaras et al. (1966). The calculation of roughness indices is covered in section 3.1.6.

Onstad (1984) investigated the effects of slope gradient and surface roughness on various properties of the soil surface. The roughness was characterised by the Random Roughness coefficient (RR). For the surface depression store volume, an empirical relationship was developed which relates the maximum surface depression storage (DS) in cm to RR in cm and slope expressed as a percentage (β):

$$DS = 0.1122RR + 0.031RR^2 - 0.012RR.\beta$$

Equation 2.2

This relationship shows that roughness has the largest effect on DS at low slopes. The storage volume decreases rapidly as slope increases.

The relationship between RR, β and the percentage surface area of the depressions was investigated. The surface area of depressions is important because the depth of the surface water will determine the eroding capability of a raindrop impact and the percentage of the soil surface which is exposed to the full force of the raindrops. This can lead to depressions becoming sediment sinks and the formation of sediment crusts. The area covered by surface water will determine the amount of infiltration that occurs at the infiltration capacity. The relationship between RR and the surface area (SA) can be expressed as:

$$SA = 0.152RR - 0.008RR^2 - 0.008RR.\beta$$

Equation 2.3

The surface area changes very little with slope for relatively smooth surfaces. For rough surfaces, the range of SA is from 0.5 on low slopes to near zero on steep slopes.

2.5.3 Topographic Factors

The two main characteristics of the topography that influence the infiltration rate are the surface gradient and aspect. Surface gradient and roughness determine the depth of the surface depression store and hence are important in conditions where the infiltration rate is less than the input rate such that ponding occurs. The depth of ponding will increase to the point when it overflows from the surface depression store and at this point overland flow occurs (Dingman 1994). The overland flow rate is positively related to slope and negatively related to roughness, this is discussed further in section 2.6.

Gradient

The effect of slope gradient has been reported as being both positively (AbuAwwad and Shatanawi 1997) and negatively (Poesen 1984; Govers 1991) related to runoff. However, a number of studies have found no significant relationship between slope gradient and runoff (Lal 1976; Mah et al. 1992). These studies have been undertaken on plots and small catchments in the field and using laboratory experiments. The variation between experimental techniques has been cited as a possible reason for the discrepancies in the results (Fox et al. 1997).

It was reported by Poesen (1984) that the amount of runoff decreased with increasing slope gradient and was based upon laboratory rainfall simulation experiments on a soil susceptible to surface crusting. This was related to the decrease in the amount of energy delivered by the rainfall with increasing slope angle, which resulted in a decrease in the surface crust depth and hence a greater infiltration capacity.

It has been found that an increase in the slope angle can also result in an increase in the amount of rills on a surface (Bryan and Poesen 1989). These rills cut through the surface crust and thus enable infiltration into the more permeable soil matrix below, therefore enhancing the negative relationship between slope gradient and runoff.

Working on field plots under natural rainfall, Govers (1991) found that slope gradient had a significant influence in increasing the infiltration capacity of soils. This was related to the increase in the infiltration capacity with the formation of macropores resulting from the soil surface cracking. The formation of the cracks was related to solar energy receipt and hence was a function of both aspect and surface gradient.

An increase in slope gradient can lead to an increase in runoff in two ways. There is a negative relationship between slope gradient and surface depression storage (Onstad 1984). This reduces the amount of infiltration excess required to fill the surface depression store and reduces the time required for runoff to be initiated (De Ploey et al. 1976). An increase in slope gradient results in greater overland flow velocities due to the greater potential energy (Knighton 1984; Chaplot and

Le Bissonnais 2000). These factors combine to give greater flow velocities and hence lower transmission losses.

Chaplot and Le Bissonnais (2000) investigated the relationship between runoff and slope gradient on a soil prone to crust formation using a combination of rainfall simulation and natural rainfall events. The infiltration rate was calculated from the amount of runoff. It was found that as the slope gradient increased from 2 to 8 percent, the infiltration rate decreased from 1 mm hr^{-1} to 0.45 mm hr^{-1} for low intensity natural rainfall and from 15 mm hr^{-1} to 5 mm hr^{-1} under intense (50 mm hr^{-1}) simulated rainfall. The increased runoff was related to the increase in flow velocity. There were no rills present which have been associated with the negative relationships between slope gradient and runoff reported above.

AbuAwwad and Shatanawi (1997) investigated the relationships between basin characteristics and discharge in Muwaqar region of Jordan. Flood measurements were carried out using rectangular sharp-crest contracted weirs and a water height recorder to measure the water height above the crest weir. It was found that increasing watershed slope increased total volume of runoff water, volume of runoff water per unit area and runoff coefficient due to the reduction in infiltration, evaporation and depression storage losses as the slope of the watershed increased. However, as the basin area increased, the runoff coefficient decreased.

Aspect

Aspect influences the amount of rainfall and the solar radiation received. Aspect influences the amount of rainfall received on a slope because of the east wind direction during many storms in Spain. Therefore the rainfall intensity received on slopes with an eastern aspect is greater (Alonso-Sarria et al. 2002). The solar radiation receipt is influenced by the aspect. For example, on the first of April at mid-day, a 10 ° slope in southern Spain with a north aspect would receive 1,040 W m^{-2} whereas a south facing slope would receive 1,259 W m^{-2}, not accounting for atmospheric effects. This difference in energy receipt effects the potential evaporation rates and soil development processes. This leads to differences in soil moisture and vegetation growth.

Kutiel et al. (1998) studied the effects of aspect along a climatic gradient in Israel. It was found that the sites with a southern aspect were dominated by stones and bare patches whereas the northern aspect slopes were dominated by vegetation and biogenetic crusts. This would result in greater runoff generation on the southern slopes due to their lower infiltration capacities.

Cerdá et al. (1995) studied the effect of aspect on runoff production in Valencia, SE Spain, using rainfall simulation techniques. On a slope with a southern aspect, runoff was produced before it was produced on a slope with a northern aspect. The runoff coefficient from the north facing slope was 8 % compared to 12 % on the south facing slope. On the north facing slope Cerdá et al. (1995) found that the low aggregate stability, low vegetation cover and low litter cover led to the

crusting of the soil surface. This crusting impeded the infiltration of the water. On the south facing slope, the aggregate stability was lower but the infiltration rate was higher due to the presents of macropores. The extent of soil surface cracking has been found to be dependent on solar isolation and hence is sensitive to slope aspect (Govers 1991).

Cammeraat and Imeson (1998) found that the aggregate stability was greater on north facing slopes than on south facing slopes. This was for a variety of sites in south eastern Spain and southern France. The greater aggregate stability on the north facing slopes would result in less crust formation and hence greater infiltration rates.

Summary

The slope gradient has been found to have a positive and negative influence on the generation of runoff. The decreases in runoff have been related to the ability of the soil surface to form rills which cut through the surface crust exposing the material below with a greater infiltration capacity. The increase in runoff has been related to the increased overland flow velocity on steeper slopes reducing the amount of time available for transmission losses to occur.

The aspect of the surface determines the amount of solar radiation received. This in turn determines the soil moisture and the long term development of the soil and the vegetation cover. Therefore, very different hydrological conditions are developed on slopes with different aspects and hence lead to the observed differences in runoff generation.

2.5.4 Changes in Infiltration Capacity over Time

On both the time scale of a storm event and over many months and years, the infiltration capacity will change. On the time scale of a storm event, the changes in the infiltration capacity are related to the changes in soil moisture. Over a series of storms, the surface roughness will change due to the breakdown of soil aggregates, and leads to the formation of a soil crust. Therefore, the infiltration capacity will decrease. Seasonal changes are related to macropore formation by surface cracking (Cerdá 1999).

The roughness of the soil surface can either increase or decrease during a storm event (Magunda et al. 1997). Surface sealing processes tend to reduce the roughness whilst erosional processes tend to increase the roughness through the initiation of rills. The rate of smoothing is greater for soils with low initial moisture content due to the lower aggregate stability (Van Wesemael et al. 1996). The most important effects of a decrease in soil surface roughness are an increase in the velocity and erosive power of runoff, a decrease in flow depth and a decrease in detention storage (Van Wesemael et al. 1996).

Zobeck and Onstad (1987) evaluated several relationships between the decrease in the surface roughness and the total rainfall energy. They proposed Equation 2.4 to describe the decrease in roughness.

$$\frac{RR}{RR_0} = a^{(bKEPR)}$$

Equation 2.4

Where RR_0 is the initial RR, a and b are coefficients and KEPR is the total kinetic energy of rainfall (MJ ha $^{-2}$) or total amount of rainfall (mm). The best prediction that Zobeck and Onstad (1987) found accounted for 76 % of the variation. The coefficients used in their study were a = 0.886 and b = 0.026.

Magunda et al. (1997) investigated the changes in surface roughness induced by rainfall on four soils from Minnesota and Uganda. The surface roughness was measured before and after each storm and it was found that the roughness decreased during each storm, as shown in Table 2.3. The roughness was described using the RR, LD and LS indices, which are described in chapter 3. The results indicated that aggregate breakdown was the dominant process in seal formation.

Soil	**Index**	**Cumulative rainfall (mm)**		
		0	63	126
Barnes loam	RR	5.9	4.32	9.97
	LD	8.58	6.57	5.68
	LS	0.52	0.32	0.23
Renova silt loam	RR	9.71	8.42	6.46
	LD	11.1	9.57	7.47
	LS	0.57	0.49	0.26
Kabanyolo clay	RR	5.7	5.46	5.44
	LD	10.32	9.8	9.28
	LS	0.54	0.43	0.32
Kachwekano clay	RR	10.07	8.92	6.13
	LD	15.43	11.42	8.54
	LS	0.64	0.58	0.44

Table 2.3 Changes in roughness with cumulative rainfall

Van Wesemael et al (1996) working in Almeria, SE Spain, found that the presence of stones had a large effect on the changes in roughness with cumulative rainfall. For soils with small rock fragments (1.7 – 2.7 cm) the RR decreased during the first 17.5 mm of rainfall and then increased (Figure 2.12a). For soils with large rock fragments (7.7 cm) the RR increased with cumulative rainfall (Figure 2.12b). This was explained by two mechanisms which are simultaneously active: the breakdown of aggregates and the washing of fine particles in the depressions between the stones. Until the 17.5 mm point, soil aggregates are still abundant and dominate the surface roughness. After this point, the aggregates are mostly destroyed and roughness is determined by the protruding rock fragments.

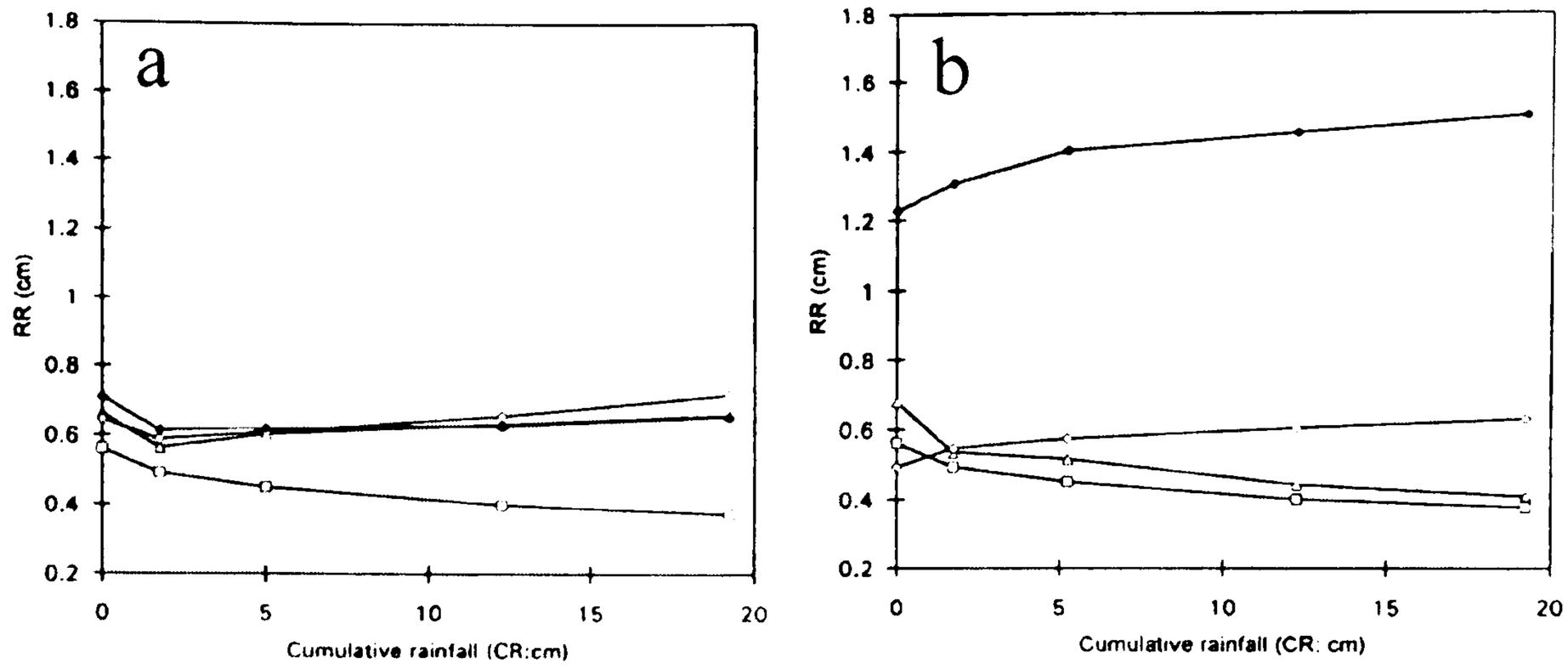

Figure 2.12 Changes in roughness over time from Van Wesemael et al (1996)

Seasonal Time Scales

The clay minerals in soils will swell when wet and shrink when dry. During wet periods, the particles swell, reducing surface porosity and permeability and hence greatly reducing the infiltration capacity. During dry periods, polygonal cracks will develop resulting in very high infiltration rates (Dingman 1994). Therefore, on seasonal or storm timescales, the infiltration capacity of the soil can significantly change.

Cerdá (1999) found that the amount of water entering the soil via macropores varied on an annual cycle. Using rainfall simulation and ring infiltrometers in eastern Spain, it was found that the range of infiltration rates increased from 6.8 – 11.8 mm hr^{-1} during the winter to 11.6 – 18.9 mm hr^{-1} during the summer. This increase in infiltration was related to the development of wide and deep macropores during the summer.

Over the course of a year, due to the variations in temperature and soil moisture availability, the vegetation cover will change. This will result in different responses to the same storm event at different times of the year. The reduction in leaf cover will result in greater rainfall energy reaching the soil surface and can lead to increased crust formation. The removal of the shading effect of vegetation will result in greater soil surface evaporation. Many large storm events occur at the end of the summer. The reduced vegetation cover makes the surface more susceptible to erosion. Therefore, the amount of discharge and the geomorphic impact of the same storm occurring at the end of the summer is greater than if it occurred at the start of the summer.

2.6 Overland flow

If the rate of rainfall is greater than the current infiltration capacity, water will pond on the surface. If the amount of ponded water exceeds the surface depression storage capacity, overland flow will occur. This flow will be influenceed by a number of forces. Gravity acts as the main driving force and there are a range of forces that transmit frictional effects onto the flow.

Most studies considering overland flow divide the system into two process domains, rill and inter-rill flow (Meyer and Wischmeier 1969). Rill flow is characterised by concentrated flow within a defined channel. The precise definition of a rill as opposed to a small gully is vague with a continuum of forms (Poesen et al. 2002). Inter-rill flow occurs with a branching pattern as the water flows around obstacles. The flow is shallow and there may be localised flow concentration.

Due to the complex and chaotic nature of flow dynamics, it is beyond the scope of this work to discuss the direct interactions between the opposing forces. To model these processes, a friction coefficient is often used. Therefore, the equations describing flow velocities will be introduced here, rather than in chapter 5, so that the interactions between surface properties and flow dynamics may be discussed.

Three main equations exist for determining the flow velocity. The Chezy (Equation 2.5) and Manning (Equation 2.6)) equations are both steady state and were originally developed for rivers.

$$v = C\sqrt{Rs}$$

Equation 2.5

$$v = \frac{R^{\frac{2}{3}} s^{\frac{1}{2}}}{n}$$

Equation 2.6

Where v is the flow velocity, C and n are roughness coefficients, R is the hydraulic radius and s is the slope of the energy gradient.

The third relationship is given by the Darcy-Weisbach equation (Equation 2.7). This has the advantage of being able to describe laminar, transitional and turbulent flow and the friction factor is dimensionless.

$$v = \sqrt{\frac{8gRs}{ff}}$$

Equation 2.7

Where ff is the friction factor and g is the gravity constant.

It has been observed that overland flow on desert surfaces may consist of a combination of laminar, transitional and turbulent flow (Abrahams et al. 1986). In these situations, the Darcy-Weisbach equation is the most appropriate since it is able to describe all of these flow conditions (Baird 1997). For this reason, the Darcy-Weisbach equation has been used in many studies of semi-arid hydrology (Scoging et al. 1992; Abrahams et al. 1994) and much work has been

undertaken to relate the friction factor to the flow dynamics and the properties of the surface (Abrahams and Parsons 1991; Gilley et al. 1992).

The friction factor in Equation 2.7 is dependent upon the resisting forces and the flow dynamics (Baird 1997). The resisting forces arise from the grain roughness, the bedform roughness (Gilley et al. 1992) and the rainfall roughness (Shen and Li 1973). Each of the separate components of the friction factor are assumed to be additive (Gilley et al. 1992). The effect of rainfall roughness was found to significantly influence total hydraulic resistance for small flows on smooth surfaces (Shen and Li 1973). However, for most natural overland flow conditions, it is expected that rainfall roughness will have negligible effect on the total hydraulic resistance (Gilley et al. 1992)

Many studies have expressed the friction factor as a function of dimensionless discharge given by the Reynolds number (*Re*).

$$Re = (vR)/k_v$$

Equation 2.8

Where R is the hydraulic radius and k_v is the kinematic viscosity. For flow over a smooth surface or where all the roughness elements are submerged by the flow, the relationship between *ff* and Re shows two distinct linear relationships with *ff* decreasing with increasing Re. The relationship within the laminar flow section is given by $ff = 1000\ Re^{-1}$ and in the turbulent section, $ff = 1000\ Re^{-0.2}$ (Abrahams et al. 1989).

When the flow is transitional, the relationship is far less clear. Abrahams et al. (1990) and Gilley et al. (1992) found that there were two forms of the relationship between *ff* and Re. The first is a linear relationship and in the second relationship, *ff* tended to increase to a maximum value and then decrease with increasing *Re*. This non-linear form was related to a change in the surface roughness with flow depth. As the flow depth rises, there is an increase in roughness as the flow comes into contact with more roughness elements. Once the flow depth is able to submerge the roughness elements, the friction decreases and hence *ff* decreases. It was found by Abrahams et al. (1994) that the form of the relationship between *ff* and *Re* was non-linear for grassland sites and negatively linear for rangeland. This difference was related to the flow not being able to over top the greater roughness heights on the grassland.

Abrahams et al. (1994) found that the relationships between *ff* and *Re* are of limited value for the prediction of flow resistance at sites other then where they were developed. The surface form generates the form and wave resistance sections of the *ff*. Therefore, the *ff* should be related to surface form characteristics such as the percentage gravel cover (Abrahams et al. 1992). Abrahams et al. (1994) found that 69.5 % of the variation in *ff* can be explained by basal plant stem and litter cover on grassland and that 56.3 % of the variation in *ff* can be explained by gravel cover at a

gravel site. A relationship between the percentage gravel cover and the *ff* was presented, as shown in Equation 2.9.

$$\log ff = -5.34 + 3.14 \log \%gr$$

Equation 2.9

The inclusion of *Re* in the analysis improved the explanation by 5.4 % on the grassland and by 7.6 % on the gravel site. It was concluded that the extra effort involved in determining the exact relationship between *ff* and *Re* for a site was not worth the additional expense (Abrahams and Parsons 1994).

2.6.1 Transmission Losses

As water flows across a surface, part of the water may be infiltrated. This loss of water during flow is termed the transmission loss. The rate of transmission loss is influenceed by the same factors that influence infiltration with the addition of the depth of water. The amount of transmission loss on an inter-rill area is determined by the infiltration capacity of the soil. The water in a channel will have greater water pressure and this leads to an increase in the infiltration rate. The effect of transmission losses is that the discharge tends to decrease downstream. The amount of discharge lost in ephemeral channels is summarised in Table 2.4. Transmission losses can cause a significant decrease in the discharge hydrograph and hence are a vital component of a flow routing model (Shannon et al. 2002).

There have been few studies considering transmission losses in rills. Parsons et al. (1999) used a field flume to investigate the transmission loss rates at Jornada, New Mexico and Walnut Gulch, Arizona. At the Jornada site, the rills had a sand bed and an infiltration rate of 554.4 mm hr^{-1} was recorded. This compared to 115.8 - 139.2 mm hr^{-1} in the inter-rill areas. The rills at the Walnut Gulch site had a gravel bed and an in rill infiltration rate of 306 mm hr^{-1} was recorded. This compared to 31.2 mm hr^{-1} in the inter-rill areas.

Study area	Measured transmission loss	Source
Queen Creek, Arizona	49.9 %	Babcock and Cushing (1941 cited in Shannon et al. 2002)
Mojave River Basin, California	77.2 % in 1969 88.2 in 1982	Buono and Lang (1980 cited in Shannon et al. 2002)
Tucson Basin, Arizona	70 %	Burkham (1970 cited in Shannon et al. 2002)
Homestead Creek – Fowlers Creek, NSW, Australia	13.2 % per km with Sub bank full flow and 5 – 6.9 % for bank full and over bank flow	Dunkerley and Brown (1999)
Goba River, South Africa	75 % and 22 % of the flow in two separate events	Hughes and Sami (1992)

Table 2.4 Transmission losses for semi-arid ephemeral channels, adapted from Shannon et al. (2002)

2.7 Hillslope Scale Runoff

There are two key factors that influence the generation of runoff at the hillslope scale: slope length and the spatial patterns of runoff generating areas on a hillslope. The slope length effects are discussed in section 2.7.1 and the spatial patterns are discussed in section 2.7.2.

2.7.1 Slope Length

The importance of slope length in determining the erosion rate has long been recognised. The slope length factor forms one of the components of the Universal Soil Loss Equation (Morgan 1995). However, the relationship between slope length and runoff is more complex. A number of studies have reported a decrease in runoff per unit area with increasing slope length (Yair and Lavee 1985; Lal 1997; Gabriels 1999; Van de Giesen et al. 2000). The decrease in the runoff coefficient on longer slopes can be related to the greater amount of time that the water has to infiltrate into the soil. Therefore, infiltration capacity of the soil, the susceptibility of the soil to crust formation and the land management all have a significant effect on the form the slope length and runoff coefficient relationship. Longer slopes on soils with low infiltration capacities generate more runoff and the runoff coefficient increases with slope length. However, longer slopes with high infiltration capacities decrease the generation of runoff and the runoff coefficient decreases with slope length (Lal 1997). Once slopes pass a critical threshold, there is sufficient volume of runoff for rill formation to occur (Truman et al. 2001). Since the rill can be considered as a small channel, this has the effect of reducing the hillslope length.

Yair and Lavee (1985) reported a modelling study of the effects of slope length on runoff generation. The deterministic model simulated runoff using the infiltration excess mechanism with spatially varying parameters. Under steady rainfall conditions they found that the area contributing to runoff increased over time. For fixed duration storms, the runoff coefficient decreased with increasing slope length. This shows that the upper sections of longer slopes do not contribute water to the slope base. A series of experiments were conducted using varying rainfall characteristics and slope lengths. It was found that uniformity in runoff generation across the whole slope was only found for storms with rainfall intensities greater than 9 mm hr^{-1} and for durations greater than 45 minutes.

Lal (1997) undertook a series of experiments to evaluate the effects of slope length on runoff on an Alfisol in Nigeria. The experiments were undertaken over a four year period on six slopes between 10 m and 60 m in length at 10 m intervals. The relationship between slope length and runoff was found to vary according to the land management and the rainfall characteristics. On slopes under conventional tillage, no relationship was found, whereas under a no-till management system there was a significant decrease in the runoff coefficient with slope length (Figure 2.13). However, under certain conditions, the relationship was more complex. The runoff coefficient was found to decrease with increasing slope length up to 50 m, however, at slope lengths greater than

50 m, the runoff coefficient increased to a level equivalent to a 20 m slope. This may be related to the greater volume of water on the longer slopes enabling the formation of rills. The rills effectively decrease the distance to the channel and the effective slope length.

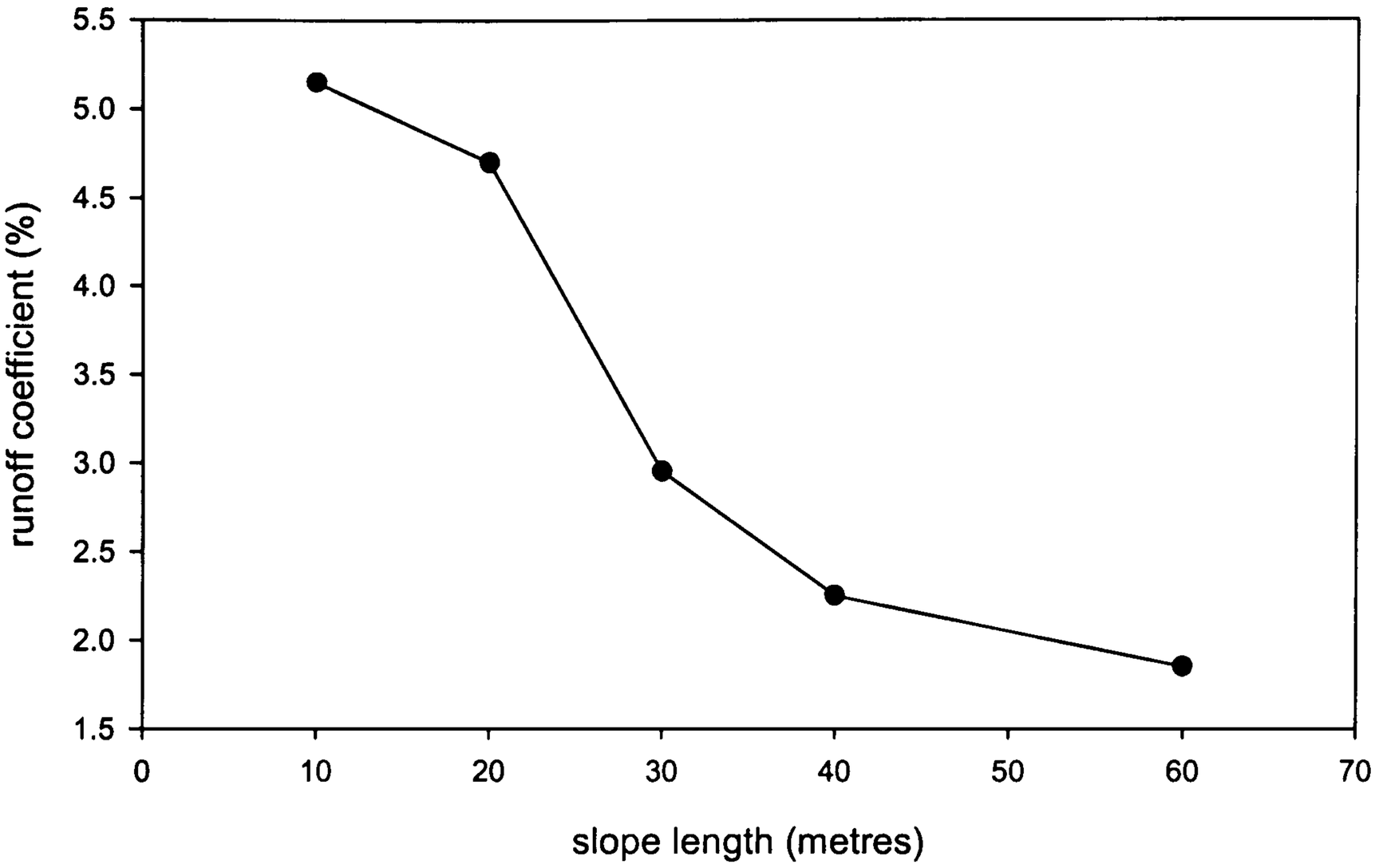

Figure 2.13 Decrease in the runoff coefficient in relation to slope length (Lal 1997)

Gabriels (1999) investigated the impact of slope length on runoff generation for two different soils. The slope lengths considered ranged between 0.3 and 0.9 m and the slope were subjected to 90 minutes of rainfall at an intensity between 22 and 75.5 mm hr^{-1}. The two soils considered were a sandy loam and a loamy sand. It was found that the decrease in the amount of runoff per unit with increasing slope length varied between the two soils. The decrease in runoff per unit area could be modelled by Equation 2.10.

$$r = l^n$$

Equation 2.10

Where r is the amount of runoff, l is the slope length and n is an exponent. It was found that n = -0.32 for the sandy loam and -0.29 for the loamy sand. This difference was related to the crust forming ability of the soil with the soils least prone to crusting having the greatest decrease in runoff per unit area. This is due to the greater infiltration capacities and greater stability of infiltration rates on the soils not prone to crusting.

Chaplot and Le Bissonnais (2000) investigated the relationship between plot size, slope gradient and runoff. This was undertaken on a soil prone to surface seal formation under a combination of rainfall simulation and natural events. Two plot sizes were investigated, 10 m^2 and 1 m^2. It was found that the 10 m^2 plot gave only slightly greater amounts of discharge than the 1 m^2 plot over the range of slope gradients 2 – 8 %.

Van de Giesen et al. (2000) studied the generation of runoff from slope lengths of 1.25 m, 12 m and for whole watersheds in central Cote d'Ivoire in 1996. They found a clear reduction in the runoff coefficient with an increase in the slope length. For a 1 m^2 area slope, the runoff coefficient was between 30 % and 50 % whereas at the watershed scale (130 ha), the runoff coefficient was 4 %. It was found that the amount of runoff produced from the 1.25 m and 12 m slopes varied significantly between storms. The variability was related to the temporal dynamics of the storm event.

Joel et al. (2002) measured runoff from plots of two different sizes under natural rainfall conditions. The large size plot measured 10 m by 5 m and the small plot was 0.5 m by 0.5 m. It was found that the large plots on average had a runoff coefficient only 40 % of the small plots. However, the minimum rainfall intensity required to produce runoff was found to be independent of the plot size.

Wainwright and Parsons (2002) considered the relationships between the temporal variation of the rainfall, the spatial variation of infiltration capacities across a hillslope, the slope length and the runoff coefficient measured at the base of the slope. The authors proposed the hypothesis that the temporal structure of the storm event will influence the runoff coefficient due to runoff generated in one section of the storm being infiltrated during another part of the storm. This effect relates to the temporal discontinuities discussed in section 2.3.1. The modelling was undertaken using a distributed hydrological model and 5 measured storm events. The authors found that on a slope with spatially uniform infiltration rates, there was a decrease in the runoff coefficient with increasing slope length. However, the authors report that this decrease does not occur when constant intensity rainfall is used. The rate of decrease in the runoff coefficient was found to be greater slopes with spatially variable infiltration characteristics than on slopes with uniform infiltration rates. The authors conclude that temporal variation in rainfall intensity is a significant factor in controlling the scale dependency of the runoff coefficient. The authors recommend that models of semi-arid hydrological systems include temporally variable rainfall since if constant intensity rainfall is used, the runoff coefficient will be under predicted and certain runoff generating events may be missed.

2.7.2 Spatial Patterns

At the scale of a hillslope, there is spatial variation in the infiltration rates (Lyford and Qashu 1969). The processes of runoff and run-on lead to dynamic interactions between the different zones. These interactions significantly influence the large-scale hydrological response and cause the hillslope scale runoff to be significantly different to what it would be without the interactions (Fiedler et al. 2002). The relative importance of the interactions is positively related to the spatial variability (Fiedler et al. 2002).

Undisturbed semi-arid sites tend to develop a structured two phase system of vegetated and bare areas. Patterning in vegetation has been observed in the semi-arid areas of Australia, Niger, Mexico and Spain (Sanchez and Puigdefabregas 1994; Seghieri et al. 1997; Valentin et al. 1999; Dunkerley 1999). As discussed in section 2.5.2, the presence of vegetation can greatly increase the relative infiltration capacity compared to the inter-scrub bare areas. Therefore, during a storm event, runoff is generated in the bare areas and flows down slope until it reaches a vegetated area where it is infiltrated. This greatly increases the available water for the vegetation. It has been suggested by Cerdá (1997) that as the climate becomes drier, the size of the bare areas increases. These interactions between the bare and vegetated areas are complex and makes the prediction of runoff from the whole slope very complicated (Cerdá 1997). During the initial stages of a storm event, the soil surface layer in both the vegetated and bare areas may produce infiltration excess runoff. However, in the later stages of the storm, the soil in the bare areas may become saturated and the majority of the runoff is then generated in the bare areas. This is very important in generating large amounts of runoff and hence creating a significant runoff response (Puigdefabregas and Sanchez 1996). The response of the hillslope can not be determined solely by the cover of bare and vegetated areas, but the spatial configuration of these areas needs to be considered in up-scaling (Morgan 1995; Fitzjohn et al. 1998; Cammeraat and Imeson 1999).

In semi-arid environments the scattered distribution of both sources and sinks of runoff inhibit the continuity of the flow over long distances even under extreme conditions (Bergkamp 1998). Puigdefabregas et al. (1998) have shown that the spatial pattern of soil moisture is hard to predict. There may be isolated pockets of greater soil moisture on the slope and soil moisture does not always increase downslope (Puigdefabregas et al. 1998). However, as the soil moisture increases, the likelihood of a connection being made between sources of runoff increases (Fitzjohn et al. 1998). It is therefore possible to define a threshold wetness level above which landscape units connect such that flow may reach the channel (Fitzjohn et al. 1998).

2.8 Land Use and Management

The management of the land has a significant effect on its hydrological properties. Recent trends in southern Europe have included the contradicting patterns of agricultural expansion and land abandonment (Allen 2001). There has been a large expansion of almond monocultures in south-east Spain over the last few decades of the twentieth century (Grove 1996). In the Murcia region of Spain, the area devoted to this crop increased from 33,123 ha in 1970 to 69,645 ha in 1980 (Poesen et al. 1997). This expansion has moved agriculture onto steep slopes with shallow, stony soils.

The agricultural areas in many semi-arid areas are ploughed 2 – 5 times a year with a duckfoot chisel plough (Poesen et al. 1997). This removes any vegetation and greatly increases the infiltration capacity, thus increasing the available water for the crop. The action of ploughing

results in the movement of rock fragments to the soil surface (Wijdenes et al. 1997) and redistributes the fragments across the slope (Van Wesemael et al. 2000). This leads to shallow stony soils near the hilltops with high infiltration rates, low overland flow and high evaporation rates. This is in contrast to the soils in the valley bottom which are deeper, less stony but with a greater surface stone cover (Van Wesemael et al. 2000).

Since the 1950's there has been rural depopulation in many rural areas in southern Europe with areas losing up to 50 % of their population (Douglas et al. 1994). The outward migration was to industrial jobs and since the 1960's to the tourism industry on the coasts. This reduced the labour available for agriculture and has led to a reduction in the intensity of land use and later to the abandonment of agricultural land (Douglas et al. 1994).

Many agricultural areas have been abandoned in recent years (Ruecker et al. 1998). In 1990, between 10 % and 20 % of the area that was active agricultural land had been abandoned (Grove 1996). In the Alpujarra region of southern Spain, the upper slopes have been abandoned leading to a reduction in the margin of cultivation from 1800 m to 1600 m (Allen 2001). The period directly after abandonment is characterised by greater runoff and erosion rates. As the vegetation stabilises on the abandoned field, the runoff and erosion rates decrease (Ruecker et al. 1998).

The hydrological response to land abandonment is complex and non-linear. Lasanta et al. (2000) investigated the hydrological characteristics of a site in the Central Ebro Depression, north east Spain for five years after abandonment. They found that 6 months after abandonment the site gave 0.2 ml s^{-1} discharge after 897 seconds under simulated rainfall. After two years the discharge had risen to 1.4 ml s^{-1} and the time to runoff had decreased to 211 seconds. After five years, the discharge had decreased to 1.1 ml s^{-1} but the time to runoff had remained similar at 210 seconds, (Figure 2.14). The initial runoff rates are low due to the high infiltration capacities of the soil. Over time, a crust will develop, reducing the infiltration capacity and hence leading to an increase in the runoff. During this period, the vegetation cover is low and hence is exposed to erosion. In the following years, the land is colonised by vegetation and the average infiltration capacity increases.

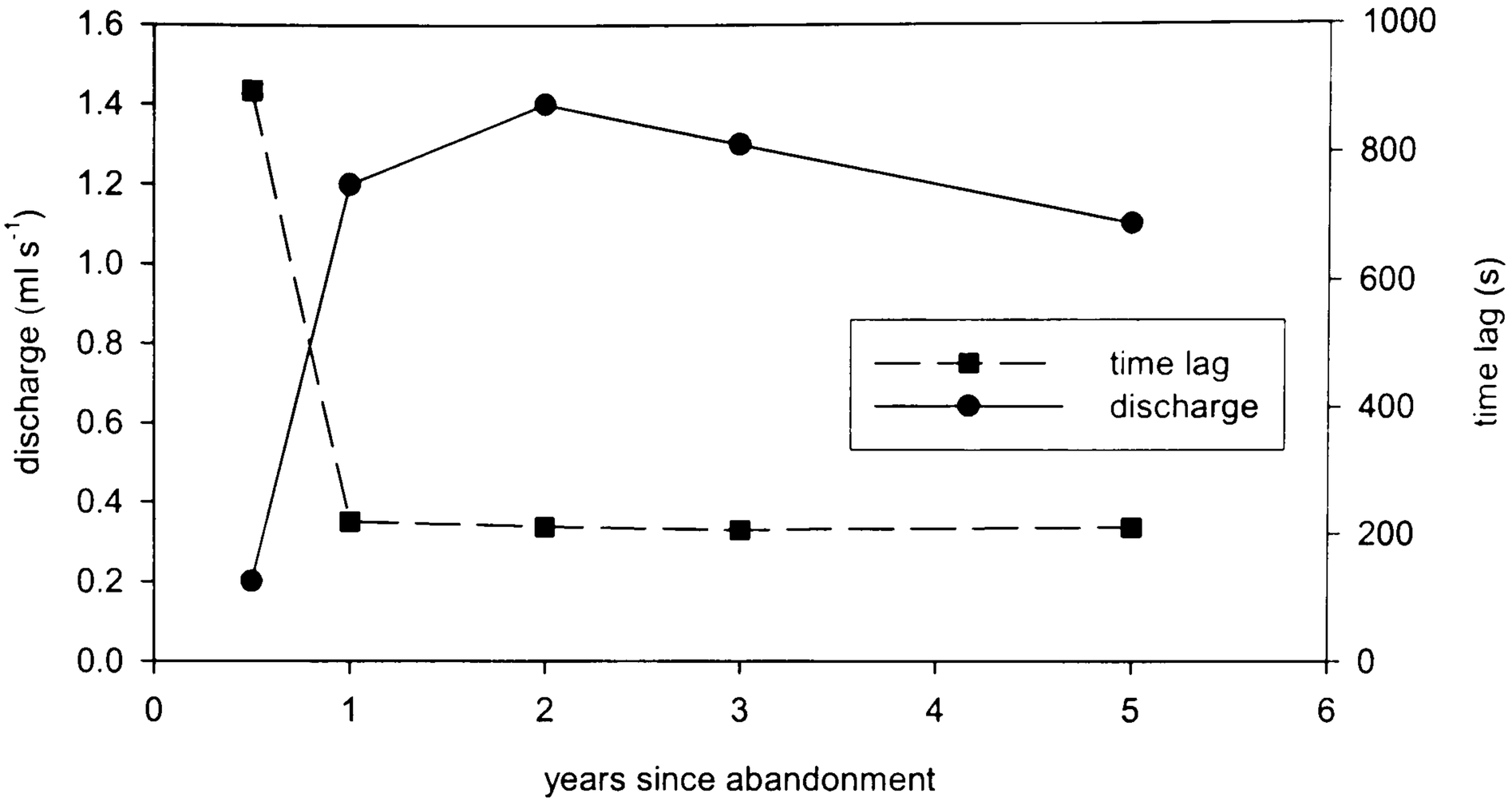

Figure 2.14 Impact of land abandonment on hydrological behaviour (Lasanta et al. 2000)

2.9 Summary

Semi-arid areas are characterised by potential evaporation rates that far exceed the precipitation and cover 17.7 % of the global land surface. The Mediterranean landscape has a complex geological, pedological and management history. This has given high spatial variability in many hydrological properties at the landscape scale. This is coupled with highly variable rainfall and results in a landscape that has a non-uniform response to rainfall events.

The Mediterranean basin is located between two contrasting climatic zones, the temperate maritime climate of Europe and the arid subtropical desert climate of Africa. This leads to hot dry summers with mild wet winters. Large scale climate systems control the switch between the dominance of these two climate zones. This leads to strong seasonality in temperature and rainfall. There is high inter-annual and spatial variability in rainfall.

At the time scale of a storm event, the key hydrological processes influencing the generation and transmission of runoff are interception, infiltration and overland flow. The nature of each of these processes is summarised in turn.

The process of interception influences both the timing and quantity of the water reaching the soil surface. The process can reduce the amount of water reaching the ground by evaporation. Water may reach the soil surface as canopy drainage or stem flow. Stem flow concentrates flow resulting in intensities many times greater than the rainfall and may, therefore, generate localised runoff.

The relationship between the rainfall intensity and the infiltration rate is the key factor in determining the amount of runoff generated. Representative rates of infiltration in many semi-arid environments are 50 - 70 mm hr^{-1}. Due to the low annual rainfall and the high potential evaporation rates, the soils are at or below the residual soil moisture (field capacity) for the

majority of the year. Therefore, the main runoff generating mechanism is infiltration excess (Hortonain) overland flow.

Many factors can influence the infiltration capacity of a soil. These may be categorised by their spatial scale of operation. They have been grouped into point scale factors, plot scale factors and topographic scale factors. The majority of research that has been undertaken has concentrated on the point and plot scales. There is a scarcity of research that has been under taken at the hillslope scale.

The infiltration capacity is strongly controlled by the soil texture and moisture content. This is due to greater capillary tension in smaller pore spaces. Water will move into the soil structure under gravity and due to matrix potential. As the soil moisture increases, the soil matrix potential decreases and hence the infiltration capacity is reduced. This results in the final infiltration capacity being the saturated conductivity of the soil. Under intense rainfall, the infiltration into the soil may be rapid. This can result in the entrapment of air within the soil matrix and a reduction in the infiltration capacity of 70 – 90 %.

Macropores form efficient channels through which water may infiltrate. This can result in an order of magnitude increase in the infiltration capacity. Macropores are formed by many different processes including soil cracking, rock fragments, roots and biota activity.

The development of a soil crust can significantly decrease the infiltration capacity of the soil. This may result in an infiltration capacity of one third that of a non-crusted area. Soil crusts form by the breakdown of aggregates by mechanical action and by microbiological processes.

As the scale moves from the point to the plot scale, the effects of vegetation, rock fragments and surface roughness become important. The presence of vegetation will increase the infiltration capacity. This is due to the development of better soil structure from the greater organic matter, the protection from crust formation by the canopy and the development of macropores by the root system. These factors can lead to an infiltration capacity three times that found in the inter-plant area.

Rock fragments can have both a positive and negative impact on the infiltration capacity. If rock fragments are resting on the surface, they protect the soil from crusting processes, resulting in an increase in the infiltration capacity. If the rock fragments are embedded into the soil then they reduce the area over which infiltration can occur leading to a reduction in the infiltration capacity.

The surface roughness influences the amount of water that can be held in the surface depression store. With a larger surface depression store, greater amounts of infiltration excess will be required to generate runoff. As the ponding depth increases, the area of ponded water will also increase.

This can result in an increase in the infiltration rate since a greater area is infiltrating at the infiltration capacity.

The topography influences the infiltration capacity in a number of ways. Slope gradient has been reported as having both positive and negative relationships with the infiltration capacity and runoff generation. An increase in slope gradient leads to a reduction in the depth of the surface depression store. This reduces the amount of infiltration excess required to generate runoff. With other factors being equal, the velocity of the flow is positively related to slope gradient leading to a positive relationship. However, the increase in flow velocity increases the erosive power of the flow. This may enable the runoff to erode through a surface crust and expose the material below which has a far greater infiltration capacity. This leads to an increase in the overall infiltration capacity.

Aspect influences the amount of solar energy received at a point. This has implications for water availability, vegetation growth and weathering processes. This leads to lower infiltration rates on slopes with a southern aspect than a northern aspect.

The infiltration capacity of a soil must not be considered as constant in space or time. All of the factors outlined above have a spatial distribution and will vary over time. During a storm event, the breakdown of aggregates will influence the surface roughness. On a seasonal time scale, the opening of desiccation cracks and the changes in the vegetation cover will alter the infiltration capacity.

Once runoff has been generated, it will move across the surface as overland flow. The flow velocity is related to the slope gradient, flow hydraulics and surface friction. As the water moves across the surface, part will be removed as transmission losses. In semi-arid environments, the transmission losses are often over 50 % and result in a decrease in flow in the downstream direction. Therefore, the position and movement of a storm over a catchment can have significant impacts on the size of the flood produced.

When the amount of discharge from a hillslope is considered, rather than the generation of runoff at the point scale, the dynamics of the system change. There are important, complex interactions between the runoff source areas and the runoff sinks. This means that the spatial configuration of different hydrological zones is important for determining the discharge from the whole slope.

As the slope length increases, the amount of runoff generated tends to decrease. This is related to the short bursts of high intensity rainfall generating runoff for short periods of time and hence the overland flow travel distances are short and the runoff may not, therefore, reach the channel.

Land management has a significant effect on the hydrological properties of the soil. The main agricultural land uses in the Mediterranean are tree crops, wheat and vines. The soils under crops

are ploughed 2 – 5 time per year. The removal of the vegetation cover greatly increases the infiltration capacity and increases the surface stone cover. Current trends in agriculture are for the abandonment of marginal areas and the intensification of production in the more favourable areas. The definition of marginal land is strongly dependent on the subsidies received from the EU. The abandonment of land results in an initial increase in runoff due to the lack of vegetation and the bare soils on which crusts can form. As the area is colonised by vegetation, the average infiltration capacity increases and hence runoff decreases.

2.10 Conclusions and Research Gaps

Runoff generation in semi-arid environments is dominated by the infiltration excess mechanism. This is due to the low water content of the soils for most of the year and the intense rainfall events. The key factors influenceing the infiltration rate are the vegetation cover, rock fragments, surface roughness and soil crusting. The key factors influenceing the transmission of runoff are the surface gradient and the surface roughness. Therefore, these factors need to be considered when investigating the key controls on runoff generation in the field.

The majority of research undertaken on the generation of runoff in semi-arid areas has been focused on the point and plot scales. There are only a few studies that consider hillslope and landscape scale runoff generation. The complex spatial patterns of these factors results in a dynamic system with many interactions between the different hydrological zones. Therefore, the hillslope scale runoff is difficult to predict from the point scale measurements since the spatial arrangement of hydrological properties will influence the transmission of runoff. The hillslope scale runoff will be influenced by the topographic factors of slope gradient and slope length. It is important to understand the hydrological behaviour at this greater scale since it is the discharge from hillslopes, rather than points, which determines the flood magnitude.

The up-scaling of runoff generation from the point and plot scales to the scale of the hillslope and small catchments is important for understanding the origin of channel flow. A few studies have addressed this problem with large scale rainfall simulation and monitoring of natural catchments. It would be scientifically valuable to extend the understanding of hillslope and small catchment scale runoff generation and transmission presented in these studies.

The temporal dynamics of the runoff generating storm event have received little attention in the literature. This is an important aspect of the runoff generation process in semi-arid environments and should be investigated further.

Little work has been undertaken on the origin of discharge within a catchment. By understanding the origin of discharge, the key generating areas can be identified for different storm events. This knowledge will greatly aid land use planning within semi-arid catchments. By understanding the

controls on runoff at a larger spatial scale, the modelling and prediction of flood risk within semi-arid catchments can be improved.

Therefore, this research will consider the generation and transmission of runoff at the spatial scale of hillslopes and small catchments at the temporal scale of a storm event. This will focus on the amount and origin of water reaching the channel.

3 Field Site and Techniques

3.1 Introduction

The aim of this chapter is to describe the study site and the field and laboratory techniques used. The selection of the study area is discussed in section 3.2. The geology, land use and vegetation characteristics of the catchment are described in section 3.3 and the selection of experimental locations is presented in section 3.4. The rainfall regime is described in section 3.5 and considers the recent climate in the area covering the last 40 years and the detail of the storms experienced in the study area. The field and laboratory techniques are described in section 3.6 and covers the measurement of surface roughness, soil properties, land cover composition and infiltration characteristics.

3.2 Study Area Selection

The study area selected for this research is the Rambla de Nogalte catchment located in Almería and Murcia, south-east Spain (37° 35' N, 01° 56' W). The location of the catchment is shown in Figure 3.1, the detail of the channel network within the catchment is shown in Figure 3.2 and a photograph of the upper section of the catchment is shown in Figure 3.3. The Rambla de Nogalte catchment was selected because of spatial contrasts in its response to an extreme storm event in September 1997 (Bull et al. 2000), which is discussed in more detail in section 3.5.5. The catchment has a history of catastrophic flooding and the last extreme flood event occurred in 1973 and killed many people in the town of Puerto Lumbreras (Shannon et al. 2002). The area is also typical of many semi-arid catchments in the Mediterranean basin.

The Rambla de Nogalte is a broad wandering gravel bed ephemeral channel surrounded by steep hills with the relief being greater on the southern side of the catchment. This area has many steep convex slopes. The total catchment area is 177 km^2 with an altitude range from 464 m to 1204 m A.M.S.L.

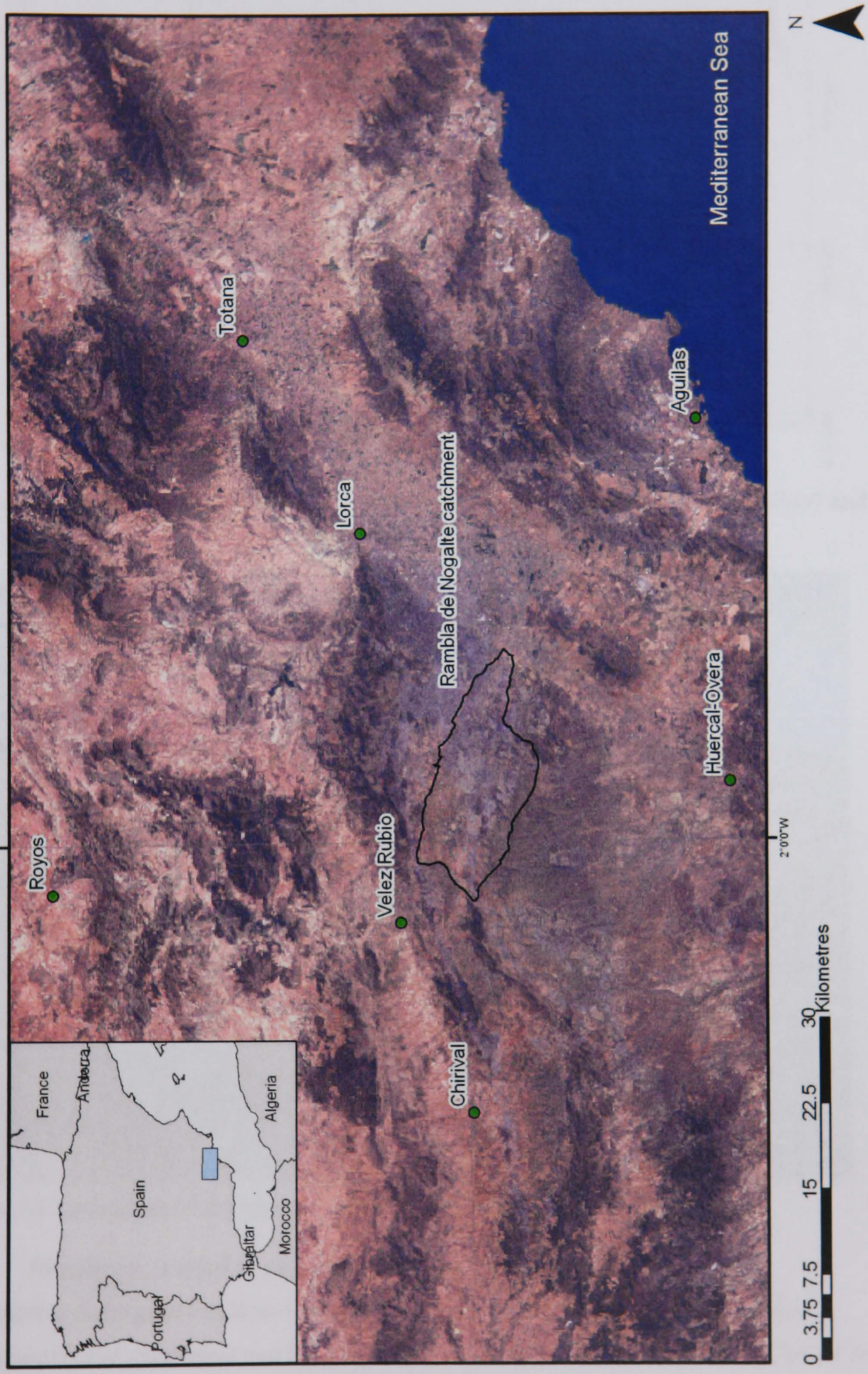

Figure 3.1 Location of the Rambla de Nogalte catchment. Landsat 7 visible image acquired on 08/08/2000 and provided by the Landmap Project (www.landmap.ac.uk).

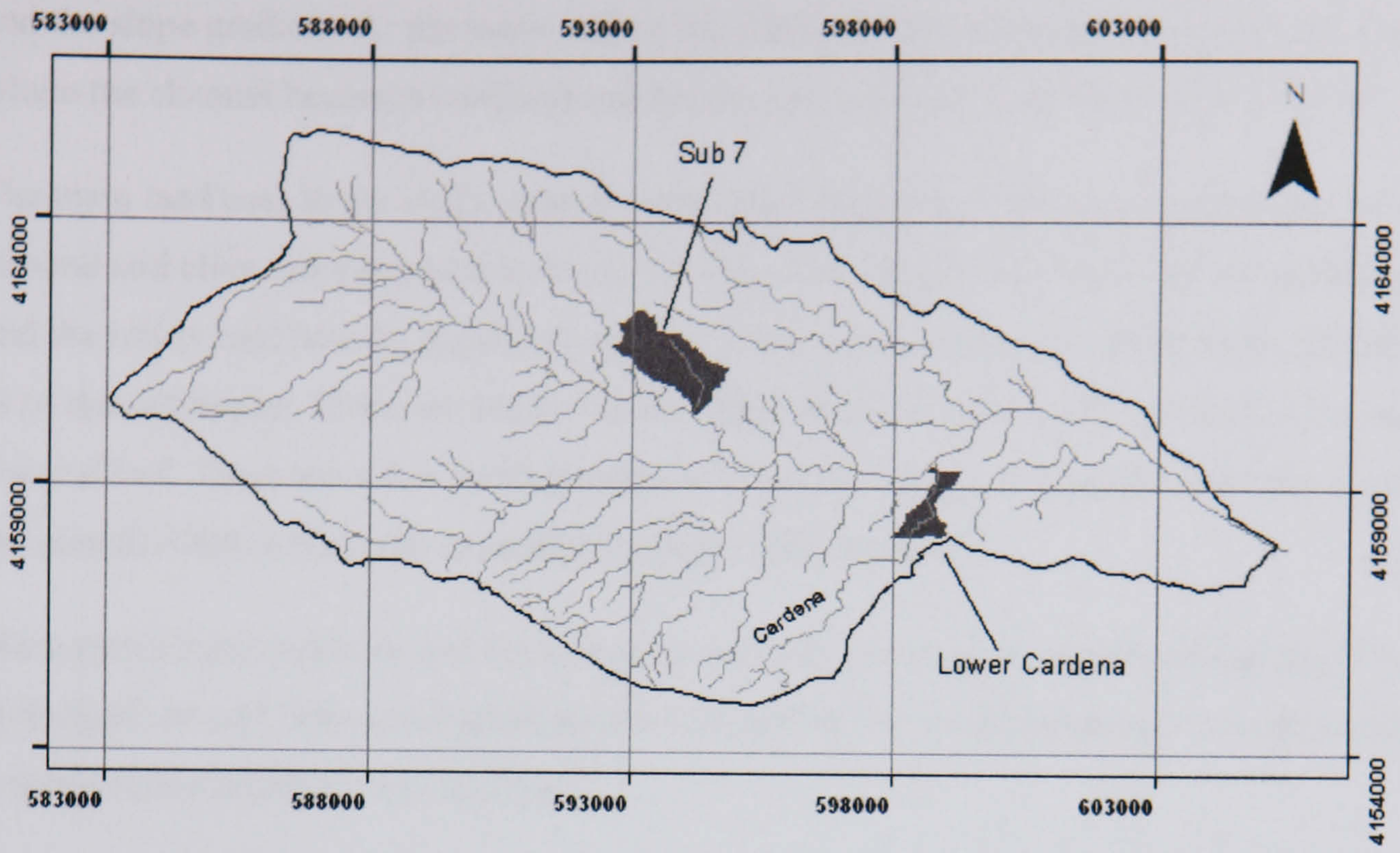

Figure 3.2 Detail of the Rambla de Nogalte catchment showing the location of the Sub7 and lower Cardena Sub-catchments.

Figure 3.3 Photograph of the upper section of the catchment

3.3 Geology, Land Use and Vegetation

The Rambla de Nogalte catchment consists of metamorphic rocks and conglomerates, dominated by red mica schist and local outcrops of blue mica schist (Figure 3.3). The red mica schist has a greater iron content than the blue, hence the difference in colour. The soils developed from the red mica schist are relatively deep but those on the blue mica schist are shallow with sparse vegetation cover. The pattern of soil depths is modified by both the land use

and the slope gradient. At the lower end of the catchment there are some Quaternary deposits where the channel becomes confined and braids across a large fan (Thornes et al. 1999).

The main land uses in the study areas are tree crops and scrub. The main agricultural land use is almond and olive cropping which covers 61.4 % of the catchment. The trees are widely spaced and the soil is kept bare by regular ploughing. There are a number of wheat fields, covering 2.5 % of the catchment. These are located in the upper section of the catchment and in the main channel bed. There are a few small patches of vines, covering 1.4 % of the catchment, although the area devoted to this crop expanded between 1998 and 2001.

Most agricultural slopes do not have terraces and are smoothed by regular ploughing. From field investigations and from aerial photographs it is possible to see the remnants of past terrace systems across much of the catchment.

The areas not under current active agriculture are covered by a natural scrub (matorral) or mature trees. The scrub covers 30 % of the catchment and the trees cover 0.2 %. The mature trees are either oak (*Quercus coccifera* L.) or Aleppo Pine (*Pinus halepensis* L). The scrub is composed of anthyllis (*Anthyllis cytisoides* L), grasses, rosemary (*Rosmarinus* L) and thyme (*thymus* L). The vegetation density varies from 10 % to 80 % but is near zero on recently abandoned areas.

3.4 Selection of Experimental Locations

The selection of sites in the field was based upon a stratified random scheme (Walford 1995) using land use, geology and slope as the defining criteria. The Rambla de Nogalte catchment is dominated by two land use types - active tree crops and scrub. The geology can be divided into two main categories, red and blue schists. Both sloping and flat sites were investigated. The combinations studied are listed in table Table 3.1 and their locations are shown in Figure 3.4. It was not possible to study a scrub site on a flat slope as all flat areas are under active agriculture. An extra scrub on blue schist site was studied in the Cardena Sub-catchment for two reasons. Firstly, during a recent flood event, the Cardena catchment generated far greater volumes of runoff than other sections of the Rambla de Nogalte catchment. Secondly, there is a greater amount of quartz in the schist at this site which may influence the hydrological characterises of the soils.

Site Number	Land use	Geology	Gradient
1	Tree Crops	Red Schist	10 º
2	Scrub	Blue Schist	15 º
3	Tree Crops	Blue Schist	2.5 º
4	Tree Crops	Blue Schist	25 º
5	Scrub	Red Schist	20 º
6	Tree Crops	Red Schist	3 º
7	Scrub	Blue Schist (Cardena)	10º

Table 3.1 Combinations of land use, geology and slope gradient at the field sites

The location of the sites was determined in the field by the selection of a region of the catchment with the required combination of factors from map and GIS data. A vantage point was then chosen where sites could be evaluated from a distance and a suitable area selected. The final location of the site was then chosen in the area selected ensuring that it was representative of the desired combination.

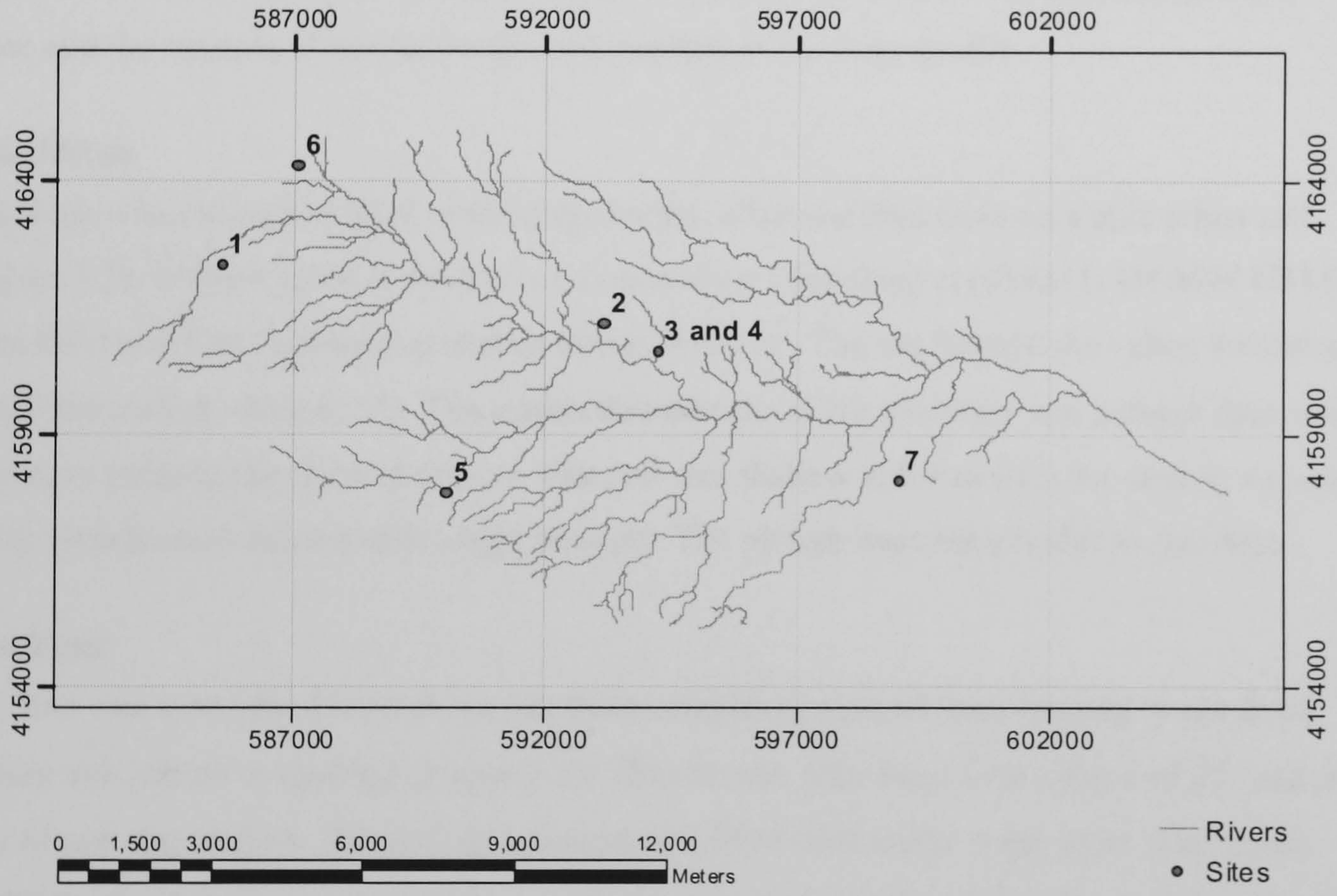

Figure 3.4 Experimental locations

The size of the sites was determined by the variability of the ground cover, so that there was a similar amount of variability within each plot. The spacing between the plant individuals was used to define the size of the sites. Therefore, tree crop sites had approximately four by four trees and the scrub sites had four cycles of plant – bare areas.

3.4.1 Site Details

Site One

Site one (0585600, 4162350 UTM) was a sloping (10°) ploughed field on a red schist containing nine almond trees (Figure 3.5). The site was located at the top of a slope, approximately 10 m from the drainage divide and covered an area of 138.9 m^2. The plough furrows ran across the slope with the contours. The soil was stony and approximately 0.3 m deep. The stone content was greater in the base of the furrows.

Site Two

Site two was a scrub slope on blue schist (0593150, 4161200 UTM) covering an area of 37.8 m^2 (Figure 3.5). The dominant vegetation was *anthyllis* L. with a small number of *thyus* L. individuals. There was a large spacing between the individual plants leading to a two-phase system of bare and vegetated areas. There was field evidence that the area had been under agriculture in the recent past. A number of almond trees are located with the same patch of scrub and the remains of terrace levels were evident in the slope profile.

Site Three

Site three was a ploughed field containing almond, olive and fruit trees on a blue schist soil (Figure 3.5). It was located at the base of a steep slope (Site four) at (059241, 4160640 UTM). Sites three and four together covered an area of 4500 m^2. The site formed the valley bottom and hence had a slight slope (2.5°). Ten metres downstream of the site there was a check dam which may have reduced the slope of the site. The soil was shallow at 0.4 m with the underlying schist being weakly consolidated with a high porosity. The plough lines ran parallel to the slope.

Site Four

Site four was a ploughed field above site three containing almond trees ranging in age from mature individuals to saplings (Figure 3.5). The site was very steep with a slope of 25° and an area of convergent flow. The soil was shallow at 0.16 m with a thin, weak crust. There was evidence of soil movement down slope with many linear features running down slope with high stone cover. The plough lines followed the slope and deviated around trees. This has resulted in an accumulation of soil behind and to the sides of the trees of approximately 0.5 m of extra soil.

Site Five

Site five was a scrub slope located on red schist (0590050, 4157842 UTM). The slope of the site was 20° and covered an area of 57.8 m^2 (Figure 3.5). The dominant vegetation was *thymus* L., widely spaced, with many dead or dormant individuals. Two types of areas in between bushes could be identified: areas with grass and areas with high stone cover. The areas with high stone cover may be related to a higher frequency of overland flow. There were many flow paths on

the surface and there was one small gully, approximately 0.3 m deep. There were many mounds and ridges on the site possibly from sediment capture by vegetation and relic terrace features. Both the areas above and below the site had evidence of past terracing and adjacent areas were under active agriculture.

Site Six

Site six was an almond field located on a red schist soil (0587200, 4165300 UTM) and had an area of 326 m^2 (Figure 3.5). The site had a slight slope (3°) with a convergent flow pattern. Three types of soil surface could be identified. These were crusted soils, soils with broken crusts and compacted soils. The surface had been smoothed rather than ploughed into furrows. The soil crust was weak and thin. The compacted soils were the result of bulldozer tracks and ran mainly perpendicular to the slope.

Site Seven

Site seven was located on a scrub slope (10°) on a blue schist (0599000, 4158100 UTM) and had an area of 15.5 m^2 (Figure 3.5). There were three main plant types, *anthyllis* L., *thymus* L. and *romero* L. with a few large and many small individuals. The areas in between the plants were very stony with very little soil. There was evidence of past terracing and ploughing. Many of the plants were arranged in parallel lines across the slope, where past ploughing may have created areas with greater water storage capacity.

Site 1

Site 2

Sites 3 and 4

Site 5

Site 6

Site 7

Figure 3.5 Photographs of the field sites

3.5 Rainfall Characteristics

The rainfall characteristics have been investigated at three temporal scales. The first scale represents the local climate and is examined using a 30 year rainfall record from a local weather station. The second scale considers the storm scale rainfall within the catchment. This gives information on the distribution of storm sizes, durations and the length of time between storms. The final scale investigates the structure of the rainfall within the storm event.

3.5.1 Long Term Daily Analysis

The nearest meteorological station to the Rambla de Nogalte with an available daily long term record is located in Lorca (1.7 °W 37.8 ° N), 16 km from the catchment. This record has daily information on precipitation and temperature and has been analysed for the period 1958 - 1987. The average monthly precipitation and temperatures are shown in Figure 3.6 with the standard error of the mean. There is high inter-annual variability of annual rainfall totals with the coefficient of variation being 2.82.

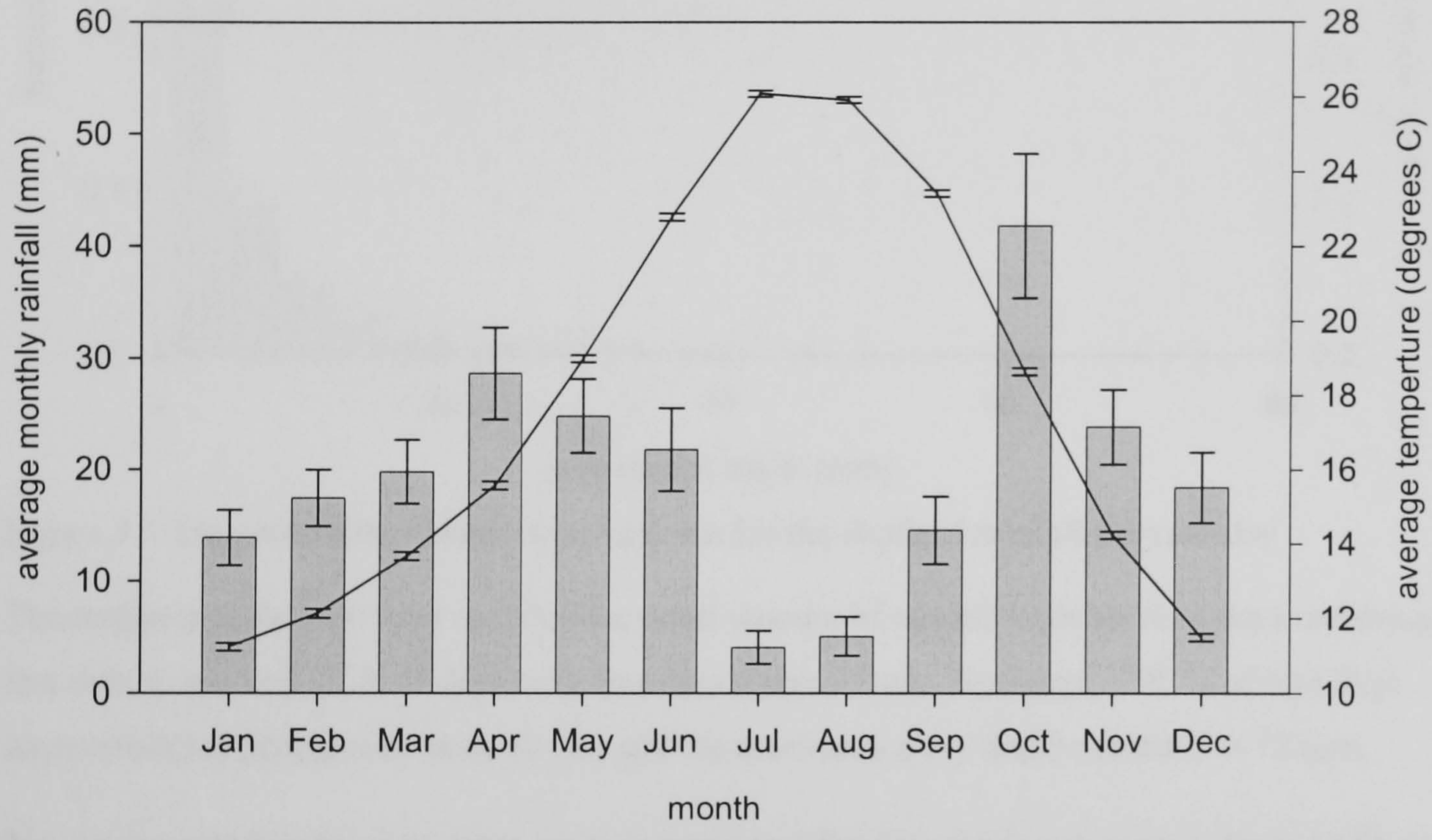

Figure 3.6 Average monthly precipitation and temperature for Lorca covering the period 1958 - 1987

The climate shows strong seasonality with maximum temperatures and minimal rainfall occurring in July and August. The hydrological year runs from August to July with two peaks in rainfall occurring in April and October. The rainfall in October mainly results from convectional storms whereas the April rainfall results from frontal storms (Romero et al. 1998).

If the statistical properties of the time series are to be investigated, it is important to consider whether the climate has been stationary over the time period of the climatic record. In order to investigate this factor, the time series was broken down into three time periods, each relating to a decade. The non-parametric Kruskal-Wallis H test was used to determine if there are significant differences in the sets of data. The test returned a value of 14.48 for precipitation and 180 for average temperature, both of which are significant at the 99.9 % level. This indicates that there are differences in the climate over this time period on the time scale of decades. This may relate to high inter annual variability in the rainfall (Figure 2.5) or to a changing climate as a result of anthropogenic induced climatic change.

Over the period of the record, 10.5 % of the days can be classed as rain-days. The probability distribution function for the depth of rainfall on these days is shown in Figure 3.7

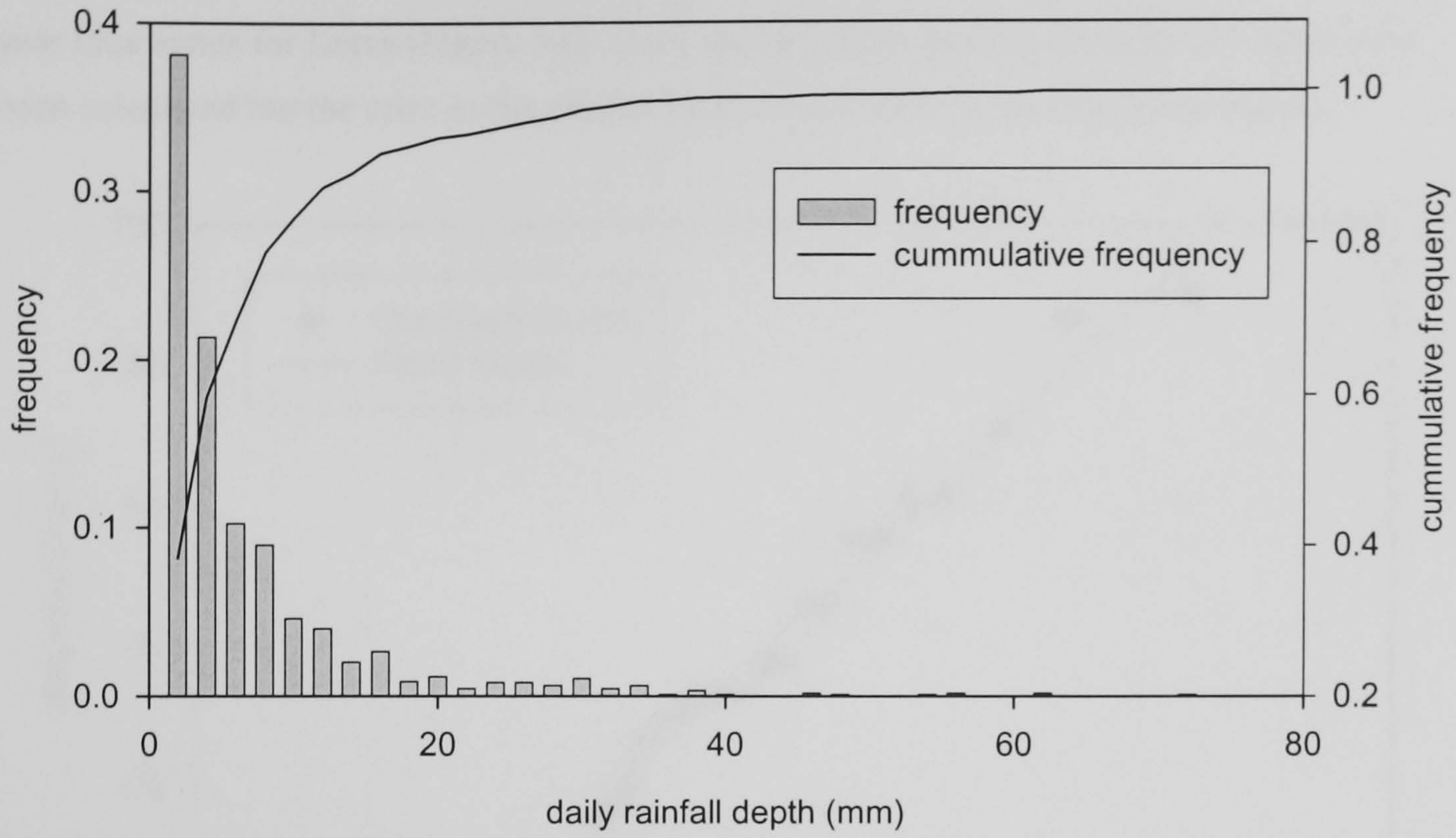

Figure 3.7 The probability distribution function for the depth of rainfall per rain-day

The majority of the rain days only have a small amount of rainfall with 60 % of days receiving less then 4 mm and 70 % of days have less than 6 mm of rain. However, 0.95 % of rain days have rainfall depths greater than 40 mm and the maximum daily depth recorded is 72 mm.

The temporal structure of the time series is important for determining the antecedent conditions for runoff generation. This property can be investigated using the temporal autocorrelation of the series, as shown in Figure 3.8.

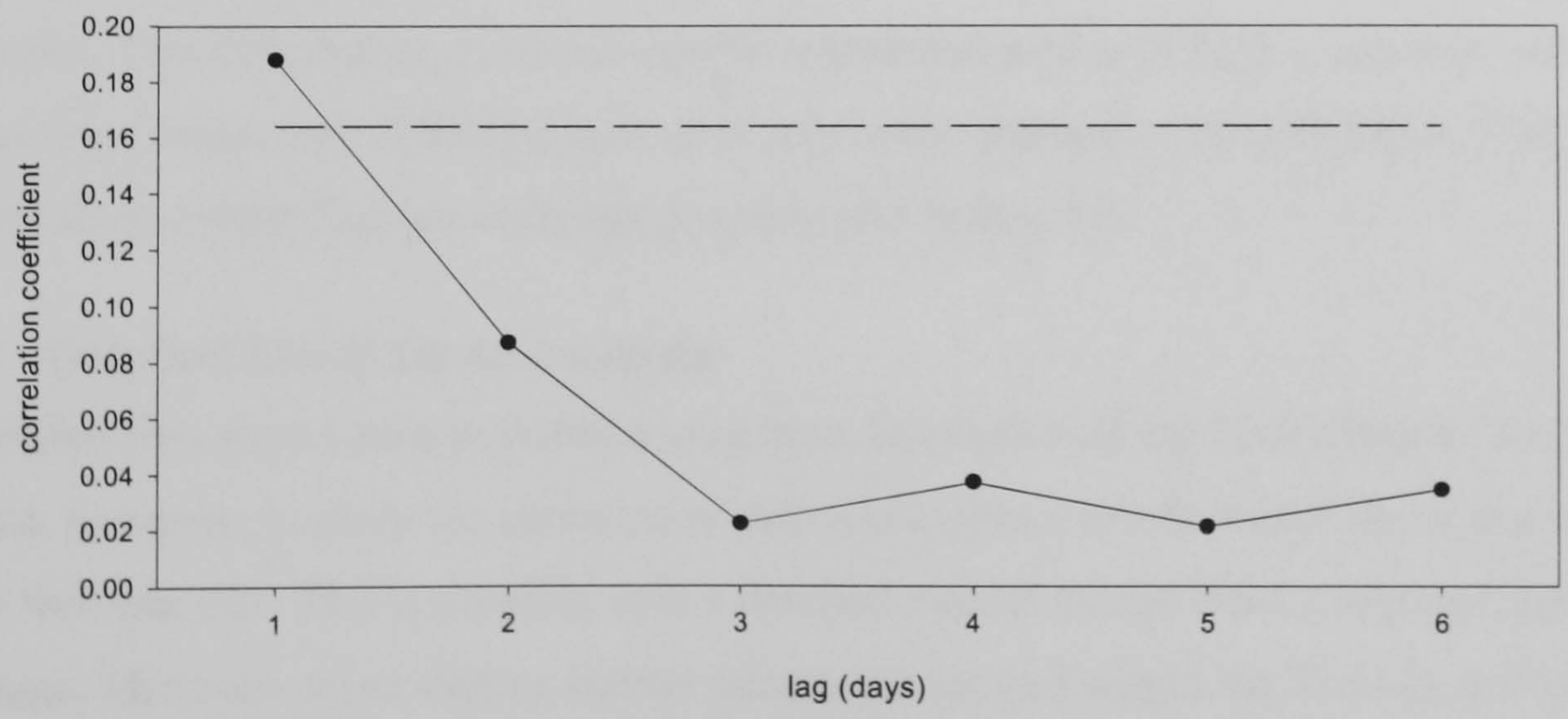

Figure 3.8 Temporal autocorrelation of daily rainfall for Lorca. The dashed line shows the 95 % significance level

The temporal autocorrelation at a lag of one day returns a value of 0.19 and can be considered significant at the 95 % level. Lags beyond this are not significant.

Rainfall during a certain day can be considered as having a probability of exceeding a certain depth. This is normally described by the average amount of time between events of a certain size, and is expressed as the return period of the storm. This has been calculated using the 30 year time series for Lorca (Figure 3.9). Daily rainfall return periods of up to 100 years have been calculated but the error in the estimation increases with increasing return period.

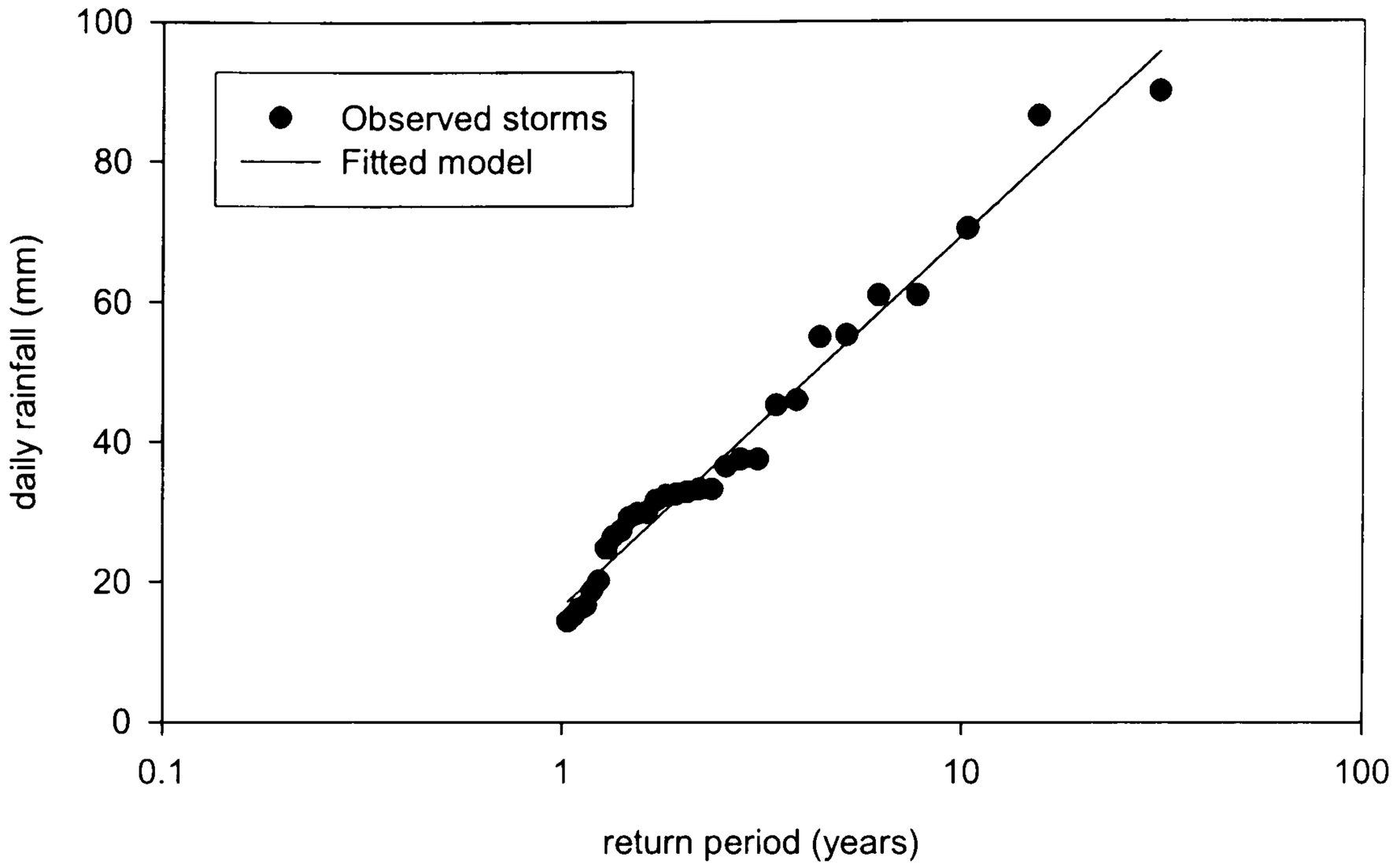

Figure 3.9 Return periods of daily rainfall for Lorca

The daily rainfall depth increases rapidly over a range of years from two to twenty. A daily rainfall depth of 60 mm has a return period of only seven years while a depth of 75 mm has a return period of 15 years. The estimated depth of a 100 year return period event is 122 mm, an increase of 61 % in depth for a fourteen fold increase in the return period compared to the 15 year event. This distribution of storms results in frequent storms of high magnitude with storms with a longer return period delivering a relatively small increase in rainfall depth. This leads to frequent flood events that can endanger property and human life.

3.5.2 Detailed Short Term Analysis

The rainfall data from Lorca provides a long term description of the local climate. It is not possible, however, to study the structure of individual storms events which occur at a time scale of less than one day. This is possible with a detailed rainfall record from a tipping bucket raingauge. There are seven tipping bucket raingauges located within the Rambla de Nogalte catchment (Figure 3.10). These record every 0.2 mm of rainfall and the data is recorded as the

number of tips within a single minute. The data analysed was collected between 25 March 1997 and 30 December 2000 thus giving observations over 1376 days[1].

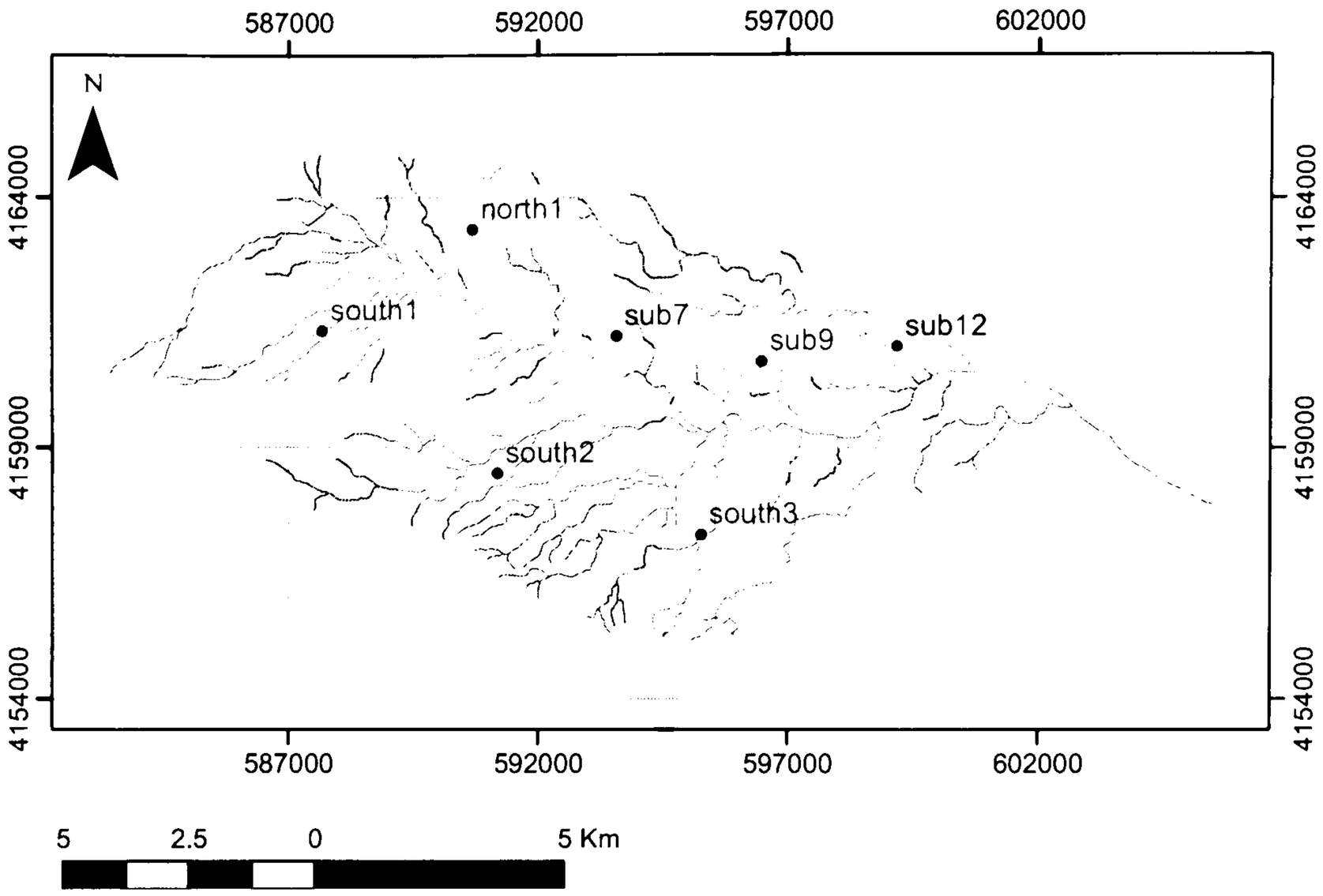

Figure 3.10 Location of raingauges within the Rambla de Nogalte catchment

The raingauge in Sub 7 is located at a central location within the catchment and has therefore been taken as representative and detailed analysis of the data presented. The analysis of the spatial organisation of rainfall patterns is presented in section 3.5.4.

To examine the storm characteristics, it is first necessary to break the rainfall record down into discrete storm events. A time period of 24 hours without rainfall was selected as the criterion required to separate individual events. This duration was selected as it will take approximately this long for the catchment to dry out following the previous event and will ensure the soil moisture state is similar at the start of each storm. For the Sub 7 rain gauge, this gives 163 discrete storm events with total rainfall depths ranging from 0.2 mm to 90 mm.

Figure 3.11 shows the probability distribution functions (pdf) for the storm duration, mean rainfall intensity and the length of gaps between storms.

[1] Unpublished data, Department of Geography, Kings College London.

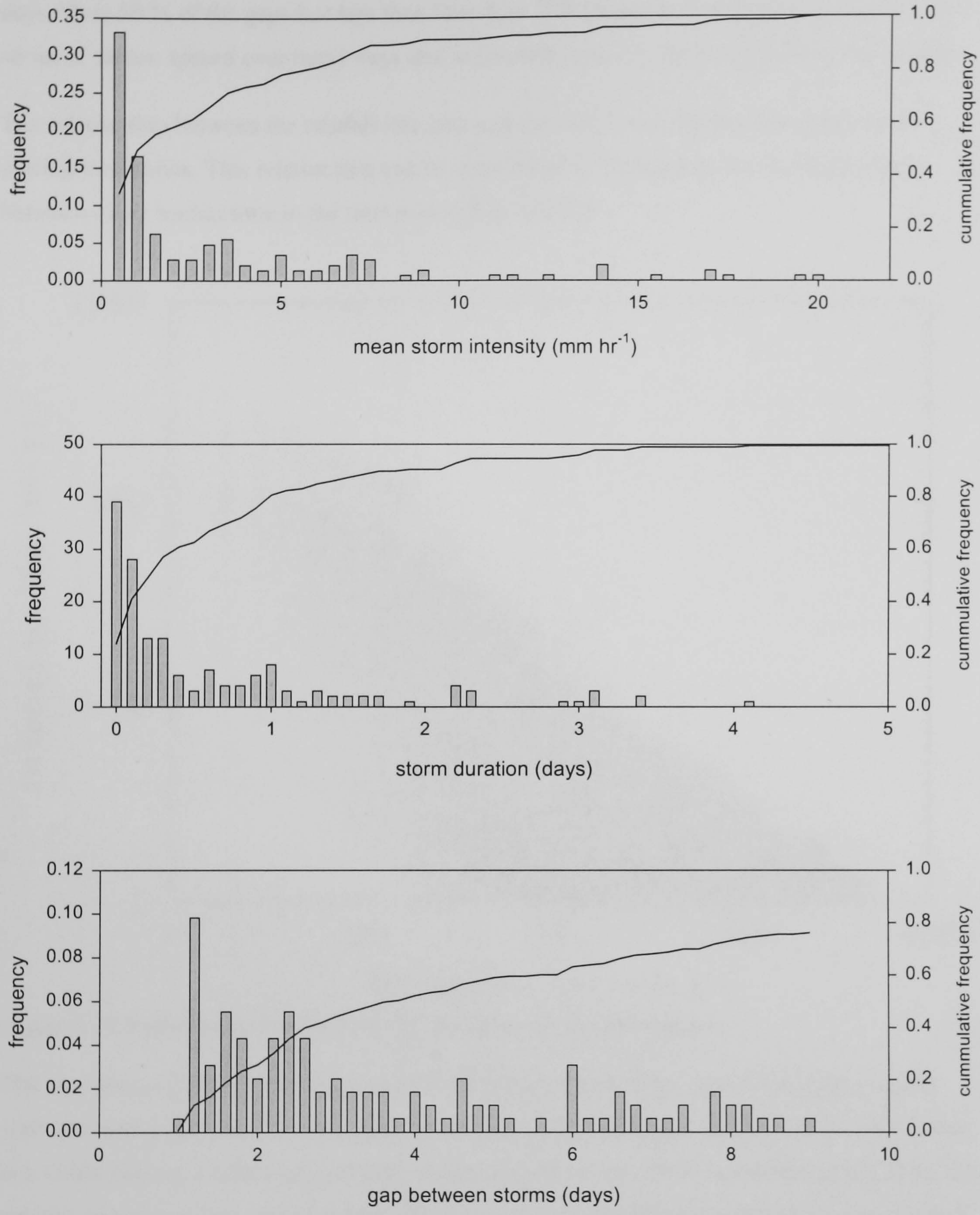

Figure 3.11 Probability distribution functions for mean rainfall intensity, storm duration and the length of gaps between storms for the Sub 7 rainfall record

Figure 3.11 shows that over 55 % of storms have mean rainfall intensities less than 1.5 mm hr^{-1}. However, 4.14 % of storm events have mean intensities of greater than 15 mm hr^{-1}. Figure 3.11 shows that most storms are short lived. Nearly 50 % of storms last for less than 4.8 hours. However, 5 % of storm last for three days or more. Figure 3.11 shows that the length of time

between storms varies across a large range with 20 % of the gaps lasting for greater than ten days. Over 50 % of the gaps last less than four days. This suggests that there are periods with a series of storms spread over many days and individual storms located within long dry periods.

The relationship between the rainfall intensity and duration is an important property of the rainfall time series. This relationship can be considered by calculating the rainfall intensity between every bucket time in the time series (Figure 3.12).

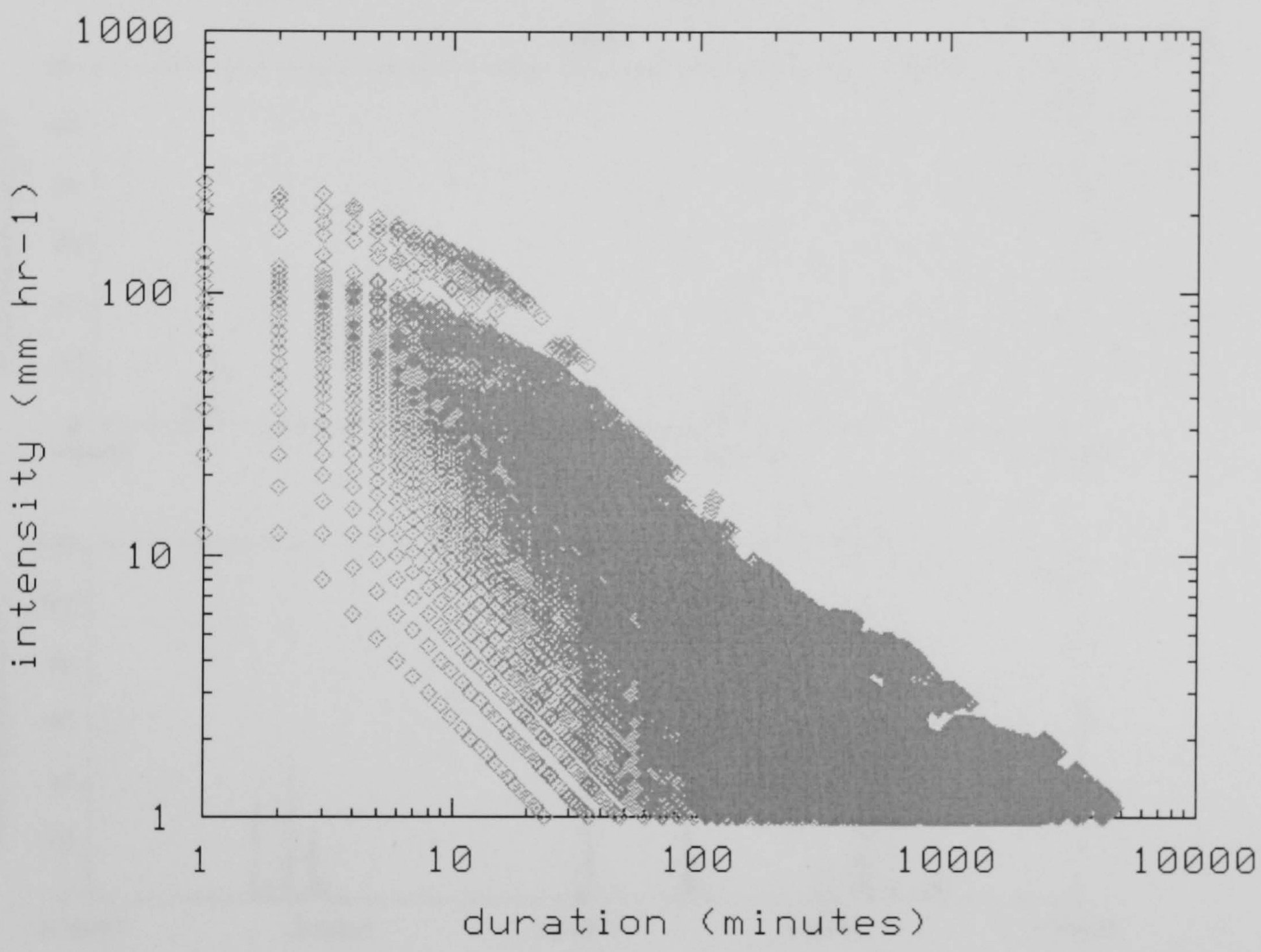

Figure 3.12 Relationship between rainfall duration and rainfall intensity

The maximum rainfall intensities occur for short durations and the intensity declines rapidly with increasing duration. The maximum recorded rainfall intensity was 264 mm hr^{-1} or 4.4 mm in a single minute. At the high intensity, short duration section of the parameter space, there is a separation between two sets of points. This may relate to the difference between spring frontal storms and the late summer, higher intensity convectional storms. The scarcity of data points at the low end of the intensity and duration ranges is due to the 0.2 mm tip depth of the rain gauge used for the data collection.

3.5.3 Individual Storm Structure

To consider the structure of the storm, the six longest storms were extracted from the time series (Table 3.2) and sample storms are shown in Figure 3.13.

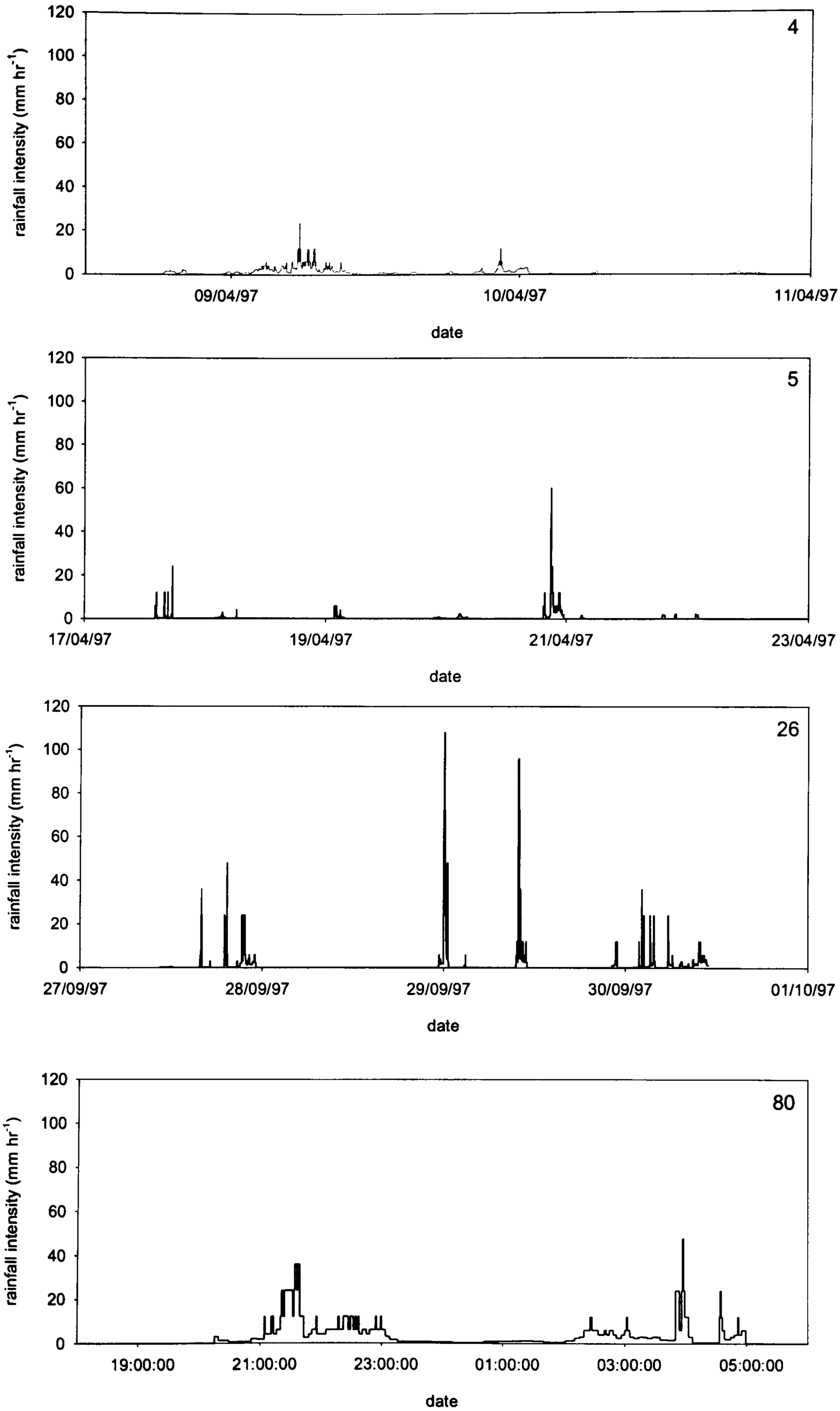

Figure 3.13 Sample storms recorded at the Sub 7 rain gauge

Storm Number	Start	Length (days)	Depth (mm)	Maximum intensity (mm hr^{-1})
4	08/04/97 16:19	2.2	46.2	24
5	17/04/97 14:01	6.8	46.6	60
26	27/09/97 10:27	3.0	88.2	108
73	18/09/98 05:31	1.1	36.2	48
80	05/11/98 04:04	3.0	44.8	24
82	01/12/98 20:07	2.9	44	24
152	21/10/00 03:09	4.0	90	72

Table 3.2 Seven largest storms on the detailed record for Sub 7

From these figures, it is clear that a rain storm is delivered in a number of pulses over a long time period. The rainfall may be classified into pulse rainfall and background low intensity rainfall. The spring storms have a greater amount of low intensity rainfall, e.g. storm 4, whereas late summer storms may be entirely made up of high intensity rainfall, e.g. storm 26.

Rainfall intensities greater than 12 mm hr^{-1} have been classified as belonging to a pulse. This depth relates to more than one bucket tip occurring within a minute and hence gives greater accuracy on the recorded intensities. The pdf is shown in Figure 3.14.

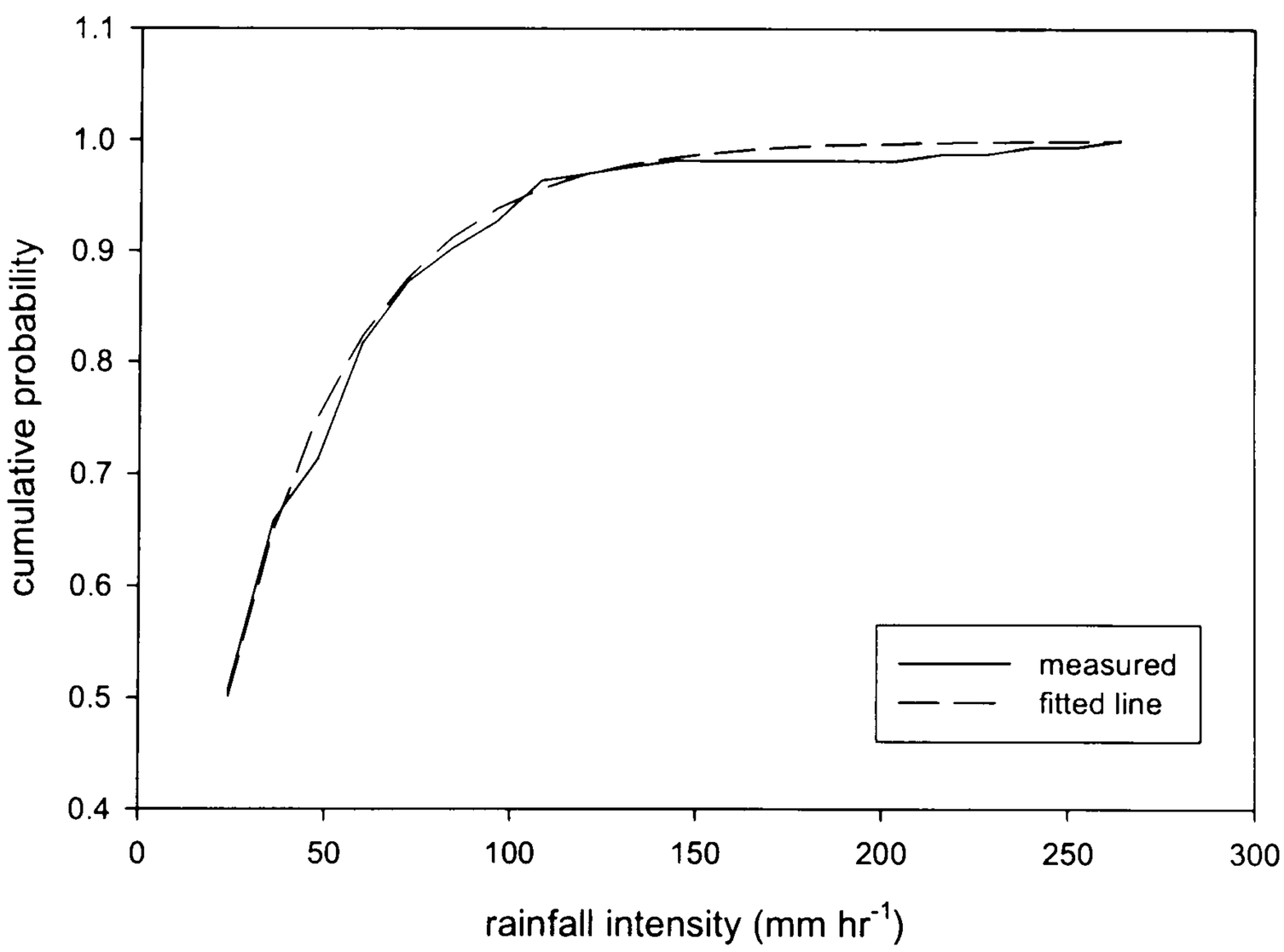

Figure 3.14 Probability distribution function of per minute pulse rainfall intensities

The distribution of the pulse rainfall intensities (rf_i) (mm hr^{-1}) can be modelled using Equation 3.1.

$$rf_i = \frac{1}{a}\ln(1 - prob).60$$

Equation 3.1

Where $1/a$ is the mean per minute rainfall intensity, a is a coefficient and *prob* is the probability of that rainfall intensity. For the rainfall record, $a = 1.74$ giving an r^2 value of 0.98. This relationship will enable the generation of stochastic rainfall with a realistic intensity distribution.

3.5.4 Spatial Patterns

The spatial patterns of rainfall have been considered in four ways. For the hydrological year 1997 – 98 the number of rain days and the total rainfall volume were calculated. For a large storm in September 1997, the peak rainfall intensity and the storm total have been calculated. Since the small scale spatial variability is not known, it is not possible to derive a continuous surface. Therefore, the values have been interpolated over the catchment using a block kriging algorithm (Figure 3.15).

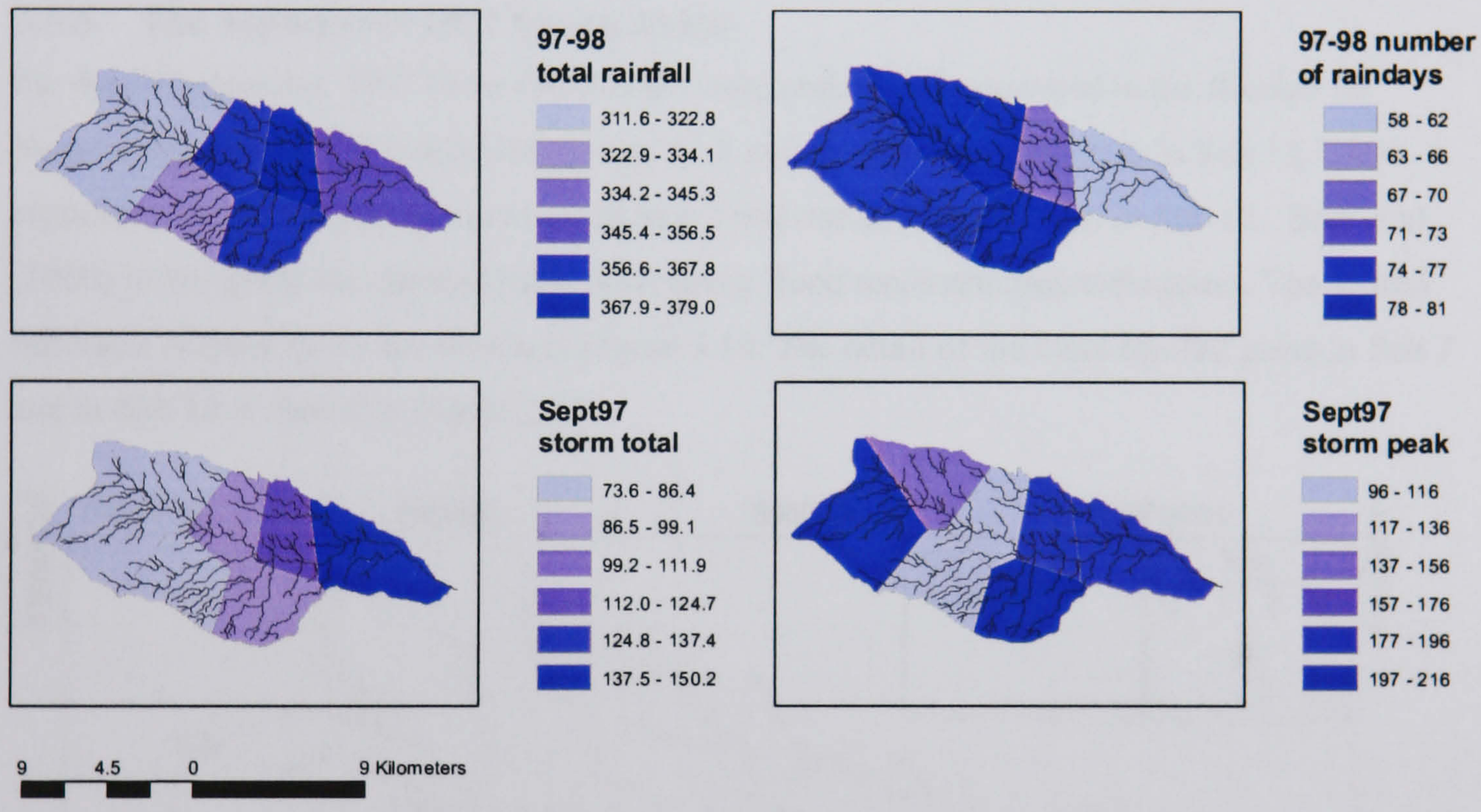

Figure 3.15 Spatial patterns of rainfall for the 1997 – 1998 hydrological year and for a storm in September 1997

From all four measures of the rainfall characteristics, it is clear that there are differences in the rainfall. However, there is not a systematic pattern across the catchment.

For the hydrological year 1997 – 98 the central section of the catchment received the greatest total rainfall at over 355 mm, whereas the upper sections received between 311 and 322 mm. The lower section received between 345 and 356 mm, however this was delivered in the minimum number of rain days, 58. The upper sections received less rainfall, but this was distributed over a greater number of days, between 74 - 75 days. This suggests more intense storms in the lower catchment and more prolonged rainfall in the upper catchment. This may relate to the greater mean elevation in the upper catchment. The lower catchment may receive more convectional storms originating in the low lying Guadalentin basin.

The spatial structure of the storm event which occurred in September 1997, discussed in section 3.5.5, shows a clear relationship with total storm depth. The greatest amounts of rainfall occurred in the lower sections of the catchment. The maximum depth was recorded at the Sub 12 gauge at 150.2 mm. This is more than twice than that received at the south 2 gauge which received 73.6 mm.

The maximum rainfall intensity of 216 mm hr^{-1} for the September 1997 storm was recorded at both ends of the catchment, in south 1 and south 3. There is, however, a cluster of high peak intensities at the lower section of the catchment. The pattern of storm rainfall depth and peak intensities relates to the meso-scale climatic conditions at the time of the storm. The path of the convectional storm cells may, therefore, have been more closely focused on the lower section of the catchment.

3.5.5 The September 1997 Storm Event

On the 29 September 1997 there was a high magnitude storm event within the Rambla de Nogalte catchment. The rainfall depth was 51.4 mm in Sub 7 and 76.8 mm in Sub 12. This represents a one in 5 year storm event in Sub 7 and one in 14 year event in Sub 12. Bull et al., (2000) investigated the channel peak flows using flood reconstruction techniques. The spatial estimates of peak flows are shown in Figure 3.16. The detail of the main rainfall pulse in Sub 7 and in Sub 12 is shown in Figure 3.17.

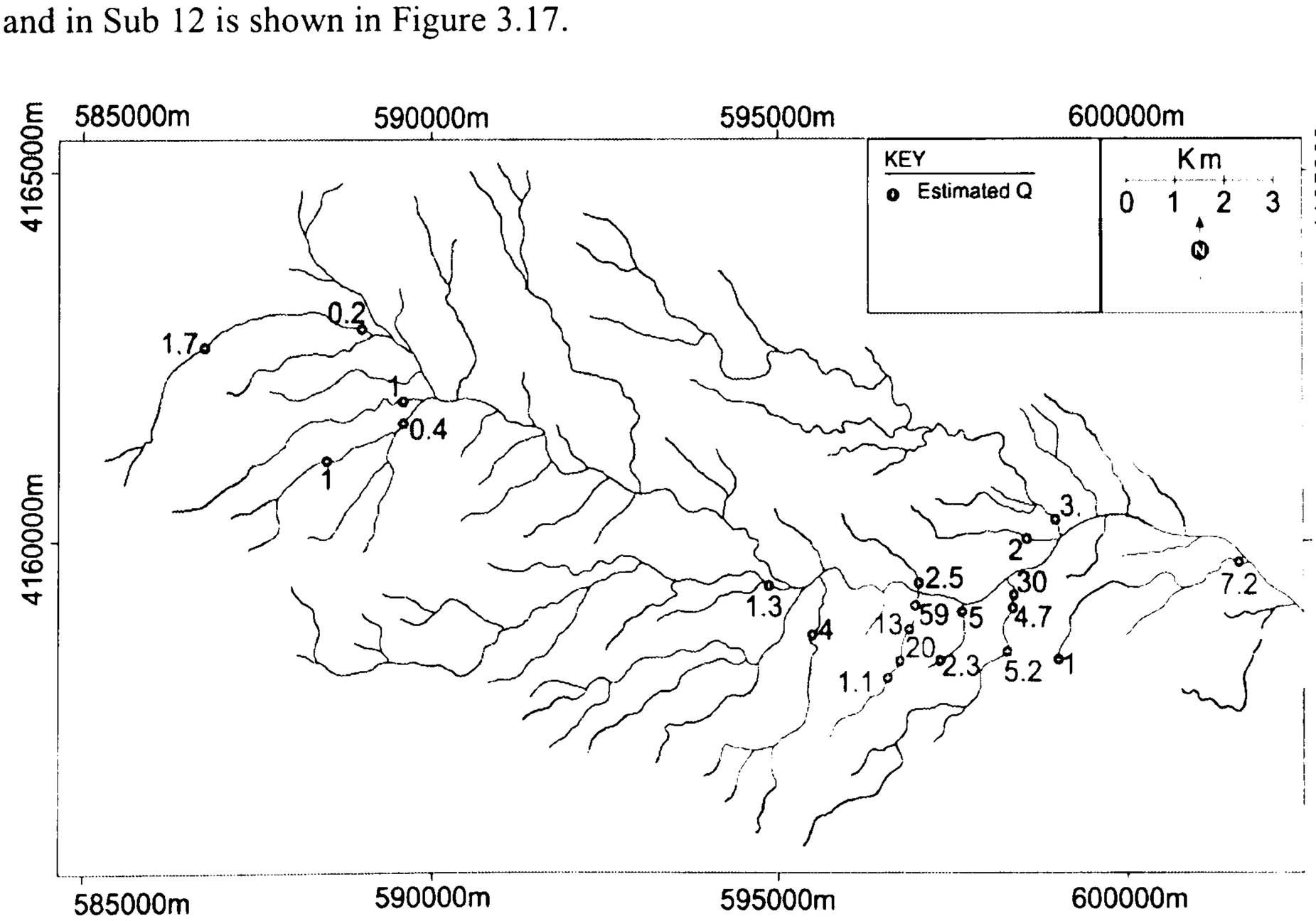

Figure 3.16 Variation in rainfall intensity for the 29 September 1997 and estimated discharges for the Rambla de Nogalte. Modified from Bull et al. (2000).

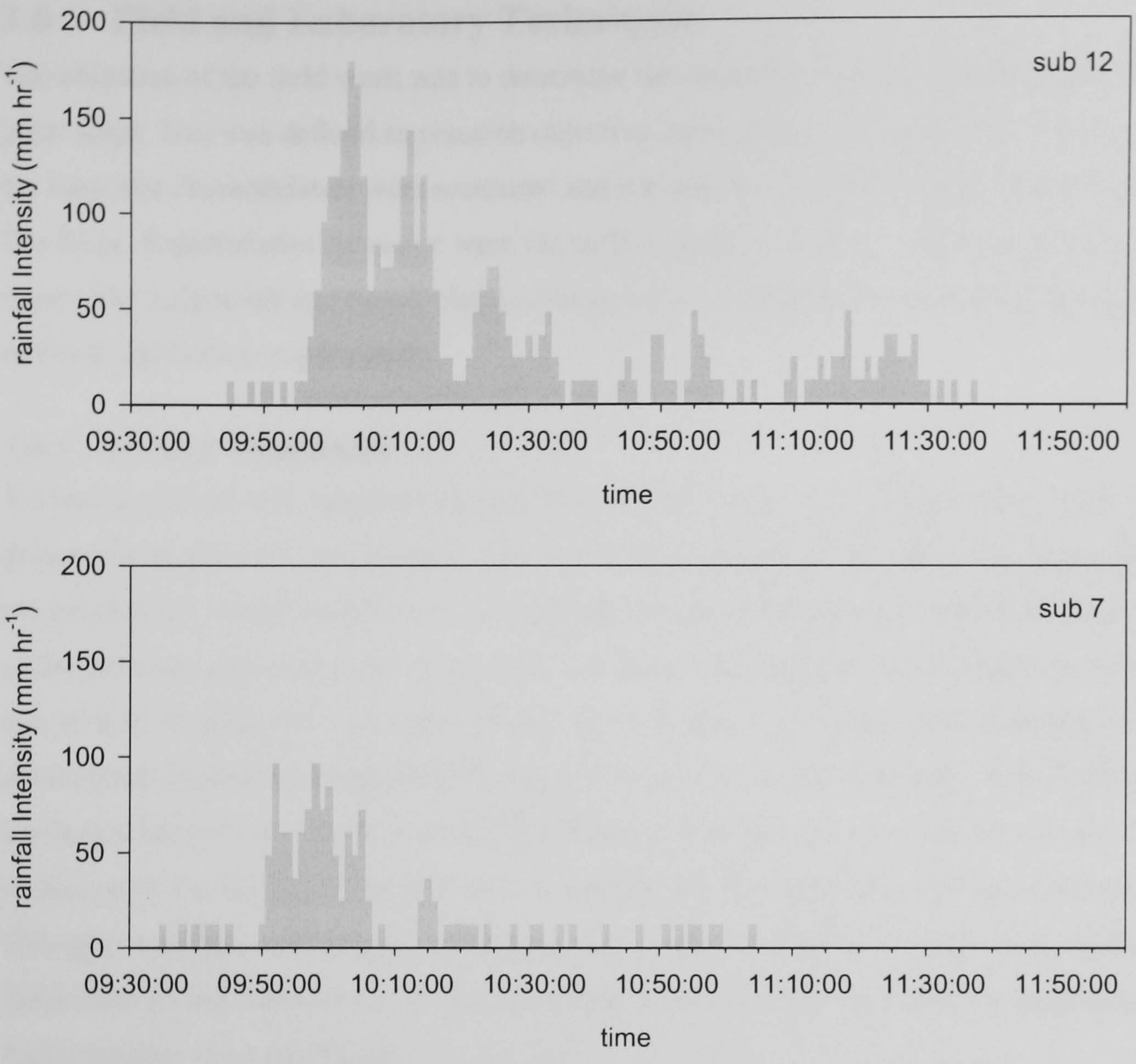

Figure 3.17 Detail of the main rainfall pulse from the 29 September 1997 storm event for Sub 7 and Sub 12

The range of maximum discharges varies across the catchment with large differences over short distances. Although there were spatial differences in the maximum intensity and the total rainfall, these differences alone are insufficient to explain the variations in discharge. Bull et al. suggested that certain combinations of land use, topography and geology were required to generate significant runoff. Sub-catchments characterised by steep, gorge like terrain and Sub-basins where agriculture had been abandoned produced the greatest flood discharges.

3.5.6 Summary of Rainfall Characteristics

The rainfall in the Rambla de Nogalte catchment is characterised by episodic, high intensity storm events. The return period for a storm event with a high rainfall depth is short, with the one in eight year storm event producing 60 mm. The storms consist of a series of rainfall pulses which may be separated by no rainfall in the case of convective storms or low intensity rainfall in the case of frontal storms. The instantaneous rainfall intensities are extremely high with a maximum intensity recorded of 264 mm hr^{-1} for a single minute. There is high spatial variability in rainfall on the temporal scales of individual storms and annual totals. This variability in rainfall will be translated into variability in the generation and transmission of runoff.

3.6 Field and Laboratory Techniques

The objective of the field work was to determine the controls on the generation of runoff at the point scale. This was defined as research objective one in chapter 1. At each of the field sites, the local site characteristics were measured and the nature of the infiltration regime investigated. The local characteristics measured were the surface roughness, soil properties and the surface cover. The infiltration and runoff characteristics were investigated using rainfall simulation and minidisk infiltration experiments.

3.6.1 Surface Roughness

Surface roughness was measured using a pin meter (Cremers et al. 1996) (Figure 3.18). The device has 86 pins of 6 mm diameter with the centres spaced 10 mm apart. The meter was placed over the surface and the pins lowered into contact with the soil. The profile from the top of the pins was then traced onto paper and the slope of the meter recorded. Eighteen profiles spaced 0.05 m apart were recorded with the pins running in the down-slope direction. This gave detailed information on a regular 0.05 m spaced grid. The recorded profiles were digitised and the height values were snapped to their grid location. The heights were then corrected for the variations in the lengths of the pins and for the slope of the meter when the data was collected. This gave a surface with height values relative to a horizontal plane. A linear trend surface was fitted through the data and the residuals calculated. It is from this data that the roughness characteristics were calculated.

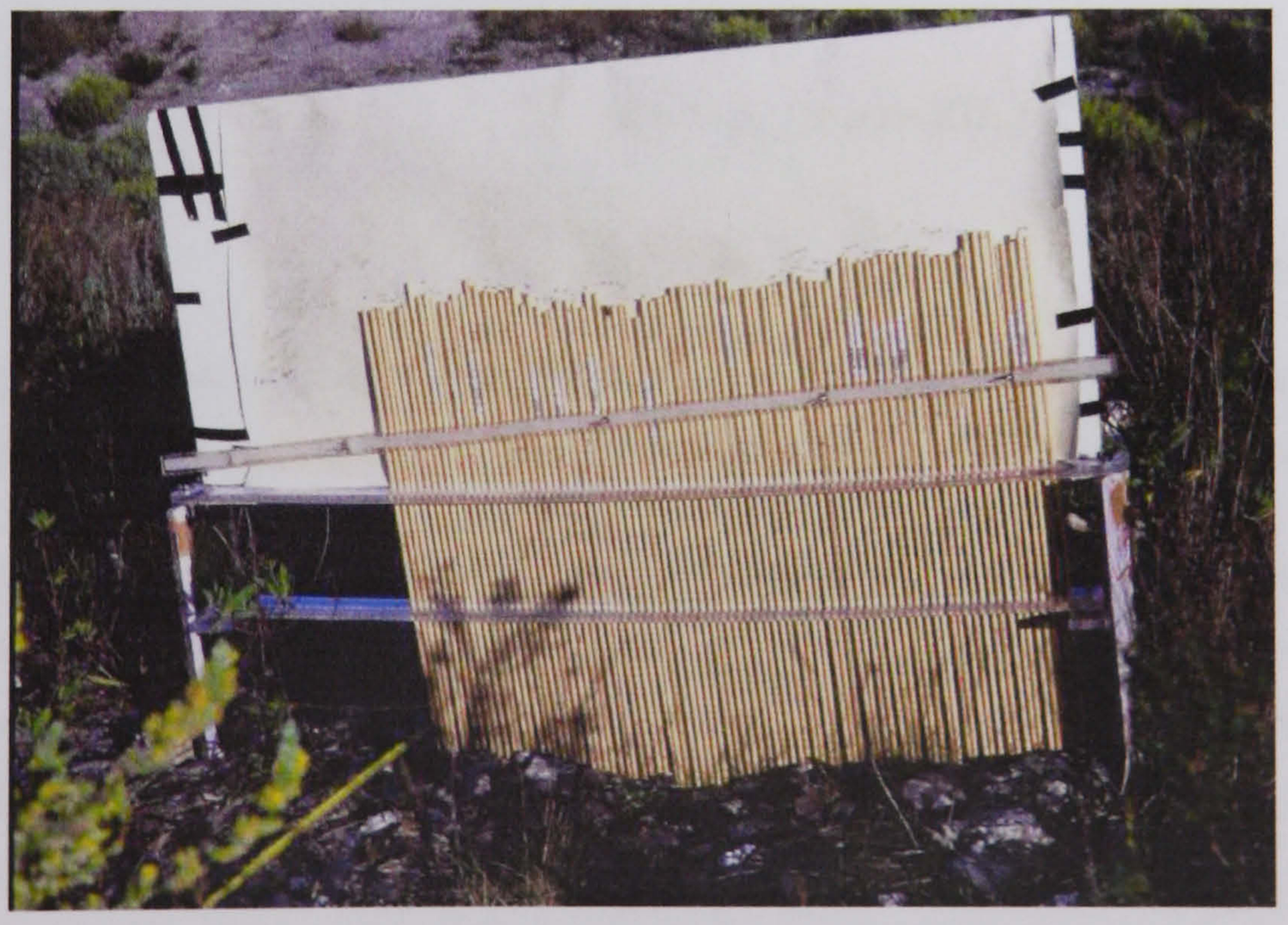

Figure 3.18 Photograph of the pin-meter used to measure surface roughness

Indices

Many indices for the description of surface roughness have been developed. The Random-Roughness (RR) index developed by Allmaras at al. (1966) is the most frequently quoted (Hansen et al. 1999). It is calculated as follows:

1. All elevation data are transformed to a natural logarithm scale.

2. Contributions from the oriented roughness and slope are removed.

3. The upper and lower 10 % values are excluded from the data set.

4. The RR is then obtained as the product of the standard deviation of the remaining logarithmic transformed data and the overall arithmetic mean of the elevations.

The introduction of this index constituted a major advance in describing the surface roughness (Römkens and Wang 1986). However, the statistical nature of the index limits its ability to describe the spatial structure of the surface, the quantification of roughness related to surface characteristics and limited its use in describing hydrological processes (Römkens and Wang 1986). The index is not sensitive to the spacing between the sample points.

Geostatistical Approach

A powerful set of techniques for the understanding of the spatial variability is geostatistics. For many variables that vary spatially, statistical inferences from regression equations are not valid since these deterministic functions have no generality (Oliver and Webster 1986). Since many features are essentially random but spatially dependent it is possible to describe them using stochastic functions of their spatial location (Oliver and Webster 1986) using the 2D semivariance function, Equation 3.2 (Carbonneau et al. 2003):

$$\gamma(p,q)=\frac{1}{2(N-|p|)(M-|q|)}\sum_{i=1+\frac{|p|-p}{2}}^{N-\frac{|p|+p}{2}}\sum_{j=1+\frac{|q|-q}{2}}^{M-\frac{|q|+q}{2}}[Z(i+p,j+q)-Z(i,j)]^2$$

Equation 3.2

Where $\gamma(p, q)$ is the semivariance, p and q are the lags in the x and y directions, M and N are the dimensions of the surface in the x and y directions and $Z(i, j)$is the elevation at point (i, j).

This is expressed as a semivariogram and can be used as a method of measuring, presenting and modelling the variations between spatial properties (Hypanen 1996). The form of the semivariogram gives information on the scale and the magnitude of the variations (Oliver and Webster 1986). The aspects of the semivariogram of interest are the range, the sill and the nugget. The range defines the distance where the maximum variance is reached, this being the distance where the variables stop correlating with each other. The sill is the value of the semivariance at the range. The nugget is the value of semivariance at zero distance, this is often considered the measurement error or bias (Hypanen 1996) and may be related to variations occurring at a spatial scale below the sampling frequency.

Linden and Doren (1986) developed two roughness indices based upon classical geostatistics, termed LS and LD. These indices considered the relation between neighbouring points and hence are directly related to the spatial structure of the sampled points and are sensitive to differences in roughness.

The calculation of LS and LD are based upon the mean absolute elevation differences, ΔZh, defined as:

$$\Delta Z_h = \sum_{i=1}^{n} \frac{|Z_i - Z_{i+h}|}{n}$$

Equation 3.3

Where Z_i is the elevation of a point and Z_{i+h} is the elevation of a point at lag distance h from point Z_i. The relationship between ΔZ_h and the lag distance ΔX_h was obtained from a linear regression of their reciprocals, Equation 3.4.

$$1/\Delta Z_h = a + b(1/\Delta X_h)$$

Equation 3.4

Where a and b are fitted constants. The lag spacing was limited to a maximum of 0.2 m. The indices were then defined as:

$$LD = 1/a$$

Equation 3.5

$$LS = 1/b$$

Equation 3.6

Linden et al. (1988) found that the best predictor of detention storage was a combination of the LD and LS indices:

$$(LD * LS)^{0.5}$$

Equation 3.7

The LS and LD indices are physically based, however, the regressions required to calculate them to some extent neglect important characteristics of the soil surface as reflected in the exact difference in level between adjacent points (Hansen et al 1999).

3.6.2 Soil Properties

Soil samples were taken from each different cover type both from the crust and the Sub-surface material. This gave two samples at each of the eleven rainfall simulation plots resulting in 22

samples in total. These samples were then analysed for soil moisture, organic matter, bulk density and the particle size distribution.

Samples of a known volume were collected for the determination of the bulk density. This was achieved by driving a cylinder of known volume (78.5 cm^3) into the soil. Care was taken not to compact the soil in this process and that the cylinder was completely full. The bulk density was calculated according to Brady (1990) from Equation 3.8.

$$BD = \frac{dw}{vol}$$

Equation 3.8

Where *BD* is the bulk density, *dw* is the dry weight of the soil and *vol* is the volume of soil. The porosity (p) of the soil was then calculated from Equation 3.9.

$$p = \frac{BD}{PD}$$

Equation 3.9

Where *PD* is the particle density. The particle density was calculated by measuring the amount of water displaced by a sample of bed rock material and dividing it by the sample weight.

Where significant organic matter content was present, the percentage content was determined by the loss on ignition technique. The material with the organic material removed was then used for the particle size analysis.

To determine the particle size distribution, the samples were reduced in size through the use of a quartering box to gain a sample of approximately 40 g. This was then dry sieved through 2 mm and 1.5 mm sieves. A Sub-sample was then taken from the < 1.5 mm material and mixed with calgon (5 %) on a watch-glass to break down any aggregates. This material was then analysed using laser diffraction in a Coulter LS 230 over the range 0.04 – 2000 µm. For each Sub-sample three runs were performed to ensure consistency in the results. For every tenth sample, three different Sub-samples were taken to ensure that the Sub-sampling technique was not introducing any bias or errors.

3.6.3 Determination of Cover

The cover of the sites was assessed at two scales: at the scale of the whole site and over a number of smaller plots within the site. The position of the each significant plant was surveyed. The plant structure was simplified into two measurements; the plant height, and the crown diameter. This information was then imported into a GIS system to calculate the area of the site covered by vegetation.

The cover at the plot scale was recorded for each different cover type within the site at the rainfall simulation plots. This was done by photographing the surface from a height of 1.45 m using a 50 mm lens onto 35 mm film. This gave ground coverage of 1 m by 0.65 m. The image was then scanned[2] and overlaid with 100 stratified random points. The cover at these points was determined by eye and classified into soil, stones and biomass.

3.6.4 Infiltration

For the investigations into the soil infiltration capacity and the controls upon the infiltration rate two techniques have been used. The first is rainfall simulation, described in section 3.6.5, and the second is minidisk infiltration, described in section 3.6.6.

3.6.5 Rainfall Simulation

The rainfall simulator is a spray type simulator based on the design of Cerdá et al. (1997a). This design was chosen for a number of reasons. The simulator was designed for operation in rugged terrain and has been used in semiarid environments for over a decade with good results (Cerdá et al. 1997a). The nozzle based system is able to generate high intensity rainfall similar to natural storm events with a return period of 5 - 10 years. The design is simple and lightweight, enabling ease of movement between plots in the field and transportation to the study catchment from the UK.

Water is pumped under pressure into a horizontal pipe mounted above the plot. The nozzle is located on the underside of this pipe such that the water fills the pipe and flows out through the nozzle. The nozzle used was a Lechler 460.648. The rainfall intensity is controlled through the water pressure at the nozzle. A pressure gauge is located on the top of the pipe and the controls are located on the ground next to the pump.

The rainfall is delivered to a bounded plot located 1.7 m below the nozzle. Strips of metal bound the top and sides of the plot. At the bottom of the plot there was a Trough Runoff Collector (TRC). This spans the full width of the plot and routes the runoff into the collector. The experimental set up is shown in Figure 3.19.

Experimental Procedure

At each experimental site, two storms were performed. The storm rainfall intensity was approximately 75 mm hr^{-1} for 25 minutes. The second storm was performed 1 hour after the end of the first storm. This was to investigate the effects of antecedent soil moisture on the generation of runoff. The runoff volume was measured every minute during the rainfall and until the runoff ceased. The slight variations in water pressure at the nozzle, and hence in simulated rainfall intensity, were recorded. The plots were 0.25 m^2 and the shape was either

[2] Image scanned at 1360 dpi, 24-bit colour depth on a CanoScan FD 2710F film scanner.

square or round depending on the surface conditions. The round plots were used where the soil was not strong enough to support the square plot. This is because the square plot has the whole lower side exposed to collect runoff.

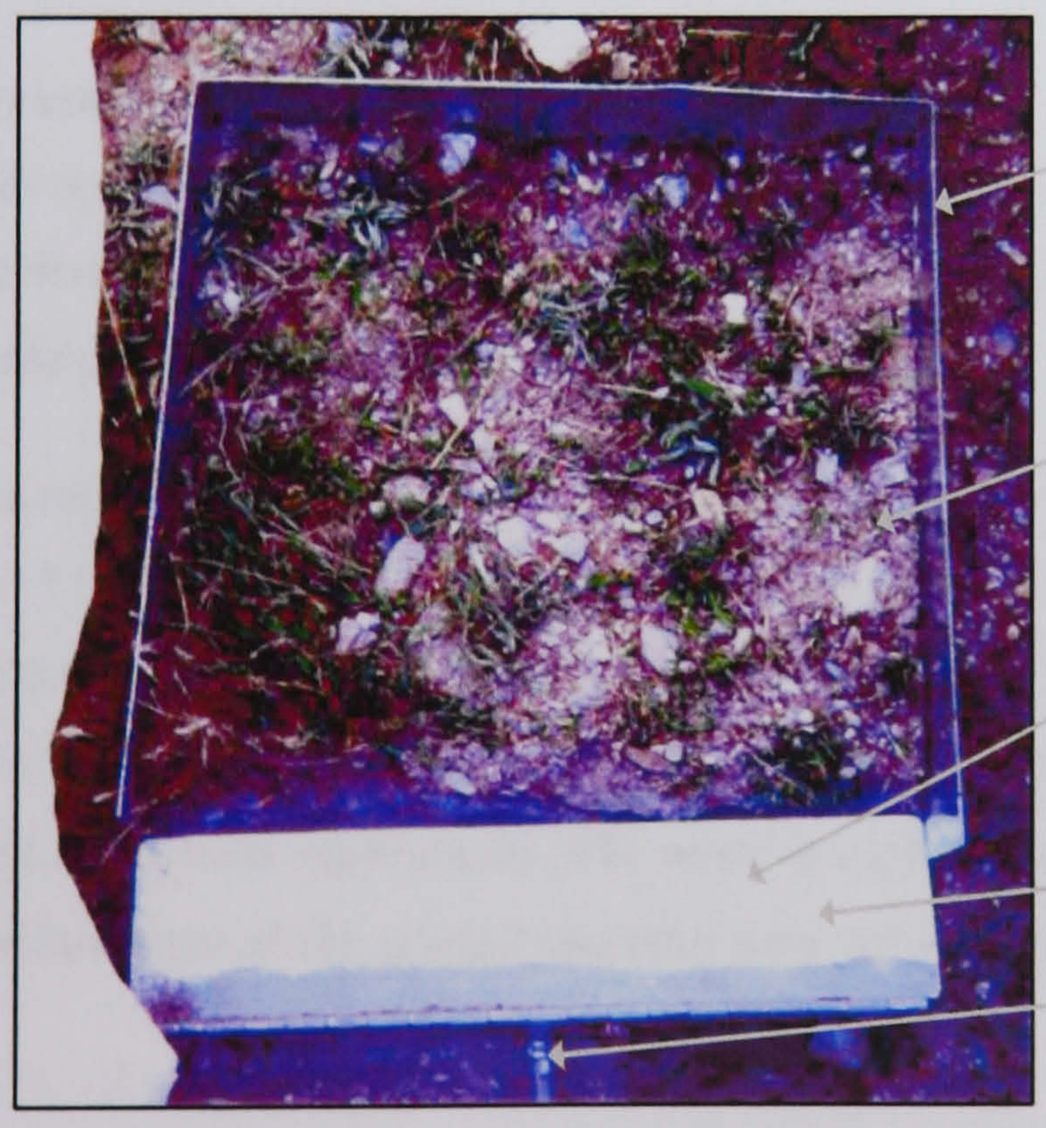

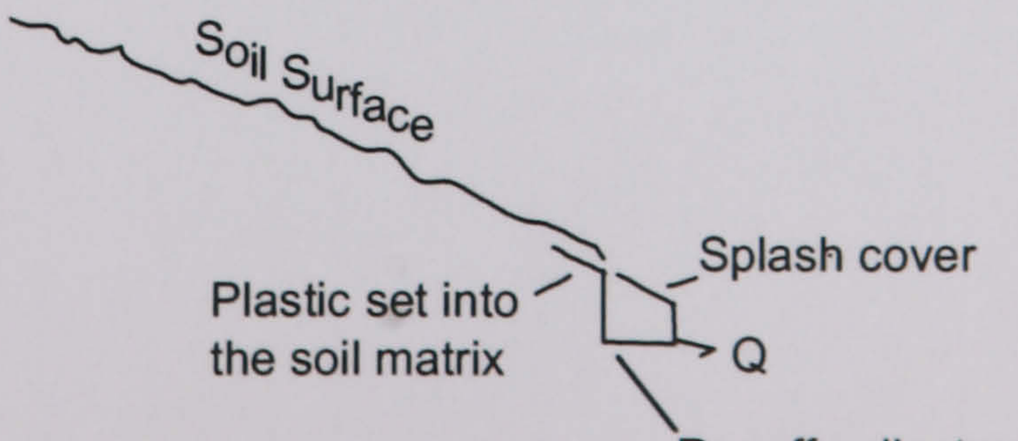

Figure 3.19 Rainfall simulator set up

Applicability of Rainfall Simulation

It is not possible to use natural storm events due to their infrequent nature and because of the spatial and temporal variations in storm characteristics. It is also very difficult to ensure the same initial conditions for each runoff experiment. These factors, coupled with the cost of monitoring the plot for long periods of time, make it impractical to rely on natural storms. Therefore, although the simulated rainfall differs from natural rainfall it is the best way to investigate runoff generation processes under rainfall. The knowledge of the discrepancies between the simulated and natural rainfall enables the critical analysis of the results gained using the technique.

The objective of rainfall simulation is to produce rainfall with characteristics as close to natural rainfall as possible. It is important to appreciate the effects of any deviations between the natural and the simulated rainfall. It is also important that the simulated rainfall is constant over space and time such that any variations in measurement are due to differences in the surface and not simulator variability. Four aspects of the simulated rainfall were investigated with their potential effects on runoff generation discussed. The four aspects are the relationship between pressure and rainfall intensity, the temporal and spatial variability of rainfall intensity and the drop size distribution.

Pressure – Intensity Relationships

During the operation of the rainfall simulator, the rainfall intensity is managed by controlling the water pressure at the nozzle. To understand how much water reaches the ground, knowledge of the relationship between the pressure at the nozzle and the rainfall intensity is required.

The relationship between pressure and intensity was investigated over the pressure range 0.4 bar to 0.7 bar with a spacing of 0.1 bar. The simulator was run for 25 minutes and the rainfall collected in 529 (23*23) collectors with a radius of 11 mm arranged in a grid pattern. These were 1.7 m below the nozzle and covered an area of 0.5 m x 0.5 m, identical to the plot size used in the field experiments. The water in each collector was then measured and the mean and standard error of the rainfall intensity were calculated (Figure 3.20).

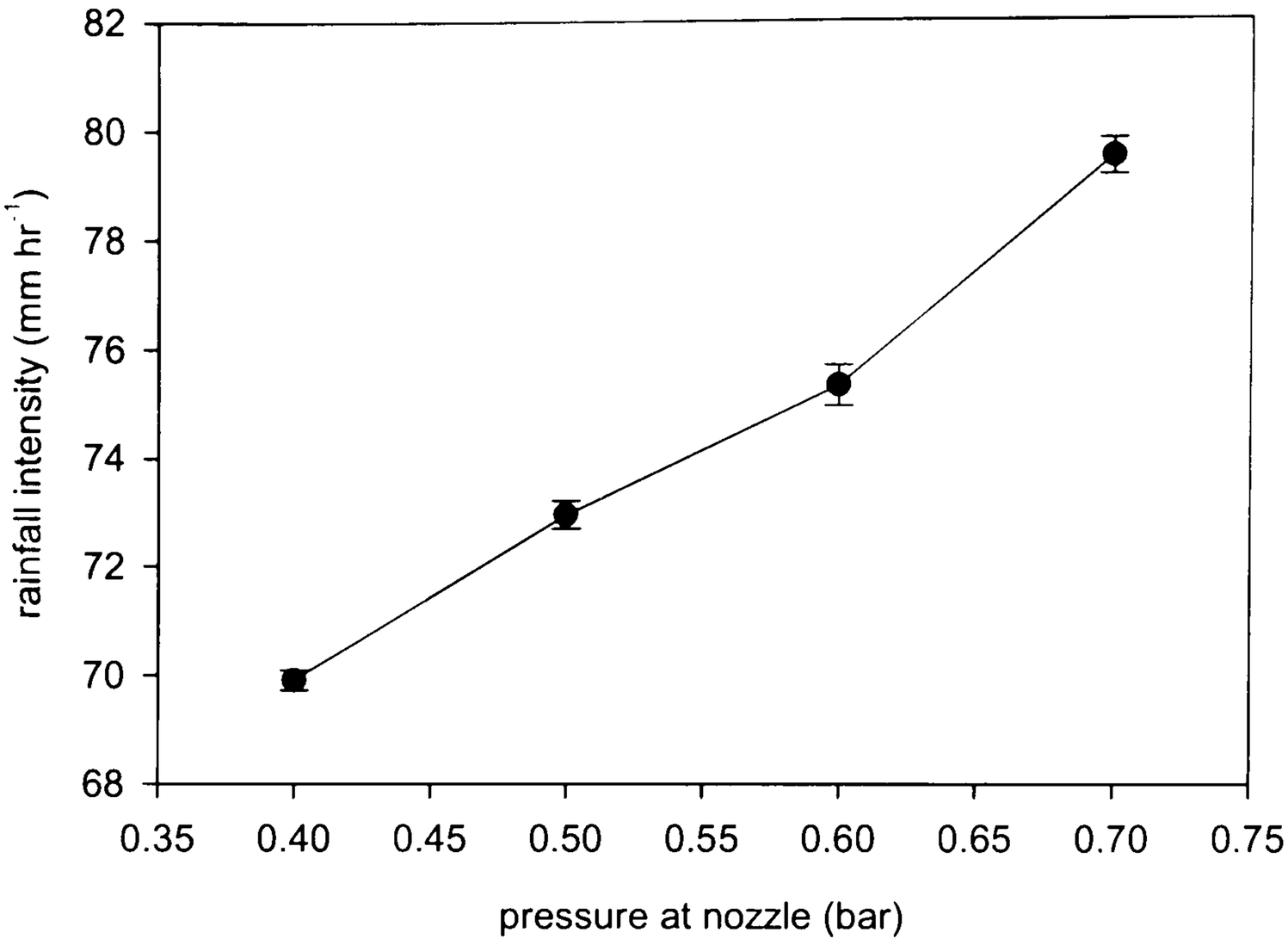

Figure 3.20 Changes in rainfall intensity with changes in pressure, error bars show standard error of the mean

The rainfall intensity increases from 69.9 mm hr^{-1} at 0.4 bar to 79.5 mm hr^{-1} at 0.7 bar at an almost linear rate. The variability of the intensity increases with the pressure to 0.6 bar and then decreases slightly.

Temporal Variability of Intensity

It is important that the intensity of the simulated rainfall does not vary with time. Factors which can lead to variations in the rainfall intensity include variations in the power supply (12 volt battery) and the efficiency of the pump in relation to the head of water in the reservoir.

The temporal variability of the rainfall intensity was investigated using a tipping bucket raingauge located 1.23 m below the nozzle. The top of the gauge was closer to the nozzle than in the pressure intensity relationship, hence the higher intensities. This difference does not influence the shape of the distribution, only the mean. The simulator was run for an hour and the time of the bucket tipping was logged to a precision of one second. The cumulative histograms for 0.4 bar, 0.6 bar and 0.7 bar are shown in Figure 3.21. The mean, standard deviation and the coefficient of variation (COV) were calculated for each pressure, as shown in Table 3.3.

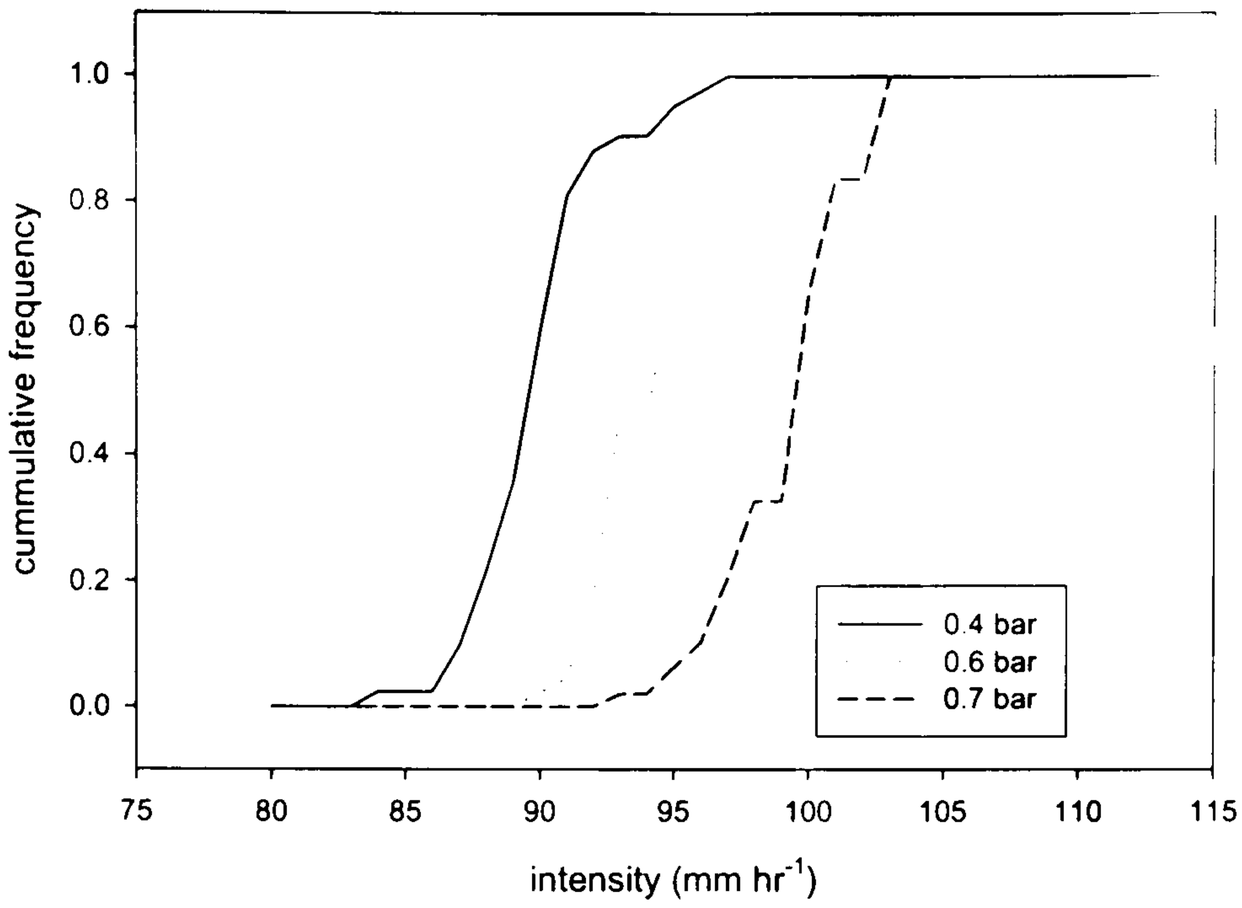

Figure 3.21 Histograms of simulated rainfall intensities at different nozzle pressures.

	0.4 bar	**0.6 bar**	**0.7 bar**
Mean mm hr^{-1}	89.57	94.07	99.15
Stdev	2.54	2.16	2.34
COV	0.03	0.02	0.02

Table 3.3 Temporal variability of rainfall at different nozzle pressures

The standard deviation is very low in comparison to the mean, as shown in the COV and the steepness of the cumulative histogram curves. Therefore, the rainfall intensity is fairly stable over time.

Spatial Variability of Intensity

The spatial pattern of rainfall intensity is important because if it is not uniform, certain parts of the plot will generate more runoff due to the greater rainfall intensity making the results prone to errors.

The experimental set-up was the same as for the pressure - intensity relationship experiments. The location of each collector in the grid was recorded and the intensity values were interpolated using a kriging algorithm to give the grids shown in Figure 3.22. There is a considerable amount of spatial variation in the rainfall intensity. The main direction of the variation is between the left and right sides of the plot with higher intensities on the right side. The variability within the plot increases with intensity and the greatest change in spatial pattern occurs between 0.5 bar and 0.6 bar.

Possible reasons for this asymmetrical spray pattern are that the nozzle characteristics tend to push more water out of one side or that the delivery of the water to the nozzle, which includes a right angle bend, are forcing the water out of the nozzle in a non-uniform way. The direction from which the water is delivered is from the side with the higher intensities. To test the first of

these ideas, the nozzle was turned through 180° and the pattern of intensities measured again. The same trend with higher intensities on the right hand side was recorded.

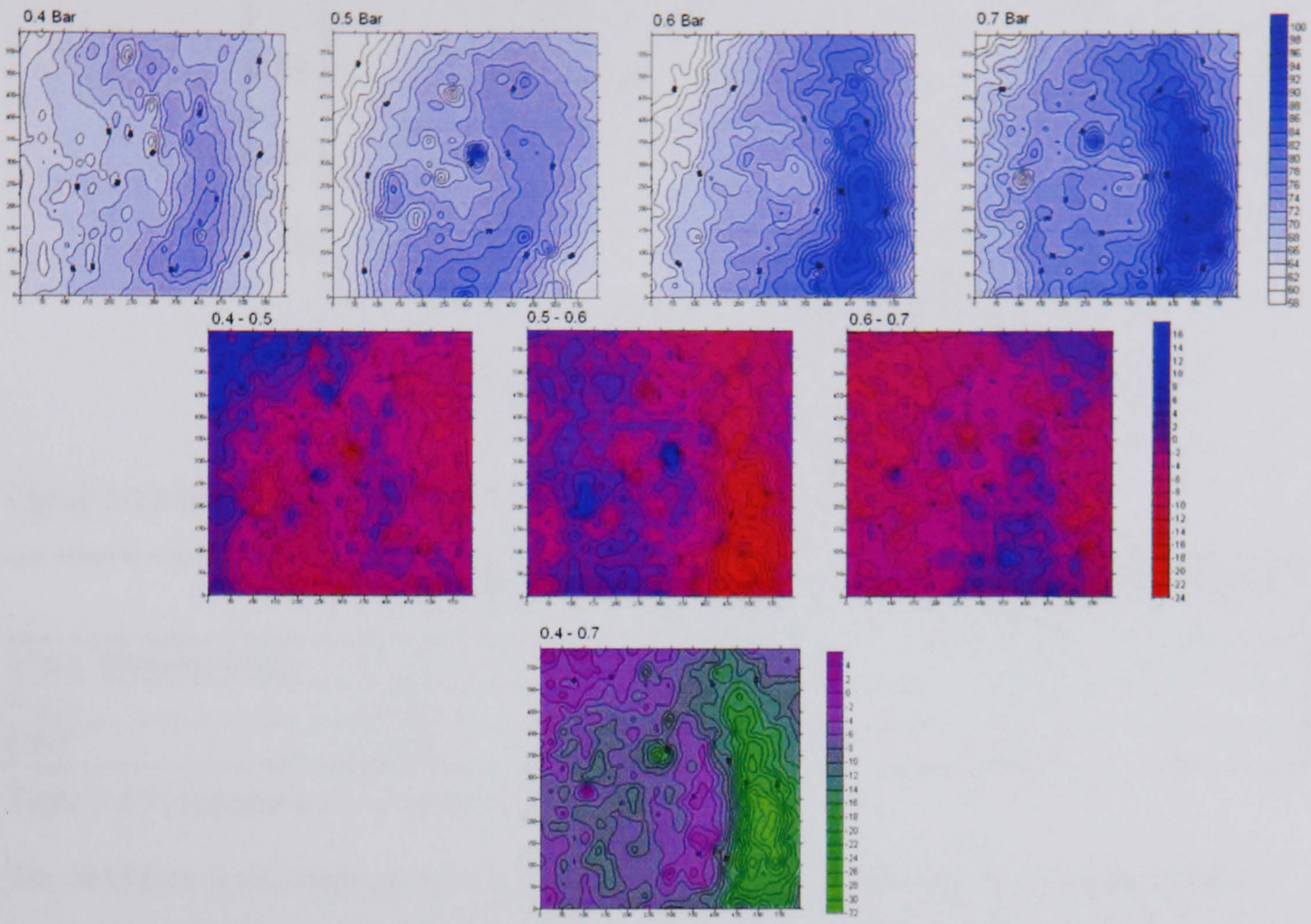

Figure 3.22 Changes in the spatial pattern of intensity with increases in pressure

Drop Size Distribution

The drop size distribution of the simulated rainfall was measured using the paper staining technique (Brandt 1989). The drop size distributions of simulated rainfall were measured at 0.5 bar at both the centre and the edge of the spray cone. These distributions were then compared with measured drop size distribution from a frontal rainstorm on 05 May 2001 in the Rambla de Nogalte catchment. These distributions are shown in Figure 3.23 and the moments of the distributions are shown in Table 3.4.

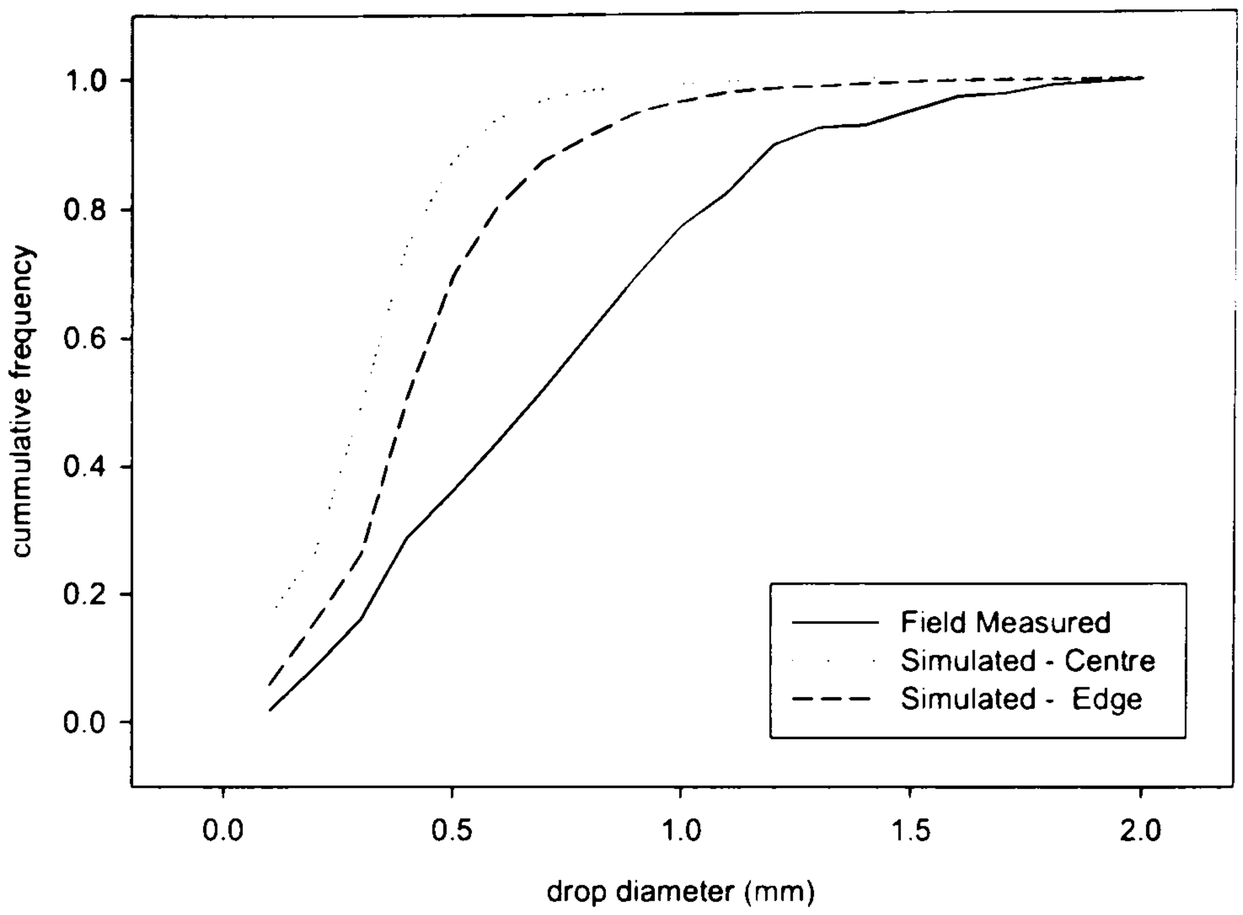

Figure 3.23 Measured and simulated rain drop size distributions

	Field Measured	**Simulated, centre of cone**	**Simulated, edge of code**
Mean diameter (mm)	0.72	0.44	0.31
Stdev	0.42	0.26	0.20
COV	0.58	0.59	0.62

Table 3.4 Comparison of measured and simulated rainfall

The field-measured raindrops have a greater mean and standard deviation than either of the simulated distributions. The drop size distribution at the edge of the cone has a smaller mean and standard deviation than at the centre of the cone. The differences between the simulated rainfall and the natural rainfall relate to the huge differences in the drop forming processes. During natural rainfall, individual drops will coalesce to form larger drops. The simulated rainfall drops are formed under pressure in the nozzle and this gives smaller drop sizes. The changes in the drop size distribution in different parts of the spray cone relate to the distribution of exit velocities from the nozzle. The drops at the edge of the cone have greater velocities and hence large drops are unstable and break down into small drops.

To test if the simulated rainfall has a statistically similar variance to the field measured rainfall and if the distributions are consistent within the spray cone, F tests where performed. The F statistic for the comparison of the centre of the cone and the field-measured distributions was 4.503. This is greater than the critical value of 1.167 (df 230, 2430; 95 % significance level) and hence it is statistically unlikely that the two samples are from the same underlying distribution. The F statistic for the comparison of the distributions from the centre and the edge of the cone was 1.745. This is greater than the critical value of 1.086 (df 1158, 2430; 95 % significance level) and hence it is statistically unlikely that the two samples are from the same underlying distribution.

The smaller drops in the simulated rainfall will deliver less kinetic energy to the soil surface. This will influence the changes in the soil surface during the rainstorm. There will be less reduction in the surface roughness and less surface sealing since fewer aggregates will be broken down. The detachment of soil particles by raindrops will also be less due to the reduction in kinetic energy, leading to reduced erosion.

Summary of Rainfall Simulation

The rainfall simulator used is restricted to a limited range of intensities due to the pressure at the nozzle required for drop formation. This ranges from 70 – 80 mm hr^{-1}. There are spatial variations in the delivered rainfall intensity although the temporal variability is low. There is a systematic spatial pattern of intensities with a range of intensities from 58 to 100 mm hr^{-1} across the plot at 0.7 bar. The drop size distribution is statistically different from the field measured distribution and varies across the plot.

Rainfall simulation does not provide a perfect reproduction of natural rainfall and there are a number of problems associated with the technique. Despite these problems, it is still the best available technique for the investigation of infiltration and runoff generation (Neff 1979).

3.6.6 Minidisk Infiltration

A series of minidisk infiltrometer experiments was conducted on each different cover type within each site. There are a number of different methods to measure soil hydraulic conductivity with a disk infiltrometer. The method proposed by Zhang (1997) has been used in this research. The infiltrometer is filled underwater and the stopper inserted in the top. To ensure good contact between the disk and the soil surface, a thin layer (approximately 3 mm) of wet sand was placed in-between the infiltrometer and the soil surface. The infiltrometer was then placed on top of the sand and the volume change was recorded every 30 seconds for five minutes. When the change in volume was insufficient to allow accurate measurement, the time between measurements was increased.

To determine the soil conductivity, the method requires that the measured cumulative infiltration against time is fitted to the function:

$$I = \left(C_1 t + C_2 \sqrt{t}\right)$$

Equation 3.10

Where C_1 and C_2 are fitted coefficients. The hydraulic conductivity (K) is then calculated from:

$$K = \frac{C_1}{A}$$

Equation 3.11

A is computed from:

$$A = \frac{11.65\left(n^{0.1} - 1\right)\exp\left[a\left(n - 1.9\right)ah_0\right]}{\left(\alpha r_0\right)^{0.91}}$$

Equation 3.12

Where n and α are the Van Genuchten parameters for the soil, r_o is the disk radius, h_o is the suction at the disk surface and a is a coefficient. For $n >= 1.9$, $a = 2.92$, for $n < 1.9$, $a = 7.5$. The Van Genuchten parameters for the 12 texture classes of soil were obtained from Carsel and Parrish (1988). The minidisk infiltrometer used had a radius of 1.59 cm and a suction rate of 2.0 cm.

The data gained from the use of minidisk infiltrometers complements the rainfall simulation data in a number of ways. The use of the minidisk infiltrometer does not require the disturbance of the soil surface. It is, therefore, possible to study the effects of soil crusts on the infiltration rate. The area over which the infiltration is measured is small, 0.02 m in diameter. This allows the investigation of the variability of infiltration rates at the scale below that considered by the rainfall simulation plots.

Minidisk Summary

Minidisk infiltration techniques provide rapid information on the infiltration capacity of the soil. They do not require the disturbance of the soil surface and hence are well suited to the consideration of the impacts of soil crusting. They do not, however, simulate the processes associated with raindrop impact, such as crust formation.

3.6.7 Comparison of Rainfall Simulation and Minidisk Infiltration

Rainfall simulation has been used as it is able to reproduce many of the processes occurring during a natural rain storm. These processes include impact of raindrops on the soil surface and the subsequent aggregate break down and surface sealing. It is possible to consider the changes in the runoff generation during the storm and between storms at the same location with different initial conditions. The inclusion of plot scale factors such as surface roughness, vegetation and slope gradient are also possible.

There are a number of limitations with rainfall simulations. The first of these is the need to build a bounded plot to capture the generated runoff. This breaks the surface crust and can create macropores which greatly increase the infiltration capacity of the soil. Each simulation uses approximately 100 litres which may be difficult to obtain in a semi-arid environment. As the simulator runs at a set rainfall intensity, the information obtained is on the infiltration rate rather than the infiltration capacity. The final factor is the time required to perform a simulation

experiment. To set up the plot and run two simulations may take over four hours. This, therefore, limits the number of sites that can be examined.

The minidisk infiltration technique has a number of advantages over rainfall simulation. Firstly, the experiments only take 5 minutes to perform and it is possible to perform a number of experiments in parallel. This rapid data collection enables the investigation of variability of the infiltration capacity. The water use is approximately 100 ml, three orders of magnitude less than rainfall simulation. The technique gives information on the infiltration capacity of the soil. It is not required to build a bounding plot and hence it is possible to examine the effects of surface crusting on the infiltration capacity.

The technique does not include the effect of raindrop impact, surface roughness, interception by vegetation or surface gradient effects. This means that the different techniques are giving information on different parts of the infiltration process. Therefore, the results should not be considered directly comparable. However, each of the techniques is strong where the other is weak. This, therefore, creates a powerful combination for understanding the controls on the infiltration rate.

3.6.8 Summary

Through the investigation of the surface roughness, soil properties and vegetation cover, it will be possible to consider the main controls on the infiltration rate. The use of both rainfall simulation and minidisk infiltration experiments gives a balanced picture of the infiltration process. The rainfall simulation enables the study of infiltration under semi-natural conditions with rain drop impact and surface seal processes. The use of the minidisk experiments enables the consideration of the variability of the infiltration capacity. The results and analysis of the field data is presented in chapter 4.

4 Field Results

4.1 Introduction

The aim of the field investigations was to identify the key variables controlling runoff generation in the Rambla de Nogalte catchment. From the discussion of semi-arid hydrology in chapter 2 a short list of controlling factors has been compiled. These are the vegetation cover, rock fragments, gradient, roughness and surface crusting. These factors are influenceed by the geology and manipulated by land management. The relationships between these factors and the results from the rainfall simulation and minidisk infiltration experiments are investigated through the use of statistical techniques. The details of the sites investigated and the techniques used are given in the previous chapter. The original data is given in appendix 1 and on the CD.

4.2 Site and Soil Characteristics

Two spatial scales of investigation were used. The first is termed the site scale which refers to the location where the smaller scale experiments were clustered. The size of the sites varied according to the spatial variability of the ground cover such that scrub sites were approximately 5 by 5 m and agricultural sites were approximately 15 by 15 m. The second scale is the plot scale, which is approximately 0.5 by 0.5 m. This refers to the area used for the rainfall simulation and the measurement of surface roughness.

4.2.1 Surface Cover

At the plot scale the cover composition of vegetation, bare soil and stones was measured. At the site scale, the vegetation cover was measured for each rainfall simulation plot. The site level cover results are shown in Table 4.1 and the plot level in Table 4.2.

Site	Main vegetation types	Vegetation cover (%)	Number of individuals
1	Almonds	7.45	9
2	Anthylsis	16.9	151
3	Almonds and olive	2.28	11
4	Almonds and olive	8.08	13
5	Anthylsis and thymus	15.8	75
6	Almonds	7	12
7	Anthylsis and thymus	12.3	51

Table 4.1 Site level vegetation cover

Simulation plot	Soil (%)	Stones (%)	Biomass (%)
Site 1 Tree crops	56.9	39.7	3.4
Site 2 Bush	2	0	98
Site 2 Inter bush	28.1	8.8	63.2
Site 3 Tree crops	0.0	98.6	1.4
Site 4 Tree crops	49.95	50.05	0.0
Site 5 Bush	7.0	2.0	91.0
Site 5 Inter bush - grass	23.0	39.0	31.0
Site 5 Inter bush – stones	8.0	57.0	35.0
Site 6 Compacted	68.0	32.0	0.0
Site 6 Crusted	56.0	44.0	0.0
Site 7 Scrub	0.0	88.9	11.1

Table 4.2 Surface cover at each of the rainfall simulation plots

Many of the plots have a percentage surface stone cover greater than the percentage stone content of the soil as a whole. This uneven distribution of stones may have resulted from the down washing of fines from the surface layer to lower in the soil profile. The soils developed on the blue schist are poorly developed and contain many large rock fragments. These fragments dominate the surface cover, especially at sites 3 and 7.

The surface stone cover can be related to the surface gradient (Figure 4.1). A linear regression model has been fitted to the data and gave an r^2 value of 0.25. There is an overall trend for lower stone cover on plots with high slope gradients. The large amount of scatter relates to the differences in stone cover as a result of the land management.

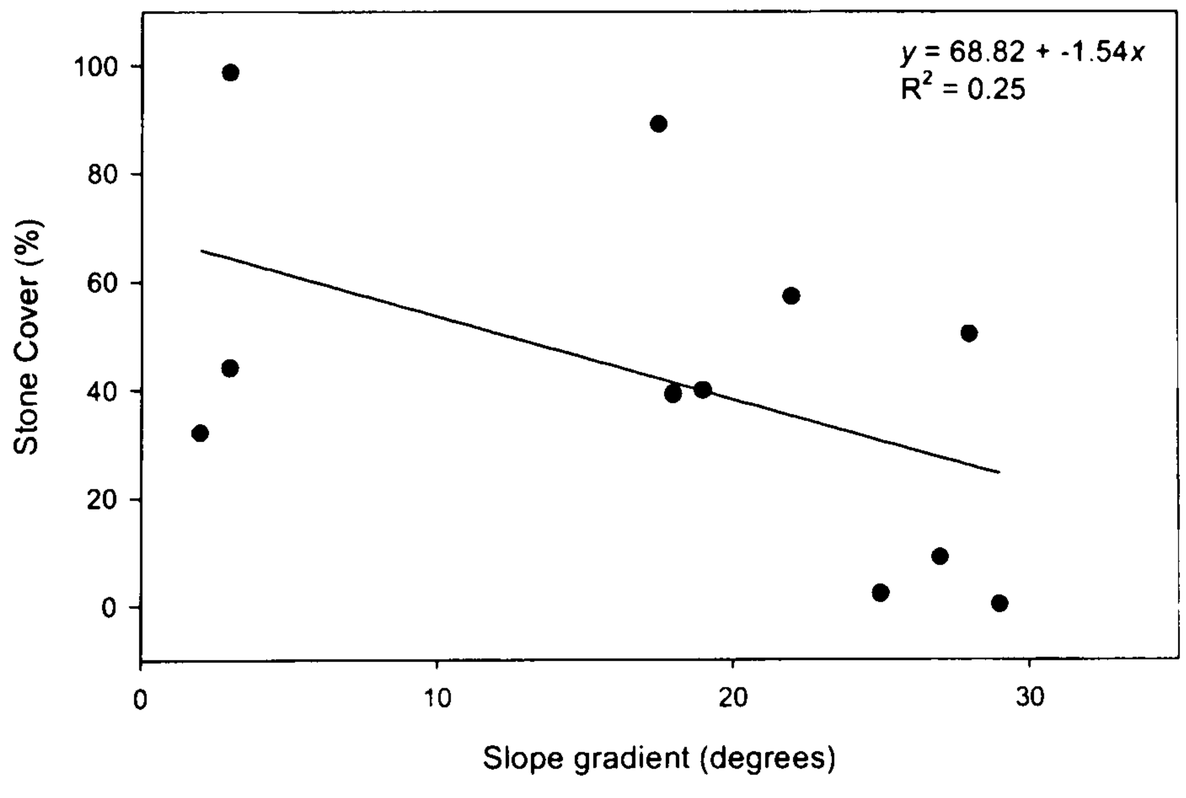

Figure 4.1 Relationship between slope gradient and surface stone cover

4.2.2 Soil Properties

At each rainfall simulation plot a soil sample was taken and analysed for the particle size distribution and the porosity. Details are given in Table 4.3 and a ternary plot of all the soil sampled analysed is shown in Figure 4.2. The details on the methods used are given in chapter 3. The soil texture, excluding the gravel content, classifies the majority of the soil as a sandy loam according to the British Standards Institution classification system.

Simulation	Gravel (%)	Sand (%)	Silt (%)	Clay (%)	Porosity (%)
Site 1 Tree crops	52.84	30.06	15.43	1.66	46.23
Site 2 Bush	39.58	42.27	16.50	1.18	54.05
Site 2 Inter bush	52.56	36.27	10.14	0.82	52.10
Site 3 Tree crops	56.97	32.84	9.20	0.80	43.86
Site 4 Tree crops	69.01	22.21	7.97	0.87	46.65
Site 5 Bush	41.94	43.94	12.99	0.73	49.28
Site 5 Inter bush - grass	53.91	44.01	1.90	0.17	49.28
Site 5 Inter bush – stones	45.16	51.61	2.97	0.20	50.20
Site 6 Compacted	50.45	31.44	16.23	1.38	54.18
Site 6 Crusted	34.87	37.10	24.77	1.94	57.25
Site 7 Scrub	59.24	33.22	7.07	0.32	47.26

Table 4.3 Soil properties at each of the rainfall simulation plots

All sites are characterised by high gravel content and low clay content. The average gravel content on the blue schist is 55.5 % compared to 46.5 % on the red schist. This is reflected in the average porosity values, with the red schist having a higher average porosity of 51.1 % compared to 47.8 % for the blue schist. The greater porosity in the red schist soils enables more water to be stored in a set volume of soil. This increase in storage has the effect of reducing the amount of runoff generated by saturation excess. However, macropores form around the edges of stones embedded in the soil surface and can greatly increase the infiltration capacity of the soil. These macropores will reduce the amount of runoff generated by the infiltration excess process and increase the probability of soil saturation and the generation of saturation excess runoff.

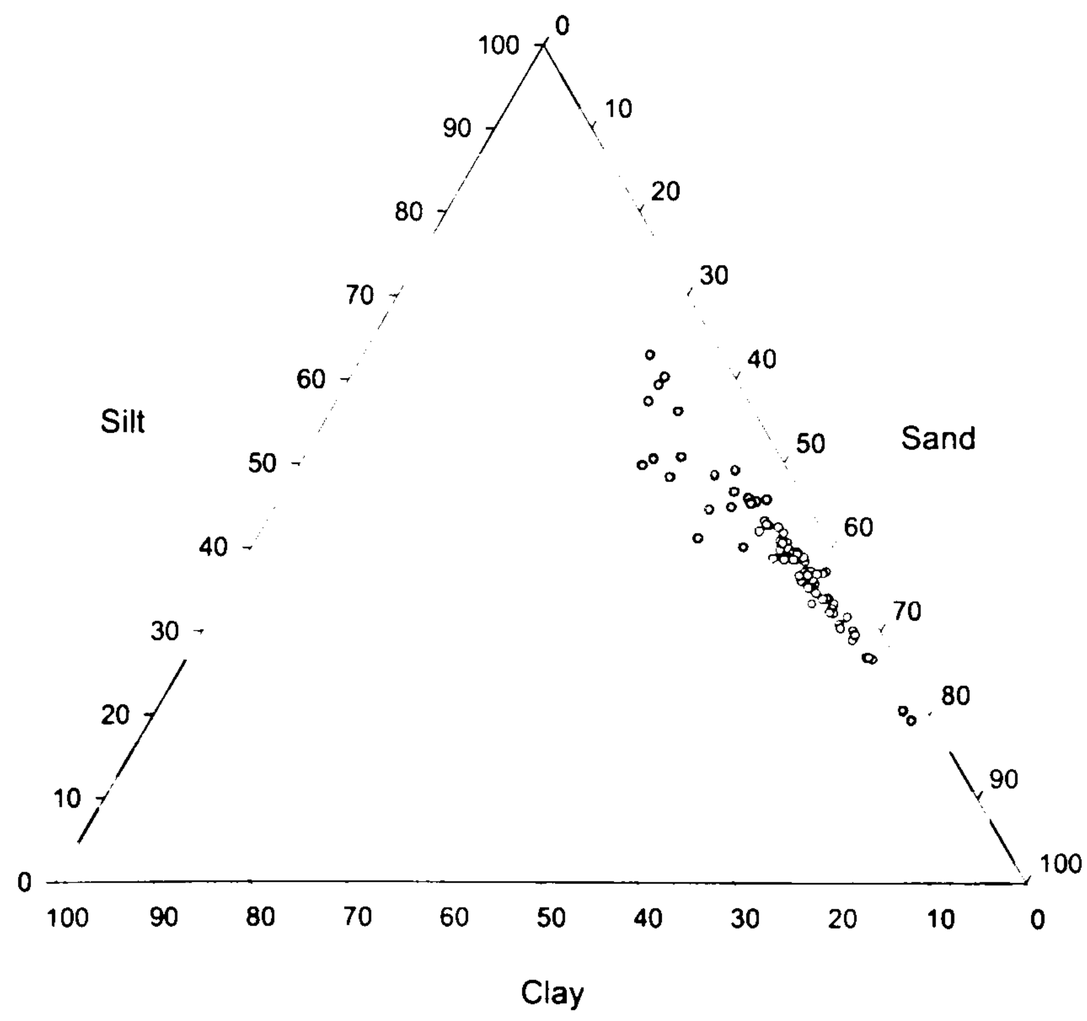

Figure 4.2 Ternary plot of soil texture from across the Rambla de Nogalte catchment

4.2.3 Surface Roughness

Detailed measurements of the surface roughness were undertaken at each site. Details of the measurement technique are given in chapter 3. The large scale roughness was removed from

each surface by fitting a 2D plane to the data and calculating the residuals. The deviations from this surface have been used in the analysis. Sample surfaces are shown in Figure 4.3 for site 1 (ploughed almond field), site 5 (scrub) and site 6 (ploughed and flattened almond field).

The land management of the agricultural sites manipulates the roughness through ploughing of the surface. The relationship between the orientation of the plough lines and the contours influences both the amount of depression storage and flow direction. If the plough lines are perfectly aligned with the contours, then water will be equally distributed along the furrows and hence large volumes of water can be stored. However, if the alignment is slightly out, the water will flow along the furrows and accumulate at a low point. This will then enable the over topping of the furrow and the water will flow down slope.

The surface roughness from the scrub sites and from site 6 (ploughed and flattened) does not contain the orientated roughness of the ploughed sites. The surface can be thought of as a set of small interconnected basins. As the surface depression store fills, these basins will reach their capacity and as they overflow, connections are made between them. These connections enable the transmission of flow across the surface as runoff. The spatial configuration of these basins will determine the runoff response to rainfall for different surfaces with the same amount of surface depression storage. For example, if a large basin is located at the lower edge of the plot, this will take much of the upslope runoff to fill and hence, discharge from the plot will change from negligible to almost all the plot when the large basin fills. If the same basin is located at the top of the plot, most of the plot can contribute runoff without being influenceed.

The Random Roughness coefficient (RR), as defined in section 3.6.1, enables the comparison of the magnitude of the roughness at the different sites (Table 4.4). The site with the highest RR is the tree crop site on the red schist (site 6) and the site with the lowest RR is the tree crop site on the blue schist (site 3).

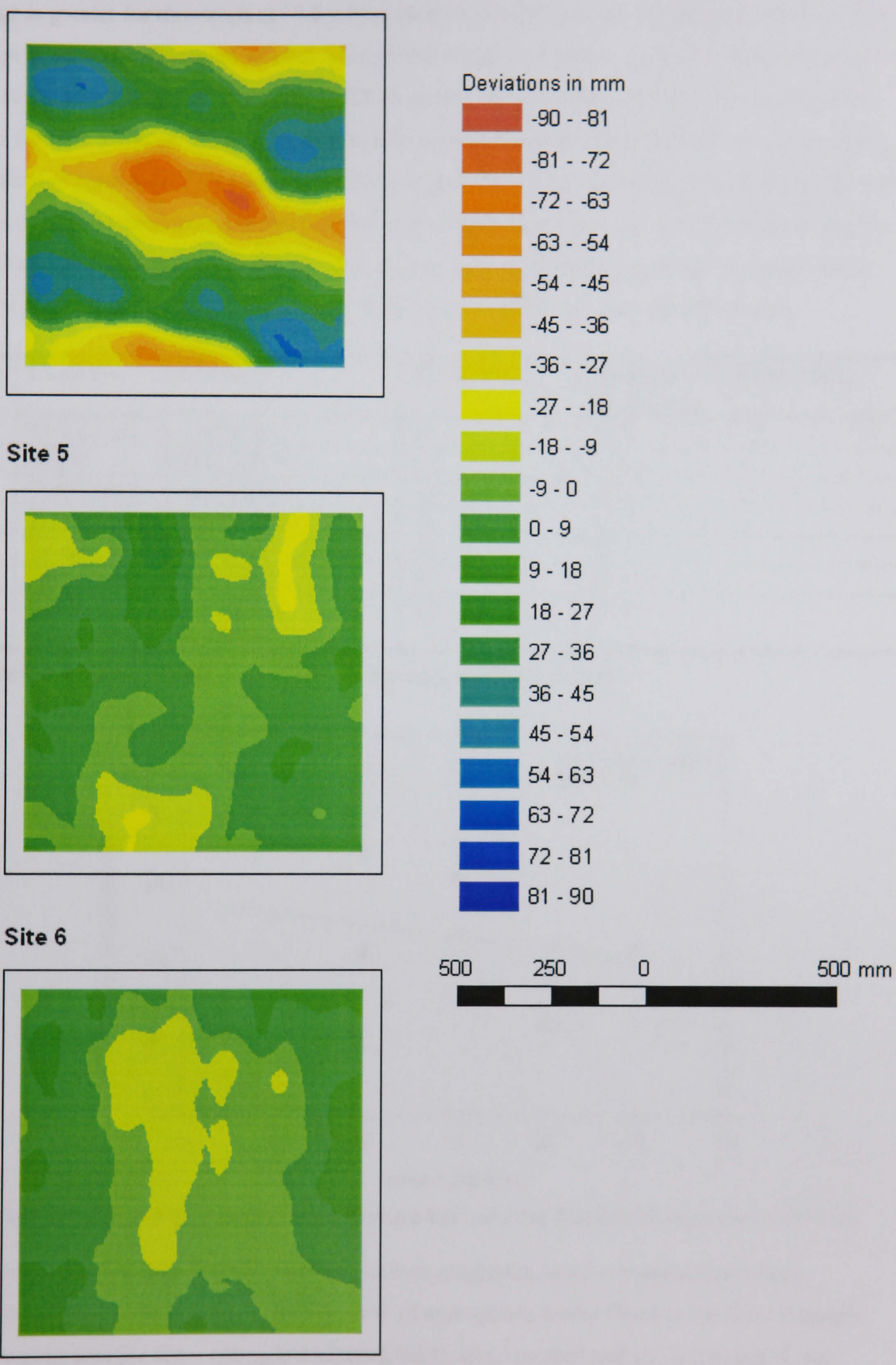

Figure 4.3 Example soil roughness surfaces for site 1 (ploughed almond field), site 5 (scrub) and site 6 (ploughed and flattened almond field). Roughness is shown as deviations from a best fit plane (in mm).

The average RR is greater for scrub slopes at 51.5 than for tree crops at 45.7. However, the range is greater for tree crops at 77.6 with a maximum of 88.2 compared to scrub slopes with a range of 46 and a maximum of 69.2. This greater range is probably due to the manipulation of the surface by ploughing. The average RR is greater for red schist surfaces at 51 compared to 46.1 for blue surfaces. There is an overall relationship for decreasing RR with increasing slope gradient (Figure 4.4). This relationship is more pronounced for the scrub slopes than for the tree crop sites. A linear regression model was fitted to the data and gave an r^2 value of 0.04. The low r^2 value can be related to the fact that the roughness is dependent on land use, geology and the slope gradient. This dataset is too small to separate the effects of each of these factors.

Site	Land use	Geology	Gradient (°)	Random Roughness (RR) coefficient
1	Tree Crops	Red Schist	10	41.7
2	Scrub	Blue Schist	15	62.3
3	Tree Crops	Blue Schist	2.5	10.6
4	Tree Crops	Blue Schist	25	42.5
5	Scrub	Red Schist	20	23.2
6	Tree Crops	Red Schist	3	88.2
7	Scrub	Blue Schist (Cardena)	10	69.2

Table 4.4 Random roughness coefficients for each experimental site

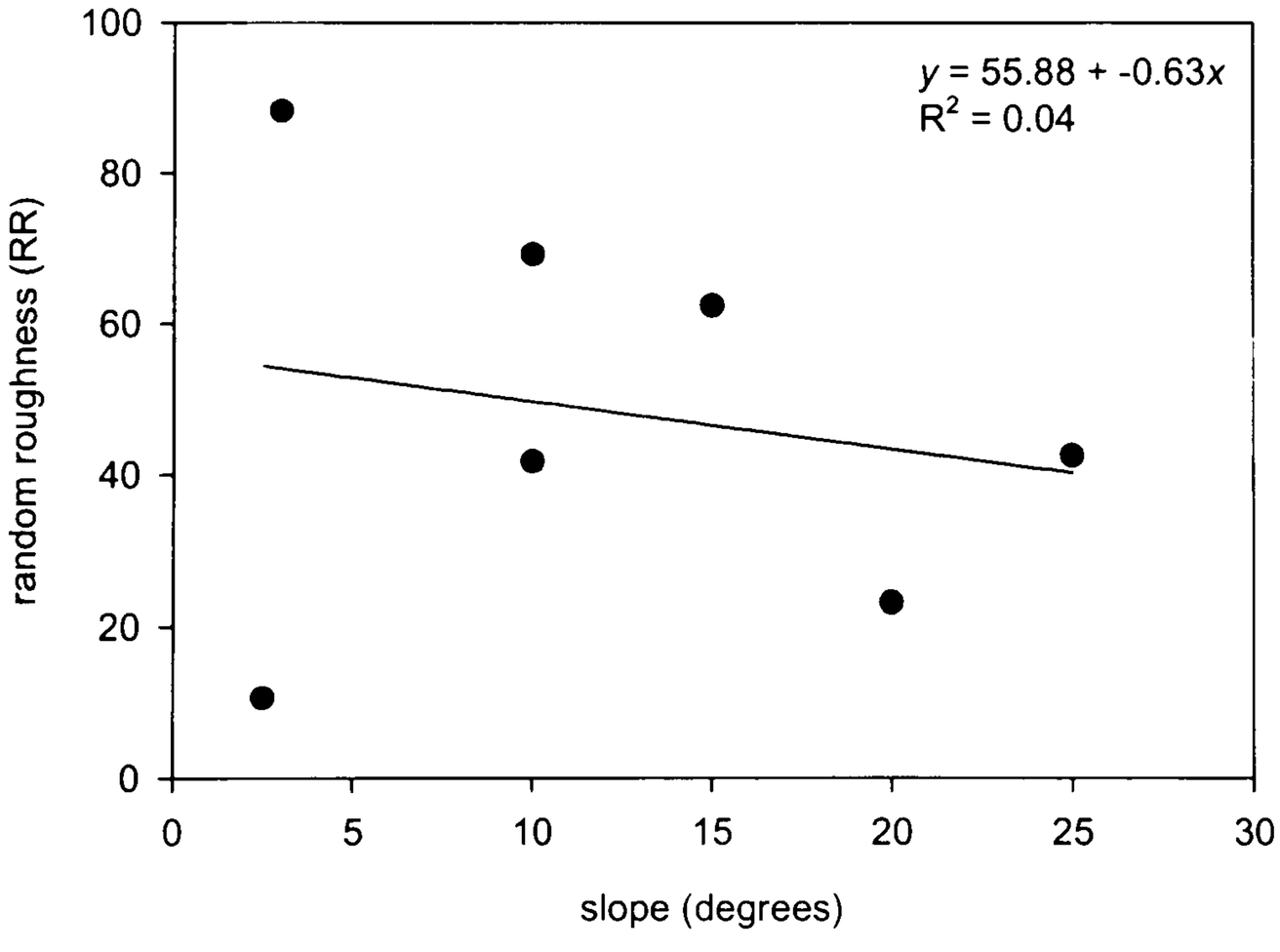

Figure 4.4 Relationship between the surface gradient and the Random Roughness coefficient

To investigate the spatial structure of the surface roughness, semivariograms have been calculated within the limits of reliability and an appropriate model fitted to the data. Example semivariograms for site 1 (ploughed almond field), site 5 (scrub) and site 6 (ploughed and flattened almond field) are shown in Figure 4.5 and the parameters of the fitted models for all sites are given in Table 4.5. The models were fitted using a minimisation of sum of squares

algorithm. A number of different models were investigates and the model with the bet fit was selected.

Site 1

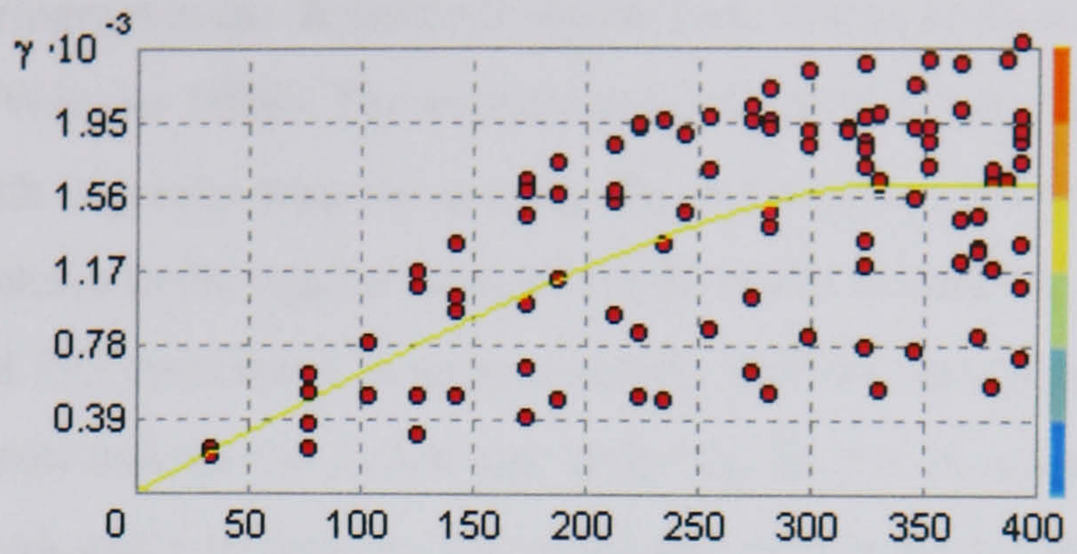

Site 5

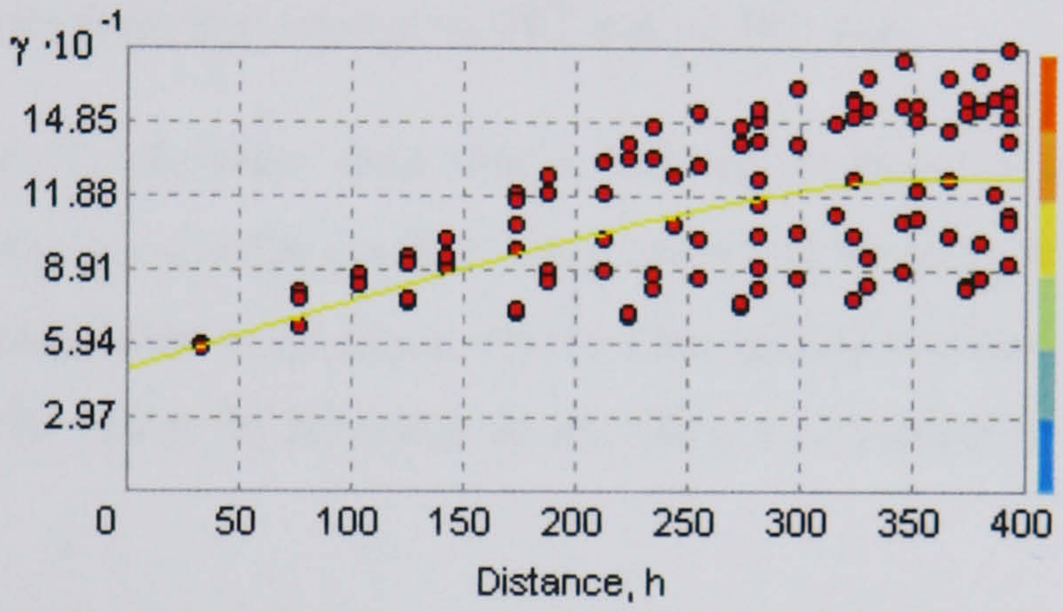

Site 6

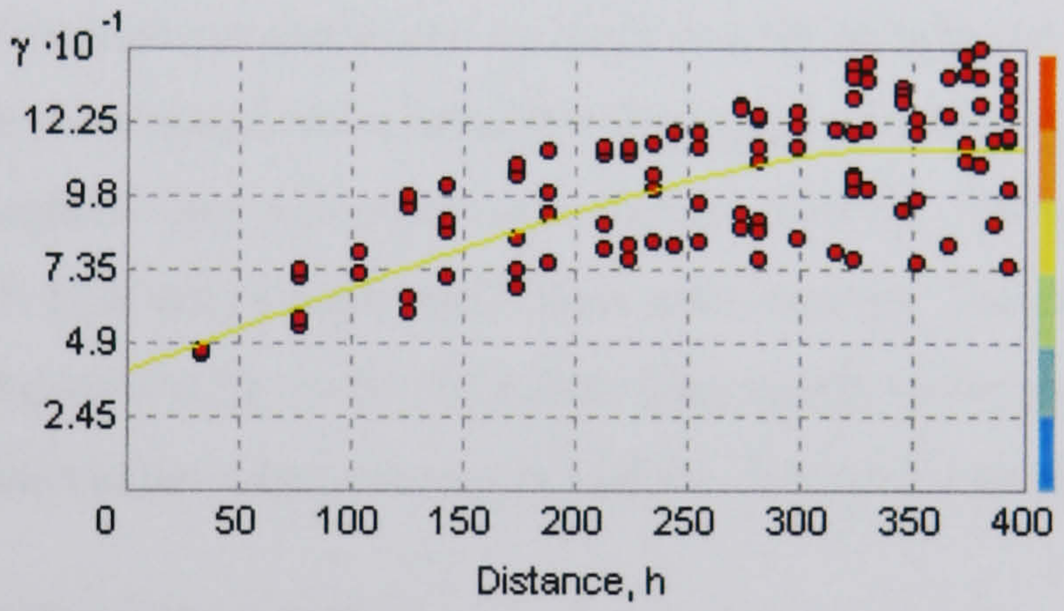

Figure 4.5 Example semivariograms for site 1 (ploughed almond field), site 5 (scrub) and site 6 (ploughed and flattened almond field)

Site	Land use	Geology	Gradient (°)	Model	Nugget	Range	Sill
1	Tree Crops	Red Schist	10	Circular	0	325	1617
2	Scrub	Blue Schist	15	Circular	1185	395	584
3	Tree Crops	Blue Schist	2.5	Hole-effect	174	250	230
4	Tree Crops	Blue Schist	25	Circular	96	261	116
5	Scrub	Red Schist	20	Circular	49	357	78
6	Tree Crops	Red Schist	3	Circular	39	334	74
7	Scrub	Blue Schist (Cardena)	10	Circular	61	395	258

Table 4.5 Parameters of the models fitted to the semivariograms of the soil surface roughness

The semivariograms fit either the circular or hole-effect models. With the hole-effect model, the current point may be related to another point 100 mm away, not related to a point 150 mm away but again be related to a point 200 mm away. This suggests a repeating pattern in the spatial structure. For site 3 this will result from the ploughing of the soil surface between the trees. The

remaining sites fit a circular model whereby the roughness stops being related to the current point beyond a certain distance.

The range of the semivariogram is the distance at which there ceases to be any spatial dependence (Oliver and Webster 1986). The average semivariogram range distance on scrub surfaces is 382 mm, which is greater than the average for tree crops of 292 mm. The shorter range on the tree crops relates to the regular reorganisation of the surface by ploughing. The average range distance of 292 mm relates to approximately half the furrow spacing and hence is the distance from the furrow base to the furrow top. After the field is abandoned and it reverts to a semi-natural scrub, the plough line features will erode and diffuse across the surface. This increases the range distance from the average of 292 mm to 382 mm.

The average range distance for the blue schist sites is 325 mm whereas the average range for red schist sites is 338 mm. The very similar average range values on the different geologies suggests that the land management is the key control on the spatial structure of the surface roughness at this scale. The values for the range do not show a consistent relationship with the plot slope.

The nugget of the semivariogram represents the variance at a lag distance of zero. This can be seen as a function of both the amount of non-spatially structured variation in the surface and variations occurring at a spatial scale below the measurement interval. The nugget effect does not vary significantly with land use or slope, but it does with geology. The average nugget on the blue schist is 379, compared to 29 on the red schist. This relates to the greater stone content in the blue schist soils which cause large changes in surface elevation over short distances.

4.3 Infiltration Characteristics

The infiltration characteristics were investigated using two techniques: rainfall simulation and minidisk infiltration experiments. Full details of the techniques are given in chapter 3.

4.3.1 Rainfall Simulation Results

The rainfall simulation experiments consisted of 25 minutes of rainfall at 73.3 mm hr^{-1}. The results from the experiments undertaken on scrub sites are given in Figure 4.6, and the result from experiments at agricultural field sites are given in Figure 4.7. The dry initial conditions simulations are shown in solid lines and the wet initial conditions simulations are shown in dashed lines. The field measured values from the rainfall simulation experiments are given in Appendix 1.

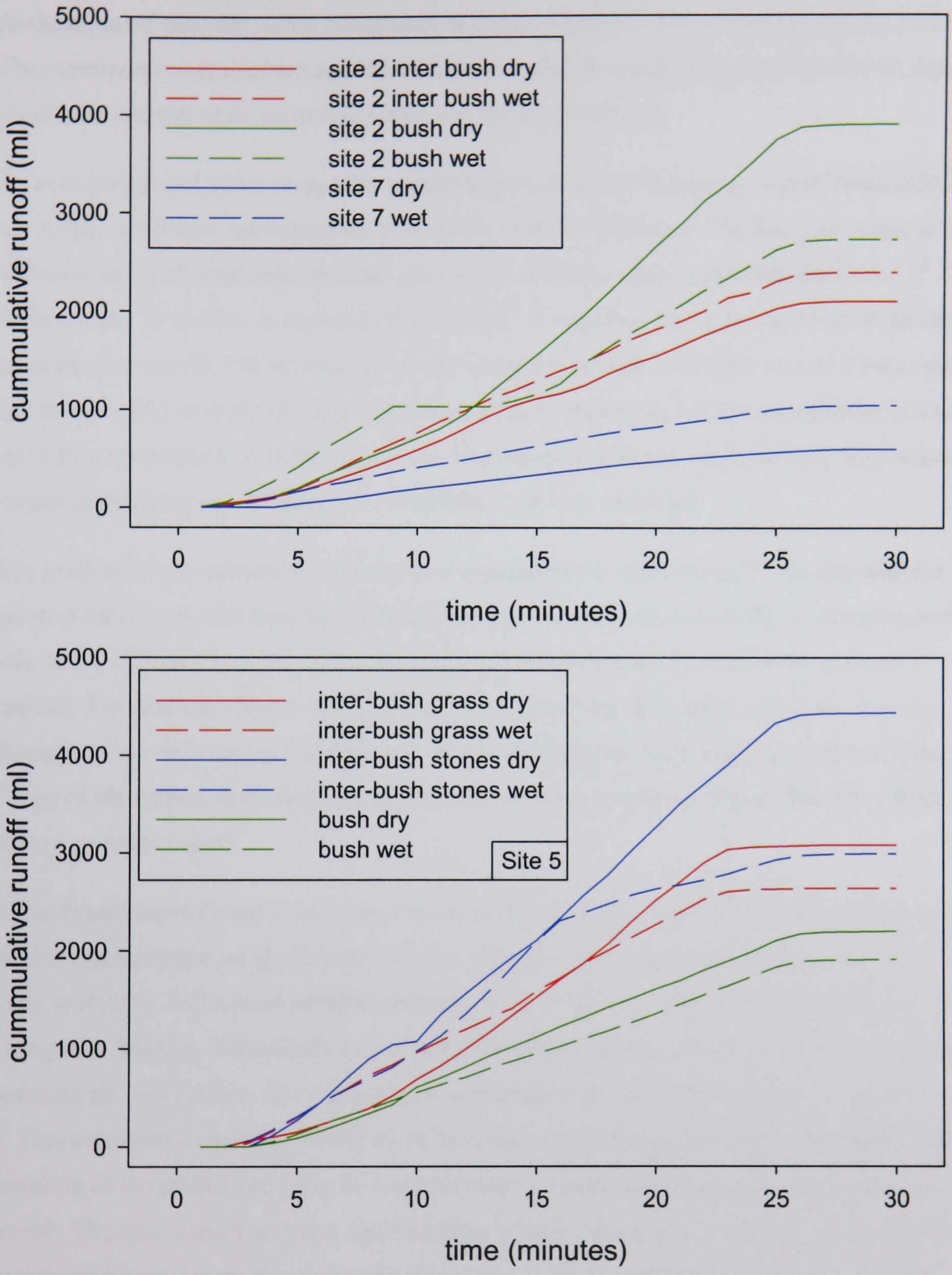

Figure 4.6 Rainfall simulation results from scrub surfaces

All of the scrub sites generate runoff shortly after the start of the rainfall. The experiment over a vegetated plot on site 2 gave the shortest time to runoff at 45 s for dry initial conditions and 32 s for wet initial conditions. The bare plot generated runoff after 49 s on dry initial conditions and after 42 s for wet initial conditions. Site 7 required the longest time to generate runoff at 256 s on dry initial conditions and 250 on wet initial conditions. All of the experiments at site five on the red schist soil required longer than site 2 on the blue schist. At site 5, the experiment over a vegetated plot took 180 s to generate runoff on dry initial conditions and this increased to 210 s

for wet initial conditions. The experiment over the bare surface with stones took 180 s to produce runoff with dry initial conditions, and this reduced to 108 s with wet initial conditions. The experiment over the bare surface with grass took 180 s to produce runoff with dry initial conditions and this reduced to 160 s with wet initial conditions.

At all experimental plots, except the vegetated plot on site 2, the time to runoff decreased on the wet initial conditions run compared with the dry initial conditions. The decrease is due to the reduction in infiltration capacity with greater soil moisture and the possible formation of a surface crust. Therefore, at the start of the rainfall, the surface has been conditioned for the rapid generation of runoff. The increase in time observed at the vegetated plot on site 2 may relate to air entrapment during the dry initial conditions run lowering the infiltration capacity and hence increasing the amount of runoff generated. During the wet initial condition run, there was no longer any trapped air and hence the infiltration capacity increased.

The gradient of the cumulative runoff curve represents the rate of runoff. The site with the greatest runoff rate was the stone covered bare plot at site 5. The site with the lowest runoff rate was on the bare plot at site 7. Most plots show a constant runoff rate after ten minutes of rainfall. The first ten minutes of rainfall is used to condition the surface. This involves the increase of the soil moisture and hence a lowering of the infiltration capacity. This enables the filling of the surface depression store. Once these stages have been completed, the surface is able to generate runoff.

Three experiments do not have a linear increase in cumulative runoff. The first is the experiment on the vegetated plot on site 2, which shows a change in the runoff rate after 12 minutes. The main *anthysis* L. bush covered approximately 50 % of the plot and when the runoff rate changes, it doubles. This relates to the canopy overflowing thus doubling the amount of water reaching the soil surface. The second is the experiment on the inter-bush area with grass at site 5. This cumulative runoff curve shows an increase in runoff rate over time. This relates to a lowering of the infiltration capacity with cumulative infiltration and hence the increase in runoff. The final experiment that does not have a linear increase in cumulative runoff is the wet initial conditions run on the vegetative plot at site 2. This is related to the blocking of the outflow pipe by material transported from the soil surface. However, the sections of the curve either side of the blockage are linear.

The simulated rainfall lasted for 25 minutes (22 minutes on the inter-bush with grass experiment at site five). Most plots show a small amount of runoff in the first minute following the cessation of rainfall followed by negligible runoff. Site 7, on the very stony surface in the upper Cardena, shows a far slower decrease in runoff which lasts for 3 minutes following cessation of rainfall.

The experiment which gave the greatest volume of runoff was the dry initial conditions simulation on the inter-bush with stones plot at site 5. This is closely followed by the dry initial conditions simulation on the bush plot at site 2. The lowest runoff volume was obtained from the dry initial conditions simulation at site 7. At all of the experiments at sites 5 and 7 and the bush experiment at site 2, the dry initial conditions experiments gave greater runoff volume than the wet initial conditions. This may relate to air entrapment during the dry initial conditions experiment. When water infiltrates into a dry soil at relatively high rates, the soil air is displaced by the water and becomes compressed ahead of the wetting front. This displaced soil air can significantly lower the infiltration capacity (Wang et al. 1998). During the one hour period between the experiments, the water in the upper layers of the soil is able to move down through the soil profile and the air is able to escape. Hence, the upper layers are now wet without the trapped air. This has the effect of increasing the infiltration capacity of the soil and can explain the observed lower runoff volumes on the wet initial conditions simulations.

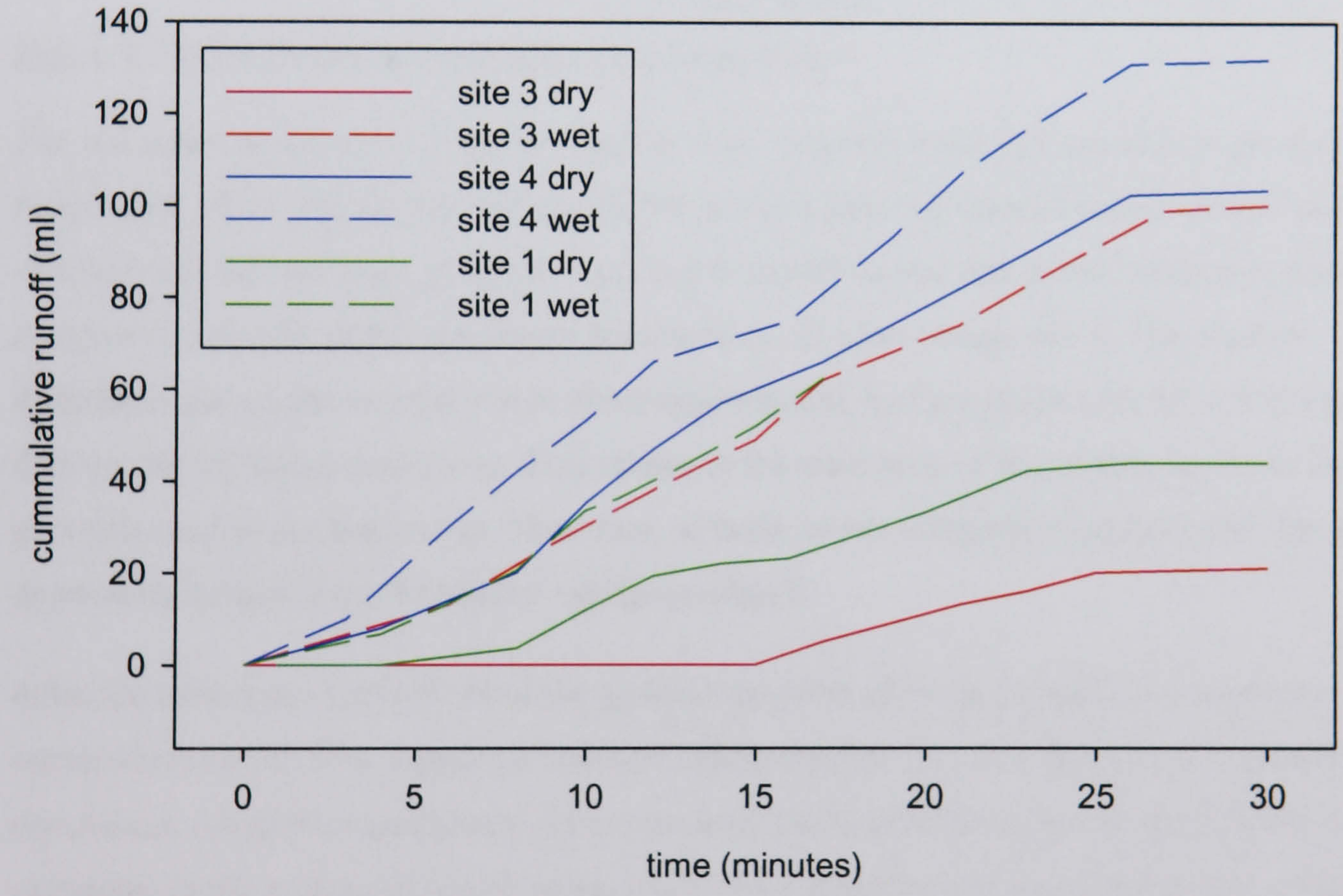

Figure continued on next page.

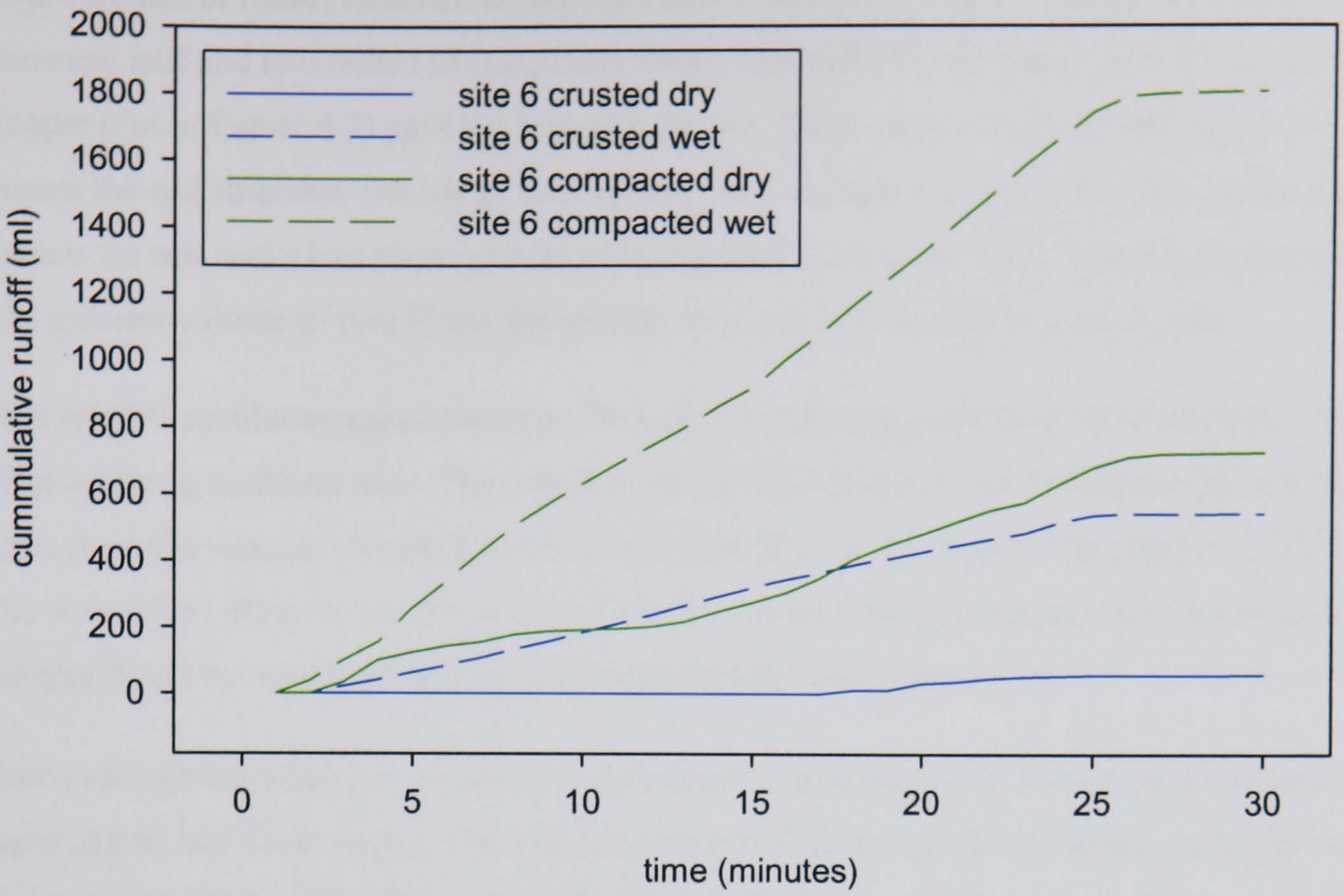

Figure 4.7 Rainfall simulation results agricultural fields

The red schist plot at site 1 gave the shortest time to runoff under dry conditions, producing runoff after 180 s. The crusted red schist plot at site 6 gave the longest time to runoff at 1020 s although this was on a low gradient. The time to runoff for the wet initial conditions simulation compared to the dry initial conditions decreased on all plots except site 1. The greatest difference was on the crusted plot at site 6 where runoff was produced after 68 s, 952 s earlier than on the dry initial conditions. This relates to the saturation of the surface layers in the previous rainfall simulation run. Therefore, with the lower infiltration capacity and low surface depression storage, runoff could be rapidly produced.

After the initiation of runoff, all of the agricultural plots show an overall linear increase in cumulative runoff. This suggests a constant infiltration rate over the duration of the rainfall simulation. All of the curves have deviations from the overall linear trend. These relate to the variations in the routing of runoff across the surface whereby water may be held in a small surface dam resulting in a decrease in discharge, and then released resulting in an increase in discharge.

The experiment at site 1 with wet initial conditions ended prematurely due to the disintegration of the plot. This resulted from the formation of a water table above the bedrock and the soil at the front face of the plot failing and flowing out as a small mud flow. This shows the rapid vertical water movement in these ploughed fields and the possibility of mass failure in the form of mud flows given sufficient rainfall.

The volumes of runoff obtained during the rainfall simulations on the agriculture plots are between half and two orders of magnitude lower than those on the scrub plots. Sites 1, 3 and 4 (upper plot in Figure 4.7) gave the lowest volumes. These sites were ploughed regularly and hence the soil structure was loose. Site 6 (lower plot in Figure 4.7) was on a low gradient site where the soil was a two phase system of crusted and compacted soils. The compacted soil gave the greatest volume of runoff and the amount of runoff was similar to a scrub plot.

The rainfall simulation experiments performed in scrub sites gave far greater amounts of runoff than on the agricultural sites. The runoff from the experiment on the compacted soil at site 6 gave a similar amount of runoff as a low runoff producing scrub plot. The greater runoff from the scrub sites relates to the formation of a surface crust. On agricultural sites, this crust is broken down by regular ploughing and results in less runoff generation.

Due to the strong influence of land use, the impact of geology has been separated out into both agricultural and scrub slopes. The average total runoff from agricultural plots in greater on the red schist at 540 ml (SE 279) compared to 89 ml (SE 24) on the blue schist. The average total discharge from red schist scrub slopes is greater at 2875 ml (SE 363) opposed to 2131 ml (SE 485) on the blue schist scrub slopes. However, due to the limited number of samples and the structuring of the sampling scheme, these values must be treated with care. Much of the high average runoff volume from the red schist on agricultural land results from the experiments taken on compacted soil. A clearer picture is given by the minidisk infiltration results where more measurements were taken and hence there is a better representation of the variability in the system.

4.3.2 Minidisk Infiltration Results

Minidisk infiltration experiments were undertaken at each of the cover types covered by the rainfall simulation experiments and in the channels. The mean and coefficient of variation (COV) for each plot is given in Table 4.6. The field measured values from the minidisk infiltration experiments are given in Appendix 1.

Site	Land use	Geology	Mean (mm hr^{-1})	COV	*n*
1	Agriculture	Red	13.8	1.00	12
2	Scrub	Blue	11.6	1.04	12
3	Agriculture	Blue	41.4	1.07	13
4	Agriculture	Blue	37.2	0.65	12
5	Scrub	Red	15.7	1.76	11
6	Agriculture	Red	71.4	0.91	10
7	Scrub	Blue	5.9	3.10	6
8	Channel bed	Blue	51.5	1.24	36
9	Channel bed	Blue	10.6	0.80	53
10	Channel bed	Blue	34.2	1.06	30

Table 4.6 The mean and coefficient of variation (COV) of infiltration capacity from the minidisk infiltration experiments

Agricultural sites have the highest infiltration capacities with a maximum mean rate of 71.38 mm hr^{-1}. The scrub sites have lower infiltration capacities with a minimum mean of 5.91 mm hr^{-1}. The experiments conducted at channel bed sites have infiltration capacities between the agricultural sites and the scrub with a mean of 32.1 mm hr^{-1}. The greater infiltration capacities on the agricultural sites relate to the removal of any surface crust by the regular ploughing. This manipulation of the surface also decreases the bulk density, hence allowing greater infiltration.

There is not a consistent relationship between the land use or geology and the COV. The site with the highest variability is site 7 with a COV of 3.1. This site has almost complete stone cover and hence the surface variability in infiltration capacity is expected to be high. Site 9 is the channel bed in Sub catchment 9 and has the lowest variability with a COV of 0.8.

4.3.3 Infiltration Characteristics Summary

The rainfall simulation experiments showed that there are large differences in the infiltration rates between the land cover types considered. The greatest infiltration rates were measured on the agricultural sites. The regular ploughing of these soils removes the surface crust and increases the soil porosity and hence leads to the increase in the infiltration capacity. The rainfall simulation experiments conducted on scrub sites found far lower infiltration capacities. It was found that there are significant differences between the infiltration characteristics on the inter-bush areas and the vegetated areas. This will lead to a spatial pattern of runoff sources and sinks.

The minidisk infiltration experiments also showed that the greatest infiltration capacities are found on the agricultural sites with lower rates recorded on the scrub sites. The experiments showed that there is significant local variation in the infiltration capacities. However, the variation does not vary significantly with geology or land use. This may relate to the finite sample being unable to fully capture the variability of the infiltration capacities.

4.4 Controls on Runoff Generation

The aim of this analysis is to determine the most significant controls on the generation of runoff to enable the prediction of the spatial pattern of runoff generation at the larger scale. It will also aid the development and parameterisation of a mathematical simulation model of runoff generation. This model will enable the investigation of the influence of flow connectivity upon the amount of water leaving the slope.

The rainfall simulation data has been analysed by decomposing the hydrograph and relating the component parts to the plot characteristics. This is presented in section 4.4.1. The minidisk data has been analysed using Mann-Whitney U tests to consider the differences between the main sampling factors. This is presented in section 4.4.3.

4.4.1 Analysis of Rainfall Simulation Results

From the literature, a number of important factors in controlling the form of the hydrograph have been identified. These can be grouped into storm characteristics, surface characteristics and soil properties. To quantitatively assess the relationships between plot properties and the runoff hydrograph form, the hydrograph was decomposed into a number of parts, Figure 4.8, and is described below.

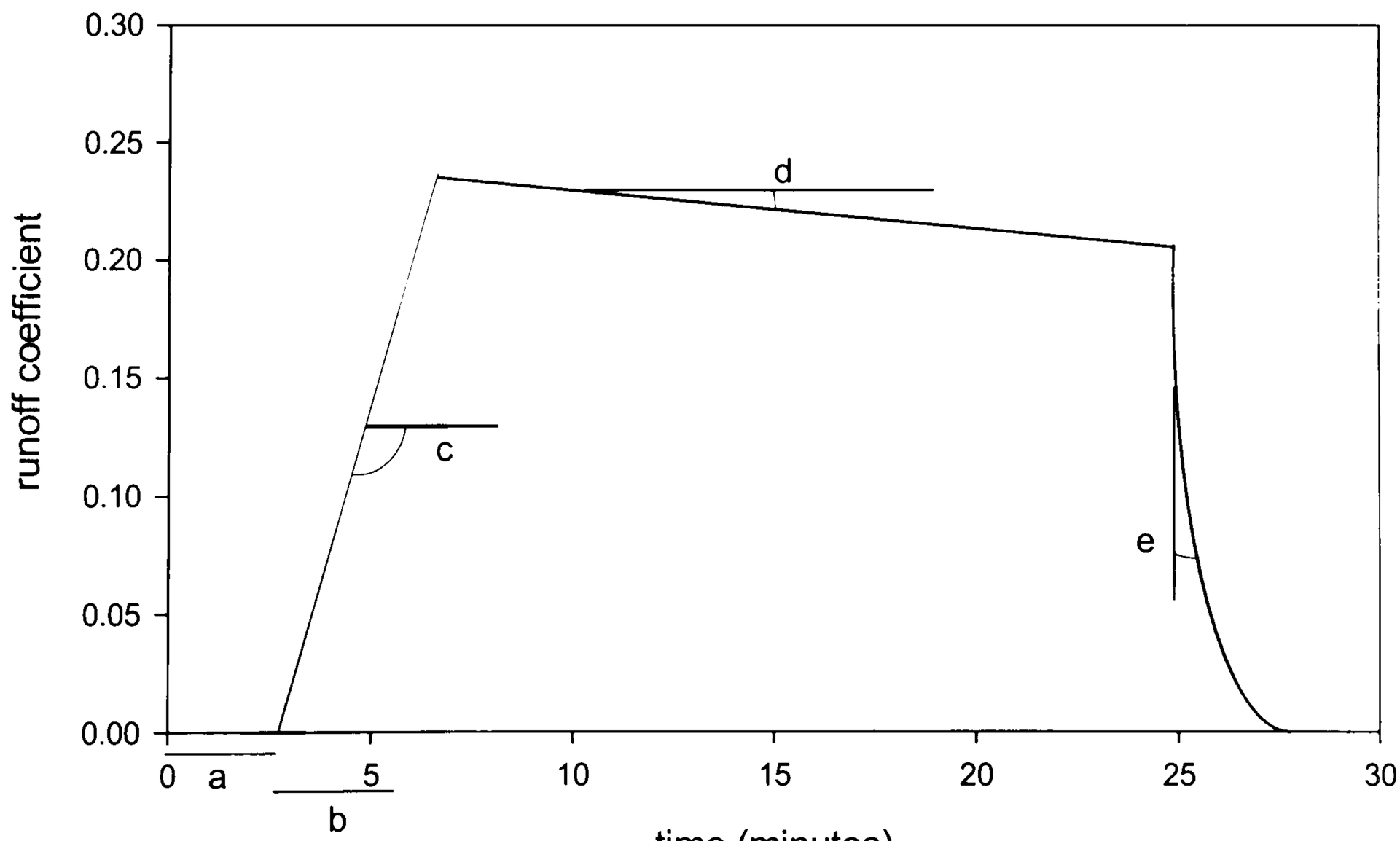

a = time to runoff
b = time to peak runoff
c = slope of rising limb
d = slope of back
e = slope of receding limb

Figure 4.8 Model of the runoff hydrograph

Time to ponding

The time to ponding is defined as the time in seconds from the start of the rainfall until the water is ponding on the soil surface. At this point the rainfall rate is exceeding the current infiltration rate and the water is being held by the surface roughness.

Time to runoff

The time in seconds from the start of the rainfall until water leaves the plot. The depth of the ponded water is sufficient to overcome the resistance of the surface roughness

Depth of rainfall required to generate runoff

Strongly associated with the time to runoff is the depth of rainfall required to generate runoff. This is a function of the time to runoff, the rainfall intensity, the infiltration rate and the depth of the detention store.

Time to peak runoff

This is the time in seconds from the start of runoff until the initial peak runoff.

Mean runoff coefficient

The mean runoff coefficient is the ratio of received rainfall to the amount of runoff for the whole rainfall event.

Peak runoff coefficient

The peak runoff coefficient is calculated in the same way as the mean runoff coefficient but only considers the measurement period with the greatest amount of runoff.

Slope of rising limb

The slope of the rising limb was determined by fitting a linear regression model to the values of the runoff coefficient. The range over which the model was fitted is defined by the start of runoff until the initial peak, as used in the time to peak runoff. The slope term of the model was then used in the analysis.

Slope of back

The slope of the back was determined by fitting a linear regression model to the values of the runoff coefficient. The range over which the model was fitted was defined as the peak runoff and the cessation of rainfall. The slope term of the model was then used in the analysis. This variable gives information on the changes in runoff rates during the rainfall event.

Slope of receding limb

The slope of the receding limb was determined by fitting an exponential model to the rc values after the cessation of rainfall. The slope term was used in this analysis. This variable gives information on the time required for runoff to cease following the end of rainfall.

Evolution of the runoff coefficient during the storm

The runoff coefficients were calculated at 5, 10, 15, 20 and 25 minutes after the start of rainfall to give an insight into how the importance of different factors change during the rainfall event.

In order to determine which factors have the most significant influence on the form of the runoff hydrograph, a bivariate correlation analysis was performed. The majority of the data is non-normally distributed and has a low n value, therefore, the non-parametric Spearman's Rank correlation coefficient has been used. Scatter plots of the relationships with significant correlations (>95 %) are shown in Figure 4.9. The correlation matrix is shown in Table 4.7, the relationships which are significant at the 95 % level are highlighted in light grey and those significant that the 99 % level are highlighted in dark grey.

Table 4.7 Correlation matrix of plot properties and runoff characteristics from the rainfall simulation experiments

Hydrograph parameters		*Storm Characteristics* Rainfall Depth	Run length	Intensity	*Cover Composition* Soil	Stones	Biomass	*Plot Characteristics* Slope	Roughness	Soil Depth	*Soil Matrix Composition* Stones	Sand	Silt	Clay	Bulk Density
Time to ponding	Correlation Coefficient				0	0		0		0	0	0	0		0
	sig. (2-tailed)				1	1		1		1	1	1	1		1
	n	4	4	4	4	4	4	4	2	4	4	4	4	4	4
Time to runoff	Correlation Coefficient	-0.434	0	**-.600(**)**	-0.241	**.611(**)**	-0.442	-.529(*)	.643(*)	0.138	-0.088	0.011	0.081	-0.156	**.508(*)**
	sig. (2-tailed)	0.072	1	**0.009**	0.336	**0.007**	0.066	0.024	0.045	0.584	0.728	0.965	0.749	0.536	**0.031**
	n	18	18	18	18	18	18	18	10	18	18	18	18	18	18
Time to peak runoff	Correlation Coefficient	0.432	0.239	0.382	0.171	**-.549(*)**	**.574(*)**	**.725(**)**	-0.368	-0.039	-0.338	0.468	0.151	0.132	-0.128
	sig. (2-tailed)	0.073	0.34	0.118	0.498	**0.018**	**0.013**	**0.001**	0.295	0.877	0.17	0.05	0.548	0.603	0.612
	n	18	18	18	18	18	18	18	10	18	18	18	18	18	18
Rainfall required to generate runoff	Correlation Coefficient	-0.434	0	**-.600(**)**	-0.241	**.611(**)**	-0.442	-.529(*)	**.643(*)**	0.138	-0.088	0.011	0.081	-0.156	.508(*)
	sig. (2-tailed)	0.072	1	**0.009**	0.336	**0.007**	0.066	0.024	**0.045**	0.584	0.728	0.965	**0.749**	0.536	**0.031**
	n	18	18	**18**	18	**18**	18	18	**10**	18	18	18	**18**	18	**18**
Slope of rising limb	Correlation Coefficient	-0.127	-.424(*)	0.185	-0.186	-0.059	0.24	-0.297	-0.257	-0.2	0.119	-0.089	-0.031	0	-0.27
	sig. (2-tailed)	0.574	0.049	0.41	0.407	0.795	0.282	0.179	0.375	0.371	0.596	0.694	0.892	1	**0.224**
	n	22	22	22	22	22	22	22	14	22	22	22	22	22	22
Slope of back	Correlation Coefficient	0.075	-0.025	0.118	0.227	-0.208	-0.057	-0.06	0.292	0.247	0.155	-0.166	0.087	0.273	**-0.126**
	sig. (2-tailed)	0.74	0.912	0.602	0.309	0.352	0.801	0.79	0.31	0.268	0.492	0.46	0.699	0.218	**0.576**
	n	22	22	22	22	22	22	22	14	22	22	22	22	22	22
Slope of receding limb	Correlation Coefficient	-0.518	.	-0.518	-0.447	0.532	-0.237	-0.363	0.632	-0.564	-0.025	0.303	-0.43	-0.52	**.768(*)**
	sig. (2-tailed)	0.154	.	0.154	0.227	0.141	0.539	0.337	0.252	0.113	0.948	0.428	0.248	0.152	**0.016**
	n	9	9	9	9	9	9	9	5	9	9	9	9	9	**9**
Runoff coefficient (Rc)	Correlation Coefficient	0.167	-0.349	.504(*)	-0.121	-.469(*)	**.581(**)**	0.271	-.656(*)	-0.314	-0.063	0.19	0.024	0.257	-0.351
	sig. (2-tailed)	0.457	0.111	0.017	0.59	0.028	**0.005**	0.222	0.011	0.155	0.782	0.397	0.916	0.248	0.109
	n	22	22	22	22	22	**22**	22	14	22	22	22	22	22	22
Peak Runoff Coefficient	Correlation Coefficient	0.238	-0.299	**-.555(**)**	0.044	-.532(*)	.591(**)	.444(*)	-0.488	-0.293	-0.163	0.369	0.118	**.443(*)**	-0.294
	sig. (2-tailed)	0.286	0.176	**0.007**	0.847	0.011	**0.004**	0.039	0.076	0.186	0.469	0.091	0.601	**0.039**	0.185
	n	22	22	**22**	22	22	**22**	22	14	22	22	22	22	**22**	22
Rc t5	Correlation Coefficient	0.24	-0.194	.470(*)	-0.125	-0.419	.535(*)	0.272	-0.514	-0.342	-0.002	0.19	-0.048	0.183	-0.277
	sig. (2-tailed)	0.283	0.388	0.027	0.58	0.052	0.01	0.221	0.06	0.12	0.994	0.397	0.833	0.414	0.212
	n	22	22	**22**	22	22	22	22	14	22	22	22	22	22	22
Rc t10	Correlation Coefficient	-0.079	-0.388	0.218	-0.074	-0.38	0.417	0.278	**-.736(**)**	-.535(*)	-0.255	0.395	0.103	0.067	-0.007
	sig. (2-tailed)	0.728	0.074	0.33	0.743	0.081	0.054	0.211	**0.003**	0.01	**0.252**	0.069	0.648	**0.768**	**0.975**
	n	22	22	22	22	22	22	22	**14**	22	**22**	22	22	**22**	**22**
Rc t15	Correlation Coefficient	0.116	-0.369	.454(*)	-0.126	**-.436(*)**	**.601(**)**	0.375	**-.729(**)**	-.445(*)	-0.193	0.365	0.056	0.271	**-0.233**
	sig. (2-tailed)	0.607	0.091	0.034	0.575	**0.043**	**0.003**	0.086	**0.003**	0.038	0.39	**0.095**	0.806	**0.223**	**0.296**
	n	22	22	22	22	22	**22**	22	**14**	22	22	22	22	**22**	**22**
Rc t20	Correlation Coefficient	0.153	-0.411	.536(*)	-0.04	**-.566(**)**	.523(*)	.440(*)	**-.685(**)**	-0.384	**0.012**	0.176	-0.026	0.364	**-0.227**
	sig. (2-tailed)	0.497	0.058	0.01	0.861	**0.006**	0.013	0.041	**0.007**	0.077	**0.959**	0.432	0.908	0.095	**0.31**
	n	22	22	22	22	**22**	22	22	**14**	22	22	22	22	22	**22**
Rc t25	Correlation Coefficient	**.544(**)**	0.18	**.556(**)**	-0.006	**-.616(**)**	.506(*)	.485(*)	-.573(*)	-0.255	0.039	0.194	**-0.011**	0.241	**-0.295**
	Sig. (2-tailed)	**0.009**	0.422	**0.007**	0.977	**0.002**	0.016	0.022	0.032	0.252	0.864	0.386	**0.963**	**0.279**	**0.183**
	n	22	22	**22**	22	22	22	22	14	22	22	22	**22**	22	**22**

** Correlation is significant at the .01 level (2-tailed).
* Correlation is significant at the .05 level (2-tailed).

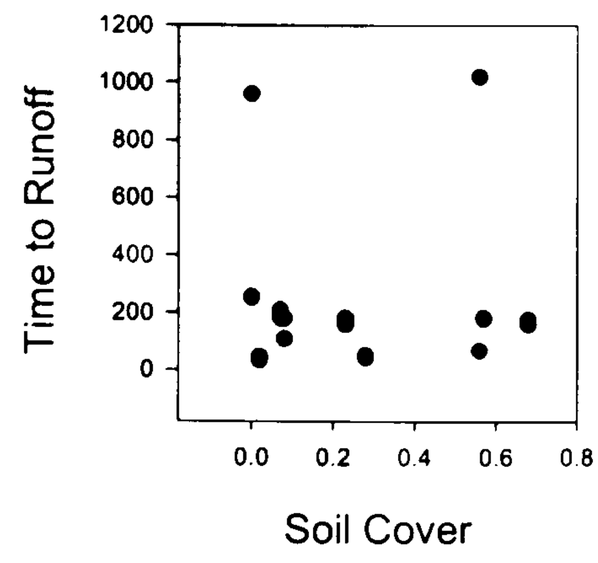

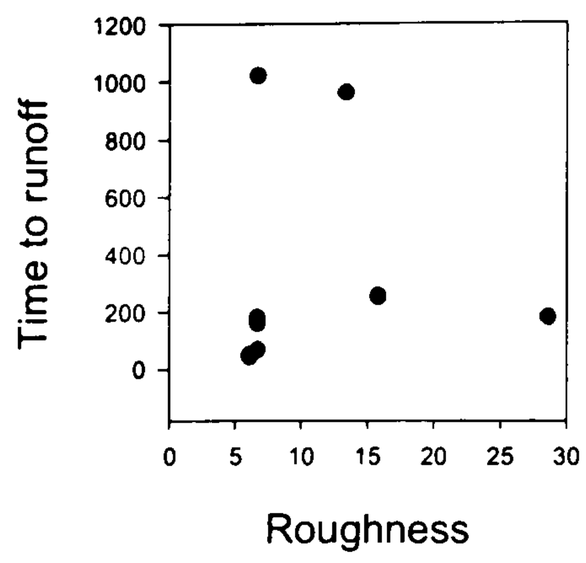

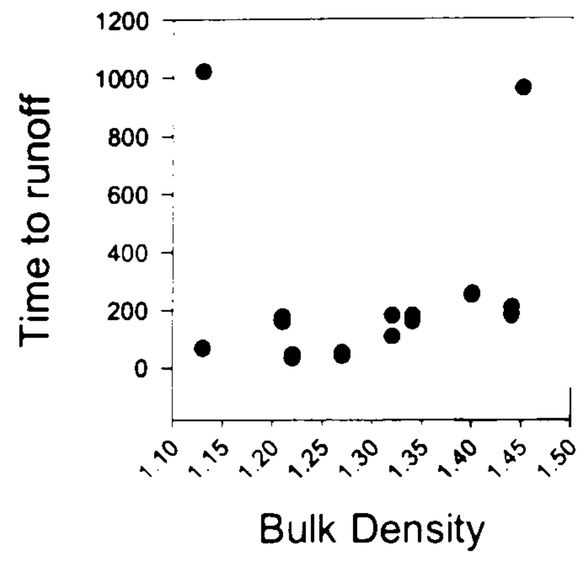

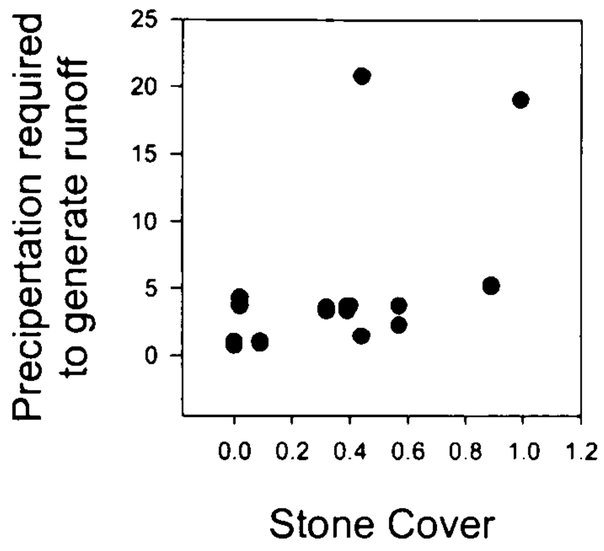

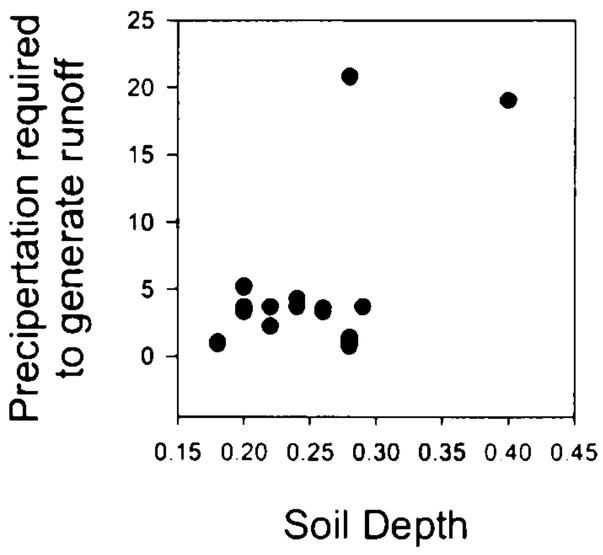

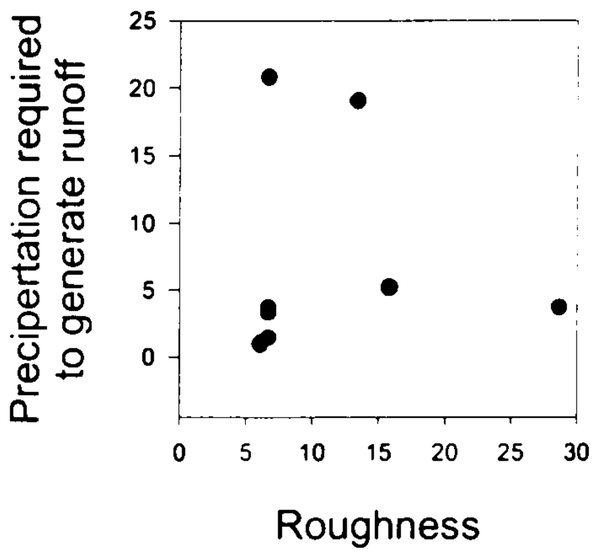

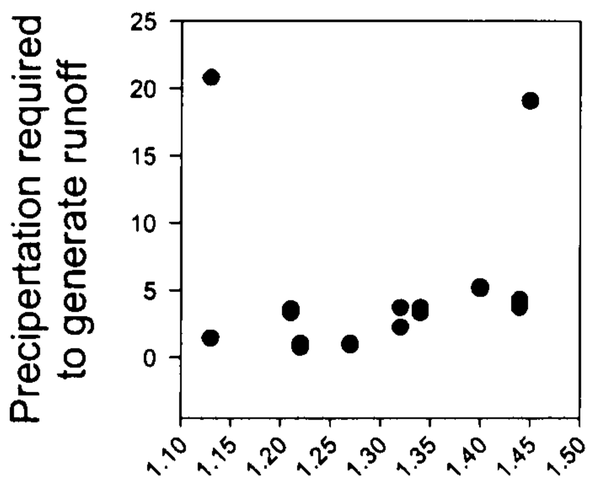

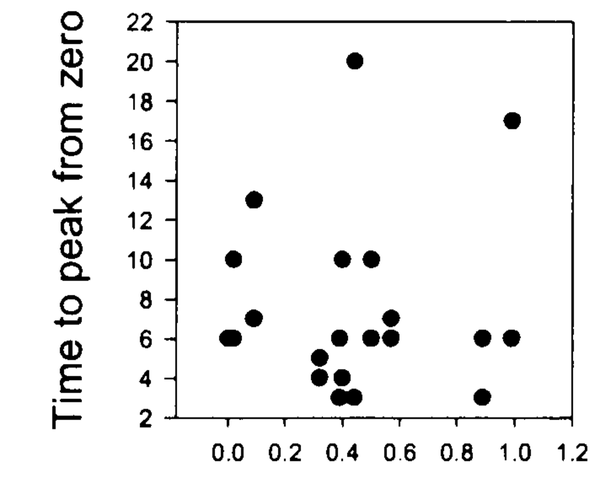

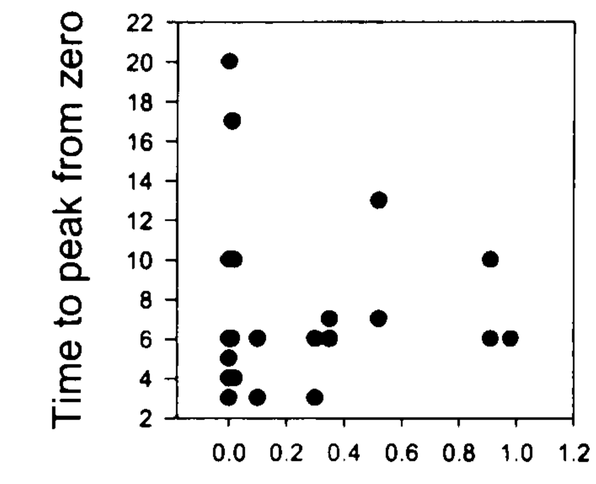

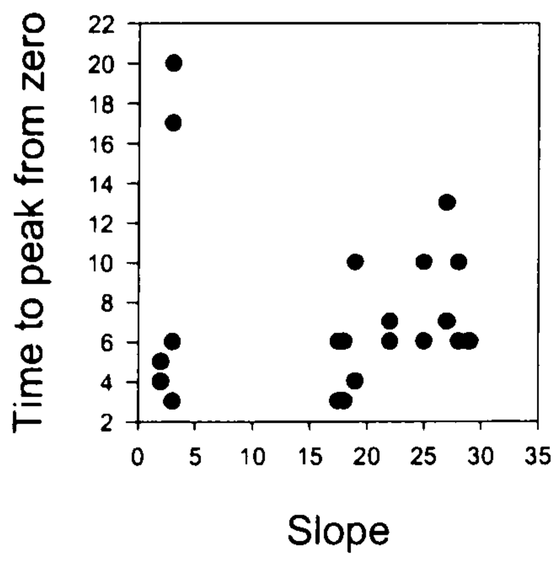

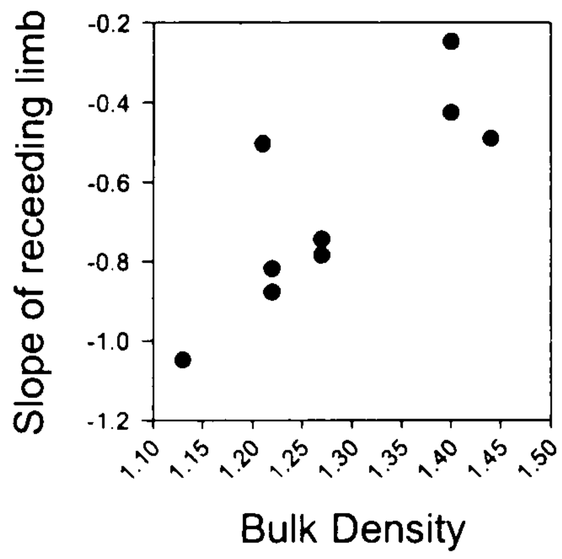

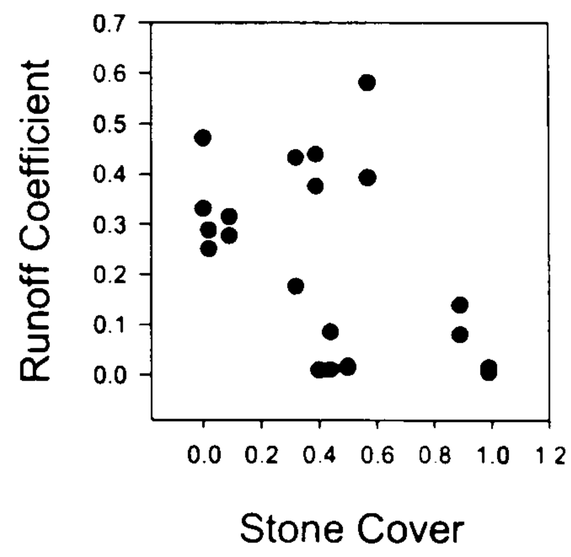

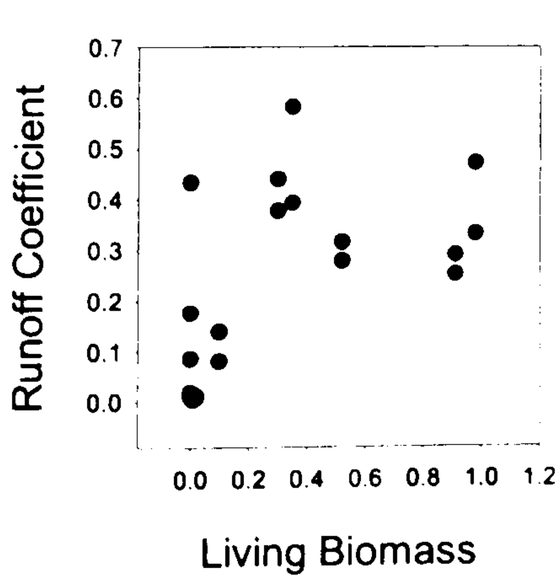

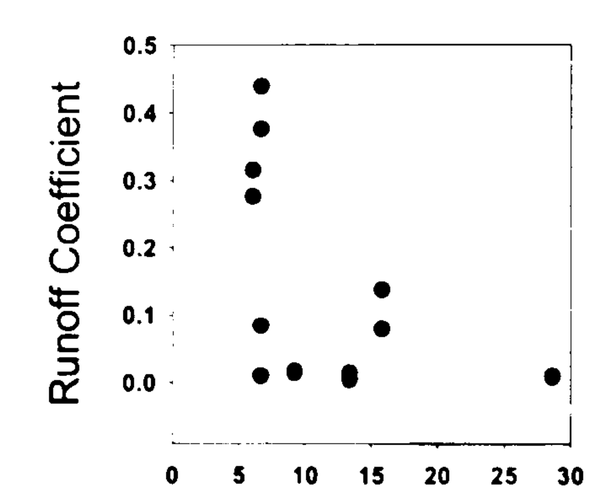

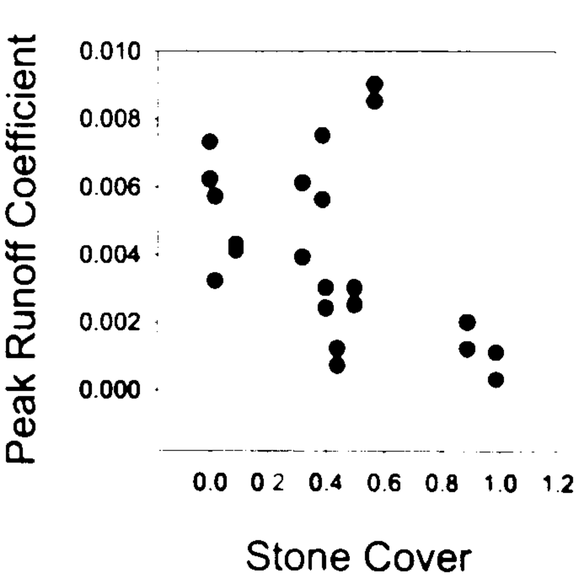

Figure continued on next page.

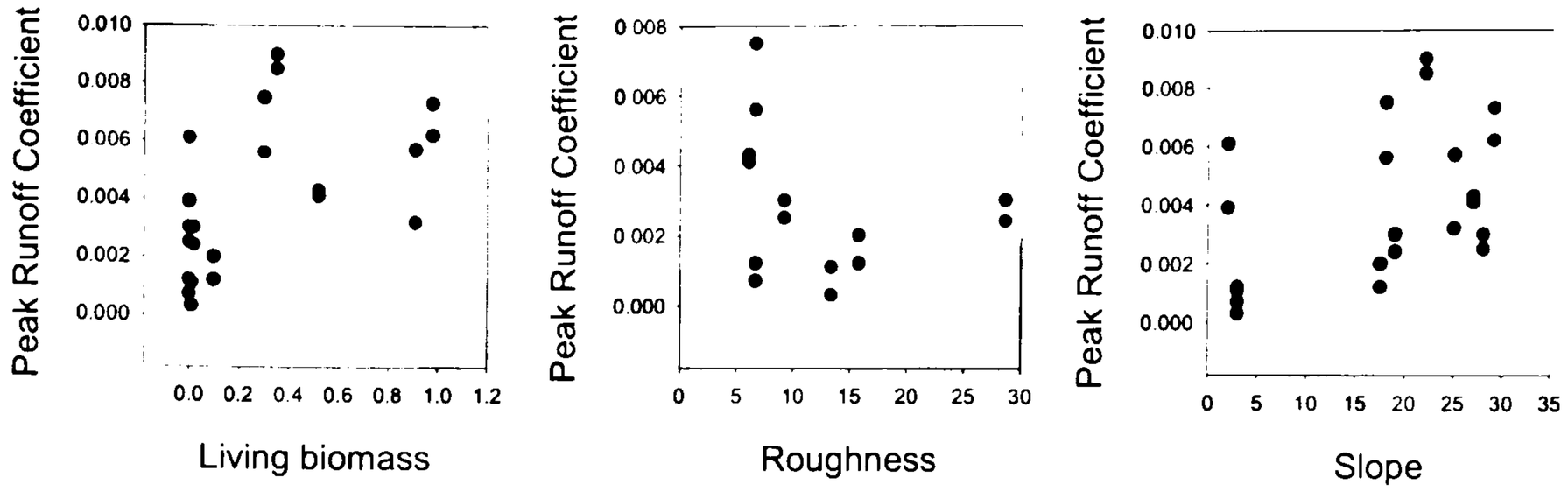

Figure 4.9 Scatter plots of significant (>95 %) correlation relationships

The effects of rainfall intensity variations were not investigated as part of the fieldwork. Due to slight variations in the parameter value during fieldwork, it was included in the analysis. The range of values is very small and hence no conclusions about the effects of rainfall intensity upon the form of the runoff hydrograph can be drawn from this dataset.

From the correlation matrix it can be seen that the factors which influence the greatest number of hydrograph parameters are the surface cover of stones (5) and the slope of the plot (4). The surface cover of biomass (3), the surface roughness (3), and the bulk density of the soil (3) have a lesser influence while the storm length (1) and the clay content (1) have a marginal influence. The surface cover of soil, dead biomass, stone, sand and silt content of the soil had no significant correlations with any of the hydrograph properties. The numbers in the brackets relates to the number of hydrograph form properties the factors are significantly related to.

Stone Cover

The surface stone cover has been found to be related to the time to runoff (0.61, sig. 0.01), the depth of rainfall required to generate runoff (0.61, sig. 0.01), the mean runoff coefficient (-0.47, sig. 0.05), the peak runoff coefficient (-0.53, sig. 0.01) and the time to peak runoff (-0.55, sig. 0.05).

The relationship between the time to runoff and the surface stone cover and the relationship between the depth of rainfall required to generate runoff and the stone cover are positive and linear with a large amount of scatter. As the stone cover increases, the detention storage and the number of macropores will increase. This will lead to a longer time to runoff on plots with

higher stone cover. With greater stone cover, there is an increase in the detention storage and the number of macropores. Therefore, a greater amount of water is required to fill these stores before runoff is initiated.

There is a large amount of scatter and no obvious trend in the relationships between the mean and peak runoff coefficients and the surface stone cover. The scatter is far greater when the stone cover is between 30 % and 60 %. The relationship between the time to peak runoff and the surface stone cover shows a negative trend with a large amount of scatter. The negative trend may be approximated by either a linear or a logarithmic model. As the amount of surface stone cover increases, the amount of scatter decreases. Therefore, the importance of stone cover is proportional to percentage cover.

Slope Gradient

The slope gradient was found to be related to the time to runoff (-0.53, sig. 0.05), the depth of rainfall required to generate runoff (-0.53, sig. 0.05), the time to peak runoff (0.73, sig. 0.01) and peak runoff coefficient (0.44, sig. 0.05).

The relationship between the slope gradient and the depth of rainfall required to generate runoff shows a negative trend with three outliers. Either a linear or logarithmic regression model could be fitted to the data. Further information on the effects of slopes between 5° and 15° would be required to determine the form of this relationship.

The relationship between the peak runoff coefficient and the surface gradient shows a large amount of scatter and no visible trend. Due to the sampling scheme, no slopes between 5° and 15° were sampled. The range of scatter is as great in the lower slope values as in the high slope values suggesting that there is no trend in the data.

The relationship between the time to peak runoff and the surface gradient shows significant scatter with a positive linear trend. This is due to the lower surface depression store depths at greater slope gradients and the increase in flow velocity across the plot. There is greater scatter at lower slope values with a stronger trend for steeper slopes. Therefore, the effect of slope is proportional to the gradient with higher gradients having the most influence.

Biomass Cover

The surface cover of biomass has been found to be related to the mean runoff coefficient (0.58, sig. 0.01), the peak runoff coefficient (0.59, sig. 0.01) and the time to peak runoff (0.57, sig. 0.01).

The relationship between the mean runoff coefficient and the surface biomass cover shows a logarithmic trend with significant scatter. The trend reaches a plateau after the biomass cover

reaches 30 %. This suggests that the mean runoff coefficient is very sensitive to change in the living biomass cover below 30 % and far less sensitive above this point.

The relationship between the peak runoff coefficient and the cover of biomass shows a large amount of scatter. The values are generally higher at greater cover values, but without an overall trend. There is the possibility of two process domains, with there being a different range of values at plots with cover values below 20 % to those over 20 %.

The relationship between the time to peak runoff and the cover of biomass shows significant scatter and possibly three separate domains. The first of these relates to the plots with slight vegetation cover, <10 %. In this domain there is a large amount of scatter and the biomass has little effect on the time to peak runoff. The second domain ranges from 10 % - 50 % cover where there is a strong positive linear relationship. The third domain is between 80 % and 100 % cover where there is a large amount of scatter and no obvious trend.

Surface Roughness

The surface roughness was found to be significantly related to the time to runoff (0.64, sig. 0.05), the depth of rainfall required to generate runoff (0.64, sig. 0.05), and the runoff coefficient (-0.66, sig. 0.01). The surface roughness was characterised by the Random Roughness coefficient (RR).

The relationship between time to runoff and RR shows a large amount of scatter. There is a general positive trend. However, due to the limited amount of data, it is not possible to assess the form of the relationship. The lower times to runoff at the higher roughness values may be related to land management, especially ploughing of the soil.

The relationship between the RR and the depth of rainfall required to generate runoff, shows a cluster of values around RR≈7 and four significant outliers. There is no apparent overall trend in the data.

The relationship between the mean runoff coefficient and the RR shows a negative linear or possible logarithmic trend with a large amount of scatter. At low roughness values (RR≈8) there is a larger amount of scatter than at greater roughness values (RR≈15). This suggests that the influence of roughness is greater at high roughness values.

Soil Bulk Density

The bulk density of the soil was found to be related to the time to runoff (0.51, sig. 0.05), the depth of rainfall required to generate runoff (0.508, sig. 0.05) and the slope of the receding limb (0.77, sig. 0.05).

The relationship between the bulk density of the soil and the time to runoff is positive linear with two significant outliers. In terms of the porosity of the soil, as the soil approaches solid rock, the time to runoff increases and as the soil has more pore space, the shorter the time to runoff. This may seem counterintuitive however, the samples with the high bulk densities resulted from a greater volume of stones in the soil. These stones create macropores around their edges and hence can increase the infiltration capacity of the soil.

The relationship between the bulk density of the soil and the depth of rainfall required to generate runoff, shows a positive linear trend with significant scatter and two outliers. The reasons for the direction of this trend will be due to the stone content of the soil influenceing the bulk density measurements, similar to the relationship between the time to runoff and bulk density. The larger macropore storage component will require a greater depth of rainfall before runoff is initiated.

The slope of the receding limb was found to be significantly correlated with the bulk density of the soil (0.768, sig. level 0.02). There is a positive linear trend between the data series. Since the bulk density of the soil is inversely related to the porosity, the relationship may be expressed in terms of the porosity. As the porosity decreases, the time to cessation of runoff increases.

Evolution of the Runoff Coefficient during the Storm

The times during the storm event when different parameters have a significant (>95 %) correlation with the runoff coefficient (*rc*) are shown in Figure 4.10. During the initial period, the only parameter which has a significant effect on the *rc* is the living biomass cover (0.535, sig. 0.01). The living biomass cover will influence the runoff hydrograph through the interception of water, hence reducing the amount of water reaching the ground.

After ten minutes, the key parameters have changed to the surface roughness (-0.736, sig. 0.003) and the soil depth (-0.535, sig. 0.01). During this period the living biomass cover is not significantly correlated but it is before and after this period. The surface roughness starts to be significantly related and continues to be until the end of the rainfall event. The correlation coefficient drops from -0.769 (sig. 0.003) after ten minutes to -0.573 (sig. 0.032) after 25 minutes.

After 15 minutes the biomass cover is significantly correlated again and the surface stone cover starts to be significantly correlated. All of these parameters continue to be significantly correlated until the end of the rainfall event. The correlation coefficient for the surface stone cover increases from -0.436 (sig. 0.043) after fifteen minutes to -0.616 (sig. 0.002) after 25 minutes. The correlation coefficient for biomass decreases from 0.601 (sig. 0.003) after fifteen minutes to 0.506 (sig. 0.016) after 25 minutes.

After 20 minutes the soil depth ceases to be significantly correlated with the rc. The slope of the surface starts to be significantly correlated (0.44 sig. 0.041) and after 25 minutes the correlation coefficient increases to 0.485 (sig. 0.022).

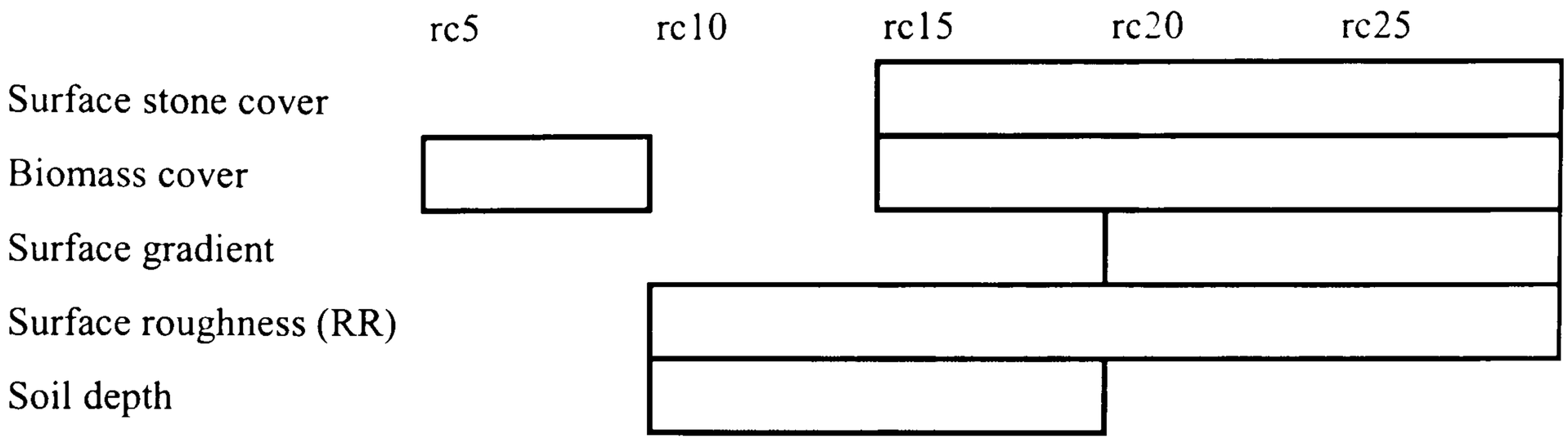

Figure 4.10 Changes in the significant factors controlling runoff generation during the storm

Since natural storm events are very short in duration, the factors that influence the runoff coefficient in the early part of the simulated storm are more important. The surface roughness influences the depth of the surface depression stores and hence controls the amount of infiltration excess required to generate runoff. During the first five minutes, most surfaces are filling the depression store. It is during the five to ten minute period that the surface depression store has filled enough to allow large areas of the surface to contribute runoff. The importance of the size of the surface depression store remains for the rest of the storm event.

The soil depth will control the change in soil moisture with cumulative infiltration. The infiltration rate as determined by the soil moisture in the first five minutes was probably greater than the simulated rainfall intensity. During the five to fifteen minute period, the changes in the soil moisture influence the infiltration capacity and hence has a significant effect on the runoff coefficient. Beyond fifteen minutes, the soil may have been infiltrating at its saturated conductivity rate. Therefore, the addition of more rainfall will not influence the soil moisture or the infiltration capacity.

The biomass cover influences the runoff coefficient in the first five minutes through the interception of rainfall. The lack of a correlation in the five to ten minute period relates to the filling of the canopy store in the first five minutes. The significance of the vegetation in the rest of the simulated storm relates to the effect the vegetation has on the soil. The greater biomass and aggregate structural stability means that the surface is less prone to crusting processes. The vegetation roots can develop macropores and hence increase the infiltration capacity. Therefore, it is able to maintain a greater infiltration capacity in the later stages of the storm.

4.4.2 Infiltration and Soil Moisture

As was discussed in chapter 2, there is a physical relationship between the soil moisture and the infiltration rate. This is related to the relationships between the soil moisture and the soil matrix

potential and the soil moisture and the hydraulic conductivity of the soil (Dingman 1994). It is possible to describe the changes in the infiltration capacity using a simplification of the Green and Ampt (1911) equation (Kirkby 1975), Equation 4.1.

$$i_c = a + \left(\frac{b}{\theta}\right)$$

Equation 4.1

Where i_c is the infiltration capacity of the soil (mm hr^{-1}), a and b are coefficients and θ is the percentage soil moisture. The saturation conductivity of the soil is given by $a + b$.

For each of the rainfall simulation experiments it is possible to reasonably estimate θ at each measurement interval. This is possible with knowledge of the soil porosity, soil depth and the amount of runoff. To remove random variations in the discharge related to surface properties, the infiltration rate and soil moisture have been taken as 5 minute averages. Equation 4.1 was then fitted to the measured infiltration rate and the calculated soil moisture using a minimum sum of squares algorithm. Sample plots are shown in Figure 4.11 and the predicted a and b coefficients and the significance level values are given in Table 4.8.

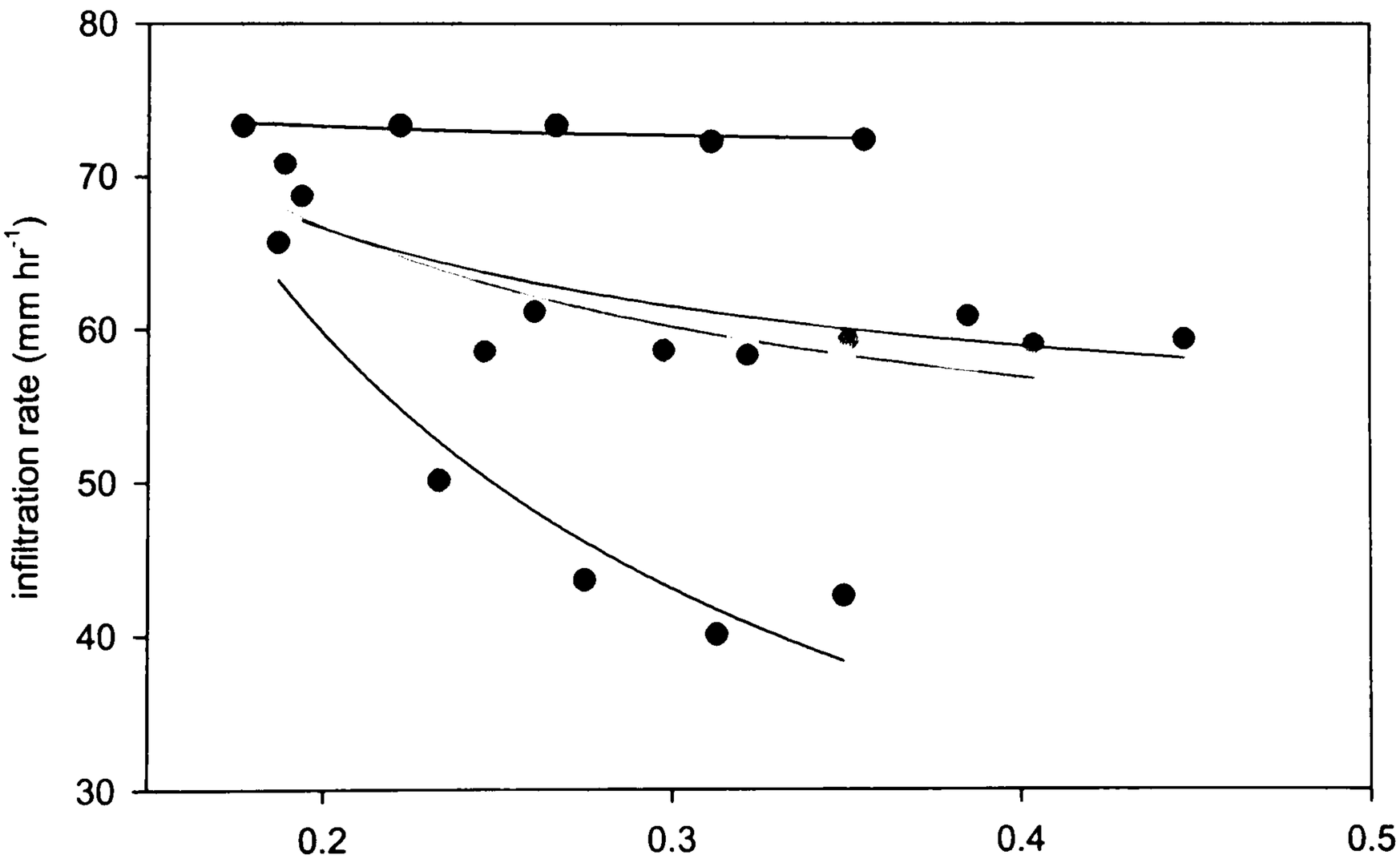

Figure 4.11 Relationship between measured infiltration rate and the calculated soil moisture

Site and plot	Initial conditions	Geology	Land Use	Slope	*a*	*b*	r^2
1 Almond field	Dry	Red	Agriculture	Steep	72.6	0.1	0.51
1 Almond field	Wet	Red	Agriculture	Steep	73.6	-0.3	0.12
2 Inter-bush	Dry	Blue	Scrub	Steep	51.2	3	0.75
2 Inter-bush	Wet	Blue	Scrub	Steep	41.4	11.8	0.41
2 Bush	Dry	Blue	Scrub	Steep	12.4	11.2	0.97
2 Bush	Wet	Blue	Scrub	Steep	44.7	8.7	0.16
3 Almond field	Dry	Blue	Agriculture	Flat	70.8	0.1	0.65
3 Almond field	Wet	Blue	Agriculture	Flat	69.6	0.6	0.33
4 Almond field	Dry	Blue	Agriculture	Steep	72.7	0.1	0.11
4 Almond field	Wet	Blue	Agriculture	Steep	72.2	0.4	0.04
5 Inter-bush stones	Dry	Red	Scrub	Steep	9.6	10	0.91
5 Inter-bush stones	Wet	Red	Scrub	Steep	55	0.6	0
5 Inter-bush grass	Dry	Red	Scrub	Steep	32.3	6.6	0.57
5 Inter-bush grass	Wet	Red	Scrub	Steep	50.6	4.1	0.06
5 Bush	Dry	Red	Scrub	Steep	47	3.9	0.67
5 Bush	Wet	Red	Scrub	Steep	41.5	12	0.69
6 Crusted	Dry	Red	Agriculture	Flat	71.4	0.3	0.6
6 Crusted	Wet	Red	Agriculture	Flat	65.4	1.8	0.33
6 Compacted	Dry	Red	Agriculture	Flat	59.1	1.8	0.35
6 Compacted	Wet	Red	Agriculture	Flat	30.9	11.4	0.61
7 Inter-bush	Dry	Blue	Scrub	Flat	69.9	0.7	0.31
7 Inter-bush	Wet	Blue	Scrub	Flat	67.2	0.2	0

Table 4.8 Predicted *a* and *b* coefficients and the significance level values for the relationship between measured infiltration rate and the calculated soil moisture

All of the agricultural sites (1, 3, 4 and 6) have low *b* values suggesting that the infiltration rate was not responding to the increase in the soil moisture. This is shown by the site 6 plot in Figure 4.11. The negative *b* parameter recorded for the site 1 wet initial conditions simulation relates to an increase in the infiltration capacity with increasing soil moisture. In order to get an accurate representation of the infiltration capacity of the soil, the simulated rainfall needs to be delivered at an intensity greater than the infiltration capacity. At the agricultural sites this probably was not the case and hence the low *b* and r^2 values. Therefore, the infiltration capacity can be viewed as greater than 75 mm hr^{-1}. The minidisk infiltration experiments are able to give more information on the infiltration capacity at these sites.

The most accurate relationship between Equation 4.1 and the field data was for the dry initial conditions experiment at the scrub site 2 with bush land cover, this gave an r^2 value of 0.97. The scrub site 5 also gave reasonable results with an r^2 of 0.91 for the dry inter-bush with stones simulation and an r^2 value of 0.69 for the wet bush experiment. As the difference between the predicted saturated infiltration rate ($a+b$) increases and the intensity of the simulated rainfall becomes greater, the fit of the model improves. This suggests that the model would work better

on the agricultural sites if greater rainfall intensities were used. Therefore, the low r^2 values should not been seen as a deficiency in the equation but in the rates of simulated rainfall.

4.4.3 Analysis of Minidisk Infiltration Results

To investigate the controls on the infiltration capacity, the minidisk infiltration results have been analysed using the Mann-Whitney U test. This non-parametric test was selected because the data is not normally distributed. The analysis has been undertaken at two spatial scales. Firstly, the differences between landscape scale factors are considered. These are the effects of land use and geology. The second scale is the difference between topographic elements within the landscape considering the differences between hillslopes and channel beds. The combination has been divided into two, the first considering all hillslopes and the second considering bare scrub sites. This distinction is made since bare scrub can be seen as analogous to channel beds as it is not under active agriculture and there are not the effects of vegetation. The combinations considered and the test results are given in Table 4.9.

Test combination	**Land use (scrub and agriculture)**	**Geology (red and blue)**	**All hillslopes and channel beds**	**Bare hillslopes and channel beds**
Mann-Whitney U	317.5	2501	4190	2573
Asymp. Sig. (2-tailed)	0.00	0.56	0.39	0.42

Table 4.9 Mann-Whitney U test results for minidisk infiltration results

At the landscape scale, the difference between agricultural crops and scrub slopes is able to completely separate the two sets of infiltration capacities. The difference between the soils derived from the red and the blue schist is able to explain 44 % of the variability of the infiltration capacity. The difference between all hillslope infiltration capacity values and the channel bed is able to explain 61.2 % of the variability. When only bare hillslope values are compared with channel infiltration values, this reduces to 58 %.

4.5 Summary

The surface roughness is influenceed by both the land use and the geology. The land use controls the magnitude of the roughness due to the ploughing of the soil. The geology influences the spatial structure of the surface. Surfaces derived from the blue schist have a longer range distance on the semivariogram than surfaces derived from the red schist. This suggests that the red schist soils have greater cohesion and hence are able to retain their ploughed form whereas the blue schist soils spread more under gravity.

The infiltration rates on agricultural sites were found to be greater than those on scrub sites. The average infiltration rate on agricultural plots from the rainfall simulation experiments was 67.34 mm hr^{-1} and 49.62 mm hr^{-1} on scrub sites. The minidisk infiltration experiments have a lower

mean infiltration capacity for agricultural sites at 40.96 mm hr^{-1} and for scrub sites at 11.07 mm hr^{-1}.

The time to runoff was found to be shorter on scrub surfaces than on agricultural fields. There was very little difference found between the different geologies. There is a negative relationship between the time to runoff and the surface gradient.

The form of the discharge hydrograph from the rainfall simulation experiments is controlled by the surface cover, roughness and gradient. The surface cover of biomass influences the early part of the discharge hydrograph whilst the surface stone cover and roughness influence the runoff in the later parts of the storm.

The infiltration rate on scrub slopes can be related to the soil moisture by Equation 4.1. A match between Equation 4.1 and agricultural sites was not found due to the simulated rainfall intensity being less than the infiltration capacity of the soil. Therefore, the infiltration rate of agricultural soil can be considered to be greater than 70 mm hr^{-1}.

The minidisk infiltration experiments show that there is high variability in the infiltration rates on all surfaces. Land use was able to completely separate the sets of infiltration experiments on scrub and agriculture whilst geology was able to explain 44 % of the variability in the infiltration capacity. Channel beds have a similar range of infiltration capacities to those of bare hillslopes.

From the analysis of the field investigations of the key controls on infiltration characteristics, it has been found that the key areas producing runoff are steep scrub slopes. The management of agricultural areas increases the infiltration capacity and hence reduces their ability to generate runoff. The impact of land management is greater than the influence of geology and slope gradient influences the generation of runoff regardless of the land management.

4.6 Implications for Model Development

The field results have been used to guide model development. This creates an important link between the real world processes and the abstraction of these complex processes in the model. This link has been achieved in two ways. Firstly, the field results influence the selection of the processes and parameters that should be included in the model. Secondly, the field experiments give a consistent set of parameter values.

The aim of the model is to consider runoff generation and connectivity at the spatial scale of hillslopes and small catchments. The field experiments were undertaken at a far smaller scale because of practical limitations, as discussed in section 1.3. In order to convert between the two scales, hierarchical theory has been used (Bergkamp 1998). A model representing the rainfall simulation plots is nested within a hillslope model which has a spatial distribution of cells with

a flow routing algorithm moving water between them. The rainfall simulation experiments form the basis for parameterising the cells and the minidisk experiments give insight into the variability of infiltration rates.

The results of the rainfall simulation experiments show that the surface roughness, gradient, soil moisture and stone cover are the key controls on the generation of runoff at the plot scale. Therefore, each of these factors needs to be implicitly or explicitly incorporated into the model structure. Surface roughness and slope gradient influence the generation of runoff by determining the depth of the surface depression store. The depth of the surface depression store needs to be calculated for many combinations of slope gradient and surface roughness. Therefore, this relationship must be investigated in detail as part of the modelling work and the results explicitly incorporated into the model. The surface gradient influences the amount of runoff by increasing the overland flow velocity and, therefore, this relationship needs to be explicitly incorporated into the model structure. Soil moisture is a dynamic property of the soil that varies on the time scale of a storm event. From the field work, it was found that there are two classes of soil behaviour in relation to soil moisture. Generally, the scrub sites showed a decrease in infiltration rate with increasing soil moisture whereas agricultural sites showed no significant change in the infiltration rate with changes in the soil moisture. Both of these behaviour types can be explicitly modelled using Equation 4.1 which relates the infiltration rate to the soil moisture. The processes leading to the effects of the surface cover of stones on the infiltration rate operate on a spatial scale finer than the rainfall simulation plot. Since Equation 4.1 uses the infiltration rate over an area rather than for a point it is able to represent processes occurring over the spatial scale that the data was collected (Beven 2000). The amount of stone cover can be related to the surface gradient and the land use. Therefore, by using the parameters from Table 4.8 for sites with different slope gradients and land uses, the effects of the stone cover are implicitly incorporated into the model.

The rainfall simulation experiments found that there are strong differences in infiltration characteristics between bush and inter-bush plots on scrub plots. Therefore, within the model, a distinction must be made between these two surfaces. The arrangement of the vegetation on a hillslope has been shown to influence the hydrological behaviour of a hillslope (Cerdá 1997). The vegetation pattern can be considered as the result of a stochastic process. When investigating the effects of the vegetation pattern, it is important to consider many realisations of this process.

The minidisk infiltration experiments showed that there is a significant variation in the infiltration capacity within a single site. The spatial pattern of the infiltration capacity will effect the distribution of runoff sources and sinks. The greatest source of variation relates to the vegetation effects which will be included in the model parameterisation. To determine the large

scale controls on hillslope scale runoff, this small scale noise has been excluded from the model parameterisation. This should increase the signal strength of the key relationships.

Within each of the experimental sites, there are complex patterns of surface cover and topography. The flow routing algorithm needs to be able to represent the distribution of flow across these surfaces.

The parameter values obtained from the field investigations are subject to a degree of uncertainty and the abstraction of reality into a model structure introduces another layer of uncertainty. Sensitivity analysis and the use of many realisations of stochastic processes are able to decrease the uncertainty associated with the model. However, these uncertainties should be considered when interpreting the model results.

The model, therefore, needs to have the following properties:

- A distributed structure with each cell relating to a rainfall simulation plot.
- Each cell requires information on:
    - Land use
    - Slope gradient
    - Vegetation cover
- The flow routing algorithm needs to be able to handle the complexity of the spatial distribution of controlling factors.
- The surface roughness and vegetation pattern may be considered stochastic processes. Therefore, relationships should be tested using many realisations of these processes.
- The uncertainty associated with the parameterisation should be considered when interpreting the model results.

5 Model Development

5.1 Introduction

A modelling approach has been adopted to investigate the dynamics of runoff generation and overland flow connectivity. This approach has the advantages of being able to improve our understanding about the system state and response in both space and time. This information can then be analysed to consider how the system dynamics are changing throughout the storm and between storms. Natural storms are sporadic and high magnitude, runoff producing storms are infrequent making field based studies difficult. Although it is possible to use rainfall simulation over small plots, applying the same techniques over whole hillslopes is expensive and impractical. The use of the modelling approach enables the generation of storms of defined characteristics within the model. The approach also enables the generation of many different realisations of stochastic processes, such as flow path configurations and vegetation patterns. Although many of these advantages could be achieved with fieldwork, it would require a very long term, very high budget research project, which is far beyond the scope of this research. The model developed in this chapter has the advantage of being based on the results of field based experiments. This solid foundation aids the model development and parameterisation.

The model aims are defined in section 5.2. The modelling framework is developed in section 5.3. The vertical and horizontal hydrological structure is discussed in section 5.4. The selection of the process representation equations and algorithms is in section 5.5. The generation of stochastic storms is presented in section 5.6 and the generation of stochastic grid is in section 5.7. The model implementation is discussed in section 5.8. The assessment of the model is described in section 5.9. Details of the model availability are in section 5.10. The model development summary is presented in section 5.11.

5.2 Model Aims

The aim of the model is to simulate numerically the generation of runoff and to route this flow across a surface. The model should have the following properties:

- The model should contain the relevant hydrological fluxes for a semi-arid environment.

- In line with the aim of this research, the model should consider processes operating at the temporal scale of a single storm.
- The range of spatial scales to be considered will range from small plots through hillslopes to small catchments.
- The model should be compatible with external software. This allows for the visualisation and processing of model data.

5.3 Modelling Framework

There are a number of different frameworks available for the development of a hydrology model. These relate to the different methods of representing space and time within the model. There are two main methods of representing space in hydrology models: lumped and distributed. In the lumped approach, the whole catchment is considered as a single modelling element with one set of model parameters. This is computationally inexpensive but gives limited insight into the hydrological system dynamics. In the distributed approach, the area is divided into a large number of small modelling elements. Each modelling element has its own set of parameter values and hence the variability of the natural world can be captured more realistically. These elements are connected together by horizontal fluxes to route the water through the system. This approach gives greater spatial detail on the distribution of the state of the hydrological system. The explicit inclusion of connections between different parts of the landscape means that the distributed approach is well suited to the investigation of connectivity issues that are key to understanding runoff generation in semi-arid regions.

There are two main methods of handling the fluxes between the modelling elements: finite element and finite difference. Both methods describe a continuous data field with the finite element method using an irregular data structure and the finite difference approach using a regular data structure. The selection of the most appropriate approach is discussed in section 5.4.2.

Water within a modelling system can be represented in continuous or discrete forms. In a continuous form, the amount of water in a store is represented as a continuous, floating point, variable. This allows high resolution to be achieved on the amount of water stored at a certain location. Under the discrete representation, parcels of water containing a finite volume of water are routed through the system. This has the advantage that the origin and flow paths of a parcel can be recorded and analysed. The main disadvantage of the discrete approach is the amount of computer storage space required for all the parcels in the system. Therefore, this limits the spatial and temporal scales of application to a small plot. Thus, for the spatial scale of hillslopes and small catchments, a continuous representation is the most suitable and will be used in this

model. However, the advantages of the parcel based approach are coupled with the developed continuous representation model in chapter 8.

5.4 Model Hydrological Structure

To aid the discussion of the model, it has been named the Connectivity of Runoff Model (CRUM). The model has been implemented in 1D and 2D forms with different levels of process representation in the different versions. CRUM-1D is a one-dimensional representation of a single hillslope flow path. This can be used to investigate some of the fundamental relationships in hillslope hydrology relating to the generation of overland flow and the connections between these flows. CRUM-2D is a two-dimensional representation of a hillslope allowing for flow convergence and divergence. This version includes a dynamic infiltration capacity and overland flow velocity. The majority of the research has been undertaken using CRUM-2D. As detail has been added to the model during the development, it is hoped that more subtle characteristics of the system behaviour will be revealed.

The CRUM model is supported by two other models. The generation of storm events is modelled by a stochastic storm generator, stormG. This is described in section 5.6. The creation of grids with stochastic patterns is modelled by the stocHAstic GRID generator (HAGRID). This is discussed in section 5.7.

The model structure is divided into two parts, the vertical and the horizontal components. The vertical structure considers the interception of rainfall, infiltration and the generation of runoff. The structure of the vertical exchanges is developed in section 5.4.1. The horizontal model structure controls the distribution of runoff across the surface. At each point in the horizontal structure, the vertical structure is represented. The development of the horizontal structure is discussed in section 5.4.2 and the integration of the two process domains is discussed in section 5.4.3.

5.4.1 Vertical Model Structure

From the review of processes in chapter 2, a simplified version of the surface hydrological response has been developed in Figure 5.1. This includes the processes relevant for a semi-arid environment at the time scale of a single storm event. At each model iteration, the water is routed through this cascade of stores.

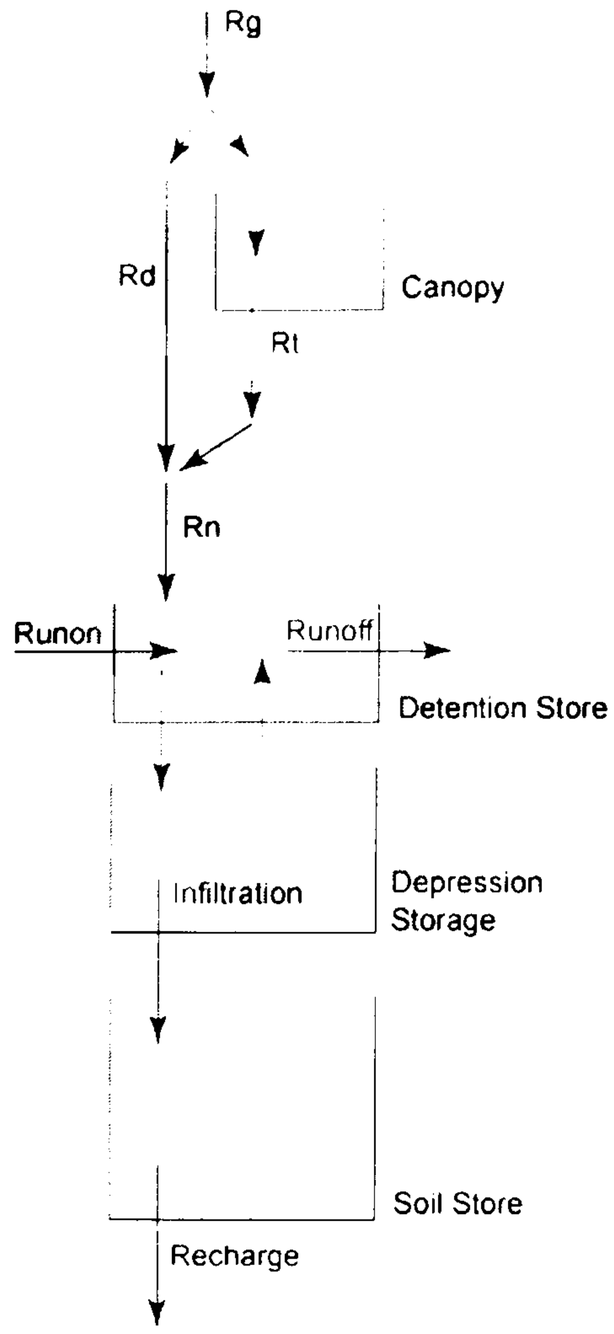

Figure 5.1 Vertical model structure showing hydrological stores and fluxes

The gross rainfall, *Rg*, is first routed through the canopy, a certain percentage of the rainfall will fall directly through the canopy, *Rd*, and the canopy intercepts the remainder. The water stored on the canopy will drain as through fall, *Rt*, and this combined with *Rd* gives the net rainfall, *Rn*.

The next store is the surface detention store which represents water held on the soil surface above the depression storage, this is the flowing water layer. The runoff from upslope areas is routed into the surface detention store and the runoff from the vertical cascade is routed out of the surface detention store. The surface detention store drains into the depression store which is turn overflows back into the surface detention store. Water from the depression store then infiltrates into soil store. Water then drains out of the bottom of the soil store as recharge and is lost from the system.

5.4.2 Horizontal Model Structure

Many methods of dividing space into modelling elements have been developed. Within each of these elements the vertical structure is represented. These methods are the finite difference approach using raster grids, finite element approaches using Triangular Irregular Network (TIN) meshes and polygon based spatial representations. Each method has its own strengths and relies on different amounts of knowledge about the surface being described. The data structures for the CRUM models will be required to handle different type of data, including terrain, runoff pathways and vegetation patterns.

The most widely used method in geoscience is the raster grid structure. This is a grid of data points systematically spaced to describe the surface. The values at each point may either be a point value or an area average for the region the cell covers. Much data is available in this format including terrain data, remotely sensed images and rainfall radar data. This format has the advantage of being a computationally efficient method of storing data since the format fits well with the computers own internal storage. Many algorithms have been developed for extracting secondary parameters from the grid such as slope, aspect (Burrough and McDonnell 1998) and flow direction (Costa-Cabral and Burges 1994). However, the raster data structure does have a number of disadvantages. It is not able to handle abrupt changes in the surface except with a very fine grid. In the case of an elevation surface, this would result in lower slopes and a smoother terrain than reality. In areas where the representative scale of the surface is highly variable, the selection of the grid resolution is a compromise between accuracy and cost. The results of many grid operators are dependent on the grid size with different grid resolutions giving different results for the same surface (Cho and Lee 2001).

The Triangular Irregular Network (TIN) data model overcomes many of the problems with the raster data format. It is able to adjust the sampling density to the local surface. It is possible to include linear features in the TIN model such as drainage divides. With the raster structure the position of such features is only approximated since their locations must be assigned to the nearest cell, whereas with the TIN structure features are precisely located. It is possible to calculate most of the topographic attributes with the TIN model that are possible with the DEM structure. There are problems with the identification of the upslope connection of a facet, which can only be overcome by the visual inspection and manipulation of the TIN (Moore et al. 1993). Since the data structure is based on an irregular structure, the structures for topography and vegetation would not match up. Although it is possible to overlay the two datasets, this would result in a surface with a very high number of facets. This removes one of the main advantages of the TIN structure. This will also increase the computational cost since there are more model cells and a greater number of interactions. The storage of data using the TIN structure is not as efficient as the raster structure. The calculation of runoff pathways is complicated if the water is routed to more than one other facet.

Many workers have considered the landscape to be composed of polygonal units which can be used as the basis for hydrological modelling (Kite and Kouwen 1991; Flügel 1995; 1997; Becker and Braun 1999). These units represent the natural basic elements of a landscape and have a uniform homogeneous or quasi-homogeneous hydrological behaviour in the vertical domain (Becker and Braun 1999). There are distinct differences between adjacent areas and the internal variations within each unit is far greater than the variations between units. It is therefore appropriate to model such areas as separate units.

The definition of landscape units requires detailed spatial data sets and an understanding of the relevant factors controlling hydrological response. If the defined units are very small, the determination of the amount of runoff partitioned to each of the units' neighbours becomes very complicated due to the complex nature of the joining edges. It is possible to define a unit that is contained within another unit, thus forming a runoff loop. If each unit routes runoff into the channel network and extends to the watershed, many of the routing problems are removed. To apply a unit based approach successfully, the definition of the units should be strongly based on the hydrological structure of the study catchment.

The use of a non-systematic data structure requires knowledge of the nature of the system under study. Since the dynamics of the spatial patterns of runoff connectivity are not well understood, a systematic data structure is best suited to the analysis. The raster grid structure is a systematic format. It also has the advantages of being computationally efficient, of the availability of algorithms available for extracting parameters from the surface and of the number of available tools for pre and post processing of the data. Therefore, a raster grid-based structure has been selected for CRUM. Once information on the main controls of the generation of runoff have been defined, the landscape unit approach is used to delimit hydrological similar areas. The delimitation of the hydrologically similar areas is presented in chapter 8.

5.4.3 Integration of Vertical and Horizontal Processes

The order in which the processes are computed within the modelling framework for CRUM is shown in Figure 5.2. It is important to ensure that the model remains computationally stable, Courant criterion is maintained and that numerical diffusion is minimised. This is achieved by relating the time length of the model iteration to the hydrological activity in the system. The measure of activity used is the slope of the water surface. When the model predicts that there will be a large amount of flow, the slope of the water surface within the model will increase. Therefore, to maintain a realistic water surface, the model iteration length is decreased. The length of the current iteration is given by Equation 5.1.

$$l_n = \frac{l_c}{\beta_m n}$$

Equation 5.1

Where l_n is the new length, l_c is the current length β_m is the maximum water surface slope and n is a positive integer. The length of the iteration is therefore updated dynamically while the model is running. This approach has been limited to a minimum time step of 5 Hz since the system was found to be stable at this resolution even with significant flow. The normal time step used is 1 second since this gives the required detail in the discharge hydrograph. The use of

model iteration lengths between 1 and 0.2 seconds ensures that the Courant criterion is maintained and that numerical diffusion is minimised.

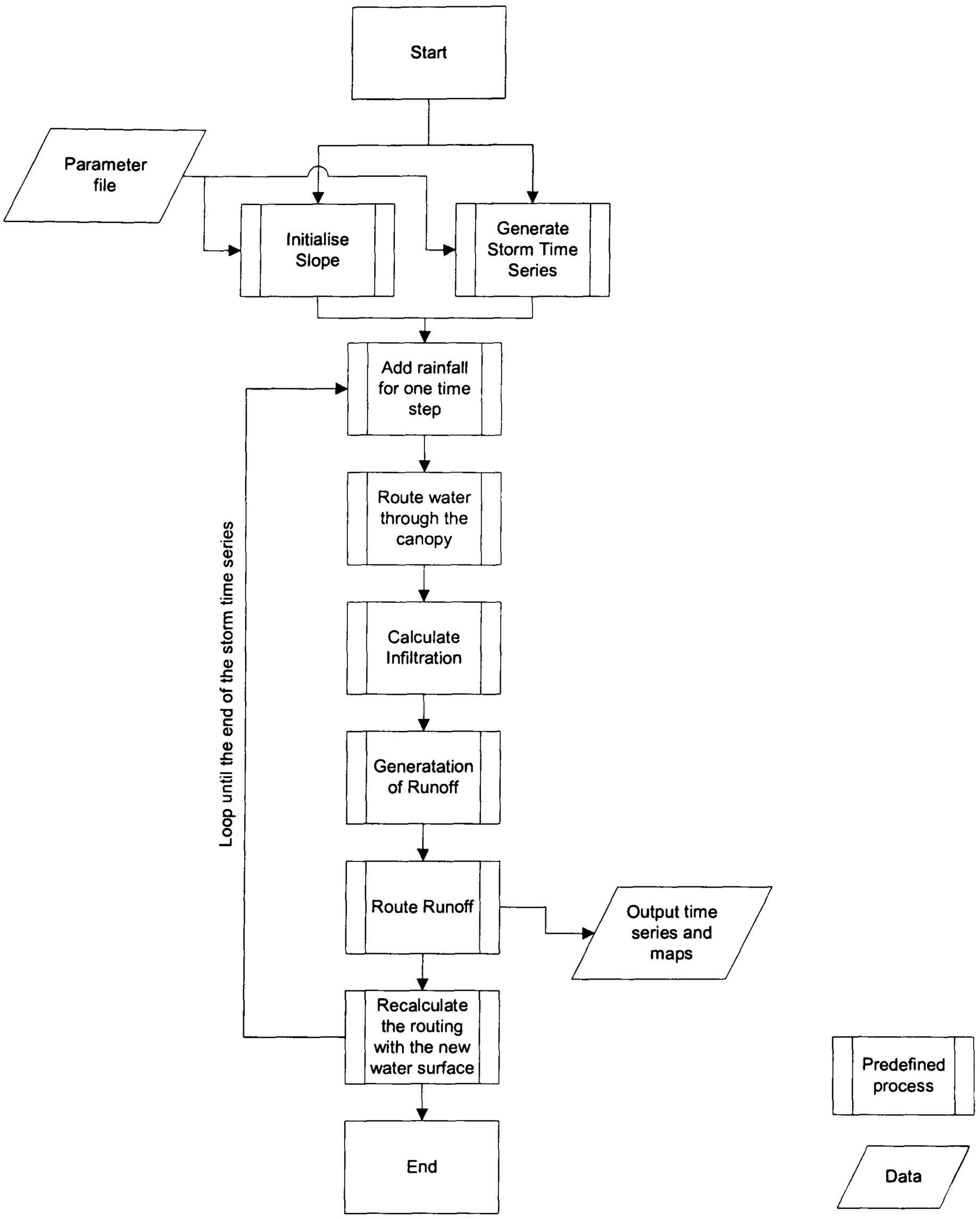

Figure 5.2 Model processing order

5.5 Selection of Process Equations

Each of the fluxes shown in Figure 5.1 and the spatial distribution of overland flow requires an equation or algorithm to model the process. For each process, the requirements for the representation have been defined, the relevant literature reviewed and the equation or algorithm selected.

5.5.1 Interception

The presence of vegetation influences the amount of water reaching the soil surface. The change in the amount of water reaching the ground results from the storage of water on the plant elements and the subsequent evaporation. On the temporal scale of the simulation modelling, water that is intercepted by the vegetation may be considered as lost from the system.

The requirements for a model of rainfall interception have been defined as:

- The model should be dynamic, giving output at the same temporal scale as the rainfall data.
- Due to the fragmented vegetation pattern, the model should work on the scale of the individual plant not whole canopies.
- The model parameters should have physical meaning and be simple to measure or be available in the literature.

Many models of rainfall interception have been developed for temperate and tropical forest canopies (Rutter 1971, Calder et al. 1986). There is only a limited amount of work that has been undertaken on semi-arid shrub vegetation. Each of the main models will be reviewed and applications of these models to semi-arid environments, where available, are presented.

Physical Models of Interception

The simplest physical model of rainfall interception views the canopy as a non-leaking store. The rainfall is divided into direct throughfall and intercepted water. The intercepted fraction fills the canopy store until it overflows. This is the approach taken in the Patternlite model and has been applied to south-eastern Spain and Greece (Mulligan and Reaney 2000). The modelling of interception in the CASC2D model (Johnson et al. 2000) follows similar lines with the exception that after the canopy story has filled, only a percentage of the water will drain.

Rutter et al. (1971; 1975) developed a model of interception based on physical properties. The model acts as a water balance with a canopy store and a stem flow store. The Rutter model forms the interception component of the Systéme Hydrologique Europeen (SHE) (Abbott et al. 1986) which has been applied to semi-arid areas (Andersena et al. 2001). The water balance of the canopy is given by:

$$\sum R_g = \sum D + \sum E + \sum T_d + p_t + \Delta C$$

Equation 5.2

Where R_g is the gross rainfall, D is the drainage, T_d is the direct throughfall, E is the evaporation, p_t is the stemflow and ΔC is the change in canopy store.

The evaporation loss from the canopy is assumed to occur at the rate of potential evaporation when the canopy is wet, calculated from the Penman-Monteith equation. Drainage is related to the amount stored through an exponential relationship that follows the observations of Leonard (1967):

$$D = ds(\exp(bC))$$

Equation 5.3

Where *ds* and *b* are coefficients and *C* is the canopy storage.

Therefore while the canopy is wetting up the direct through fall is less than gross rainfall. The *ds* parameter accounts for all of the processes not explicitly handled in the model such as wind speed. Rutter et al. (1971) found *a* to equal 3.7 for Corsican pine and *ds* could be determined by:

$$ds = (3.17 * 10^{-5})S$$

Equation 5.4

The use of the exponential relationship means that the model violates the physical boundary conditions of the drainage process, when $S=0$, $D\neq 0$ (Massman 1980). To overcome this, Rutter et al. (1971) defined a rate of 0.002 mm min^{-1} as the cessation of drainage. The *ds* parameter will vary between storm events due to changing meteorological conditions (Massman 1980).

Domingo et al. (1998) applied a modified version of the Rutter model to *Anthyllis cytisoides* L., *Retama sphaerocarpa* L. and *Stipa tenacissima* L. in Almeria, SE Spain. The main adaptations to the model for individual plants rather than complete canopies centre on the determination of the boundary layer conductance. This term strongly influences the evaporation loss and hence the interception loss. The modelled results were compared with field measured results and the model was able to explained 94 % of the observed interception loss.

Analytical Models of Interception

In light of the complexities of the interception process, Gash (1979) and Mulder (1985) developed an analytical solution to the problem. The Gash model assumes that all of the rain falls in a single storm onto a dry canopy. Evaporation is assumed constant over time and space and assumed negligible from stems. The Mulder model differs from the Gash model in that it does not assume that the rainfall occurs in a single storm. Instead, the number and duration of storms coupled with the daily rainfall are used to define an equalised distribution over the whole day. There is a difference in evaporation between the wetting up, saturation and drainage stages of the canopy. Both models were developed for continuous forest canopies. The application of these models to individual shrubs would be a significant change from the original conditions.

Navar et al. (1999) applied the Gash model to the Tamaulipan matorral thornscrub of north-eastern Mexico. The thornscrub differs from the mattoral of SE Spain, being approximately 2 m tall and quite dense. They found that the modelled interception loss differed only slightly from the 12 month validation series. The measured series had an interception loss of 18.3 % (83.6mm) compared with the modelled loss of 18.4 % (84.1mm).

Stochastic Models of Interception

Calder (1986; 1996) developed a model which was a 'significant step forward' (Pearce 1987) in the modelling of the interception process. Calder was able to model the complexity of the process through probabilistic theory based upon the size of the raindrops. The model was able to replicate the asymptotic wetting of the canopy observed by (Aston 1979). The model relates the mean number of raindrops retained on the canopy, n, to the mean number of strikes per element, m, given in Equation 5.5. The model was later refined (Calder, 1996) to include a two-layer canopy representation whereby drops could be re-intercepted. Evaporation was described by redefining m as a state variable to represent the equivalent number of strikes per element.

$$n = q\left(1 - e^{-m}\right) + e^{-m} \sum_{x=1}^{r} (x - q) \frac{m^x}{x!}$$

Equation 5.5

Where q is the maximum number of drops which can be retained on the canopy and r is the largest integer $< q$.

It has been shown that under conditions of heavy rainfall the model can become unstable (Hall 1992). This can be overcome by using either a very small or variable time step or an implicit solution method.

The Calder model has been applied successfully in tropical environments (Calder et al. 1986) but has not been applied to many semi-arid areas. The model has been applied to a plantation of Eucalypus in a semi-arid region of southern India (Hall et al. 1992). They verified the model using a small data set of three storms (total depth of 22 mm) and found that the model performed well, except at high intensities, explaining 85.6 % of the overall variance.

Of the available interception models, the storage based models of Mulligan and Reaney (2000) and Johnson et al. (2000) are the most suitable for semi-arid shrub interception on the single storm time scale. This is due to the ease of parameterisation and physical realism. The analytical models of Gash and Mulder were developed for the interception loss over long time scales. Therefore they would not be able to predict the per moment dynamics of interception and throughfall required. The Calder stochastic model performed well in temperate and tropical forest environments but has not been applied to many semi-arid environments. The detail of the model and the computational expense are too great for the current study. It is beyond the scope

of this research to undertake a detailed investigation on semi-arid rainfall interception in order to parameterise and verify the Calder model. The modified Rutter model of Domingo et al. (1998) performed well at simulating the interception by a semi-arid shrub during a single storm. However, as was shown by the results from the rainfall simulation experiments, there is a strong switch in the runoff generation from bush plots. This is consistent with a simple store filling and overflowing. The values of storage depth presented by Domingo et al. can be used to parameterise this model. Therefore, a simple storage model will be used for the modelling of interception.

5.5.2 Infiltration

The relationship between the rate at which the rainfall can enter the soil and the rainfall intensity is the essential process in determining the generation of runoff. It is important therefore to model this process accurately.

For the modelling of the infiltration rate, a number of requirements have been defined:

- The equation needs to relate the infiltration capacity to soil water storage to due to distributed nature of the model. This is due to water entering a cell from both rainfall and run-on sources.

- Due to the distributed nature of the model, the infiltration equation needs to be computationally inexpensive since the value will be updated at each model iteration.

- The equation parameters should be simple to obtain and have physical meaning.

Approaches to Modelling Infiltration

Two main approaches to modelling infiltration can be found in the literature. The first set of models aims to calculate the infiltration rate based upon soil physics. The second set of models calculates the infiltration rate empirically based upon either the time since the start of the rain event or the current state of the soil moisture store. These approaches are called time-based and storage based respectively (Baird 1997).

Physically Based

The Richards equation (Richards 1931) was derived by combining Darcy's Law for unsaturated flow with the conservation of mass (Equation 5.6). The 1D form of this equation is the basic theoretical equation for vertical unsaturated flow in a homogeneous porous medium. It is used in numerical modelling of infiltration and redistribution by dividing the soil into thin layers and applying it to each layer sequentially at very small time increments.

$$\frac{\partial\theta}{\partial t} = \frac{\partial}{\partial z}\left(K(\theta) + K(\theta)\frac{\partial\Psi(\theta)}{\partial z} \right)$$

Equation 5.6

Where θ is the soil moisture, t is the time, z is the vertical distance, K is the hydraulic conductivity defined for each layer in the soil and Ψ is soil matrix potential.

Since the equation is highly non-linear, it is normally solved using low-order numerical techniques such as finite difference or finite element methods, which are computationally expensive (Miller et al. 1998). Many algorithms are available for finding solutions to the Richards equation (Parlange et al. 1997; Miller et al. 1998). However, each technique represents a compromise between computational efficiency and accuracy (Kirkby et al. 1996).

The Richards equation models flow into a homogeneous porous medium. Semi-arid soils have a high stone content and contain macropores and hence the key assumption of homogeneity is invalidated. Since the input rates at the soil surface vary spatially due to differences in soil crusts and vegetation cover, the Richards equation should be applied in 3D. This would result in a huge computational cost and large field data requirements and would still would not give a complete solution for macropore flow.

Kunze and Nielsen (1983) compared the infiltration rates calculated by the Richards equation with observations from a light clay soil. The solution to the Richards equation was achieved using a simple algebraic equation using a finite difference iterative solution. They found 'fair agreement' between the measured and modelled infiltration profiles. The maximum wetting distances exceeded the experimental results by 0 cm after 64 minutes, 4 cm after 226 minutes and by 14 cm after 467 minutes. They found that the reduction of $\Delta\theta$ improved the accuracy of the procedure.

The MEDALUS Slope Catena Model (Kirkby et al. 1996) uses the Richards equation to model the infiltration rate. The soil hydraulic properties were allowed to vary with depth and dynamically with soil organic matter and soil dispersion thus enabling the incorporation of surface sealing influences. The applied solution divided the surface into a number of statistical zones and calculated infiltration rates in each of these zones. Thornes et al. (1996) applied the MEDALUS Slope Catena Model to runoff plots in Abanilla, Murcia, SE Spain. They found that under large rainfall events, the model did not perform well, only explaining 17.7 % of the overland flow discharge from the base of the plot. If the large storms are removed, the percentage explained increased to 63 %.

Empirically Based

Philip (1957) obtained an approximate analytical solution to the Richards equation by assuming a delta function change in diffusivity for the soil across the wetting front (Beven 2000). The cumulative infiltration it can be approximated by:

$$i_t = S_p t'^{0.5} + K_p t', \qquad 0 < t' < t_w - t_p$$

Equation 5.7

Where S_p is the sorpivity of the soil, which is related to the suction at the wetting front, t_p is the time to ponding and t' is given by $t - t_p$. The S_p term can be approximately given by (Manley 1977):

$$S_p = \left(2 K_s \psi_f\right)^{0.5}$$

Equation 5.8

Where Ψ_f is the effective tension at the wetting front. The equation assumes that the water is ponded on a deep homogeneous soil with uniform initial wetness. The effect of the sorptivity term decreases with time resulting in the final infiltration rate being equal to the saturated conductivity. The Philip equation was found to give an excellent fit for infiltration into uniform soils over short periods. However, due to the inclusion of time in the equation, the goodness of fit reduced over longer periods of time (Kirkby 1985).

Green and Ampt (1911) developed an equation based upon Darcy's Law and the conservation of mass in a finite difference formulation. This allowed for a more holistic view of the infiltration process than the Richards equation (Dingman 1994). The model assumes that the soil is homogeneous to an indefinite depth with a horizontal surface. It is also assumed that the infiltrating wetting front forms a sharp jump in moisture content from the initial constant moisture ahead of the wetting front to saturation at the front. The infiltration rate is calculated from:

$$i_t = K_s \left[1 + \frac{h_0 + \Psi_f}{z_f} \right]$$

Equation 5.9

Where h_0 is the depth of ponded water on the soil surface, z_f is the vertical depth of the wetting front It is possible to approximate the Green and Ampt parameter from soil texture data (Rawls et al. 1983). The assumptions in the Green and Ampt equation may not be compatible with many semi-arid soils. The presences of macropores and Sub-surface layers violate the assumption that the soil is uniform (Seyfried 1991). Beven (1984) developed a version in which the hydraulic conductivity declines exponentially with depth. This contrasts with the infiltration

model developed by Mulligan (1996) for a semi-arid environment in which the hydraulic conductivity declines linearly with depth.

Mein and Larson (1973) developed an equation based upon the Green and Ampt equation, the GAML equation:

$$V_{t_0} = \frac{\Psi_f . Md}{(p/K_s) - 1}$$

Equation 5.10

Where V is the amount of infiltration prior to runoff and Md is the moisture deficit. After the onset of runoff, the infiltration rate i_t is defined by:

$$i_t = K_s \left[1 + \left(\Psi_f . Md / V_t\right)\right]$$

Equation 5.11

Swartzendruber and Hillel (1975) developed the equation:

$$i_t = Bt^{-n} + A$$

Equation 5.12

Where A is the final constant infiltration capacity and B and n are constants. When $n = 0.5$ the equation is very similar to the Philip (1957) curve (Scoging and Thornes 1980).

Kirkby (1975) suggested that the infiltration rate could be related to the soil moisture and proposed a storage based simplification of the Green and Ampt equation (Kirkby 1985):

$$i_t = a + \frac{b}{\theta}$$

Equation 5.13

This equation was used in a distributed model which featured run-on between model cells (Kirkby 1990). The use of the storage term in Equation 5.13 gives a number of advantages. It enables the equation to model the infiltration rate over areas rather than points. This is of great help in scaling the model since the storage term can relate to an area of 1 cm^2 or 1 km^2 (Beven 2000). The use of a changing soil moisture term allows the equation to be applied to irregular rainfall time series.

Scoging and Thornes (1980) investigated the performance of the GAML, Swartzendruber and Hillel and the simplified Green and Ampt infiltration equations in a semi-arid environment. The authors undertook 73 experiments using a ponded infiltration test and 80 experiments using a sprinkler based rainfall simulator. The experiments were undertaken at two field sites in semi-arid Spain: around Soria, central Spain and Ugijar, Granada province. Both sites are described

in detail in Thornes (1976). They found that the simplified Green and Ampt model fitted better to the observed data than either the GAML or Swartzendruber and Hillel models.

Although the Richards equation would give the most accurate description of the infiltration process into a homogeneous medium, semi-arid soils are not homogeneous. This accounts for the poor results observed with semi-arid soils. The computational expense involved in finding a solution makes it unsuitable for distributed modelling. The other equations do not have this problem. The time based Green and Ampt infiltration equation model outperformed other equations under test conditions in a semi-arid environment. The Kirkby storage version has greater physical meaning and can be applied to areas, distributed modelling and irregular rainfall time series. The model parameters can be easily derived from rainfall simulation experimental results and retain physical meaning.

In section 4.4.2, the rainfall simulation results from the field experiment were fitted to the storage based Green and Ampt infiltration equation model. The r^2 values from fitting the equation (Table 4.8) are low with the model fit being strongest on scrub slopes and weakest on agricultural slopes. The low r^2 values may relate to the simulated rainfall intensity being less than the infiltration capacity of the soil. Therefore, the water was infiltrating at the rainfall intensity rather then at the infiltration capacity. Therefore, the low r^2 values may be a result of the rainfall simulation experiment procedure rather than a deficiency in the storage based Green and Ampt model. All of the relationships between soil moisture and infiltration rate show either no change in infiltration rate with increasing soil moisture (rainfall delivered at a rate less then the infiltration capacity) or a general trend for decreasing infiltration capacity with increase soil moisture. Thus showing the same relationship as in the storage based Green and Ampt model. There is much scatter in the per minute infiltration rates which results in the low r^2 values. The storage based Green and Ampt infiltration equation model is based on soil physics, as described in Section 2.5.1 and Figure 2.9 and hence has a strong theoretical basis. Therefore, due to its strong theoretical basis and agreement with field results when certain criteria are met, the storage based simplification of the Green and Ampt infiltration equation has been selected for use the in the CRUM model.

5.5.3 Overland Flow Velocity

The different equations for determining overland flow velocity were discussed in chapter 2. From this discussion, the Darcy-Weisbach equation (Equation 5.14) was selected since it is able to describe laminar, transitional and turbulent flow and the friction factor is dimensionless.

$$v = \sqrt{\frac{8gRs}{ff}}$$

Equation 5.14

Where *ff* is the friction factor, *g* is the gravity constant, *R* is the hydraulic radius and *s* is the slope of the energy gradient. Following Abrahams et al. (1992), the friction factor, *ff*, is related to the surface cover rather than the flow hydraulics.

5.5.4 Overland Flow Routing

The movement of water across a surface is determined by the local variations in slope. The routing of water may lead to the concentration of flow into channels or the dispersion of flow. The requirements of a flow routing algorithm have been defined as:

- The algorithm must be computationally efficient since the flow routing will change dynamically as the water surface changes. Therefore, the flow routing map must be updated at each model iteration.

- The algorithm will be applied at the hillslope scale and hence needs to handle convergent and divergent flow (Abrahams et al. 1992).

Five main flow direction algorithms can be found in the literature: D8, Rho8, FD8, DEMON and Dinf. Each of these methods will be discussed in chronological order of development and the differences in the algorithms is illustrated in Figure 5.3. This shows the flow accumulation as calculated by each algorithm and shaded by equal area. The original DEM has a horizontal resolution of 50 m and is part of the Ordnance Survey (UK) raster Panorama topography data set and represents part of southern Warwickshire, UK.

D8

The single flow path algorithm developed by O'Callaghan and Mark (1984) is termed D8 (deterministic eight node). The algorithm considers the slopes to the eight neighbouring cells and assigns the flow direction to the cell with the steepest slope. This algorithm has been widely used (Costa-Cabral and Burges 1994) and is the only flow direction algorithm available in Arc Info.

The main problem with this algorithm is that flow is assigned to only one of the eight directions separated by 45° (Tarboton 1997). This leads to parallel flow lines in hillslopes. For example, if a hillslope has aspects ranging from 338° to 22°, all of the cells would be assigned as flowing due north. This assignment of flow to one direction means that the algorithm is incapable of modelling flow dispersion (Gallant and Wilson 1996).

Figure 5.3 Differences in flow accumulation for the different flow direction algorithms

In special cases where the eight neighbours all have the same slope, such as a on a flat plain the original algorithm assigned the drainage direction to the first direction encountered working clockwise from north with the maximum slope. The algorithm was modified by Lea (1992) to improve the handling of this special case. A surface is fitted to the local cells and if no immediate neighbour is lower, the analysis window is expanded until a lower cell is found.

The flow accumulation for the example DEM calculated with D8 is shown in Figure 5.3. It is possible to see many parallel flow paths and that the flow paths are always in one of the eight directions.

Rho8

In order to resolve the problem of parallel flow lines created by D8, Fairfield and Leymarie (1991) developed a stochastic version of D8, termed Rho8. The probability of the flow being assigned to a certain direction is given by:

$$p_i = \frac{-1s_i}{\sum_{i=1}^{8} -1s_i} \qquad s <= 0$$

Equation 5.15

Where p_i is the probability of the flow going in direction i and s_i is the slope in direction i.

For example, on a planar slope with an aspect of 15° all of the cells will flow due north flow is the flow direction is calculated using D8,. However, using Equation 5.15 a proportion of the cells will flow north-east and the rest flow north resulting in an overall flow direction closer to 15°.

The Rho8 algorithm is capable of producing more realistic flow networks (Gallant and Wilson 1996) but like D8, it is not capable of modelling flow dispersion. The stochastic nature of the algorithm results in many cells without an upslope connection hence distorting the distribution of contributing areas (Gallant and Wilson 1996). The algorithm produces a different flow path network each time it is run, which is generally undesirable (Gallant and Wilson 1996). Ahnert (1994) states that 'the reintroduction of some randomness into a model equation which was previously freed from random influences…appears to be an illogical step backwards in the methodological research sequence'.

The flow accumulation for the example DEM calculated with Rho8 is shown in Figure 5.3. In comparison to the D8 map, some of the parallel flow lines have been broken down, for example in the top right of the map.

FD8

The FD8 algorithm was initially developed by Quinn et al. (1991) and expanded upon by Rieger (1993) and Holmgren (1994). This algorithm is a multiple flow direction version of D8 and hence allows the dispersion of flow. On hillslopes flow is distributed to all of the lower neighbouring cells and in channels flow is only routed to single cells. The amount of flow assigned to each cell is determined on a slope-weighted basis as proposed by Quinn et al. (1991) and Freeman (1991). The fraction of flow given to neighbour i is given by:

$$F_i = \frac{\beta_i^v}{\sum_{i=1}^{8} \beta_i^v}$$

Equation 5.16

Where β_i is the slope from the central node to neighbour i and v is a positive constant.

The v constant can be seen as a flow concentration factor, the greater the value of v, the greater the flow concentration (Holmgren 1994). If the value is taken as $v = 1$, then the algorithm works in the same way as Quinn et al. (1991) and if $v \rightarrow \infty$ the algorithm will work in a similar way to a single flow path algorithm. Freeman (1991) found that $v = 1.1$ gave the most accurate results for artificial cone surfaces. However, Holmgren (1994) recommends values of $v = 4$ - 6 for distributed modelling. Quinn et al. (1995) found that values of $v > 10$ gave a single flow direction approximation and that $v = 100$ was equivalent to the single flow direction algorithm.

The FD8 algorithm gives a realistic distribution of contributing areas in upslope areas while eliminating the parallel lines created by D8 (Gallant and Wilson 1996). This algorithm tends to causes considerable dispersion of flow in valley bottoms which is undesirable since stream lines tend to be well defined (Gallant and Wilson 1996). This can be overcome by switching to a single flow path algorithm when the contributing areas exceeds a certain value, this however can lead to a bump in the frequency distribution of the contributing area (Gallant and Wilson 1996). In studying dispersal areas, Endreny and Wood (2001) found that FD8 was far less sensitive to errors in the DEM than D8 or DEMON. A disadvantage of FD8 is that distributed modelling can be computationally more expensive due to the larger number of connections involved (Gallant and Wilson 1996).

The flow accumulation for the example DEM calculated with FD8 ($v = 1.1$) is shown in Figure 5.3. The diffusive nature of the algorithm is clearly shown in the figure. The problem of parallel flow lines has been removed. However, the definition of channels is not as strong as with D8 or Rho8.

DEMON

The method developed for raster DEMs by Lea (1992) and Costa-Cabral and Burges (1994) is conceptually similar to the stream tube approach of Moore et al. (1991) developed for contour based DTMs. The implementation of this algorithm by Costa-Cabral and Burges (1994) is called DEMON (DEM network extractiON).

The assignment of the single flow direction is according to the aspect of the cell. The flow routing is two dimensional, thus allowing for the effects of topography on the flow path width. The flow paths remain constant over a planar slope, increases in size on divergent terrain and

decrease on convergent terrain (Costa-Cabral and Burges 1994). The computational expense of DEMON is similar to FD8 and gives results of similar quality (Gallant and Wilson 1996).

A weakness of the approach is that the process of fitting a surface to the local cell neighbourhood for every possible combination of elevation values is complex. The coding therefore requires the separate handling of many special cases (Tarboton 1997).

The flow accumulation for the example DEM calculated with DEMON is shown in Figure 5.3. The map shows more defined concentrated flow features, this is especially visible in the left half of the map.

Dinf

Tarboton (1997) developed a method (Dinf) that takes the advantages of DEMON through the assignment of a single flow direction to each cell. The direction is represented as a continuous variable between 0° and 360°. The direction is determined by fitting a 3 by 3 pixel triangular window centred on the focus cell. The use of a triangular window avoids the approximation of fitting a surface (Tarboton 1997).

The flow accumulation for the example DEM calculated with Dinf is shown in Figure 5.3. The map shows more pronounced flow lines and less diffusive flow than either FD8 or DEMON.

Neither D8, Rho8 nor Dinf fulfil the criterion that the algorithm must be able to handle divergent flow and hence are not suitable for this application. The main advantage of DEMON is that it is able to model flow in channels more accurately than FD8. However, since the algorithm will be applied to hillslopes and not to entire catchments, this advantage is not of great importance. The FD8 algorithm is straightforward to implement since it does not require special code to handle unusual situations, like DEMON. The use of multiple flow paths does increase the computational expense but the improved representation of the process justifies this expense. The v exponent value has been set at 2 thus allowing for flow dispersion on the hillslope. Therefore, FD8 has been used within the model.

5.6 Storm Generation

For the Rambla de Nogalte catchment there is a detailed rainfall record. This record covers three years with over 180 individual storm events. However, these storms only cover a small percentage of the possible range of storm characteristics. Through the use of a stochastic storm generator, it is possible to control the characteristics of the storm and generate many realisations of the same storm.

The current work requires a rainfall generator to create per minute rainfall intensities for a defined storm length and intensity. Rectangular Pulse Model (RPM) and Monte Carlo based

storm generators are considered the most appropriate for this research. The Rectangular Pulse Model approach uses constant rainfall intensity for a set period of time. This approach is useful for considering the effects of slope characteristics on the discharge hydrograph since the rainfall is constant. The RPM approach has been used in many hydrological applications (e.g. Khaliq and Cunnane 1996; Cameron et al. 2000). In contrast to the RPM, the Monte Carlo model selects random rainfall intensities from a distribution function. The Monte Carlo approach has been used for hydrolgical models of semi-arid environments (e.g. Mulligan 1996). This type of model assumes that the there is no temporal auto-correlation in the rainfall time series. The model experiments are concerned with the surface response to heavy rainfall. The Monte Carlo models uses a distribution function fitted to the intense rainfall sections of the time series. This distribution function is given in Figure 3.14 and is given by Equation 5.17.

$$rf_i = \frac{1}{a}\ln(1 - prob).60$$

Equation 5.17

Where rf_i is the rainfall intensity (mm hr^{-1}), $1/a$ is the mean per minute rainfall intensity, a is a coefficient and *prob* is the probability of that rainfall intensity.

5.7 Stochastic Pattern and Surface Grid Generation

The creation of grids with stochastic patterns and surfaces is modelled by the stocHAstic GRID generator (HAGRID). This model is able to generate two types of stochastic grids, random terrain and vegetation patterns. The generator was used to create large numbers of patterns with defined characteristics. This enables the investigation of the effect of the nature of the pattern rather than the response of a single realisation of a pattern.

The creation of random terrain is achieved by generating independent random elevations across a surface and then adding a separate slope component. This simulates small scale random roughness variations on the surface and is suitable for the generation of individual plots and the small hillslopes.

The generation of vegetation patterns follows the algorithm presented by Tischendorf and Fahrig (2000). This algorithm is capable of generating vegetation patterns with variable amounts of fragmentation. A cell is chosen at random on the surface and the probability of it being defined as vegetated is a function of the surrounding vegetation and the value of the *frag* parameter. A uniform random number is chosen and if it is less than the *frag* value, then the cell will become vegetated. However, if the cell has a vegetated neighbour, the cell will become vegetated. This, therefore, creates the clustering in the vegetation pattern. By the visual comparison of the generated patterns and field measured patterns, it was found that *frag* values of 0.05 – 0.3 gave realistic results.

5.8 Implementation

The model is based on a modular structure using object orientated design principles. The main components of the model are shown in Figure 5.4.

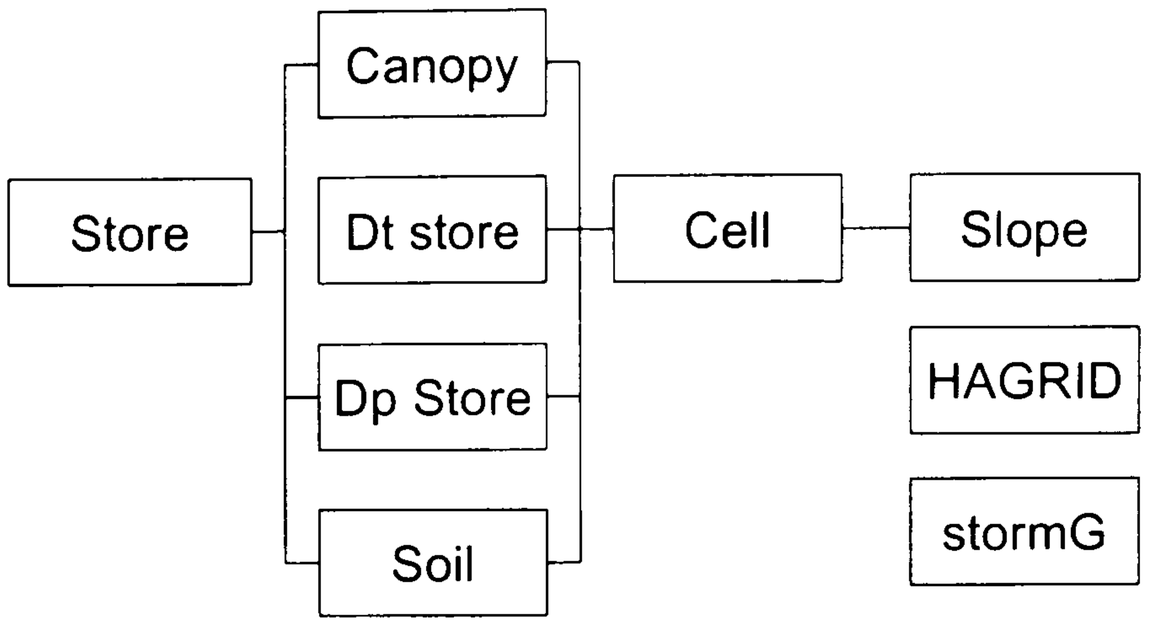

dp store = The surface depression store
dt store = the detention store on top of the surface depression store

Figure 5.4 Class structure for CRUM

The object orientated philosophy has been used opposed to procedural programming methods since if a complicated problem is modelled using procedural programming methods it can result in a model that is difficult to understand, to critique, to debug and to modify. This makes it difficult to advance or to reuse parts of the model (Reynolds and Acock 1997). The aim of object orientated design and programming is to break down a complicated problem into a number of smaller, simpler problems. In object orientated design the emphasis is on the objects in a system and the interactions between these objects. The objects are normally defined by the physical objects in the system. Each object has information on its state (member variables) and knows how to perform certain processes (member functions). For example, a soil store object knows the current soil moisture and is able to calculate the current infiltration capacity. The combining of data and methods in an object is known as encapsulation. Another key aspect of object orientated design is the ability for objects to inherit the member functions and member variables of other objects. This makes the variables and functions available to the new, specialised version of the object. This has the advantage of being economical with coding and reducing the possibilities for errors. For example, the store object is inherited by the soil object to give the soil store. In order to create objects, classes are written. A class may be seen as a template for creating objects of a certain type.

5.8.1 Classes Used for CRUM

The fundamental hydrological class is the store (C_Store). This abstract class ensures conservation of mass while water is added or removed. Three of the stores in the vertical cascade inherit this class and add their own process representation. These classes are the depression storage (C_dt_store), soil (C_Soil) and the canopy (C_Canopy) classes.

The cell class (C_Cell) models the vertical cascade using instances of the canopy, puddle, depression storage and soil objects. The rainfall is received by the cell object and routed through each of the objects in the vertical cascade. With the raster spatial data structure, the cell object represents the base spatial unit, a single raster of the grid.

The slope class (C_Slope) takes the vertical model of the Cell class and spatialisises it in one or two dimensions. This class models the distribution of the runoff generated in the cell class. Many of the input and output capabilities are handled by the slope class.

There are two stochastic process classes for the modelling of storms (C_stormG) and terrain (C_hagrid). Each of these classes generates process realisations based on defined parameters.

The model manager class (C_modelmgr) controls the execution of the model. This class owns instances of slope, storm generator and terrain generator objects. The class controls the generation of the terrain and storms and then uses this data to run the model. The characteristics of the storm, terrain and slope configuration are controlled by a parameter file.

The CRUM model has been written in C++ using the GNU Compiler Collection (GCC) C++ compiler under Linux and Microsoft Visual C++ 6.0 under Windows NT 4 and XP. The C++ language was chosen over other object orientated languages due to its high speed of computation (Stroustrup 1997).

The storage and visualisation of spatial data is handled by ArcInfo 8.1. Grid based data is imported and exported using the ArcAsciiGrid format and vector data is outputted using the Arc Generate format. This enables the rapid exchange of data between the GIS system and the model. This use of the GIS and the coded model enables the utilisation of the complex functions that are implemented in the GIS and the specialised modelling routines that are not.

5.9 Model Assessment

There are many ways in which a simulation model can be assessed. The conventional, positive approach is to compare the model output with an observed dataset. If the model has been incorrectly structured or if there are errors in the computer code, the simulated results would diverge from the observed dataset (Lane and Richards 2001). However, if the model predictions are in line with the observations, it does not necessary mean that the model is valid since it is possible to be generate the 'correct' output for the wrong reasons (Beven 1996). Therefore it is only possible to prove that a model is unsuitable through falsification and not that it is a valid representation of the system under study.

For this study, a detailed time series of runoff generation and channel flow was not available. Therefore it has not been possible to undertake the conventional, positive approach to model assessment. However, it is still possible to assess the model in a number of ways including the

comparison of model predictions with expectations (Lane and Richards 2001). The assessment of the CRUM model has been undertaken in five ways: The comparisons of the model predictions and the expected outputs is presented in section 5.9.1, the mass balance checking is presented in section 5.9.2, the error testing of the computer code is presented in section 5.9.3, the comparison of peak flow predictions are presented in 5.9.4 and the sensitivity analysis is presented in section 5.9.5.

5.9.1 Model Predictions and Expectations

In order to compare the model predictions with a set of expected results, a simple surface and storm have been used, Table 5.1. From the characteristics of the surface and the storm event, it is possible to calculate the timing and amount of runoff during the storm event. The calculated values and the values prediction by the model are shown in Table 5.2.

Characteristic	**Value**
Grid Size	100 by 100 m
Cell Size	1 m
Terrain type	Independent random elevations
Maximum flow path length	116 m
Soil Depth	Constant at 0.2 m
Storm intensity	120 mm hr^{-1}
Infiltration characteristics	All water infiltrate until store is full
Storm length	200 time steps
Overland flow velocity	One cell per time step

Table 5.1 Characteristics of the theoretical surface and storm

Characteristic	**True value**	**Model**
Time to runoff	Rainfall rate / Soil depth 0.002 / 0.2 = 100 time steps	100 time steps
Time to peak runoff	Time to runoff + Maximum flow path length 100 + 116 = 216	216 time steps
Peak discharge	Number of cells * rainfall rate 100^2 * 0.002 = 20	20 m^3 time $step^{-1}$
Time to end of runoff	Time of end of rainfall + maximum flow path length 300 + 116 = 416	416 time steps

Table 5.2 Comparison of predicted and simulated hydrograph properties

As can be seen from Table 5.2, the model is able to reproduce accurately the characteristics of the runoff hydrograph. This shows that the conservation of mass within the model is being maintained and that the water is being routed correctly.

5.9.2 Mass Balance

It is very important that all of the water within the model can be accounted for since this ensures that the model is no generating or losing water during the simulation. Within CRUM water may

be held and accounted for as one of the stores or fluxes in Table 5.3. The mass balance is calculated using the parameters in Table 5.3 and Equation 5.18.

Store or flux	Code	Simulated Volume (m^3)
Initial water on slopes	*a*	63.8
Total rainfall	*b*	201.7
Total on canopy at end	*c*	0.706
Recharge total	*d*	57.3
Water on slopes at end	*e*	157.6
Flow off map	*f*	0
Total discharge	*g*	50.6

Table 5.3 Parameters used in the mass balance calculation and a simulated set of modelled fluxes and stores.

$$MB = \frac{out}{in} = \frac{c+d+e+f+g}{a+b}$$

Equation 5.18

Where *MB* is the mass balance of the model. From the example shown in Table 5.2 it can be seen that $MB = 1$ and hence the mass balance of the model is maintained. At the end of each model run, the mass balance is checked and reported. This therefore ensures that the model is still conserving mass when different model configurations are used.

5.9.3 Error Testing of Computer Code

The error checking of the computer code has been undertaken through the comparison of the model predictions with the externally calculated results and through the checking of the mass balance within the model. These two forms of assessment will give a good insight into the numbers of errors within the model code. Since the model predictions and expectation matched and the mass balance was maintained, as shown in Table 5.3, it can be assumed that there are no significant errors in the computer code.

5.9.4 Comparison with Observed Flows

Due to the irregularity and scarcity of storm events producing channel flow in the Rambla de Nogalte, a detailed time series of runoff generation and channel flow is not available. However, there are a number of peak discharge estimates from a storm in September 1997 (Bull et al. 2000). The model predictions for this storm in comparison to these estimates are discussed in detail in chapter 8. The model predicts a lower peak discharge than was observed. This may be due to the spatial variations in the rainfall with the observed rainfall location being outside the catchment or the limited detail of the DEM failing to capture significant flow structures.

5.9.5 Sensitivity Analysis

Sensitivity analysis considers the effect of changing model parameters on the model output. The model parameters may be divided into two categories, physical and empirical parameters. The

physical parameters include slope gradient, slope length, vegetation cover and storm intensity. These factors are investigated in chapters 6 and 7. The empirical factors relate to the process representation equations. These are the friction factor (*ff*) of the Darcy-Weisbach equation and the flow concentration parameter in the FD8 routing algorithm. The sensitivity analysis was performed using a 50 by 50 m slope with a gradient of 6 ° and a storm that lasted 5 minutes at 75 mm hr^{-1}. The sensitivity of total discharge to changes in the friction factor (*ff*) and the flow concentration factor is shown in Figure 5.5.

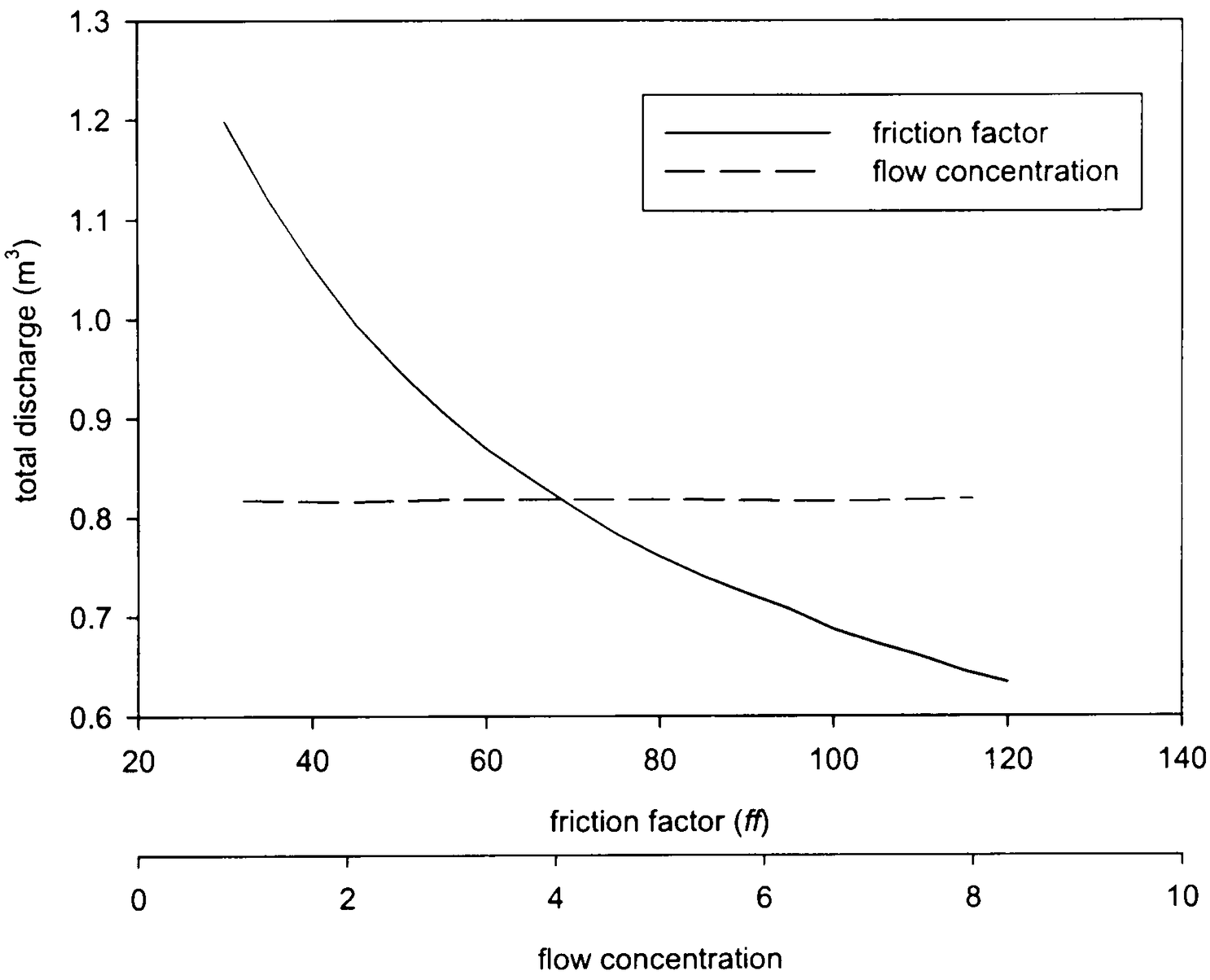

Figure 5.5 Sensitivity of the total discharge to changes in the friction factor and flow concentration factor

The model is sensitive to changes in the friction factor and not to changes in the flow concentration factor. The response to changes in the friction factor is non-linear with greater runoff at lower friction factor values. Since the flow velocities will be greater at lower friction factor values, it is reasonable that there will be greater total discharge. The insensitivity of the total discharge to the flow concentration relates to the diffusive nature of the flow across the hillslope. The introduction of greater flow organisation may change the nature of the sensitivity.

It is expected that there will be interactions between the different factors in the model. For example, the sensitivity to the friction factor will be related to the slope length, gradient and storm duration. To investigate the model response across the full parameter space of the model is extremely computationally expensive. Even to consider a small sub-section of the parameter space is currently beyond the available computational resources.

5.9.6 Model Assessment Conclusions

The model is able to generate simulation results that are in line with the expected results for a theoretical hillslope and storm. The model does not gain or lose water as has been shown by the maintenance of the model mass balance. The correct timing of flows and the maintenance of the model mass balance show that there are not significant errors in the computer code. The comparison of the model predictions with observed data has been limited by the available data. The model sensitivity to the friction factor and flow concentration factor show that the model responds in a logical way to changes in these parameters. The different aspects of the model assessment presented in sections 5.9.1 - 5.9.5 show that the CRUM model is suitable for the investigation of the generation and connectivity of runoff in a semi-arid environment.

5.10 Model Availability

A copy of the model and the details of the parameter file format can be obtained from:

www.geog.leeds.ac.uk/projects/s.reaney/

5.11 Summary

The Connectivity of Runoff Model (CRUM) has been developed for the investigation of the controls on runoff generation and flow dynamics in semi-arid environments. The model is divided into vertical and horizontal components and distributed on a grid structure. The model has been designed using an object orientated approach. This creates a modular model that is simple to modify, to debug and to reuse.

The vertical component represents interception, puddle storage, surface depression storage, soil moisture storage and recharge. The interception is modelled by a non-leaking store that covers a percentage of the horizontal area. Once this store fills and overflows, all of the rainfall will reach the soil surface. The infiltration of water is modelled by a simplified Green and Ampt equation based on the soil moisture status. The water that is not able to be infiltrated is first held in the surface depression store. Once this store overflows, runoff is generated.

The horizontal interactions occur only as overland flow since through flow is negligible in the study area. The flow routing between the grid cells uses the FD8 algorithm since this allows for flow concentration and dispersion.

The model has been internally verified for the conservation of mass and flow routing. It was not possible to perform an external verification since no suitable data set was available. It was found that the model was sensitive to changes in the Darcy-Wesibach friction factor but not to changes in the flow concentration factor of the FD8 algorithm. The sensitivity to surfaces and storms are covered in the following chapters.

6 Surface Controls on the Discharge Hydrograph

6.1 Introduction

The aim of this chapter is to consider the controls that the surface characteristics impose on the form of the discharge hydrograph. These controls will be considered at a range of levels of abstractions and spatial scales. The one dimensional slope model (CRUM-1D) represents the greatest level of model abstraction from reality. Working at this level of abstraction it is possible to consider some of the fundamental controls on the amount of runoff that leaves the base of the slope. The two dimensional modelling has been undertaken at two spatial scales, the plot and the slope scale. A plot is an area of approximately 0.5 by 0.5 m. At this scale, a greater amount of physical realism is introduced to enable to investigation of the controls on the surface depression storage. The slope scale represents an entire hillslope from the drainage divide to a channel at the slope base. This spatial scale uses the greatest amount of physical realism with the inclusion of such factors as vegetation, infiltration and overland flow routing velocities. As the model incorporates more processes, it is possible to investigate subtle aspects of the system behaviour in more detail.

The model results from a one dimensional slope are presented in section 6.2. The two dimensional plot scale results are presented in section 6.3, which covers the relationship between surface gradient, roughness and the amount of surface depression storage for scrub and ploughed surfaces. The two dimensional hillslope scale results are presented in section 6.4, which includes the individual influence of slope length, gradient, flow path configuration, infiltration rates, vegetation effects and slope form on the discharge hydrographs. Section 6.5 considers the interactions between slope length and gradient and between vegetation and slope gradient. Section 6.6 briefly covers other possible factors that influence the discharge hydro but are beyond the scope of this model to consider. The discussion of the result is in section 6.7 and the conclusions are in section 6.8.

6.2 One Dimensional Slope Results

The effects of slope length and soil store size distribution on discharge from the base of the slope were investigated using CRUM-1D. The model configuration consisted of a 1D series of cell objects with each cell routing into the next cell down slope. For each cell to generate runoff, the soil store must overflow. The model was run both with fixed depth and variable depth soil stores. The model time step is defined as the time required for overland flow to cross a cell. The structure of the model is described in detail in chapter 5.

The cell spacing is related to the distance of the spatial autocorrelation length of the soil store size. These distances are not well documented in the literature. Field observations suggests that appropriate values are of the order of 1 m for agricultural land, and 5-10 m for scrub areas, related to the regularities or patch sizes in the land surface. In this section, a distance of one m is used. The distribution of soil depths has been approximated using an exponential model.

6.2.1 The Effects of the Soil Store Size Distribution

The effect of the distribution of the sizes of the soil stores was investigated by comparing the differences in discharge between uniform and variable depth stores. The rainfall intensity was set at 0.003 m per time step (ts) for 128 ts on a slope of 256 cells. From the field investigations, a mean soil depth of 0.2 m was selected as representative. The variable depth stores were based on an exponential distribution with a mean of 0.2 m. The uniform depth cells had a soil store size of 0.2 m. The mean discharge timing from 10,000 variable store size slope realisations and from the uniform store size slope are shown in Figure 6.1.

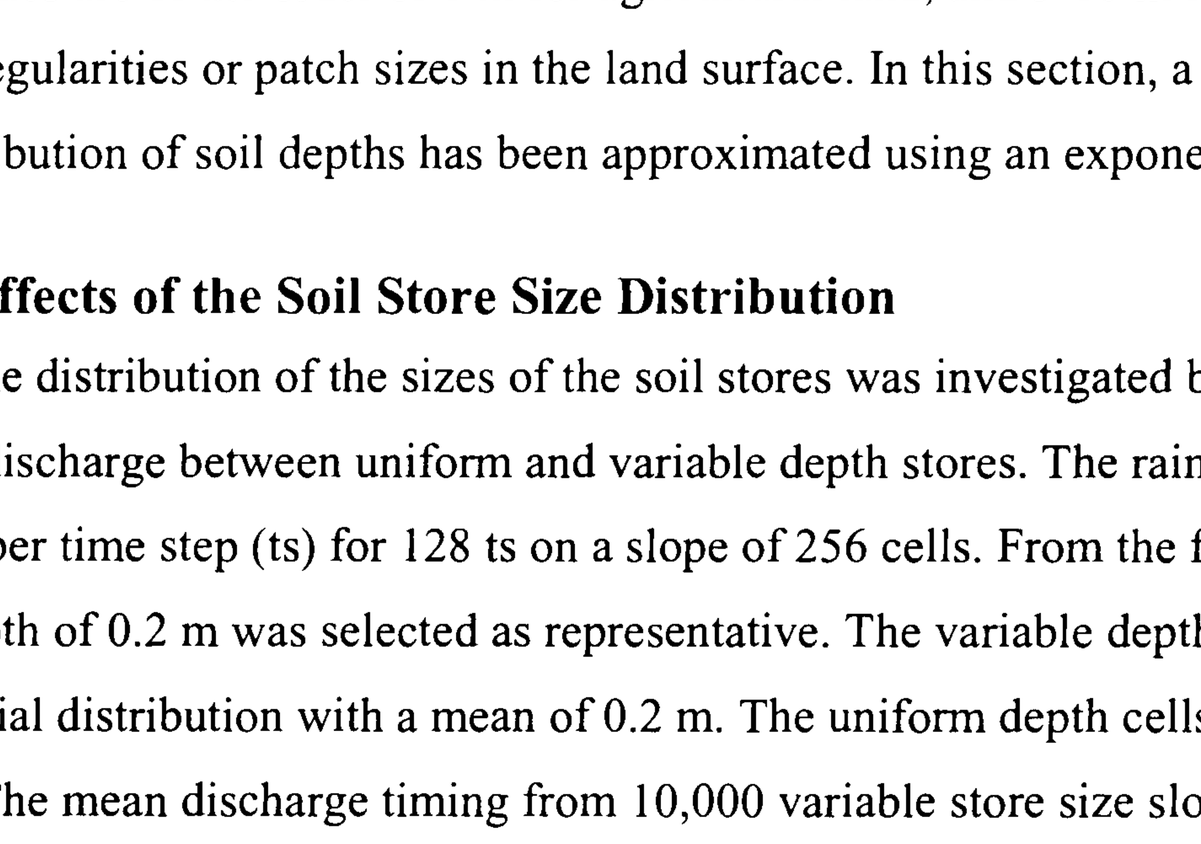

Figure 6.1 Effects of the soil depth distribution on runoff

The variable depth slope produces runoff sooner than the fixed depth slope. This is because the smaller buckets located near the base of the slope will produce discharge earlier since they require less rainfall to generate runoff and the travel times to the slope base are small. The smaller the standard deviation of the soil depths, the more sharply defined the time of the first

slope discharge will be. This will therefore give a more uniform catchment response. The point at which the uniform soil store depth slope starts to produce discharge is the point when all of the soil stores are filled. The increase in discharge from this time is controlled by the travel times from the point of generation to the slope base.

After the cessation of rainfall, the time until the cessation of runoff is controlled by the slope length, since the runoff generated at the top of the slope will take one time step to cross each cell. The discharge from the variable soil store slope decreases more rapidly than from the uniform bucket slope. This is because it is possible to have soil stores which are larger than the total depth of rainfall delivered. Therefore, not all of the slope will be connected and contributing runoff. If less of the slope is connected, the decrease in runoff will be steeper.

6.2.2 Slope Length

The effect of the length of the slope was investigated for slope lengths of 32, 64 and 128 cells, which are typical for the field area. The soil store sizes were based upon an exponential distribution with a mean of 0.2 m. The mean discharge timing from 10,000 stochastic slope realisations in relation to slope length is shown in Figure 6.2.

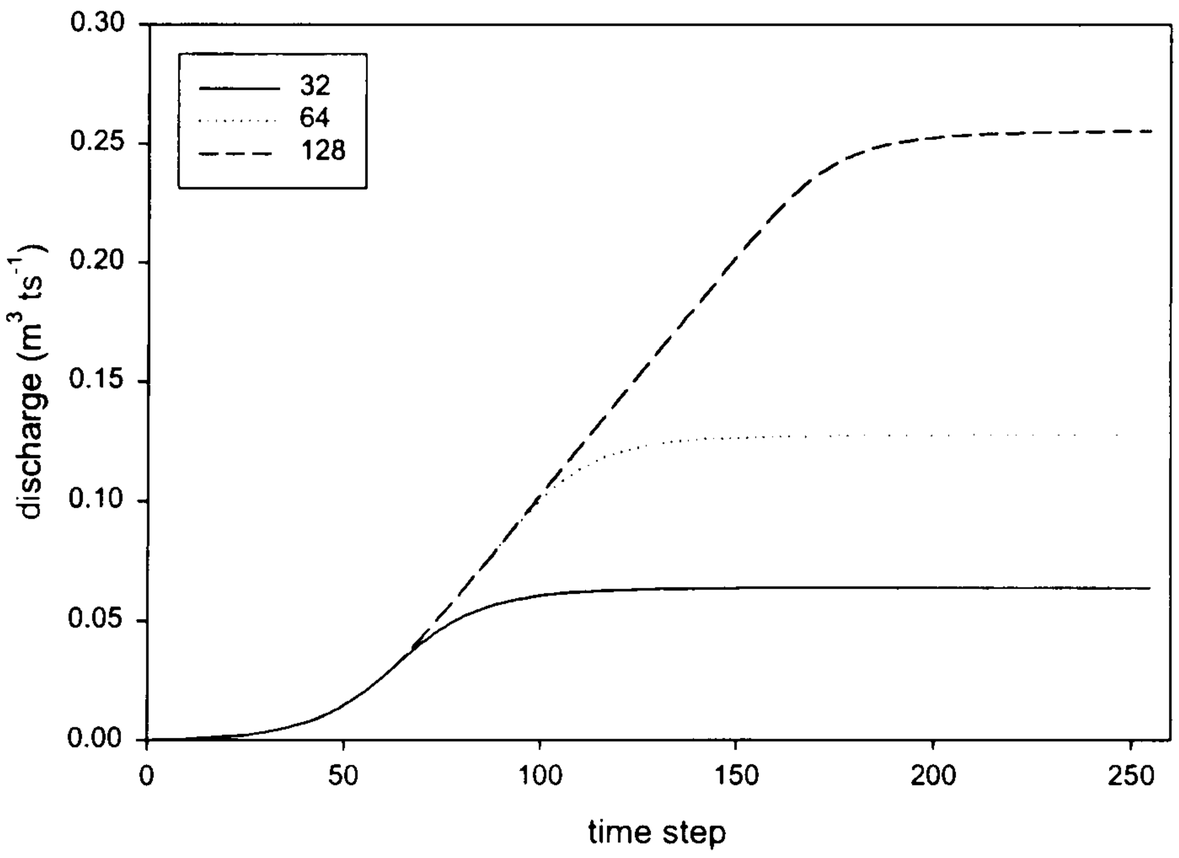

Figure 6.2 Influences of slope length on discharge

As the slope length increases it takes proportionally longer for the discharge to reach its equilibrium value. Therefore, on longer slopes it is more likely that the slope will cease to be generating runoff before the runoff reaches the base of the slope. This leads to infiltration of runoff further down the slope. This will have the effect that these lower sections of the slope will rapidly produce runoff if another storm occurs soon after and if evaporative losses are minimal.

6.2.3 Timing of Discharge

The discharge hydrographs shown in Figure 6.2 show the average discharge from many realisations of the soil depths. This smoothing hides the variability in the discharge from each slope realisation. Figure 6.3 shows the discharge hydrographs from a number of individual slope realisations of a 64 cell slope. Although, each hydrograph reaches the same end point with the entire slope contributing runoff, there is a variety of ways in which this point is reached. To consider the effect that these different paths have, it is useful to consider two factors: the first of these is the probability at each time step that there will be any discharge from base of the slope. The second is the probability at each time step that all of the slope will be contributing runoff. These probability curves are shown in Figure 6.4 for slope lengths of 32, 64 and 128 model cells.

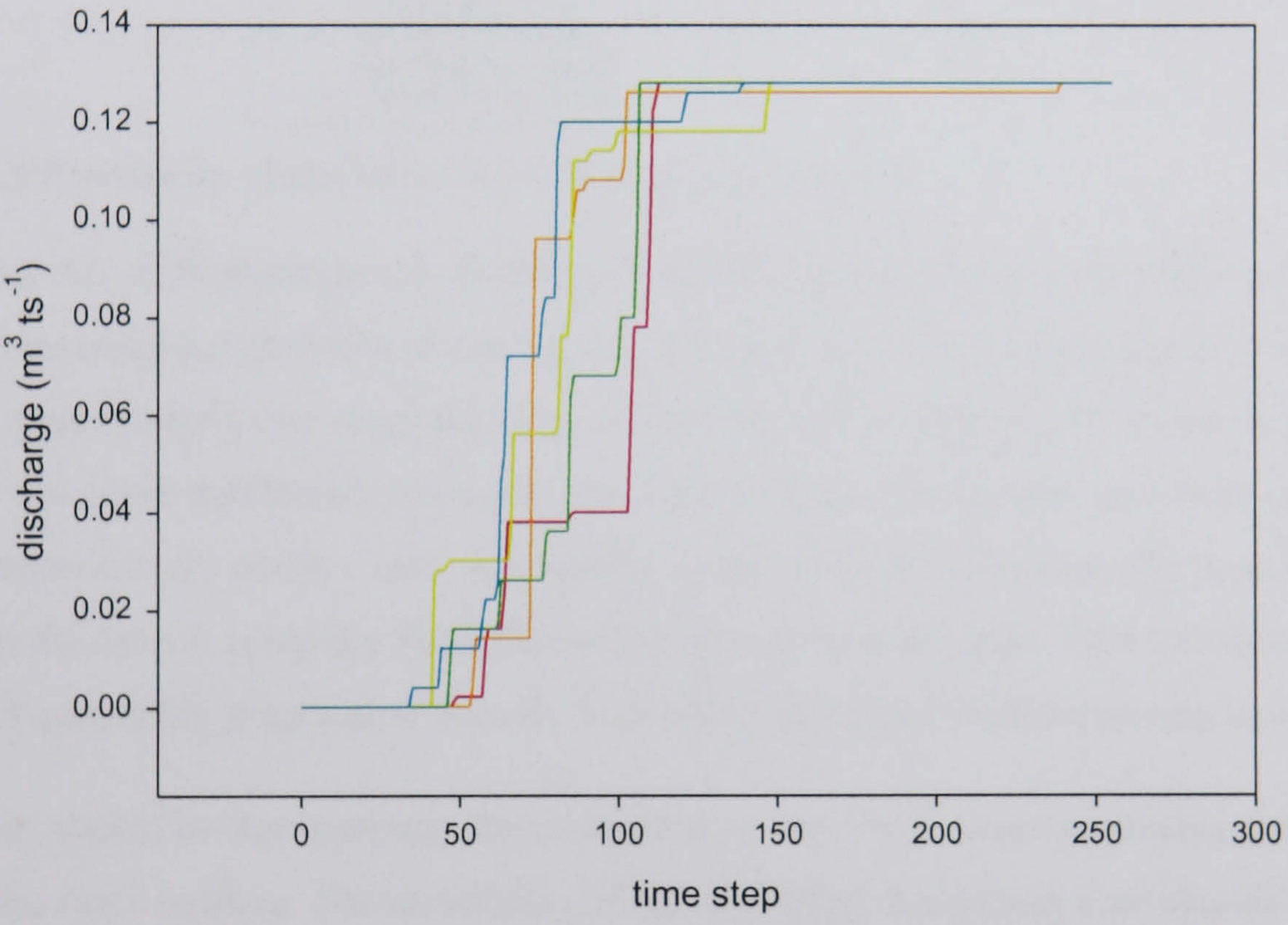

Figure 6.3 Discharge hydrographs. Each line represents an individual stochastic slope realisation

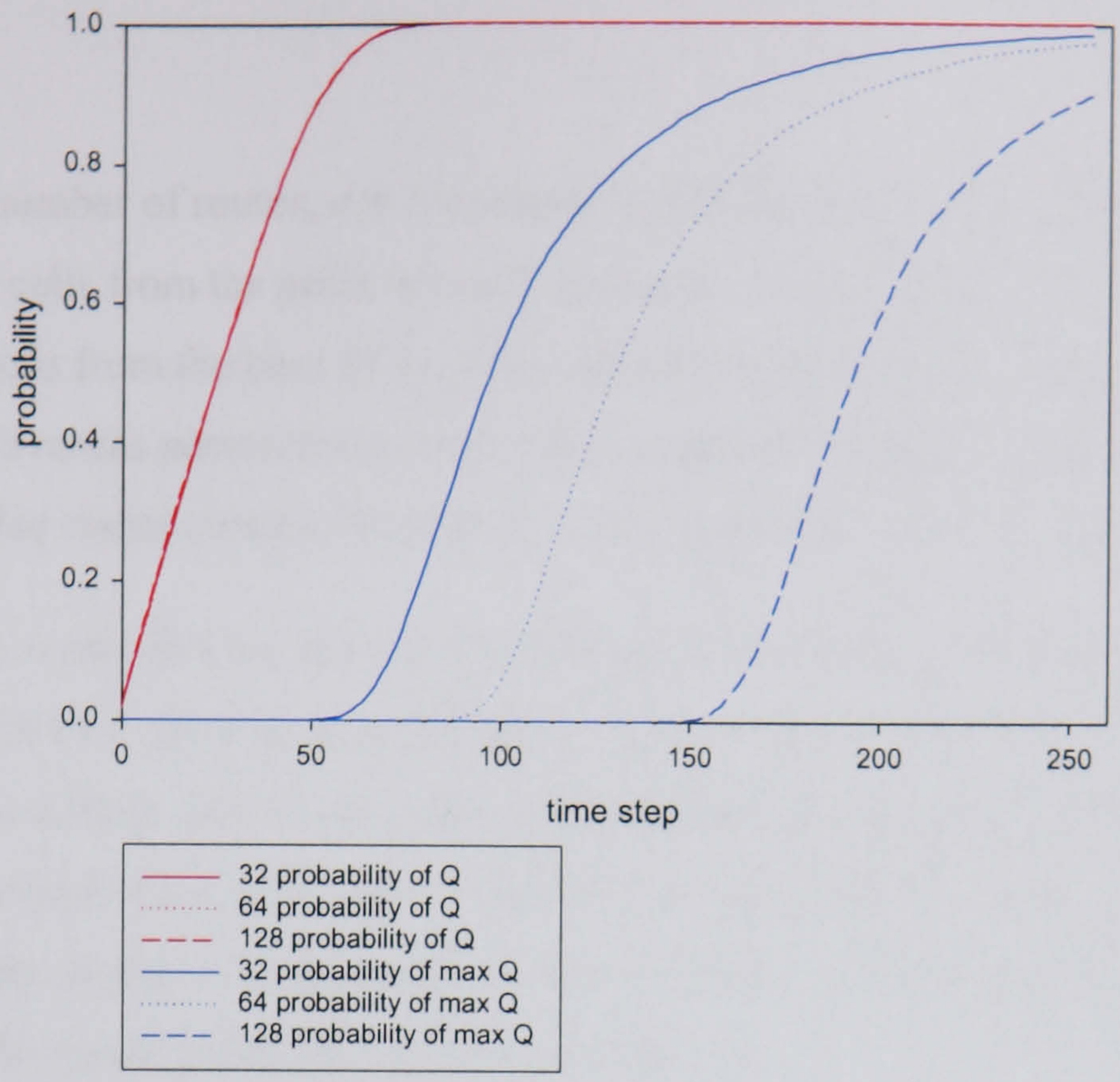

Figure 6.4 Probability of discharge for different slope lengths

The probability of there being any discharge from the slope is shown in the red curves. These steep curves reach a probability of one by the 95th time step. Each of the three curves is overlain, thus showing that the probability of discharge is not related to the slope length. The shape of this curve will be determined by the depth of the cells closest to the slope outflow. A small number of very shallow cells will rapidly produce runoff. However, if a deep cell is located at the base, it is rapidly filled due to the run-on from up slope. This therefore increases the runoff generating potential of the cell. This effect decreases with decreasing upslope area.

The curves shown in blue represent the probability of the whole slope producing runoff that reaches the slope outflow. The probability of full discharge at a certain time step decreases with increasing slope length. All of the curves are shallower and none of the curves reaches a probability of one. This is because this hydrograph property is sensitive to the spatial distribution of soil depths across the whole slope rather than in the lowest few cells. If a deep cell is located in the upper part of the slope, even with run-on, it may never produce runoff since its upslope area is small.

6.3 Two-Dimensional Plot Results

As the system representation is changed from one to two dimensions, the system complexity increases significantly. For example, the number of possible flow routes down a 1D slope is one, with each cell only routing into one other. However, with the multiple flow directions on a 2D surface, the number of possible routes from a single cell can be given by:

$$n_r = d^p$$

Equation 6.1

Where n_r is the number of routes, d is the number of directions the flow could be routed in and p is the number of cells from the point of runoff generation to the slope outflow. Therefore, for a cell located 50 cells from the base of the slope with three possible down slope cells, there are over 723 possible routes across the surface. This is assuming single flow path routing. The number of possible routes using a multiple flow path algorithm will tend towards infinity.

On a 1D slope, it is possible for one cell to dominate the response of the entire slope since all of the upslope runoff must pass through that point. For example, a cell with an above average elevation, such as a bush, will act as a dam. With the huge number of possible flow routes on a 2D surface, it is possible for flow to be routed around such obstacles. This increase in possible connection patterns enables the formation of flow networks and has a significant effect on the connectivity of the runoff producing areas on a slope.

6.3.1 Effects of Slope and Roughness on Depression Storage

From the rainfall simulation experiments, the surface roughness has a strong effect on both the timing and amount of generated runoff. The aim of these experiments is to investigate the relationship between the plot gradient, surface roughness and surface depression storage. The surface roughness was generated from the positive half of an exponential distribution. The slope was then added to the surface as a separate component. The mean of the distribution, α, can be related to the Random Roughness (RR) coefficient (in m) of Allmaras et al. (1966) (Equation 6.2) as described in chapter 3.

$$RR = 0.657\alpha \qquad (r^2\ 0.999)$$

Equation 6.2

The model cells were spatialised on a grid structure over the plot. The horizontal scale of each cell was 0.01 m and the grid extent was 50 by 50 giving the same spatial extent as the rainfall simulation plots. The depression storage was calculated by raining onto the surface and allowing water to flow into the depressions. No infiltration of water was allowed during the simulation. The rainfall continued until there was no further increase in the amount of water stored on the surface. This approach is similar to that of Onstad (1984).

The relationship between slope, roughness and depression storage was investigated over the range of slopes from 0° to 40° and for α values of 0.004, 0.006, 0.008, 0.012 and 0.016. The results are shown in Figure 6.5.

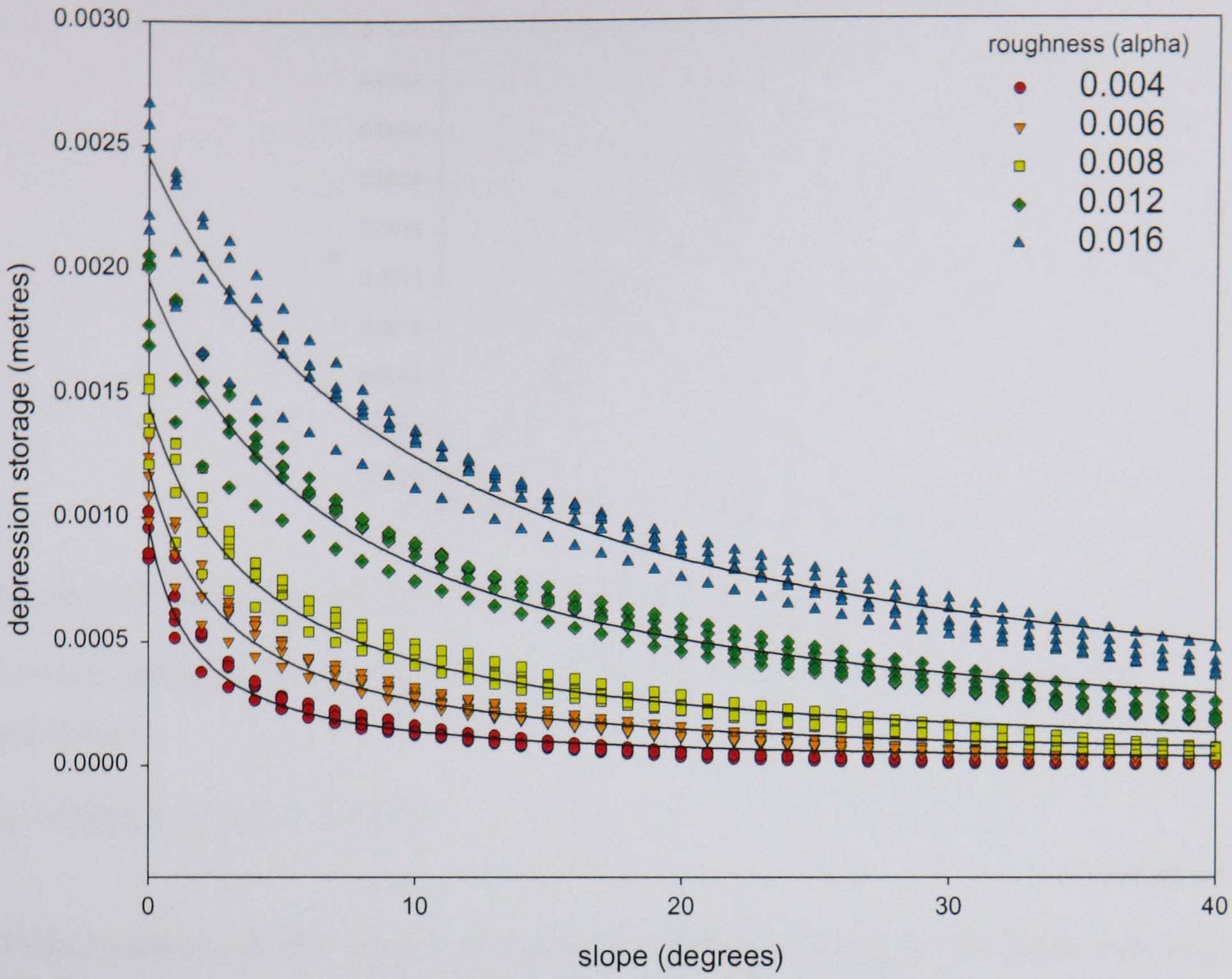

Figure 6.5 The relationship between surface slope, roughness and depression storage

The trend in all of the data series is for a decrease in the depression storage with an increase in slope. This is due to the reduction in volume of the depressions as they are tilted. As the roughness increases the amount of depression storage also increases. With greater roughness, the mean and maximum size of depression increases leading to the greater storage. All of the data series have a curved decrease in storage to a point where the surface is influenceed less by increases in slope gradient. The point at which this insensitivity starts is at greater slope gradients for higher roughness values. As the roughness increases, the absolute scatter in the data series also increases. However, the COV of storage depths decreases with increasing roughness. Curves were fitted to the data using Equation 6.3.

$$dp = \frac{a}{\beta}$$

Equation 6.3

Where a is a coefficient and β is the surface slope of the surface in degrees. The relationship between a and α are shown in Figure 6.6.

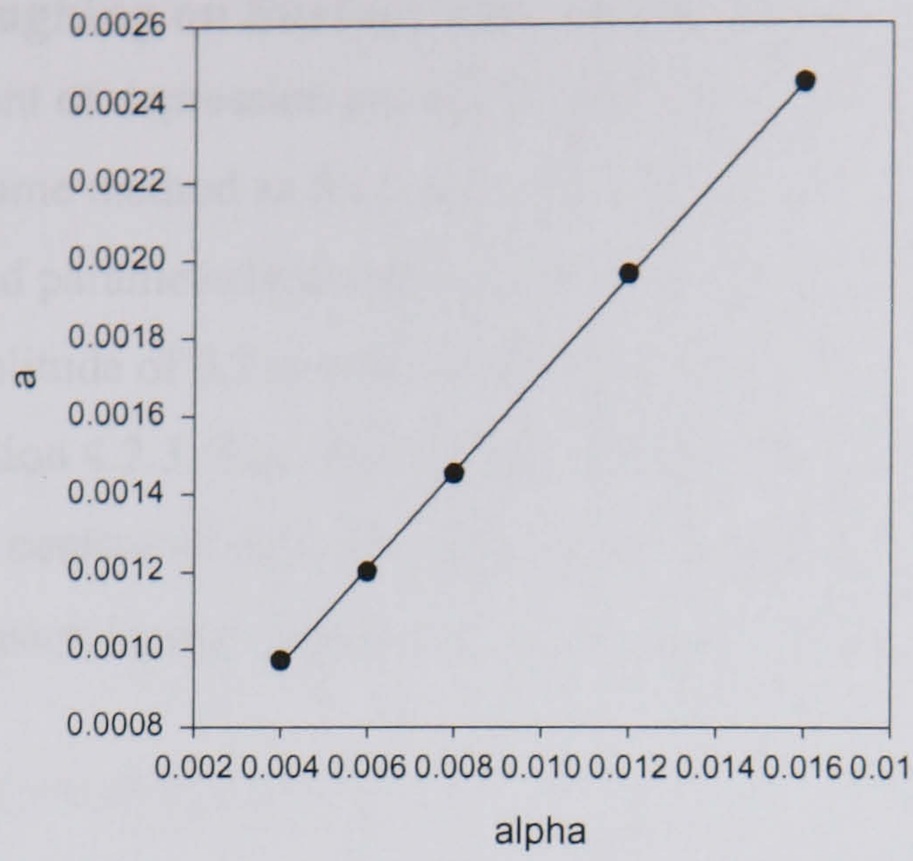

Figure 6.6 Relationships between the roughness (α) and the a coefficient

Linear regression lines were fitted to the relationships between *a* and α. This gives the relationship:

$$a = 0.0005 + 0.1242\ \alpha \quad (r^2\ 0.999)$$

Equation 6.4

These equations can then be used to calculate the depression storage for any given slope and roughness within the range defined above. The surface defined by these equations is shown in Figure 6.7.

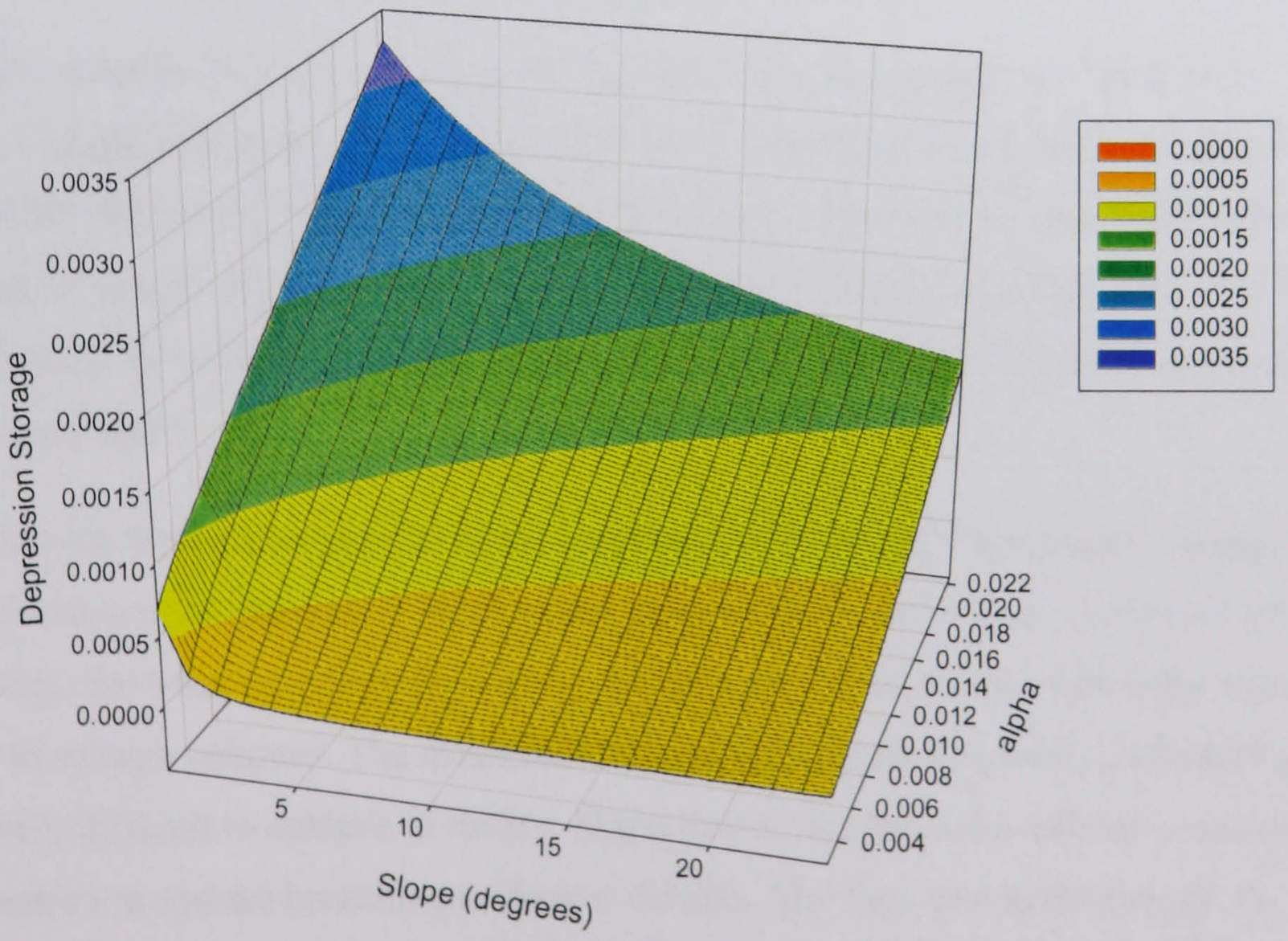

Figure 6.7 The statistical relationship between surface slope, roughness and depression storage

This relationship can be used to characterise the Sub-model unit depression storage as it varies with gradient. This is then used in the slope scale modelling as a key relationship in CRUM-2D.

6.3.2 Effects of Ploughing on Surface Depression Storage

The effects on the amount of depression storage caused by the ploughing of the surface were investigated using the same method as for scrub slopes. The characteristics of the furrows were measured in the field and parameterised using a sine wave and a separate roughness component. The furrows had an amplitude of 0.2 m and a wavelength of 0.4 m, as was found from the field results presented in Section 4.2.3. The relationship between the furrow direction and the contour was varied from perfect contour ploughing to plough lines perpendicular to the contour in step of 15°. The mean depression storage depths from 20 surface realisations is shown in Figure 6.8.

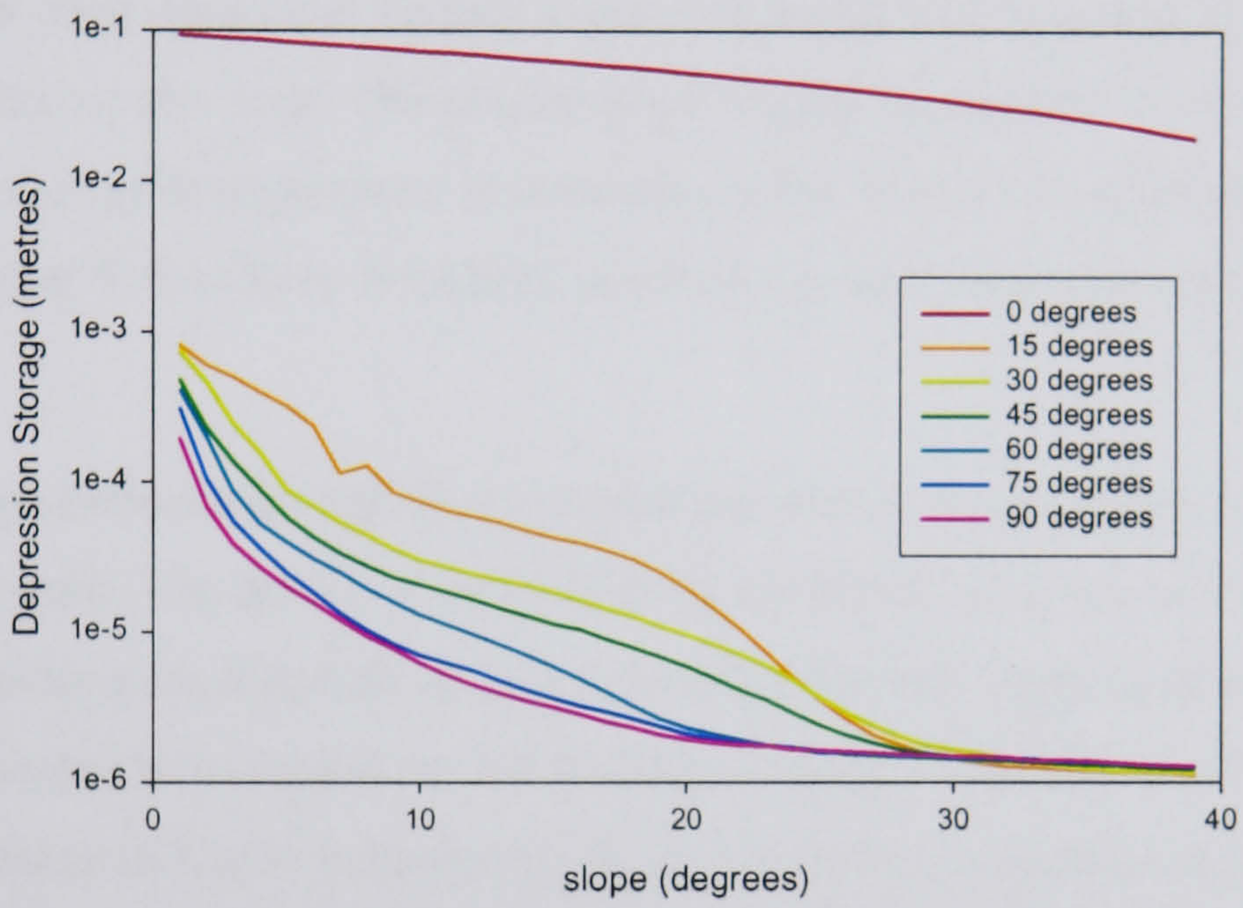

Figure 6.8 Effects of plough line direction on depression storage

The greater the angle between the furrow and the contours, the steeper the decrease in depression storage with slope. The surfaces become less sensitive to changes in slope above a gradient of 30°. However, the depression storage value for slopes of greater than 8° are less than 0.1 mm and for slopes of greater than 23°, the depression storage is less then 0.01 mm. These depths are below the resolution of most tipping buck rain gauges (0.2 mm) and hence can be considered negligible.

The surface with the furrows parallel to the contours has far greater depression storage. This is because the water must increase in depth to the point where it can breach the furrow top. On the other surfaces, the water is able to flow along the contour to the outflow, hence the strong difference in storage volumes. The modelled situation reflects perfect contour ploughing which would be very difficult to achieve in reality. Slight deviations from the contour would result in flow concentration and the breaching of furrow divides. The flow would then erode the top of the furrow. Both of these factors would lead to a reduction in the depression storage.

The very low levels of depression storage are related to the decrease in storage area from the furrows and to the concentration of flow in the furrow bottoms. This flow concentration enables

the flow to overcome the micro-roughness and connect with the plot outflow. The greater organisation in the surface leads to greater connectivity of overland flow.

6.4 Two-Dimensional Slope Results

This section considers the processes occurring at the spatial scale of a hillslope. This is considered to extend from a drainage divide at the top of the slope to a channel at the slope base. The change in spatial scale means that a number of new factors become important in determining the generation and transmission of runoff. The presence of vegetation influences the infiltration rate and the amount of rainfall reaching the soil surface through the process of interception. The slope dependent surface depression storage investigated in section 6.3.1 is now distributed across the slope. The greater slope lengths mean that the overland flow velocities become of great importance in determining the form of the discharge hydrograph. As discussed in chapter 5, the Darcy-Weisbach equation has been implemented to model flow velocities.

To aid comparison between the different model experiments, the same base size and shape surface has been used. The details of the base slope and storm are given in Table 6.1 and Figure 6.9 shows the discharge hydrograph and the depression storage. From field investigates, this slope has been created to be typical for the Rambla de Nogalte catchment. The slope length of 50 m and at 6° relates to slopes found in the field. The surface roughness relates to the values measured in the field as presented in Section 4.2.3. The soil depth is related to surface gradient using a linear regression model fitted to the field data. The infiltration model parameters relate to results from the rainfall simulation experiment on the bare area with stones on a scrub site (5), as shown in Table 4.8. A set storm of 75 mm hr^{-1} for five minutes has been used for all the experiments in this section. This rainfall pulse is related to a low frequency, high magnitude storm event. From the rainfall record analysed in chapter 3, 0.6 % of rainfall occurs at this intensity or above. The rate of 75 mm hr^{-1} was used in the rainfall simulation experiments and hence links the two sets of experiments. The peak discharge is 0.008 $m^3 s^{-1}$ and the total discharge is 0.76 m^3 giving a runoff coefficient of 4.87 %. These values are used throughout this section and the changes are noted in each section.

Parameter	Value
Slope size	50 by 50 m
Cell size	1 by 1 m
Slope gradient	6°
Surface roughness	Independent random elevations based on an exponential distribution with a mean of 1 mm
Soil depth	Related to slope, giving a depth of 0.288 m at six degrees
Initial soil moisture	45 %
Vegetation	None
Infiltration parameters ($mm\ hr^{-1}$)	a = 11 b = 9
Friction factor, *ff*	75
Storm length	5 minutes
Storm intensity	75 $mm\ hr^{-1}$

Table 6.1 Base slope and model parameters

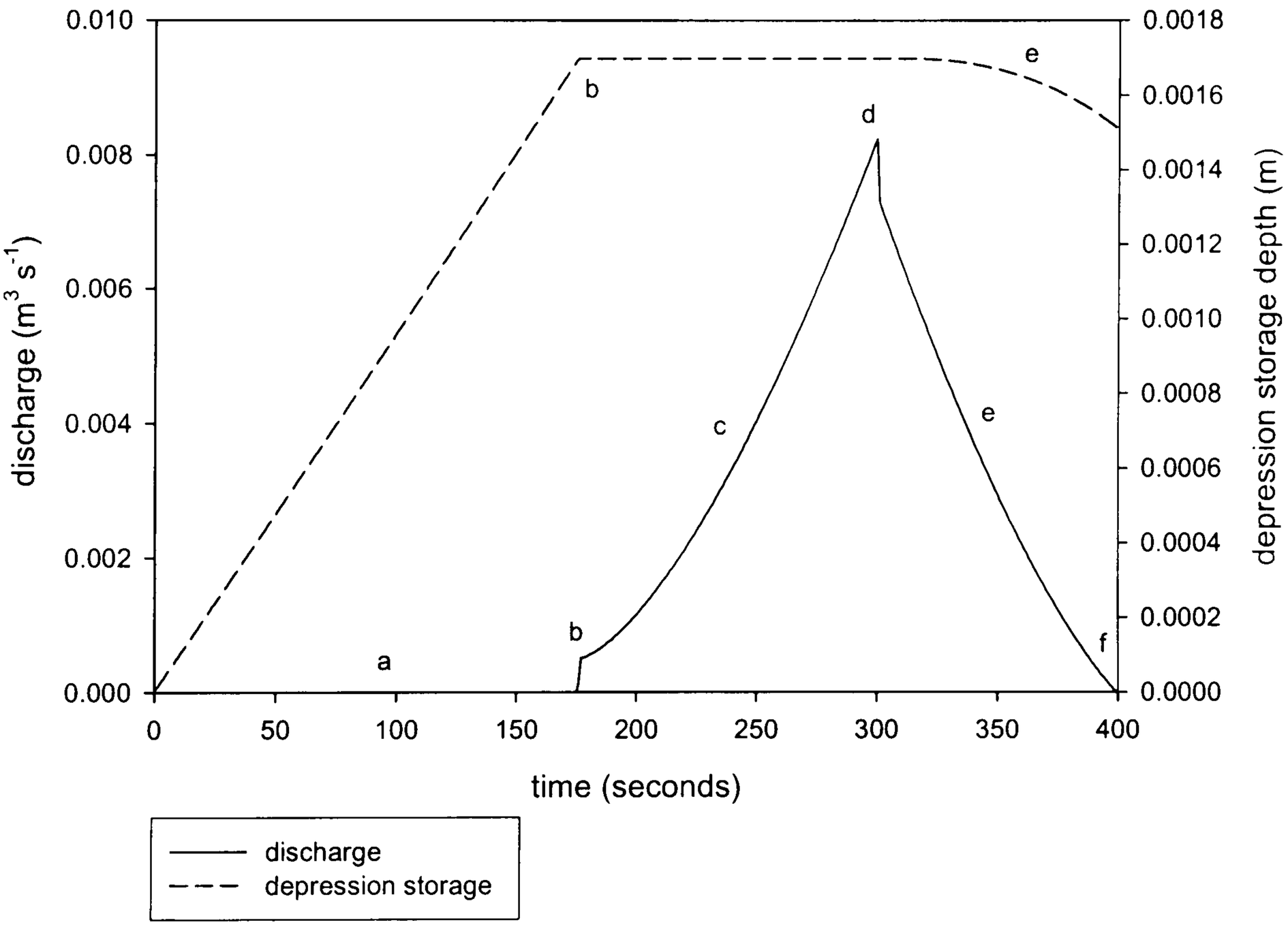

Figure 6.9 Discharge hydrograph from the base surface

The hydrograph form may be broken down into a number of sections. Section a represents the time to runoff. During this period, the infiltration excess is able to fill the surface depression store. At point b, part of the depression store is full and runoff is initiated. The step increase in discharge relates to the overflowing of the depression store and rainfall being converted directly to runoff. The rising limb c is related to increase in the area contributing to the discharge and the decreasing infiltration rate. At point d the rainfall ceases and there is a switch from rainfall generated runoff to flow controlled runoff. This accounts for the sharp decrease in the discharge. During the following section e the discharge is decreasing due to transmission losses and the

reduction in the area contributing runoff. The amount of water in the depression store is decreasing thus disconnecting parts of the slope and hence reducing the area able to contribute runoff. The slope of section e is related both to the transmission losses and the decrease in the amount of area contributing to discharge. The final point f marks the cessation of runoff. At this point, the water on the slope is held either in the surface depression store or in the soil moisture store. Over time, the water in the surface depression store will infiltrate and the soil store will drain. This therefore returns the system to its initial state.

6.4.1 Slope Length

Slope length is a universal parameter of every point in the landscape which influences the distance to the channel and the contributing area to a runoff generating point. The distance to the channel is important since it controls the time required to reach the outflow and hence determines the time available for runoff to be lost as a transmission loss. The upslope contributing area determines the amount of run on and hence the soil moisture store. This influences the infiltration rate and the amount of runoff which will be generated.

The effect of the slope length on the amount of discharge has been investigated. This is an extension of the 1D modelling of the effects of slope length. From analysis of the DEM of the catchment, the range of slope lengths was defined as 5 m to 400 m. The hydrographs for slopes between 5 and 50 m are shown in Figure 6.10.

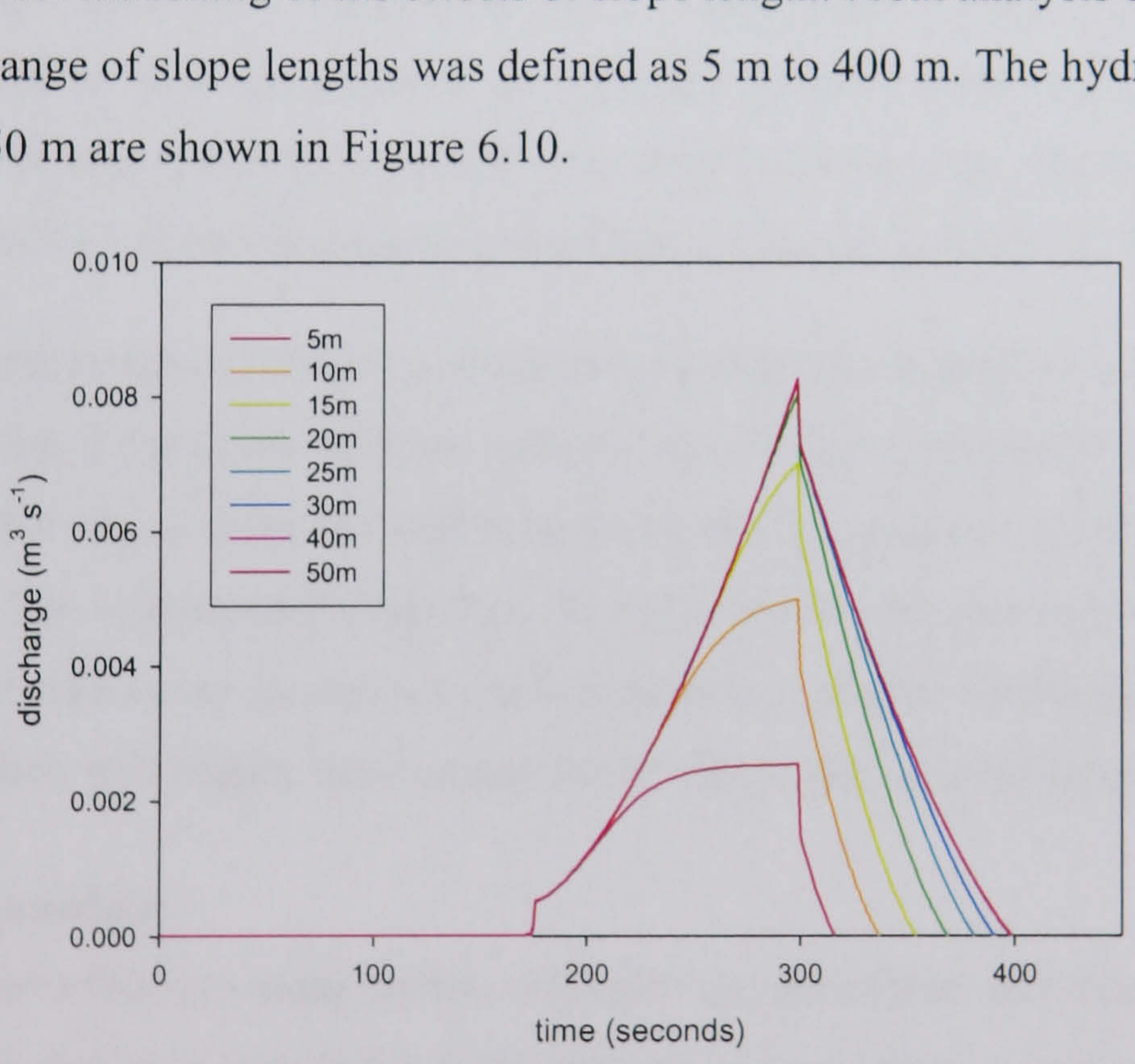

Figure 6.10 Effects of slope length on hydrograph form

The simulations with slope lengths greater than 20 m show the same rising hydrograph limb and the same peak discharge. The slopes with shorter lengths have shorter travel times to the slope base. Therefore, the runoff generated on a larger percentage of the slope is able to leave the slope as discharge. As the slope length increases, the slope of the receding limb decreases thus resulting in a longer time until the cessation of rainfall. The relationship between slope length and the runoff coefficient for slope lengths from 5 to 400 m are shown in Figure 6.11.

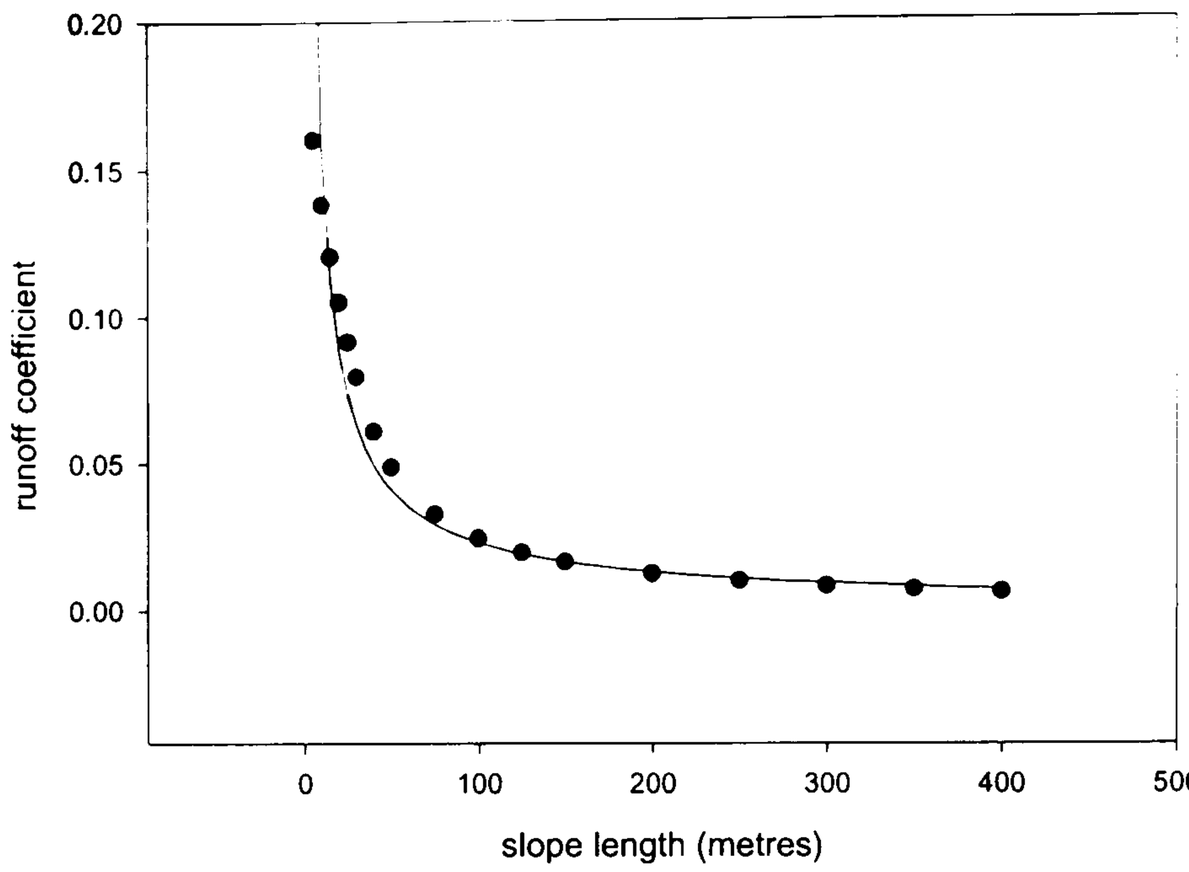

Figure 6.11 Effects of slope length on the runoff coefficient

The relationship shows a curvilinear decrease in the runoff coefficient with increasing slope length. A regression model can be fitted to the data of the form:

$$rc = a.slen^{b}$$

Equation 6.5

Where a and b are coefficients. For this storm, a = 1.0874 and b = -0.8383. This relationship will be influenceed by the slope gradient, the infiltration characteristics and the storm characteristics. The interaction between the slope length and the slope gradient is investigated in detail in section 6.5.1 and the interactions with the storm characteristics in chapter 7.

The decrease in the runoff coefficient with increasing slope is caused by transmission losses as the runoff flows down the slope. With an overland flow velocity of about 0.1 m s^{-1}, it will take over 16 minutes for runoff generated 100 m from the base to reach the slope outflow. Since flow only occurs for ~100 seconds after the end of the storm, the maximum distance it can travel is ~10 m. As the water moves over the soil surface, it will be infiltrated. The introduction of concentrated flow will reduce these transmission losses, and is investigated in section 6.4.3.

6.4.2 Slope Gradient

The slope gradient influences many factors related to the generation and transmission of overland flow. As shown in section 6.3.1, the amount of water that can be held in depression storage decreases with increasing slope gradient. From field results, it was shown that the soil depth decreases with increasing slope gradient. The energy available for overland flow increases with slope gradient, and hence the overland flow velocity increases. The relationships between these factors and slope gradient are shown in Figure 6.12. The effect on the surface depression storage is taken from Equation 6.3. The effect on the overland flow velocity is calculated from the Darcy-Weisbach equation. The effect on soil depth is taken from a regression model based on field measurements.

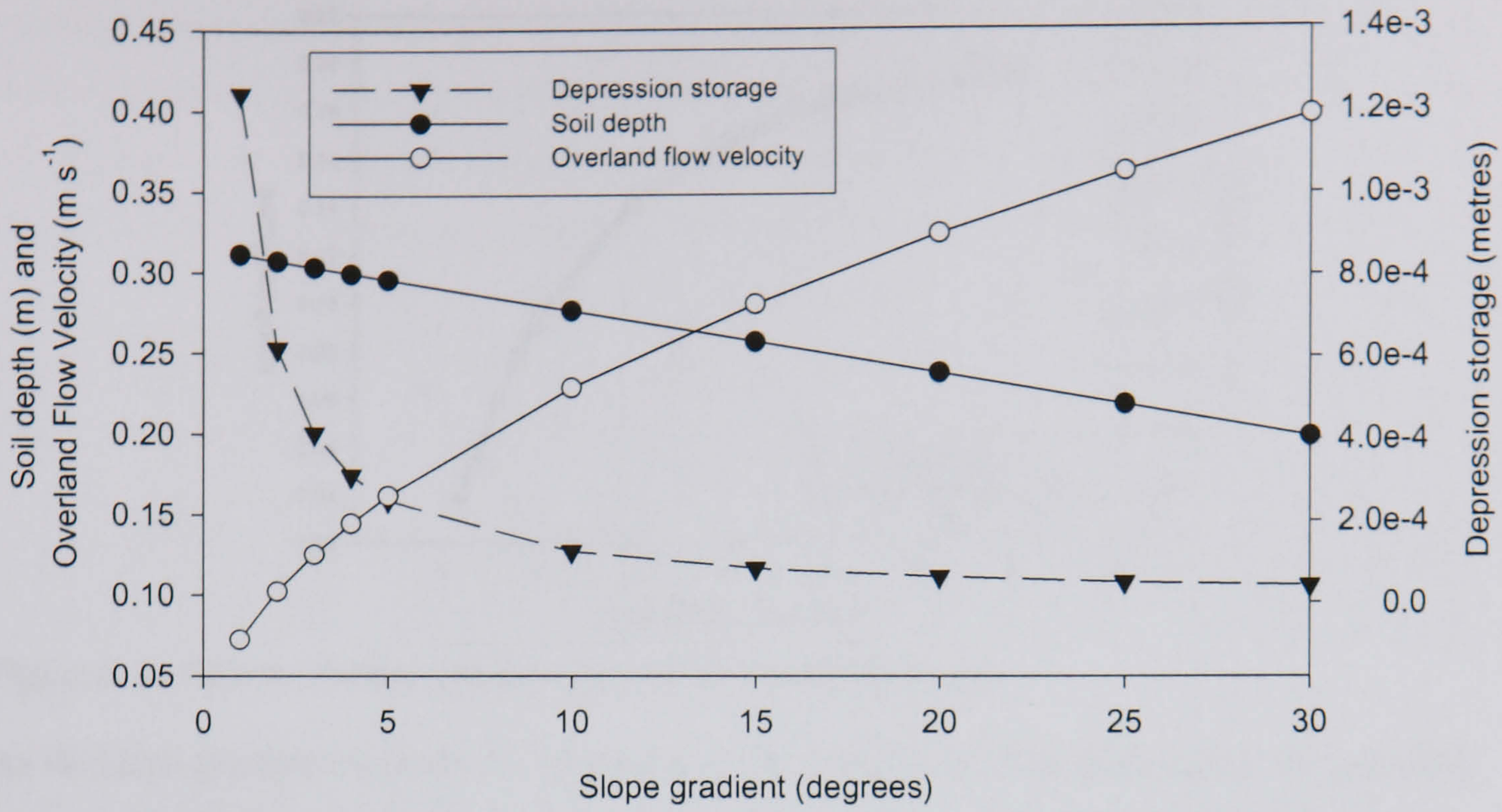

Figure 6.12 Effects of slope gradient on depression storage, soil depth and overland flow velocity

The surface depression storage and the overland flow velocity are very sensitive over the range 0° to 5° and the depression storage is extremely sensitive over the range 0° to 2°. The soil depth is related linearly to the surface gradient and hence is not sensitive over a particular range. The effect of slope gradient on the hydrograph form is shown in Figure 6.13 and the effect on the total and peak discharge is shown in Figure 6.14.

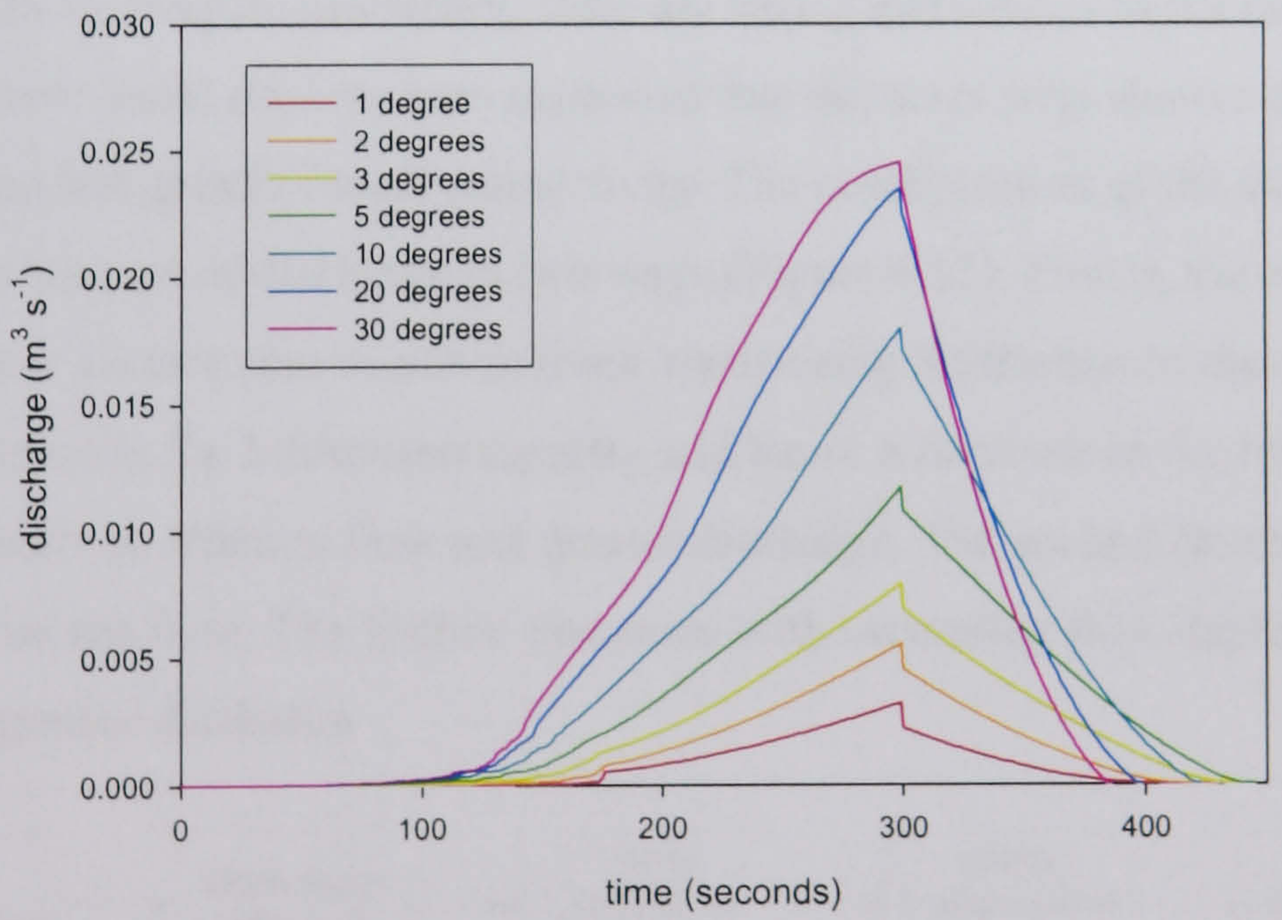

Figure 6.13 Effects of slope gradient on the hydrograph form

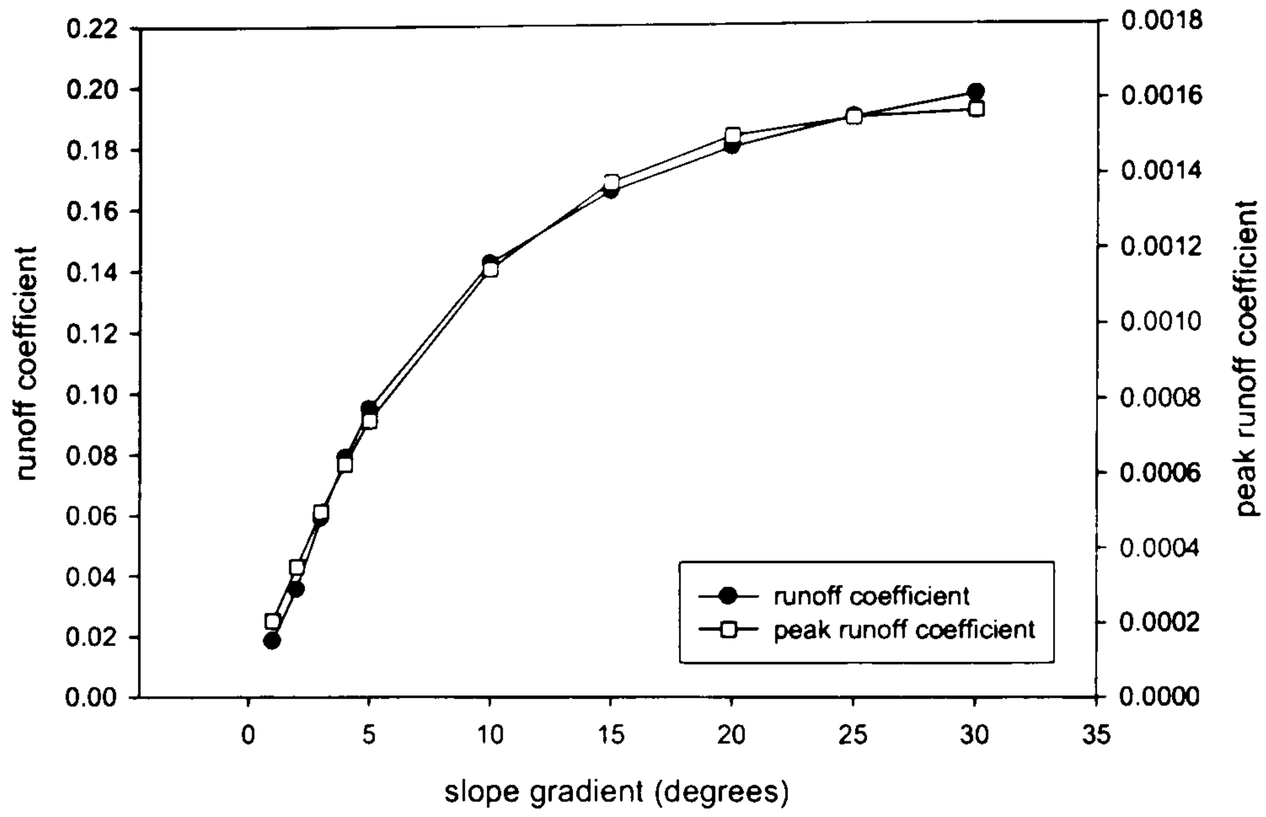

Figure 6.14 Effects of slope gradient on total and peak discharge

As the slope gradient increases the steepness of the rising limb of the hydrograph, the peak and total discharge increase. These increases are greatest over the range 1° to 5°, as predicted by Figure 6.12. On the steeper slopes, the soil depth is less. Hence, there is a greater reduction in the infiltration capacity with the same amount of rainfall. The decrease in depression storage means that less infiltration excess is required to initiate overland flow. The increase in the flow velocity results in the runoff reaching the base of the slope in less time, hence the steeper rising hydrograph limbs.

6.4.3 Flow Paths

Across the Rambla de Nogalte catchment, there are strong differences in the distance to an area of concentrated flow. Field observations suggested that the areas with shorter distance to the flow concentration had greater runoff connectivity. The configuration of the surface flow paths will influence the amount of discharge in two ways (Figure 6.15). Firstly, the concentration of water into a smaller surface area results in more water being infiltration in these areas. This in turn leads to decrease in the infiltration capacity and hence a decrease in the transmission losses. This therefore results in efficient flow and greater discharge. The second factor relates to the friction imposed on the flow. The friction decreases with increasing flow depth, resulting in faster flows and greater discharge.

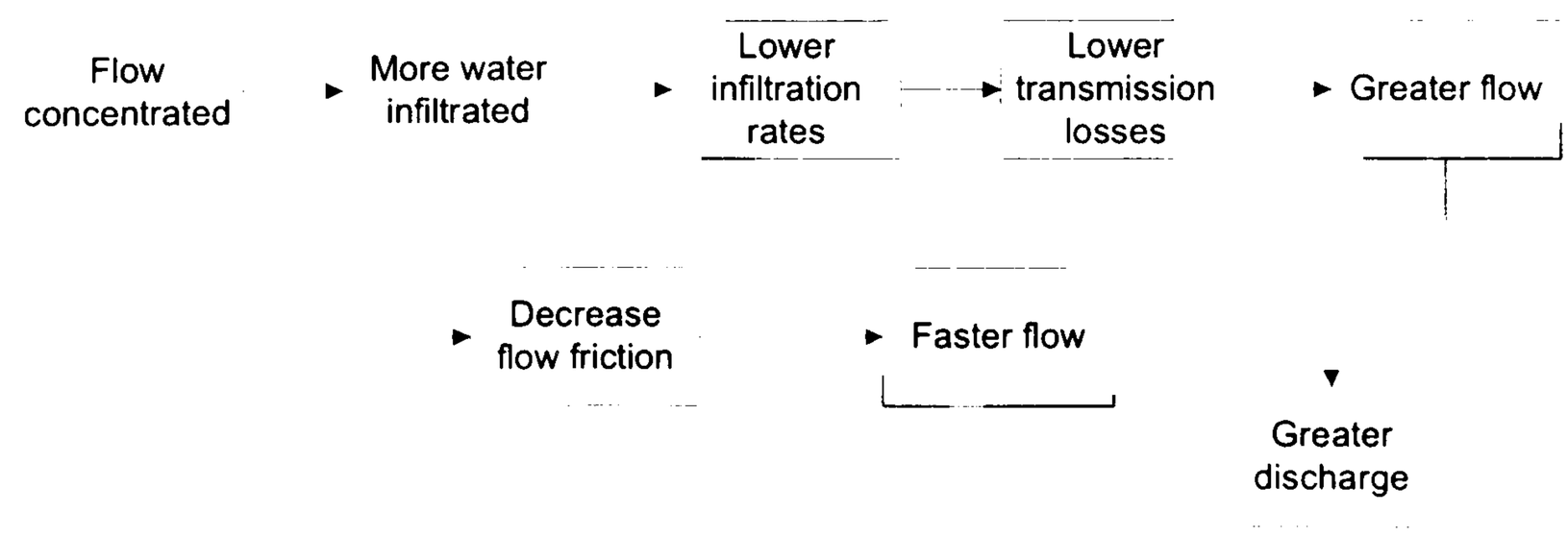

Figure 6.15 Effects of the surface flow path configuration

A series of surfaces was created with a range of distances to the nearest channel. The surfaces were created using a sine wave and a separate slope component. As the wavelength was decreased, so too was the amplitude, thus creating surfaces with a similar slope gradient. Sample surfaces are shown in Figure 6.16. The discharge hydrographs are shown in Figure 6.17.

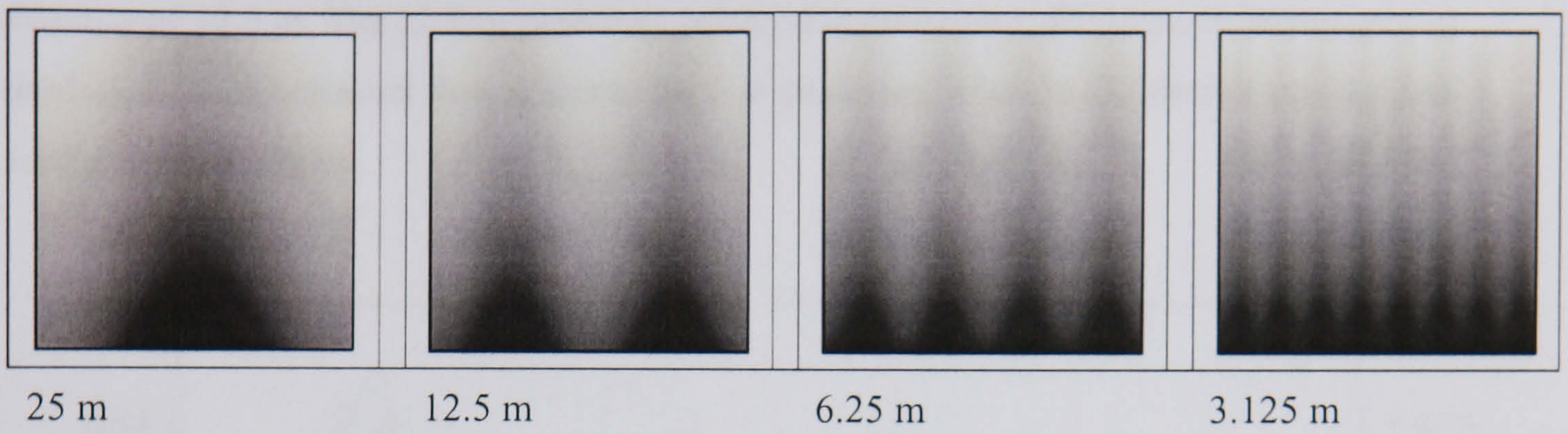

Figure 6.16 Different distances to the nearest channel

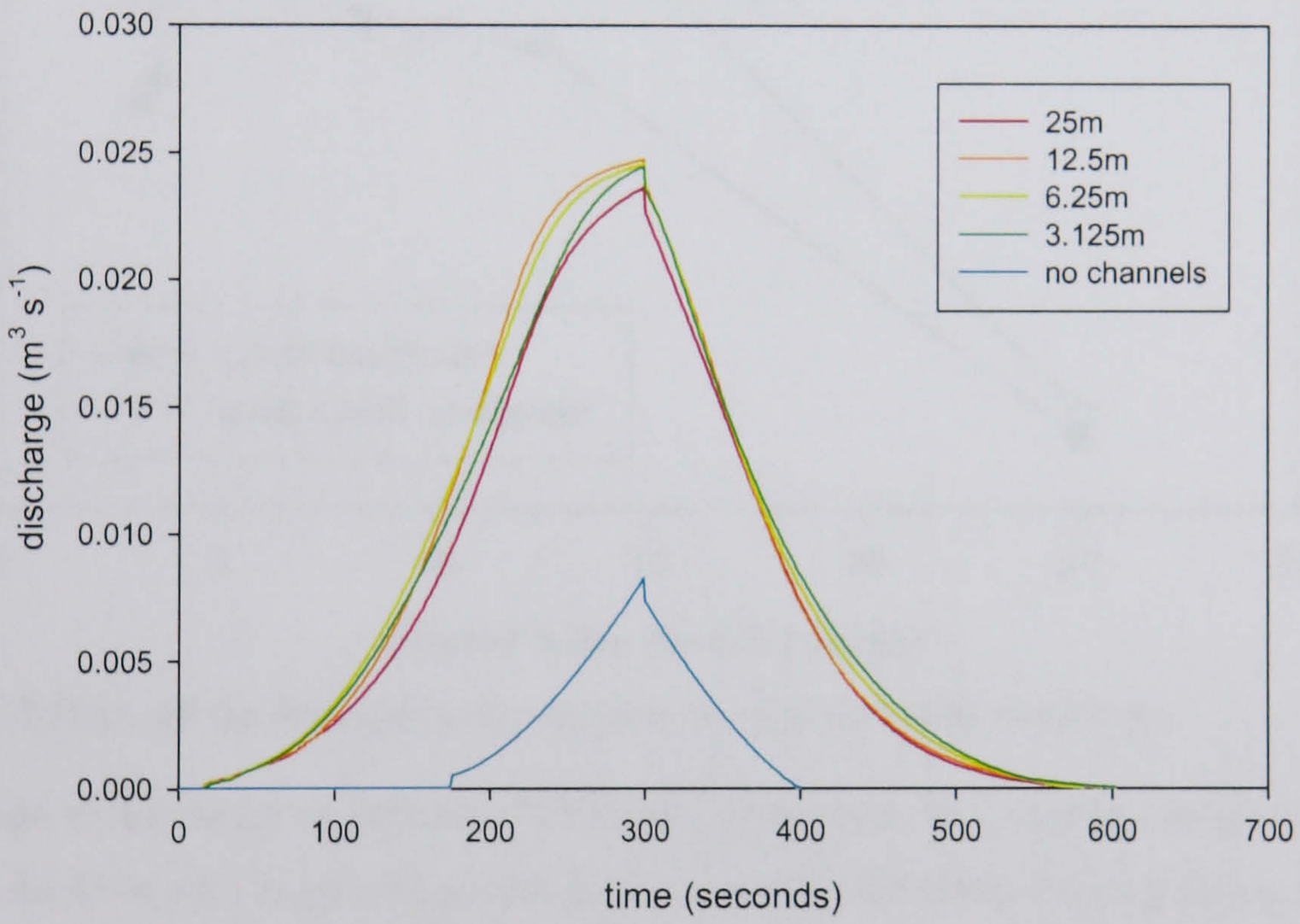

Figure 6.17 Effects of the distance to the channel on discharge

The introduction of flow convergence onto a surface through the presence of channels results in a significant increase in both total and peak discharge when compared to a surface without flow convergence. The introduction of channels creates slopes on the surface that have gradients greater than 6 °. This therefore decreases the surface depression storage and hence the amount of infiltration excess required to initiate runoff. This accounts for the shorter time to runoff. The flow concentration increases the flow depth and hence the flow velocity. The maximum velocity on the flat surface is 0.067 m s^{-1} whilst on the surface with a single channel, the maximum velocity increases to 0.3 m s^{-1}.

The runoff coefficient reaches it maximum value for a surface with a distance to the channel of 5 m (Figure 6.18). Distances greater and less than 5 m give a lower runoff coefficient. This suggests that there is an optimal spacing for channels for this storm. If the channels are spaced

closer together than this value, then there is not enough runoff generated to create efficient channel flow. If the channels are further apart, then the flow is too shallow to create efficient channel flow and more water is lost on the slope as transmission losses.

The peak runoff coefficient values show two peaks, one at a distance of 5 m and the second at a distance of 12.5 m. The 12.5 m peak may relate to there being sufficient catchment area to produce efficient channel flow whereas the 5 m peak may relate to the shorter travel times across the side slopes.

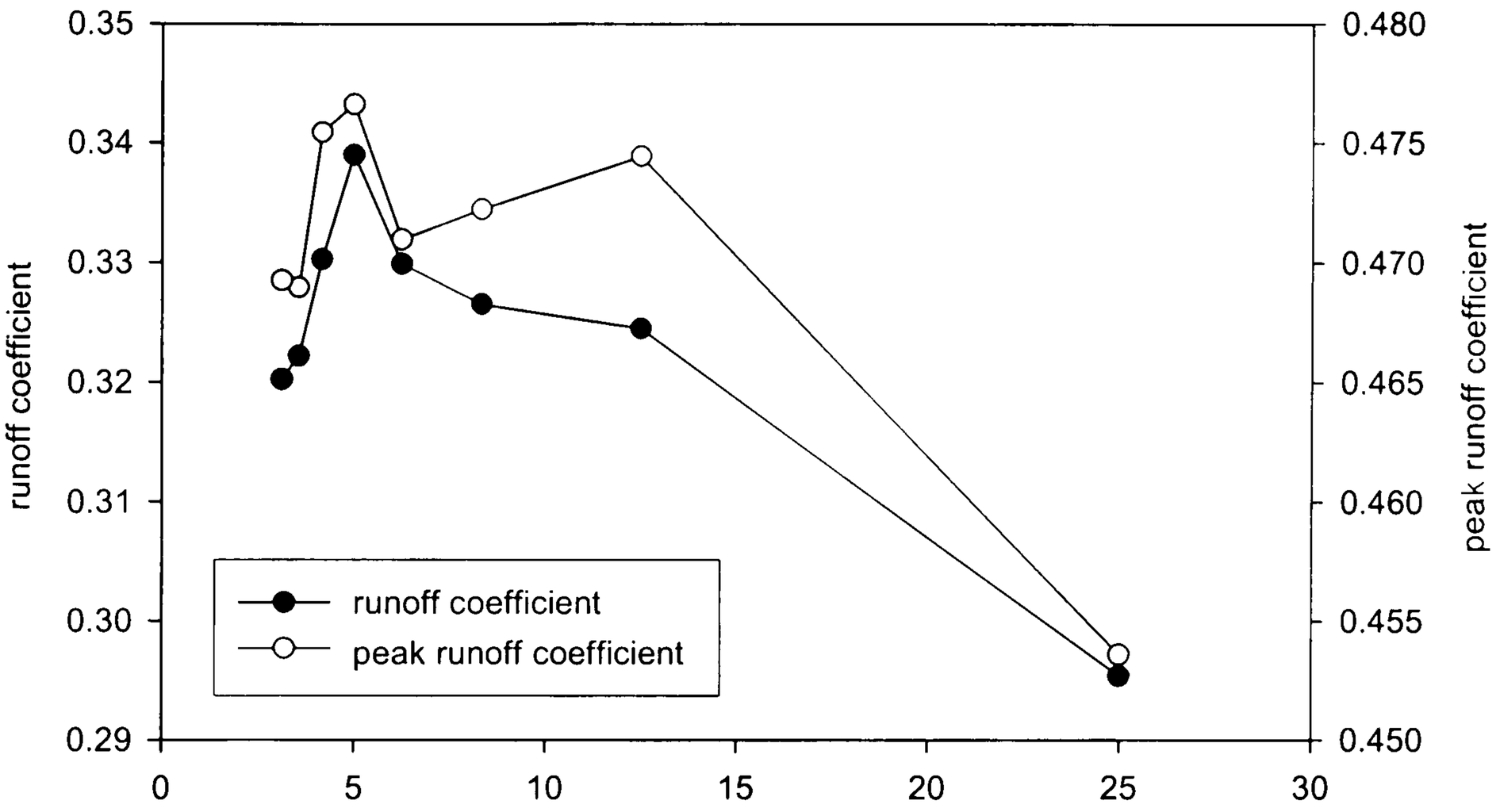

Figure 6.18 Effects of the distance to the channel on total and peak discharge

The reduction in discharge on surfaces with larger distances to the channel can be related to the increase in the flow path length. This increase is caused by the water flowing across the slope to the channel before flowing down slope. Therefore, there is a greater amount of transmission loss and hence lower discharge. This can be related to the slope length experiments in section 6.4.1 since the introduction of channels onto the slope manipulates the distribution of slope lengths.

6.4.4 Infiltration Rates

The infiltration rate influences the time until the runoff is generated, the time until the depression storage overflows and the transmission losses of the overland flow. The combined result of these effects means that the infiltration rate has a significant control on the discharge from the slope. The parameters of the simplified Green and Ampt equation were investigated over the range derived from the rainfall simulation experiments, Section 4.4.2 and as shown in Table 4.8. This gave the range of values a = 10 - 75 and b = 1 - 12. This therefore gave a minimum steady state infiltration rate of 16.7 mm hr^{-1} and a maximum rate of 155 mm hr^{-1}. The

effects on the runoff coefficient are shown in Figure 6.19 and the effects on peak runoff coefficient are shown in Figure 6.20.

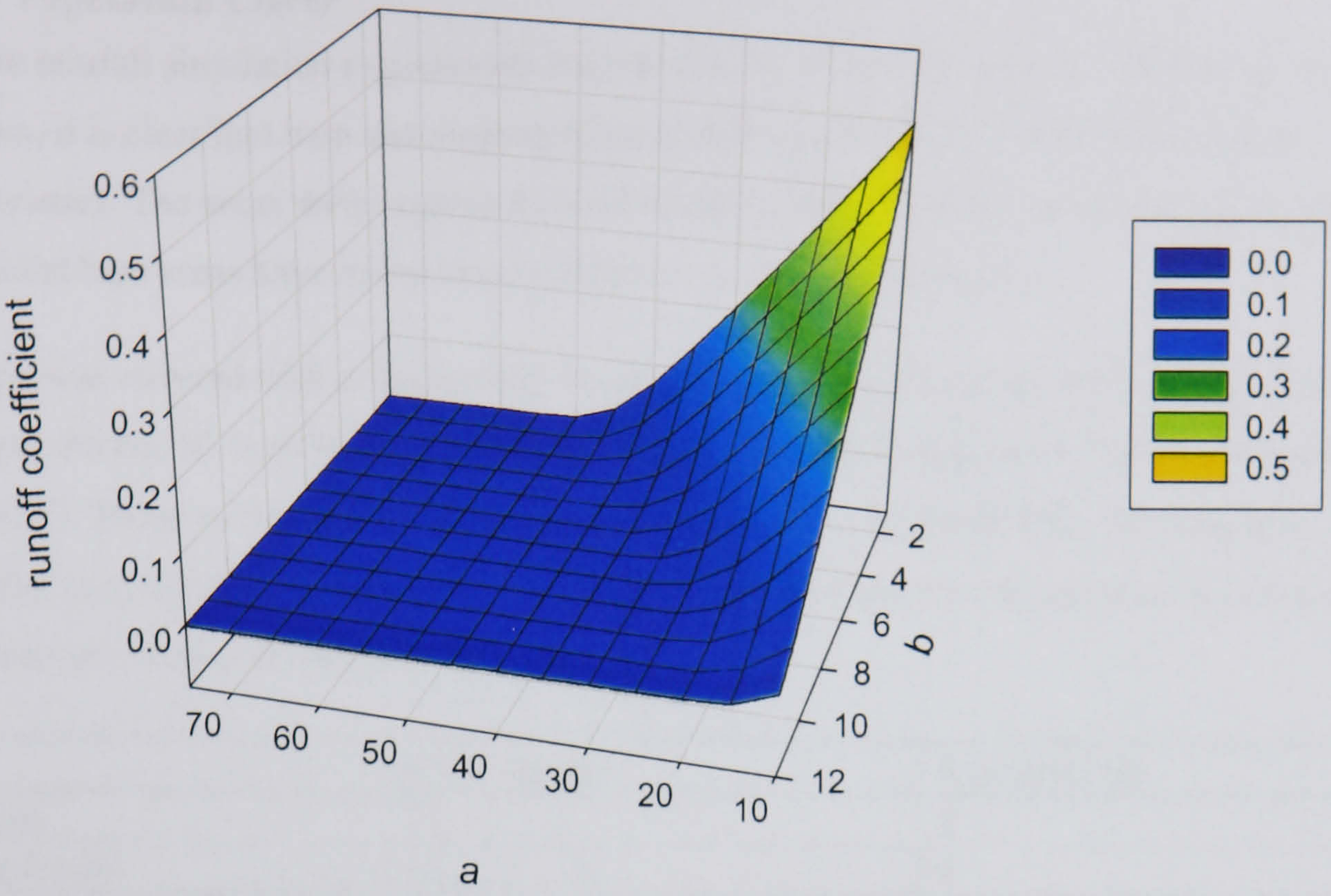

Figure 6.19 Effects of infiltration characteristics on total discharge

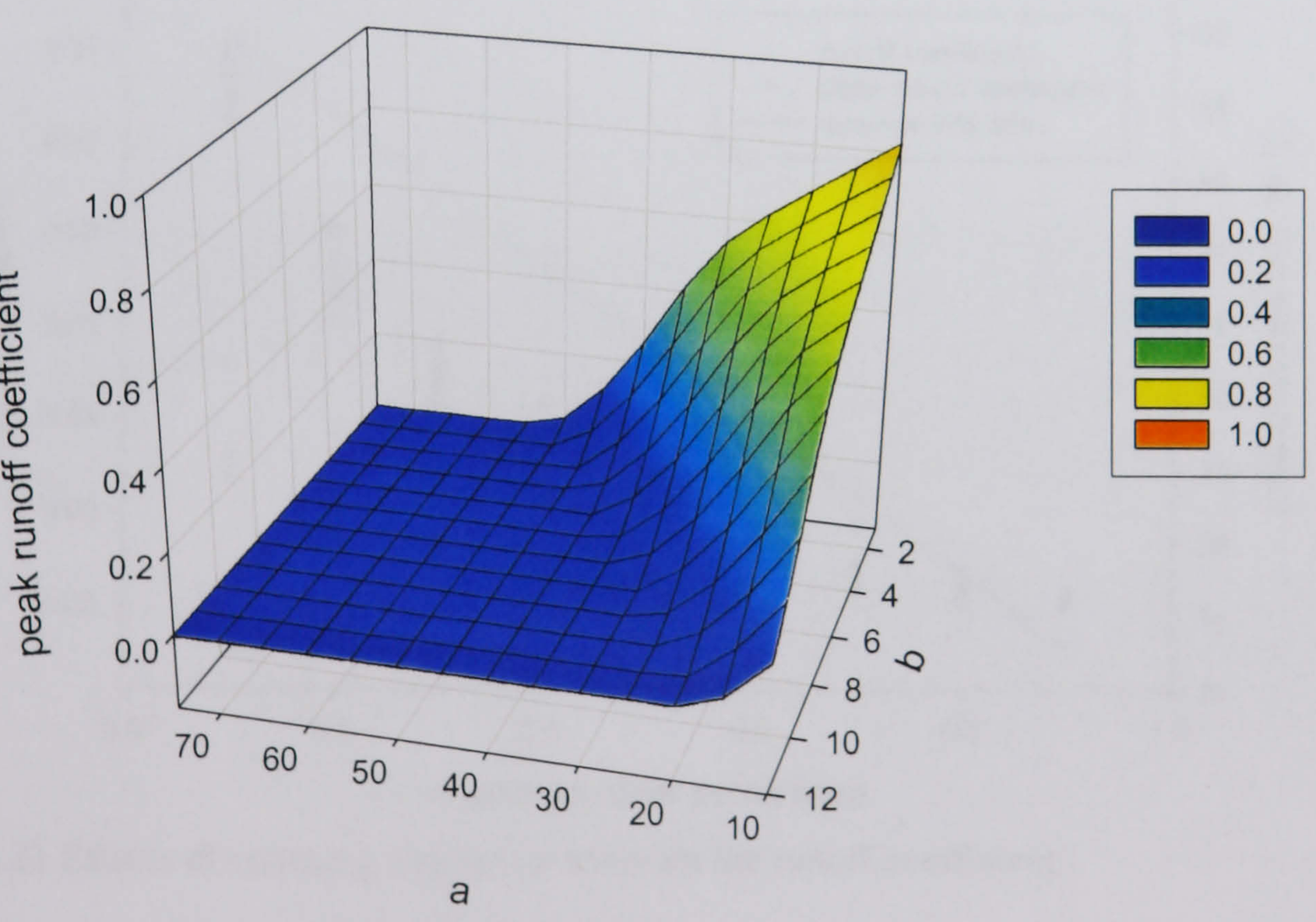

Figure 6.20 Effects of infiltration characteristics on peak discharge

It is clear from Figure 6.19 and Figure 6.20 that over much of the parameter space of the infiltration equation, there is no runoff generated for this storm. The change in the storm runoff coefficient increases linearly above a threshold infiltrate rate. However, the increase in the peak runoff coefficient is curvilinear. This is due to the higher peak runoff being sourced from a

larger spatial area. Therefore, the travel distances increase and hence the sharpness of the runoff peak decreases.

6.4.5 Vegetation Cover

From the rainfall simulation experiments and the review of the literature on infiltration in semi-arid areas, it is clear that bare and vegetated areas have significantly different infiltration characteristics. The areas with vegetation have higher infiltration rates and hence act as runoff sinks whilst bare areas have lower rates and hence act as runoff sources.

The slope was covered with a fragmented vegetation pattern with a *frag* value of 0.25. The cover varied from 10 % to 90 % with the infiltration equation (Equation 4.1) parameter values in Table 6.2. These values are from the field results from site 5 (Table 4.8). The average infiltration rates across the slope for the different vegetation covers and the peak and total runoff coefficients are shown in Figure 6.21.

	***a* parameter**	***b* parameter**
Bare areas	11	9
Vegetated areas	46	4

Table 6.2 Infiltration model parameters for bare and vegetated area

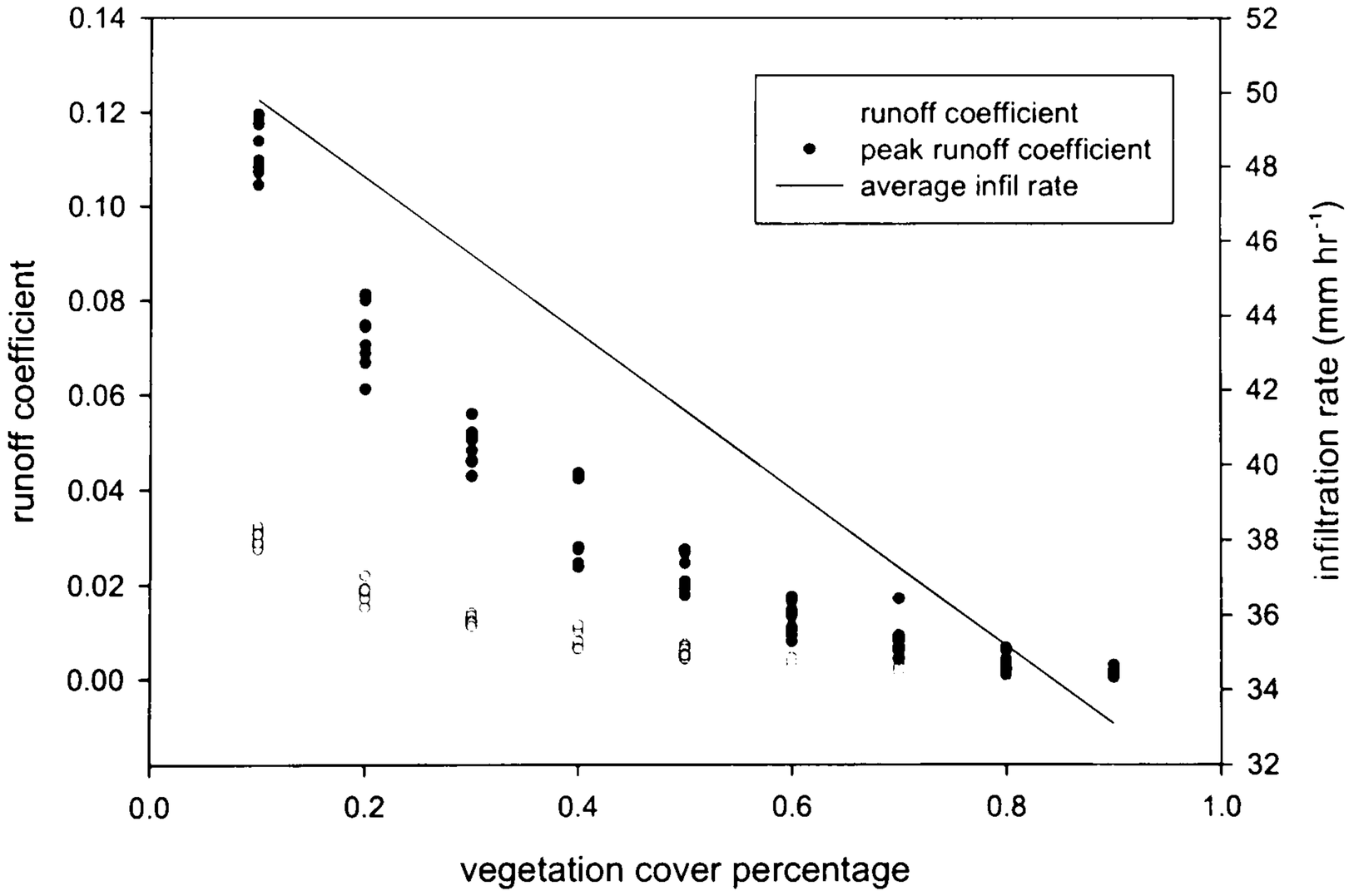

Figure 6.21 Effects of changing vegetation cover on the runoff coefficient

Although there is a linear decrease in the average infiltration rate, the decrease in both the peak and total runoff coefficients is non-linear. The steepest part of the curve is between vegetation cover values of 10 % to 40 %. With vegetation covers values greater than 40 %, there is less change in the amount of discharge. Therefore, the presence of a two phase infiltration pattern has significant effects on the connectivity of the runoff and hence the discharge. This effect comes from the spatial configuration of runoff sources and sinks across the slope. The effect of

the vegetation pattern is investigated in section 6.4.6 and the effects of vegetation clustering in section 6.4.7.

6.4.6 Vegetation Patterns

The spatial configuration of vegetated and bare areas on a hillslope has been shown to influence the amount of runoff generated (Bromley et al. 1997a). This is because the vegetated and bare areas have significantly different infiltration characteristics. The infiltration values assigned to the different areas have been determined from the analysis of field results, Table 6.2. To aid the comparison, the discharge from a slope with an averaged uniform infiltration rate is presented. In the discussion, the percentage deviations from this hydrograph are given in the brackets.

The patterns investigated all have 50 % vegetation cover and are shown in Figure 6.22. The patterns are organised into four sets. Patterns 1 and 2 are reversed versions of each other, one with all of the vegetation in the lower part of the slope and the other with it in the upper part. Patterns 3 to 6 are considering the effects of vegetation banding or tiger strips (Thiéry et al. 1995) on the discharge. The width of the bands is 5 m. The difference between patterns 3 and 4 is the conditions next to the base of the slope. Pattern 5 is rotated through 90 ° to give bands running in the same direction as the flow paths. Pattern 6 is a combination of patterns 3 and 5 to give a chess board effect. Pattern 7 has a contained area of vegetation while pattern 8 is the inverted image of pattern seven. Patterns 9 and 10 are considering the effects of clustering. Pattern 9 is a near random distribution while pattern 10 has a large amount of clustering. The effects of fragmentation are further investigated in section 6.4.7.

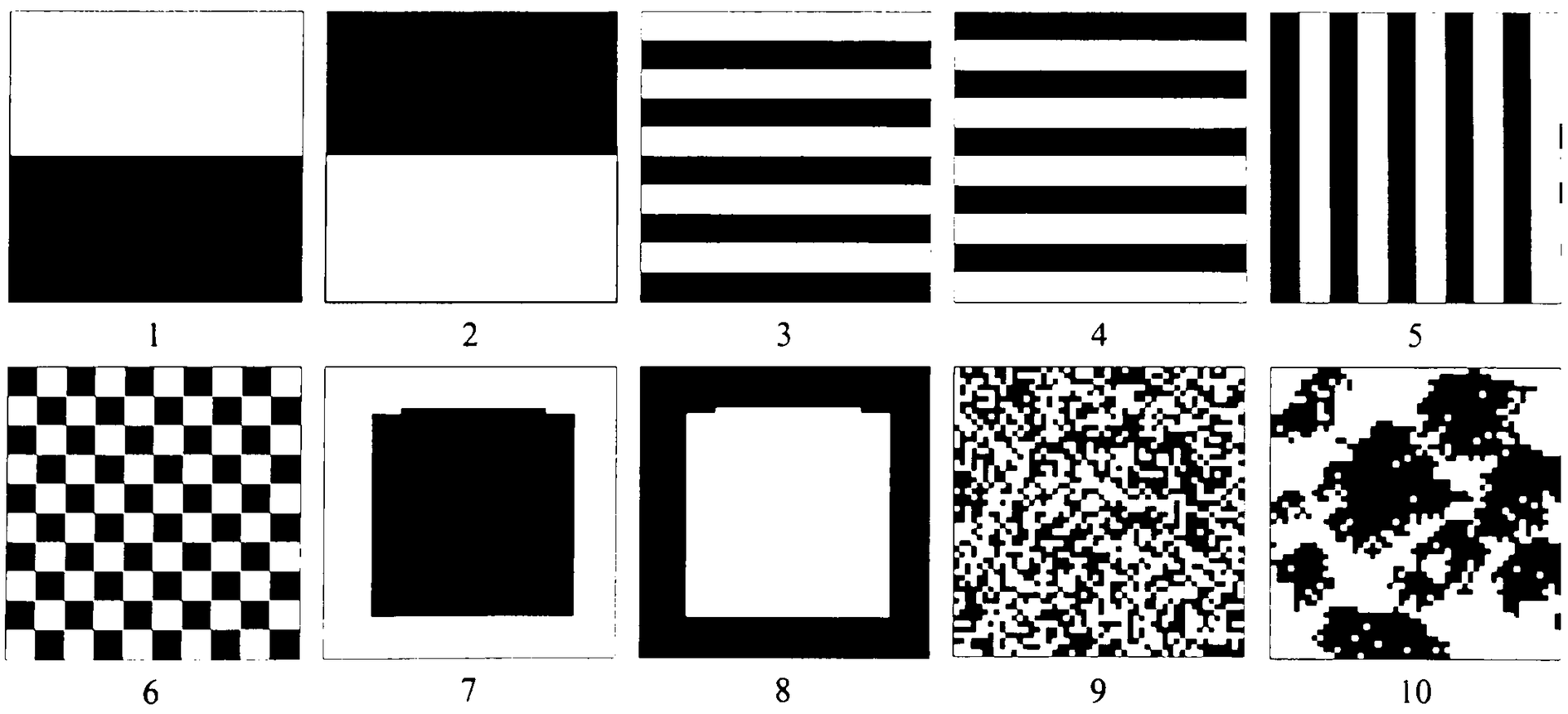

Figure 6.22 Vegetation patterns (black represents vegetation)

Pattern	Runoff coefficient (%)	Peak runoff coefficient (%)	Total Q % of no pattern	Peak Q % of no pattern
No pattern (average infil)	0.4	3.7	100	100
1	0.0	0.0	0.0	0.0
2	4.6	15.8	1098.1	429.1
3	0.0	0.0	0.0	0.0
4	1.6	4.8	385.2	131.9
5	1.2	4.5	281.9	122.9
6	0.7	2.4	178.8	64.9
7	2.8	9.1	660.0	247.7
8	0.0	0.0	0.0	0.0
9	0.4	1.5	100.4	40.7
10	1.5	5.7	368.7	154.6

Table 6.3 Total and peak discharge values for different vegetation patterns

The introduction of areas with different infiltration rates results in significant changes in both total and peak discharge. The discharge hydrographs from patterns 3 through 6 and patterns 9 and 10 are shown in Figure 6.23.

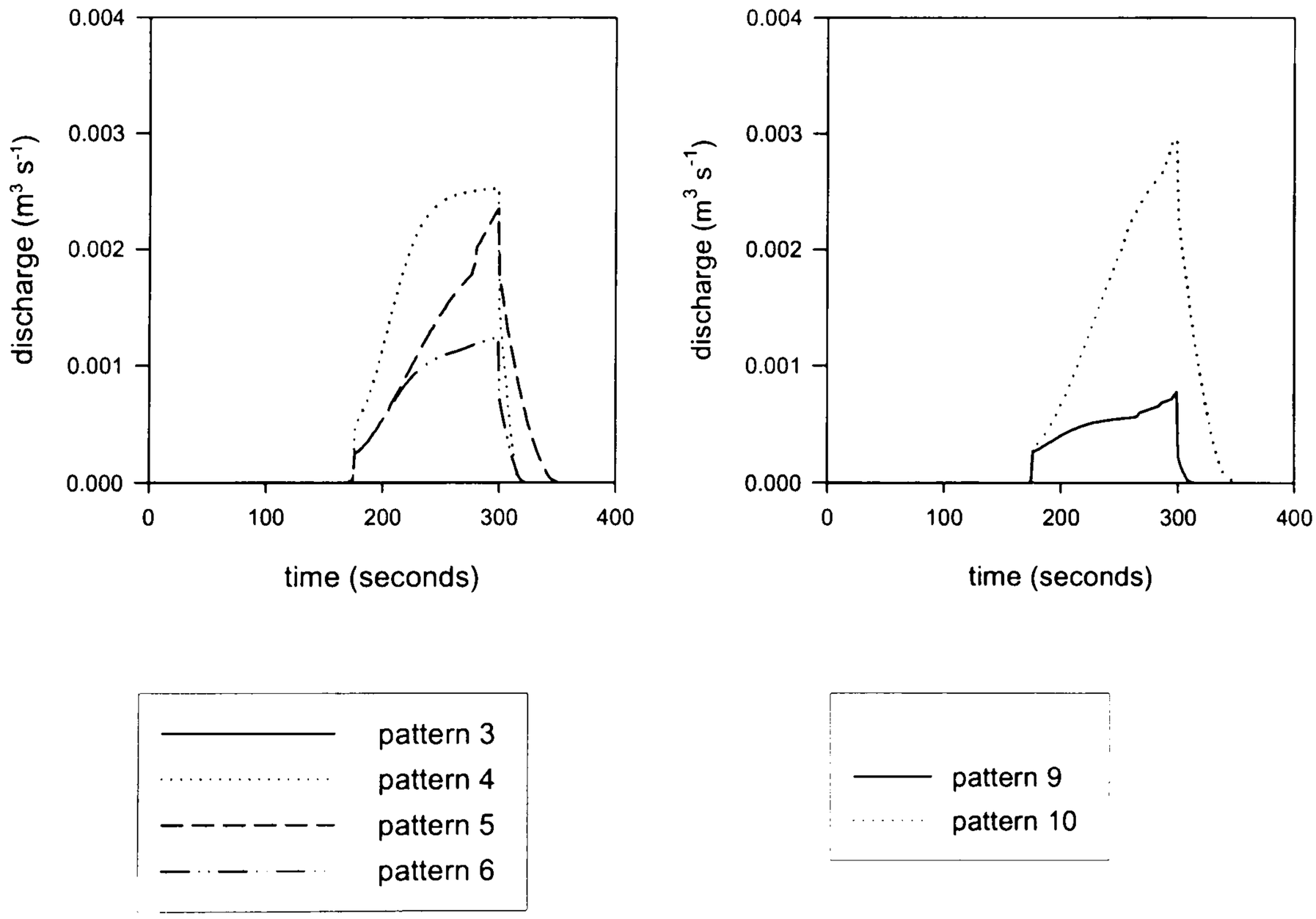

Figure 6.23 Discharge hydrographs from different vegetation patterns

There are very strong differences in the discharge hydrographs produced by patterns 1 and 2. Pattern 1, with the vegetation on the lower part of the slope, did not produce any runoff. The vegetated area is able to infiltrate all of the runoff generated in the bare area. Pattern 2, with the bare area at the base of the slope, gave a runoff coefficient of 4.6 %, 1098 % greater than for the

average infiltration conditions. Since no runoff sink is located down slope of the bare area, the runoff source is strongly connected to the outflow.

The hydrographs for patterns 3 to 6 differ in all sections of their discharge hydrographs. Pattern 6 did not produce any runoff, since the 5 m wide strip of vegetation was large enough to absorb all of the runoff generated upslope. Pattern 4 has the highest runoff coefficient at 1.6 % (385 %) and the highest peak runoff coefficient at 4.8 % (131 %). All of the runoff generated on the 5 m bare strip is directly connected to the outflow and hence the greater amount of runoff which is able to leave the slope. From Figure 6.23 it can be seen that pattern 4 generates a hydrograph with a steep rising limb. Patterns 5 and 6 both have vegetation cover of 50 % at the slope out flow. Pattern 5 gave a runoff coefficient of 1.2 % (282 %) and pattern 6 gave a runoff coefficient of 0.7 % (179 %). The early stages of both hydrographs are the same but then the rising limb of pattern 5 continues to rise whilst the rising limb of pattern 6 declines. This is associated with the large amount of bare area which is directly connected to the outflow on pattern five.

This set of results shows that the discharge is highly sensitive to the land use at the slope base. Pattern 3 has no bare areas at the slope base and has the minimum discharge. Pattern 4 has 100 % of bare areas at the slope base and has the maximum discharge. Both patterns 5 and 6 have 50 % bare areas at the slope base. On pattern 6, the bare area only extents for 5 m upslope whereas for pattern 5 it extends to the top of the slope and hence pattern 5 has the higher discharge.

Pattern 7 has a total runoff coefficient of 2.8 % (660 %) whilst pattern 8 did not produce any discharge. This can also be related to the land cover at the base of the slope. Pattern 7 has a bare area at the base of the slope and hence the much greater discharge.

Patterns 9 and 10 consider the effect of clustering on the discharge. Pattern 9 has a total runoff coefficient of 0.4 % (100 %) and a peak of 1.5 % (41 %). The small scale random pattern of vegetation gives a total discharge almost identical to the averaged conditions. However, the peak is significantly reduced. Pattern 10 has a higher total runoff coefficient of 1.5 % (369 %). This may be related to the large bare area connected to the slope outflow.

These experiments show that the infiltration characteristics at the slope outflow are very important in determining the discharge from the whole slope. A narrow buffer strip is able to absorb all of the runoff generated upslope. The width required to do this will depend upon the upslope area and the characteristics of the storm event. This interaction is discussed in chapter 7.

In order to quantify the importance of changes in the land cover in relation to the distance from the slope outflow, a two m band of vegetation was placed at varying distance from the slope outflow. The runoff coefficients are shown in Figure 6.24.

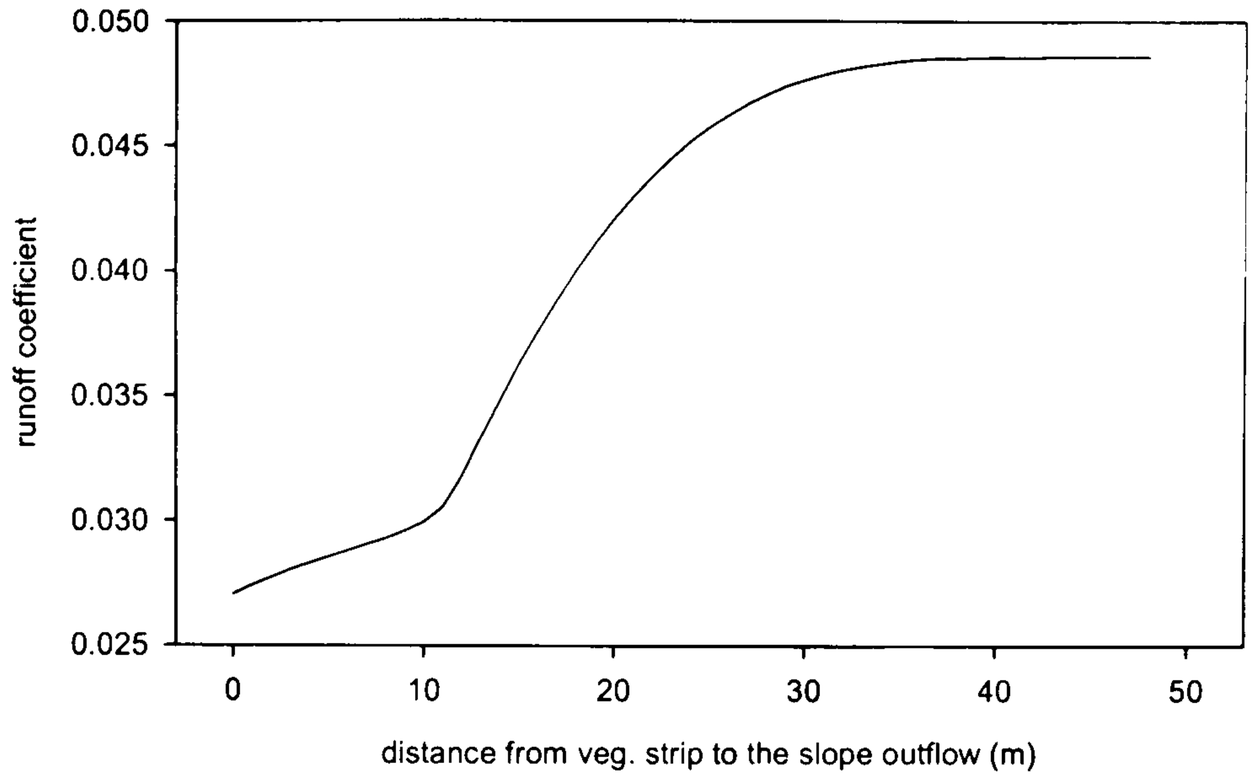

Figure 6.24 Effects of a strip of vegetation at varying distances from the slope outlet

There is a non-linear response in the total discharge to the position of the vegetation strip on the slope. As the strip moves further from the outflow there is an increase in the total discharge. This is related to the increase in the area directly connected to the slope outflow. The change is behaviour as the strip moves more than 12 m relates to the size of the source area. When the strip is located in the lower 12 meters of the slope, it is located within the source area. Once it moves out of the source area, its impact is decreased and the discharge is able to significantly increase.

6.4.7 Vegetation Clustering

The clustering of the vegetation was shown to have an effect on the peak and total discharge from a slope in section 6.4.5. In this section, the effect of changing the clustering from a random pattern to highly clustered is investigated. The fragmentation parameter, frag, of the vegetation pattern generator was varied from 0.05 to 0.5 and sample pattern realisations are shown in Figure 6.25. Since the generated patterns are stochastic, 1,000 frag values were selected from a uniform distribution. The runoff coefficient from each surface plotted against the frag value is shown in Figure 6.26.

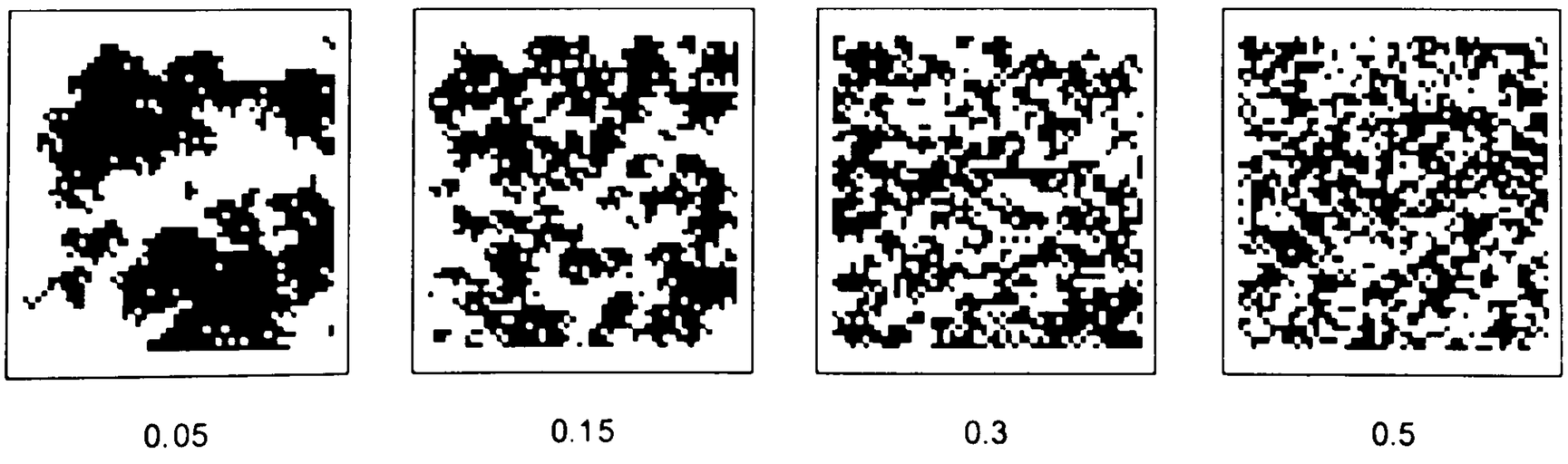

Figure 6.25 Sample vegetation pattern realisations (black represents vegetation)

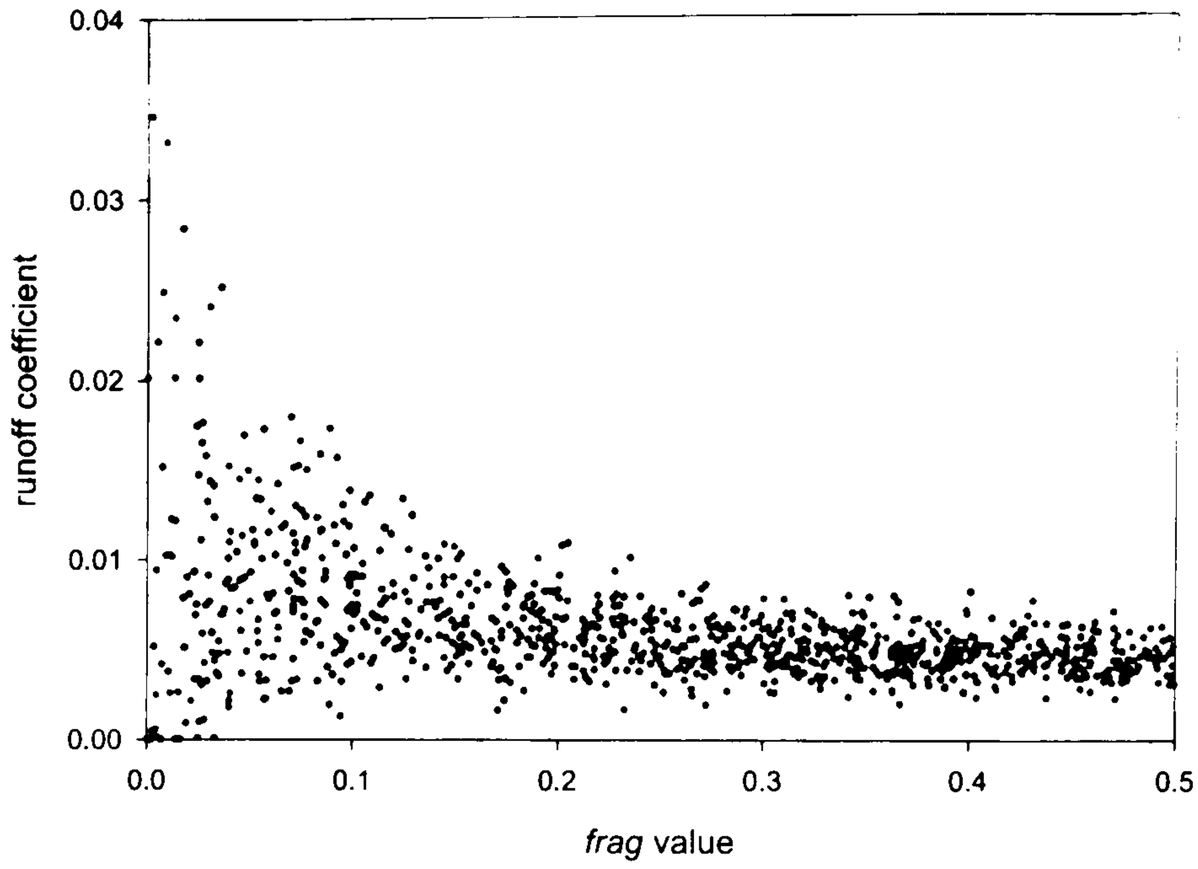

Figure 6.26 Runoff coefficient from different amount of vegetation clustering

The greatest variability and both the minimum and maximum runoff coefficient occur at the smallest value of frag. This relates to the vegetation patterns with the greatest amount of clustering. Therefore, all of the vegetation may occupy the upper slope thus connecting the runoff source areas directly to the slope outflow. It is also possible that the vegetation may occupy the lower slope, thus absorbing the runoff generated upslope. As the patterns become more fragmented, the variability of the runoff coefficient decreases and the standard deviation decreases. However, the mean remains constant at ~0.4 %. At frag values above 0.2 there is little change in the distribution of runoff coefficient values.

6.4.8 Slope Form

The experiments investigating the effect of slope gradient in section 6.4.2 showed that gradient had a significant effect on the slope discharge. Those experiments were undertaken using a linear slope which is different to many natural slopes. The introduction of different slope forms may influence the discharge through the introduction of flat, runoff sinks at the base of the slope or by producing greater amount of discharge from steeper part of the slope. This section investigates the presence of a floodplain at the base of the slope. The floodplain width was varied from zero to 50 m (100 % of the slope). The discharge hydrographs are shown in Figure 6.27 and the effects on the peak and total runoff coefficient are shown in Figure 6.28.

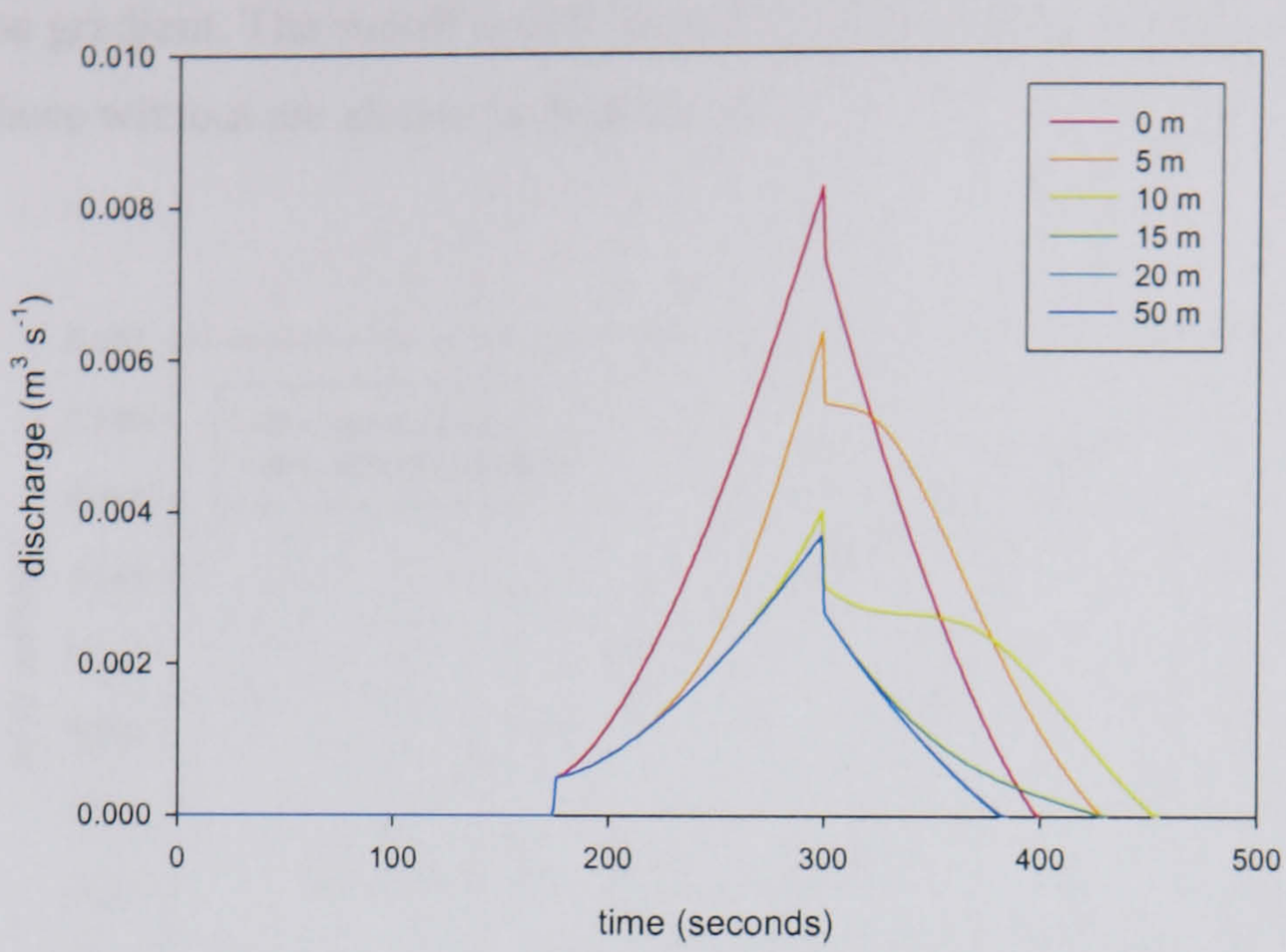

Figure 6.27 Effects of the floodplain size on discharge on the discharge

The introduction of two separate slope gradients on the surface results in the generation of a bulge in the receding limb of the discharge hydrograph. The bulge relates to runoff generated on the steep, upper section of the slope arriving at the outflow. The size of the bulge in relation to the end of rainfall peak varies with the size of the floodplain with the maximum size occurring on the slope with a 10 m floodplain.

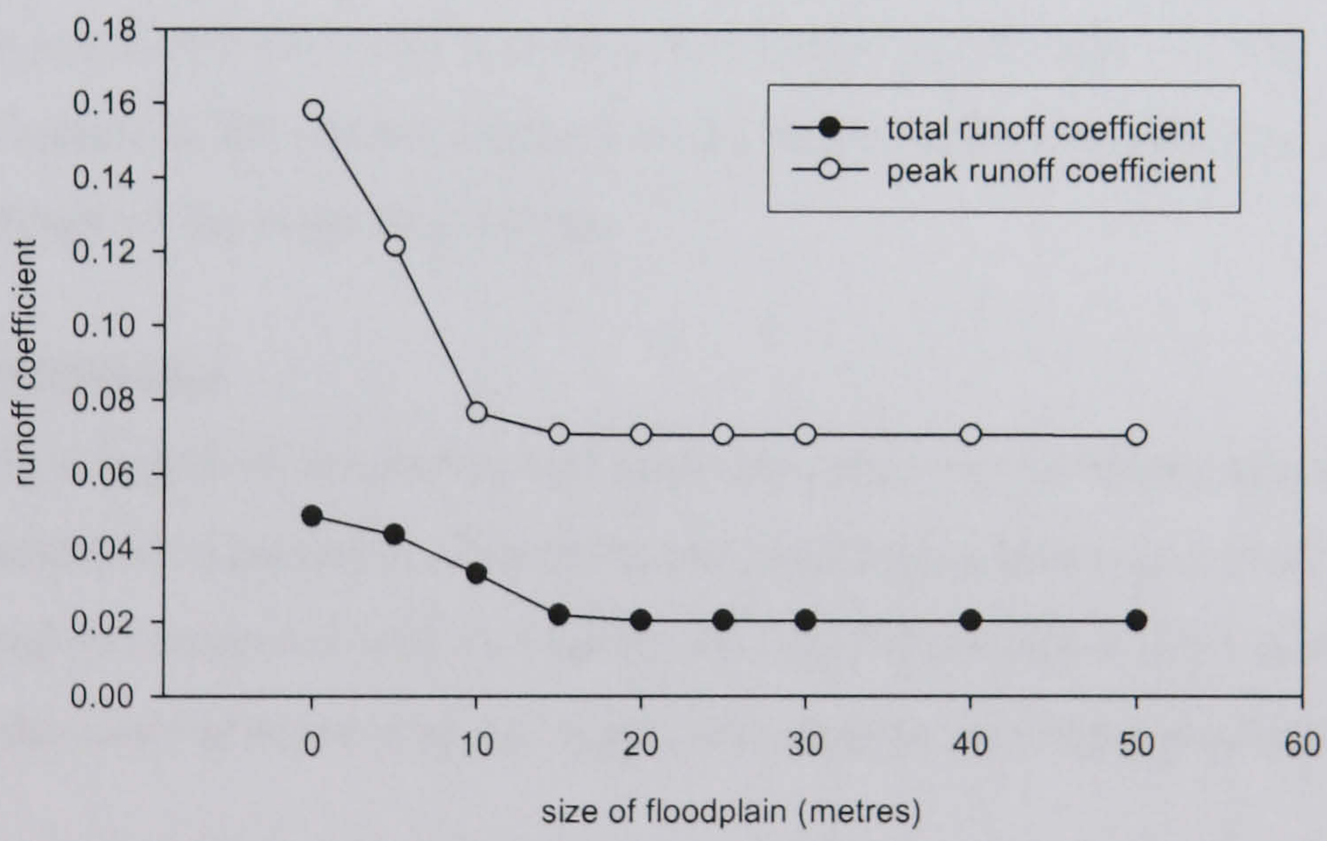

Figure 6.28 Effects of the floodplain size on the runoff coefficient

The peak runoff coefficient declines steeply with increasing floodplain width until a width of 15 m. At this point, the runoff generated on the steep upper section does not reach the outflow during the storm and hence does not increase the peak size. This water then flows out after the end of the rainfall and leads to the bulge in the receding limb mentioned above. The total runoff coefficient decreases with increasing floodplain width up to 20 m. For slopes with floodplains above this length, there is very little decrease in the total runoff coefficient.

The introduction of a floodplain decreases the average slope gradient. Therefore, these reductions in runoff through the introduction of a floodplain must be related to those from the

reduction in slope gradient. The runoff coefficients for the average slope gradient with a floodplain and those without are shown in Figure 6.29.

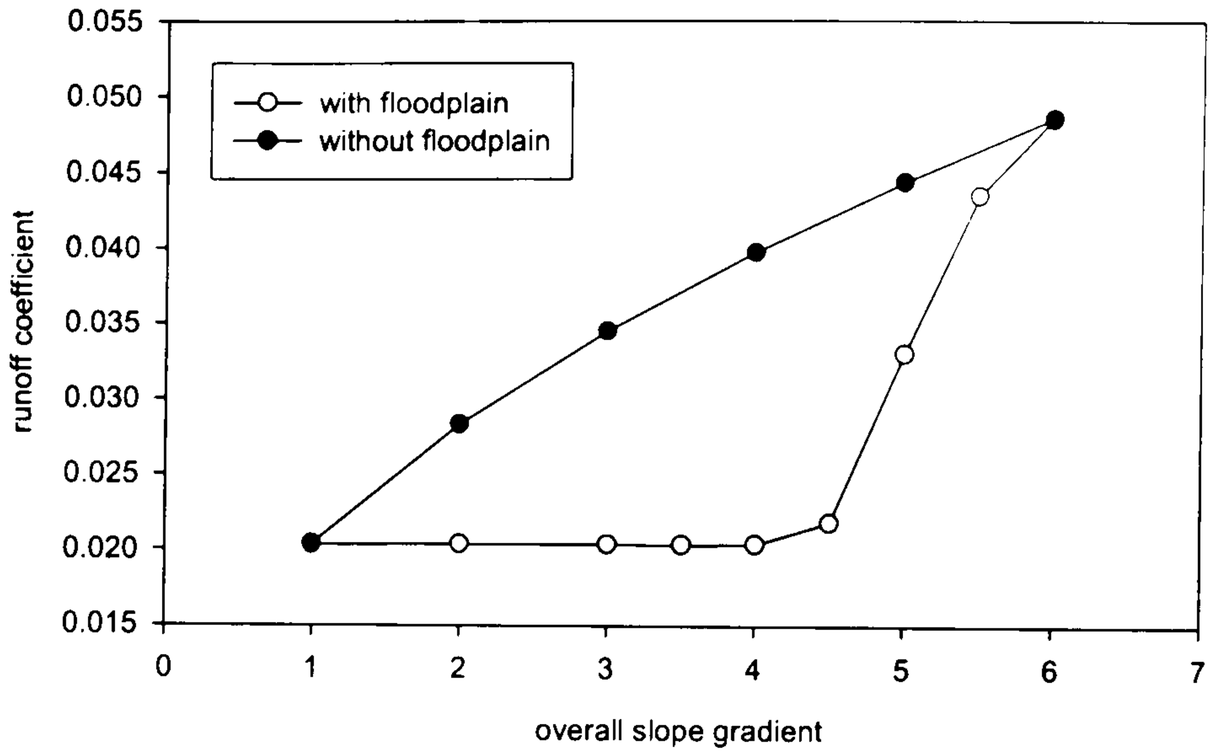

Figure 6.29 Effects of floodplain compared to the reduction in slope gradient

The introduction of the floodplain results in a significant reduction in the runoff coefficient from the slope. The introduction of a 10 m floodplain gives a 25 % reduction in the runoff coefficient. The slopes with floodplains of above 20 m behave like a slope with a linear slope of 1 °. The upper, steeper, slope where much of the runoff will be generated is disconnected from the slope outflow and all of the runoff is produced from the lower slope. As was shown in section 6.4.6, the nature of the surface adjacent to the slope outflow is critical in determining the hydrological response of the slope as a whole.

6.5 Combinations

Since there is a high degree of interaction and inter-dependencies between parameters, each should not be considered in isolation. Therefore, the interactions between a number of the factors investigated in section 6.4 will be considered. The factors that will be considered are the slope length and the slope gradient and the vegetation patterns and slope gradient.

6.5.1 Slope Length and Slope Gradient

Both the slope length and the slope gradient showed a significant effect on the total and peak discharge. Slope length has a negative relationship with the runoff coefficient while the slope gradient has a positive relationship. The interactions between these factors are shown in Figure 6.30.

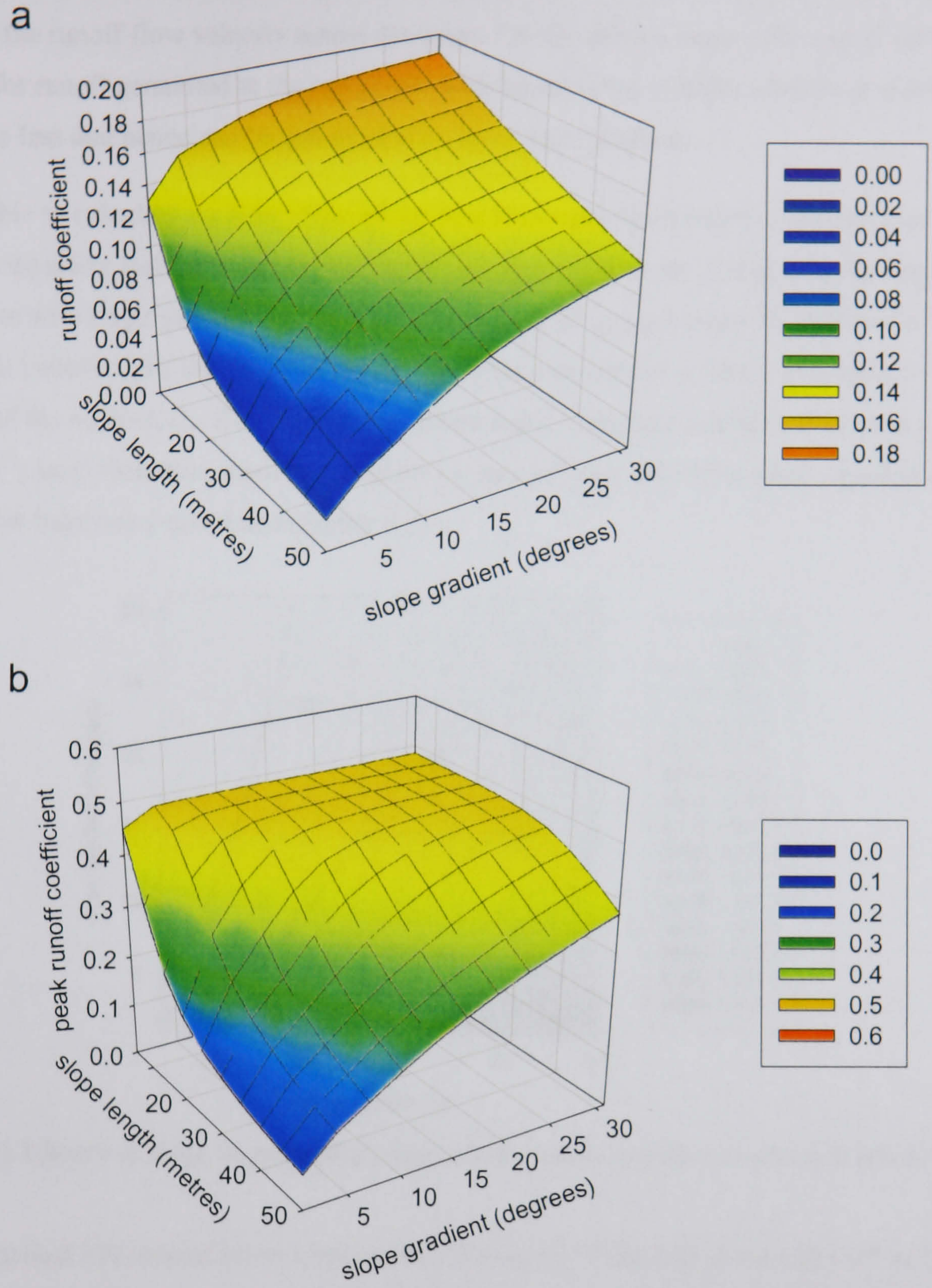

Figure 6.30 Effects of slope length and slope gradient on (a) the runoff coefficient and (b) the peak runoff coefficient

The results in Figure 6.30a show an increase in the runoff coefficient with increasing slope gradient and decreasing slope length. The runoff coefficient is sensitive to changes in the slope gradient below 5°, however this sensitivity decreases with increasing slope length. As the slope gradient increases, the runoff coefficient increases, therefore a longer high gradient slope will behave like a shorter, lower gradient slope. Figure 6.30b shows that the peak runoff coefficient responds to slope length and gradient in a similar way to the total runoff coefficient. However, the peak runoff coefficient is only influenced by increases in slope gradient up to a threshold gradient. Above this point, the peak runoff coefficient does tend to increase with increasing slope gradient. The threshold slope gradient is dependent upon the slope length with longer

slopes reaching the threshold at a higher slope gradient. The location of this threshold can be related to the runoff flow velocity across the slope. On the shorter slopes, the runoff velocity required for runoff generated at the top of the slope travel to the outflow within the storm duration is less and hence can be achieved at a lower slope gradient.

It is possible to calculate the time required for runoff to reach the outflow using the Darcy-Weisbach equation and the time required to fill the depression store. The size of the depression store varies with slope gradient and the time required to fill it is given by the difference between the rainfall intensity and the infiltration rate. The maximum travel distance was taken as the diagonal of the surface, i.e. from top left to bottom right. Using the rainfall intensity as above (75mm hr^{-1}) and infiltration model parameters (41mm hr^{-1} at $\theta = 0.3$) the times required to reach the out flow have been calculated (Figure 6.31).

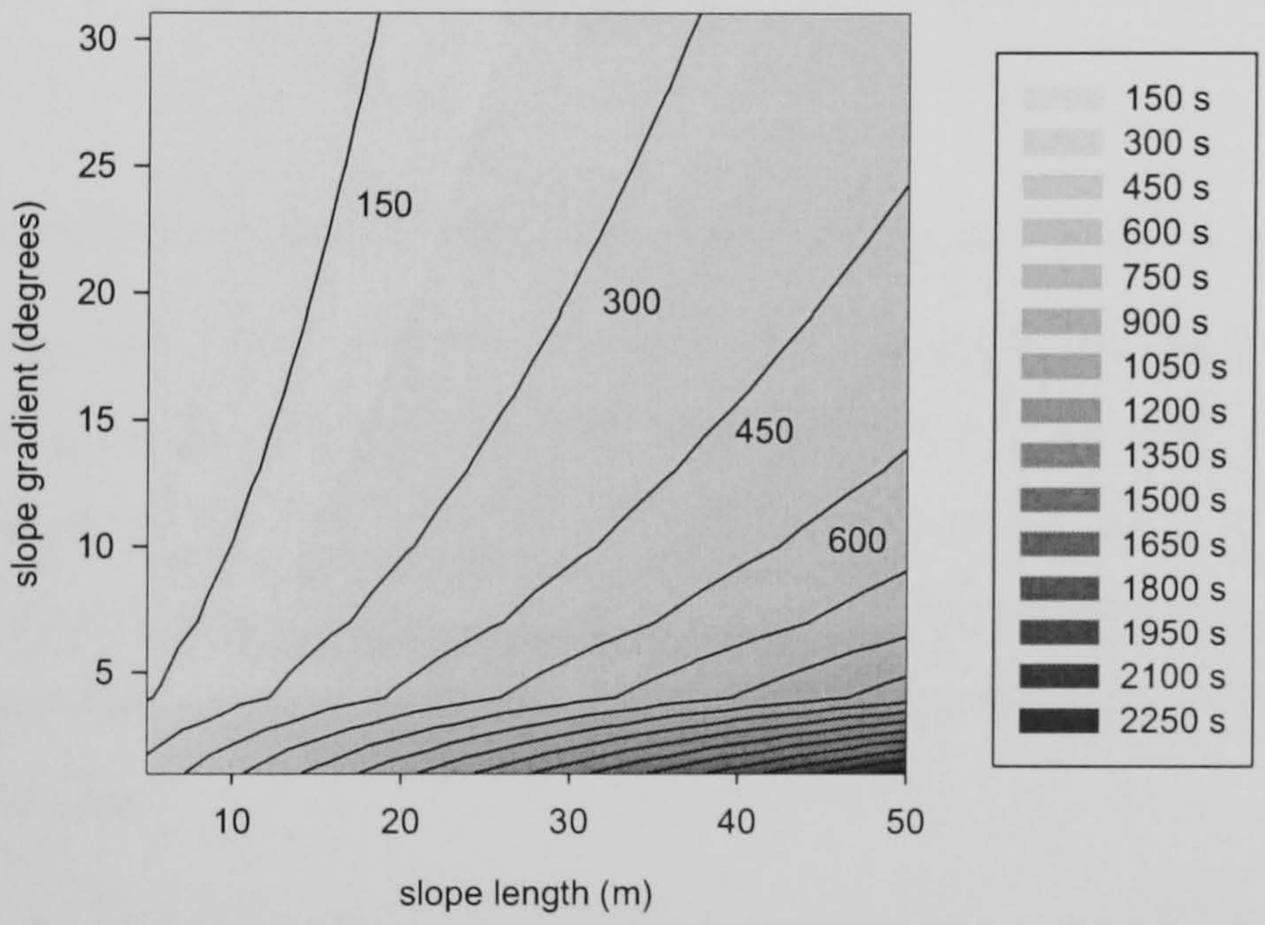

Figure 6.31 Effects of slope length and gradient on the maximum time required to reach the out flow

For the standard 300 second storm used in this chapter, all of the area to the right of the 300 second isoline would not produce runoff from the whole slope. Therefore, slopes with these combinations of length and gradient would not be able to produce their maximum peak discharge. The slopes effectively behave like short slopes which reduces the catchment area. This therefore reduces the contributing area and thus the size of the flood. This relationship can be mapped out across a whole catchment to give information on the storm length required to give maximum peak runoff.

6.5.2 Vegetation and Slope Gradient

In section 6.4.6 it was shown that a strip of vegetation at the base of the slope is able to absorb all of the runoff generated on the slope above it. This therefore, disconnects the slope from the channel network. The size of vegetation strip required to disconnect the slope will depend upon the amount of runoff generated. This in turn will be dependent on the slope gradient and the

storm characteristics. The effects of slope gradient and buffer strip width on the runoff coefficient is presented in Figure 6.32.

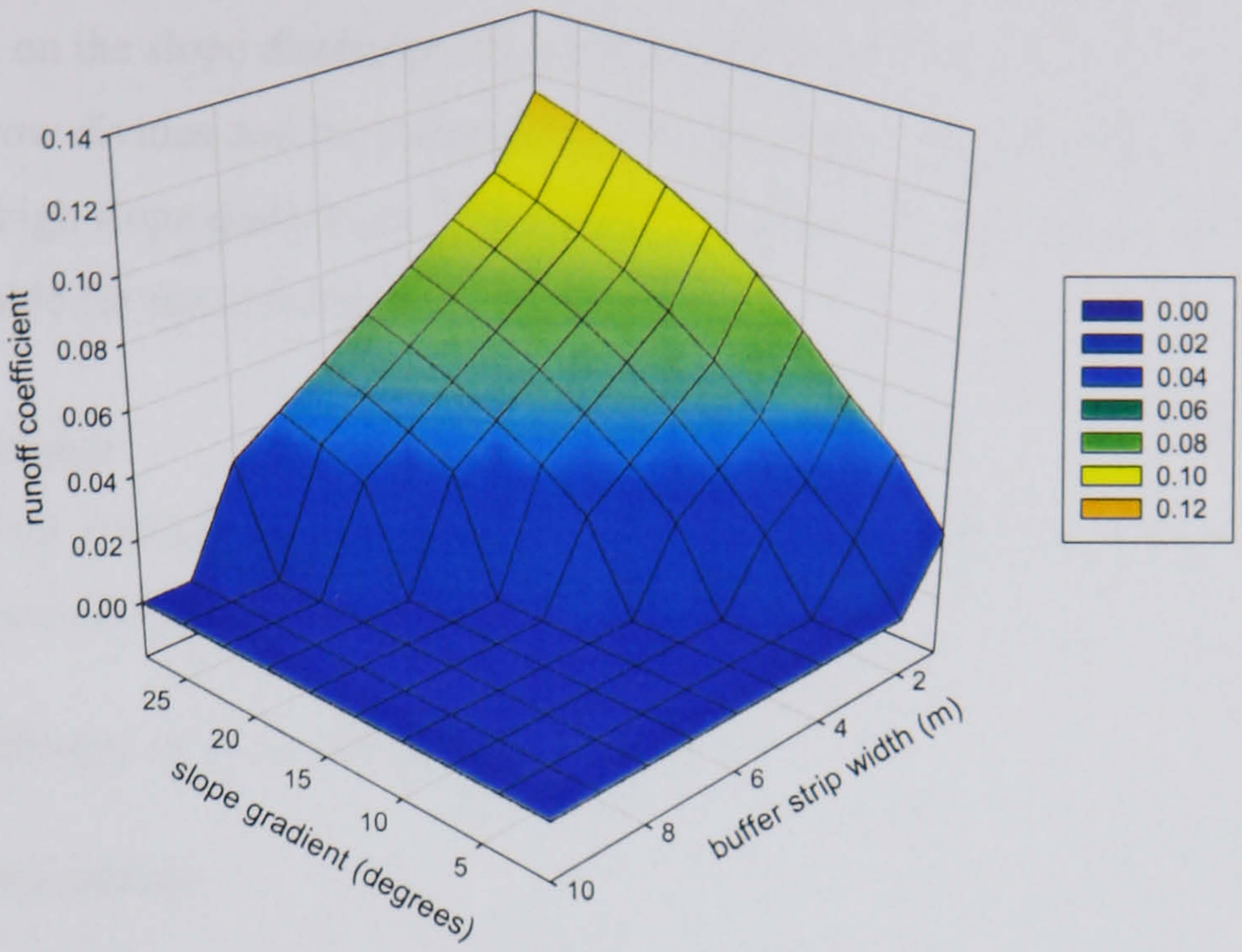

Figure 6.32 Effects of slope gradient and buffer strip width on the runoff coefficient

As the width of the buffer strip increases, the slope gradient required to generate enough runoff to break through the buffer also increases. For a buffer strip of one m, a slope gradient of only one degree is required to break through. For a buffer strip of ten m, only slopes with gradients greater than ten degrees that are able to generate discharge. As the slope gradient increases, the width of the buffer strip required to disconnect the upper slope from the outflow increases linearly (Figure 6.33).

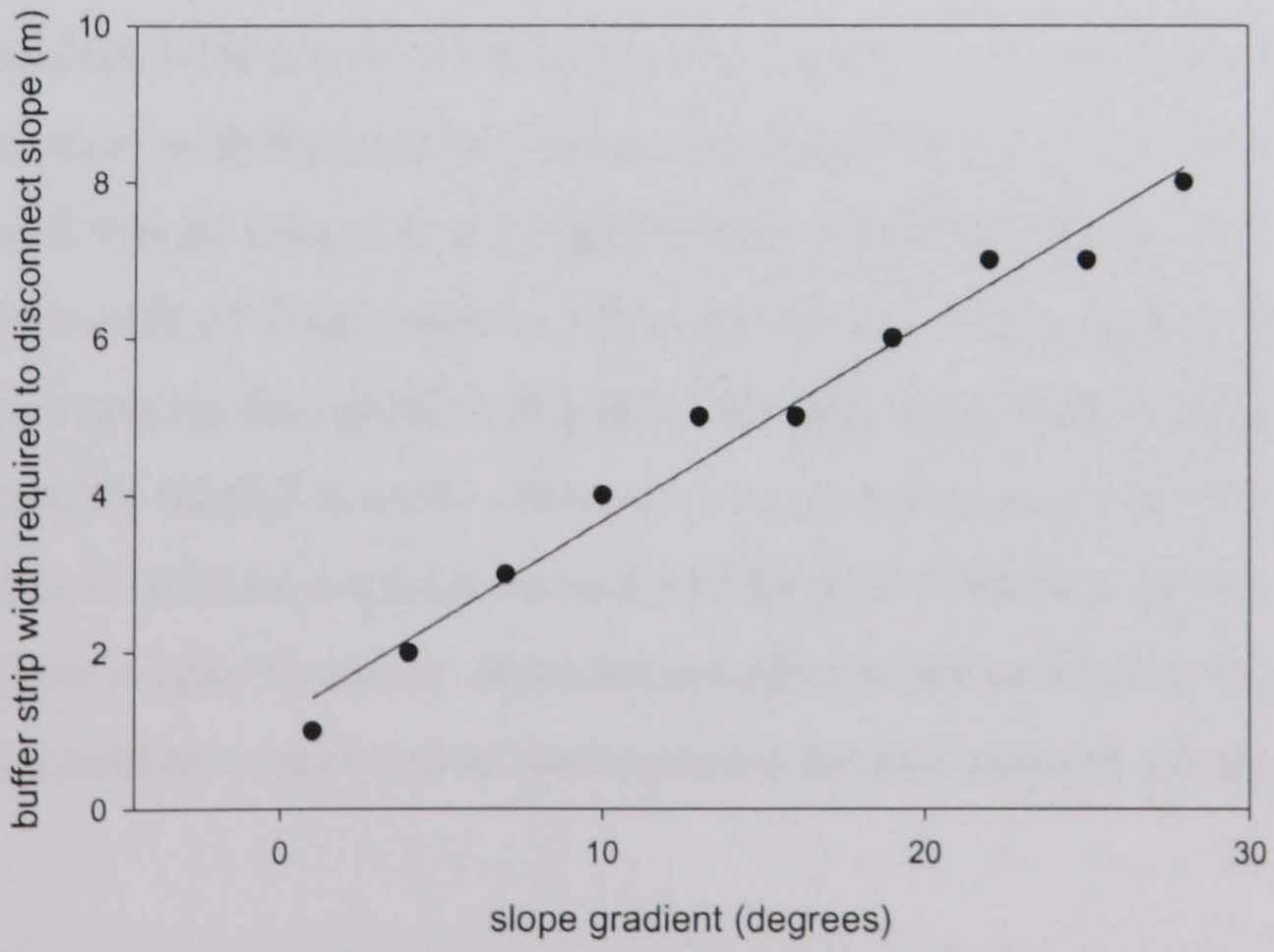

Figure 6.33 Buffer strip width required to disconnect the upper slope

These results show that the area at the slope base is key for determining if the rest of the slope will connect to the channel. The size of the area that determines this behaviour varies with the slope gradient.

6.6 Other Factors

The characteristics of the surface presented here are considered important but they not represent a complete list of factors. For example, the ploughing direction at the slope scale will have a significant effect on the slope discharge. One of the main mechanisms in this relationship is the breaching of furrow divides and the subsequent erosion. This produces effective channels on the slope and hence high slope discharges. CRUM-2D does not represent the erosion process and hence is not suitable for the investigation of this factor.

6.7 Discussion

From the modelling results presented, three main themes have been revealed as important in controlling the discharge. These are:

- The distribution of flow path lengths
- The slope gradient
- The spatial organisation of the slope

Each of these themes will be discussed in turn.

6.7.1 The Distribution of Flow Path Lengths

The importance of slope lengths is shown in a number of the modelling experiments presented. The slope length influences the total amount of discharge from the slope by determining the amount of transmission loss from the overland flow. As the slope length increases, the distance that water must flow over the infiltrating surface increases. Hence, the longer the slope, the greater the time available for transmission losses and leads to lower runoff coefficients. These results are in agreement with the field results presented by findings presented by Lal (1997), Gabriels (1999) and Van de Giesen et al. (2000) and the modelling results of Yair and Lavee (1985) and overall results of Wainwright and Parsons (2002). Wainwright and Parsons (2002) found that the "decrease (in the runoff coefficient with increasing slope length) does not occur when constant intensity rainfall is used". However, the modelling experiments results presented in this chapter utilised constant intensity rainfall and did find a decrease in the runoff coefficient with increasing slope length. However, since the simulation continued after the cessation of rainfall, the storm could be considered to have variable rainfall intensity due to the period of no rainfall.

This work has also shown that it is not the broad scale slope length that is the key control on the amount of water reaching the channel, but the distance to a flow concentration. As was shown in some of the results presented by Lal (1997), on the longer slopes where rills were able to form, the runoff coefficient increased. This is due to the decrease in the distance to a flow

concentration. Therefore, to fully appreciate the impact that slope lengths have on catchment hydrology, measurements need to be taken at an appropriate scale to capture the small scale flow concentrations.

The one-dimensional modelling investigation of slope length does not show the decrease in discharge due to transmission loss. However, it shows the effect of travel time on the timing of the peak discharge. The two-dimensional slope modelling is able to suggest that the decrease in runoff is due to the transmission losses. This effect is also shown in the investigation of the infiltration rates leading to the curvilinear relationship between the infiltration rate and the total discharge.

The distribution of slope lengths within a catchment will have a significant effect on the catchment discharge. The distribution of slope lengths will be influenceed by the topography and the land management. The topography will influence the drainage density, which will be strongly related to the distribution of slope lengths. Catchments with a high drainage density have a shorter average slope length and hence higher discharge. Land management influences the distribution of slope lengths through the introduction of artificial breaks on the slope in the form of roads, terraces, irrigation channels and check dams. Each of these landscape features potentially disconnects the catchment area upslope from the lower slope. In the case of irrigation channels and roads, the generated runoff is efficiently transported to another point in the catchment where it may be stored or released as a concentrated point source.

The slope lengths can be extracted from a DEM and a map of the efficient channels through the use of a GIS. This enables the estimation of the likely catchment scale runoff coefficient and the identification of the areas of the catchment which would give the highest slope discharges.

6.7.2 Slope Gradient

The slope gradient influences a number of parameters which have a strong influence on the generation and transmission of overland flow. The slope gradient influences the amount of energy available for overland flow, hence increasing the overland flow velocity. An increase in the slope gradient decreases the depression storage and the soil depth.

The slope gradient was found to have a consistent relationship with the surface depression storage at the plot scale for scrub slopes. It is possible to fit a family of curves to predict this important relationship. This enables the prediction of this key parameter in the slope scale model. The relationship between the surface roughness, gradient and surface depression storage are similar to those reported by Onstad (1984).

From the investigation of the effects of slope gradient on the slope discharge, it was found that both the peak and total discharge are positively related to the slope gradient. The slope gradient

effect interacts with the slope length effects. An increase in the slope gradient increases the runoff coefficient. Thus, a longer slope will have the same runoff coefficient as a shorter slope at a lower gradient.

This relationship is in line with the results found by AbuAwwad and Shananawi (1997) for basin scale runoff in Jordan. The reduction in infiltration, as shown by the greater runoff, is also comparable with the results reported by Chaplot and Le Bissonnais (2000) where an increase in runoff was found for increased slope gradient under natural and simulated rainfall. However, the results are in conflict with those reported by Poesen (1984) and Bryan and Poesen (1989) where an increase in slope gradient resulted in a decrease in runoff. This was reported as being due to the erosion of the surface crust exposing the material below which had a greater infiltration capacity. This process is not included in the model and hence should be considered as a possible modification.

The depth of the surface depression store is very sensitive to slope gradients less than 5 °. Since the surface depression store has a strong influence on the generation and transmission of runoff, this factor influences many other experiments. From a 50 m DEM of the Rambla de Nogalte catchment, 56 % of slopes are less than 5 ° and 67 % are less than 6 °. Therefore, there will be considerable variation in discharge among these similar slopes.

The model considers the slope of the surface at the spatial scale of one metre. As the spatial scale changes, the measurement of slope also changes. This is important when up-scaling the results for slope gradient to the landscape scale.

The slope gradients are manipulated through land management practices such as terracing and ploughing. The building of terraces reduces the surface slope to effectively zero over most of the hillslope. The regular ploughing of the slopes to remove non-crop vegetation moves large amounts of material down slope and in-fills the valley bottom. This reduces the slope gradient and increases the size of the valley bottom, thus reducing the slope length. The construction of check dams alters the valley floor slope gradient.

6.7.3 Spatial Organisation

The spatial organisation of the slope can be considered in terms of the surface roughness / topography or in terms of the spatial arrangement of infiltration characteristics. The surface depression storage was found to be related to the surface roughness. A family of curves can be fitted to the data to predict this important parameter. This set of results supports the findings of Onstad (1984). The high order roughness introduced by plough lines was found to be sensitive to the relationship between the plough line direction and the contours. If the plough lines are slightly off the contour, flow concentration occurs resulting in far greater discharge from the base of the slope. The furrows concentrate the depression storage into a small area, thus

reducing the average depression storage. The greater organisation of the surface leads to an increase in the connectivity of overland flow.

The importance of the spatial organisation of the slope upon runoff generating characteristics has been shown in the timing of the runoff in the one dimensional results and in the consideration of the spatial patterns of vegetation. From the one dimensional results, the step change in the amount of discharge from a slope (Figure 6.3), is related to the threshold soil moisture level suggested by Fitzjohn et al. (1998). Before the step change, the soil moisture level is below the threshold and the runoff producing areas on the upper parts of the slope remain unconnected. If the storm was to stop at this point, the amount of runoff reaching the channel would be low. However, if the storm continues past this threshold point, far greater amounts of runoff will reach the channel.

The importance of vegetation patterns in the functioning of semi-arid environments has long been recognised (Cerdá 1997). The results presented in sections 6.4.5 to 6.4.7 show the impact of the vegetation cover on the amount of runoff leaving the slope. The model results show that the response of hillslopes with a fragmented vegetation cover is non-linear and complex, supporting the findings of Cerdá (1997) and showing that the spatial pattern of vegetated and bare areas, on a slope with the same vegetation cover, can have a significant impact on the amount of runoff reaching a channel at the base of the slope. This supports the comments of Morgan (1995), Fitzjohn et al. (1998) and Cammeraat and Imeson (1999) that the spatial configuration of the vegetation patterns needs to be considered when upscaling from the hillslope to landscape scale.

The importance of an individual model cell in determining of the amount of discharge is related to its location on the slope. Cells located nearest the channel have the greatest influence while cells located at the top of the slope have the least influence. Therefore, a change in land use close to the channel will have a greater influence than a corresponding change on the upper slope sections.

From the one-dimensional analysis, it was shown that the cells located at the base of the slope control the timing of the onset of slope discharge. However, it is the characteristics of all of the cells on the slope that determines if the contributing area will extend to the top of the slope. The investigations of the effects of the vegetation patterns on discharge found that it was the 5 - 10 m strip at the base of the slope which was the most important factor in determining the slope discharge.

The results from the influence of vegetation patterns are applicable at a large scale to the effects of spatial patterns of land use. This is because there are similar differences in the infiltration

characteristics between scrub slopes and active agriculture as there are between bare and areas of uncultivated vegetation.

6.8 Conclusions

The results from the modelling experiments show that three surface factors are important in determining the form of the discharge hydrograph. These are the slope length, the slope gradient and the hydrological characteristics at the base of the slope. The importance of these factors has been shown at a number of levels of abstraction and at a range of scales. An increase in the slope length decreases the runoff coefficient for the slope. This is due to transmission losses following the cessation of rainfall. An increase in the slope gradient gives an increase in both the total discharge and the peak discharge. This is due to the reduction in the soil depth and the surface depression storage and the increase in flow velocity. This increase in velocity decreases the time available for transmission losses and hence leads to the increase in the discharge. The introduction of two contrasting infiltration regimes on a slope can alter the total discharge and the peak discharge from a slope. The discharge is sensitive to the configuration of the contrasting areas at the base of the slope. A small change in this area will lead to a large change in the discharge whereas a large change on the upper sections of the slope will give a small change in discharge. Of these three themes, slope length is the most universal and has the greatest effect. These relationships will be influenced by the nature of the storm driving the generation of runoff. These issues are discussed in chapter 7.

7 Storm Controls on the Discharge Hydrograph

7.1 Introduction

The aim of this chapter is to consider the control that the characteristics of the storm event impose on the amount of runoff and the form of the discharge hydrograph. The factors considered are the rainfall intensity, duration, variability and the temporal structure of the storm. The method used to separate individual storm events used in chapter 3 was a minimum period of 24 hours with no rainfall. This time period has been selected since it will allow the hydrological system sufficient time to return to dry conditions. Therefore, the initial conditions are the same for each storm. Each storm event is made up from a number of rainfall pulses and it is these pulses that generate runoff. A pulse is defined as a period of rainfall separated by one hour without any rainfall. The pulses have been modelled in three ways. Firstly, a Rectangular Pulse Model (RPM) has been used (section 7.2). The rainfall pulse has a constant intensity for a defined duration and is the same model as used in chapter 6. The second approach considers the controls that the timing of the rainfall hydrograph has on the discharge hydrograph using defined storm hydrographs (section 7.3). The third approach uses a Monte Carlo based generator to deliver the rainfall at varying intensities (section 7.4). For both constant and variable rainfall, the effects of the varying storm characteristics upon the base slope, slope length, and slope gradient have been investigated. For constant rainfall, the effect of the vegetation buffer strip width has also been investigated.

7.2 Constant Rainfall

The constant rainfall intensity experiments used the Rectangular Pulse Model (RPM) to generate the rainfall intensities. This delivers rainfall at a constant intensity for a defined length of time. Full details of the storm generators are given in chapter 5.

The range of rainfall intensities and pulse durations used in this chapter are derived from the analysis of the rainfall record in chapter 3. Rainfall durations range from 1 minute to 132 minutes and intensities from 0 to 56.1 mm hr^{-1}. However, the pulses contain instantaneous intensities much greater than the mean. The maximum recorded instantaneous intensity was 264

mm hr^{-1} for one minute. The lower values of these ranges are highly unlikely to generate discharge and hence have been removed from the analysis. To fully explore the parameter space, the range of intensities has been set as 10 – 90 mm hr^{-1} and the duration from 5 to 140 minutes. The use of stochastic rainfall in section 7.4 will include the effects of high instantaneous intensities.

7.2.1 Base Slope

The RPM rainfall pulses have been used on the same base slope as in chapter 6. This slope is 50 by 50 m with a slope gradient of 6 °. The infiltration characteristics represent a bare scrub slope. The full details of the slope are given in Table 6.1. The total rainfall depth and the runoff coefficients are shown in Figure 7.1. From the analysis of storm depth return periods in chapter 3, a rainfall depth of 122 mm relates to a one in one hundred year storm event. The maximum rainfall depth relates to a one in many thousands of years storm event. It is not possible to calculate the return period for this rainfall depth with the data set available. These return periods will be different for other regions of the world and hence it is valuable to include these more extreme storms in the analysis.

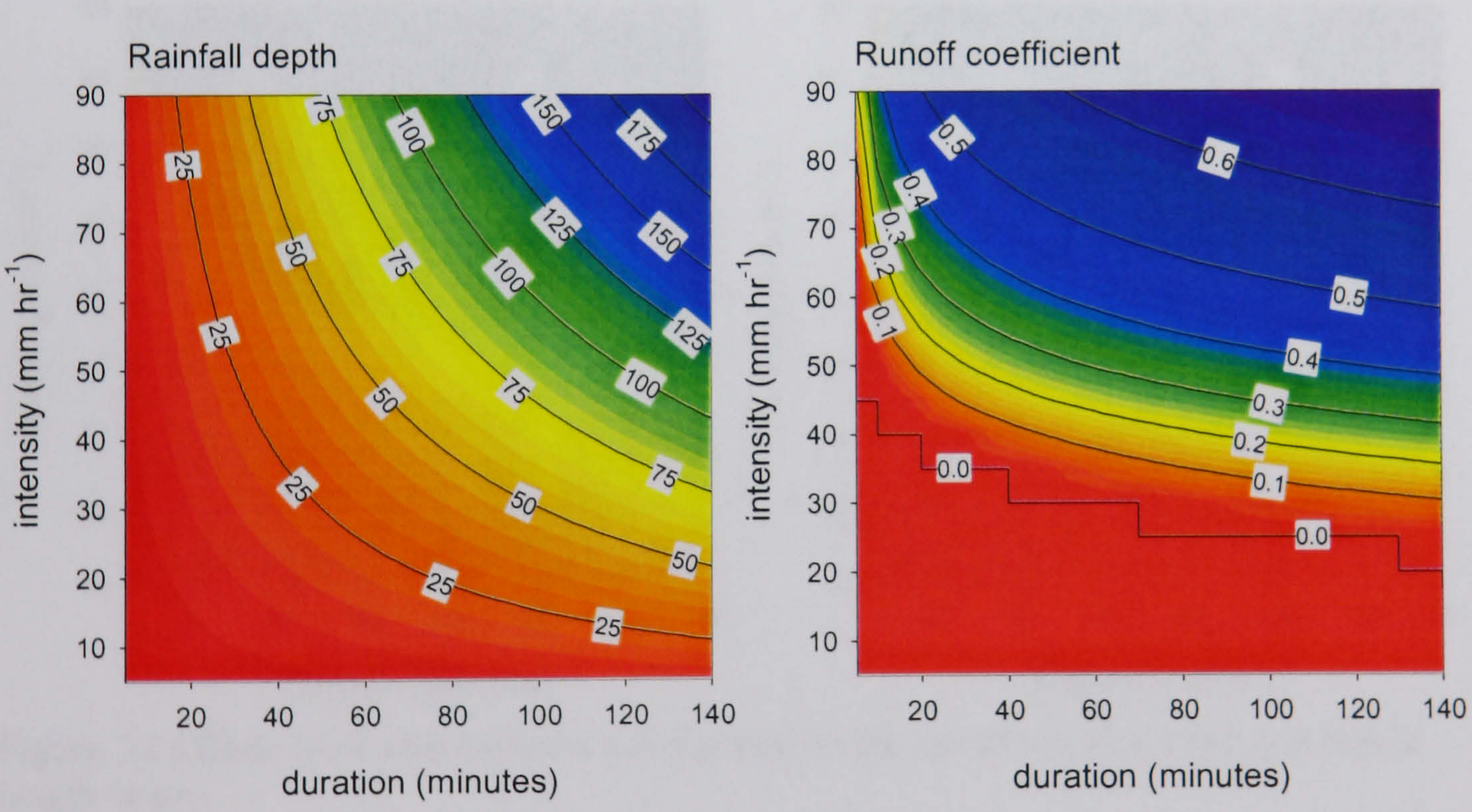

Figure 7.1 Effects of rainfall intensity and duration on the runoff coefficient from the base slope

There is a linear relationship between the rainfall duration, intensity and the rainfall depth. However, the runoff coefficient is more sensitive to changes in both the rainfall intensity and duration in different parts of the parameter space. The greatest sensitivity to the rainfall duration is over the range 5 – 20 minutes. The discharge is most sensitive to the rainfall intensity between runoff coefficients of 10 % to 30 % and is less sensitive above this region.

Part of the storm water is used to decrease the infiltration rate and to fill the surface depression store and then a percentage of the remainder can be converted into runoff. The first part is a constant depth for a certain surface and therefore is not dependent upon the storm duration. As

the storm duration increases, the percentage of the storm water which is able to be converted into runoff increases. For short storms, most of the storm water will be used to condition the surface for runoff generation. Therefore, the amount of runoff is very sensitive to changes over the range 5 – 20 minutes, but the sensitivity then decreases for longer duration pulses.

The response to changes in rainfall intensity is connected to the infiltration rate. Since the rainfall intensity has to be greater than the infiltration rate to initiate runoff, the slope will be sensitive to changes in the rainfall intensity. As the amount of water stored in the soil increases the infiltration rate decreases, and hence there is an increase in the runoff coefficient with increasing storm duration.

7.2.2 Slope Length

It was shown in chapter 6 that the slope length has a significant effect on the amount of discharge for a given storm. The slope lengths have been investigated over the range 5 – 45 m and two-dimensional slices from the parameter space for 5 and 45 m are shown in Figure 7.2.

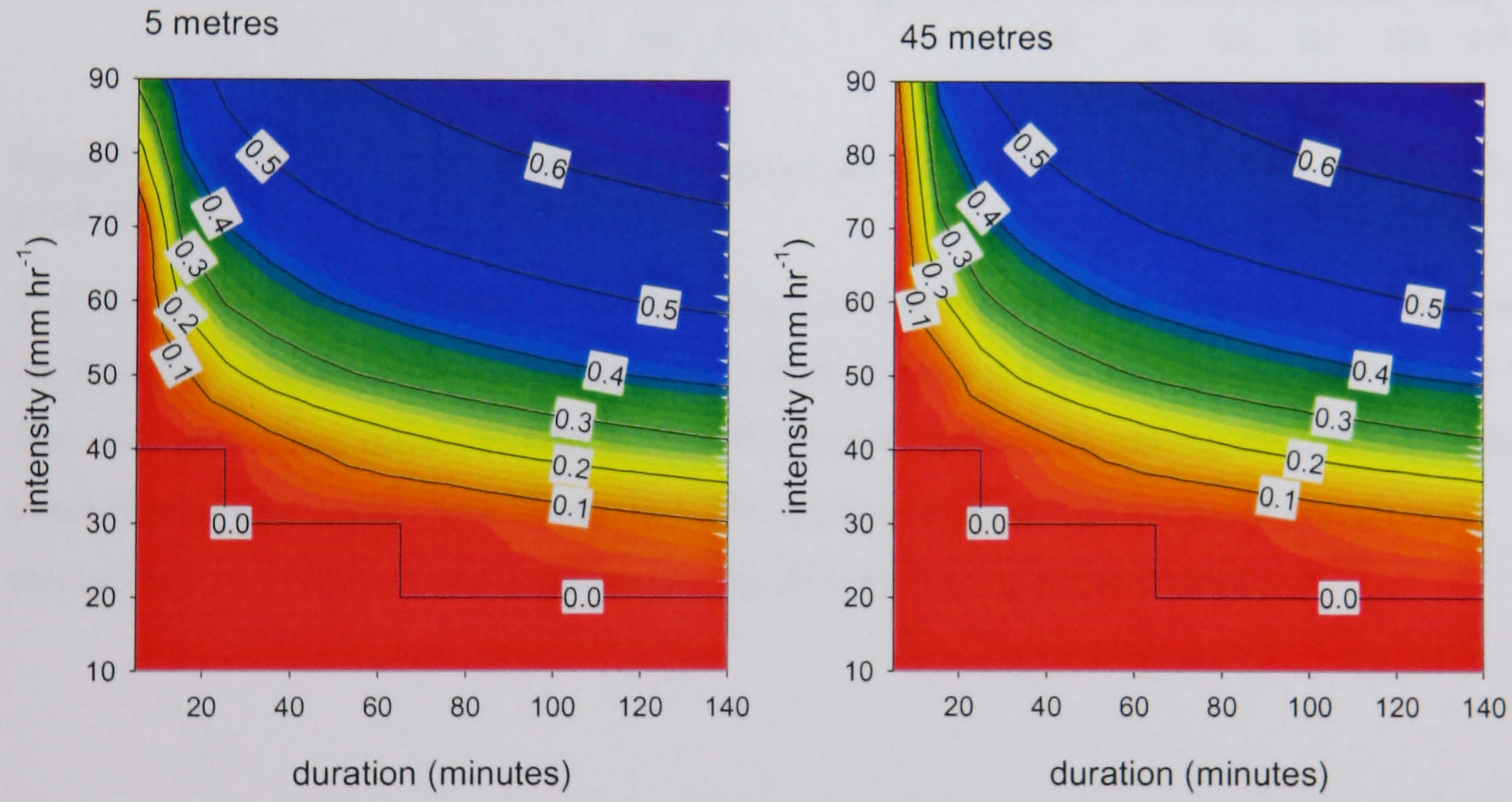

Figure 7.2 Effects of rainfall intensity and duration on the runoff coefficient from different length slopes

The slope length influences the amount of discharge by controlling the travel distances from the runoff generation point to the outflow. For the longest storm duration, assuming a flow velocity of 0.1 m s^{-1}, flow can travel 840 m. This distance is much further than the slope lengths considered. The greatest sensitivity to changes in the slope length occurs at short storm duration, less than 15 minutes, where the possible travel distances are shortest. The constant rainfall means that once runoff is generated, it will flow across the surface until the rainfall ceases, thus resulting in longer travel distances. Variability in the rainfall time series allows the infiltration of runoff down slope and this is explored in section 7.4.

7.2.3 Slope Gradient

It was shown in chapter 6 that the slope gradient has a significant effect on the amount of discharge for a given storm. The slope gradient has been investigated over the range 5 ° – 30 ° and two-dimensional slices from the parameter space for 5 ° and 30 ° are shown in Figure 7.3.

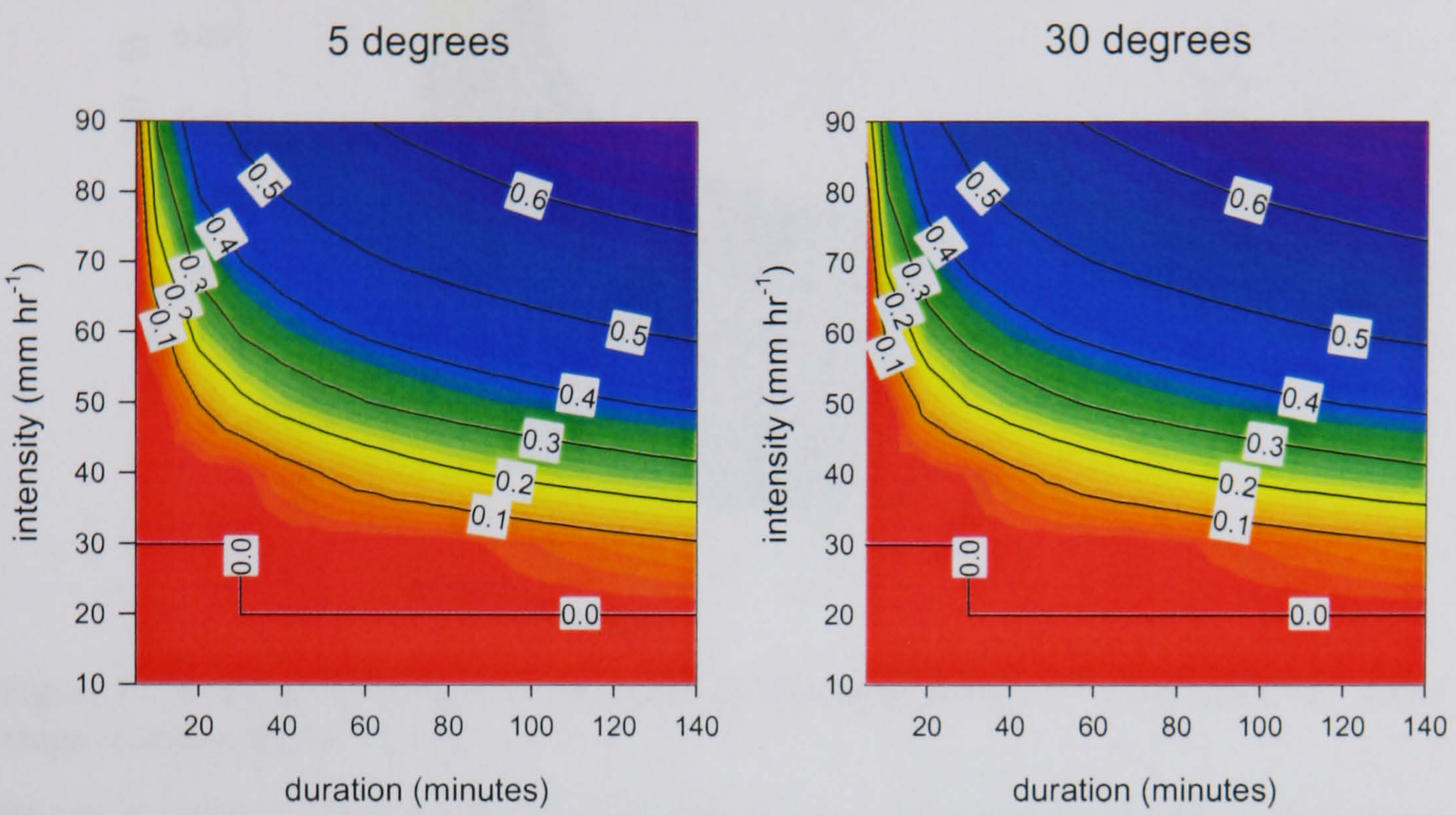

Figure 7.3 Effects of rainfall intensity and duration on the runoff coefficient from different slope gradients

The overall difference between the two surfaces shown in Figure 7.3 is slight. Figure 7.4 shows the absolute increase in the runoff coefficients from increasing the slope angle from 5 ° to 30 °. The main area where there are differences in the runoff coefficient is during short storms with rainfall intensities greater than 50 mm hr^{-1}. The increase in discharge decreases rapidly with increasing storm duration and decreases slowly with increasing storm intensity.

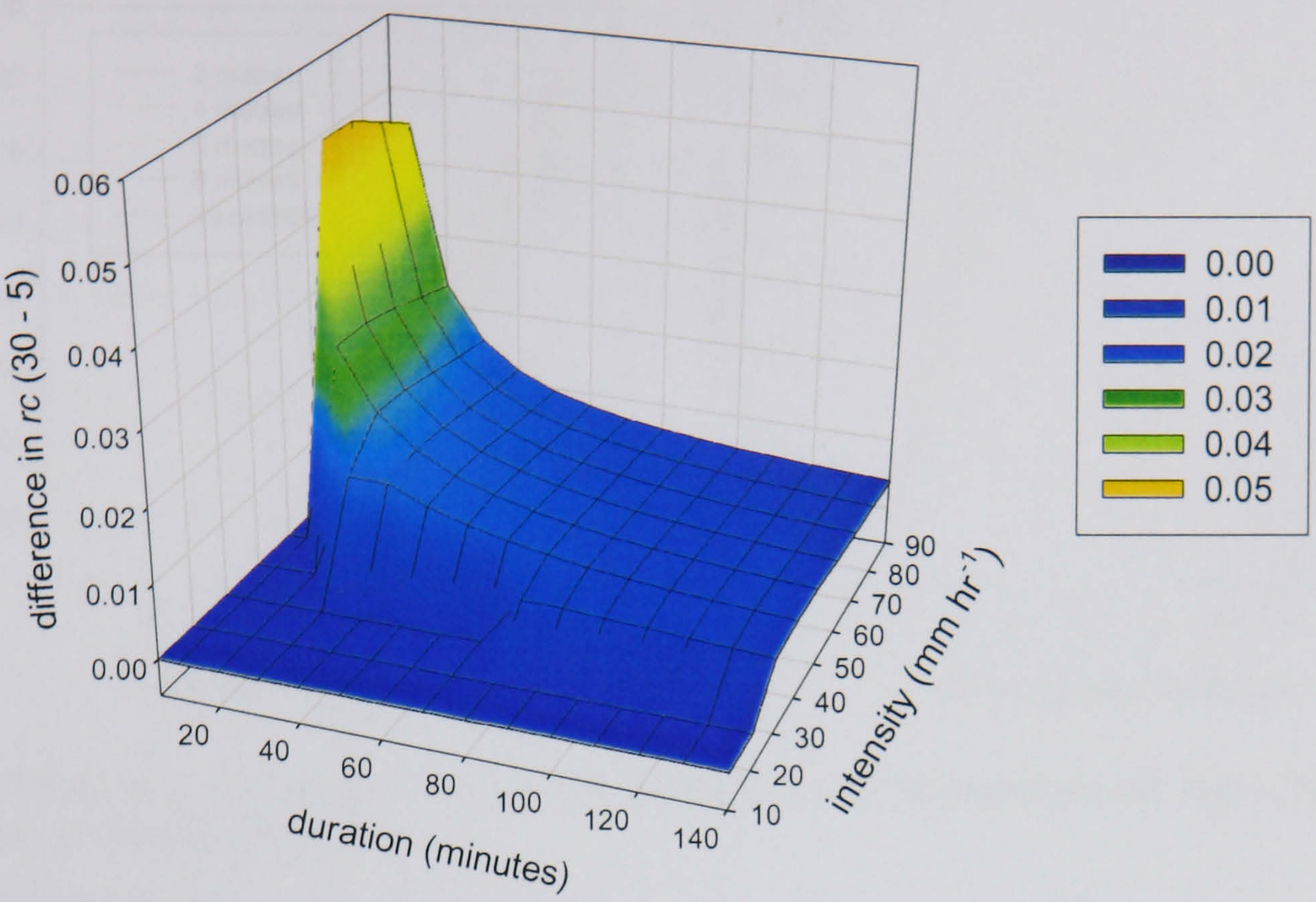

Figure 7.4 Absolute differences in the runoff coefficient between a 5 ° slope and a 30 ° over a range of storm pulses

The slope gradient influences the amount of discharge by decreasing the surface depression storage and increasing the overland flow velocity. The changes in the surface depression storage will influence the amount of water required to condition the surface to generate runoff. As explained in section 7.2.1, this will have the greatest effect during shorter storms, as shown in Figure 7.4. The changes in the overland flow velocity will reduce the time from runoff generation to it reaching the outflow. If this time is expressed as a percentage of the total storm, it will decrease with increasing storm length. Therefore, changes in the flow velocity will have the greatest impact during short storms.

7.2.4 Vegetation Buffer

It was shown in chapter 6 that the presence of a buffer strip of vegetation at the base of the slope can have a significant effect on the discharge. The efficiency of the strip and the size of buffer required to disconnect the slope will be influenced by the storm characteristics. The runoff coefficients from a ten minute storm at varying intensities and from a 70 mm hr^{-1} storm at varying durations are shown in Figure 7.5. The complete runoff coefficients surfaces for slopes with buffer strip widths of two and ten m are shown in Figure 7.6.

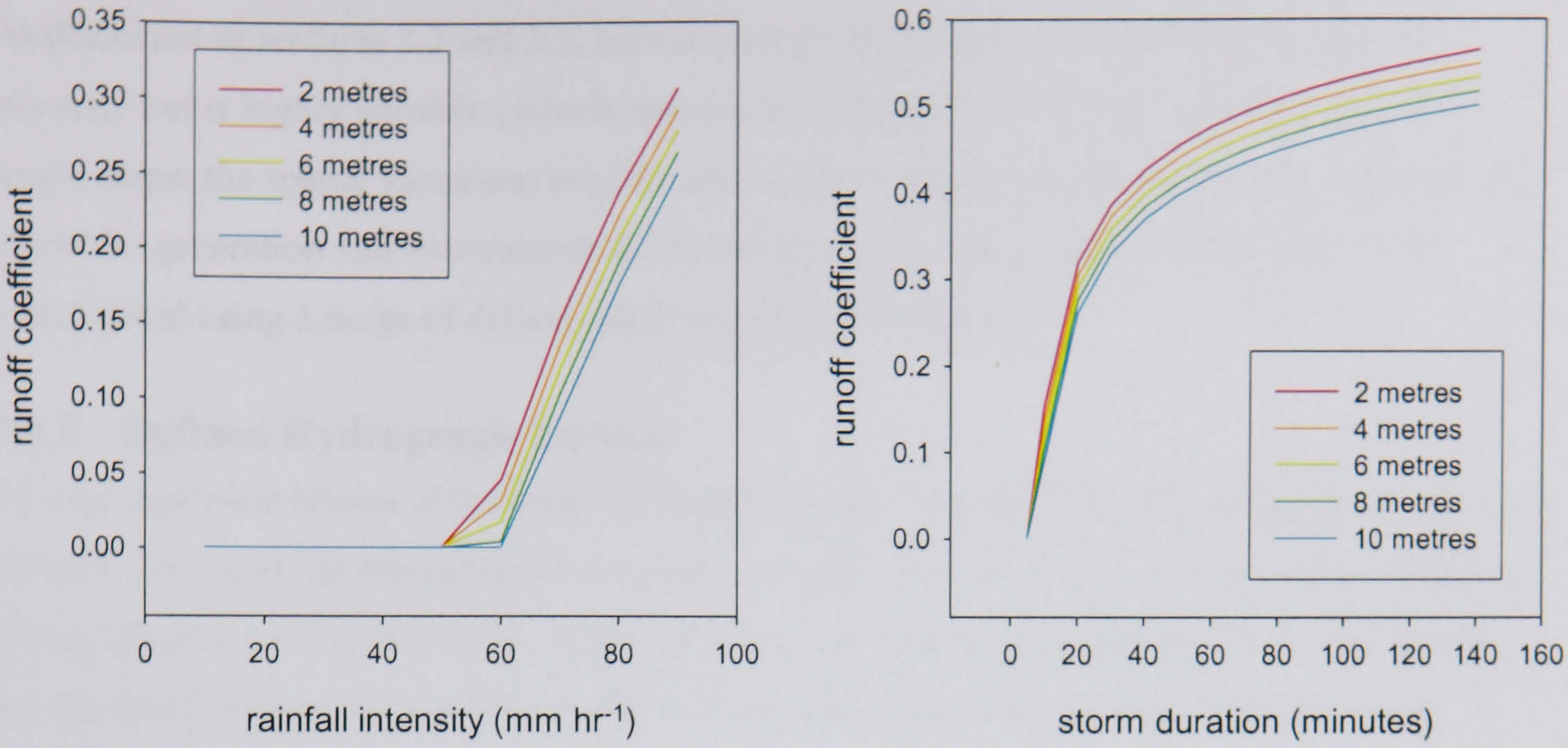

Figure 7.5 Runoff coefficients from a ten minute storm at varying intensities and from a 70 mm hr^{-1} storm at varying durations

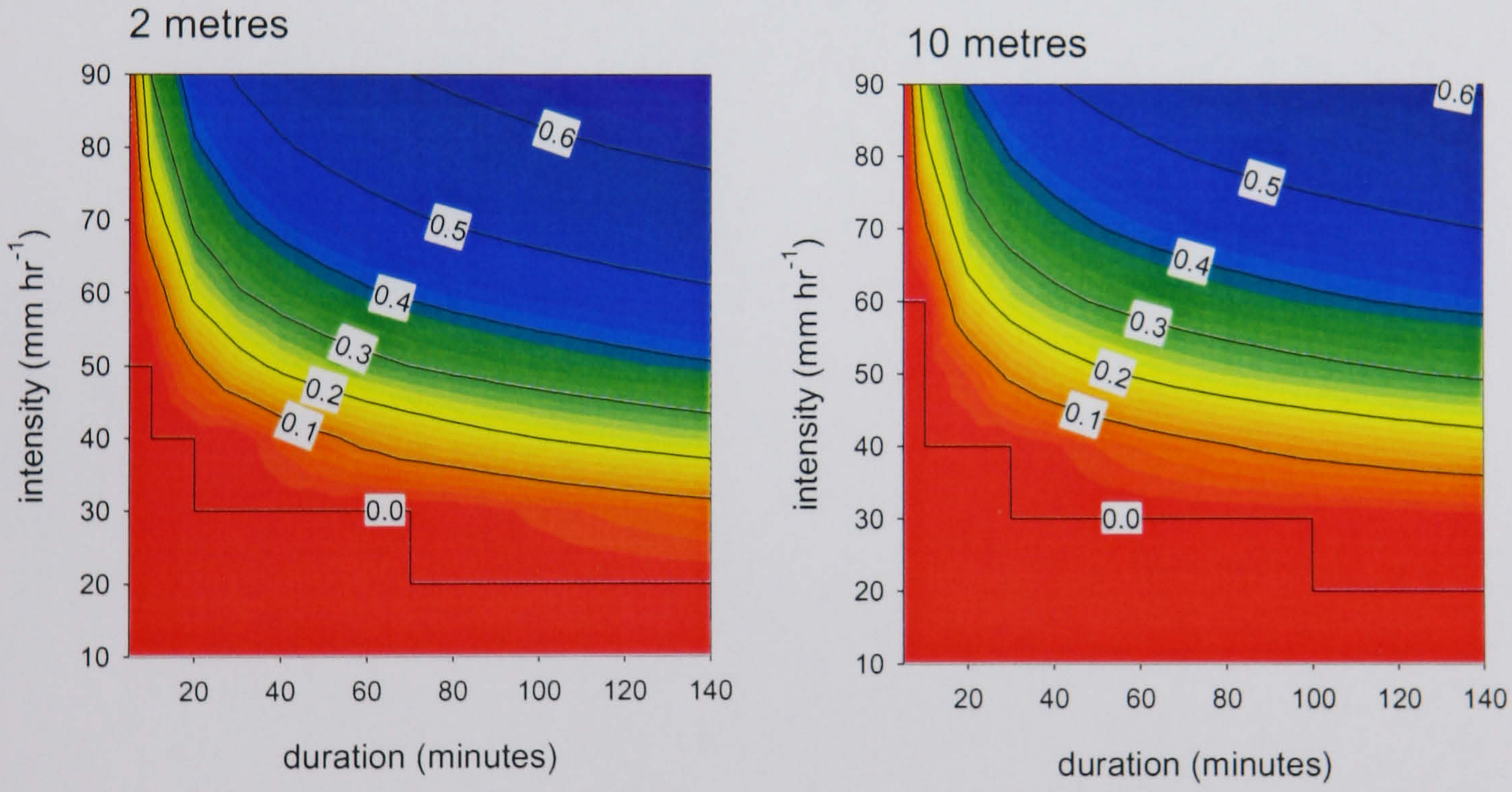

Figure 7.6 Effect of buffer strip width on discharge from different storm events

For all storm events, an increase in the width of the vegetative strip decreases the amount of discharge from the slope. As the width of the strip increases, the amount of rainfall required for the slope to connect to the outflow increases. For a strip of 2 m, it requires over 10 minutes of rainfall at 40 mm hr^{-1} however, with a strip of 10 m it requires 40 minutes of rainfall for the runoff to break through the buffer strip. At a rainfall intensity of 20 mm hr^{-1} it requires 70 minutes to break through on a 2 m strip opposed to 100 minutes on a 10 m strip. The total discharge and the time to break through can be considered in terms of the cumulative rainfall depth. As the rainfall depth increases, it is able to fill the storage in the vegetation strip thus reducing its infiltration capacity. This therefore connects the upper slope to the outflow.

7.3 Storm Hydrograph Form

As discussed in sections 2.3 and 3.5, natural rainfall does not occur at a constant rainfall intensity but is highly variable on both spatial and temporal scales. At the spatial scale of a single slope, the spatial variations may be considered negligible but the temporal variations will affect the generation and transmission of runoff across the slope. These effects have been investigated using a range of defined storm hydrograph patterns.

7.3.1 Defined Hydrograph Patterns

To investigate the effects of the storm hydrograph form on the discharge hydrograph, a series of defined storm hydrograph patterns have been used (Figure 7.7). These storms all deliver 80 mm of rainfall over a two hour period. Although this is an extreme rainfall event, it is able to bring out the differences in the storm hydrograph form. The storm characteristics and the runoff coefficients are shown in Table 7.1.

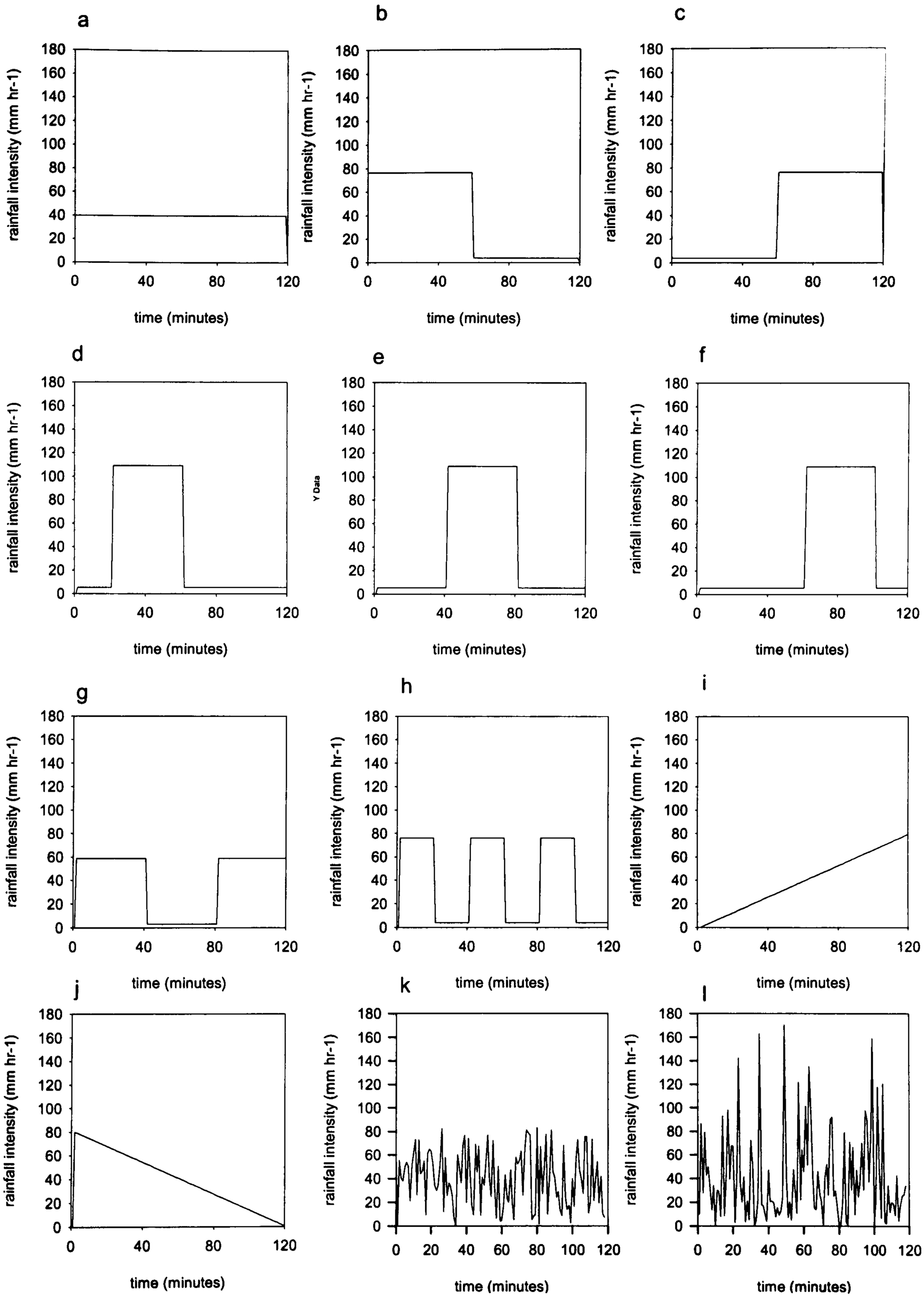

Figure 7.7 Defined storm hydrographs

Storm	Max intensity	Mean intensity	COV	Runoff Coefficient
a	40.0	40	0.00	25.3 %
b	76.2	40	0.91	51.4 %
c	76.2	40	0.91	47.6 %
d	109.1	40	1.23	57.9 %
e	109.1	40	1.23	56.9 %
f	109.1	40	1.23	55.8 %
g	58.5	40	0.66	39.4 %
h	76.2	40	0.91	44.8 %
i	80.0	40	0.58	37.1 %
j	80.0	40	0.58	35.2 %
k	83.2	40	0.60	26.2 %
l	170.3	40	0.95	26.9 %

Table 7.1 Storm intensity characteristics and runoff coefficients

Storm pattern *a* has a constant rainfall of 40 mm hr^{-1} and gives the lowest runoff coefficient at 25.3 %. The initial infiltration rate is greater than 40 mm hr^{-1}, therefore, a large percentage of the rainfall is being used to increase the soil moisture and hence decrease the infiltration rate. The maximum rainfall intensity in storms *b* and *c* increases to 76.2 mm hr^{-1} and the runoff coefficient also increases to 51.4 % for storm *b* and 47.6 % for storm *c*. Storm *b* gives slightly more discharge than storm *c* and this can be related to the rainfall after the main pulse aiding the transmission of flow.

Storms *d*, *e* and *f* all have a maximum rainfall intensity of 109.1 mm hr^{-1} and give runoff coefficients of over 55 %. The difference between the storms is the location of the high intensity rainfall pulse within the storm event. Storm *d* has the high intensity pulse at the start of the storm and has the highest runoff coefficient of the subset whilst storm *f* has the high intensity pulse at the end of the storm and has the lowest runoff coefficient. The increase in runoff can be related to the rainfall after the main pulse aiding the transmission of flow.

Storm *g* has two high intensity rainfall pulses and maximum rainfall intensity of 58.5 mm hr^{-1} and storm *h* has three high intensity rainfall pulses and maximum rainfall intensity of 76.2 mm hr^{-1}. Although storm *g* has high intensity rainfall for 66 % of the storm events, it gives less runoff (rc = 39.4) than storm *h* (rc = 44.8) which has high intensity rainfall for 50 % of the storm. The greater runoff coefficient can be related to the greater rainfall intensity in storm *h*.

Storms *i* and *j* have a linear change in rainfall intensity with a maximum intensity of 80 mm hr^{-1}. Storm *i* has a linear increase in intensity and storm *j* has a linear decrease in rainfall intensity. Storm *i* gives the higher runoff coefficient at 37.1 % opposed to 35.2 % and can be related to the wetting up of the soil before the higher intensity, runoff generating rainfall.

Storms *k* and *l* are variable rainfall with storm *l* having the greater amount of variability. Storm *k* has a maximum rainfall intensity of 83.2 mm hr^{-1} and storm *l* has a maximum intensity of

170.3 mm hr^{-1}. Despite the large difference in the maximum intensities, they give similar runoff coefficients with storm *k* giving 26.2 % and storm *l* giving 26.9 %. These values are only slightly greater than from storm *a* with constant rainfall. This suggests that the runoff which was generated during the high intensity is rapidly infiltrated during subsequent low rainfall intensity periods. This shows the importance of the temporal structure of the storms.

The effects of the maximum rainfall intensity and the coefficient of variation (COV) of the per minutes intensities on the runoff coefficient have been investigated using linear regression. Figure 7.8.

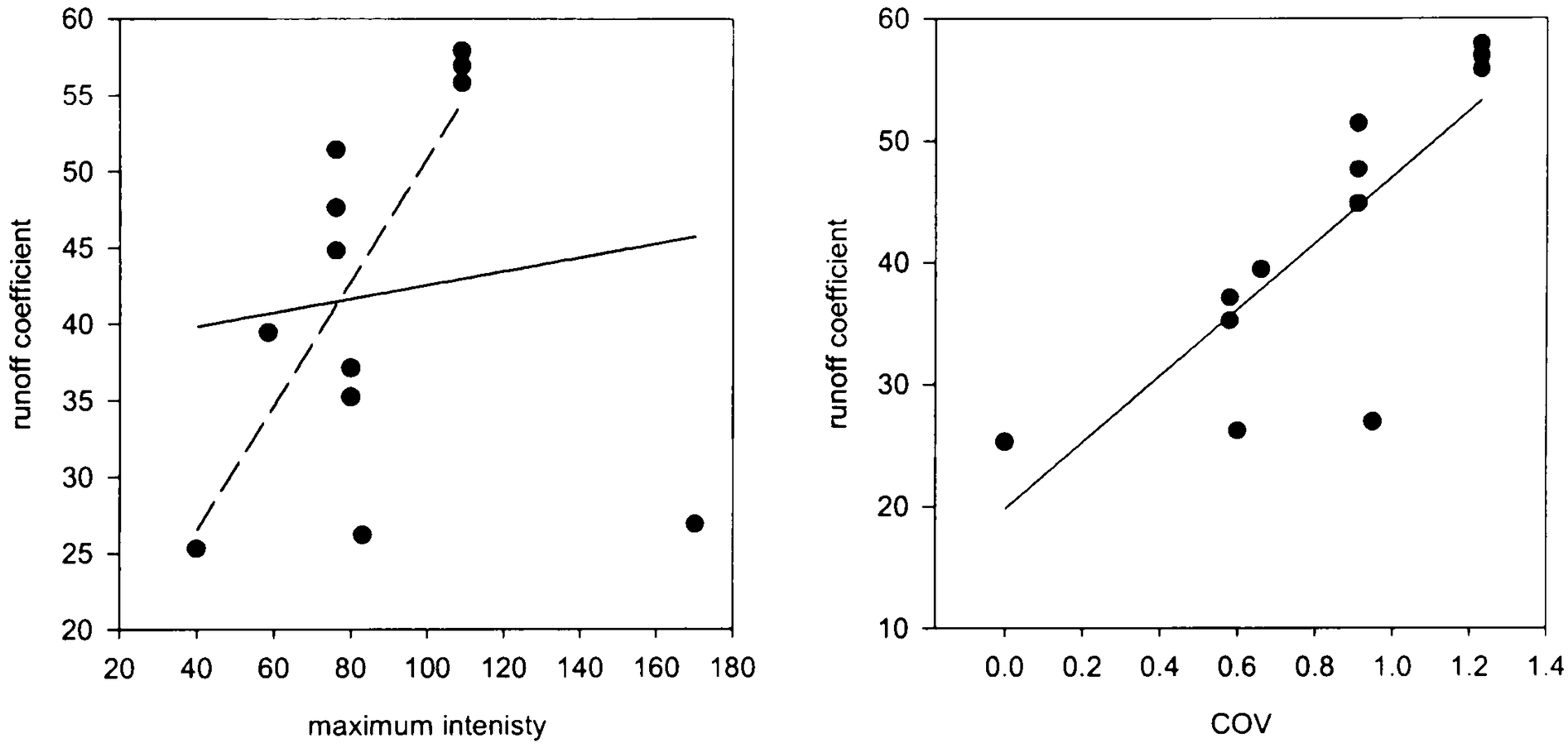

Figure 7.8 Effect of the maximum intensity and the COV on the runoff coefficient

Both the maximum rainfall intensity and the COV show a positive relationship with the runoff coefficient. However, COV is able to explain 64.18 % of the variation in the runoff coefficient whilst the maximum rainfall intensity is able to explain 1.48 % of the variability (solid line). However, if the outlier at a maximum intensity of 170.3 mm hr^{-1} is excluded, the maximum rainfall intensity is able to explain 55.4 % of the variability (dashed line). This suggests that the variability of the per minute intensities within the storm has a greater effect on the amount of discharge than the maximum rainfall intensity. This will be investigated further in section 7.4 using stochastic rainfall with variable per minute rainfall intensities.

The position of a high rainfall intensity pulse within the storm has been shown to influence the amount of discharge. The position of the pulse relates to the antecedent soil moisture conditions at the start of the storm and the conditions during the overland flow after the main rainfall pulse. This is investigated further in section 7.3.3 by running a series of rainfall pulses.

7.3.2 Slope Length and Gradient

It is valuable to assess the importance of the surface characteristics over a range of rainfall time series. In chapter 6 it was shown that the discharge is most sensitive to the slope length and

slope gradient. The hydrological response of surfaces with varying slope gradients and slope lengths was assessed for each of the defined hydrographs in Figure 7.7. The slope lengths were varied from 1 to 50 m and the slope gradients from 1 ° to 30 °. The effect of the slope gradient is shown in Figure 7.9 and Figure 7.10. The effect of slope length is shown in Figure 7.12 and Figure 7.13.

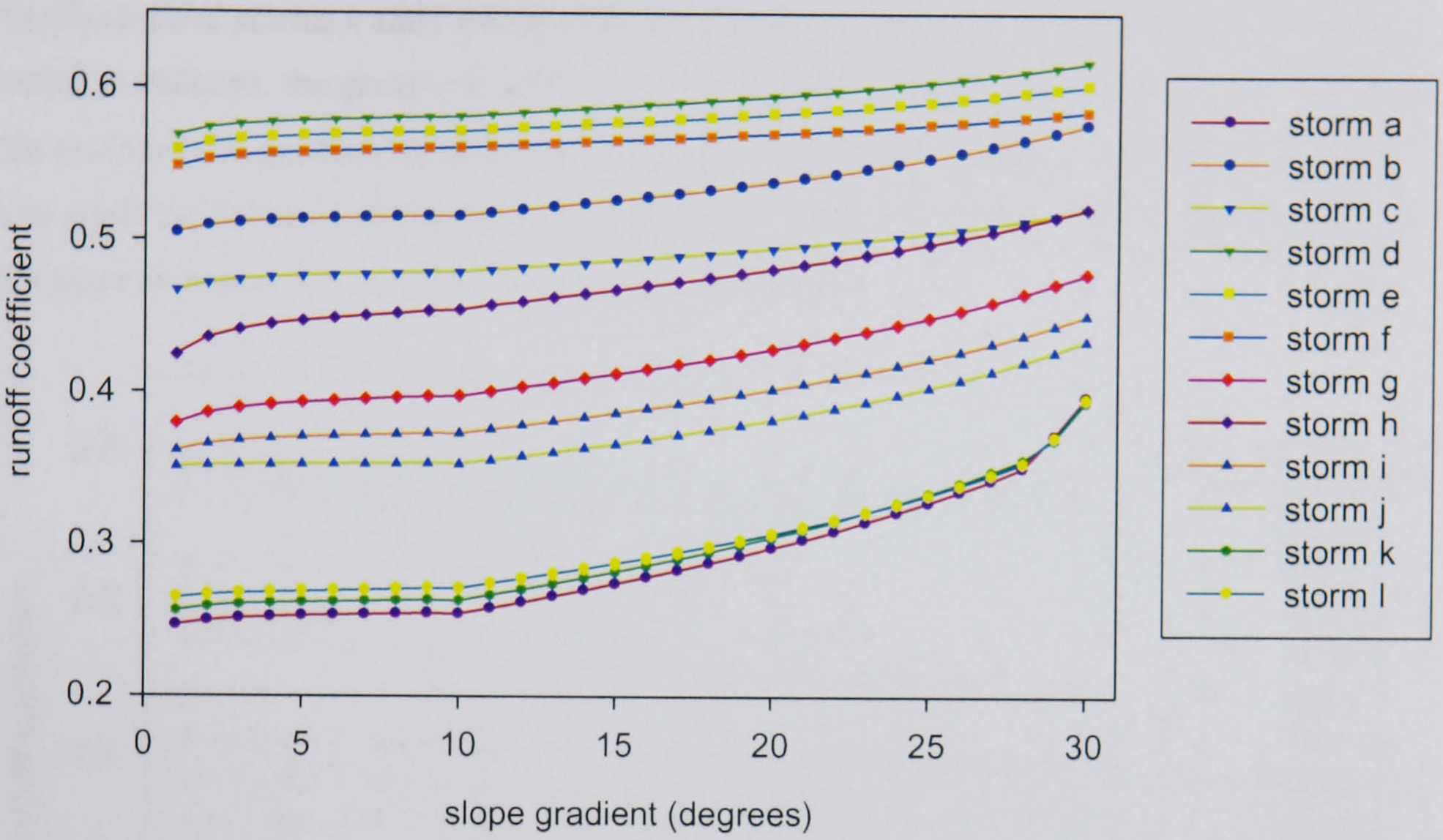

Figure 7.9 Effect of slope gradient on the runoff coefficient over a range of storm hydrographs

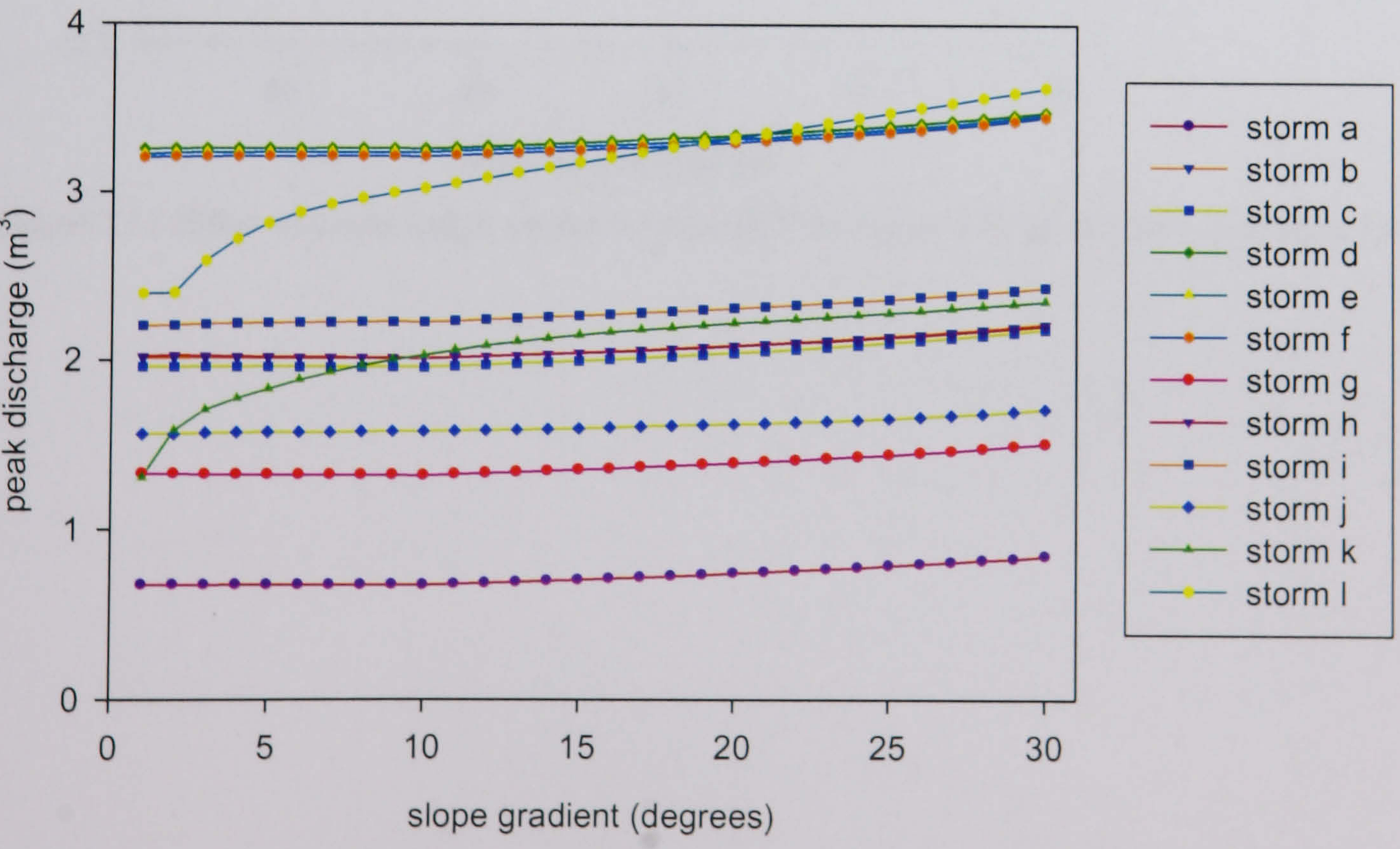

Figure 7.10 Effect of slope gradient on peak discharge over a range of storm hydrographs

Across all the of the different storm forms, there is a trend for an increase in the runoff coefficient and peak discharge. This supports the results in chapter 6 with the short, constant intensity storm.

Most of the different storm forms show a linear response to increases in the slope gradient. This is with the exception of storms *a*, *k* and *l* which show a non-linear response in the overall runoff coefficient and storms *k* and *l* which show a non-linear response in the peak discharge. For the runoff coefficient, the greatest sensitivity is on steep slopes with gradients above 28 ° whereas the sensitivity to gradient for the peak discharge is between 2 ° and 5 °. The sensitivity to the low gradients for peak discharge reflects the results found in chapter 6. The linear response of the other storms is in contrast to the results from chapter 6.

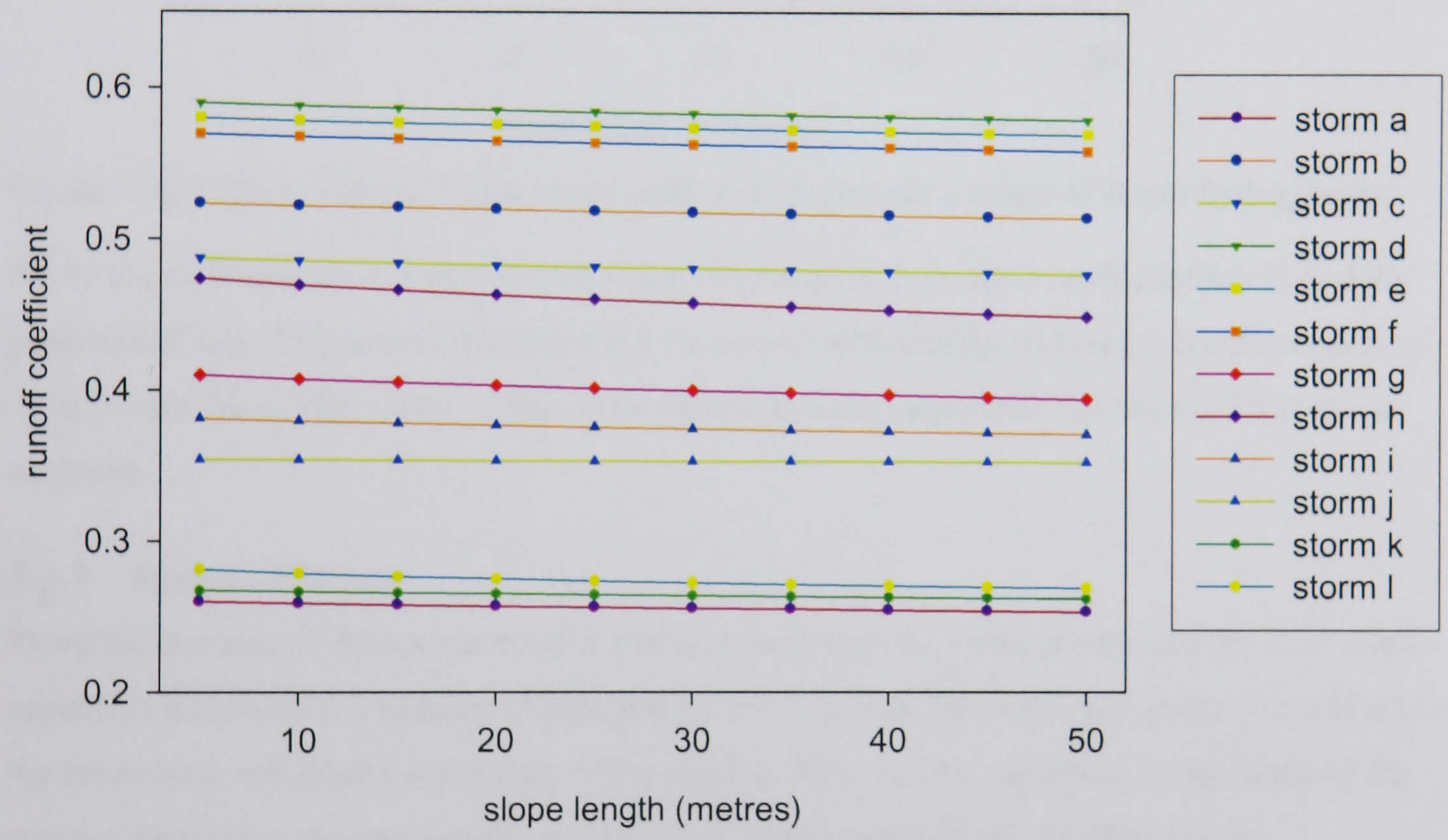

Figure 7.11 Effect of slope length on the runoff coefficient over a range of storm hydrographs

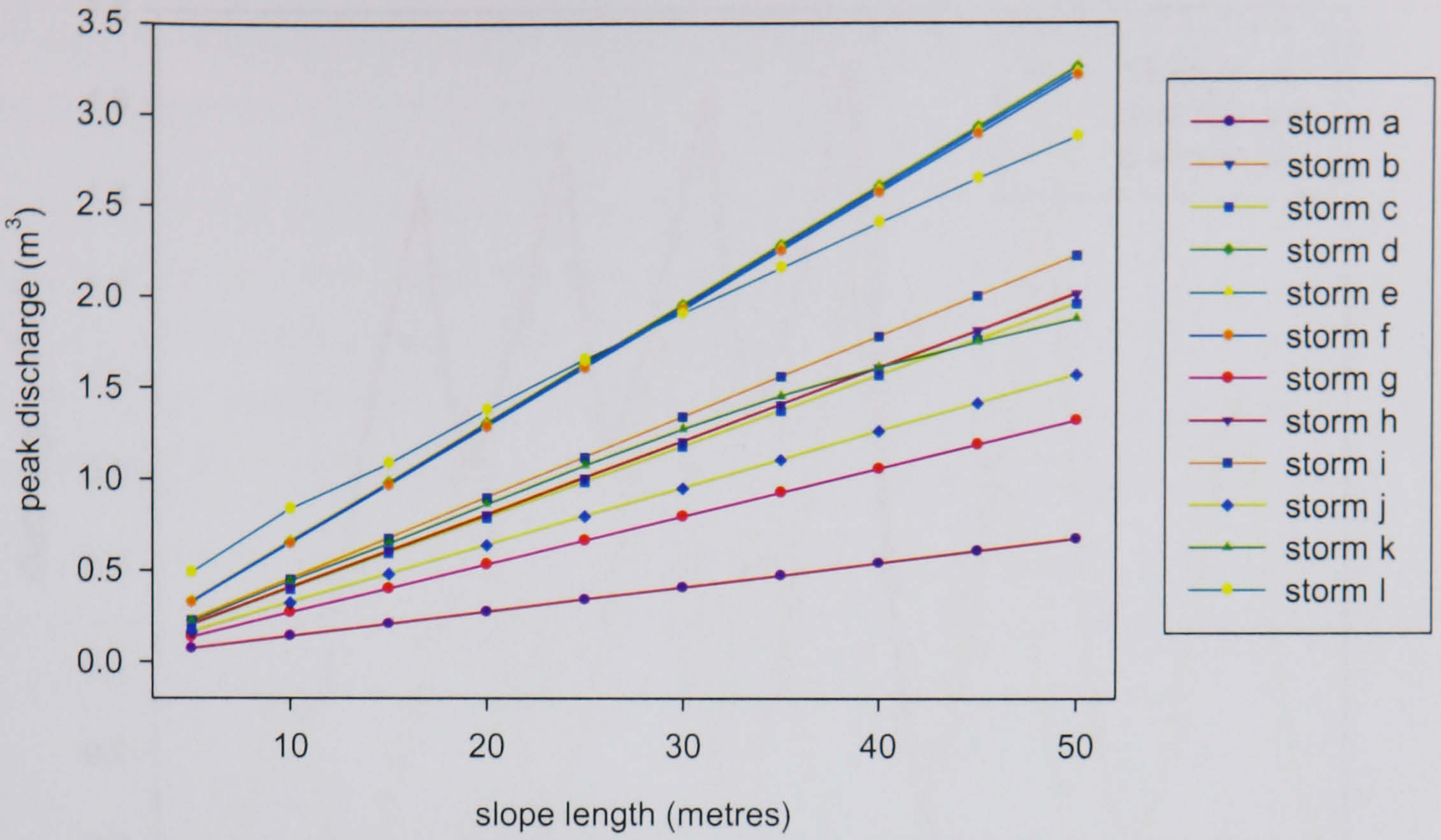

Figure 7.12 Effect of slope length on the peak discharge over a range of storm hydrographs

All of the different storm forms shown linear responses to both the runoff coefficient and the peak runoff rate. This shows that there is a consistent relationship with slope length regardless of the storm form. The nature of the storm determines the magnitude but not the form of the response.

7.3.3 Series of Pulses

From the analysis of the natural rainfall patterns in chapter 3, it was shown that the total storm rainfall is delivered in a number of separate pulses. The time between each pulse will influence the antecedent conditions at the start of the rainfall. This will be expressed in the depth of the surface depression storage and the soil moisture which controls the infiltration rate.

The same rainfall pulse that was used in chapter 5 (75mm hr^{-1} for five minutes) has been repeated five times with a varying gap of no rainfall. The discharge hydrographs for gaps of one, three and five minutes are shown in Figure 7.13. Although the rainfall intensity in all of the rainfall pulses is constant between the different storms, the mean storm intensity decreases with the increasing gap between pulses.

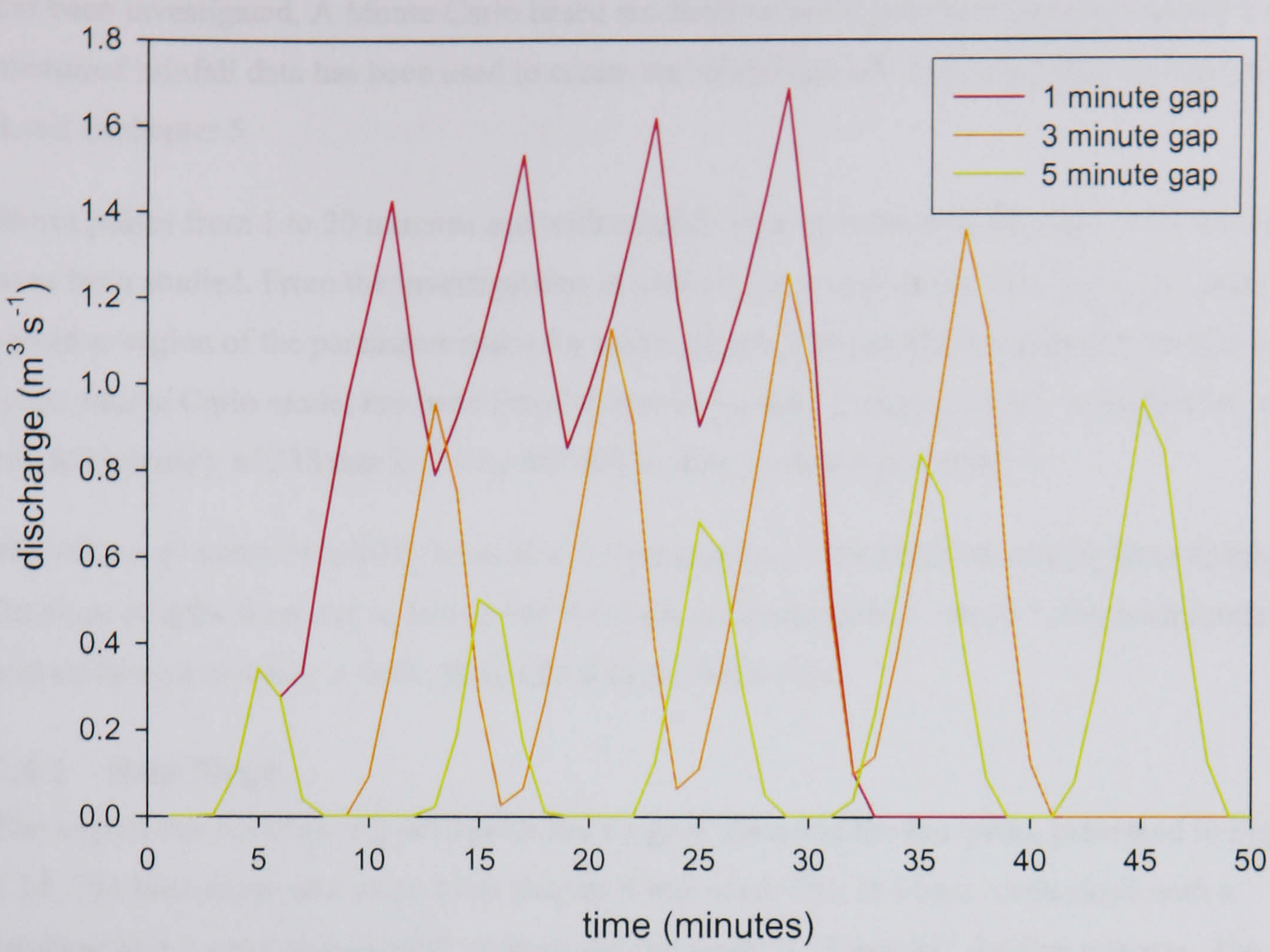

Figure 7.13 Effects of the length of the gap between storm pulses on discharge. Note: All three series have a peak at 5 minutes but are obscured by the 5 minute gap line.

As the cumulative amount of rainfall increases, the runoff coefficient per rainfall pulse increases. This shows the importance of the antecedent soil moisture and soil surface conditions on the generation and transmission of runoff. As the total rainfall depth increases, the soil moisture increases, thus reducing the infiltration capacity. The reduction in the infiltration capacity decreases the time required for the surface depression store to fill and hence for runoff to be generated.

The discharge from the slope subjected to the rainstorm with five minutes between storm pulses always returns to zero before the next pulse of rainfall. There is sufficient time for the water on the surface to enter the surface depression store or to infiltrate and hence for runoff to stop. The amount and peak runoff increases with each successive pulse and can be related to the decrease in the infiltration rate with the cumulative infiltration. The rainfall time series with one minute between the pulses gives the maximum amount of discharge. Due to the short time between the rainfall pulses, there is not enough time for the runoff generating areas to become disconnected from the slope outflow. This therefore leads to the continuous discharge from the slope outflow.

7.4 Stochastic Rainfall

The investigations in section 7.3 incorporated variability within storms using RPM derived rainfall. This suggested that the rainfall variability may be a significant control on the amount of runoff generated. To explore this further, the impact of rainfall variability at the minute scale

has been investigated. A Monte Carlo based stochastic rainfall generator parameterised from measured rainfall data has been used to create the rainfall pulses. This generator is described in detail in chapter 5.

Storm pulses from 1 to 20 minutes and with rainfall intensities from 40 mm hr^{-1} to 90 mm hr^{-1} have been studied. From the investigations in section 7.2, it was shown that this is the most sensitive region of the parameter space for storm pulses. The rainfall intensity distribution used in the Monte Carlo model has been fitted to real storm data. This gives a 0.1 % probability of a rainfall intensity of 238 mm hr^{-1}. The full distribution is shown in chapter 3.

The effects of storm variability have been investigated with the fixed base slope from chapter 6, for slope lengths from one to 100 m and for slope gradients from 1 ° to 30 °. For both rainfall and surface parameters, a uniform distribution has been used.

7.4.1 Base Slope

The impact that variable rainfall has on discharge is shown in the box plots, presented in Figure 7.14. The base storm and slope from chapter 6 was used. This is a bare scrub slope with a gradient of 6 ° and a slope length of 50 m and the storm is 75 mm hr^{-1} for five minutes. The Monte Carlo generator was used to produce 200 realisations of the storm pulse. The RPM generator always produces the same discharge hydrograph. This is shown by the single line in Figure 7.14. The Monte Carlo generator produces a distribution of slope discharge values.

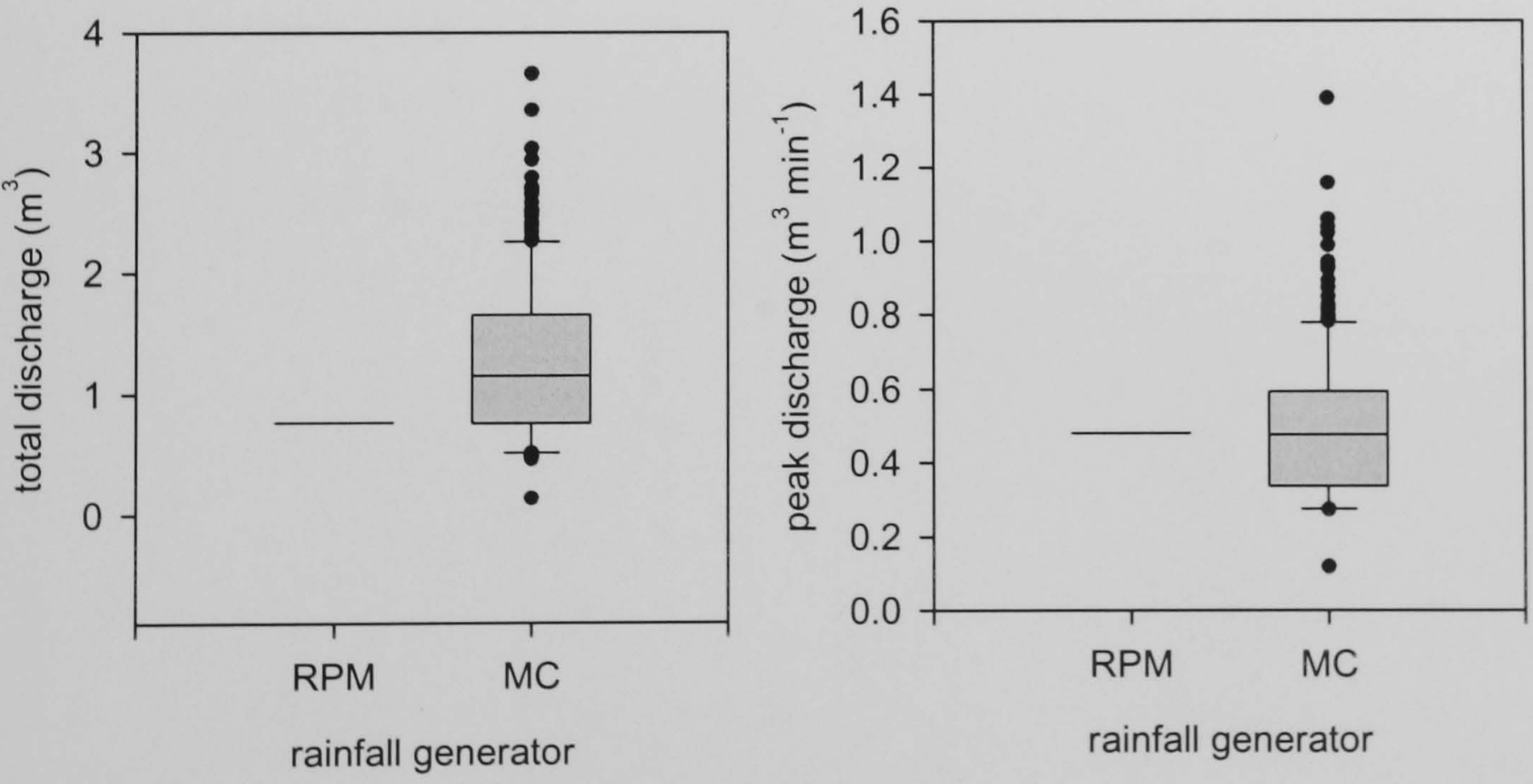

Figure 7.14 Box plots of the differences in runoff from variable and constant rainfall

For the total discharge, the introduction of variable rainfall leads to an increase in the median discharge. The maximum discharge volume simulated was 3.65 m^3; this is 480 % greater than with constant rainfall. However, 25.9 % of the simulations produced a discharge volume less than the constant rainfall, with the minimum simulated discharge at only 0.46 m^3.

The median peak discharge is very similar between the constant and variable rainfall and hence 51.2 % of the simulations gave discharges less than the constant intensity rainfall. There is a greater spread of values with the variable rainfall, to a maximum of 1.38 m^3 min^{-1}.

To investigate which properties of the rainfall pulse control the amount of discharge that leave the slope, the surface was subjected to 1000 storm realisations of varying intensity and duration. The relationship between the nature of the storm and the characteristics of the slope discharge are shown in Figure 7.15.

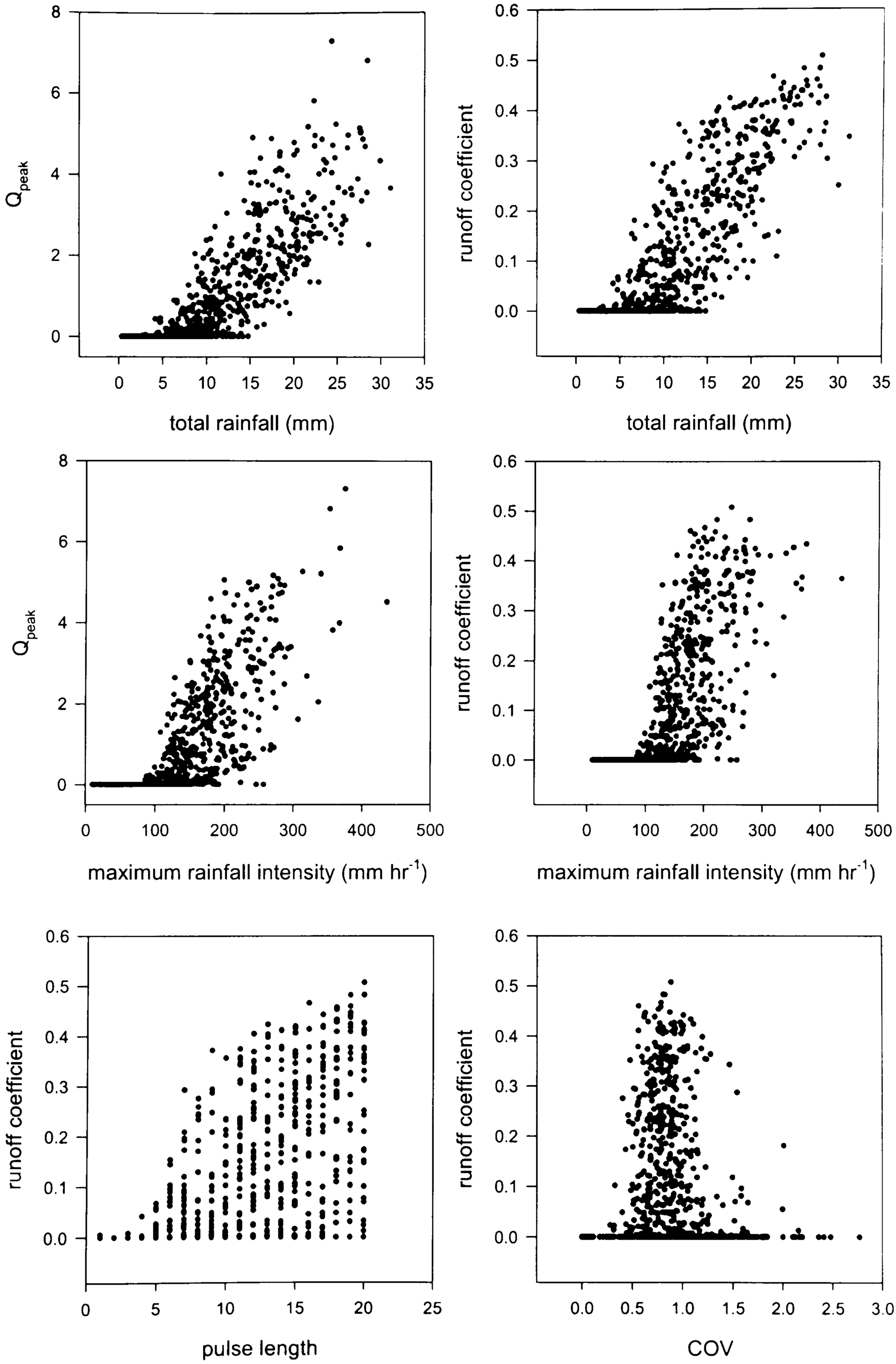

Figure 7.15 Effect of storm characteristics on the discharge characteristics

The total rainfall depth shows a positive relationship with both the peak discharge and the runoff coefficient. The increase in the peak discharge and the runoff coefficient is related to the decrease in infiltration rate with cumulative rainfall and hence the increase in runoff production. There is a large amount of scatter in the *y* axis on both plots. For a total rainfall depth of 15 mm, the peak discharge varies from 0 to 4.8 m^3 min^{-1} and the runoff coefficient varies from 0 to 38 %. This spread of values relates to the range of intensities within the pulse and the temporal structure of the storm pulse.

The maximum rainfall intensity shows threshold behaviour for both the peak discharge and the runoff coefficient. The maximum rainfall intensity must be greater than the infiltration rate of the soil to produce any runoff. The infiltration rate at the start of the simulation run is 55 mm hr^{-1} whereas the runoff threshold is at 84 mm hr^{-1}. This difference relates to the infiltration excess required to fill the surface depression store. If only a small amount of water overflows from the depression store, it is likely that it will be infiltrated further down slope. This threshold therefore relates to the amount of infiltration excess required to form a connection between the runoff generating points and the outflow.

Above the threshold there is a positive relationship between the maximum rainfall intensity and both the peak discharge and the runoff coefficient. There is, however, a large amount of scatter with many pulses with high maximum rainfall intensities giving no runoff. At a maximum rainfall intensity of 240 mm hr^{-1}, the peak discharge varies from 0 to 5 m^3 min^{-1} and the runoff coefficient varies from 0 to 50 %. The maximum rainfall intensity only describes a single minute within the rainfall pulse. This minute is expected to relate to the peak discharge but not so well with the runoff coefficient which is a pulse scale measure. The response to the maximum intensity minute will be determined by the antecedent conditions which are in turn related to the position of the high intensity minute within the storm event.

As the pulse length increases, there is an increase in the range of runoff coefficients. The rate of increase in the maximum runoff coefficient rises above a pulse length of five minutes and levels off after 13 minutes. The increase at five minutes relates to the time required to fill the surface depression store and for the runoff to reach of the outflow. The levelling off of the range of runoff coefficients at 13 minutes relates to the total travel times across the surface. With a slope length of 50 m, it will take approximately 8.5 minutes to reach the outflow from the top of the slope. The remainder of the time is connected to the time required to generate runoff.

With the defined storm hydrograph patterns in section 7.3.1, the coefficient of variation (COV) was found to be strongly related to the runoff coefficient. For the stochastic rainfall pulses, it does not show the same behaviour. There are lower and upper limits beyond which there is minimal discharge from the slope. The lower limit is at 0.5 and the upper limit is at 1.25

although there are a number of outliers. Between these limits there is a large range of runoff coefficient values ranging from zero to 50 %. This therefore suggests that the temporal structure, as well as the variability, plays a significant role in the generation of runoff.

7.4.2 Storm versus Slope Characteristics

The spatial distribution of runoff can be related to the spatial pattern of rainfall characteristics and the spatial pattern of surface characteristics. The relative role of the storm and surface factors has been investigated using statistical analysis.

Surfaces with varying slope lengths, slope gradients and the base slope were subjected to 1000 storm realisations. Each storm realisation has been characterised by a number of statistical properties relating both to the storm duration and intensity and to the variability of the rainfall within the storm pulse. In order to assess the importance of the different storm characteristics, the correlation coefficients between the characteristic and the peak discharge and the runoff coefficient have been calculated (Table 7.1). Due to the high *n* value (1000), it is possible to use the Pearson correlation coefficient. Correlations significant at the 99 % level and above are marked with an asterisk.

	Base slope		**Varying slope gradient**		**Varying slope length**	
	Peak discharge	**Runoff coefficient**	**Peak discharge**	**Runoff coefficient**	**Peak discharge**	**Runoff coefficient**
Slope Gradient			0.09*	0.03		
Slope Length					0.18*	-0.10*
Pulse Length	0.52*	0.53*	0.47*	0.49*	0.46*	0.52*
Range	0.73*	0.71*	0.70*	0.68*	0.64*	0.69*
Minimum intensity	-0.12*	-0.12*	-0.12*	-0.13*	-0.15*	-0.16*
Maximum intensity	0.75*	0.73*	0.73*	0.71*	0.66*	0.71*
Mean intensity	0.57*	0.58*	0.53*	0.56*	0.44*	0.50*
Pulse depth	0.84*	0.85*	0.78*	0.81*	0.72*	0.81*
Standard Deviation	0.59*	0.58*	0.58*	0.58*	0.52*	0.57*
Skew	0.11*	0.08	0.09*	0.05	0.11*	0.10*
Kurtosis	0.06	0.02	0.07	0.01	0.09*	0.06
COV	-0.04	-0.06	-0.02	-0.05	0.02	0.02

Table 7.2 Correlations between storm characteristics and discharge for varying slopes

For the base slope, the rainfall pulse depth explains 72 % of the variability in the runoff coefficient and 71 % of the variability in the peak discharge. This is related to the conditioning of the soil to give runoff by the early section of the rainfall to give lower infiltration rates and hence higher runoff. The maximum rainfall intensity explains 56 % of the variability in the peak discharge and 53 % of the variability in the runoff coefficient. This is contrasted with the mean

rainfall intensity only explaining 33 % of the variability in the peak discharge and only 34 % of the variability in the runoff coefficient.

Of the statistical moments related to the variability of the rainfall, the standard deviation is significantly related to the peak discharge and the runoff coefficient and the skewness is only significantly related to the peak discharge. The kurtosis and the COV are not significantly related to either discharge hydrograph characteristic.

The variability in the slope gradient is able to explain 1 % of the variability in the peak runoff. It is not, however, significantly related to the overall runoff coefficient. The introduction of variable slope gradients reduces the influence of all of the storm characteristics on the discharge hydrograph with the exception of the minimum rainfall intensity which increases by less than 1 % in explaining the runoff coefficient.

The variability in the slope length is able to explain 3 % of the variability in the peak discharge and 1 % of the variability in the runoff coefficient. The introduction of variable slope lengths reduces the influence of the pulse length, intensity range, maximum and mean. There is a slight increase in the importance of the minimum rainfall intensity. The skewness becomes significantly related to the runoff coefficient explaining 1 % of the variability and the kurtosis becomes significantly related to the peak discharge explaining 0.8 % of the variability. This increase in the importance of the variability of the rainfall is related to the infiltration of run on. Constant high intensity rainfall will allow runoff to travel further whereas variable rainfall will allow the infiltration of runoff during low intensity rainfall.

The main control on the amount of discharge from a slope is the storm characteristics. However, the surface form can account for up to 3 % of the variability in discharge over a range of storms. These surface factors should be considered as significant controls on discharge generation since it is the surface factors that will determine the spatial pattern of runoff across a catchment.

7.5 Discussion

The modelling results show that there are two key storm characteristics that determine the runoff coefficient for individual storm events: the relationship between the rainfall intensity and surface conditions and the temporal structure of the rainfall intensities within the storm event. It is helpful to consider the temporal dynamics of runoff generation as a four stage process. This view of the runoff generation process is discussed in section 7.5.1. The relationships between the rainfall intensity and the surface properties are discussed in section 7.5.2 and the impact of the temporal fragmentation of high intensity rainfall is discussed in section 7.5.3.

7.5.1 The Four Stages of Runoff Generation

The generation of runoff at the point scale can be viewed as a four stage process with the storm event moving the runoff generating system sequentially between the different stages. The stages are:

1. The rainfall intensity is less than the infiltration capacity. During this stage, all the rainfall will infiltrate and the increase in soil moisture will cause a reduction in the infiltration capacity.

2. The rainfall intensity is greater than the infiltration capacity but the amount of water held in surface detention is less than the depth of the surface depression store.

3. The rainfall intensity is greater than the infiltration capacity and the amount of water held in surface detention is greater than the surface depression store capacity. During this stage, runoff is generated.

4. The rainfall intensity is less than the infiltration capacity but the amount of water held in surface detention is greater than the surface depression store capacity. During this stage, no new runoff will be generated but overland flow will continue.

The location of the stages within the parameter phase space is shown in Figure 7.16. As a storm event progresses, it will create a path through this parameter phase space, as shown in Figure 7.16. The characteristics of the path taken through the phase space will determine the amount of runoff generated, the time available for the transmission of runoff across the surface and hence the amount of runoff that is able to leave the slope as discharge. The path that the storm takes through the phase space will be determined by both the surface characteristics and the nature of the storm. The amount of discharge from the slope will be determined by both the amount of time spent in stage 3 and the structure of the rainfall during this period. The structure of the rainfall will determine if the storm will move between stages 2 and 3 or remain in stage 3 for a long time period.

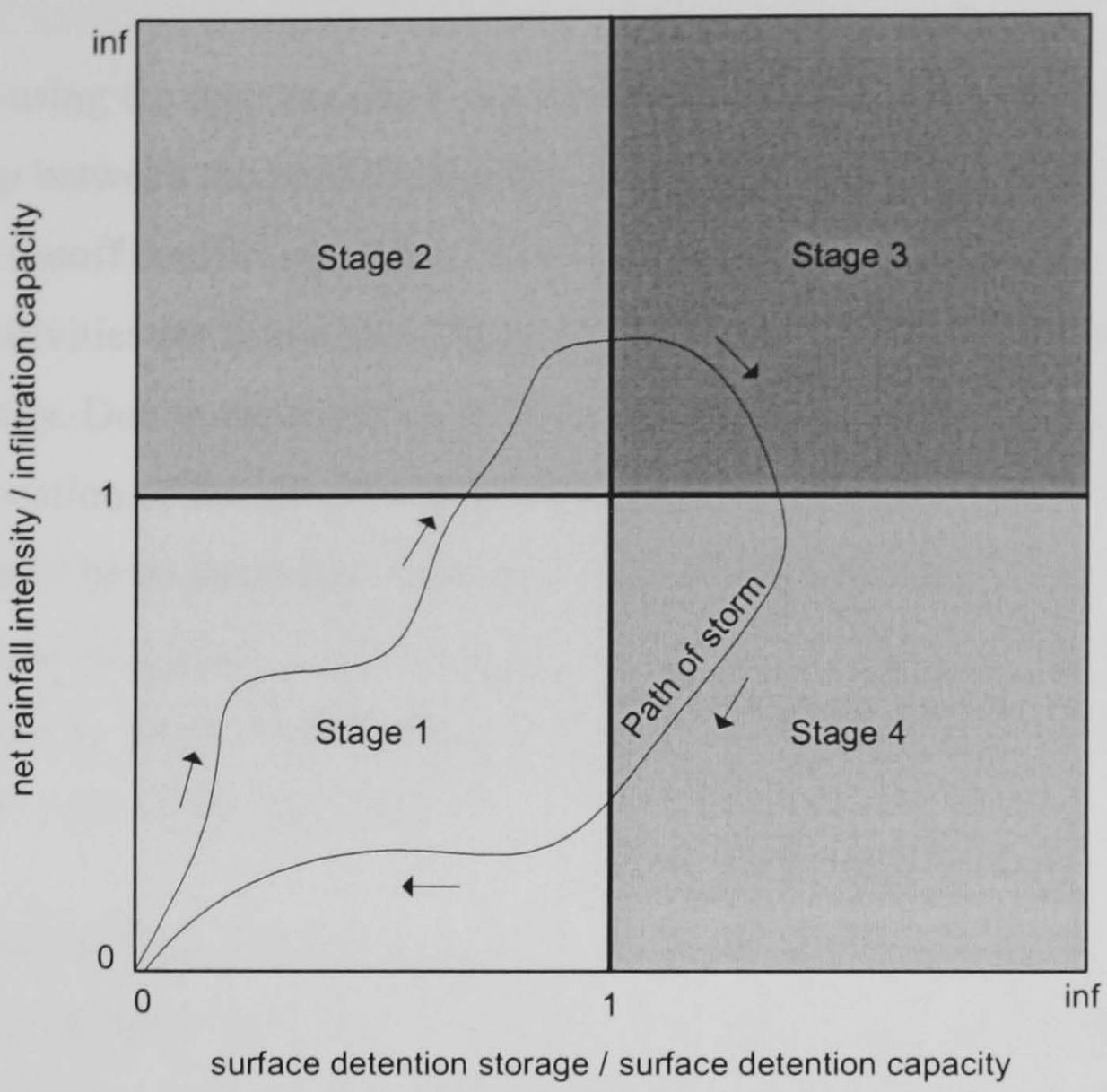

Figure 7.16 The location of the four stages of runoff generation within the parameter phase space

The time taken to move through stage 2 is dependent upon the depth of the surface depression store and the fragmentation of high intensity rainfall. As was shown in chapter 6, this is related to the soil roughness and the local slope gradient. As the slope gradient increases, the depression storage decreases, reducing the amount of water required to pass through stage 2. The simulation results shown in section 7.2.3 show, for example, that an increase in the slope gradient from 5 ° to 30 ° may increase the runoff coefficient by up to 8 %.

The time required for the system to leave stage 1 will be strongly related to the antecedent soil moisture. With wetter conditions, the infiltration capacity will be lower and hence less rainfall will be required to move the system into stage 2. When a high intensity pulse of rainfall occurs in a system which is already in stage 2, 3 or 4, almost all of the water in the pulse will be converted into runoff. If a similar pulse falls on a dry, stage 1, soil surface, much of the rainfall enters the soil and / or surface depression store before moving the system into stage 3 when runoff is generated.

7.5.2 Rainfall Intensity and the Surface Conditions

In chapter 6 the key surface controls on the amount of water leaving a slope were shown to be the distribution of flow path lengths, slope gradient and the spatial organisation of the slope. The modelling experiments presented in chapter 7 show how the relationships presented in Chapter 6 are modified by the rainfall characteristics.

General

The experiments using the Rectangular Pulse Model (RPM) rainfall show that there is a non-linear relationship between the rainfall intensity and duration and the runoff coefficient. The sensitivity of the runoff coefficient varies across the intensity – duration parameter phase space. The greatest sensitivities are found when there is a balance between the infiltration capacity and the rainfall intensity. Due to the reducing infiltration capacity with increasing cumulative infiltration, the location of the sensitive area moves with increasing volume of rainfall delivered. Therefore, there will be an interaction between the distribution of storm characteristics and the surface hydrological properties. A small change in the characteristics of the storms, through driving only a small response in the hydrological system within the phase space, can result in a significant change in the runoff generated.

The Distribution of Flow Path Lengths

The effect of the distribution of flow path lengths has been investigated in the experiments on the effect of slope length. It was found that the greatest sensitivity to the changing rainfall characteristics was for storms of less than 15 minutes. The runoff generation system must remain in stage 3 or 4 along the entire pathway for flow transmission to occur. For storms with durations less than 15 minutes, only a small percentage of the flow normally reaches the slope outflow. As storm duration increases, the percentage reaching the outflow increases and hence the system sensitivity decreases. Analysis of the relationship between rainfall duration and intensity is presented in Figure 3.11. If a rainfall intensity of 70 mm hr^{-1} is taken to be the threshold for runoff generation, the maximum observed rainfall duration at this intensity is 25 minutes, with the majority of pulses much briefer. Therefore, the runoff generated in these shorter pulses will not reach the slope outflow. The impact of the number and temporal arrangement of multiple rainfall pulses is discussed further in section 7.5.3.

Yair and Lavee (1985) considered a number of storm intensities and durations across a range of slope lengths. They found that a threshold rainfall depth had to be exceeded before any runoff was able to leave the slope and a higher threshold for uniform generation of runoff across the slope. These thresholds were dependent upon the rainfall characteristics and the slope length. The results presented in Figure 7.2 show similar differences in response to those found by Yair and Lavee (1985). The infiltration characteristics used in the experiments presented in this chapter differ significantly from those used in the model of Yair and Lavee (1985) due to the differences in the arid environment modelled by Yair and Lavee and the semi-arid environment under consideration in this chapter. The experiments presented here extend the work of Yair and Lavee (1985) by considering a greater range of storm lengths and intensities and by application to semi-arid rather than arid hydrological conditions.

Lal (1997) found that the form of the relationship between the slope length and the runoff coefficient varied significantly between storm events. He proposed that this variation depended on interactions between the slope length, rainfall characteristics and land management. The results presented in section 7.3.2 using the defined hydrograph patterns show that there is a consistent relationship between the slope gradient and the runoff coefficient. For all storms considered there is a decrease in the runoff coefficient with increasing slope length. However, the gradient of the decrease varies between storms. This contrasts with the findings of Lal (1997) who found that the form of the slope length and runoff coefficient relationship varied between storms. Lal found that there was an increase in the runoff coefficient with increasing slope lengths at short slope lengths, followed by a decrease in the runoff coefficient at longer slope lengths. This more complex relationship was not generated by any of the model experiments performed. The changes in the runoff coefficient reported by Lal may relate to the formation of rills during the storm event. The amount of rill initiation will depend upon the amount of runoff generated and the erosive power of the rainfall. The generation of a rill network significantly alters the distribution of flow path lengths leading to a reduction in the mean path length. This reduction increases the runoff connectivity and hence leads to the observed increase in the slope scale runoff coefficient.

Slope Gradient

The relationship between the slope gradient, rainfall characteristics and runoff coefficients have been investigated using constant intensity rainfall, defined rainfall hydrograph patterns and stochastic rainfall. The modelling experiments using constant intensity rainfall found a consistent relationship with the runoff coefficient increasing linearly with an increase in slope gradient for a given storm. However, the defined storm hydrograph patterns show that certain storms generate a non-linear relationship between the slope gradient and the runoff coefficient. This is most clearly expressed for the *h, j* and *l* hydrograph forms in Figure 7.7. These three hydrograph forms have the greatest amount of variability in the rainfall intensities. Therefore, the runoff generation system will be moving between stage 2 and stage 3. This results in runoff infiltrating while the system is in stage 2. As the slope gradient increases, the flow velocity increases and the runoff is able to travel further whilst the system is in stages 3 and 4. This shows that it is the potential travel distances whilst the system is in stages 3 and 4 that are the key factor in determining the runoff coefficient.

The experiments using stochastic rainfall showed that the characteristics of the storm are able to explain far more of the variability in the runoff coefficient than the slope gradient. The slope gradient is able to explain 0.8 % of the variability in the peak discharge and 0.01 % of the variability in the runoff coefficient. However, the rainfall pulse depth is able to explain 65.6 % and the rainfall variability expressed through the standard deviation is able to explain 33.6 % of

the variability in the runoff coefficient. This shows the greater importance of the rainfall characteristics over the slope gradient.

The modelling results presented in this chapter considering the effect of slope gradient on the runoff coefficient agree with the field results of AbuAwwad and Shananawi (1997) with greater runoff being found on steeper slopes. The modelling results contrast with the rainfall simulation experiments of Chaplot and Le Bissonnais (2000) who found a decrease in runoff with increasing slope gradient. The decrease observed by Chaplot and Le Bissonnais (2000) related to a breakdown of the surface crust resulting in an increase in the infiltration capacity. The dynamics of crust formation and rill initiation should be considered in future versions of CRUM.

Spatial Organisation of the Slope

The modelling experiments investigating the effect of spatial organisation of the infiltration characteristics across the slope considered the impact of a variable width vegetated buffer strip on the runoff coefficient across a range of storms. The modelling results showed that the buffer strip width required to disconnect the upper slope from the outflow increased with increasing storm depth. By relating these results to the distribution of storm rainfall depths for a region, it would be possible to design effective buffer strips for erosion and pollutant capture whilst minimising the amount of productive land that is lost to the buffer strips. These buffer strips can reduce flood flows and improve water quality by disconnecting the pollutant source areas from the channel.

7.5.3 Temporal Structures of the Rainfall Intensity

The temporal structure of the rainfall time series determines the amount of time which the runoff generating system spends in stages 3 and 4 of the runoff generation phase space. Therefore, the temporal structure of the rainfall time series is a key control on the development of connectivity across a slope and hence the amount of runoff able to reach the slope outflow. This supports the field results report by Van de Giesen et al. (2000) who found that the runoff coefficient varied between storms with different temporal dynamics.

This importance of the timing of a high intensity pulse is clearly shown in the investigations of the effect of the storm hydrograph form (section 7.3). The highest runoff coefficient was obtained by a high intensity pulse followed by a long period of low intensity rainfall. The low intensity rainfall helps to keep the system in stage 4, hence allowing greater flow. For the experiments utilising a series of rainfall pulses, the length of the gap between pulses determines how much the system can dry out or how many stages back the system is able to move. For the series with a one minute gap, once the system has reached stage 3, it oscillates betweens stages 3 and 4 until the end of the rainfall. The gap is insufficient to allow the system to move back

into stage 2. The series with a five minute gap always returns to stage 2 before the next storm pulse. This is shown by the cessation of discharge during the gap. This clearly shows the importance of the antecedent conditions at the time of the main rainfall pulse within a storm. If the land surface is conditioned for runoff generation, the runoff generation system can rapidly move into stage 3 and hence a greater amount of runoff can be generated.

The importance of the temporal structure of the rainfall time series is clearly demonstrated by the Monte Carlo based simulation results. From the Monte Carlo generation of 200 storms with the same rainfall depth and duration, it was found that the amount of runoff leaving a slope with a length of 50 m was highly variable. The majority of the realisations gave a greater runoff coefficient than the constant rainfall intensity. However, 25.9 % of the realisations gave a lower total discharge and 51.2 % of the realisations gave a lower peak discharge. These results contrasts with the findings of Wainwright and Parsons (2002) who found that the use of variable intensity rainfall always resulted in an increase in the amount of runoff leaving a slope. The results presented here show that the temporal structure can both increase and decrease the amount of runoff leaving a slope during a storm event.

The investigations into which factors of the rainfall series have the greatest control on the runoff coefficient are presented in section 7.4. The modelling results showed that although many statistical properties of the time series are related to the runoff coefficient, no one statistical property was able to explain the variations in the runoff coefficients. The statistical properties do not directly consider the temporal structure of the rainfall time series. The variability of the per minute rainfall intensities, expressed by the standard deviation, is able to explain 33.6 % of the variability in the runoff coefficient. With more variable rainfall, the periods with runoff generating rainfall become more fragmented. This allows the system to move back into stage 2 or 1. This finding suggests that the temporal structure, as well as the variability, plays a significant role in the determination of the runoff coefficient.

The variability of the 1 – 5 minute rainfall intensities is important when considering the significance of convective driven rainfall events as opposed to frontal driven events. Convective events have short bursts of high intensity rainfall with little build up, whereas frontal storms have rainfall over many days which conditions the ground surface for runoff generation. The frontal storms, therefore, produce relatively more runoff and discharge at lower rainfall intensities.

As the slope gradient increases, the sensitivity to the fragmentation of high intensity rainfall decreases. This decrease in sensitivity can be seen from the reduction in the majority of the correlation coefficients in Table 7.2 comparing slope with uniform and variable gradients. This decrease in sensitivity is because runoff is able to travel further due to the greater flow velocities

so that a greater percentage of the generated runoff reaches an effective channel. Therefore, it is not the absolute time which is the key factor in determining the amount of runoff that leaves a slope but the potential flow distances. These distances are a function of both storm characteristics and the surface properties.

These findings regarding the temporal structure of the rainfall intensities within the storm event support the comments of Yair and Lavee (1985) who found that the properties of the rainfall time series were able to explain the observed discontinuities in the runoff from arid and semi-arid catchments in Israel. The importance of the variability in rainfall intensities was shown in the work by Wainwright and Parsons (2002). This work extends their findings through the Monte Carlo analysis of storm properties. This enables the investigation of a greater amount of the parameter phase space. The Monte Carlo analysis suggests that many simple statistical properties of the time series can be related to the amount of discharge. However, each of these relationships contains a large amount of scatter, thus indicating the complexities of the runoff – run on processes occurring across the hillslope. The work on the defined hydrograph forms extends the temporal scale of investigation from 0.5 – 1 hour to 2 hours, allowing the consideration of antecedent conditions for the main rainfall pulse.

7.6 Conclusions

The response of the hydrological system to changes in the rainfall characteristics can be explained using a four stage model of the runoff generation process. These stages are: 1, all water infiltrating, 2, the surface depression store filling or emptying without runoff occurring, 3, the generation and transmission of runoff and 4, the transmission of runoff without new runoff being generated. The storm event will move the system between the four stages and the nature of the rainfall required to move between the stages is determined by the surface characteristics.

The runoff coefficient is very sensitive to changes in the duration over the range 1 to 20 minutes. This sensitivity relates to the time required to move the system in to the runoff generating stage described above. It is most sensitive to changes in the rainfall intensity over of 10 % to 30 % runoff coefficient region of the parameter space and is less sensitive above this region. The change in sensitivity relates to the interaction between the infiltration rate and the rainfall intensity. In the 10 % to 30 % region, the infiltration rate and the rainfall intensity are similar thus a small change in the rainfall intensity results in a large change in discharge. Above this region, the rainfall intensity is much greater than the infiltration rate and hence a small change does not give such a large change in the discharge.

The storm form influences the runoff coefficient and the peak discharge. Over a range of slopes lengths, the storm form controls the magnitude of the discharge but does not influence the response to changes in the slope length. Different storm forms have different responses to

changes in the slope gradient. This may be linear or non-linear with greater sensitivities at different parts of the parameter space.

The storm characteristics have a greater influence on the amount of runoff generation than the surface characteristics. The slope length is able to explain only 1 % of the variability in the runoff coefficient over a range of storms. However, for a given storm event, the surface properties will determine the spatial response of the landscape to the rainfall.

The temporal fragmentation of high intensity rainfall is important for determining the flow distances and hence the amount of runoff which leaves the slope as discharge. If the high intensity rainfall is fragmented, the runoff will be infiltrated a short distance down slope. Longer periods of high intensity rainfall allows the runoff to travel further and hence become discharge. Therefore, storms may have the same amount of high intensity rainfall but produce vastly different amounts of discharge. This shows the importance of the variable intensity rainfall when modelling semi-arid runoff generation. The amount of discharge may be greater or less than the amount that would have been produced if constant rainfall intensity is used in the model.

8 Connectivity of Flow and the Origin of Discharge

8.1 Introduction

This chapter has two aims: firstly to apply the theoretical results presented in the previous chapters to the Rambla de Nogalte catchment. These results will be used to locate the areas of high runoff generation within the catchment. The second aim is to trace the origin of the water which reaches the channel and contributes to a flood during a storm event. This work will focus on the September 1997 storm for which some information on the spatial distribution of discharges is known.

8.2 Focus Sub-Catchments

The investigations require detailed spatial information on topography and land use. This is only available for two areas of the Rambla de Nogalte catchment, Sub 7 and the lower Cardena (Figure 3.1). For the Cardena, only the lower section is available. Due to a number of large check dams, the upper section is disconnected and hence the lower section can be considered in isolation. The details of the two Sub-catchments are given in Table 8.1. The topography and land use maps are shown in Figure 8.1 for Sub 7 and Figure 8.2 for the lower Cardena.

Characteristic	**Sub 7**	**Lower Cardena**
Area	1.92 km^2	0.66 km^2
Geology	Blue schist	Blue schist with high quartz content
Land use	Almonds with a few small sections of scrub	Mainly scrub with almonds on upper sections
Slopes	Mainly low gradients with a few steep slopes.	Main channel is deeply incised leading to steep slopes beside the channel. Upper sections have low gradients

Table 8.1 Characteristics of the focus Sub-catchments

The DEMs for the Sub-catchments were interpolated from 1:5000 contour data using *topogrid* in ArcGrid. The used of *topogrid* was selected over other interpolation methods since it has been shown to produce the most accurate representation of the actual surface (Wise 1998). The pits in the DEM were removed with a put fill algorithm to give a hydrologically continuous

surface. The land use data was derived from field mapping. The infiltration characteristics for the scrub and the agricultural areas were defined from the rainfall simulation values given in table 4.8. The agricultural areas used the parameters from the rainfall simulation experiment on the almond field at site 1 and the scrub areas used the results from the experiment on vegetated plot on site 2.

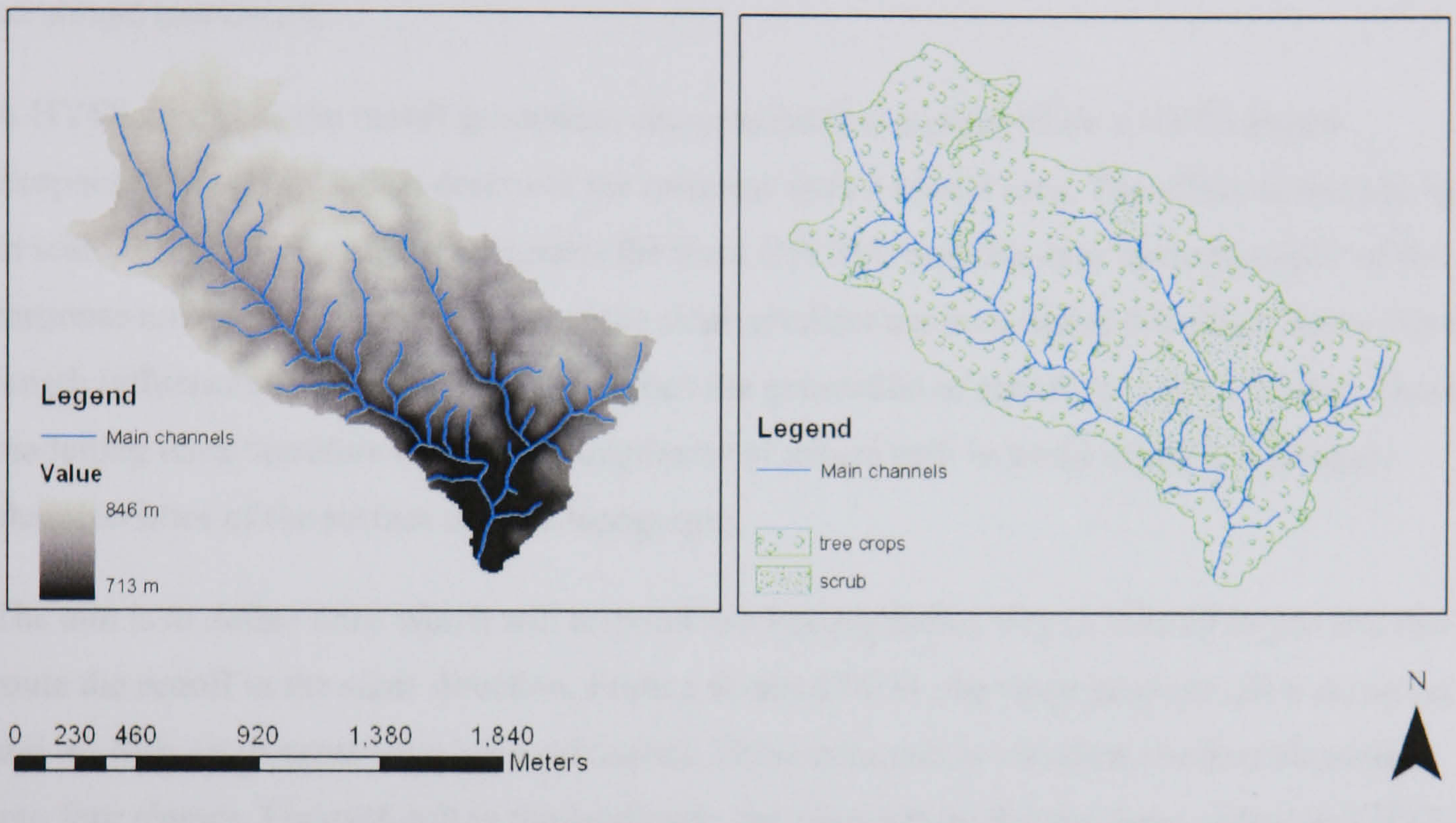

Figure 8.1 DEM and land use for the Sub 7 catchment

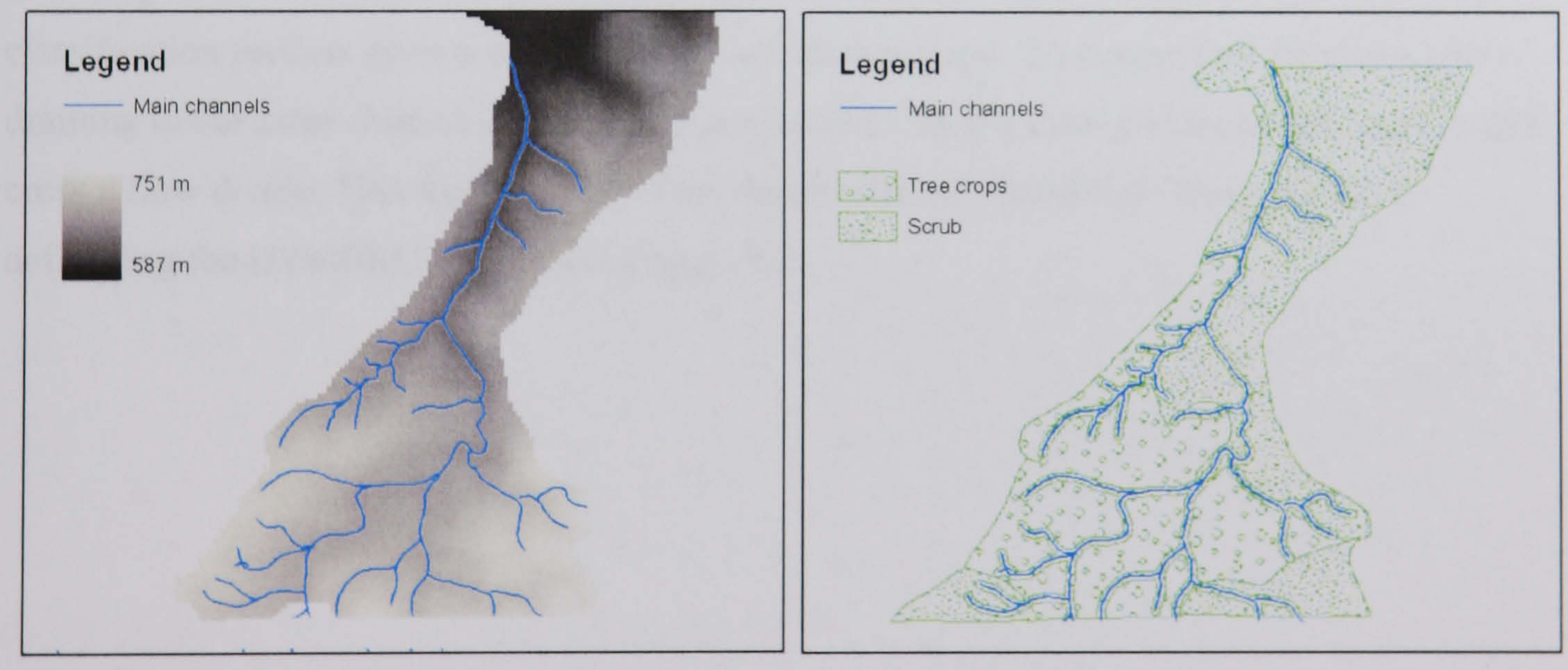

Figure 8.2 DEM and land use for the lower Cardena

8.3 Location of High Runoff Generating Areas

From the analysis of field experiments in chapter 4 and the simulation modelling in chapters 6 and 7, it has been shown that the at-a-point generation of runoff is strongly controlled by the

land use. This can be used to define Hydrologically Similar Surfaces (HYSS) (Bull et al. in press). HYSS are areas with a similar hydrological response defined by their distribution of storage and infiltration values. These are associated with land use, surface characteristics, lithology and soil properties. HYSS are defined by vertical exchanges and are independent of topography (Bull et al. in press). For Sub 7 and the Cardena catchments two predominant HYSS were identified: tree crops (almond and olive) with frequently ploughed soils and semi-natural scrubland (*matorral*).

A HYSS describes the runoff generation characteristics at a point while a HYSS Based Response Unit (HYSSBRU) describes the response over a spatial area. The effect of this change in scale is that the HYSSBRU integrates the local (HYSS) response over the topography of the response unit. Therefore, the effects of the slope gradient are included at this stage. Since slope length influences the transmission rather then the generation of runoff, it is not included. These modelling units therefore reflect the complexity of nature both in terms of the hydrological characteristics of the surface and the topography.

The aim is to define units which will respond in a homogeneous way to rainfall inputs and that route the runoff in the same direction. From a detailed DEM, the slope gradient, flow direction and the Sub-catchments have been calculated. These continuous variables are then classified into four classes. For each cell in the landscape, the class values for the slope, aspect and HYSS are combined to give a code representing the cell's hydrological response. The first digit relates to the aspect class, the second to the slope class and the final digit relates to the HYSS. This classification process gives a set of units across the landscape. To ensure that the entire unit is draining to the same channel, the units are intersected with the flow divides to split units which cross a flow divide. This then gives the final distribution of HYSSBRU. The process of defineding the HYSSBRU is shown in Figure 8.3.

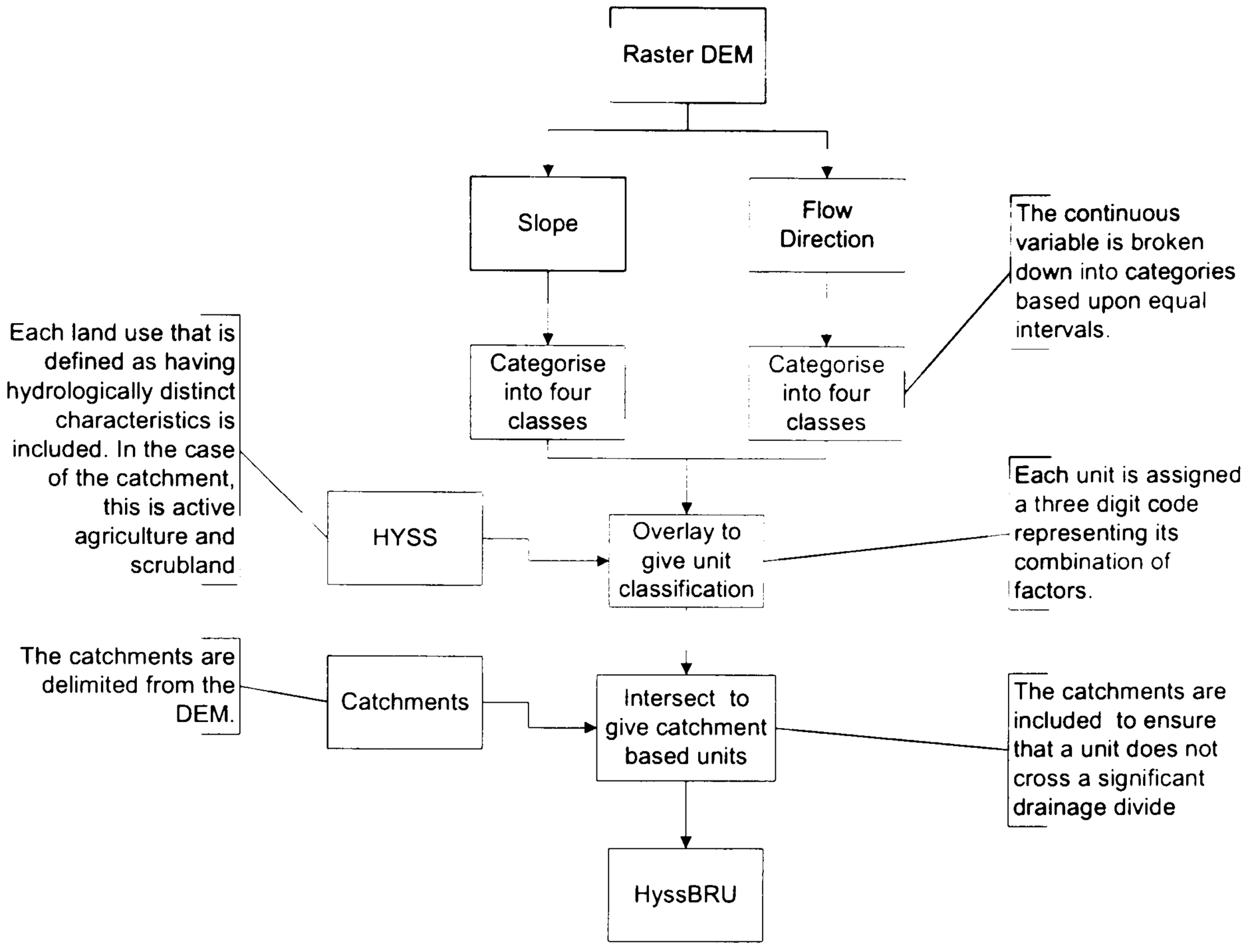

Figure 8.3 Process for defining HYSSBRU

The definition of the HYSSBRU is sensitive to the classification of the continuous variables for flow direction and slope gradient. The sensitivity to slope gradient changes dynamically with storm characteristics and hence the optimal classification also changes. An equal interval approach has been used since it is not biased towards a certain storm and hence will give a more accurate representation over the whole range of storm characteristics.

The different combinations of factors that make up the individual units have been classified in order according to the amount of runoff generation. From the field results presented in chapter 4, two key relationships were shown that are relevant to the classification of the HYSSBRU. Firstly, it was shown that scrub slopes produce more runoff than agricultural slopes and secondly it was shown that steep slopes produce more runoff than low slopes. Therefore, it can be assumed that steep scrub units will produce the most amount of runoff, that flat ploughed fields will produce the least, and that a low slope scrub unit will produce more runoff than a steep ploughed field. The classified HYSSBRU for Sub 7 is shown in Figure 8.4 and the lower Cardena are shown in Figure 8.5.

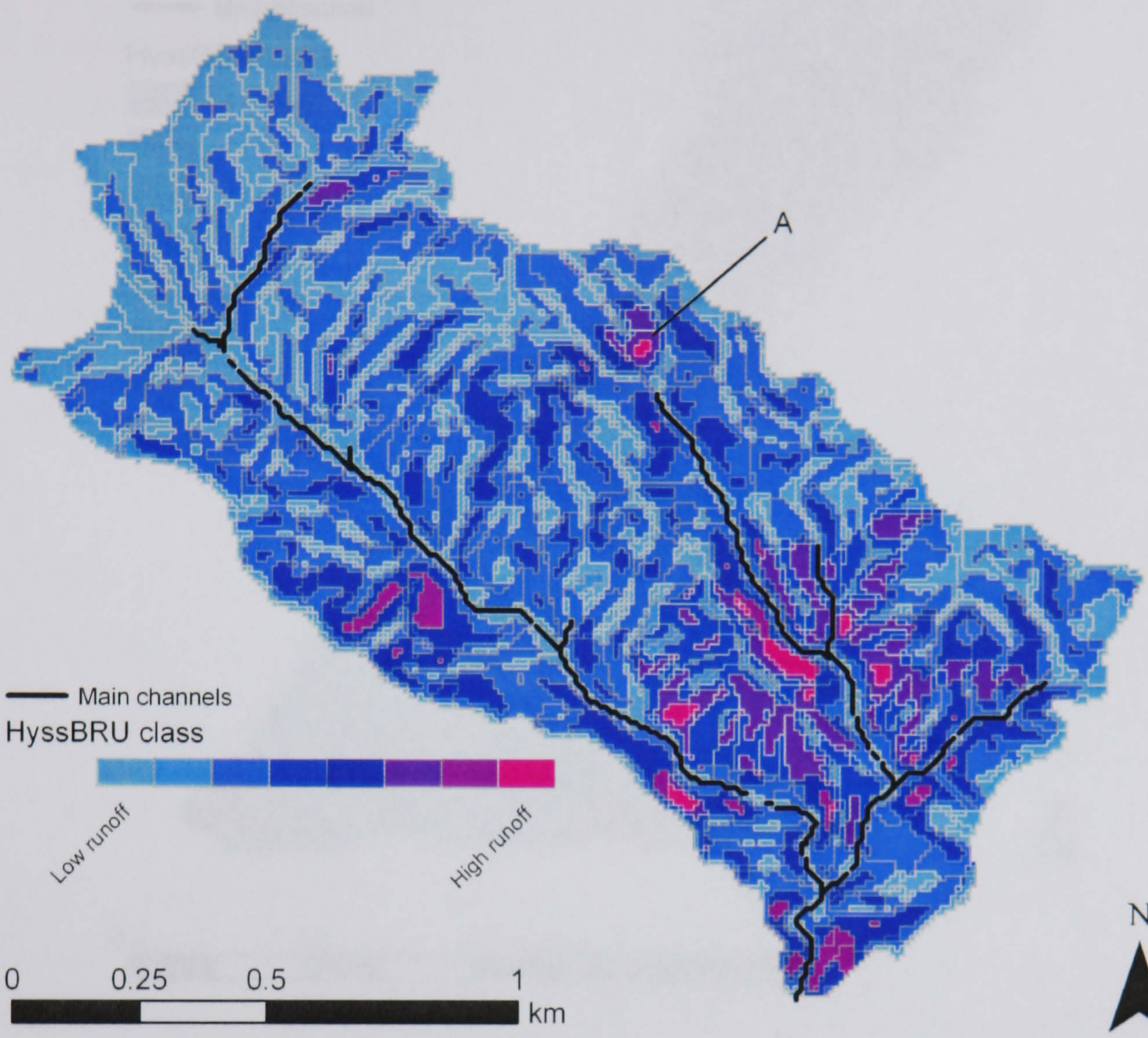

Figure 8.4 Classified HYSSBRU for Sub 7

From the application of the method to the Sub 7 catchment it can be seen that only a small fraction of the catchment is likely to produce significant amounts of runoff. Many of these areas are located away from the main channels. Since runoff producing storm events have short duration, the travel distance of overland flow is also short. Therefore, much of the generated runoff may not reach the main channel network. The mosaic pattern of units is important since if a high runoff generating unit is located above a low runoff generating unit, the lower unit may act as a runoff sink, thus removing the connection to the channel. This can be seen at point A where a potentially high runoff generating area is surrounded by potentially low runoff generating areas.

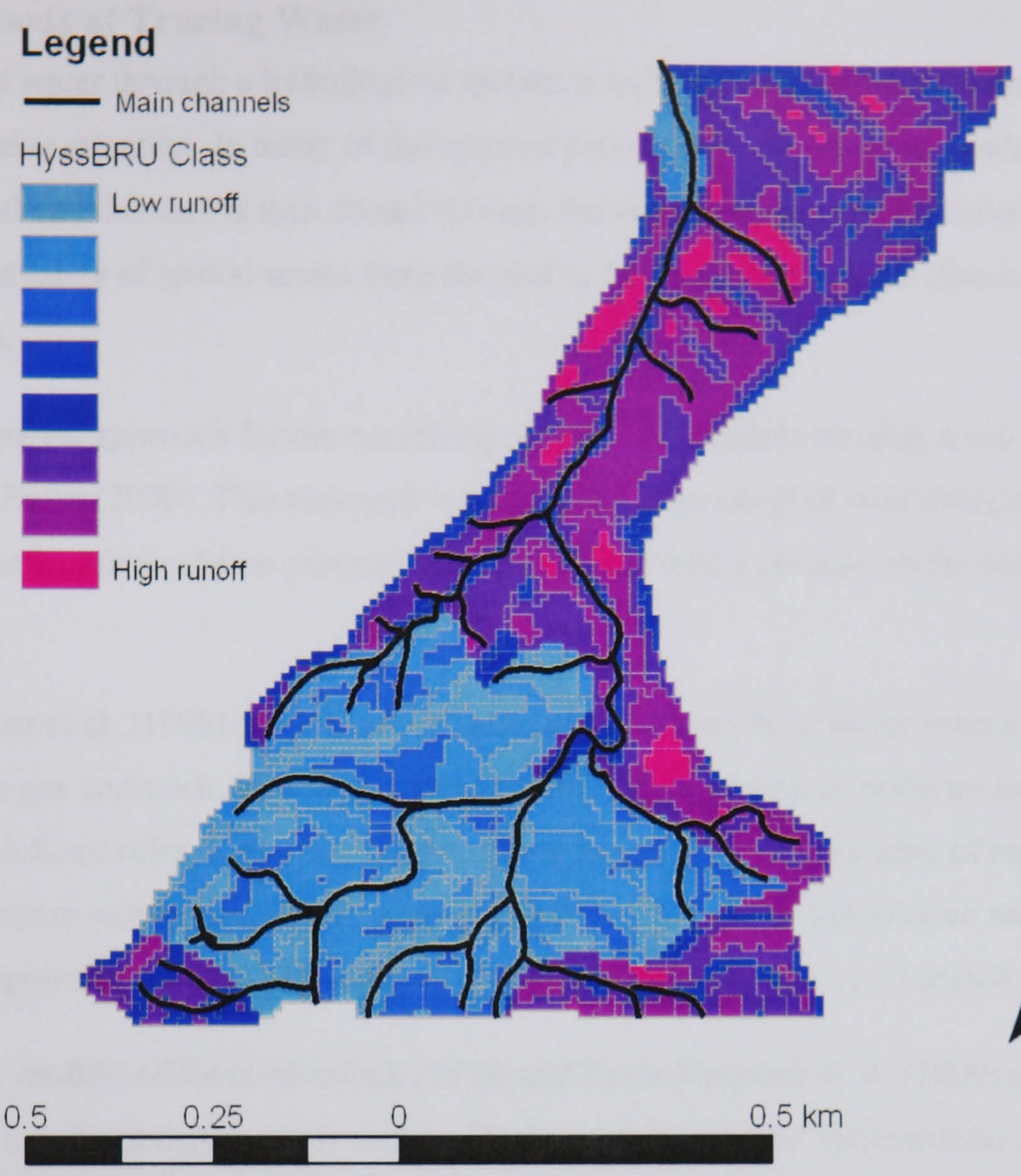

Figure 8.5 Classified HYSSBRU for the lower Cardena

The pattern of high runoff producing areas in the lower Cardena is very different to Sub 7. There is a contrast between the flat agricultural areas and the steep scrub slopes. Much of the area is likely to produce high runoff volumes and these areas have channel systems running though them. This results in the slopes being well connected to the channels and hence the runoff can be transmitted across the surface with minimal transmission losses.

8.4 Modelling Techniques for Tracing Flow

The aim of this work is to investigate the amount and *origin* of runoff reaching the channel. Many models consider the amount of water reaching the channel but do not explicitly consider where in the catchment the runoff originated. Many different spatial patterns of infiltration characteristics and topography can give the same discharge hydrograph. This is related to the problems of equifinality (Beven 1996). The use of the HYSSBRU approach enables the potential location and the potential spatial pattern of high runoff generating areas to be mapped. It does not provide information on the fate of the generated runoff or the origin of the water in the channel.

8.4.1 Methods of Tracing Water

The tracing of water through a hydrological system is an area of hydrology that has recently started to receive attention. In many of the systems presented in the literature, water is contained within a parcel and this unit is then routed through the system. These models have been developed at a range of spatial scales from the plot to the landscape and are discussed here in order of scale.

The use of a parcel approach for the modelling of water movements through a soil was presented by Ewen (2000). This approach was designed to be coupled with transport and mixing models. The infiltration scheme presented compared well with a solution to the Richard's equation.

Garcia-Sanchez et al. (1996) considered the infiltration and runoff of water from a rough surface using a lattice-gas approach. This approach considers a fluid as a set of particles that move according to defined rules. Using this model, it was found that it was capable of reproducing surface depression storage and runoff as an intrinsic result of the hydrodynamic nature of the model. This application of the lattice-gas approach is focused upon a small spatial area.

The RillGrow models of Favis-Mortlock (1998) and Favis-Mortlock et al. (2000) simulates the flow paths of raindrops across a soil surface. These models consider the generation of rills at the spatial scale of a plot of up to 2.2 m by 2.2 m. Raindrops are inserted into the model and their flow path is determined by the surface energy gradient and the location of surface depressions. The RillGrow 2 version of the model operates on true spatial and temporal scales. Infiltration and splash erosion are not implemented in the year 2000 version. The lack of an infiltrating surface makes it impossible to consider the effects of rainfall intensity on flow routing.

The model of Darboux et al. (2002) considers the connectivity of ponding on a rough soil surface. The hydrology was modelled using the conditioned walker approach. Each 'walker' carries with it a set volume of water and moves across the surface according to a steepest path algorithm. When the walker encounters a depression, it deposits part or all of its water to enable it to fill the depression and hence create an outflow path. The model was applied over varying sized grid which represented rough soil surfaces.

Shannon et al. (2002) have developed a model of ephemeral channel flow based on parcels of water. The routing of the water is determined either by the channel bed topography or by a stochastic routing algorithm. This model is able to simulate the flow within a channel reach. This sets it apart from the approaches above due to the far greater spatial scale.

Chase (1992) developed a model of fluvial erosion, transportation and deposition that operated at the spatial scale of hillslopes to mountain ranges. The surface is subjected to a number of

localised storms, termed 'precipitons', which are routed across the surface. As the precipitons move across the surface, they erode the surface and transport a slope limited amount of material. It was found that this approach could simulate complex landscapes. This approach has been extended by Haff (2001) and has been applied to a number of terrains. It was found that the model predictions for terrain change altered with different sets of model assumptions. These models treat a storm event as a single parcel which enables them to work at the landscape scale. Their most important aspect is the rule based approach to the movement of water through an environment.

The models of Chase (1992) and Haff (2001) treat a storm as one parcel whereas in the other approaches to parcel based modelling outlined above, it is the ensemble behaviour of the individual partials or parcels that gives the higher level hydrological behaviour. Although the individual paths of the particle are not recorded, it would be possible to record the paths within these frameworks. This would, however, generate a huge amount of data with high levels of redundancy. With the exception of Shannon et al. (2002), all of the models have been applied at the scale of a small soil surface plot. This restricted size is due to the huge memory requirements of representing all of the hydrology as parcels. This would be a major problem if these techniques were applied at the scale of a small catchment.

8.4.2 Tracing System Development

To overcome the problems associated with parcel based hydrological modelling and obtain information on paths of flow, a two part system has been developed. This system uses a traditional hydrological model coupled with autonomous software agents which trace the flow. Autonomous agents are units which interact with their environment and act independently of other agents (Flake 1998). These can be seen as analogous to the 'precipitons' of Chase (1992) in that they follow a simple rule set. These software agents have been termed 'hydroAgents'. The environment through which they move is generated by a hydrological model, in this case, CRUM-2D, although other models could be used.

The main difference of this approach is that the hydroAgents do not have mass like the parcel based systems. This means that there is only a one way interaction between the environment generator and the agent population. This greatly reduces the memory requirements of the system and hence enables the application of hydroAgents to large spatial scales.

As the agent moves through the environment, it records its path and the time spent in each cell. The collection of this information enables the life histories of the agents to be visualised. By investigating the paths taken by the agents which reach the channel, it is therefore possible to determine the origin of the channel runoff.

8.4.3 hydroAgent Rule Set

An agent interacts with its environment according to a rule set. In this implementation, the movements of the agents are determined using probability theory. This is defined by the follow set of equations:

$$P_i = \frac{i_v}{W_t}$$

Equation 8.1

$$P_r = \frac{r_v}{W_t}$$

Equation 8.2

$$P_n = \frac{-1\beta_n}{\sum_{n=1}^{8} -1\beta_n} \qquad \beta_n <= 0$$

Equation 8.3

P_i is the probability of the agent infiltrating; P_r is the probability of the agent leaving the cell; i_v is the volume of water infiltrating in the current time step; r_v is the volume of water leaving the cell in the current time step; W_t is the total volume of water in the surface water of the cell; P_n is the probability of the flow going in direction n and β_n is the slope in direction n.

Each of these probabilities is examined in turn. Only if the agent does not infiltrate, is the runoff probability assessed and only if the agent is leaving the cell is the flow direction algorithm used. The flow routing is based on the Rho8 algorithm.

This rule set has a one key assumption. It assumes that there is total hydrological mixing within each model cell such that an agent that has just moved into the cell has an equally probability of leaving as an agent that has been there for a number of model iterations. Due to the large number of agents, the collective response of the population will give a realistic distribution of flow paths.

The rule set used here is for the movement of water within a hydrological environment. It would be simple to write a set of rules to model the movement of sediments or pollutants. This is an area for future research.

8.5 Tracing the Origin of Channel Flow

To determine the origin of the water in the channel, software agents called hydroAgents have been developed and were described in sections 8.4.2 and 8.4.3. This approach will be used to monitor the movement of water across the landscape for three different storm events. Two

constant rainfall events have been used, the five minute storm at 75 mm hr^{-1} from chapter 6 and a storm of 60 minutes at 75 mm hr^{-1}. The third storm is the main rainfall pulse from the 29 September 1997 storm event. Three landscapes will be used, the base 50 m slope from chapter 6 and the two focus-catchments.

8.5.1 Constant Rainfall and Base Slope

The base slope and storm from chapter 6 have been used for the initial hydroAgent investigations. In this simulation, a time step of 1 second has been used and 85 hydroAgents were introduced into the model per second. The number of agents was selected since this was the maximum number that the desktop computer used for the initial experiments could handle. The distribution of flow paths lengths is shown in Figure 8.6 and the flow paths across the surface and the area contributing to discharge are shown in Figure 8.7.

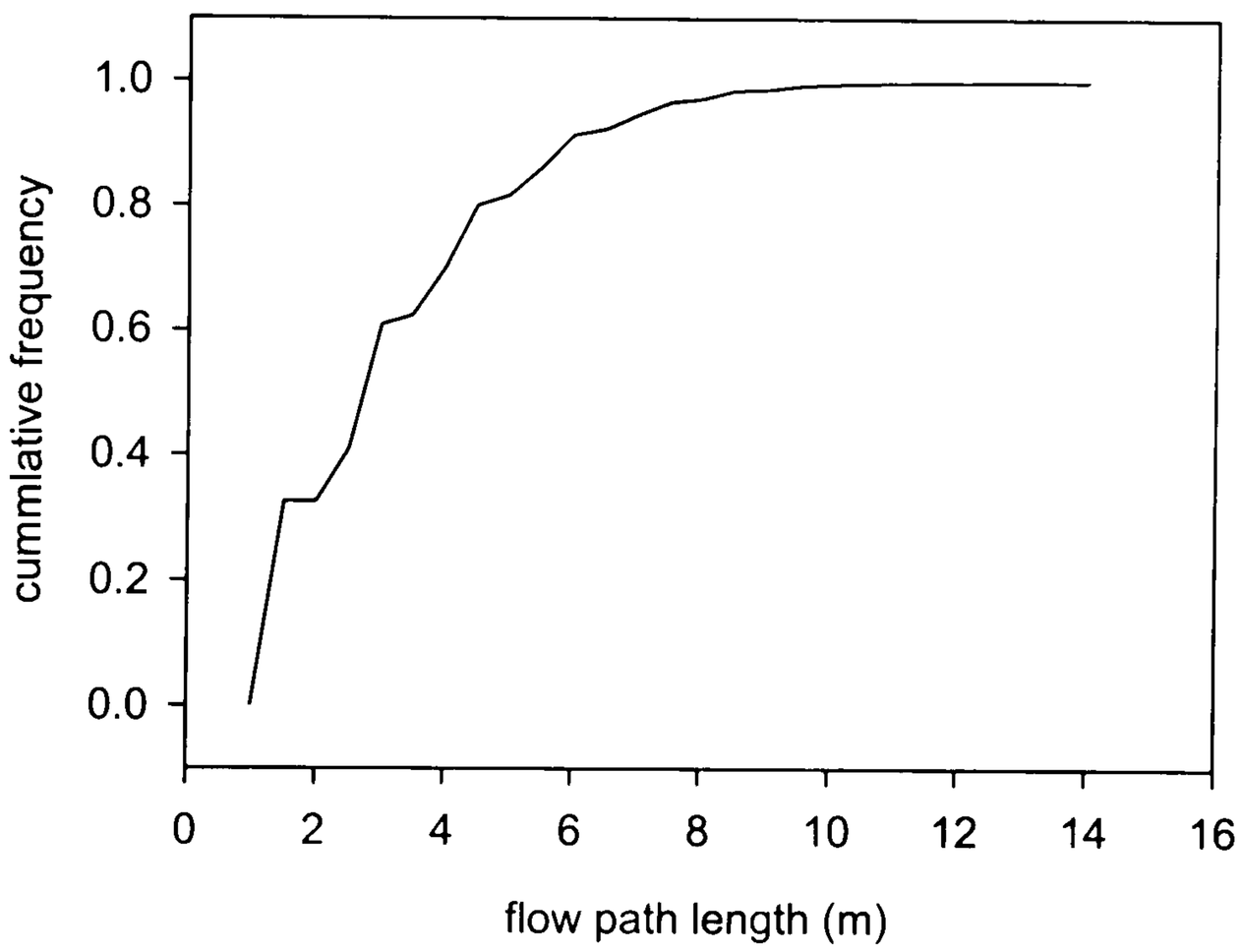

Figure 8.6 Cumulative flow path length distribution for the base slope and storm

During the five minute rainfall pulse, the average flow path length is short at 3.5 m with a maximum length of 14 m. However, 99 % of all path lengths are less than 8 m. The interaction between this distribution of flow path lengths and the distribution of distances to channels across a surface will strongly influence the strength of the connectivity and hence the amount of discharge from the surface. As shown in Figure 8.6, the maximum distance to the channel is 50 m and the mean flow path length is 3.5 m, the model therefore predicts that only a small percentage of the total surface area contributes to the discharge. If there were a number of channels within the surface, the maximum and mean distances to the channel would decrease and hence the connectivity would increase along with the discharge.

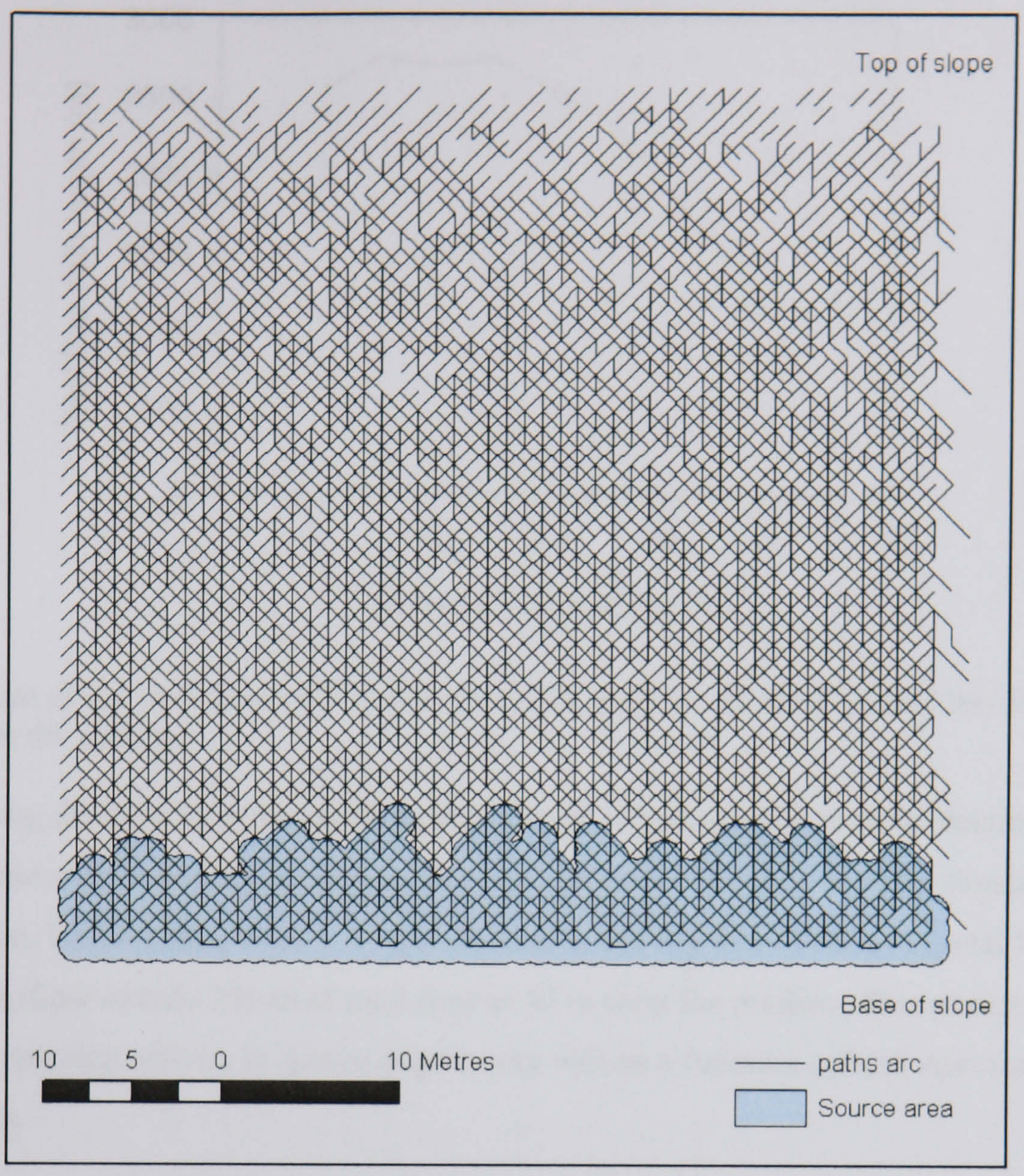

Figure 8.7 Flow paths and contributing area for the base slope and storm

The black lines show the movement of hydroAgents across the surface and the area shaded in blue shows the source of runoff that reached the main channel. Although the slope is linear, the distance from the point of runoff generation to the outflow varies across the width of the slope. The surface has a small amount of random roughness imposed upon it. This leads to the routing of flow and the creation of local flow concentrations. These flow concentrations result in more efficient flow and hence the increase in travel distance.

The contributing area width relates well with the overall distribution of flow path lengths. The maximum distance from the point of runoff generation to the outflow was 7 m. Runoff generated upslope of the contributing area is involved in the runoff generation dynamics within the contributing area. The runoff generated upslope may infiltrate within the contributing area thus increasing the soil moisture, decreasing the infiltration rate and hence increasing the probability of flow transmission within the contributing area. It is therefore useful to consider the hydrological activity in relation to distance from the outflow. This has been characterised by the sum of all flow path distances within 5 m wide polygons across the width of the surface (Figure 8.8).

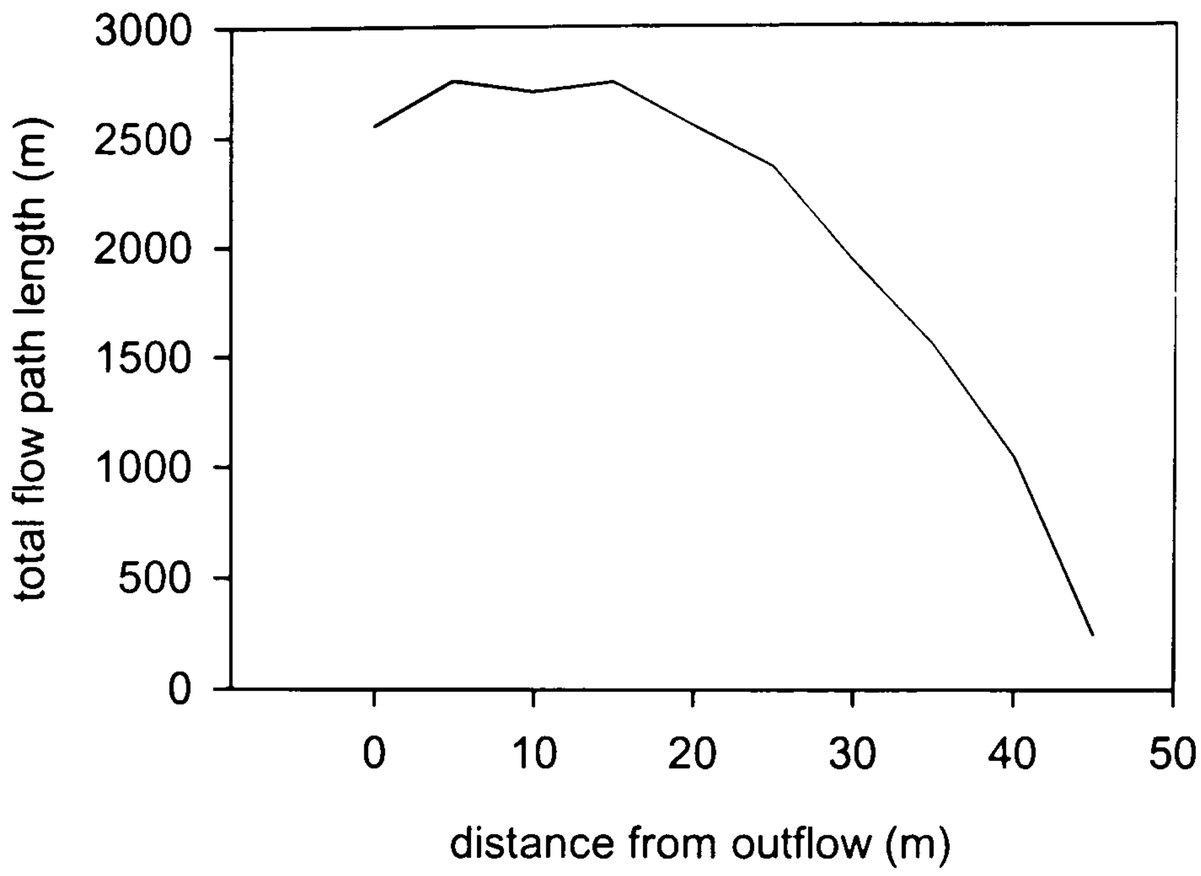

Figure 8.8 Sum of the total flow path distances within each five m band against the distance of the band from the outflow

With increasing distance from the outflow, the amount of hydrological activity decreases. For the lower section of the surface, from 0 to 20 m, the amount of activity is fairly constant with a slight variation. Beyond this, there is a rapid decline in activity from 2400 m of total flow at 15 m from the outflow to only 250 m of total flow at 45 m from the outflow. This position of this change from constant activity to decreasing activity will be a function of both storm and surface characteristics.

This shows that it is not only the area that directly contributes runoff that is important for determining the discharge but also the upslope area which helps to condition the contributing area for runoff generation and flow transmission. For the base slope and storm, an area with a width of 7 m contributed runoff. If the slope was reduced in length to 7 m, the amount of runoff would decrease since there would be no upslope area to help condition the contributing area.

It was shown in chapter 6 that the amount of discharge from the base 50 m slope was increased by the introduction of flow convergence from 4.7 % to 29.5 %. The flow patterns from a slope with one flow convergence have been investigated (Figure 8.9). It can be seen that the area contributing to flow is greatly increased. This increase is associated with the position of the efficient flow within the flow convergence. This supports the conclusion from chapter 6 that it is the distance to the nearest efficient flow that is important in determining the discharge from the slope.

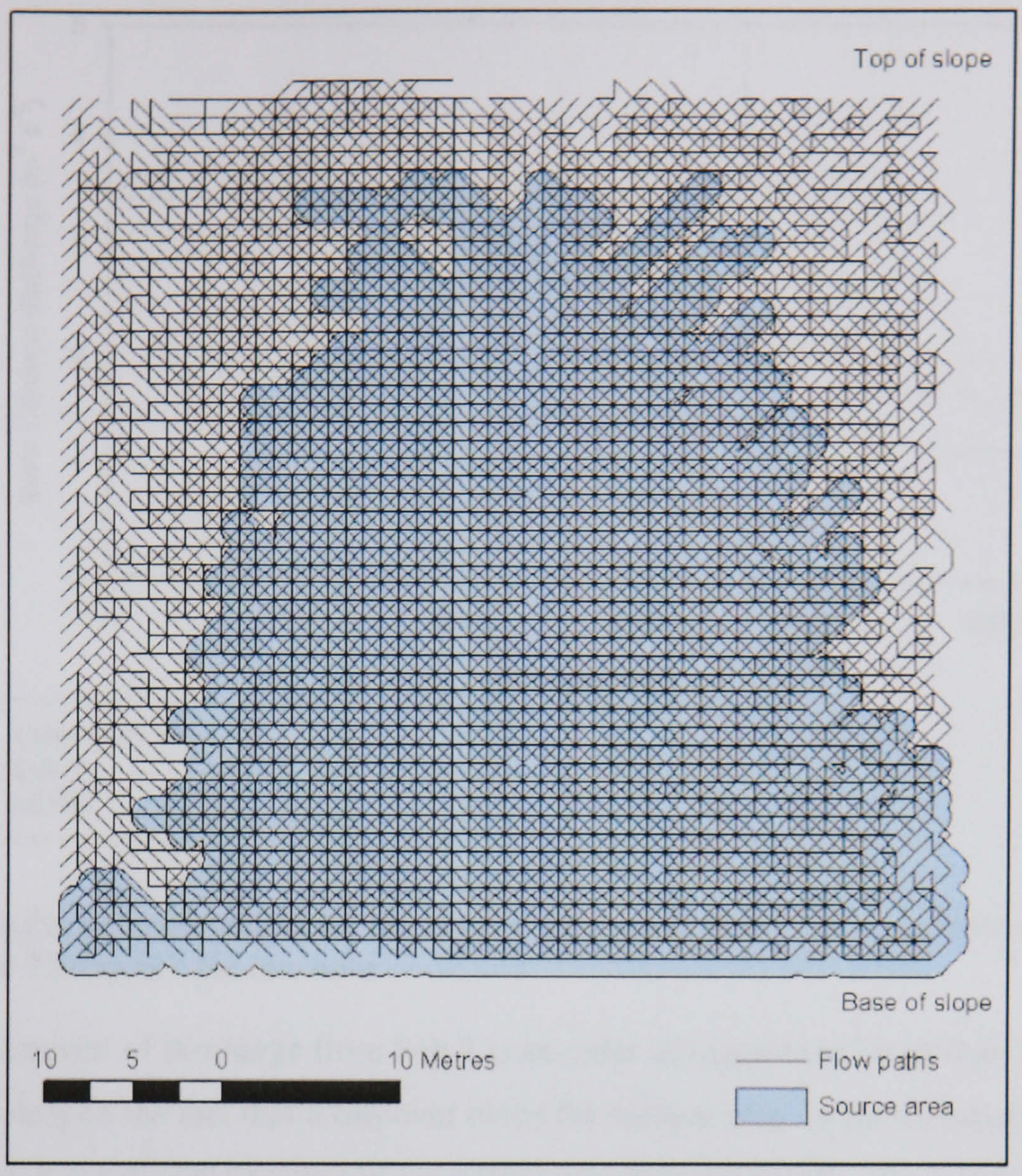

Figure 8.9 Area contributing to runoff on a slope with a convergent flow pattern

8.5.2 Constant Rainfall and Focus Catchments

To investigate the order in which different sections of the Sub catchments contribute runoff, a high magnitude storm event with constant rainfall intensity has been used. This storm event has an intensity of 75 mm hr^{-1} for 1 hour. The discharge hydrographs are shown in Figure 8.10 and the area contributing to channel flow during different time slices is shown in Figure 8.11 for the lower Cardena and in Figure 8.12 for Sub 7.

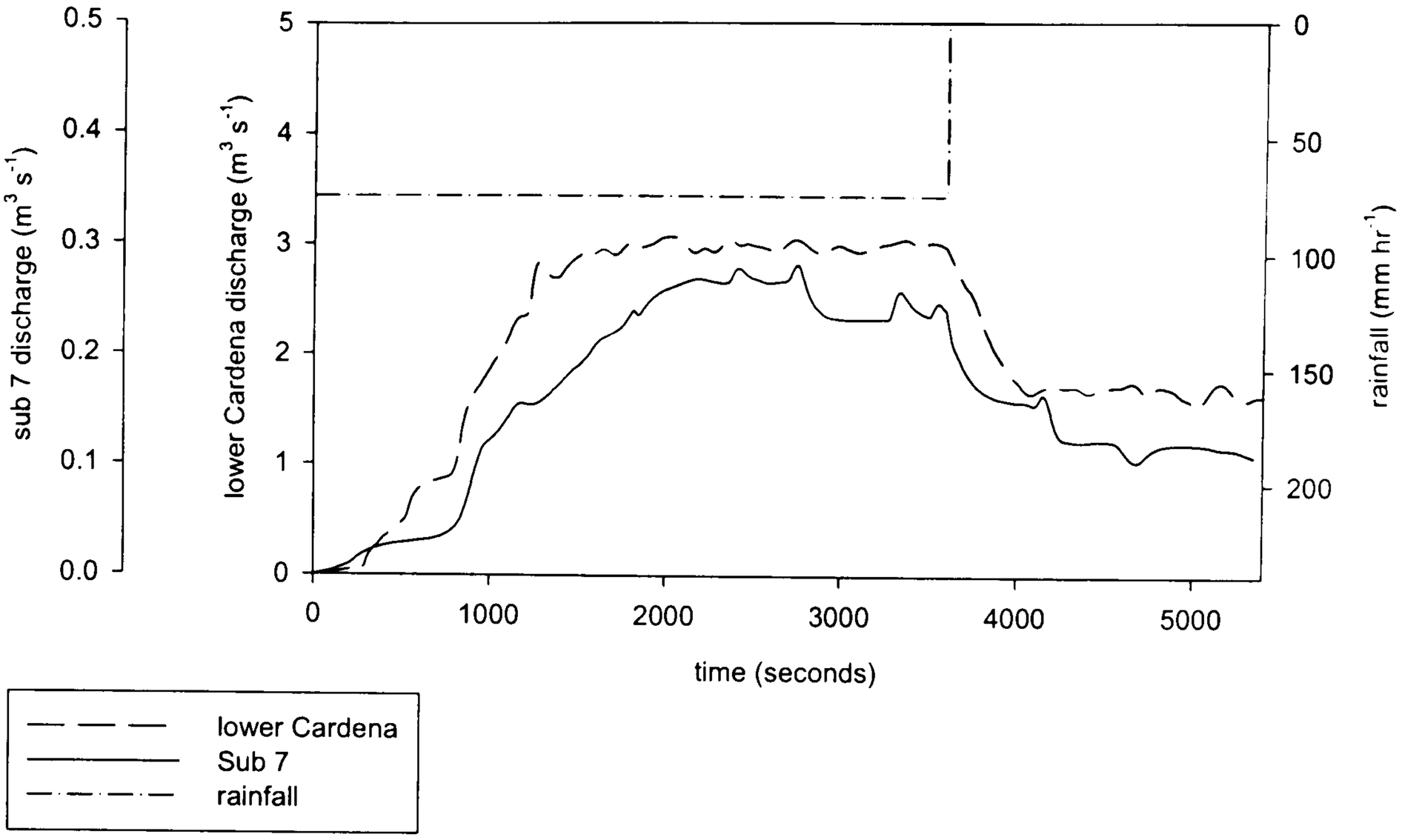

Figure 8.10 Discharge hydrographs for the lower Cardena and Sub 7 for a constant intensity rainfall event at 75 mm hr^{-1} for one hour

The simulated amount of discharge from Sub 7 is an order of magnitude lower than from the lower Cardena despite the fact that it has over twice the surface area. In the simulations, both catchments have a non-linear response to increasing cumulative rainfall. The lower Cardena has four changes in behaviour in the early stages of the storm. After 296 seconds, there is a sharp increase in the discharge. At 600 seconds, the rate of increase significantly decreases and at 800 seconds, the rate of increase in discharge increases again. After 1800 seconds the discharge stops increasing and there is little variation in the discharge rate. A similar pattern can be seen for Sub 7. Over the first 270 seconds, there is a curvilinear increase in discharge and between 270 seconds and 749 seconds; the rate of increase is low. At 750 seconds there is a large change in the rate of discharge with a step at 1200 seconds, it then remains constant up 2060 seconds

The form of the discharge hydrograph is related to the area contributing runoff and the travel times from the point of generation to the outflow. If all of the surface area starts producing runoff at the same time and there is a simple distribution of flow path lengths, then there is a smooth increase in the discharge hydrographs, as was shown in section 6.4. As the distribution of flow path lengths becomes more complex the form of the discharge hydrograph changes. If there are areas with similar distances to the outflow, then water from all these areas will arrive at once at the outflow. This will result in the step changes in discharge as shown in Figure 8.10.

Due to the spatially variable distribution of runoff generating factors, different sections of the catchment will generate runoff at different times. This then interacts with the travel time effects to give an intricate discharge hydrograph. The modelled spatial distribution of the areas

contributing to channel flow can be seen in Figure 8.11 for the lower Cardena and in Figure 8.12 for Sub 7.

The simulations suggest that the changes in the pattern of contributing areas are very different between the two focus catchments. The lower Cardena responds rapidly within the first 100 seconds of the storm and after that, there is a gradual increase in contributing area until 1000 seconds (Figure 8.13). The percentage area contributing runoff in Sub 7 has a more gradual increase. During the first 100 seconds there are very few areas contributing runoff. At the peak of discharge, the percentage of the catchment contributing is still low at 10 %. In both catchments, there is a rapid decline in the contributing area following the cessation of rainfall. This shows the importance of continued rainfall on the transmission of runoff across the surface.

In the lower Cardena, the model predicts that the main areas that contribute to runoff are the steep slopes covered with scrub. There are a number of gullies in the lower section of the catchment; much runoff is transmitted from the heads of these gullies to the channel. This shows the importance of efficient flow channels on the connections between the point of generation and the outflow. In the upper part of the catchment, the land use is dominated by agriculture and the main slopes are gentle. In this section of the catchment, the only areas contributing to channel flow are the steep scrub slopes adjacent to the channels.

The model predicts that the contributing area in Sub 7 is strongly focused on the channel network and the immediately adjacent slopes. There is a gradual increase in contributing area throughout the storm. There is a greater percentage of the channel area contributing to channel flow in the lower section of the catchment than in the upper section. This is related to the steeper slopes and the greater cover of scrub.

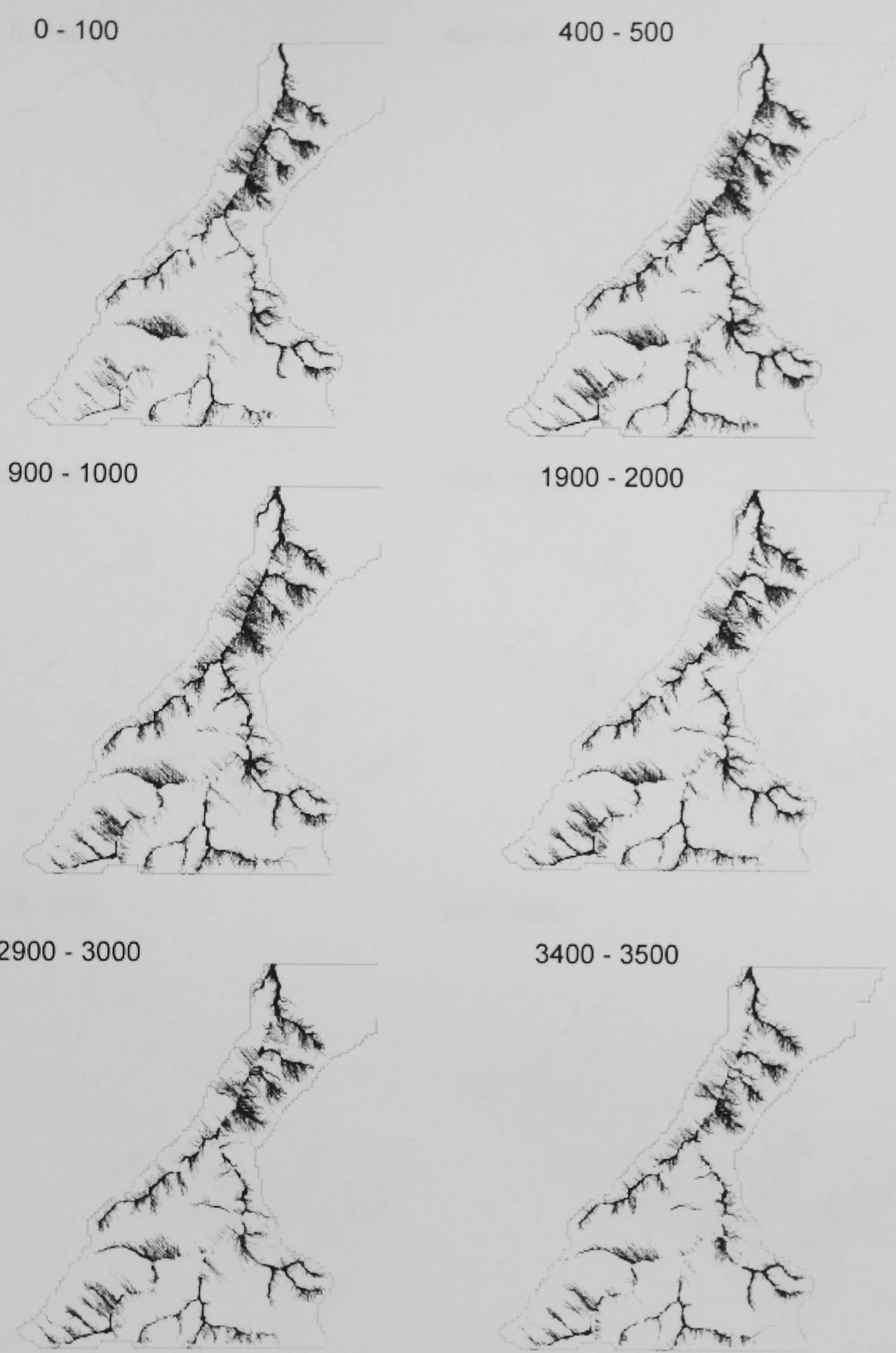

Figure 8.11 Area contributing to channel flow in the lower Cardena during a constant rainfall event at 75 mm hr^{-1} for one hour

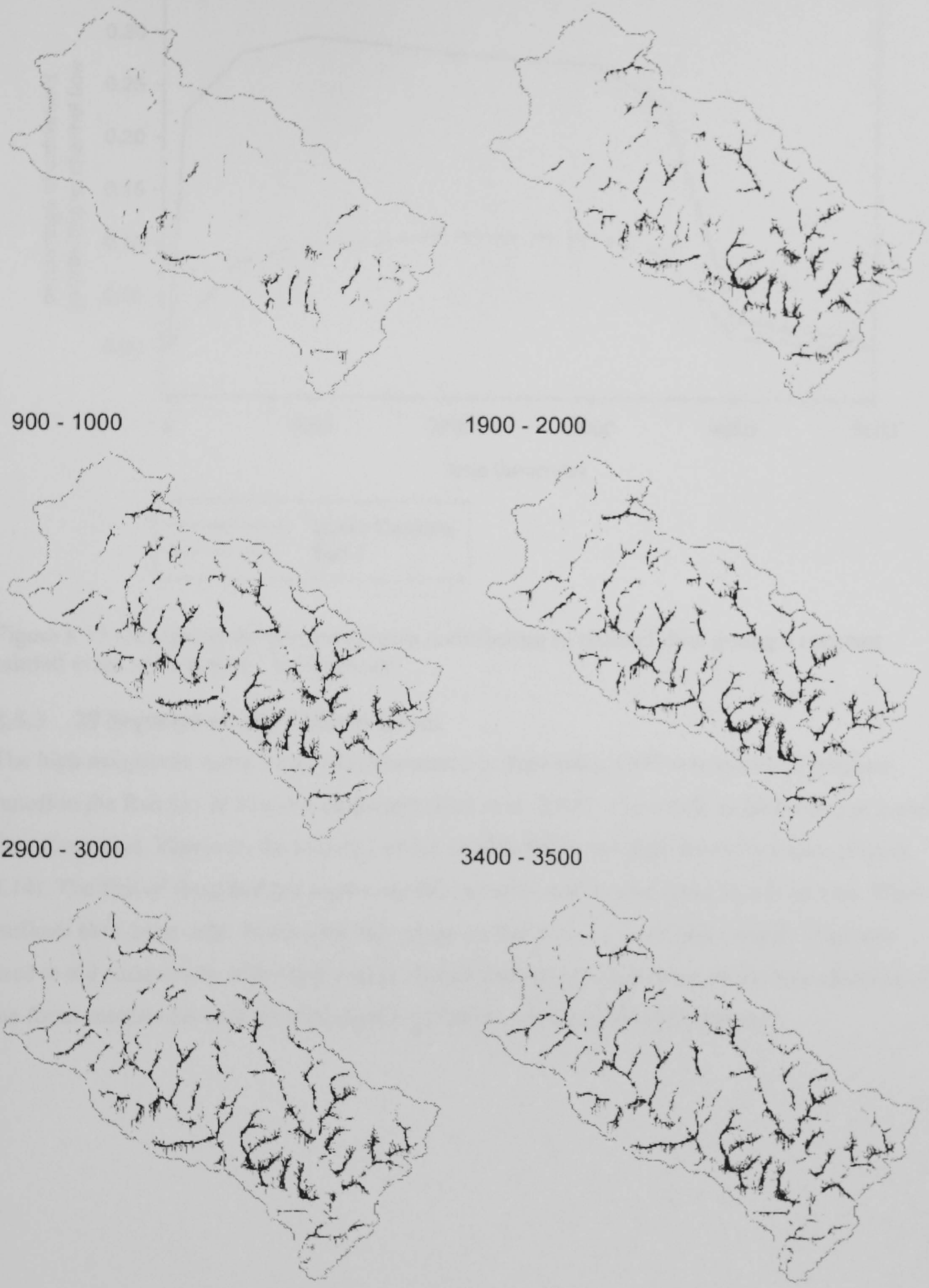

Figure 8.12 Area contributing to channel flow in the Sub 7 during a constant rainfall event at 75 mm hr^{-1} for one hour

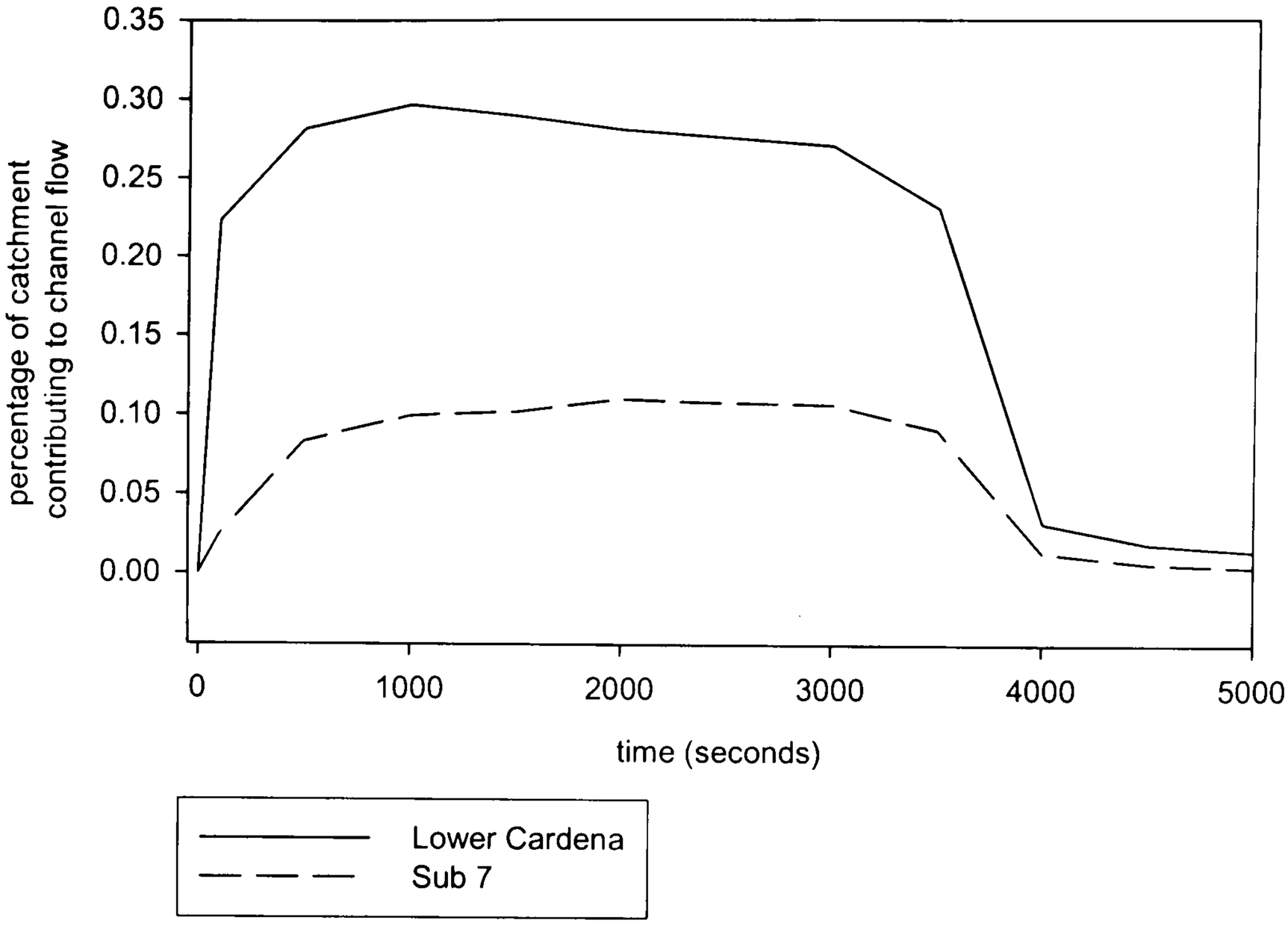

Figure 8.13 Changes in the percentage area contributing to channel flow during a constant rainfall event at 75 mm hr^{-1} for one hour

8.5.3 29 September 1997 Storm Event

The high magnitude storm event which occurred in September 1997 was shown to produce runoff in the Rambla de Nogalte catchment (Bull et al. 2000). The whole rainfall event occurred over three days. However, the majority of the rainfall fell in two high intensity pulses (Figure 8.14). The first of these had the higher rainfall intensity and is considered in this section. Three surfaces have been used. Firstly, the base slope used above and in chapters 6 and 7 has been used to aid comparison with other results. The second and third surfaces are Sub-catchments of the focus catchments with field measured infiltration rates and land use patterns.

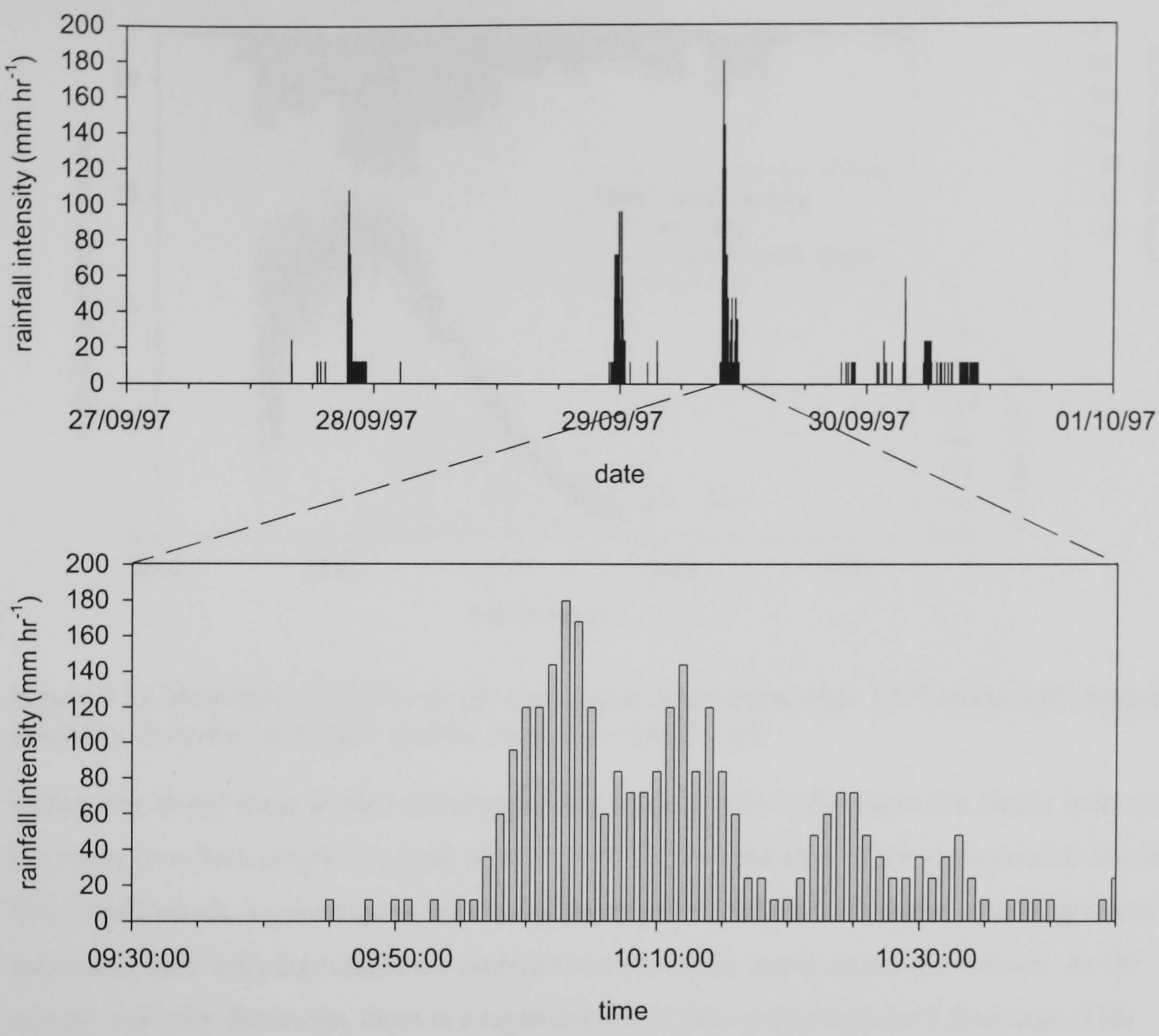

Figure 8.14 The September 1997 storm event as recorded at the Sub 12 rain gauge with detail of the main rainfall pulse.

Base Slope

The modelled discharge hydrograph and the mean flow path length for the base slope for the main section of the pulse is shown in Figure 8.15. The mean flow path lengths are plotted against the time of introduction into the system and hence relate more strongly to the rainfall intensity and are slightly offset from the discharge.

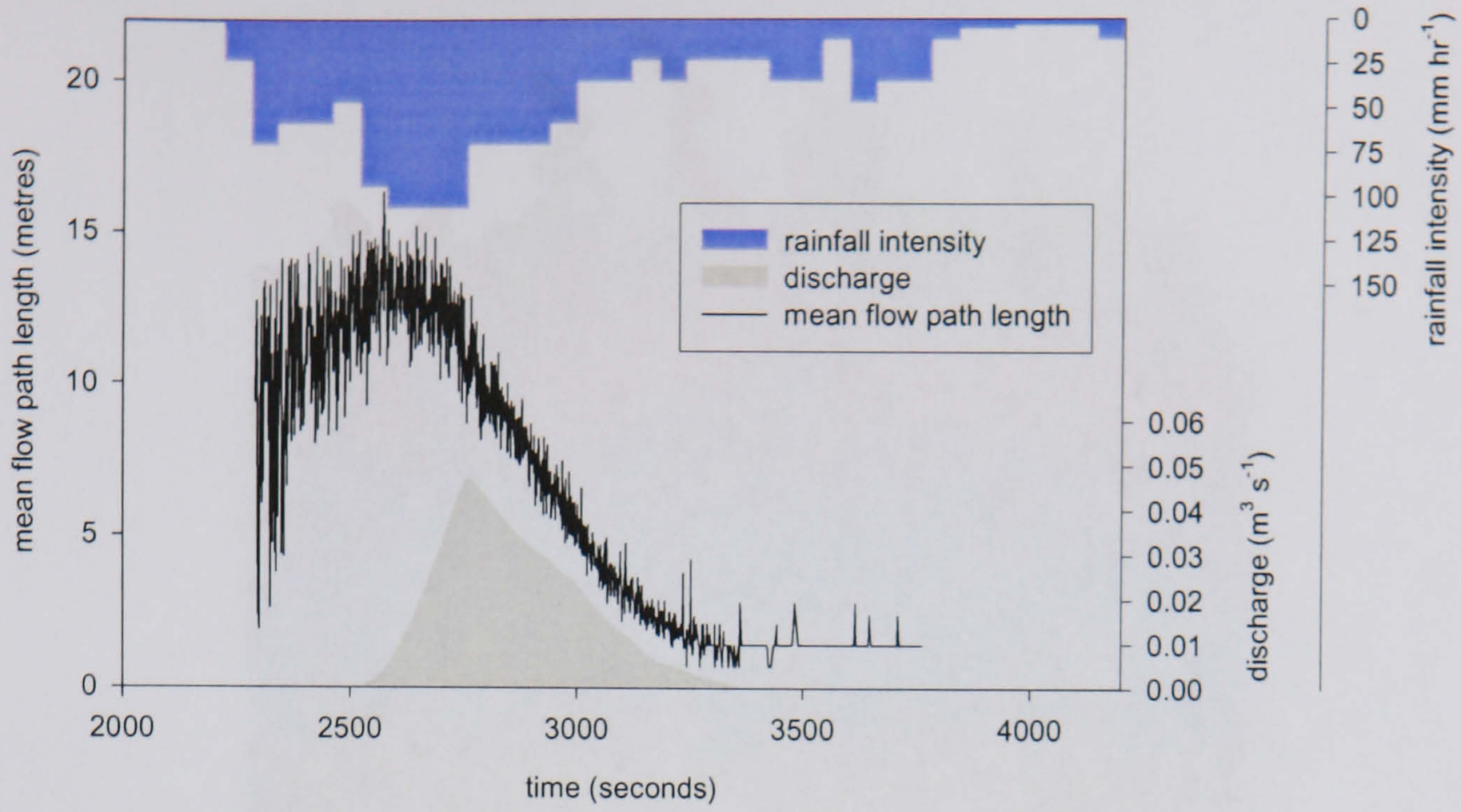

Figure 8.15 Measured rainfall from the main pulse in the September 1997 storm with modelled discharge from the base slope and the mean flow path length

During the initial stage of the rainfall pulse, the model predicts that there is a steady increase in the mean flow path length to a peak which coincides with the start of the peak rainfall intensity. The runoff which is generated at the start of the high rainfall intensity pulse has the greatest amount of time with favourable transmission conditions to move across the surface. As the rainfall intensity decreases, there is a rapid decline in flow path length and discharge. This relates to the reduced amount of water on the surface and hence the increase in the probability of infiltration. After the discharge has ceased from the slope outflow, there is still some movement of water on the slope.

The rainfall pulse event has been broken down into a number of 200 second slices. Within each of these time slices it is possible to extract the source area for discharge from the model (Figure 8.16). Each of the areas extends from the base of the slope to the exposed upper edge.

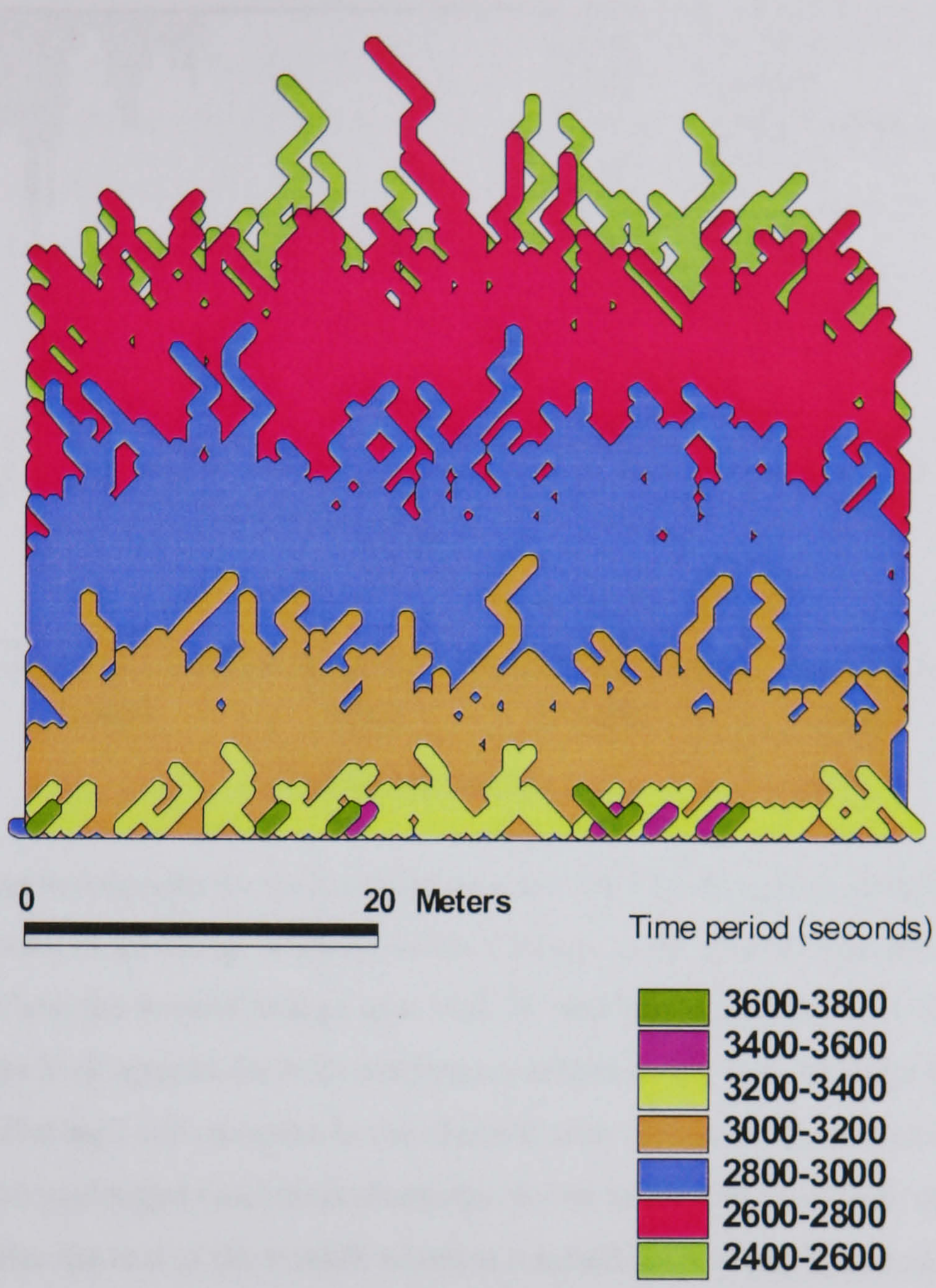

Figure 8.16 Origin of runoff during the receding hydrograph limb for the 29 September 1997 storm event on the base slope

In the first two time slices after the cessation of rainfall, there is very little change in the source area. There is then a rapid decline between 2,800 seconds and 3,400 seconds. During the final stages of discharge, there are a few areas near the base of the slope that continue to give discharge.

Real Sub-Catchments – Discharge Hydrograph

The hydroAgents approach has been applied to the two focus Sub-catchments for the 29 September storm event. The rainfall time series from the gauge in Sub 12 has been selected for the simulations. It is the closest gauge to the lower Cardena and hence should provide the most accurate time series for this location. The rainfall intensities observed in Sub 12 were much greater than those in Sub 7. Therefore, to test if it is the landscape in Sub 7 which resulted in less runoff rather than the difference in rainfall, the Sub 12 time series has been applied to Sub 7. The discharge hydrographs from the two catchments for the Sub 12 rainfall time series are shown in Figure 8.17.

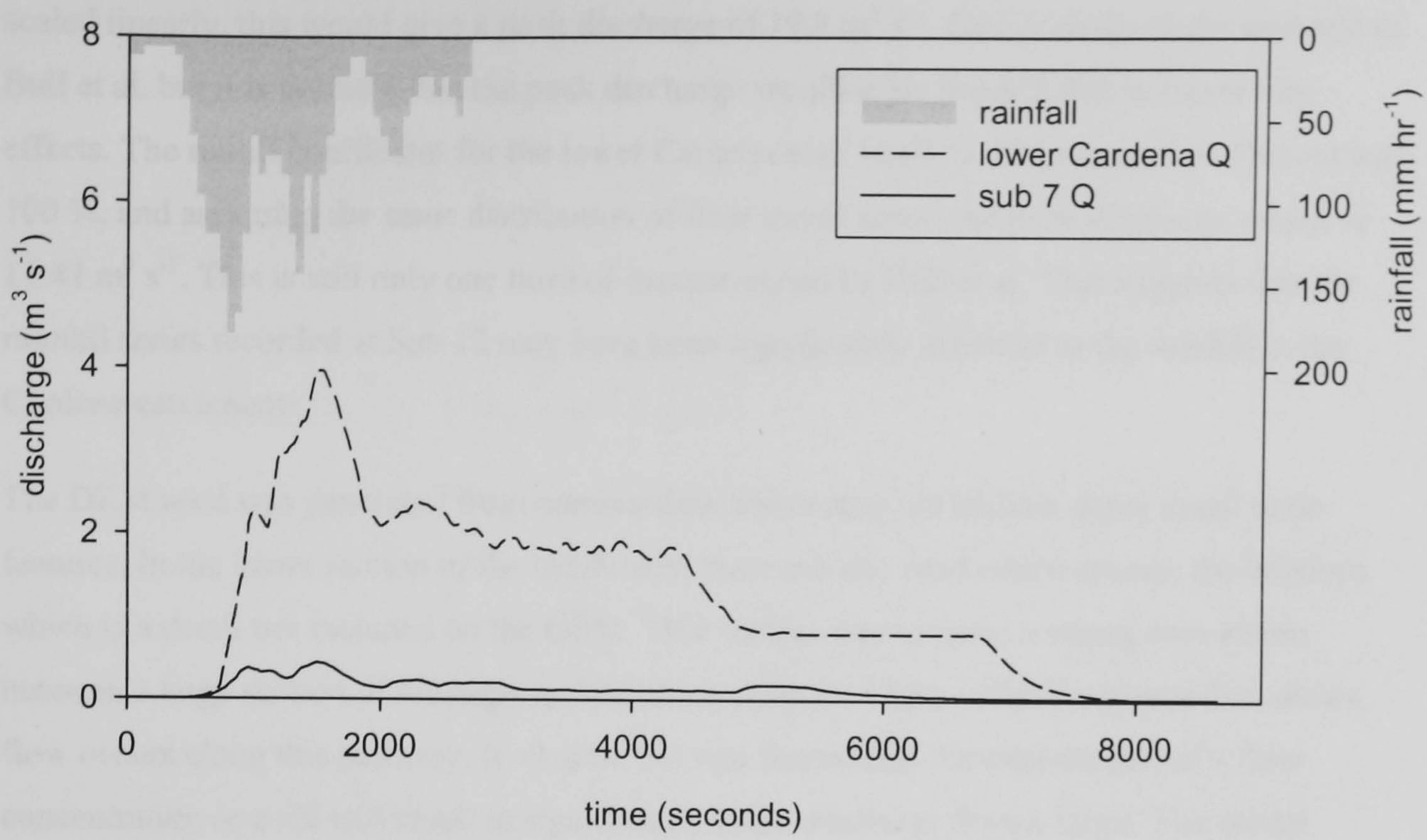

Figure 8.17 Discharge hydrographs for the lower Cardena and Sub 7 for the Sub 12 rainfall time series

The simulated amount of discharge from the lower Cardena is far greater than from Sub 7. The runoff coefficient from the lower Cardena was 34.67 % and from Sub 7 it was 1.7 %. The long tail on the discharge hydrographs for both catchments relates to the flow of water through the channel network. The high soil moisture in the channel network results in low transmission losses and hence the prolonged catchment discharge. In the lower Cardena, flow continued for 1 hour 39 minutes after the end of the rainfall whereas it lasted for 8 hours 36 minutes in Sub 7. This relates to both the longer maximum flow length in Sub 7 and the lower slope gradient creating slower flow.

Bull et al. (2000) undertook field studies of the impact of the 29 September 1997 storm event on the Rambla de Nogalte catchment. They used flood reconstruction techniques to estimate the pattern of discharge across the catchment. This is discussed in chapter 3. The relative pattern of discharge is in line with the observations of Bull et al. However, the peak discharge from the Cardena is much lower than estimated by Bull et al. The authors estimated a peak discharge of 30.6 $m^3 s^{-1}$ at the Cardena outflow whereas the model predicts a peak discharge of 3.96 $m^3 s^{-1}$. Bull et al. also estimated a peak flow of 4.7 $m^3 s^{-1}$ 250 m upstream of the 30.6 $m^3 s^{-1}$ estimate. This is more in line with the model output. There are a number of possible explanations for this difference in peak discharge estimation at the outflow between the field studies and the model output.

The model simulation only considered the lower 20 % of the Cardena catchment. It is possible that areas upstream of the section considered were contributing runoff. If we assume that all of the catchment generated runoff at the same rate as the lower section, and the peak discharge

scaled linearly, this would give a peak discharge of 19.8 $m^3 s^{-1}$. This is closer to the estimate of Bull et al. but it is unlikely that the peak discharge would scale linearly due to travel time effects. The runoff coefficient for the lower Cardena was 34.67 %. If the runoff coefficient was 100 %, and assuming the same distribution of flow travel times, the peak discharge would be 11.42 $m^3 s^{-1}$. This is still only one third of that estimated by Bull et al. This suggests that the rainfall series recorded at Sub 12 may have been significantly different to the rainfall in the Cardena catchment.

The DEM used was generated from contour data which may not include many small scale features. In the lower section of the catchment, there is a dirt road which crosses the hillslope which is a detail not included on the DEM. This surface would make a strong connection between a large section of hillslope and the main channel. There is field evidence that shows flow occurs along this pathway. In chapter 6 it was shown that the introduction of a flow concentration or a rill will result in significantly more discharge from a slope. The model configuration had a grid cell size of 2 m. At this scale, the process of rill flow is not explicitly incorporated into the model and could account for the lower modelled peak flow.

It is possible that runoff in the main Cardena channel was sourced from outside the catchment. To the east of the catchment there is a plain located above the main Cardena channel. Due to the angle of dip of the schist strata, it is possible that ground water flow or pipe flow could be sourced in this area and delivered to the main Cardena channel. There is no major field evidence of pipe outflow but there is evidence of perched water tables. The movement through the schist as piston flow would give a rapid response and would have diffuse outflow.

The model assumes that the rainfall is perpendicular to the horizontal ground surface. The main slopes in the lower Cardena are 30 ° with eastern or western aspects. Many storm events are driven by easterly winds and hence slopes with an eastern aspect receive greater amounts of rainfall. If the rainfall incident angle matches the slope angle, the increase in projected area will result in a 15 % increase in received rainfall. Although this is at the expense of the opposite hillslope, the increase in rainfall can lead to the saturation of parts of the slope and hence far greater runoff generation.

It is possible that the model is inaccurately predicting the amount, timing and transmission of flow. An extensive model calibration could be performed on the main hydrological parameters or an empirical correction factor could be applied to give a more accurate estimate of discharge. However, this would remove most of the physical basis of the model. Since the infiltration characteristics are derived from field measurements and the flow routing is from extensively used algorithms and equations, it is unlikely that the model is inaccurately predicting the

represented hydrology. Therefore, important processes may not be represented in the model such as the formation of rills during a storm event.

The final possibility for the discrepancy between the field estimate of Bull et al. and the model results is that the 30.6 $m^3 s^{-1}$ is an over estimate. If the 4.7 $m^3 s^{-1}$ value is taken as more representative, then the model peak flow of 3.96 $m^3 s^{-1}$ may be considered reasonable.

Focus Sub-Catchments – Origin of Channel Flow

In order to observe the areas contributing to channel flow during the storm event, the hydroAgents that entered the channel network have been extracted. This was done by selecting agents whose pathway intersects the channel network. The agent pathways have been divided into 100 second time slices using the time of insertion of the agent rather than the time of infiltration. The contributing areas for the 29 September 1997 storm event with the Sub 12 rainfall time series for the lower Cardena is shown in Figure 8.18 and for Sub 7 in Figure 8.19.

During the first time slice, the simulations for both catchments show a small amount of runoff reaching the channel. This is as expected since during the first 100 seconds of the storm, the soil moisture will be low and hence the infiltration capacity will be high. Therefore, little runoff will be generated.

In the second time slice, between 400 and 500 seconds, there is a strong difference in the simulated response between the two catchments. Many sections of the lower Cardena are contributing to channel flow. A number of the upper hillslopes are also contributing to channel flow but these sections are disconnected from the lower sections of the catchment. During this time slice, the first discharge is leaving the catchment. In Sub 7, it is only the areas directly adjacent to the channel that are contributing to the channel flow and no discharge is leaving the catchment.

In both catchments, the model predicts that the most extensive area contributing to channel flow occurs during the 900 – 1000 second time slice. This time slice is just after the highest intensity rainfall but is 500 seconds before the peak discharge. In the bottom section of the lower Cardena, the area contributing runoff expands and covers most of the slopes near to the drainage divide. In the upper section, the scrub slopes along the sides of the channels are contributing runoff. Some runoff is reaching the channel from agricultural areas, especially on the eastern side of the catchment. However, from the main low gradient agricultural areas in the upper section, no runoff is reaching the channel although there is hydrological activity in this area.

In Sub 7, the model predicts a massive increase in the area contributing flow to the channel. This expansion is most pronounced in the scrub land areas. In the upper section of the

catchment, with low slopes and agricultural land use, only the slopes next to the channel are contributing to channel flow.

The 1400 – 1500 second time slice occurs just before the peak discharge in both catchments. In both catchments the model predicts that there is a reduction in the area contributing to channel flow. This decrease in area is related to the reduction in catchment discharge in the time period following this time slice. In the lower Cardena, there are still many hillslopes that are active but in Sub 7 it is only the channels and the lower sections of the slopes next to the channel that are active.

In the 1900 – 2000 second and the 2400 – 2500 second time slices, the simulations show that the upper area of the lower Cardena is still contributing runoff to the channels but only from the scrub slopes along the side of the channels. These areas become disconnected from the main outflow due to transmission losses in the main channel. The steep slopes at the lower end of the catchment are still contributing runoff. In the 2900 – 3000 and the 3400 – 3500 second time slices, after the end of the rainfall, the movement is restricted to the main channels with no runoff coming off the slopes.

The simulations predict that the discharge in Sub 7 will continue for longer than in the lower Cardena. However, from 1900 seconds onwards, it is only water falling directly on the channels that is moving. This is with the exception of a small area of scrub slope in the lower section of the catchment which continues to give runoff to the channel in the 4400 – 4500 second time slice. This is due to the concentration of flow in this area leading to greater soil moisture.

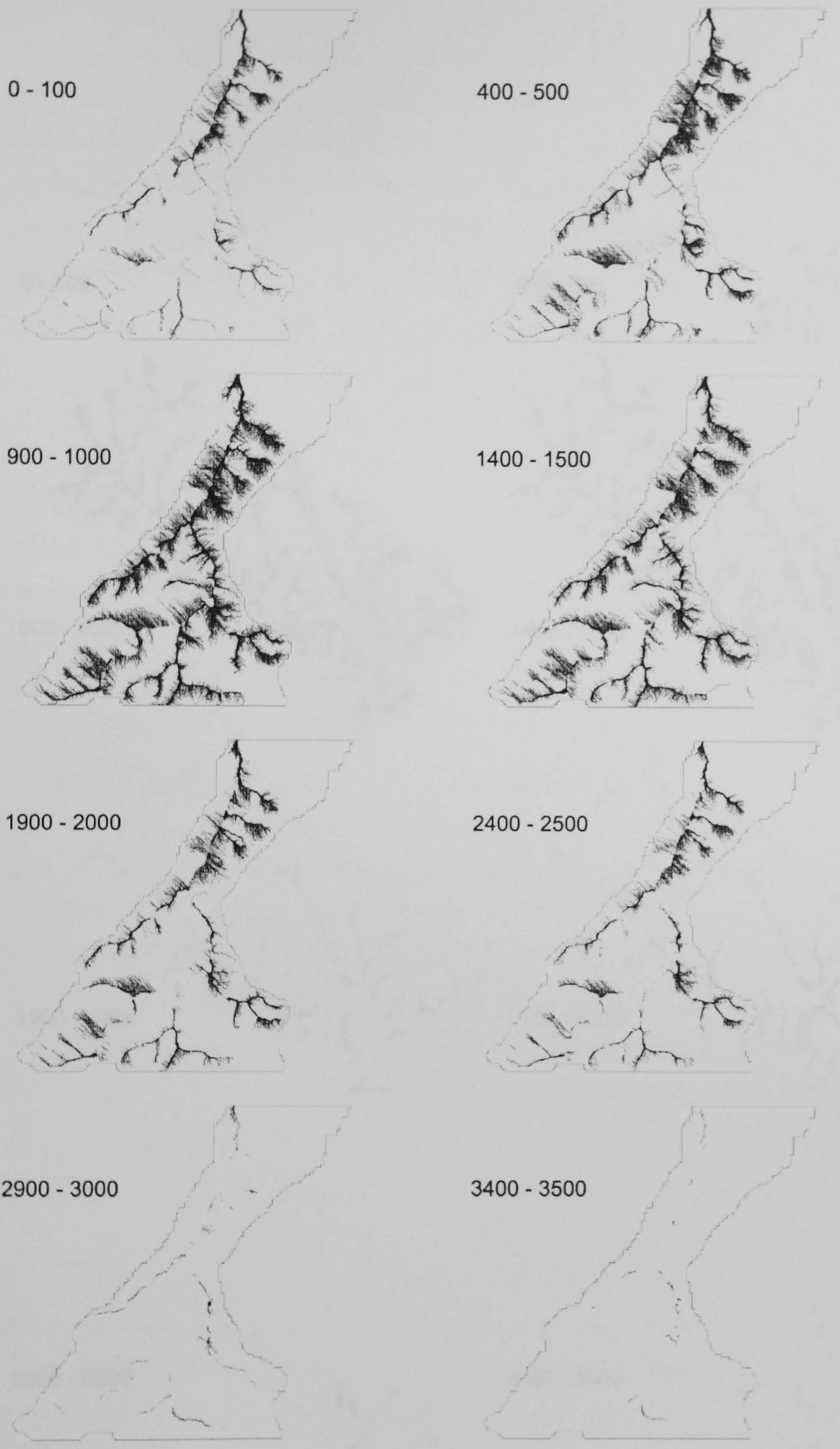

Figure 8.18 Active contributing areas for the lower Cardena for the 29 September 1997 storm event

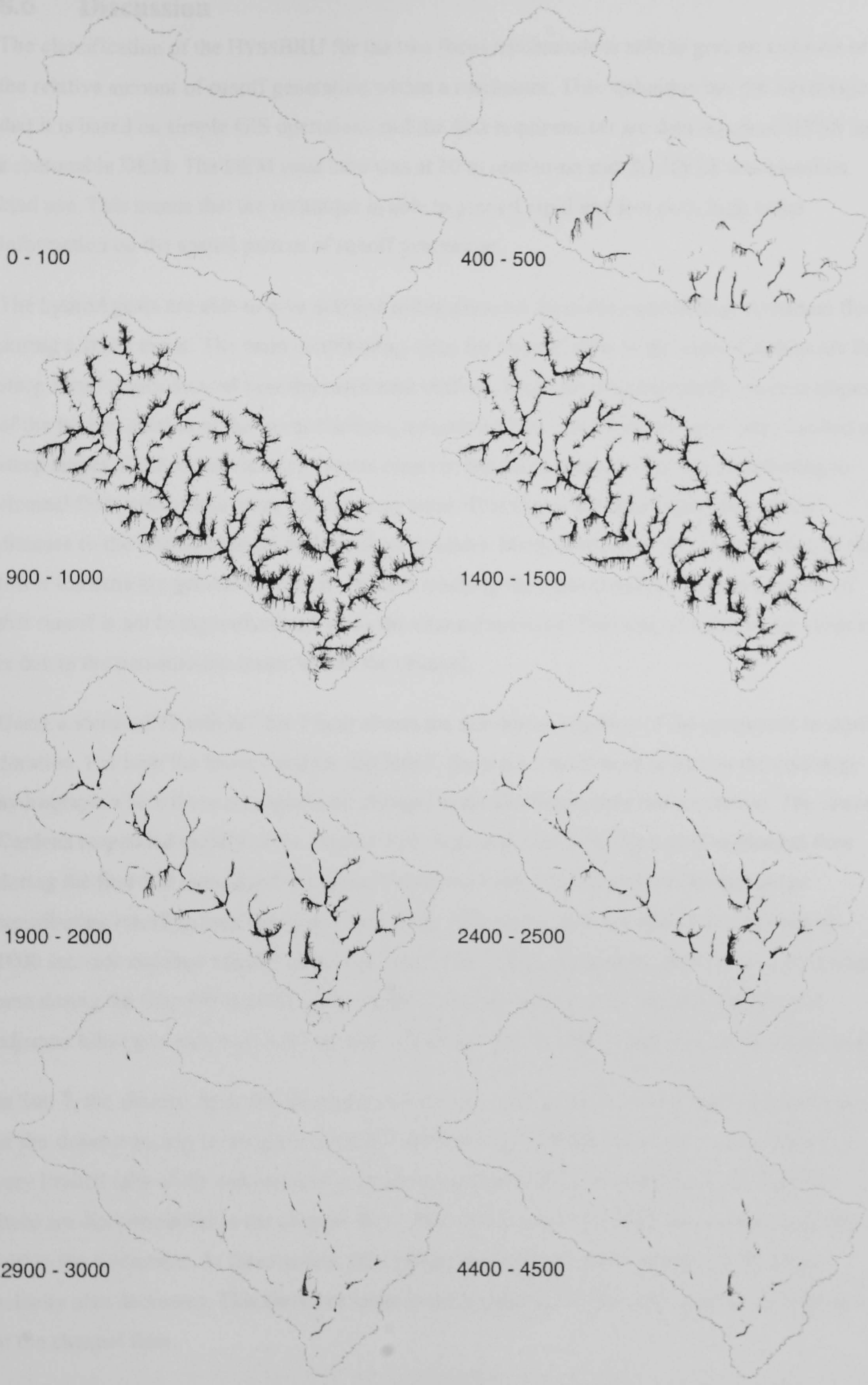

Figure 8.19 Active contributing areas for Sub 7 for the 29 September 1997 storm event

8.6 Discussion

The classification of the HYSSBRU for the two focus catchments is able to give an estimate of the relative amount of runoff generation within a catchment. This technique has the advantage that it is based on simple GIS operations and the data requirements are data layers of HYSS and a reasonable DEM. The DEM used here was at 10 m resolution and the HYSS was based on land use. This means that the technique is able to proved rapid and low cost, high value information on the spatial pattern of runoff generation.

The hydroAgents are able to give detailed information on the areas contributing to channel flow during a storm event. The main contributing areas for channel flow in the lower Cardena are the steep scrub slopes located near the catchment outflow. From the channels on the eastern slopes of the bottom section of the lower Cardena, a number of the runoff source areas were located on steep slopes at the top of channels. Areas closer to the main channel were not contributing to channel flow while these areas further away were. This shows the dual importance of the distance to the nearest channel and the slope gradient. Many sections in the upper section of the lower Cardena are generating runoff which is reaching the main channels. However, much of this runoff is not being transmitted along the channel network. This loss of water in the channels is due to the transmission losses within the channel.

Using a storm of 75 mm hr^{-1} for 1 hour shows the non-linear response of the catchment to storm duration. For both the lower Cardena and Sub 7, there are a number of points on the discharge hydrograph where there are significant changes in the discharge from the catchment. The lower Cardena responded rapidly to the rainfall with large areas contributing runoff to channel flow during the first 100 seconds of the storm. Throughout the rest of the storm the key areas contributing runoff remain the steep scrub slope. The source area expands to a maximum at 1000 seconds and then slightly decreases. Sub 7 has a slow, curvilinear increase in contributing area during the first 500 seconds of the storm. The main source areas are the channels and adjacent hillslopes and, even after an hour of rainfall, there is little expansion in the source area.

In Sub 7, the channel flow was sourced from the few small areas of scrub, from the lower parts of the slopes adjacent to the main channels and from the channels themselves. This leads to a very limited area of the catchment contributing to channel flow. As with the lower Cardena, there are discontinuities in the channel flow. This may relate to the location of the check dams within the catchment. At these points, the channel gradient decreases and hence the flow velocity also decreases. This therefore leads to the infiltration of the water and the disconnection of the channel flow.

There is good agreement between the two techniques. Many of the areas which are predicted to generate high levels of runoff by the HYSSBRU are shown by the hydroAgents to be

contributing to channel flow. High runoff generating HYSSBRU that are surrounded by areas of low runoff generation potential are shown not to connect to the channel. This can be seen at point 'A' in the Sub 7 catchment where a HYSSBRU with the highest runoff generation potential class is surrounded by lower value HYSSBRU. Using the hydroAgent technique, it can be seen that this unit does not contribute to the channel flow at any point during the storm event.

The hydroAgent technique relies upon high resolution spatial data on topography and infiltration patterns. For this research, a base spatial resolution of 2 m has been used. The DEMs were calculated from 1:5000 topographic maps. The generation of a 2 m DEM from this source data requires much interpolation. This results in a smoothed surface and a lack of detail in the channels. The structure of the channels will greatly influence the flow hydraulics and hence the amount of discharge. From the simulations, the channel detail problems can be seen where the flow ceases in the channel. This may relate to transmission losses but may also result from problems with the DEM. These problems could be overcome through the use of LIDAR for the generation of the DEM and airborne optical remote sensing for the generation of the land cover data. This would, however, drastically increase the cost of the modelling exercise. It would improve the process representation in the channels if a spatially variable model grid resolution with greater detail in the channel network was used.

The computational and memory expense of the hydroAgent technique is very high and is many millions of times greater than for the HYSSBRU approach. The large memory requirements of the hydroAgent technique relates to the density of agents required for the accurate representation of the distribution of flow paths. The requirements can be significantly reduced by only considering the fate of rainfall from a limited number of focus points rather than from the whole catchment.

The rule set used for the hydroAgents in this research relates to the movement of water through a hydrological environment. The rule set could be re-written to model the movement of sediment or pollutants through the catchment. This would be very useful in determining the fate of pollution in the environment.

The detail of the areas extracted as contributing to channel flow will be sensitive to the defined channel network. In this application of the technique, a fixed channel network was used derived from map based data. An improvement would be to dynamically generate the channel network whilst the model is running to account for channel expansion and to include the feedback between the runoff generation on the hillslopes and the state of the channel system.

Field validation of the hydroAgent technique in a semi-arid catchment could be achieved by selecting a number of key areas that connect and do not connect with the channel network and placing blocks of fluorescent tracers on the slopes and installing a number of fluocapteurs in the

channel floor. The fluocapteurs consist of a steel mesh bag containing adsorptive charcoal. The fluorescent tracers are absorbed into the charcoal and hence can be collected after the storm event. The amount of dye in the charcoal can then be determined using a spectrofluorimeter (Lange and Leibundgut 1997). This will therefore give valuable information on the points in the landscape that connect to the channel and those that do not. The method is similar to the modelling approach and hence would be a very suitable validation method. The September 1997 storm has been estimated as a 1 in 7 year event, hence, it is likely that a suitable storm event will occur in the near future.

The hydroAgent technique of flow tracing is able to give a unique picture of the origin of channel flow within a catchment. The technique can be applied at temporal and spatial scales not possible with the models discussed in section 8.4.1. The RillGrow model of Favis-Mortlock (1998) and Favis-Mortlock et al. (2000) is potentially able to give information on the origin of runoff. However, due to the representation of finite volumes of water in each parcel / agent, the huge memory requirements limit the spatial extent of the model application to a few square metres rather than the 2 km^2 area in the Sub 7 catchment to which the hydroAgent technique was applied to. The model of Shannon et al. (2002) has been applied at a more useful spatial scale, however, since it only considers the river channel, it is not able to give information on the origin of runoff within the whole catchment. The hydroAgent technique is able to trace the flow of the agents both across the hillslopes and through the fluvial environment in the channel system. The landscape evolution models of Chase (1992) and Haff (2001) operate at the landscape scale. However, due to the treatment of storms as a single parcel / agent, the fine detail is lost on both spatial and temporal scales. It would be possible to apply the hydroAgent technique at the landscape scale if coupled to a suitable hydrology model acting as the environment generator. This system could then trace the movement of water across a landscape and hence determine the origin of runoff at the landscape scale. Therefore, the hydroAgent technique developed here is a significant step forwards in both the application of agent based modelling techniques to hydrology and in the determination of the source areas within complex semi-arid catchments.

8.7 Conclusions

The location of areas which generate large amounts of runoff can be investigated using the HYSSBRU approach. This gives information on the spatial configuration of runoff generating areas within a catchment. The configuration of land use and topography give a complex pattern of HYSSBRU. The HYSSBRU approach can give rapid, low cost, high value information on the location of runoff generating areas. However, it does not give information of the fate of the generated runoff.

The application of the hydroAgents technique is able to give information on the origin of channel flow. This is achieved by tracing the software agents representing water through the catchment hydrological system back to their origin. This technique is therefore able to give a unique picture of the sources of channel flow during a storm event.

The comparison of the contributing area on the base 50 m slope with and without the flow convergence illustrates the importance of efficient flow structures on the surface in connecting larger areas of the slope to the outflow. There is a massive increase in the contributing area with the introduction of flow convergence and this explains the increases in discharge shown in chapter 5.

There are large contrasts between the two focus catchments in their response to rainfall over time as illustrated by the 75 mm hr^{-1} for an hour experiments. The model predicts that the lower Cardena responds rapidly to rainfall. Within the first 100 seconds, large areas of the catchment are predicted to be contributing to channel flow. This area expands to its maximum extent by 500 seconds. The simulated response of Sub 7 is far slower than the lower Cardena. After 100 seconds, there are only a few scattered areas which are contributing flow to the main channel. The contributing area increases slowly to a maximum after 3000 seconds. The contributing area does not extend beyond the valley floors and the immediately adjacent slopes, even after an hour of high intensity rainfall.

During the 29 September 1997 storm event, the model predicts that the lower Cardena responded rapidly to the lower intensity rainfall in the first 100 seconds of the storm event. The contributing area expands rapidly during the main high intensity rainfall pulse. In Sub 7, the model predicts that there is very little hydrological activity contributing to channel flow until the main, high intensity, rainfall pulse. The contributing area during this pulse is greater than that predicted after the hour of high intensity rainfall. The contributing area contracts rapidly after the end of the high intensity rainfall, however, channel flow continues for longer than in the lower Cardena. This may relate to the greater catchment area.

The simulations predict that the main contributing areas for the lower Cardena catchment are the steep slopes at the lower end of the catchment and the upper sections of a number of gullies. In Sub 7, the channel flow was sourced from the channels and the lower sections of the slopes directly adjacent to the channel.

9 Research Synthesis and Conclusions

9.1 Introduction

The aim of this chapter is to integrate the different aspects of the research presented in the thesis so far. The integration of field and model experiments is described in section 9.2. The implications of the research findings for semi-arid hydrology are presented in section 9.3. The recommendations for future research, both in terms of field work and modelling, are presented in section 9.4. The policy implications of the research presented in this thesis are discussed in section 9.5. The extent to which the research aims and objectives presented in chapter 1 have been achieved and the general implications of the research are discussed in section 9.6. The research conclusions are presented in section 9.7.

9.2 Integration of Field and Modelling Experiments

The development of the Connectivity of Runoff Model (CRUM) was driven and guided by the field experiment results presented in chapter 4. From the analysis of the field work results, the parameters and processes that need to be included in the model were determined. This model was used for the modelling work presented in chapters 6, 7 and 8.

The rainfall simulation experiments showed that surface roughness, gradient, soil moisture and stone cover are the key controls on the generation of runoff at the plot scale. Each of these factors has been incorporated into the model. The effects of soil moisture and stone cover on the infiltration rate have been combined through the use of the rainfall simulation experiment results to parameterise the simplified Green and Ampt equation. The surface roughness and slope gradient are spatially distributed within the model.

The up-scaling of the field results from the plot scale to the hillslope and small catchment scale was achieved through the use of hierarchical scale techniques. This approach nests many simulations of the rainfall simulation plots on a grid structure. Due to the complexity of the spatial patterns in the factors controlling runoff generation found in the field results, the routing of the overland flow between the distributed cells has to be handled with care. Therefore, the multiple flow path routing algorithm, FD8, has been implemented in CRUM. At each of the distributed cells, information on the key controls on runoff generation is required. Spatial

patterns of land use, slope gradient and vegetation cover are inputted into the model whilst the soil moisture is determined by CRUM.

The field experiments were able to give a consistent set of parameter values and parameter ranges. These parameter sets and ranges were used to parameterise the model for the simulation experiments undertaken in chapters 6, 7, and 8. The field work results gave the parameter values for the simplified Green and Ampt infiltration equation, information on the vegetation cover and structure and the spatial pattern of land use within small catchments. The range of slope gradients and lengths was obtained from a combination of fieldwork and GIS analysis.

The field results presented in chapter 4 showed that there is high variability in the infiltration rates related to the vegetation cover and land management. The analysis of the rainfall time series showed that the rainfall is highly variable. Therefore, these factors have been considered as stochastic processes with many realisations of the processes being modelled. The effects of variable vegetation patterns were presented in section 6.4 and the effect variable rainfall were presented in section 7.3 and section 7.4.

9.3 Conclusions for Semi-Arid Hydrology

From the field results and the modelling experiments, there are number of conclusions for semi-arid hydrology. These have been broken down into the general underlying themes that occur throughout the different experiments. These are discussed in section 9.3.1. The conditions required to generate a major flood are discussed in section 9.3.2. Finally, the implications of possible future changes in climate and land management are discussed in section 9.3.3.

9.3.1 General Themes

From this research, two general themes can be found throughout the different experiments. The first is the interplay between the distribution of flow path lengths generated during a storm and the distributions of flow lengths to the channel as a function of the landscape. The second theme relates to the importance of the spatial structure of hydrological areas within the landscape. Each of these themes will be discussed in turn.

Flow Path Lengths

It was shown in chapters 2 and 3 that the rainfall in many semi-arid regions and in the Rambla de Nogalte is characterised by episodic, high intensity storm events. Within these events there are short bursts of high intensity rainfall. It is during these bursts that the infiltration capacity of the soil will be exceeded and runoff will be generated. After the burst, the runoff is rapidly lost to transmission losses due to the high infiltration rates. The duration of the high intensity burst therefore will determine the time available for runoff to move across the surface.

The effect of the flow path length on the runoff coefficient has been investigated by Yair and Lavee (1985), Lal (1997), Gabriels (1999) and Van de Giesen et al. (2000) and Wainwright and Parsons (2002). It was shown in chapter 6 that it is not the broad scale slope length that is the key control on the amount of water reaching the channel, but the distance to a flow concentration. As was shown in some of the results presented by Lal (1997), who found that on longer slopes where rills were able to form, the runoff coefficient increased with increasing slope length opposed to the normally observed decrease. This is due to the decrease in the distance to a flow concentration since, once the water is in an efficient flow channel, the probability of it being lost as part of the transmission losses is greatly reduced and the flow velocity is far greater hence enabling it to leave the sub-catchment. The important aspect is not the physical distance but the time required to reach the channel due to the interplay with the duration of the rainfall burst. It was shown in chapter 6 that the slope gradient is positively related to the amount of water leaving the hillslope and reaching the channel. This is due to the increased flow velocity decreasing the time required to reach the channel. By combining the effects of slope gradient and slope length, it is possible to calculate the distribution of flow path travel times for a catchment.

The importance of the flow path length distribution has been shown in chapter 7 through the consideration of storm characteristics. The temporal structure of the rainfall can have a significant influence on the amount of runoff that leaves the slope as discharge. This has been shown with the use of defined storm hydrographs, section 7.3, and the use of stochastic rainfall, section 7.4. Using the defined storm hydrographs, it was found that the greatest amount of runoff was generated by a high intensity pulse followed by a long period of low intensity rainfall. The use of the stochastic rainfall showed that the introduction of variable rainfall intensities can reduce as well as increase the amount of runoff leaving a slope. These model results support the findings of Yair and Lavee (1985) who found that the threshold amount of rainfall required for runoff to leave a slope was related to the rainfall characteristics and the slope length. These model results also support the findings of Lal (1997) who found that the form of the relationship between the slope length and the runoff coefficient varied significantly between storm events and proposed that this variation depended on interactions between the slope length, rainfall characteristics and land management. This modelling work extends the findings of Yair and Lavee (1985) and Lal (1997) by considering a greater range of storm events.

The application of the hydroAgent technique to the two sub-catchments in chapter 8 was able to show the importance of the flow path lengths in determining the amount and locations from which runoff reaches the river channel. It was found that the main contributing areas for channel flow in the lower Cardena catchment are the steep scrub slopes located near the catchment

outflow. From the channels on the eastern slopes of the bottom section of the lower Cardena, a number of the runoff source areas were located on steep slopes at the top of channels. Some areas close to the main channel were not contributing to channel flow while suitable areas farther away were. This shows the dual importance of the distance to the nearest channel and the slope gradient.

There are two key distributions of flow travel times. The first is a function of the landscape in terms of the distance to the nearest flow concentration, slope gradient and surface roughness. These three factors will determine the distribution of travel times to the efficient flow in the flow concentration. The second key distribution is the distribution of flow travel time which is derived from the temporal structure of the storm event. It is the convolution between the landscape derived distribution and the distribution of the runoff generating times from the storm event that will determine the strength of the connectivity and hence the amount of water able to reach the channel.

Spatial Structure

From the literature review in chapter 2 and the field results in chapter 4, it has been shown that semi-arid landscapes have a two-phase pattern of infiltration characteristics at both the hillslope and the landscape scales. At the hillslope scale, there is a contrast in the infiltration characteristics between vegetated and non-vegetated areas with greater infiltration capacities being found in the vegetated areas. At the landscape scale, there is a large contrast between the scrubland areas and those under agriculture. The infiltration capacities are far greater on the agricultural land than on the scrub areas.

The importance of the pattern of infiltration on the transmission of runoff across a hillslope has been shown in the results presented in sections 6.4.5 to 6.4.7. The model results show that the response of hillslopes with a fragmented vegetation cover is non-linear and complex, supporting the findings of Cerdá (1997), and that the spatial pattern of vegetated and bare areas, on a slope with the same vegetation cover, can have a significant impact on the amount of runoff reaching a channel at the base of the slope. The model results show a decrease in discharge greater than would be expected from the area average infiltration capacity. The decrease in discharge is due to the runoff that was generated in the bare areas being infiltrated as run-on in the vegetated areas. With large patches of vegetation, there is high variability in the amount of discharge due to the sensitivity of the system to the land use at the base of the slope. As the size of the vegetation patches decreases so too does the average discharge due to the greater opportunities for runoff to be captured by down slope vegetation. This supports the comments of Morgan (1995), Fitzjohn et al. (1998) and Cammeraat and Imeson (1999) that the infiltration patterns needs to be considered when upscaling observations from the hillslope to landscape scale.

The amount of discharge that leaves a slope is sensitive to the position of surfaces with different hydrological properties. If an area with high infiltration capacity is located at the base of the slope, it will have a far greater impact on the amount of discharge from the slope than if it was located further up the slope. The form of this relationship is non-linear with the shape of the curve being related to the interplay between the storm and the slope characteristics. This is related to the concept of a threshold soil moisture level for runoff connectivity as proposed by Fitzjohn et al. (1998). The threshold value is related to the statistical distribution and the spatial distribution of the infiltration rate. The same statistical distribution of infiltration rates with different spatial distributions will result in different soil moisture threshold values.

9.3.2 Conditions Required for Flooding

For the generation of a large flood within the Rambla de Nogalte catchment, a certain set of circumstances would have to occur. These may be divided into antecedent conditions, storm characteristics and land management. Each of these will be discussed in turn.

As was shown in chapters 2 and 4, there is a negative relationship between the soil moisture store and the infiltration capacity. Therefore, the antecedent conditions at the start of the rain storm will have a significant effect on the amount of discharge, as was shown in chapter 7 for the different storm forms. Therefore, if there is sufficient rainfall before the storm, then there would be greater soil moisture and hence lower infiltration rates. The lower infiltration rates would, therefore, increase the amount and area over which runoff would be generated. This increase in area increases the connectivity of the runoff due to the longer flow path lengths. Therefore, there is an increase in the probability that runoff will reach a channel.

It was shown in chapter 7 that the storm characteristics have greater influence on the discharge hydrograph than the surface characteristics. There are two key characteristics of the storm that determine how much rainfall will be converted to runoff and reach the channel. The first of these is the rainfall intensity; this must be greater than the infiltration capacity of the soil. As was shown in chapter 4, the infiltration capacities in the Rambla de Nogalte catchment are high, in excess of 75 m hr^{-1} in agricultural areas. Far greater infiltration capacities have been reported in the literature, as detailed in chapter 2. The high infiltration capacities mean that it is only the high intensity rainfall pulses that are able to generate runoff which, therefore, leads to two issues. The first is the position of the high intensity pulse within the storm since this will influence the antecedent soil moisture during the main runoff generating phase. The second is the length of high intensity pulse. If the rainfall intensity falls below the infiltration capacity, the runoff which is flowing across the surface will infiltrate further down slope as run on. There is, therefore, an interplay between the distribution of travel times from the point of runoff generation to the channels and the distribution of storm pulse lengths. It was shown in chapter 6 that the travel times are influenceed by the slope lengths and the slope gradient. The effect of

slope length and gradient on the travel times can be seen in chapter 8 where one of the key channel flow source areas is the heads of gullies. These areas connect due to their short travel distance to an efficient flow channel due to the convergent flow pattern.

The most efficient topography for transforming rainfall to channel flow would consist of short flow path and steep slopes. This combination would minimise the time required for runoff to reach the channel since the distances would be short and the flow velocities would be high. This landscape may consist of steep slopes with an embedded rill network. This is the form of the slopes in the lower Cardena which has been shown as having a high degree of connectivity.

The most efficient way to transform rainfall into channel flow would be from a two stage high intensity rainfall pulse. The first stage of the pulse must be greater than the infiltration capacity of the soil. The high rainfall intensities will generate infiltration excess and fill the surface depression store. The second stage of the pulse must be at a greater intensity than the first. This section of the rainfall pulse may be seen as not falling on the soil surface but on the surface depression store. Therefore, almost all of the pulse would be converted into runoff. After the end of the high intensity pulse, the rainfall needs to continue at a rate greater than the infiltration capacity of the soil such that the runoff generated in the main pulse is not lost to transmission losses. The time between the start of the main pulse and the end of the pulse must be large in comparison to the flow travel times from the hillslope to the channel. A storm of this form could be possible with the observed range of rainfall intensities and durations, as discussed in chapter 3.

It was shown that land management has a significant control on the generation of runoff. The regular ploughing of tree crops greatly increases the infiltration capacity and surface roughness. Therefore, runoff is rarely produced in these areas and due to the surface roughness it is not able to travel far. The increase in the infiltration capacity as a result of ploughing is due to the removal of the surface crust and the increase in the porosity of the upper soil layer. Therefore, the timing of a storm event within the ploughing cycle can greatly influence the surface response. If the storm occurs directly after the surface has been ploughed, the infiltration capacity and the surface roughness are at their greatest and hence minimal runoff will be generated. As the time since ploughing increases, a surface crust may form and the surface roughness may decrease. The amount of change is a function of the amount of rainfall received. The surface crust will decrease the infiltration capacity and the decrease in surface roughness will decrease the surface depression storage. This means that less infiltration excess rainfall is required to generate runoff. These factors combine to increase both the amount of runoff generated and the potential flow path distance. Therefore, if a storm occurs just before the surface is ploughed, more runoff will be generated and the flow path distances will be greater. More water will, therefore, reach the channel.

The abandonment of land will have a strong influence on the hydrological properties of the soil. As described above, the cessation of ploughing will result in the formation of a soil crust. This will increase runoff due to the lower infiltration capacity. The surface roughness will decrease to start with due to the smoothing of the tillage features by rain splash. However, as rills start to form, the surface roughness will increase. The formation of a rill network will greatly increase the amount of water that can leave the surface due to the decrease in the distance to an efficient flow channel. However, the colonisation of the surface by vegetation will locally increase the infiltration rate and due to the interaction between the bare and vegetated areas by run-on, the slope discharge will rapidly decrease.

Scenario for Major Flooding

Taking into account the factors outlined above, it is possible to construct a scenario for major flood generation within the Rambla de Nogalte catchment. In the days leading up to main storm event, there needs to be a number of storm events. The rainfall is preferably delivered at a low intensity over a long time period. The low intensity rainfall would enable the water to infiltrate and increase the soil moisture, and the cloud cover will minimise the evaporation losses and help to maintain the soil moisture. The main storm needs to consist of a compound, high intensity pulse. This storm structure will create conditions for efficient transmission of the generated runoff across the soil surface. The length of the pulse must be large compared to the travel times to the channel. This storm needs to occur before agricultural field are ploughed. If areas of the catchment have been abandoned, then the storm needs to take place after the rill network has formed but before much vegetation colonisation has occurred.

9.3.3 Changes in Hydrology due to Climate and Land Use Change

Potential changes in the hydrology of the Rambla de Nogalte catchment, and in semi-arid areas in general, over the next 100 years are related to climate change, policy change and the land manager response to these changes. Each of these factors is discussed in turn.

As presented in chapter 2, the predicted change in the climate in south east Spain is up to a 2 °C increase in temperature and up to a -0.5 mm day^{-1} decrease in annual rainfall. It is predicted that there will be a reduction in spring rainfall and an increase in summer rain days. These changes in the weather patterns reduce the rainfall at the crucial time of year for plant growth and increases rainfall when potential evaporation rates are at their highest. The increased evaporation will therefore result in a reduction in the annual average soil moisture. The change in the soil moisture has implications for both runoff generation and biomass. The lower soil moisture will result in a greater depth of rainfall required to start the generation of runoff. Assuming the current storm characteristics, this would result in a reduction of runoff generation.

The lower soil moisture will strongly influence the plant growth within the region since water is already the limiting factor. The reduction in vegetation cover will lead to an increase in the crusting of the soil surface and a decrease in the average infiltration rate. The changes in the infiltration rate will, therefore, lead to an increase in both the amount of runoff generation and the amount of discharge from the slope due to the lower transmission losses. This reduction in plant growth may lead to a reduction in vegetation cover over the whole year and lead to a reduction in the average infiltration capacity. These changes will change the thresholds for runoff generation and for the formation of connections between areas in the landscape and will result in more water reaching the channel for a given storm.

With a changing climate, it is expected that the nature of the rain storm events will change. As was shown in chapter 7, subtle changes in the storm characteristics can have a large impact on the amount of water leaving a slope. If the average storm rainfall pulse duration increases, then the flow path distances will also increase leading to greater amounts of water reaching the channel. However, if the storms change to greater intensity but with shorter durations, then the amount of discharge may decrease.

The agriculture in the Rambla de Nogalte catchment under the current climate may be considered marginal. If changes in the EU's Common Agricultural Policy (CAP) reduce the profitability or if the predicted climate change moves the agriculture from marginal to non-profitable, then the land management will change. In areas which are currently non-profitable for agriculture, there has been a shift from agriculture to grazing and scrub with only the most profitable areas kept under agriculture. The other main factor is the retirement of the current farmers and the possibility that they will not be replaced due to the younger members of the population finding more profitable work elsewhere. These changes in the local economy will also remove large areas of land from agriculture.

The impact of the abandonment of land was discussed in chapter 2. It has been found to increase the amount of runoff generation at the point scale. Over time, the lack of maintenance of flow control structures at the catchment scale and the formation of channel networks on the previously cultivated areas will result in an increase in discharge from the catchment.

The future for the Rambla de Nogalte will be influenceed by local scale factors associated with retirement of farmers, EU scale factors associated with CAP reform and changes in the global climate. There is a complex interplay between these factors and the net outcome is difficult to predict.

9.4 Recommendations for Future Research

In order to further investigate the amount and origin of water contributing to channel flow during a storm event in a semi-arid environment, there are a number of recommendations for future research. These may be divided into two sections: field investigations and modelling.

9.4.1 Field Investigations

During the field work, it was only possible to consider a limited number of land use and topography combinations. Therefore, further infiltration experiments on abandoned agricultural fields and on mid gradient slope would fill out the general picture of runoff generation. The rainfall simulation experiments could be extended in two ways. Firstly, the storm characteristics considered could be extended. This should consider a greater range of rainfall intensities and storm structures. Secondly, the rainfall simulation experiments were conducted on a plot 0.5 by 0.5 m and it would be useful to extend the size of this plot to consider the effect of slope length on the runoff coefficient. This would link the field experiments with the modelling results and hence help to define the uncertainty in the modelling results.

It was shown in chapter 6 that the pattern of vegetation has a significant impact on the amount of discharge from a slope. The patterns investigated were generated stochastically and hence it would be useful to map the vegetation patterns at the hillslope scale, thus relating the stochastic pattern to the real world. The modelling that was undertaken at the catchment scale used topography derived from 1:5000 contour data. This does not include many small scale surface features that will influence the efficiency of the flow. This could be derived from photogrammetric or lidar techniques. Therefore, the collection of detailed topographic data at the catchment scale would greatly aid the model application. This would give increased detail in the flow dynamics and in the determination of the origin of flow.

9.4.2 Modelling

The modelling experiments undertaken all considered runoff generation on short time scales. Therefore, main area where CRUM-2D could be extended is to consider longer time scales. To achieve this, the model needs to incorporate evaporation and changes in the surface roughness with time. The addition of these processes will enable the investigation of the effect of the weather conditions over the days previous to the main storm on the amount of runoff generated and the formation of connected runoff generating areas.

The sensitivity of the hydrological system as represented by the model has been investigated in chapters 6 and 7. However, in this analysis, only one or two parameters were varied at once. This approach is not able to consider the interactions between different parameters. These interactions could be considered using a GLUE type approach (Beven and Freer 2001). The computational resources required for this approach were not available during this study. The

investigation of the interactions between different parameters would give greater insight into the controls on runoff generation and the formation of connected runoff generating areas.

The hydroAgents could be extended in a number of ways. The hydroAgents currently work on the same grid resolution as the environment generator. Greater detail of the flow paths could be achieved by having the agents working on their own, high resolution, spatial representation. The inclusion of a high resolution grid would remove the assumption that there is full mixing within each model cell such that each agent has equal chance of leaving the cell regardless of the time spent in that cell. The current rule set only considers the surface hydrology and could be extended to include the agents being evaporated and being lost to ground water. These changes would give increased detail on the origin of runoff during a storm event.

9.5 Policy Implications

The knowledge gained from the investigations into the key runoff generating areas within a catchment and mapping the origin of runoff could be used to direct policy. This could be used for land use and land management controls and for designing flood defences. The hydrological sensitivity of the landscape is spatially non-uniform. Therefore, the same change in different parts of the landscape will have different impacts. The knowledge gained in this research could be used to inform decisions on the changes in land use.

The maps presented in chapter 8 showing the origin of channel flow could be used to regulate the land use in these sensitive areas. Knowledge of under what circumstances different areas of the catchment generate runoff would be useful in designing flood mitigation structures.

9.6 Achievement of Research Objectives

The aim of this research was to "understand the amount and origin of water contributing to channel flow during a storm event in a semi-arid environment". To achieve this aim, four research objectives were defined. The extent to which these objectives have been achieved is discussed below.

9.6.1 Key Variables Controlling Runoff Generation in the Field

The variables controlling the generation of runoff in the field were investigated within the Rambla de Nogalte catchment, south east Spain. Two techniques were used, rainfall simulation and minidisk infiltration experiments. It was found that land management has the greatest influence on the infiltration capacity of the soil. Agricultural areas have far greater infiltration capacities than scrub areas. The form of the discharge hydrograph is strongly influenced by the surface biomass and stone cover, roughness and gradient. These factors need to be incorporated in a model of semi-arid hydrology.

9.6.2 Hydrological Model to Forecast Runoff Generation and Transmission

A grid based distributed hydrology model has been developed; the Connectivity of RUnoff Model (CRUM). This model considers the hydrological fluxes relevant for a semi-arid environment at the time space of a single storm event. The infiltration capacity is determined by the simplified Green and Ampt model based on soil moisture. The runoff is routed using the multiple flow path algorithm, FD8, and the flow velocities are calculated using the Darcy-Wesibach equation. The generation of stochastic storms has been achieved using a Monte Carlo model. This was parameterised from field data.

9.6.3 Surface and Storm Controls on the Form of the Discharge Hydrograph

It has been found that the storm characteristics exert greater control on the discharge from a slope than the characteristics of the surface. However, the surface characteristics determine the spatial response to a certain storm event. The main surface controls are the slope length, slope gradient and spatial configuration of the vegetation. Greater runoff coefficients were predicted on shorter slopes and steeper gradients. The relationship with slope gradient is supported by field experiments. The discharge from a slope was found to be sensitive to the position of vegetation on the slope. There is a non-linear relationship between the position of the vegetation on the slope and the amount of discharge. Minimal runoff was predicted with the vegetation at the base of the slope. The introduction of a fragmented vegetation pattern resulted in lower discharge than would be predicted from the spatial average infiltration capacity. This is due to the interaction between the vegetation and non vegetated areas with the runoff generated in the bare areas infiltrating in the vegetated areas.

It was found that the storm form can have a significant effect on the amount of discharge from a slope. The position of the main high rainfall intensity pulse with the storm has a significant influence and the amount of discharge. There needs to be sufficient rainfall to condition the surface for runoff generation before the main pulse. The length of the pulse is the main control on the flow path distances. The rainfall characteristics after the main pulse will determine the transmission losses and can help to extend the flow paths. There is, therefore, an interaction between the distribution of travel distances to the channel and the rainfall pulse duration. Therefore, if the rainfall is delivered in a number of short pulses, the runoff flow path lengths will be short and little water will reach the channel. However, if the rainfall is delivered in one long pulse, the travel distances will greatly increase and far more water will reach the channel.

9.6.4 The Origin of Runoff

To consider the origin of runoff during a flood event, a method of tracing water through a hydrological environment was developed. This was based upon autonomous agents, termed hydroAgents. These agents moved through an environment generated by CRUM-2D.

It was found that the lower Cardena responds rapidly to rainfall with large areas contributing to channel flow after 100 seconds of rainfall. This contrasts with Sub 7 where the catchment responses very slowly to rainfall. The main contributing areas for the lower Cardena catchment are the steep slopes at the lower end of the catchment and the top sections of a number of gullies. In Sub 7, the channel flow was sourced from the channels and the lower sections of the slopes directly adjacent to the channel.

9.7 Research Conclusions

The amount of water reaching a channel during a storm event is a function of the hillslope scale hydrological processes. This research has considered the dynamics of runoff generation and transmission at the hillslope and small catchment scale and hence is able to give insight into the system operation not possible by investigating point scale processes. It has been shown that there are two key themes in determining the amount of runoff that reaches the channel network: the interplay between the distribution of flow path lengths generated during a storm and the distributions of flow lengths to the channel in the landscape. The second theme relates to the importance of the spatial configuration of hydrological areas within the landscape.

The results from the modelling experiments show that the slope length, the slope gradient and the hydrological characteristics at the base of the slope are important in determining the form of the discharge hydrograph. An increase in the slope length decreases the runoff coefficient due to transmission losses following the cessation of rainfall. An increase in the slope gradient gives an increase in both the total and peak discharge. This is due the reduction in the soil depth, the reduction in the surface depression storage and the increase in flow velocity. This increase in velocity decreases the time available for transmission losses and hence leads to the increase in the discharge. The introduction of an area with a high infiltration capacity can significantly alter the discharge from a slope. The importance of the area is non-linearly related to the position on the slope.

The storm characteristics have a greater influence on the amount of runoff generation than the surface characteristics. The temporal structure of the rainfall intensities is important for determining the flow path distances of the overland flow. With highly fragmented rainfall, the flow paths will be short and little runoff will reach the channel. With longer periods of high intensity rainfall, the flow paths will be longer and there will be greater discharge from the slope. The discharge is most sensitive to changes in the rainfall intensity when the difference between the rainfall intensity and the infiltration capacity is small. The discharge is sensitive to changes in the duration over the range of 1 to 20 minutes. This relates to the time required to generate runoff and for it to reach the channel.

A unique picture of the source areas of channel flow during a storm event is given by the application of autonomous software agents which trace the movement of water through a catchment. The contributing area in the lower Cardena catchment was far larger than in the Sub 7 catchment. In the lower Cardena, the main areas were the steep slopes at the lower end of the catchment and the top sections of a number of gullies compared to Sub 7 where the channel flow was sourced from the channels and the lower sections of the slopes directly adjacent to the channel.

These research findings give insight to the nature of runoff generation processes at the hillslope and small catchment scale. This is important since many semi-arid areas are subject to intense rainfall and catastrophic flooding which is caused by the generation of runoff at the hillslope scale. This greater understanding can reduce the impact of flood events and hence will result in significant economic and social benefits.

A1. Field Data

A1.1 Rainfall Simulation Results

t (m)	1d	1w	2IB - d	2 IB - w	2 B -d	2 B - w	3d	3w	4d	4w	5 IBS - d	5 IBS - w
1			11	5	4	5	0	0	0	0	0	0
2			30	20	13	50	0				0	0
3			28	24	36	91	0			10	0	59
4		6.7	36	45	58	119	0		8		117	115
5			56	91	85	140	0				148	133
6		6.6	67	106	116	175	0	13		20	191	141
7			89	132	97	136	0				223	125
8	3.6	7.3	85	123	101	142	0		12	12	214	119
9			90	109	96	170	0	13			150	119
10	8.2	12.9	93	107	98		0		15	11	28	160
11		2.8	101	118	101		0				274	153
12	7.4		122	108	148		0	12	12	13	205	218
13		7.4	123	113	206		0				190	233
14	2.7		106	89	199	57	0		10		190	252
15		8.2	72	102	194	67	0	11			173	259
16	1.2		54	103	201	109				9	225	221
17		10.5	78	90	202	205	5	13	9		238	80
18			125	113	234	166					208	88
19			96	124	231	154	4			18	251	94
20	10		81	96	239	132			12		234	62
21			108	81	221	139	4	12		14	243	40
22			106	106	242	152					200	49
23	9.2		98	132	175	129	3	13	12	10	198	63
24			82	57	222	139					218	77
25			92.5	112	223	147	4				210	65
26	1.6		56	73	124	83			12.5	14	86	47
27			14	14	18	19		12			14	11
28			4	4	7	4						
29												
30	0		2	3	4	2	1	1	1	1	9	9

Continued on next page

t (m)	5 IBG - d	5 IBG - w	5 B - d	5 B - w	6 Cr - d	6 Cr - w	6 Co - d	6 Co - w	7d	7w
1	0	0	0	0		0	0	0	0	0
2	0	0	0	0		0.8	0	39	0	0
3	63	40	0	0		21	36	62	0	59
4	41	122	36	49		20	65	52	0	47
5	48.5	137	52	76		21	21	102	36	55
6		148	74	93		21	20	81	28	56
7	154	131	84	90		23	12	86	24	43
8	83.67	147	91	73		25	23	79	34	49
9	133	111	93	90		24	10	69	36	53
10	162	123	173	81		27	4.6	58	33	49
11	135	118	94	77		26	4	59	27	37
12	166	113	108	74		27	6.8	55	28	40
13	167	110	113	88		28	14	55	30	47
14	185	110	97	78		28	31	64	27	46
15	183	172	102	74		27	26	56	31	48
16	181	131	103	75		25	30	86	30	45
17	170	153	93	83		20	44	75	31	42
18	197	134	106	79	12.4	24	59	89	28	45
19	229	135	89	86		19.5	41	76	26	34
20	217	128	97	88	19	19.5	34	78	25	30
21	185	126	89	96	7.1	20	36	90	22	36
22	196	135	105	98	9.8	19	35	84	20	34
23	137	79	90	90	4.3	19	25	91	19	34
24	24	20	98	96	3.2	30	54	77	18	37
25			115	95	2.5	24	50	80	16	42
26			68	56		4.2	30	44	14	16.5
27	23	13	15	14		1.2	12	9.2	10	16.5
28									5.6	4.6
29										
30	0	0	10	8	0.3	0.1	4	5.5	4.8	4.2

Table A1.1 Rainfall simulation runoff volume (ml)

A1.2 Minidisk Infiltration Experiments

A1.2.1 Site 1

t (s)	Surface of base of furrow			Below surface, base of furrow			Furrow top, surface			Below surface, furrow top		
0	5	10	12	17	3	15	0	6	15	4	13	8
30	8	11	13.5	18	4.5	15.5	1	9	16	6	14	10
60	9	12	15	19	5.5	16			17	7	15	11
90	10	13	16.5	20	6	17	2	10	18		15.5	11.5
120	11	14	18	20.5	7		2.5			8	16.5	
150	11.5	14.5	20	21	8	19	3	11	19		17	13
180	12.5	15	21.5	22	9	18.5	3.5	11.5	20	9	18	14
210	13	16	23	22.5	9.5	19	4	12				
240	14	16.5	25	23	10	20		13	21	10	19	15
270	15	17	27	24	10.5	20.5	5		22	10.5		
300	16.5	18.5	29	25	11	21		13.5		11	20	16

Table A1.2 Minidisk experiment results from site 1. Volume of water infiltrated (ml).

A1.2.2 Site 2

t (s)	Inter bush						Bush				
0	1	0	10	22	29	29	3	5	9	16	25
30	4	2	12	26	32	32	4	6	10	18	
60	5	3	13.5	27	34	35					26
90	6	3.5	15	27.5	35.5	37			11	18.5	
120	6.5	4	16	28	36.5	39	4.5	6.5		19	
150	7.5	5.5	17	28.5	38	41			12		
180	8	6.5	18	29.5	39	43		7		19.5	
210	9	7	19	30	40	45			12.5	20	
240	10	8	20	31	40.5	47	5		13		
270	10.5	9	20.5	31.5	42	48			13.5		
300	11	10.5	22	32.5	43.5	49.5		7.5	14	20.5	26.5

Table A1.3 Minidisk experiment results from site 2. Volume of water infiltrated (ml).

A1.2.3 Site 3

t (s)	base of furrow			Below base of furrow			In furrow				Furrow top		
0	0	3	2	5	4	3	2	2	18	2	4	1	10
30	3	4.5	6	7		8	7	7	24	9	6		11
60	5	5.5	7	8	10	10.5	10	10	29	15	7.5	4	12
90	7	7	8	9	12	13	13	12	35	21	8.5		12.5
120	8.5	7.5	9	10	15.5	15	16	14.5	40	26	10	5	13
150	10	8	10.5	12	18	17	18	17	45	33	11	5.5	13.5
180	11	9	12	13	20	19	20	19.5	50	37	12	6	14
210	12	10	13.5	14.5	22.5	21	22	22	55	43	13.5	7	15
240	13	10.5	15	15.5	24	22	23.5	24	60	47	15	7.5	
270	14.5	11.5	16.5	16.5	26.5	23	25	26.5	65	53	16	8	16
300	16.5	13	18.5	18	28	25	26.5	29	70	58	17.5	9	

Table A1.4 Minidisk experiment results from site 3. Volume of water infiltrated (ml).

A1.2.4 Site 4

t (s)	crust	crust	Sub crust	Sub crust	slope crust	Sub crust	Sub crust	crust	below crust	crust	crust	below crust
0	8	6	2	10	4	1	3	6	2	4	3	2
30	9	9	9	15	9	7	10	7	8	6	5	7
60	10	10	13	20	10	10	14	7.5	12.5	7	7	11
90	10.5	11	17	23	12	13.5	18	8	16	8	8	15
120	12	11.5	21	26	13	17	22	9	20	9		19
150	13	12	24	29	14	20	25.5	10	23	10	9	22
180	14	12.5	27	31.5	15	23	29	11	26	11	10	25
210	15	13	31	34	16	26	32	11.5	29	12	12	27.5
240	16	14	34	37	17	29	36	12	32	13	13	30
270	16.5	15	37	39	18.5	32	39	13	35	13.5	14	32
300	18	15.5	40.5	41	19.5	35	43	13.5	37.5	14.5	15.5	35

Table A1.5 Minidisk experiment results from site 4. Volume of water infiltrated (ml).

A1.2.5 Site 5

t (s)	Bush				IB-G			IB-S			
0	3	11	22	11	7	10	9	3	18	9	19
30	4	11.5	23	15	7.5		11	7.5	22	13	22
60	5	12	24	16	8	10.5	12.5	8	23.5	15	23.5
90	5.5		24.5	17			13.5	8.5	24.5	17	24.5
120	6		25	18	8.5	11	15	10	26	18.5	25.5
150			26	20	9	13	16	11	27	20	27
180	7		27.5		10	14	17	12.5	28.5	22	27.5
210			29	21	10.5	14.5	18	13.5	30	23	29
240	7.5	12.5	30	22	11	15	19	15	31	24	30
270	8		31	23	12		20	16	32	25	31
300	8	13	32	24	13	15.5	21.5	17	34	27	32

Table A1.6 Minidisk experiment results from site 5. Volume of water infiltrated (ml).

A1.2.6 Site 6

t (s)	Compacted soil			On soil crust			Material below crust		
0	2	12	28.5	13	6	5	14	5	1
30	4	15	32	17.5	9	7	26	20	12
60	5	17	33.5	20	11	10	34	34	18
90	6	18	35	23	13	11	41	46	24
120	7	20	36	25.5	15	13.5	46	58	28
150	8	21	37	28	16	15	52	69	33
180	9	21.5	38	30	18	17	58	81	37
210	9.5	24	39	33	20	19	64	91	41
240	10	25	40	35	21.5	20.5	68	100	45
270	11	27	41	37	23	22	74		49
300	11.5	28.5	42	40	25	24	79		53

Table A1.7 Minidisk experiment results from site 6. Volume of water infiltrated (ml).

A1.2.7 Site 7

t (s)	IB	IB	IB	B	B	B
0	0	3	12	1	3	6
30	2	4	14	2		8
60	3		15.5			
90	3.5	4.5	16.5		3.5	
120	4	5	17.5			8.5
150	5	5.5	18			9
180	5.5	6	18.5		4	
210	6		19			
240	7	7	19.5			
270	7.5		20	2.5	4.5	9.5
300	8	7.5				

Table A1.8 Minidisk experiment results from site 7. Volume of water infiltrated (ml).

A1.3 Soil Texture

Simulation	Soil Depth (m)	Stones (%)	Sand (%)	Silt (%)	Clay (%)	Bulk Density
1d	0.29	44.69	38.67	14.95	0.65	1.34
1w	0.29	44.69	38.67	14.95	0.65	1.34
2 B w	0.28	60.43	30.63	7.97	0.52	1.22
2 B d	0.28	60.43	30.63	7.97	0.52	1.22
2 IB w	0.18	45.46	41.67	11.62	0.37	1.27
2IB d	0.18	45.46	41.67	11.62	0.37	1.27
3d	0.4	74.99	20.59	3.98	0.35	1.45
3w	0.4	74.99	20.59	3.98	0.35	1.45
4d	0.16	50.05	37.64	11.18	0.60	1.41
4w	0.16	50.05	37.64	11.18	0.60	1.41
5 B d	0.24	25.50	55.38	17.60	0.71	1.44
5 B w	0.24	25.50	55.38	17.60	0.71	1.44
5 IBG d	0.2	49.65	36.06	12.94	0.70	1.34
5 IBG w	0.2	49.65	36.06	12.94	0.70	1.34
5 IBS d	0.22	42.06	43.47	13.04	0.62	1.32
5 IBS w	0.22	42.06	43.47	13.04	0.62	1.32
6 Co d	0.26	53.28	30.79	14.22	1.36	1.21
6 Co w	0.26	53.28	30.79	14.22	1.36	1.21
6 Cr d	0.28	34.70	33.12	28.73	1.12	1.13
6 Cr w	0.28	34.70	33.12	28.73	1.12	1.13
7d	0.2	59.24	33.22	7.07	0.32	1.40
7w	0.2	59.24	33.22	7.07	0.32	1.40

Table A1.9 Soil texture information from the rainfall simulation plots

A1.4 Surface Cover

Simulation	Soil (%)	Stones (%)	Living biomass (%)	Dead Biomass (%)	Slope (°)
1d	56.9	39.7	2.0	1.5	19
1w	56.9	39.7	2.0	1.5	19
2 B w	2	0	98	0	29
2 B d	2	0	98	0	29
2 IB w	28.1	8.8	52.0	11.1	27
2IB d	28.1	8.8	52.0	11.1	27
3d	0.0	98.6	1.4	0.0	3
3w	0.0	98.6	1.4	0.0	3
4d	49.95	50.05	0.00	0.00	28
4w	49.95	50.05	0.00	0.00	28
5 B d	7.0	2.0	91.0	0.0	25
5 B w	7.0	2.0	91.0	0.0	25
5 IBG d	23.0	39.0	30.0	1.0	18
5 IBG w	23.0	39.0	30.0	1.0	18
5 IBS d	8.0	57.0	35.0	0.0	22
5 IBS w	8.0	57.0	35.0	0.0	22
6 Co d	68.0	32.0	0.0	0.0	2
6 Co w	68.0	32.0	0.0	0.0	2
6 Cr d	56.0	44.0	0.0	0.0	3
6 Cr w	56.0	44.0	0.0	0.0	3
7d	0.0	88.9	10.0	1.1	17.5
7w	0.0	88.9	10.0	1.1	17.5

Table A1.10 Surface cover composition information from the rainfall simulation plots

Reference List

Abbott, M. B., Bathurst, J. C., Cunge, J. A., O'Connell, P., and Rasmussen, J. 1986: An introduction to the European Hydrological System Systéme Hydrologique Europeen, 'SHE', 2: structure of a physically-based, distributed modelling system; *Journal of Hydrology*, 87, 61 - 77

Abrahams, A. D., Parsons, A. J., and Hirsch, P. J. 1992: Field and laboratory studies of resistance to interrill overland flow on semi-arid hillslopes, southern Arizona; in (eds.) Parsons, A. J. and Abrahams, A. D, UCL Press, London, 438

Abrahams, A. D., Parsons, A. J., and Luk, S. H. 1986: Resistance to overland flow on desert hillslopes; *Journal of Hydrology*, 88, 343 - 363

Abrahams, A. D., Parsons, A. J., and Luk, S. H. 1989: Distribution of depth of overland flow on desert hillslopes and its implications for modeling soil erosion; *Journal of Hydrology*, 106, 177 - 184

Abrahams, A. D. and Parsons, A. J. 1991: Relation between infiltration and stone cover on a semi-arid hillslope,Southern Arizona; *Journal of Hydrology*, 122, 49 - 59

Abrahams, A. D. and Parsons, A. J. 1994: Hydraulics of interrill overland flow on stone-covered desert surfaces; *Catena*, 23, 111 - 140

Abrahams, A. D., Parsons, A. J., and Luk, S. 1990: Field experiments on the resistance to overland flow on desert hillslopes; in (eds.) Walling, D. E., Yair, A., and Berkowicz, S., *Erosion, transport and deposition processes.(Proceedings of the Jerusalem Workshop, March-April 1987). International Association of Hydrological Sciences Publication number 189*, 1 - 18

Abrahams, A. D., Parsons, A. J., and Wainwright, J. 1994: Resistance to overland-flow on semiarid grassland and shrubland hillslopes, Walnut Gulch, Southern Arizona; *Journal of Hydrology*, 156, 431 - 446

AbuAwwad, A. M. and Shatanawi, M. R. 1997: Water harvesting and infiltration in arid areas affected by surface crust: examples from Jordan; *Journal of Arid Environments*, 37, 443 - 452

Agassi, M., Morin, J., and Shainberg, I. 1985: Effect of raindrop impact energy and water salinity on infiltration rates in sodic soils; *Soil Science Society of America*, 49, 186 – 190

Agassi, M. and Levy, G. J. 1991: Stone-cover and rain intensity: effects on infiltration, erosion and water splash.; *Australian Journal of Soil Research*, 29, 565 - 575

Ahnert, F. 1994: Randomness in geomorphological process response models; in (ed.) Kirkby, Mike, *Process models and theoretical geomorphology*, John Wiley and Sons Ltd, Chichester, 3 - 21

Allen, H. 2001: *Mediterranean Ecogeography*; Pearson Education Limited, Harlow, 263 pages

Allmaras, R., Burwell, R., Larson, W., and Holt, R. 1966: Total porosity and random roughness of the interrow zone as influenced by tillage; *United States Department of Agriculture Conservation Research Report*, 7 - 22

Alonso-Sarria, F., Lopez-Bermudez, F., and Conesa-Garcia, C. 2002: Synoptic conditions producing extreme rainfall events along the Mediterranean coast of the Iberian Peninsula; in (eds.) Bull, L and Kirkby, M., *Dryland Rivers: Hydrology and geomorphology of semi-arid channels*, John Wiley and Sons, Chichester, 351 - 372

Andersena, J., Refsgaard, J., and Jensen K 2001: Distributed hydrological modelling of the Senegal River Basin - model construction and validation; *Journal of Hydrology*, 247

Aston, A. R. 1979: Rainfall interception by eight small trees; *Journal of Hydrology*, 42, 383 - 396

Baird, A. J. 1997: Overland flow generatation and sediment mobilisation by water; in (ed.) Thomas, D. S. G., *Arid zone geomorphology*, John Wiley & Sons, Ltd, Chichester, 165 - 184

Barry, R. and Chorley, R. 1992: *Atmosphere, weather & climate*; Routledge, London, 392 pages

Becker, A. and Braun, P. 1999: Disaggregation, aggregation and spatial scaling in hydrological modelling; *Journal of Hydrology*, 217, 239 - 252

Bergkamp, G. 1998: A hierarchical view of the interactions of runoff and infiltration with vegetation and microtopography in semiarid shrublands; *Catena*, 33, 201 - 220

Bergkamp, G., Cammeraat, L. H., and Mertinez-Fernandez, J. 1996: Water movement and vegetation patterns on shrubland and an abandoned field in two desertification threatened areas in Spain; *Earth Surface Processes and Landforms*, 21, 1073 - 1090

Bergkamp, G., Cerdà, A., and Imeson, A. C. 1999: Magnitude-frequency analysis of water redistribution along a climate gradient in Spain.; *Catena*, 37, 129 - 146

Beven, K. 1984: Infiltration into a class of vertically non-uniform soils; *Hydrological Sciences Journal*, 29, 425 - 434

Beven, K. 1996: Equifinality and uncertainty in geomorphological modelling; in (eds.) Rhoads, B. and Thorn, C., *The Scientific Nature of Geomorphology*; John Wiley and Sons, Chichester, 289 - 313

Beven, K. 2000: *Rainfall-Runoff Modelling: The Primer*; John Wiley and Sons, Chichester, 360 pages

Beven, K. 2002a: Runoff generation in semi-arid areas; in (eds.) Bull, L and Kirkby, M., *Dryland rivers, Hydrology and geomorphology of semi-arid channels*, John Wiley and Sons, Chichester, 57 - 105

Beven, K. 2002b: Towards a coherent philosophy for modelling the environment; *Proceedings of the Royal Society London A*, 458, 2465 - 2484

Beven, K. and Freer, J. 2001: Equifinality, data assimilation, and uncertainty estimation in mechanistic modelling of complex environmental systems using the GLUE methodology; *Journal of Hydrology*, 249, 11 - 29

Beven, K. and Germann, P. 1982: Macropores and water-flow in soils; *Water Resources Research*, 18, 1311 - 1325

Blackburn, W. H. 1975: Factors influencing infiltration and sediment production of semiarid rangelands in Nevada.; *Water Resources Research*, 11, 929 - 937

Bradford, J. M. and Huang, C. 1992: Mechanisms of crust formation: physical components; in (eds.) Summer, M E and Stuart, B A, *Soil Crusting : Chemical and Physical Processes*, Lewis Publishers, Florida, 55 - 72

Brady, N. 1990: *The nature and properties of soils*; Maxwell Macmillan International, 968 pages

Brandt, C. J. 1989: The size distribution of throughfall drops under vegetation canopies.; *Catena*, 16, 507 - 524

Bresson, L.-M. and Boiffin, J. 1990: Morphological characterization of soil crust development on an experimental field; *Geoderma*, 47, 301 - 325

Bromley, J., Brouwer, J., Barker, A. P., Gaze, S. R., and Valentin, C. 1997a: The role of surface water redistribution in an area of patterned vegetation in a semi-arid environment, south-west Niger; *Journal of Hydrology*, 198, 1 - 29

Bromley, J., Brouwer, J., Barker, A. P., Gaze, S. R., and Valentin, C. 1997b: The role of surface water redistribution in an area of patterned vegetation in a semi-arid environment, south-west Niger; *Journal of Hydrology*, 198, 1 - 29

Bryan, R. and Poesen, J. 1989: Laboratory experiments on the influence of slope length on runoff, percolation and rill development; *Earth Surface Processes and Landforms*, 14, 231

Bull, L., Kirkby, M., and Shannon, J. in press: Predicting Hydrological Response Units (HRUs) in semi-arid environments; *Advances in Monitoring and Modelling*

Bull, L., Kirkby, M., Shannon, J., and Hooke, J. 2000: The impact of rainstorms on floods in ephemeral channels in southeast Spain; *Catena*, 38, 191 - 209

Burrough, P. A. and McDonnell, R. A. 1998: *Principles of Geographical Information Systems*; Oxford University Press, Oxford, 333 pages

Calder, I. R. 1986: A stochastic model of rainfall interception; *Journal of Hydrology*, 89, 65 - 74

Calder, I. R. 1996: Dependence of rainfall interception on drop size: 1. Development of the two-layer stochastic model; *Journal of Hydrology*, 185, 363 - 378

Calder, I. R., Wright, I. R., and Murdiyarso, D. 1986: A study of evaporation from tropical rain forest - West Java; *Journal of Hydrology*, 89, 13 - 31

Camarada, A. and Segura, F. 2001: Flood events in Mediterranean ephemeral streams (ramblas) in Valencia region, Spain; *Catena*, 45, 229 - 249

Cameron, D., Beven, K., and Tawn, J. 2000: Modelling extreme rainfalls using a modified random pulse Bartlett-Lewis stochastic rainfall model (with uncertainty); *Advances In Water Resources*, 24, 203 - 211

Cammeraat, L. H. and Imeson, A. C. 1998: Deriving indicators of soil degradation from soil aggregation studies in SE Spain and S France; *Geomorphology*, 23, 307 - 321

Cammeraat, L. H. and Imeson, A. C. 1999: The evolution and significance of soil-vegetation patterns following land abandonment and fire in Spain; *Catena*, 37, 107 - 127

Carbonneau, P. E., Lane, S. N., and Bergeron, N. E. 2003: Cost-effective non-metric close-range digital photogrammetry and its application to a study of coarse gravel river beds; *International Journal of Remote Sensing*, 24, 2837 - 2854

Carsel, R. and Parrish, R. 1988: Developing joint probability distributions of soil water retention characteristics; *Water Resources Research*, 24, 755 - 769

Cerdá, A. 1995: Spatial distribution of infiltration on the matorral slopes in a Mediterranean environment, Geoves, Spain; in (eds.) Fantechi, R., Pete, D., Blabanis, P., and Rubio, J., *Desertification in an European context: Physical and socio-economic aspects*, European Commision, Brussels, 427 - 436

Cerdá, A. 1997: The effect of patchy distribution of Stipa tenacissima L. on runoff and erosion; *Journal of Arid Environments*, 36, 37 - 51

Cerdá, A. 1998: Changes in overland flow and infiltration after a rangeland fire in a Mediterranean scrubland; *Hydrological Processes*, 12, 1031 - 1042

Cerdá, A. 1999: Seasonal and spatial variations in infiltration rates in badland surfaces under Mediterranean climatic conditions; *Water Resources Research*, 35, 319 - 328

Cerdá, A. 2001: Effects of rock fragment cover on soil infiltration, interrill runoff and erosion; *European Journal of Soil Science*, 52, 59 - 68

Cerdá, A., Ibanez, S., and Calvo, A. 1997a: Design and operation of a small and portable rainfall simulator for rugged terrain; *Soil Technology*, 11, 163 - 170

Cerdá, A., Imeson, A. C., and Calvo, A. 1995: Fire and aspect induced differences on the erodibility and hydrology of soils at la-Costera, Valencia, southeast Spain; *Catena*, 24, 289 - 304

Cerdá, A., Schabel, S., Ceballos, A., and Gomez-Amelia, D. 1997b: Soil hydrological response under simulated rainfall in the Dehesa land system (Extremadura, SW Spain) under drought conditions; *Earth Surface Processes and Landforms*, 23, 195 - 209

Chaplot, V. and Le Bissonnais, Y. 2000: Field measurements of interrill erosion under different slopes and plot sizes; *Earth Surface Processes and Landforms*, 25, 145 - 153

Chase, C. G. 1992: Fluvial Landsculpting and the Fractal Dimension of Topography; *Geomorphology*, 5, 39 - 57

Cho, S. M. and Lee, M. 2001: Sensitivity considerations when modeling hydrologic processes with digital elevation model; *Journal of the American Water Resources Association*. 37, 931 - 934

Corte-Real, J., Sorani, R., and Conte, M. 1998: Climate change; in (eds.) Mairota, P. Thornes. J., and Geeson, N, *Atlas of Mediterranean Environment in Europe: The Desertification Context*, Wiley, Chichester, 34 - 37

Costa-Cabral, M. C. and Burges, S. 1994: Digital elevation model networks (DEMON): A model of flow over hillslopes for computation of contributing and dispersal areas; *Water Resources Research*, 30, 1681 - 1692

Cremers, N., van Dijk, P., de Roo, A., and Verzandvoort, M. 1996: Spatial and temporal variability of soil surface roughness and the application in hydrological and soil erosion modelling; *Hydrological Processes*, 10, 1035 - 1047

Darboux, F., Davy, P., and Gascuel-Odoux, C. 2002: Effect of depression storage capacity on overland-flow generation for rough horizontal surfaces: water transfer and scaling; *Earth Surface Processes and Landforms*, 27, 177 - 191

De Ploey, J. and Poesen, J. 1985: Aggregate stability, runoff generation and interrill erosion; in (eds.) Richards, K. S., Arnett, R. R., and Ellis, S., *Geomorphology and Soils*, Allen and Unwin, London, 99 - 120

De Ploey, J., Savat, J., and Moeyersons, J. 1976: The differntial impact of some soil loss factors on flow, runoff creep and rainwash; *Earth Surface Processes*, 1, 151 - 161

Descroix, L., Viramontes, D., Vauclin, M., Barrios, J. L. G., and Esteves, M. 2001: Influence of soil surface features and vegetation on runoff and erosion in the Western Sierra Madre (Durango, Northwest Mexico); *Catena*, 43, 115 - 135

Dingman, S. L. 1994: *Physical Hydrology*; Prentice Hall, New Jersey, 575 pages

Doerr, S. H., Shakesby, R. A., and Walsh, R. P. D. 1996: Soil hydrophobicity variations with depth and particle size fraction in burned and unburned Eucalyptus globulus and Pinus pinaster forest terrain in the Agueda Basin, Portugal; *Catena*, 27, 25 - 47

Domingo, F., Sanchez, G., Moro, M. J., Brenner, A. J., and Puigdefabregas, J. 1998: Measurement and modelling of rainfall interception by three semi-arid canopies; *Agricultural and Forest Meteorology*, 91, 275 - 292

Douglas, T., Kirkby, S., Critchley, R., and Park, G. 1994: Agricultural terrace abandonment in the Alpujarra, Andalucia, Spain; *Land Degradation and Rehabilitation*, 5, 281 - 291

Dunkerley, D. and Brown, K. 1999: Flow behaviour, suspended sediment transport and transmission losses in a small (Sub-bank-full) flow event in an Australian desert stream; *Hydrological Processes*, 13, 1577 - 1588

Dunkerley, D. L. 1999: Banded chenopod shrublands of arid Australia: modelling responses to interannual rainfall variability with cellular automata; *Ecological Modelling*, 121, 127 - 138

Eldridge, D. J. 1993: Effect of ants on sandy soils in semi-arid eastern Australia: Local distribution of nest entrances and their effect on infiltration of water; *Australian Journal of Soil Research*, 31, 509 - 518

Eldridge, D. J. 1994: Nests of Ants and Termites Influence Infiltration in a Semiarid Woodland; *Pedobiologia*, 38, 481 - 492

Emerson, W. W. 1995: Water retention, organic C and soil texture; *Australian Journal of Soil Research*, 33, 241 - 251

Endreny, T. A. and Wood, E. F. 2001: Representing elevation uncertainty in runoff modelling and flowpath mapping; *Hydrological Processes*, 15, 2223 - 2236

Esteban-Parra, M., Rodrigo, F., and Castro-Diez, Y. 1998: Spatial and temporal patterns of precipitation in Spain for the period 1880 - 1992; *International Journal of Climatology*, 18, 1557 - 1574

Ewen, J. 2000: Moving packet model for variably saturated flow; *Water Resources Research*, 36, 2587 - 2594

Fairfield, J. and Leymarie, P. 1991: Drainage networks from grid digital elevation models; *Water Resources Research*, 27, 709 - 717

Farres, P. 1978: The role of time and aggregate size in the crusting process; *Earth Surface Processes*, 3, 243 - 254

Favis-Mortlock, D. 1998: A self-organizing dynamic systems approach to the simulation of rill initiation and development on hillslopes; *Computers & Geosciences*, 24, 353 - 372

Favis-Mortlock, D. T., Boardman, J., Parsons, A. J., and Lascelles, B. 2000: Emergence and erosion: a model for rill initiation and development; *Hydrological Processes*, 14, 2173 - 2205

Fiedler, F. R., Frasier, G. W., Ramirez, J. A., and Ahuja, L. R. 2002: Hydrologic response of grasslands: Effects of grazing, interactive infiltration, and scale; *Journal of Hydrologic Engineering*, 7, 293 - 301

Fitzjohn, C., Ternan, J. L., and Williams, A. G. 1998: Soil moisture variability in a semi-arid gully catchment: implications for runoff and erosion control; *Catena*, 32, 55 - 80

Flake, G. 1998: Autonomous Agent and Self-Organization, *The computational beauty of nature: Computer explorations of fractals, chaos, complex systems, and adaptation*, A Bradford Book, The MIT Press, Cambridge, Massachusetts, 261 - 279

Flügel, W. A. 1995: Delineating hydrological response units by geographical information system analysis for regional hydrolgogical modelling using PRMS/MMS in drainage basin of the river Brol, Germany; *Hydrological Processes*, 9, 423 - 436

Flügel, W. A. 1997: Combining GIS with regional hydrological modelling using hydrological response units (HRUs): An application from Germany; *Mathematics and Computers in Simulation*, 43, 297 - 304

Fox, D. M., Le Bissonnais, Y., and Bruand, A. 1998: The effect of ponding depth on infiltration in a crusted surface depression; *Catena*, 32, 87 - 100

Fox, D. M., Bryan, R. B., and Price, A. G. 1997: The influence of slope angle on final infiltration rate for interrill conditions; *Geoderma*, 80, 181 - 194

Freeman, T. 1991: Calculating catchment area with divergent flow based on a regular grid; *Computers and Geoscience*, 17, 413 - 422

Gabriels, D. 1999: The effect of slope length on the amount and size distribution of eroded silt loam soils: short slope laboratory experiments on interrill erosion: *Geomorphology*, 28, 169 - 172

Gallant, J. C. and Wilson, J. P. 1996: TAPES-G: A grid based terrain analysis program for the environmental sciences; *Computers and Geosciences*, 22, 713 - 722

Garcia-Sanchez, L., Di Pietro, L., and Germann, P. 1996: Lattice-gas approach to surface runoff after rain; *European Journal of Soil Science*, 47, 453 - 462

Gash, J. H. C. 1979: An analytical model of rainfall interception by forests; *Journal of the Royal Meteorological Society*, 105, 43 - 55

Gilley, J., Flanagan, D., Kottwitz, E., and Weltz, M. 1992: Darcy-Weisbach roughness coefficients for overland flow; in (eds.) Parsons, A. J. and Abrahams, A. D, *Overland flow*, UCL Press, London, 25 - 52

Gomez, J. A., Giraldez, J. V., and Fereres, E. 2001: Rainfall interception by olive trees in relation to leaf area; *Agricultural Water Management*, 49, 65 - 76

Goodess, C. M. and Palutikof, J. P. 1998: Development of daily rainfall scenarios for southeast Spain using a circulation-type approach to downscaling; *International Journal of Climatology*, 18, 1051 - 1083

Goodess, C., Mariani, L., Palutikof, J., Menichini, V., and Minardi, G. 1998: Estimating Future Climates in the Mediterranean; in (eds.) Mairota, P, Thornes, J., and Geeson, N, *Atlas of Mediterranean Environment in Europe: The Desertification Context*, Wiley, Chichester, 38 - 43

Goodrich, D., Lane, L. J., Shillito, R., Miller, S., Syed, K., and Woolhier, D. 1997: Linearity of basin response as a function of scale in a semi-arid watershed; *Water Resources Research*, 33, 2951 - 2965

Govers, G. 1991: A field study on topographical and topsoil effects on runoff generation.; *Catena*, 18, 91 - 111

Green, W. and Ampt, G. 1911: Studies in soil physics. Part I. - The flow of air and water through soils; *Journal of Agricultural Science*, 4, 1 - 24

Greene, R., Chartres, C., and Hodgkinson, K. 1990: The effect of fire on the soil in a degraded semi-arid woodland, I: physical and micromorphological properties; *Australian Journal of Soil Research*, 28, 755 - 777

Grove, A. 1996: Physical, Biological and Human Aspects of Environmental Change, vol. Contract number EV5V 0128, MEDALUS II Report, European Commission pp 39 - 64

Haff, P. 2001: Waterbots; in (eds.) Harmon, R and Doe, W, *Landscape Erosion and Evolution Modeling*, Kluwer Academic / Plenum Publishers, New York, 239 - 275

Hall, R. L. 1992: An improved numerical implementation of the Calder stochastic model of rainfall interception – a note; *Journal of Hydrology*, 140, 389 - 392

Hall, R. L., Calder, I., Rosier, P., Swaminath, M., and Mumtaz, J. 1992: Measurements and modelling of interception loss from a Eucalyptus plantation in southern India; in (eds.) Calder, I R, Hall, R L, and Adlard, P G, *Growth and Water Use of Forest Plantations. Proceedings of the International Symposium on the Growth and Water Use of Forest*

Plantations, Bangalore, 7-11 February 1991, John Wiley and sons, Chichester, 270 - 289

Hall, R. L., Calder, I. R., Gunawardena, E. R. N., and Rosier, P. T. W. 1996: Dependence of rainfall interception on drop size .3. Implementation and comparative performance of the stochastic model using data from a tropical site in Sri Lanka; *Journal of Hydrology*, 185, 389 - 407

Hangen, E., Buczko, U., Bens, O., Brunotte, J., and Huttl, R. F. 2002: Infiltration patterns into two soils under conventional and conservation tillage: influence of the spatial distribution of plant root structures and soil animal activity; *Soil and Tillage Research*, 63, 181 - 186

Hansen, B., Schonning, P., and Sibbesen, E. 1999: Roughness indices for estimation of depression storage capacity of tilled soil surfaces; *Soil and Tillage Research*, 52, 103 - 111

Herwitz, S. and Slye, R. 1995: Three dimensional modelling of canopy tree interception of wind driven rainfall; *Journal of Hydrology*, 168, 205 - 226

Holmgren, P. 1994: Multiple flow direction algorithms for runoff modelling in grid based elevation models: An empirical evaluation; *Hydrological Processes*, 8, 327 - 334

Hughes, D. and Sami, K. 1992: Transmission losses to alluvium and associated moisture dynamics in a semi-arid ephemeral channel system in South Africa; *Hydrological Processes*, 6, 45 - 53

Hypanen, H. 1996: Spatial autocorrelation and optimal spatial resolution of optical remote sensing data in boreal forest environment; *International Journal of Remote Sensing*, 17, 3441 - 3452

Imeson, A. C., Verstranten, J. M., Van Mulligen, E. J., and Sevink, J. 1992: The effects of fire and water repellency on infiltration and runoff under mediteranean type forest; *Catena*, 19, 345 - 361

IPCC 2001: *Climate Change 2001: The scientific basis : contribution of Working Group I to the third assessment report of the Intergovernmental Panel on Climate Change*; Cambridge University Press, New York, 881 pages

Joel, A., Messing, I., Seguel, O., and Casanova, M. 2002: Measurement of surface water runoff from plots of two different sizes; *Hydrological Processes*, 16, 1467 - 1478

Johnson, B., Julien, P., Molnar, D., and Watson, C. 2000: The two-dimensional Upland erosion model CASC2D-SED; *Journal of The American Water Resources Association*, 36, 31 - 42

Khaliq, M. N. and Cunnane, C. 1996: Modelling point rainfall occurrences with the Modified Bartlett-Lewis Rectangular Pulses Model; *Journal of Hydrology*, 180, 109 - 138

Kirkby, M. 1975: Hydrograph modelling strategies; in (eds.) Peel, R, Chisholm, M, and Haggett, P, *Processes in Human and Physical Geography*, Heinemann, London, 69 - 90

Kirkby, M. 1985: Hillslope hydrology; in (eds.) Anderson, MG. and Burt, TP, *Hydrological Forecasting*, John Wiley and sons, Chichester, 3 - 37

Kirkby, M. 1990: A simulation model for desert runoff and erosion, *Erosion, transport and deposition processes (Proceedings of the Jerusalem Workshop, March-April 1987)*, 87 - 104

Kirkby, M., Baird, A., Biamond, S., Lockwood, J., McMahon, M., Mitchell, P., Shao, J., Sheehy, J., Thornes, J., and Woodward, F. 1996: The MEDALUS slope catena model: A physically based process model for hydrology, ecology and land degradation; in (eds.) Brandt, C. and Thornes, J., *Mediterranean Desertification and Land Use*, John Wiley and Sons, 303 - 354

Kite, G. W. and Kouwen, N. 1991: Watershed modeling using land classification; *Water Resources Research*, 28, 3193 - 3200

Knighton, D. 1984: *Fluvial Forms and Processes*; Arnold, 218 pages

Kunze, R. J. and Nielsen, D. R. 1983: Comparison of soil water infiltration profiles obtained experimentally and by solution of Richards' equation; *Soil Science*, 135, 342 - 349

Kutiel, P., Lavee, H., and Ackermann, O. 1998: Spatial distribution of soil surface coverage on north and south facing hillslopes along a Mediterranean to extreme arid climatic gradient; *Geomorphology*, 23, 245 - 256

Lal, R. 1976: Soil erosion of Aldisols in western Nigeria. Effects of slope, crop rotation and residue management; *Geoderma*, 16, 363 - 375

Lal, R. 1997: Soil degradative effects of slope length and tillage methods on alfisols in western Nigeria. III. Soil physical properties; *Land Degradation & Development*, 8, 325 - 342

Lane, S. and Richards, K. 2001: The 'Validation' of Hydrodynamic Models: Some Critical Perspectives; in (eds.) Anderson, M and Bates, P, *Model Validation: Perspectives in Hydrological Science*, John Wiley and Sons, Chichester, 413 - 438

Lange, J. and Leibundgut, C. 1997: Using artificial tracers to study water losses of ephemeral floods in small arid streams; in (eds.) Leibundgut, C, Gunn, J, and Dassargues, A, *Karst Hydrology (Proceeding of Workshop W2 held at Rabat, Morocco, AprilMay 1997*, IHAS Publication Number 247, 31 - 40

Lasanta, T., Garcia-Ruiz, J. M., Perez-Rontome, C., and Sancho-Marcen, C. 2000: Runoff and sediment yield in a semi-arid environment: the effect of land management after farmland abandonment; *Catena*, 38, 265 - 278

Le Bissonnais, Y. 1990: Experimental study and modelling of soil surface crusting processes.; *Catena Supplement*, 17, 13 - 28

Le Bissonnais, Y. 1996: Aggregate stability and assessment of soil crustability and erodibility: I. Theory and methodology; *European Journal of Soil Science*, 47, 425 - 437

Lea, N. J. 1992: An aspect driven kinematic routing algorithm; in (ed.) Abrahams, A. D, *Overland Flow: Hydraulics and Erosion Mechanics*, Chapman and Hall, New York, 393 - 407

Leonard, J. and Andrieux, P. 1998: Infiltration characterisitcs of soils in Mediterranean vineyards in Southern France; *Catena*, 32, 209 - 223

Leonard, R. E. 1967: Mathematical theory of interception; in (eds.) Sopper and Lull, *Forest Hydrology*, Pergamon, Oxford, 131 - 136

Li, T., Xiao, H. L., and Li, X. R. 2001: Modeling the effects of crust on rain infiltration in vegetated sand dunes in arid desert; *Arid Land Research and Management*, 15, 41 - 48

Linden, D. and Van Doren, D. 1986: Parameters for characterizing tillage-induced soil surface roughness; *Soil Science Society of America*, 50, 1560 - 1565

Linden, D., Van Doren, D., and Allmaras, R. 1988: A model of the effects of tillage-induced soil surface roughness on erosion, *Proceedings of the 11th International Conference of the International Soil and Tillage Research Organization. Edinburgh, 1*, 373 - 378

Lopez-Bermudez, F., Conesa-Garcia, C., and Alonso-Sarria, F. 2002: Floods: Magnitude and frequency in ephemeral streams of the Spanish Mediterranean region; in (eds.) Bull, L and Kirkby, M., *Dryland Rivers: Hydrology and Geomorphology of Semi-Arid Channels*, John Wiley and sons, Chichester, 329 - 350

Lyford, F. P. and Qashu, H. K. 1969: Infiltration rates as influenceed by desert vegetation.; *Water Resources Research*, 5, 1373 - 1376

Magunda, M., Larson, C., Linden, D., and Nater, E. 1997: Changes in microrelief and their influences on infiltration and erosion during simulated rainfall; *Soil Technology*, 10, 57 - 67

Mah, M., Douglas, L., and Ringrose-voase, A. 1992: Effects of crust development and surface slope on erosion by rainfall; *Soil Science*, 154, 37 - 43

Manley, R. 1977: The soil mositure component of mathematical catchment simulation model; *Journal of Hydrology*, 35, 341 - 356

Massman, W. J. 1980: Water storage on forest foliage: A general model; *Water Resources Research*, 16, 210 - 216

Mein, R. G. and Larson, C. L. 1973: Modelling infiltration during a steady rain.; *Water Resources Research*, 9, 384 - 394

Meyer, L. and Wischmeier, W. 1969: Mathematical simulation of the process of soil erosion by water; *Transactions of the American Society of Agricultural Engineers*, 12, 754 - 758

Miller, C. T., Williams, G. A., Kelley, C. T., and Tocci, M. D. 1998: Robust solution of Richards' equation for non uniform porus media; *Water Resources Research*, 34, 2599 - 2610

Moore, I. D., Grayson, R. B., and Ladson, A. R. 1991: Digital terrain modelling: a review of hydrological, geomorphological, and biological applications.; *Hydrological Processes*, 5, 3 - 30

Moore, I. D. and Larson, C. 1979: Estimating micro-relief surface storage from point data; *Transactions of the American Society of Agricultural Engineers*, 10478

Moore, I. D., Lewis, A., and Gallant, J. C. 1993: Terrain attributes: estimation methods and scale effects.; in (eds.) Jakeman, A. J., Beck, M. B., and McAleer, M. J., *Modelling change in environmental systems.*, John Wiley & Sons Ltd., Chichester, 189 - 214

Morgan, R. P. C. 1995: *Soil erosion and conservation*; Longman, Essex, 198 pages

Mulder 1985: Simulating interception loss using standard meteorological data; in (eds.) Hutchison and Hicks, *The Forest-Atmosphere Interaction*, 177 - 196

Mulligan, M. 1996: Modelling the complexity of land surface response to climate variability in Mediterranean environments; in (eds.) Anderson, M. and Brooks, S.: *Advances in Hillslope Processes*: John Wiley and Sons, Chichester, 1099 - 1149

Mulligan, M. and Reaney, S. 2000: PatternLite, A policy relevant version of Pattern for Modulus; in (eds.) Engelen, G, van der Meulen, M. Hahn. B. Uljee. I, Mulligan. M. Reaney, S, Oxley, T, Blatsou, C, Mata-Porras, M, Kahrimanis, S, Giannoulopoulos. P. Mazzoleni, S, Coppola, A, Winder. N. van der Leeuw, S, and McIntosh. B. S.. *MODULUS: A Spatial Modelling Tool for Integrated Environmental Decision Making. Final Report, The Modulus Project, EU-DGXII Environment (IV) Framework. Climatology and Natural Hazards Programme, Contract ENV4-CT97-0685, July 2000*, 145 - 202

Mulligan, M. and Thornes, J. in press: Catena versus cellular approaches to hydrological modelling through the plant communiy in seasonally dry and dry environments; Journal of Hydrology

Navar, J., Carlyle-Moses, D. E., and Martines, A. 1999: Interception loss from the tamaulipan matorral thornscrub of north-eastern Mexico: an application of the Gash analytical interception loss model; *Journal of Arid Environments*, 41, 1 - 10

Navar, J., Mendez, J., Bryan, R. B., and Kuhn, N. J. 2002: The contribution of shrinkage cracks to bypass flow during simulated and natural rainfall experiments in northeastern Mexico; *Canadian Journal of Soil Science*, 82, 65 - 74

Neff, E. 1979: Why rainfall simulation?, *Proc. Rainfall Simulator Workshop, Tucson, Ariz. March 7-9, 1979, USDA-SEA Agr. Rev. and Manuals. ARM-W-IO.*, 3 - 7

Nicolau, J. M., Sole, A., Puigdefabregas, J., and Gutierrez, L. 1996: Effects of soil and vegetation on runoff along a catena in semi-arid Spain; *Geomorphology*, 297 - 309

O'Callaghan, J. F. and Mark, D. M. 1984: The extraction of drainage networks from digital elevation data; *Computer Vision, Graphics and Image Processing*, 28, 323 - 344

Oades, J. M. 1993: The role of biology in the formation, stabilization and degradation of soil structure.; *Geoderma*, 56, 377 - 400

Oliver, M. and Webster, R. 1986: Semi-variograms for modelling the spatial pattern of landform and soil properties; *Earth Surface Processes and Landforms*, 11, 491 - 504

Onstad C 1984: Depressional storage on tilled soil surfaces; *Transactions of the American Society of Agricultural Engineers*, 729 - 732

Pariente, S. 2002: Spatial patterns of soil moisture as affected by shrubs, in different climatic conditions; *Environmental Monitoring and Assessment*, 73, 237 - 251

Parlange, J. Y., Barry, D. A., Parlange, M. B., Hogarth, W. L., Haverkamp, R., Ross, P. J., Ling, L., and Steenhuis, T. S. 1997: New approximate analytical techique to solve Richards equation for arbitary surface boundary conditions; *Water Resources Research*, 33, 903 - 906

Parsons, A. J., Wainwright, J., Stone, P. M., and Abrahams, A. D. 1999: Transmission losses in rills on dryland hillslopes; *Hydrological Processes*, 13, 2897 - 2905

Passioura, J. B. 1991: Soil structure and plant growth; *Australian Journal of Soil Research*, 29, 717 - 728

Pearce, A. J. 1987: A stochastic model of rainfall interception - Comment; *Journal of Hydrology*, 89, 371 - 372

Philip, J. R. 1957: The theory of infiltration 4: Sorpivity and algebraic infiltration equations; *Soil Science*, 84, 257 - 264

Poesen, J. 1984: The influence of slope angle on infiltration rate and Hortonian overland flow volume; *Zeitschrift für Geomorphologié Supplementband*, 49, 117 - 131

Poesen, J., Ingelmo-Sanchez, F., and Mucher, H. 1990: The hydrological response of soil surfaces to rainfall as influenceed by cover and position of rock fragments in the top layer; *Earth Surface Processes and Landforms*, 15, 653 - 671

Poesen, J., Van Dekerckhove, J., Nachtergaele, J., Oostwoud Wijdenes, D., Verstraeten, G., and Van Wesemael, B. 2002: Gully erosion in dryland environments; in (eds.) Bull, L and Kirkby, M., *Dryland Rivers:Hydrology and Geomorphology of semi-arid channels*, John Wiley and Sons, Chichester, 329 - 262

Poesen, J. and Hooke, J. M. 1997: Erosion, flooding and channel management in Mediterranean environments of southern Europe; *Progress in Physical Geography*, 21, 157 - 199

Poesen, J. and Lavee, H. 1994: Rock fragments in top soils: significance and processes; *Catena*, 23, 1 - 28

Poesen, J., Van Wesemael, B., Govers, G., MartinezFernandez, J., Desmet, P., Vandaele, K., Quine, T., and Degraer, G. 1997: Patterns of rock fragment cover generated by tillage erosion; *Geomorphology*, 18, 183 - 197

Poesen, J., Van Wesemael, B., Bunte, K., and Sol,-Benet, A. 1998: Variation of rock fragment cover and size along semiarid hillslopes: a case-study from southeast Spain.; *Geomorphology*, 23, 323 - 335

Puigdefabregas, J., Barrio, G., Boer, M., Gutierrez, L., and Sole, A. 1998: Differential responses of hillslope and channel elements to rainfall events in a semi-arid area; *Geomorphology*, 23, 337 - 351

Puigdefabregas, J. and Sanchez, G. 1996: Geomorphological implications of vegetation patchiness on semi-arid slopes; in (eds.) Anderson, M. G. and Brooks, S. M., *Advances in Hillslope Processes*, John Wiley & Sons, London, 1027 - 1060

Quinn, P., Beven, K., Chevallier, P., and Planchon, O. 1991: The prediction of hillslope flow paths for distributed hydrolgical modelling using digital terrain models; *Hydrological Processes*, 5, 59 - 79

Quinn, P., Beven, K., and Lamb, R. 1995: The ln(a/tan beta) index: How to calculate it and how to use it within the TOPMODEL framework; *Hydrological Processes*, 9, 161 - 182

Quinton, J. N., Edwards, G. M., and Morgan, R. P. C. 1997: The influence of vegetation species and plant properties on runoff and soil erosion: results from a rainfall simulation study in south east Spain.; *Soil Use and Management*, 13, 143 - 148

Rawls, W., Brakensiek, D., and Miller, N. 1983: Green-Ampt infiltration parameters from soil data; *Journal of the Hydraulics Division, American Society of Civil Engineers*, 109, 62 - 70

Reynolds, J. F. and Acock, B. 1-1-1997: Modularity and genericness in plant and ecosystem models; *Ecological Modelling*, 94, 7 - 16

Richards, L. A. 1931: Capillary conduction of liquids through porous mediums; *Physics*, 1. 318 - 333

Rieger, W. 1993: Hydrological terrain features derived from a pyramid raster structure, *HydroGIS 93: Application of Geographic Information Systems in Hydrology and Water Resources (Proceedings of the Vienna Conference, April 1993)*, International Association of Hydrological Sciences, 201 - 210

Rodrigo, F. S., Esteban-Parra, M. J., Pozo-Vazquez, D., and Castro-Diez, Y. 2000: Rainfall variability in southern Spain on decadal to centennial time scales; *International Journal of Climatology*, 20, 721 - 732

Romero, R., Guijarro, J. A., Ramis, C., and Alonso, S. 1998: A 30-year daily rainfall data base for the Spanish Mediterranean regions: first exploratory study; *International Journal of Climatology*, 18, 541 - 560

Römkens, M. and Wang, J. 1986: Effects of tillage on surface roughness; *Transactions of the American Society of Agricultural Engineers*, 84-2026

Ruecker, G., Schad, P., Alcubilla, M. M., and Ferrer, C. 1998: Natural regeneration of degraded soils and site changes on abandoned agricultural terraces in Mediterranean Spain; *Land Degradation & Development*, 9, 179 - 188

Rutter, A. J., Kershaw, Robins, P., and Morton, A. J. 1971: A predictive model of rainfall interception in forests I: Derivation of the model from observations in a plantation of Corsican pine; *Agricultural Meteorology*, 9, 267 - 284

Rutter, J. A., Morton, A. J., and Robins, P. C. 1975: A predictive model of rainfall interception in forests. II. Generalization of the model and comparison with observations in some coniferous and hardwood stands; *Journal of Applied Ecology*, 12, 367 - 380

Sanchez, G. and Puigdefabregas, J. 1994: Interactions of Plant-Growth and Sediment Movement on Slopes in A Semiarid Environment; *Geomorphology*, 9, 243 - 260

Scoging, H., Parsons, A. J., and Abrahams, A. D. 1992: Application of a dynamic overland-flow model to a semi-arid hillslope, Walnut Gulch, Arizona; in (eds.) Parsons, A. J. and Abrahams, A. D., *Overland flow: Hydraulics and Erosion Mechanics*, UCL, London, 105 - 145

Scoging, H. and Thornes, J. B. 1980: Infiltration characteristics in a semiarid environment, IAHS 128, 159 - 168

Seghieri, J., Galle, S., Rajot, J. L., and Ehrmann, M. 1997: Relationships between soil moisture and growth of herbaceous plants in a natural vegetation mosaic in Niger.; *Journal of Arid Environments*, 36, 87 - 102

Seyfried, M. 1991: Infiltration patterns from simulated rainfall on a semiarid rangeland soil; *Soil Science Society of Amercia*, 55, 1726 - 1734

Shannon, J., Richardson, R., and Thornes, J. B. 2002: Modelling event-based fluxes in ephemeral stream; in (eds.) Bull, L and Kirkby, M., *Dryland Rivers: Hydrology and geomorphology of semi-arid channels*, John Wiley and Sons, Chichester, 129 - 172

Shen, H. and Li, R. 1973: Rainfall effect on sheet flow over smooth surface; *Journal of the Hydraulics Division, American Society of Civil Engineers*, 99, 771 - 792

Stroustrup, B. 1997: *The C++ Programming Language*; Addison-Wesley, 928 pages

Swartzendruber, D. and Hillel, D. 1975: Infiltration and run-off for small field plots under constant rainfall intensity; *Water Resources Research*, 11, 445 - 451

Tackett, J. L. and Pearson, R. W. 1965: Some characteristics of soil crusts formed by simulated rainfall; *Soil Science*, 99, 407 - 413

Tarboton, D. G. 1997: A new method for the determination of flow directions and upslope area in grid digital elevation models; *Water Resources Research*, 33, 309 - 319

Thiéry, J. M., D'Herbes, J.-H., and Valentin, C. 1995: A model simulating the genesis of banded vegetation patterns in Niger; *Journal of Ecology*, 83, 497 - 507

Thornes, J. B. 1976: Semi-arid erosional systems; *LSE Occasional paper*, 7

Thornes, J. B. 2001: Environmental crises in the Mediterranean; in (eds.) King, R, de Mas, P, and Mansvelt Beck, J, *Geography, Environment and Development in the Mediterranean*, Sussex Academic Press, Brighton, 261 - 280

Thornes, J. B., Shannon, J., and Richardson, R. 1999: Modelling flow regimes in ephemeral channels; in (ed.) Thornes, J., *Mediterranean Desertification and Land Use, MEDALUS III 1996 - 1999: Ephemeral Channels and Rivers*, 197 - 244

Thornes, J. B., Shao, J. X., Diaz, E., Roldan, A., McMahon, M., and Hawkes, J. C. 1996: Testing the MEDALUS hillslope model; *Catena*, 26, 137 - 160

Tischendorf, L. and Fahrig, L. 2000: How should we measure landscape connectivity?; *Landscape Ecology*, 15, 633 - 641

Truman, C. C., Wauchope, R. D., Sumner, H. R., Davis, J. G., Gascho, G. J., Hook, J. E., Chandler, L. D., and Johnson, A. W. 2001: Slope length effects on runoff and sediment delivery; *Journal Of Soil And Water Conservation*, 56, 249 - 256

UNEP 1992: *World atlas of desertification*; Edward Arnold, Sevenoaks, UK, 192 pages

Valentin, C., d'Herbès, J. M., and Poesen, J. 1999: Soil and water components of banded vegetation patterns.; *Catena*, 37, 1 - 24

Van de Giesen, N. C., Stomph, T. J., and de Ridder, N. 2000: Scale effects of Hortonian overland flow and rainfall-runoff dynamics in a West African catena landscape; *Hydrological Processes*, 14, 165 - 175

Van Wesemael, B., Mulligan, M., and Poesen, J. 2000: Spatial patterns of soil water balance on intensively cultivated hillslopes in a semi-arid environment: the impact of rock fragments and soil thickness; *Hydrological Processes*, 14, 1811 - 1828

Van Wesemael, B., Poesen, J., Kosmas, C. S., Danalatos, N. G., and Nachtergaele, J. 1996: Evaporation from cultivated soils containing rock fragments; *Journal of Hydrology*, 182, 65 - 82

Wainwright, J. 1996: Infiltration, runoff and erosion characteristics of agricultural land in extreme storm events, SE France; *Catena*, 26, 27 - 47

Wainwright, J., Parsons, A. J., and Abrahams, A. D. 2000: Plot scale studies of vegetation, overland flow and erosion interactions: case studies from Arizona and New Mexico; *Hydrological Processes*, 14, 2921 - 2943

Wainwright, J. and Parsons, A. J. 2002: The effect of temporal variations in rainfall on scale dependency in runoff coefficients; *Water Resources Research*, 38, art - 1271

Wainwright, J., Parsons, A. J., and Abrahams, A. D. 1999: Rainfall energy under creosotebush: *Journal of Arid Environments*, 43, 111 - 120

Walford, N. 1995: *Geographical data analysis*; John Wiley and Sons, Chichester, 446 pages

Wang, Z., Feyen, J., Van Genuchten, M. T., and Nielsen, D. R. 1998: Air entrapment effects on infiltration rate and flow instability; *Water Resources Research*, 34, 213 - 222

Wijdenes, D. O., Poesen, J., Vandekerckhove, L., and De Luna, E. 1997: Chiselling effects on the vertical distribution of rock fragments in the tilled layer of a Mediterranean soil; *Soil and Tillage Research*, 44, 55 - 66

Wilby, R. 1995: Simulation of precipitation by weather pattern and frontal analysis; *Journal of Hydrology*, 173, 91 - 109

Wilcox, B., Wood, M., and Tromble, J. 1998: Factors influencing infiltrability of semiarid mountain slopes; *Journal of Rangeland Management*, 41, 197 - 206

Williams, J. D., Dobrowolski, J. P., and West, N. E. 1999: Microbiotic crust influence on unsaturated hydraulic conductivity; *Arid Soil Research and Rehabilitation*, 13, 145 - 154

Wise, S. 1998: The effect of GIS interpolation error on the use of digital elevation models in geomorphology; in (eds.) Lane, S., Richards, K., and Chandler, J., *Landform Monitoring, Modelling and Analysis*, John Wiley and Sons, Chichester, 139 - 164

Wood, J. C., Wood, M. K., and Tromble, J. M. 1987: Import factors influencing water infiltration and sediment production on arid lands in New Mexico.; *Journal of Arid Environments*, 12, 111 - 118

Yair, A. and Lavee, H. 1985: Runoff generation in arid and semi-arid zones.; in (eds.) Anderson, M. G. and Burt, T. P., *Hydrological Forecasting.*, John Wiley & Sons Ltd., London, UK, 183 - 220

Zhang, R. 1997: Determination of soil sorpivity and hydraulic conductivity from the disk infiltrometer; *Soil Science Society of America Journal*, 61, 1024 - 1030

Zobeck, T. and Onstad, C. 1987: Tillage and rainfall effects on random roughness: a review; *Soil and Tillage Research*, 9, 1 - 20